

W. Bergman

CONF-820833

Volume 1

PROCEEDINGS of the
17th DOE NUCLEAR AIR CLEANING CONFERENCE
Held in Denver, Colorado
2-5 August 1982

**Sponsors: U.S. Department of Energy
The Harvard Air Cleaning Laboratory**

**Editor
Melvin W. First**

**Published
February, 1983**

PROGRAM COMMITTEE

W.L. Anderson
R.R. Bellamy
J.F. Bresson
C.A. Burchsted
T.O. Chee
H.L. Ettinger
W.P. Gammill
H. Gilbert
M.J. Kabat
J.L. Kovach
D.W. Moeller
T.R. Thomas

CONFERENCE CHAIRMAN

Melvin W. First
Harvard Air Cleaning Laboratory

FOREWORD

The Seventeenth DOE Nuclear Air Cleaning Conference was held in Denver, CO., August 2-5, 1982, under sponsorship of the U.S. Department of Energy (DOE) and the Harvard Air Cleaning Laboratory. Attending the conference were 260 air cleaning specialists from the United States, Belgium, Canada, the Federal Republic of Germany, France, Italy, Japan, the Netherlands, Portugal, Spain, Sweden, the United Kingdom, and Yugoslavia.

The conference agenda included sessions on the definition of nuclear power plant source terms; the behavior and transport of specific radionuclides under accident conditions; performance standards, procedures, and instruments for evaluating the efficiency of air cleaning systems; air cleaning requirements for spent fuel reprocessing; special approaches for the control of ^{14}C , radioiodine, and the noble gases; development of computer models for evaluating component failures in air cleaning systems and the performance of specific systems under normal and accident conditions; contamination control and personnel protection; repair requirements and failure rates in air cleaning systems; and problems related to quality assurance.

A meeting of the Government-Industry Committee on Filters, Media, and Media Testing was held immediately prior to the opening of the conference to provide a forum for the exchange of viewpoints between suppliers and users of air cleaning equipment and the presentation of reports by various task groups addressing specific issues and developing air cleaning standards.

A conference of this size and complexity requires the dedicated service and wise counsel of many. The Chairman of the 17th DOE Nuclear Air Cleaning Conference wishes to record his appreciation of the firm support and willing assistance provided by the Program Committee throughout the lengthy planning process and during the Conference, itself. In addition to the Program Committee, many at the Rocky Flats Plant of Rockwell International in Boulder, notably Mr. W.D. Crossland and Dr. R.E. Yoder, and each of their staffs, provided essential local support for the Conference. Administrative support for the Conference and preparation of the Proceedings was ably provided by Mrs. Joan Sullivan at the Harvard School of Public Health.

Melvin W. First
Program Chairman

TABLE OF CONTENTS

VOLUME I

FOREWORDiii

Session 1

OPENING OF THE CONFERENCE

Monday: August 2, 1982
CHAIRMAN: D.W. Moeller
Harvard School of Public Health

WELCOME by James R. Nicks, U.S.
Department of Energy 2

WELCOME AND OBJECTIVES OF CONFERENCE by Melvin
W. First, Harvard Air Cleaning Laboratory 10

KEYNOTE ADDRESS by Roger J. Mattson, U.S.
Nuclear Regulatory Commission 13

DISCUSSION 20

INVITED PAPER:

POTENTIAL AIR CLEANING PROBLEMS IN FUSION REACTORS
by J.G. Crocker, EG&G Idaho, Inc. 21

REPORT:

NUCLEAR STANDARDS AND SAFETY PROGRESS IN NUCLEAR STANDARDS
DEVELOPMENT by James F. Fish, Consultant 36

Session 2

FUEL REPROCESSING

Tuesday: August 3, 1982
CO-CHAIRMEN: J.L. Kovach
J.W. Jacox
Nuclear Consulting Service

BALANCE AND BEHAVIOR OF GASEOUS RADIONUCLIDES RELEASED
DURING INITIAL PWR FUEL REPROCESSING OPERATIONS by A.
Leudet, P. Miguel, J.P. Goumondy, G. Charrier, Commissariat
a l'Energie Atomique 40

DISCUSSION 50

17th DOE NUCLEAR AIR CLEANING CONFERENCE

TIME-DEPENDENT ANALYSES OF DISSOLVER OFF-GAS CLEANING
INSTALLATIONS IN A REPROCESSING PLANT by K. Nagle, J.
Furrer, Kernforschungszentrum Karlsruhe and G. Becker,
W. Obrowski, Y.P. Seghal, J. Weyman, Technische Univer.
Berlin 51
DISCUSSION 74

A MODEL OF IODINE-129 PROCESS DISTRIBUTIONS IN A NUCLEAR
FUEL REPROCESSING PLANT by G.J. McManus, F.A. Duce, S.J.
Fernandez, L.P. Murphy, Exxon Nuclear Idaho Co. 75
DISCUSSION 98

CARBON DIOXIDE - KRYPTON SEPARATION AND RADON REMOVAL FROM
NUCLEAR FUEL REPROCESSING OFF-GAS STREAMS by P.M. Hirsch,
K.Y. Higuchi, J. Abraham, General Atomic Company 99
DISCUSSION122

ADSORPTION OF GASEOUS RuO₄ BY VARIOUS SORBENTS II by Lj.
Vujisic, R. Nikolic, Boris Kidric Institute of Nuclear
Sciences-Vinca123
DISCUSSION130

TEST RESULTS IN THE TREATMENT OF HTR REPROCESSING OFF-GAS
by H. Barnert-Wiemer, B. Bendick, B. Juergens, A. Nafissi,
H. Vygen, Kerforschungsanlage Juelich and W. Krill, Nukem,
Hanau131

SOURCE TERM AND MATERIAL TRANSPORT

SURFACE DEPOSITION OF RADON DECAY PRODUCTS WITH AND WITHOUT
ENHANCED AIR MOTION by S.N. Rudnick, E.F. Maher, W.C. Hinds,
M.W. First, Harvard Air Cleaning Laboratory151
DISCUSSION170

FORMATION AND CHARACTERIZATION OF FISSION-PRODUCT AEROSOLS
UNDER POSTULATED HTGR ACCIDENT CONDITIONS by I.N. Tang, H.R.
Munkelwitz, Brookhaven National Laboratory172

CLOSING REMARKS OF SESSION CHAIRMAN181

Session 3

RADIOIODINE

Tuesday: August 3, 1982
CO-CHAIRMEN: T.R. Thomas
J.D. Christian
Exxon Nuclear Idaho Co.

ORGANIC IODINE REMOVAL FROM SIMULATED DISSOLVER OFF-GAS STREAMS
USING PARTIALLY EXCHANGED SILVER MORDENITE by R.T. Jubin, Oak
Ridge National Laboratory183

17th DOE NUCLEAR AIR CLEANING CONFERENCE

DISCUSSION 197

A PARAMETRIC STUDY ON REMOVAL EFFICIENCY OF IMPREGNATED ACTI-
VATED CHARCOAL AND SILVER ZEOLITE FOR RADIOACTIVE METHYL
IODIDE by H. Shiomi, Y. Yuasa, A. Tani, Nippon Atomic Industry
Group Co., Ltd. M. Ohki, T. Nakagawa, Toshiba Corp. 199

DISCUSSION 222

DATA ANALYSIS OF IN-PLACE TESTS OF IODINE FILTERS IN THE
FRENCH NUCLEAR FACILITIES by P. Mulcey, L. Trehen, J.L. Rouyer,
Institut de Protection et de Sûreté Nucléaire 223

DISCUSSION 237

IODINE FILTERING FOR FRENCH REPROCESSING PLANTS by G. Bruzzone,
J.L. Rouyer, Ph. Mulcey, A. Vaudano, Commissariat à l'Energie
Atomique 239

DISCUSSION 247

RETENTION OF ELEMENTAL RADIOIODINE BY DEEP BED CARBON FILTERS
UNDER ACCIDENT CONDITIONS by H. Deuber, J.G. Wilhelm,
Kernforschungszentrum Karlsruhe 248

DISCUSSION 277

EXPERIENCES WITH A CHARCOAL GUARD BED IN A NUCLEAR POWER PLANT
by L.C. Scholten, N.V. KEMA Laboratories 278

DISCUSSION 284

DEPOSITION OF AIRBORNE RADIOIODINE SPECIES ON SURFACES OF METALS
AND PLASTICS by M.J. Kabat, Ontario Hydro 285

DISCUSSION 297

CLOSING REMARKS OF SESSION CHAIRMAN 301

Session 4

WASTE PROCESSING

Tuesday: August 3, 1982
CO-CHAIRMEN: M.J. Kabat
C.H. Cheh
Ontario Hydro

OPENING REMARKS OF SESSION CHAIRMAN 304

OFF-GAS CHARACTERISTICS OF LIQUID-FED JOULE-HEATED CERAMIC
MELTERS by R.W. Goles, G.J. Sevigny, Pacific Northwest Lab. 305

IMMOBILIZATION OF KRYPTON-85 IN ZEOLITE 5A+ by A.B.
Christensen, J.A. Del Debbio, D.A. Knecht, J.E. Tanner,
S.C. Cossel, Exxon Nuclear Idaho Company 333

DISCUSSION 357

17th DOE NUCLEAR AIR CLEANING CONFERENCE

THE LONG-TERM STORAGE OF RADIOACTIVE KRYPTON BY FIXATION IN
ZEOLITE 5A+ by R.D. Penzhorn, H. Leitzig, K. Gunther, P. Schuster
H.E. Noppel, Kernforschungszentrum Karlsruhe385
DISCUSSION370

VOLATILIZATION AND TRAPPING OF RUTHENIUM IN HIGH TEMPERATURE
PROCESSES by M. Klein, C. Weyers, W.R.A. Goossens, SCK/CEN,
Nuclear Energy Center371
DISCUSSION380

RADIOCARBON TREATMENT SYSTEMS

PLANT FOR RETENTION OF ¹⁴C IN REPROCESSING PLANTS FOR LWR
FUEL ELEMENTS by H. Braun, Federal Ministry of the Interior,
F.R.G., H. Gutowski, Linde AG, Hollriegelskreuth, H. Bonka,
Technical Univ. Aachen, D. Gründler, GRS, Cologne381

MECHANISM OF THE CO₂-Ca(OH)₂ REACTION by V.S. Chew, C.H.
Cheh, R.W. Glass, Ontario Hydro400
DISCUSSION413

¹⁴C RELEASE AT LIGHT WATER REACTORS by C. Kunz, New York
State Department of Health414
DISCUSSION429

CARBON-14 IMMOBILIZATION VIA THE Ba(OH)₂·8H₂O PROCESS by G.L.
Haag, J.W. Nehls, Jr., G.C. Young, Oak Ridge National Lab.431
DISCUSSION454

CLOSING REMARKS OF SESSION CHAIRMAN455

Session 5

FILTRATION AND FILTER TESTING I

Tuesday: August 3, 1982
CO-CHAIRMEN: H.T. Etinger
Los Alamos National Lab.
B.V. Gerber
U.S. Army Arradcom Chemical
Systems Laboratory

VERTICAL REMOVABLE FILTERS IN SHIELDED CASING FOR RADIOACTIVE
CELLS AND PROCESS GASEOUS WASTES by M. Prinz, S.G.N.457
DISCUSSION480

DEVELOPMENT OF FILTERS AND HOUSINGS FOR USE ON ACTIVE PLANT
by S. Hackney, R.P. Pratt, U.K. Atomic Energy Authority482
DISCUSSION503

AEROSOL FILTRATION WITH METALLIC FIBROUS FILTERS by M. Klein,
W.R.A. Goossens, SCK/CEN Nuclear Energy Center504

17th DOE NUCLEAR AIR CLEANING CONFERENCE

DISCUSSION 522

EVALUATION OF PERMANENTLY CHARGED ELECTROFIBROUS FILTERS by
A.H. Biermann, B.Y. Lum, W. Bergman, Lawrence Livermore National
Laboratory 523

EVALUATION OF PROTOTYPE ELECTROFIBROUS FILTERS FOR NUCLEAR
VENTILATION DUCTS by W. Bergman, W.D. Kuhl, A.H. Biermann, J.S.
Johnson, B.Y. Lum, Lawrence Livermore National Laboratory 548

DISCUSSION 574

A NEW METHOD OF DETERMINING THE OVERALL PARTICLE DECONTAMINATION
FACTOR FOR MULTIPLE OFF-GAS CLEANING COMPONENTS IN REPROCESSING
PLANTS by J. Furrer, A. Linek, Kernforschungszentrum Karlsruhe .. 576

DISCUSSION 590

IN-SITU CONTROL OF FILTRATION SYSTEMS IN FRANCE: 5 YEARS
EXPERIENCE by J. DuPoux, Institut de Protection et de Sûreté
Nucléaire 591

DISCUSSION 601

CONTAMINATION CONTROL AND PERSONNEL PROTECTION

AIR CLEANING PHILOSOPHY IN A NUCLEAR MATERIALS FABRICATION PLANT
by F.Y. Ward, R.E. Yoder, Rockwell International 602

DISCUSSION 610

SYSTEM OPERATIONAL TESTING OF MAJOR VENTILATION SYSTEMS FOR A
PLUTONIUM RECOVERY FACILITY by F.J. Linck, Jr., Rockwell
International 612

DISCUSSION 622

CLOSING REMARKS OF SESSION CHAIRMAN 623

VOLUME II

Session 6

ADSORPTION

Wednesday: August 4, 1982
CO-CHAIRMEN: C.A. Burchsted
Oak Ridge National Laboratory
V.R. Deitz
Naval Research Laboratory

NEW ADSORBENT, SILVER-ALUMINA FOR RADIOACTIVE IODINE FILTER
by M. Kikuchi, K. Funabashi, F. Kawamura, H. Yusa, H.
Tsuchiya, Energy Research Laboratory, Hitachi, Y. Takashima,
Nuclear Power Plant Engineering Department, Hitachi 626

DISCUSSION 639

17th DOE NUCLEAR AIR CLEANING CONFERENCE

CHARCOAL PERFORMANCE UNDER SIMULATED ACCIDENT CONDITIONS
by V.R. Deitz, Naval Research Laboratory 641
DISCUSSION 650

TEDA VS. QUINUCLIDINE: EVALUATION AND COMPARISON OF TWO
TERTIARY AMINE IMPREGNANTS FOR METHYL IODIDE REMOVAL FROM
FLOW AIR STREAM by J.L. Kovach, J.J. Grimm, W.P. Freeman,
Nuclear Consulting Services 652
DISCUSSION 663

NOBLE GAS TREATMENT

EXPERIMENTS ON ADSORPTION RETENTION OF NO_x AND KRYPTON FROM
DISSOLVER OFF-GAS by H. Ringel, Kernforschungsanlage Julich 664
DISCUSSION 682

FORMATION AND BEHAVIOUR OF NITRIC OXIDES IN A CRYOGENIC
KRYPTON SEPARATION SYSTEM AND CONSEQUENCES OF USING AIR
AS PROCESS GAS by R. vonAmmon, W. Bumiller, E. Hauss, E.
Hutter, G. Neffe, Kernforschungszentrum Karlsruhe, R.R.
Hammer, Exxon Nuclear Idaho, Inc. 683
DISCUSSION 693

NOBLE GAS REMOVAL AND CONCENTRATION BY COMBINING FLUOROCARBON
ABSORPTION AND ADSORPTION TECHNOLOGIES by D.K. Little, R.S.
Eby, J.L. Norton, J.L. Patton, R.M. Schultz, J.M. Vargagona,
Oak Ridge Gaseous Diffusion Plant 694
DISCUSSION 716

PERSONNEL EDUCATION AND TRAINING

FAILURES IN AIR-CLEANING, AIR-MONITORING, AND VENTILATION
SYSTEMS IN COMMERCIAL NUCLEAR POWER PLANTS (1/1/78-12/31/81)
by D.W. Moeller, L.S. Casper Sun, Harvard School of Public
Health 768
CLOSING REMARKS OF SESSION CHAIRMAN 769

Session 7

FILTRATION AND FILTER TESTING II

Wednesday: August 4, 1982
CO-CHAIRMEN: H. Gilbert
Consultant
K.J. Freiberg
Rockwell International

REPORT OF MINUTES OF GOVERNMENT-INDUSTRY MEETING ON FILTERS,
MEDIA, AND MEDIA TESTING by W.L. Anderson, Naval Surface
Weapons Center 771

17th DOE NUCLEAR AIR CLEANING CONFERENCE

APPENDIX A.	A REVIEW OF DOE FILTER TEST FACILITY OPERATIONS 1970-1980 by C.A. Burchsted, Oak Ridge National Laboratory	775
APPENDIX B.	DOE FILTER TEST PROGRAM - POLICY FOR THE '80s by J.F. Bresson, U.S. Department of Energy	788
APPENDIX C.	A SURVEY OF HEPA FILTER EXPERIENCE by E.H. Carbaugh, Pacific Northwest Laboratory	790
	DISCUSSION	800
APPENDIX D.	POTENTIAL APPLICATION OF A SINGLE PARTICLE AEROSOL SPECTROMETER FOR MONITORING AEROSOL SIZE AT THE DOE FILTER TEST FACILITIES by G.C. Salzman, H.J. Ettinger, M.I. Tillery, L.D. Wheat, W.K. Grace, Los Alamos National Laboratory	801
	DISCUSSION	814
APPENDIX E.	OPERATIONAL EXPERIENCE USING DIETHYLHEXYLSEBACATE (DEHS) AS A CHALLENGE TEST AEROSOL IN FILTER TESTING by R.D. Gilmore, J.A. McIntyre, G.R. Petersen, Hanford Environmental Health Foundation	821
	DISCUSSION	833
APPENDIX F.	THE NEED FOR REVISING U.S. NUCLEAR REGULATORY COMMISSION REGULATORY GUIDE 1.52 IN LIGHT OF NRC-SPONSORED RESEARCH PROGRAM RESULTS AND OTHER DEVELOPMENTS by R.L. Bangart, U.S. Nuclear Regulatory Commission	836
	DISCUSSION	845
	IN-PLACE HEPA FILTER AEROSOL TEST SYSTEM by R.L. Herman, Rockwell Hanford Operations	847
	DISCUSSION	865
	IN-PLACE REALTIME HEPA FILTER TEST METHOD by F.A. Hohorst, S.J. Fernandez, Exxon Nuclear Idaho Co.	867
	DISCUSSION	881
	DOE TESTING HEPA FILTER BANKS IN SERIES by W.D. Hanson, Exxon Nuclear Idaho Company, Inc.	882
	DISCUSSION	894
	THE EFFECT OF PARTICLE SIZE VARIATION ON FILTRATION EFFICIENCY MEASURED BY THE HEPA FILTER QUALITY ASSURANCE TEST by M.I. Tillery, G.C. Salzman, H.J. Ettinger, Los Alamos National Laboratory	895
	DISCUSSION	908

17th DOE NUCLEAR AIR CLEANING CONFERENCE

PERFORMANCE OF 1000- and 1800- CFM HEPA FILTERS ON LONG EXPOSURE TO LOW ATMOSPHERIC DUST LOADINGS, III by M.W. First, J.M. Price, Harvard Air Cleaning Laboratory 909
DISCUSSION 918

MEASUREMENT AND INSTRUMENTATION

PORTABLE FILTER TESTING INSTRUMENTATION USED FOR IN-PLACE LEAK TESTING OF LARGE AIR FILTERS UP TO 38 m³ sec⁻¹ (80,000 CFM) by J.L. Kovach, B.J. Kovach, F.L. Powers, W.A. Johnson, Nuclear Consulting Services 919
DISCUSSION 936

POLYMERIC DIFFUSION AS APPLIED TO A RADIOIODINE OFF-GAS MONITOR by S.J. Fernandez, L.P. Murphy, Exxon Nuclear Idaho Company 937
DISCUSSION 948

CLOSING REMARKS OF SESSION CHAIRMAN 950

Session 8

WORKING LUNCH

Wednesday: August 4, 1982
Chairman: R.E. Yoder
Rockwell International

ENERGY AND FEAR by H. Specter, Indian Point 3 Hearing Technical Support 952

Session 9

AIR CLEANING EQUIPMENT RESPONSE TO ACCIDENT RELATED STRESS

Wednesday: August 4, 1982
CO-CHAIRMEN: R.R. Bellamy
U.S. Nuclear Regulatory Commission
J.F. Bresson
U.S. Department of Energy

METHODS FOR NUCLEAR AIR CLEANING SYSTEM ACCIDENT CONSEQUENCE ASSESSMENT by R.W. Andrae, J.W. Bolstad, W.S. Gregory, F.R. Krause, R.A. Martin, P.K. Tang, Los Alamos National Laboratory, M.Y. Ballinger, M.K. Chan, J.A. Glissmeyer, J. Mishima, P.C. Owczarski, S.L. Sutter, Pacific Northwest Laboratory, E.L. Compere, H.W. Godbee, Oak Ridge National Laboratory 990
DISCUSSION 1001

HEPA FILTER EXPERIENCE DURING THREE MILE ISLAND REACTOR BUILDING PURGES by R.R. Bellamy, U.S. Nuclear Regulatory Commission 1003
DISCUSSION 1010

17th DOE NUCLEAR AIR CLEANING CONFERENCE

SIMULATION OF FORCED VENTILATION FIRES by F.R. Krause,
W.S. Gregory, Los Alamos National Laboratory 1018
DISCUSSION 1028

FIRE TESTING OF HEPA FILTERS INSTALLED IN FILTER HOUSINGS
by S. Hackney, United Kingdom Atomic Energy Authority 1030
DISCUSSION 1048

RESPONSE OF HEPA FILTERS TO SIMULATED ACCIDENT CONDITIONS
by W.S. Gregory, R.A. Martin, Los Alamos National Laboratory,
P.R. Smith, D.E. Fenton, New Mexico State University 1051
DISCUSSION 1067

HEPA FILTER RESPONSE TO HIGH AIR FLOW VELOCITIES by V.
Ruedinger, J.G. Wilhelm, Kernforschungszentrum Karlsruhe 1069
DISCUSSION 1092

EFFECTS OF SHOCK WAVES ON HIGH EFFICIENCY FILTER UNITS by
A. Cuccuru, S. Cultrera, U. Marandola, C.A.M.E.N., Italy,
S. Lanza, University of Pisa 1093

Session 10

OPEN END

Thursday: August 5, 1982
CO-CHAIRMEN: M.W. First
D.W. Cooper
Harvard School of Public Health

THE DEVELOPMENT OF A LIGHTWEIGHT, COMPACTIBLE/DISPOSABLE
HEPA FILTER by T.T. Allan, Flanders Filters, Inc. 1110
DISCUSSION 1114

EVALUATION OF HEPA FILTERS MEETING MIL-F-51068 PURCHASED
ON THE OPEN MARKET. ARE THEY NUCLEAR GRADE? by T.T.
Allan, R.V. Cramer, Flanders Filters, Inc. 1115
DISCUSSION 1119

RECENT CHANGES IN MIL-F-51068 SPECIFICATION by G.P. Smith,
U.S. Army, Chemical Systems Laboratory 1121
DISCUSSION 1123

DEVELOPMENT AND EVALUATION OF ACID-RESISTANT HEPA FILTER
MEDIA by G.W. Brassell, W.G. Thorvaldson, Rockwell Inter-
national 1125
DISCUSSION 1133

A CHANGEABLE BED ACTIVATED CARBON FILTER WITH HIGH ACCURACY
AND EFFICIENCY by H. Stiehl, H.J. Lippold, Delbag-Luftfilter,
W. Mathewes, Kraftwerk Union AG 1134

17th DOE NUCLEAR AIR CLEANING CONFERENCE

IODINE REMOVAL BY SILVER-EXCHANGED ZEOLITE FILTERS FROM THE VESSEL OFF GAS IN TOKAI REPROCESSING PLANT by A. Kawaguchi, M. Fukushima, K. Miyahara, K. Matsumoto, Tokai Works Power Reactor & Nuclear Fuel Development Corporation1142

THE DEVELOPMENT OF MOBILE FILTRATION UNITS FOR USE IN RADIOACTIVE FACILITIES by J. Dymont, Atomic Weapons Research Est.1152

DISCUSSION1156

HIGH-EFFICIENCY CHARCOAL AIR FILTER WITH COMBUSTIBLE FRAME by J.R. Edwards, Charcoal Service Corporation1157

DISCUSSION1158

Session 11

CONTAINMENT VENTING AIR CLEANING

Thursday: August 5, 1982
CO-CHAIRMEN: W.L. Anderson
Naval Surface Weapons Center
J. D'Ambrosia
U.S. Department of Energy

EXPERIMENTAL INVESTIGATIONS OF AEROSOL FILTRATION WITH DEEP BED FIBER FILTERS by H.G. Dillman, H. Pasler, Kernforschungszentrum Karlsruhe1160

VENTURI SCRUBBING FOR FILTERED VENTED CONTAINMENT by D.W. Cooper, Harvard School of Public Health1175

DISCUSSION1182

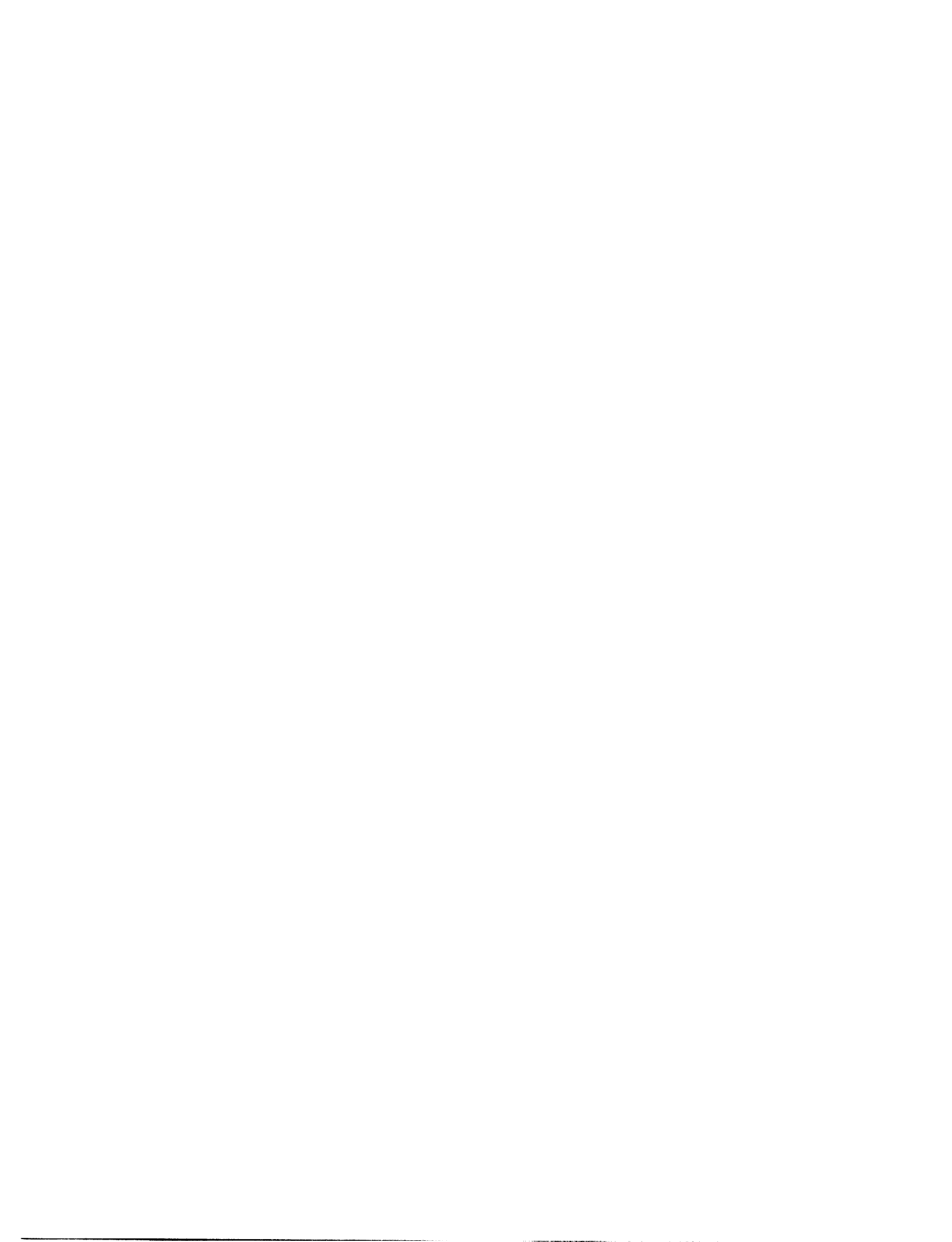
TESTING OF A PASSIVE SUBMERGED GRAVEL SCRUBBER FOR CONTAINMENT VENTING APPLICATIONS by J.D. McCormack, R.K. Hilliard, A.K. Postma, Hanford Engineering Development Laboratory1183

DISCUSSION1200

COST-BENEFIT CONSIDERATIONS FOR FILTERED-VENTED CONTAINMENT SYSTEMS by A.S. Benjamin, D.R. Strip, Sandia National Laboratory1201

INDEX OF AUTHORS AND SPEAKERS1224

LIST OF ATTENDEES1229



17th DOE NUCLEAR AIR CLEANING CONFERENCE

Session I

OPENING OF CONFERENCE

MONDAY: August 2, 1982

CHAIRMAN: D.W. Moeller
Harvard School of Public Health

WELCOME

James R. Nicks

WELCOME AND OBJECTIVES OF CONFERENCE

Melvin W. First

KEYNOTE ADDRESS

Roger J. Mattson

INVITED PAPER:

POTENTIAL AIR CLEANING PROBLEMS IN FUSION REACTORS

J.G. Crocker

REPORT

NUCLEAR STANDARDS AND SAFETY PROGRESS IN NUCLEAR STANDARDS
DEVELOPMENT

James F. Fish

17th DOE NUCLEAR AIR CLEANING CONFERENCE

DOE WELCOME

James R. Nicks, Area Manager
U.S. Department of Energy
Rocky Flats Area Office
Golden, Colorado

ON BEHALF OF THE DEPARTMENT OF ENERGY, WELCOME TO DENVER, COLORADO, THE MILE HIGH CITY, WHERE THE AIR IS THINNER, PERHAPS CRISPER BUT UNFORTUNATELY NOT CLEANER.

WE HAVE BEEN ENJOYING PERIODIC SHOWERS THROUGHOUT THE SUMMER HOWEVER YOU HAVE TIMED THIS CONFERENCE TO COINCIDE WITH EXCELLENT WEATHER CONDITIONS.

THE SURROUNDING HILLS ARE GREENER; THE MOUNTAINS BLUER AND SOME EVIDENCE OF SNOW STILL REMAINS ON THE PEAKS WEST OF THE CITY.

17th DOE NUCLEAR AIR CLEANING CONFERENCE

DENVER IS AN APPROPRIATE LOCATION FOR A NUCLEAR AIR CLEANING CONFERENCE.

WE ARE ABOUT 16 AIR MILES FROM THE DEPARTMENT OF ENERGY'S ROCKY FLATS PLANT, OPERATED BY ROCKWELL INTERNATIONAL.

PART OF OUR WORK AT THE PLANT INVOLVES CHEMICALLY PROCESSING LARGE QUANTITIES OF PLUTONIUM.

THIS INVOLVES EFFLUENT AIR-STREAM CLEANING ON A MULTIMILLION DOLLAR SCALE EVERY YEAR AT ROCKY FLATS;

A HIGH PRICE TO PAY TO GUARANTEE SUCCESS IN MEETING STRINGENT ENVIRONMENTAL AIR QUALITY STANDARDS.

WHY THE HIGH COST FOR AIR CLEANING?

OUR PLANT PROCESSING SYSTEMS ARE VERY LARGE, WHICH REQUIRES OUR EFFLUENT AIR-HANDLING SYSTEMS TO BE VERY LARGE ALSO.

THESE SYSTEMS ARE CONTINUOUSLY EXPOSED TO SIGNIFICANT CONCENTRATIONS OF PLUTONIUM AEROSOLS. MULTIPLE BANKS OF HEPA HIGH, EFFICIENT, PARTICULATE AIR FILTERS ARE REQUIRED IN THESE SYSTEMS, AND IN SPITE OF PRE-FILTERS, SOME FILTER SYSTEMS TEND TO LOAD UP SURPRISINGLY FAST.

17th DOE NUCLEAR AIR CLEANING CONFERENCE

WE HAVE ESTABLISHED A DEDICATED WORK CREW WHOSE FULL-TIME JOB IS CHANGING HEPA FILTERS AND PERFORMING IN-PLACE FILTER TESTS.

DUE TO OUR EXTENSIVE USE OF HEPA FILTERS (6000-8000 PER YEAR), WE OPERATE ONE OF THE THREE DOE HEPA FILTER TEST FACILITIES WHICH SERVICES MAINLY OUR OWN PLANT.

HOWEVER, WE ALSO TEST FILTERS FOR OTHER DOE INSTALLATIONS, AND FOR SOME NON-DOE CUSTOMERS. IN ADDITION, WE QUANTITATIVELY TEST SEVERAL THOUSAND RESPIRATOR CANISTERS EACH MONTH; WE CAN EVALUATE HEPA FILTER PERFORMANCE FOLLOWING EXPOSURE TO HIGH HUMIDITY OR HIGH TEMPERATURES, AND WE CAN FORMULATE OR ANALYZE THE FILTERING COMPONENTS.

WITH THIS BACKGROUND I WANT TO MENTION SOME THOUGHTS ON AIR CLEANING PROBLEM AREAS STILL NEEDING SOLUTIONS.

I'LL FOCUS ON TWO GENERAL AREAS:

THE FIRST IS RELATED TO SYSTEMS DESIGN AND THE HIGH COSTS FOR AIR CLEANING.

17th DOE NUCLEAR AIR CLEANING CONFERENCE

AS I SAID, OUR CURRENT AIR CLEANING SYSTEMS ARE VERY LARGE BECAUSE THEY CONTINUOUSLY "CLEAN" AIR WHICH IS NORMALLY CLEAN TO BEGIN WITH.

THIS CLEAN AIR IS IN AREAS WHICH SURROUND GLOVE BOXES AND HOT CELLS.

BASED ON OUR SAMPLING DATA, THE AIR COULD NORMALLY BE EXHAUSTED TO THE ENVIRONMENT OR RECIRCULATED WITHOUT TREATMENT.

IT IS CONTINUOUSLY CLEANED, HOWEVER, BECAUSE THIS AIR COULD BE CONTAMINATED IF RADIOACTIVE MATERIAL WERE TO BE RELEASED FROM PRIMARY CONFINEMENT STRUCTURES.

THESE AIR VOLUMES, OFTEN INHABITED BY OPERATING PERSONNEL, ARE USUALLY QUITE LARGE AND AIR CLEANUP IS EXPENSIVE.

THESE FACILITIES WERE DESIGNED BEFORE THE AGE OF ENERGY CONSERVATION.

IT SEEMS FEASIBLE TO DESIGN NUCLEAR FACILITIES WITH REDUCED AIR VOLUMES OF PRIMARY AND SECONDARY CONFINEMENT SYSTEMS, RESULTING IN SMALLER, BETTER, AND MORE ECONOMICAL CLEANUP SYSTEMS.

17th DOE NUCLEAR AIR CLEANING CONFERENCE

THE GOAL WOULD BE TO AVOID TREATING A LARGE PERCENTAGE OF THE AIR EXHAUSTED OR RECIRCULATED FROM OPERATING AREAS DURING NORMAL OPERATIONS. THE INCENTIVE IS ENERGY CONSERVATION AND THEREFORE COST SAVINGS, WITHOUT COMPROMISING HEALTH AND SAFETY.

AN ADDITIONAL REQUIREMENT IS TO DEVELOP MORE STABLE, MORE RELIABLE RADIATION DETECTION INSTRUMENTATION AND ELECTRICAL SWITCHING MECHANISMS, SO THAT UPON DETECTION OF RADIONUCLIDE RELEASE TO AN OPERATING AREA WHICH WOULD NORMALLY NOT BE FILTERED, A SIGNAL FROM THE DETECTION SYSTEM COULD BE USED TO SWITCH FROM AN UNFILTERED TO A FILTERED MODE.

THE DETECTION AND SWITCHING MECHANISMS MUST BE EXTREMELY RELIABLE.

THIS CONCEPT IS CURRENTLY BEING CONSIDERED IN SOME OF DOE'S NEWER TRITIUM-HANDLING FACILITIES, AND IS PROPOSED FOR USE IN THE WIPP.

WHEN PERFECTED, THE SAME SCHEME COULD BE MOST USEFUL IN OTHER RADIOACTIVE MATERIALS HANDLING FACILITIES.

17th DOE NUCLEAR AIR CLEANING CONFERENCE

THE SECOND AREA OF NEED IS WITH THE AIR-CLEANING DEVICES THEMSELVES. HEPA FILTERS, WITH THEIR INHERENT STRUCTURAL WEAKNESS, SERVE AS THE ONLY EFFLUENT AIR SYSTEM BARRIER BETWEEN RADIONUCLIDE PROCESS AREA AND THE ENVIRONMENT.

THEY ARE EXPECTED TO PERFORM UNDER SEVERELY ADVERSE CONDITIONS, SUCH AS CORROSIVENESS, HIGH TEMPERATURE, HIGH HUMIDITY, HIGH DUST OR SMOKE LOADING, AND POSSIBLY HIGH-PRESSURE TRANSIENTS. ITEMS SUCH AS MECHANICAL SCRUBBERS AND PRE-FILTERS DO NOT TOTALLY RESOLVE THE PROBLEMS, AND SOME OF THEM, LARGE SCRUBBERS FOR EXAMPLE, OFTEN CREATE MORE PROBLEMS THAN THEY SOLVE.

FILTERS LOAD UP, GET PUNCTURED, AND GET WET. THE ADHESIVE BURNS OR DETERIORATES AND THE FILTERS MUST BE CHANGED OFTEN.

I BELIEVE AN ACCEPTABLE AIR-CLEANING DEVICE SHOULD BE STRUCTURALLY STRONG, LONG LASTING, EFFICIENT, AND SHOULD FUNCTION DURING ALL KINDS OF ADVERSE SITUATIONS.

IT SHOULD BE RESTORABLE (CLEANABLE) AND NOT DETERIORATE.

17th DOE NUCLEAR AIR CLEANING CONFERENCE

AND, OF COURSE, IT SHOULD BE COST EFFECTIVE.

I AM AWARE OF R&D ACTIVITIES IN AT LEAST ONE OF THESE AREAS (RESISTANCE TO CORROSIVITY) BUT NOT ALL OF THEM.

I'M SURE THERE ARE OTHER AREAS IN NEED OF ATTENTION.

I WILL LOOK FORWARD WITH INTEREST TO THE REPORTS OF THE NEXT AIR CLEANING CONFERENCE TO SEE WHAT PROGRESS HAS BEEN ACCOMPLISHED IN THESE AREAS.

I APPRECIATE YOUR ATTENTION, AND I HOPE THAT THIS CURRENT CONFERENCE IS PRODUCTIVE AND SUCCESSFUL.

I WAS ASKED ABOUT A TOUR OF OUR NEW PLUTONIUM FACILITY, WHICH HAS RECENTLY GONE ON LINE.

THE AIR-CLEANING PROVISIONS IN THIS NEW FACILITY ARE INTERESTING (SOME WOULD SAY AWESOME) AND OF PROBABLE GREAT INTEREST TO THIS GROUP, HOWEVER, SECURITY CONSIDERATIONS WILL NOT PERMIT ME TO AUTHORIZE A TOUR.

AS AN ALTERNATIVE, KEN FREIBERG OF ROCKWELL INTERNATIONAL HAS PUT TOGETHER A SLIDE PRESENTATION OF FACILITY CONSTRUCTION AND SYSTEMS CHECK-OUT ACTIVITIES, WHICH HE IS WILLING TO PRESENT DURING BREAKS, LUNCH, OR AFTER DAILY

17th DOE NUCLEAR AIR CLEANING CONFERENCE

SESSIONS HAVE CONCLUDED IF THERE IS ENOUGH
INTEREST.

THIS IS A GOOD PRESENTATION, AND I RECOMMEND THAT
YOU TAKE ADVANTAGE OF KEN'S OFFER.

17th DOE NUCLEAR AIR CLEANING CONFERENCE

WELCOME AND OBJECTIVES OF THE CONFERENCE

Melvin W. First
Harvard Air Cleaning Laboratory
School of Public Health
Boston, Massachusetts

I join my colleague, Dade Moeller, in welcoming you to the 17th DOE Nuclear Air Cleaning Conference on behalf of Harvard University and the DOE, joint sponsors of this meeting.

Looking back to prior Conferences, we recollect that the very first one was intended as a mini-course on the general subject of air and gas cleaning technology by the staff of the Harvard Air Cleaning Laboratory because, in truth, at that time there was no discipline identifiable as nuclear air and gas cleaning technology and there were few specialists in any sort of air and gas cleaning technology. Largely because of a continuing interest and generous funding on the part of the Atomic Energy Commission, a sizable number of scientists and engineers became specialists in nuclear air and gas cleaning technology. Segments were located at all the major installations - Savannah River, Oak Ridge, Argonne, Brookhaven, Los Alamos, Hanford - at a number of universities such as Harvard and the University of Iowa at Ames, and at research institutions such as Battelle and A.D. Little. Perhaps, this could be called the Golden Age of nuclear air and gas cleaning science. We were highly involved with major technical problems of considerable complexity - waste disposal, incineration technology, aerosol science appropriate for liquid metal cooled nuclear reactors, reprocessing technology, and construction of installations known as LOFT and FFTF - to mention only the civilian nuclear power-related activities.

The Air Cleaning Conferences regularly reported the results of these activities, both the highly theoretical and the very practical, such as how to prevent a fire in a nuclear carbon bed, and the Proceedings became a major reference source of air and gas cleaning information here and abroad. Attendance at these Conferences by nationals of countries other than United States has grown continuously, making this a major international scientific meeting sponsored by an agency of the United States Government: in fact, the only regularly scheduled series in existence exclusively concerned with nuclear air and gas cleaning.

In the beginning, the scientists from other countries came to learn United States technology but soon they began making important contributions of their own. I think we have seen a reversal of the technical flow in recent years as our colleagues in Western Europe and Asia have forged ahead on all aspects of fuel reprocessing air and gas cleaning technology while the United States has been marking time for six years (since the beginning of the previous administration) in this important area of research and engineering. I think we can all say, "Thank goodness," for the continuing efforts of our foreign colleagues in this endeavor inasmuch as the day cannot be far off when we in the United States will find that we are in desperate need of their technology.

United States research programs have been greatly reduced in recent years and their character has altered such that our major efforts are directed toward perfecting and tidying up our technological base. As valuable as refinement of current techniques may be for improving our ability to provide effective and reliable air and gas cleaning equipment, this sort of utile activity provides few new or

17th DOE NUCLEAR AIR CLEANING CONFERENCE

innovative concepts that make it possible to leap forward instead of merely creeping ahead. The former U.S. advocacy for a strong basic research effort on nuclear air and gas cleaning technology seems to have evaporated. HEPA filter damage from handling is reported to be the most prevalent damage yet no one seems to be working on new framing technologies that will avoid this loss. Instead, worker training is advocated. What is needed is engineering re-design to make it impossible, or at least unlikely, that an ordinary worker can damage a filter during shipment and handling. Similarly missing is an engineering research effort to correct personnel error faults in air and gas cleaning systems that Dr. Moeller has been talking to us about for the past six or seven years.

A well worn joke is usually presented as an ancient curse attributable to the Persians, Greeks, the Chinese, or any other group of your choice. It says, "May you live during interesting times." The implication is clear that what historians later designate as "interesting times" are certain to be mighty hard on those condemned to live through them. There can be little question that we here are in the midst of interesting nuclear energy times and have been for about a decade. Not only are we closely beset by a persistent adverse public opinion that is unable or unwilling to make a distinction between the civilian nuclear power industry and nuclear warfare, but we must suffer the funding cutbacks that result from a failure of nerve among our leaders in the face of a clique of antinuclear zealots who have founded new secular religions that generate extraordinary commitment among their fervent, though unthinking, initiates. It is traditional to blame the news media for this state of affairs, and it is, indeed, difficult to have faith in our newspapers when most carry a daily astrology column as a counterpart to their generally inadequate reporting of what in other contexts is referred to as the "Age of Science".

Perhaps it will be more useful to ask why these periods of tumult and disease are referred to as "interesting times". In retrospect, they have stirred the innovators to rethink old habits and come forward with new solutions to old problems. This is a working out of Toynbee's theory of challenge and response, perhaps, a theory that holds that challenge and adversity bring forward the best from a civilization - or its demise when it fails to respond in productive ways.

I have the unhappy feeling that nuclear engineers and others who build, own, and operate civilian nuclear facilities tend to regard nuclear air and gas cleaning devices as unwanted and unnecessary devices that get added to their creations by force of law. When I made a statement a few years ago that nuclear air and gas cleaning systems represented the last engineering safety barrier between the reactor and the public, I was taken to task by several who insisted that the containment structure was the last barrier. Nevertheless, a reading of this Conference's program will reveal the presence of papers on the subject of vented containment and ways to decontaminate the offgases by means of air and gas cleaning technology. Surely, it is clear that here, air and gas cleaning becomes the ultimate barrier for public protection and its critical importance is unimpeachable. And surely, you and I have a clear duty to make certain that this ultimate barrier is of the utmost integrity, reliability, and efficiency. I have less concern that we might fail in this ability than I have that we will succeed splendidly, technically, but fail miserably in bringing the good tidings to our fellow citizens who have less interest in these matters than we.

Returning to my original thought that these are indeed interesting times for you and me in our professional lives, as well as in our secular lives, I hope it will be abundantly evident to all of us that we must do battle on two fronts: we must accomplish the technical advancements that will enable us to tell the public

17th DOE NUCLEAR AIR CLEANING CONFERENCE

that we have provided well for their welfare - not only with an adequate margin of safety but as low as reasonably achievable (ALARA), and we must somehow convince them that they can have confidence in our demonstrated achievements.

These Nuclear Air Cleaning Conferences continue to be a vital step in the steady development of scientific and engineering knowledge, and the professional competence that is necessary for the design, construction, and maintenance of superb nuclear air and gas cleaning systems.

We are here in Denver to advance that knowledge and skill another notch. We look forward, as we wait to hear the sixty-some technical presentations this week, to at least a few giant steps forward in our joint endeavor to develop evermore perfect air and gas cleaning systems for peaceful nuclear energy applications.

Again, I welcome you to the 17th Nuclear Air Cleaning Conference. My wish is that you will have as much pleasure attending as your Program Committee experienced while assembling the program and planning the meeting.

17th DOE NUCLEAR AIR CLEANING CONFERENCE

NRC POLICY ISSUES AFFECTING ACCIDENT EVALUATION AND AIR CLEANING SYSTEMS

Roger J. Mattson, Director
Division of Systems Integration
U. S. Nuclear Regulatory Commission
Washington, D.C. 20555

I am pleased to have the opportunity to represent the Nuclear Regulatory Commission at this conference. I am told it is the 17th in a successful series of technical interchanges of information between the nuclear industry and the government. In my prepared remarks I will describe some recent developments that may result in modifications of NRC criteria for filtration systems designed for nuclear power plant accidents. As you know, the accident at TMI-2 was the impetus for these developments. I also will mention incinerators for the volume reduction of radioactive wastes at nuclear power plants, and the importance of off-gas cleanup systems for such incineration systems. At the end I will hopefully have time for some questions of your choosing just in case we didn't anticipate all of your interests.

But before I get into those specific matters, I want to talk a little bit about a more general subject that will affect the future of reactor safety regulation. The Commission is developing a policy statement on safety goals for nuclear power plant accidents. It is described in a paper published last February for public comment. (NUREG-0880, "Safety Goals for Nuclear Power Plants: A Discussion Paper".)

After the accident at TMI-2 in March of 1979, the NRC responded to one of the recommendations of the Presidential Commission that it was "prepared to move forward with an explicit policy statement on safety philosophy and the role of safety cost tradeoffs in the NRC safety decisions." In the fall of 1980, the NRC began work on an explicit statement of the level of protection adequate to ensure public safety. That work culminated in the publication of NUREG-0880 for public comment. Both qualitative safety goals and numerical guidelines were included in the proposed safety policy.

The first qualitative safety goal reads "Individual members of the public should be provided a level of protection from the consequences of nuclear power plant accidents such that no individual bears a significant risk to life and health".

Each of us bears a continual risk of dying as the result of an accident. At any point in time our risk of dying is a function of our age, occupation, habits, leisure activities, and other factors. This first safety goal proposes that the risk of a nuclear accident not be a significant additional contributor to our risk of accidental death. The incremental risk should be sufficiently low that we would be able to go about our daily lives without special concern if we reside or work near a nuclear power plant.

The second qualitative safety goal states that "Societal risks to life and health from nuclear power plant accidents should be as low as reasonably achievable and should be comparable to or less than the risk of generating electricity by viable competing technologies".

17th DOE NUCLEAR AIR CLEANING CONFERENCE

The goal has two elements. First, the residual risks are to be compared to risks from other means of generating electricity. The comparative part of this goal implies that the risk from nuclear power-plant accidents should be comparable to or less than risk from plants using alternative means of generating electricity. Coal is the only viable alternative technology at this time, so the risk from coal-fired plants is the standard for comparison. Second, the risks should be reduced to the extent practical, considering costs and benefits of risk reduction. This simply acknowledges that society has finite resources for improvement of the quality and safety of life and that there are relative limits to what society is willing to spend to reduce risk in one area at the expense of higher risks in another area.

In addition to the qualitative goals, the safety policy proposed by NRC also contains some numerical guidelines.

There are two guidelines that address prompt mortality risk and delayed mortality risk. These guidelines state "The risk to an individual or to the population in the vicinity of a nuclear power plant site of prompt fatalities that might result from reactor accidents should not exceed one-tenth of one percent of the sum of prompt fatality risks resulting from other accidents to which members of the U.S. population are generally exposed", and "The risk to an individual or to the population in the area near a nuclear power plant site of cancer fatalities that might result from reactor accidents should not exceed one tenth of one percent of the sum of cancer fatality risks resulting from all other causes".

The 0.1% ratio of the risks of nuclear plant accidents to other risks is proposed as a reflection of the qualitative goal of no individual bearing a significant additional risk. That is, we expect that 0.1% of other accident risks is low enough that people living or working near nuclear power plants would perceive no special safety or health concern because of the plant.

One of the other risk guidelines would limit the increased risk of a delayed fatality as a result of a reactor accident to one-tenth of one percent (1 in 1,000) of the cancer risk owing to other causes. In applying the numerical guideline for delayed cancers as a population guideline, it is proposed that the population at risk be defined as the people living within 50 miles of the plant site. A substantial fraction of the population exposures from accidental releases would be expected to occur within that distance. The NRC already uses a 50-mile cutoff distance in implementing the ALARA principle embodied in Appendix I to 10 CFR Part 50 for routine reactor releases. The result of this limit on the risk to the 50-mile population is that the potential increase in delayed fatalities from all reactors at a site would be no more than a small fraction of the normal variation in the expected cancer deaths from other causes.

Our intention is that the individual and societal mortality risk guidelines be applied on a per-site rather than a per-reactor basis. Thus, persons living near multiple unit sites should be at no greater risk than those living near single unit sites. This is somewhat analogous to the way EPA's Environmental Radiation Protection Standards, 40 CFR 190, operate for normal operational releases associated with the uranium fuel cycle.

17th DOE NUCLEAR AIR CLEANING CONFERENCE

The proposed safety goals also include a benefit-cost guideline which would be used to decide whether proposed safety improvements are worth their price. Incremental reductions of risk below the numerical guidelines for societal mortality risks might be required of our licensees if they cost less than \$1,000 per man-rem averted. By most reckoning, the \$1,000 is a prudent value. Even so, our experience with its use in implementing Appendix I to Part 50 has shown it to have had little or no impact. We don't have any experience with its use for accident risk reduction to know if that will hold true in this case also.

Finally, the proposed safety goal contains a plant performance guideline for large-scale core-melt accidents. It states: "The likelihood of a nuclear reactor accident that results in a large-scale core melt should normally be less than one in 10,000 per year of reactor operation."

The controlling feature of public risk from nuclear reactor operation is the chance of serious core damage; the probability is small but the potential consequences are large. Of course there are large uncertainties in probabilistic assessments of the risk portended by infrequent reactor accidents, and in the evaluation of their consequences. Thus, the core melt guideline is not intended to serve as a speed limit. It is more of a screening criterion with uncertainty bands for use in deciding on regulatory actions in specific cases.

The proposed safety goals and numerical guidelines are not intended to displace or deemphasize the defense-in-depth approach in regulation of reactor safety. Rather, they are intended to make the regulatory process more cohesive and to provide a more systematic policy basis for considering changes to address new issues. The nature and extent of the consideration to be given to the numerical guidelines in individual regulatory decisions would depend on the nature of the issue, the quality of the data base, and the reach and limits of analyses involved in the probabilistic calculations. The proposed numerical guidelines are intended to aid professional judgment, not to substitute a mathematical formula for it.

The uses of safety goals and numerical guidelines will be proposed by the NRC staff in a detailed implementation plan being developed for Commission approval.

Now let me turn to some specific developments at NRC that will more directly affect you. You've probably heard about the first one - we are reevaluating accident source terms. In the past, the assumptions made in our evaluation of accidents have been very conservative in several respects. We are reviewing our current practices in this area and assessing the current state of technology to support changes in our practices.

Our preliminary assessment of the technical basis for source term estimates is described in NUREG-0772, "Technical Bases for Estimating Fission Product Behavior during LWR Accidents". It was published in 1981. We expect that the results of ongoing research will permit best estimate revised source terms to be formulated in early 1983. The objective of the NRC source term research programs is to develop a data base for assessing fission product release from the fuel and fission product transport from the fuel to the environment during severe core damage and core melt accidents. The programs will provide information on: (a) the release of fission products and non-radioactive aerosols from overheated and melting fuel; (b) the chemistry of the released fission products; (c) the aerosol formation mechanisms; (d) the transport behavior of fission products and

aerosols in the reactor coolant system and in the containment; and (e) the effectiveness of engineered systems in mitigating fission product releases. For today, I will just concentrate on the effects of properly accounting for the predominant chemical form of iodine released from fuel in an accident. It appears that the predominant form would be cesium iodide rather than the very much more volatile elemental form of iodine.

You all know that our regulations require us to define a "maximum credible accident" for site analysis and engineered safety feature design. Although we have used a non-mechanistic event (no specific accident sequence), certain accident characteristics have been prescribed as follows:

1. substantial melting of the core is assumed;
2. containment integrity is assumed to be established and its leak rate maintained at a value no greater than about 0.1% per day; and
3. engineered safety features designed to mitigate the consequences of the event are assumed to function.

Our current guideline for release of radioactive material to the containment atmosphere for these analyses is that 100% of the core inventory of noble gas and 50% of the iodine is initially available for release from containment via the airborne pathway. Typically, half of that iodine is assumed to plate out very rapidly on containment analyses. It is also assumed that 91% of the iodine is present in the elemental form, 5% is particulate (i.e., sorbed on aerosols), and 4% is organic.

Both the amounts and the physical and chemical forms of radionuclides released into the containment atmosphere are significant factors affecting the design of features whose purpose is to prevent release to the atmosphere. The evidence available today suggests that a far greater portion of radioiodine in the containment atmosphere would be expected to be in the form of the highly water soluble cesium iodide. This was a subject of discussion at the 16th Air Cleaning Conference. Other forms of iodine such as organic iodide, elemental iodine, and other species are only expected to constitute a small percentage of the total iodine.

Several conclusions are likely to result from reevaluation of the current accident source terms. First, the current data base may be sufficient to support revision of the accident characteristics on an interim basis. This could be accomplished by the selection of a suitably conservative accident sequence and a best estimate analysis of the consequences of that accident sequence in lieu of the present "design basis accident" or DBA.

A second result of our source term work has shed some light on the assertion that past regulatory assumptions regarding volatile radioiodine may have resulted in a misplaced emphasis in engineered safety feature (ESF) design. A review of current designs shows that many ESFs for mitigation of postulated accident sequences within the design basis accident envelope are likely to be effective for postulated accidents substantially more severe than the DBA. However, there is

17th DOE NUCLEAR AIR CLEANING CONFERENCE

substantial variation in their effectiveness under such conditions. The containment spray, ice condenser, and suppression pool systems are considered to be very effective for a broad spectrum of accidents. There is, however, one other system for which this conclusion is not necessarily valid which I'll describe shortly.

Our third conclusion is that the methodology of the Reactor Safety Study (WASH-1400), currently used to evaluate consequences of accidents more severe than the design basis, leads to source term estimates that are generally conservative. While there is insufficient information for a revision of these source term estimates, the currently available data base does support reassessment of several conclusions arising from previous consequence evaluations. That is, we expect a less dominant role for iodine, and we have a new understanding of the importance of delayed containment failure.

Finally, our current studies reinforce the conclusion that there remain large uncertainties associated with accident source term determinations. In particular, more research is needed on effects such as thermohydraulic and thermodynamic conditions in the core region; aerosol formation and deposition in the primary system; aerosol particle size distributions; and containment failure mechanisms. The uncertainties associated with current source term estimates are expected to be reduced, however, as the core melt technology matures and as currently funded or planned research programs are completed.

I expect that in the future we will be turning to an evaluation approach which attempts to more realistically model the events and consequences of a broad spectrum of accidents. For less severe accidents, we will need to be able to estimate a range of likely filtration system effectiveness and the associated probabilities. For the most severe accidents involving loss of containment integrity, the performance of filtration systems will be moot. The uncertainties in accidents between these two extremes may be significant and are dependent upon a number of factors, including the reliability of components or systems and operator reliability in taking action to terminate an accident or to mitigate its consequences.

Our source term study in recent months has identified one accident consequence mitigation system of concern. Some large containment PWRs would use recirculation filtration systems in lieu of containment sprays to cool the atmosphere and remove fission products following an accident. These recirculation systems employ moisture separators, prefilters, HEPA filters, and charcoal adsorbers in series. If our current understanding is correct, this type of filtration system would be ineffective when contaminated by high aerosol loading in the more severe (beyond design basis) accident sequences. Calculations indicate that it would take only a few minutes to accumulate one kilogram of aerosol per filter module. That amount may be sufficient to plug such systems. Thus, the copious quantities of aerosols expected to be produced may plug the filters in a short time and render them ineffective for much of the accident. Credit could not be taken for them in accident analyses. On the other hand, if an ESF filtration system is located outside of the primary containment, our improved understanding of the severe accident source term does not alter our earlier estimates of their performance. Such filtration systems outside containment include auxiliary building filtration systems in a pressurized water reactor (PWR), the standby gas treatment system in a boiling water reactor (BWR), and control room habitability systems. These systems are intended to remove airborne radioactive

materials that result from leakage from piping systems or containment. In all likelihood the total concentration of airborne radioiodine reaching these filtration systems would be less than presently assumed because of the influence of partitioning of the large CsI particulate fraction between the liquid and gaseous phases. The distribution of the iodine chemical species would be much different from that presently assumed. The fraction of elemental iodine would be reduced and the fractions of organic and particulate iodine may be increased. There would likely be more particulate fission products but the increase may not be enough to warrant significant concern for the overall effectiveness of these systems external to containment.

A change in the accident source term assumptions would require revision of Regulatory Guide 1.52, "Design, Testing, and Maintenance Criteria for Post-Accident Engineered-Safety-Feature Atmosphere Cleanup System Air Filtration and Adsorption Units of Light-Water-Cooled Nuclear Power Plants". This guide specifies typical environmental conditions for atmosphere cleanup systems designed to mitigate the consequences of DBAs. With a revision to the accident source terms, the filtration system design values for iodine buildup and adsorption, and airborne concentrations of elemental iodine, methyl iodide, and particulate iodine would have to be modified.

That concludes my remarks on reactor accidents, but before closing I would like to discuss another subject I know some of you are interested in. We have been getting a lot of questions about the cleanup of off-gas streams from incinerators designed to process radioactive wastes generated at nuclear power plants.

The NRC issued a policy statement on October 16, 1981, to encourage the volume reduction of low-level radioactive wastes. It was prompted by the limited amount of space presently available for disposal at low-level waste disposal sites and the uncertainty regarding the continued operation of the disposal sites. The Commission called upon all generators of low-level radioactive waste to reduce the volumes destined for disposal and to establish programs to implement volume reduction practices. The Commission encouraged licensees to first implement a system of administrative controls, such as planning of work activities, training, and management oversight, to minimize the volume of waste generated. Then, the Commission called for evaluation of advanced equipment, such as incinerators, to achieve even greater reductions in volume. The Commission also committed to take expeditious action on requests for licensing approval of volume reduction systems.

Even before the issuance of the policy statement, several nuclear power plants were considering the installation of radwaste incineration systems. In addition, a variety of incineration system designs have been proposed by equipment vendors, including both wet scrubbing and dry off-gas cleanup systems. Successful cleanup of the off-gas stream may be difficult in certain incinerator applications because of the many types of waste to be burned and the resulting differences in combustion products; e.g., some may be corrosive while others impair charcoal adsorbers. Power plant wastes to be incinerated may include spent ion exchange resins containing relatively high concentrations of radioactive material; solid wastes containing polyvinyl chlorides, rubber and other organics; and organic liquids such as waste oils. Thus, the incinerator off-gas system may be called upon to remove particulates, maintain the concentration of corrosive combustion

17th DOE NUCLEAR AIR CLEANING CONFERENCE

products to levels that are compatible with the materials of construction of the system, reduce non-radioactive pollutants to levels that will meet EPA or state and local regulations, and remove radioiodine to levels consistent with allowable limits established by the NRC.

Although the NRC presently does not have guidance specifically addressing the acceptability of radwaste incineration system design, much of the existing guidance is applicable, namely, Regulatory Guide 1.143, "Design Guidance for Radioactive Waste Management Systems, Structures, and Components Installed in Light-Water-Cooled Nuclear Power Plants" and Regulatory Guide 1.140, "Design, Testing, and Maintenance Criteria for Normal Ventilation Exhaust System Air Filtration and Adsorption Units of Light Water-Cooled Nuclear Power Plants".

However, since the offgas system has been the source of a significant fraction of the operational problems encountered with incinerators to date, the Commission is requesting that test or operational results be provided to demonstrate that design value decontamination factors can be achieved under anticipated operational conditions. Because of greater use of radwaste incineration systems at nuclear power plants or other locations in the future, we will be following up on the information presented at this conference with special interest. If you think we should be doing more, drop me a line and tell me what it is and why. We are open to your suggestions and will try hard to answer your questions.

That concludes my prepared remarks. I appreciate the opportunity to meet with you today. I hope you have a productive week.

DISCUSSION

BELLAMY: A core-melt accident could lead to 13,000 deaths. If a core-melt occurs once in 10,000 reactor-years, is 13,000 deaths in 10,000 reactor years acceptable?

MATTSON: You shouldn't expect 13,000 deaths from a core-melt accident. The safety features (especially the containment system) would limit the effects so that the likely consequences of the more probable core-melt accidents are no prompt fatalities.

CHRISTIAN: In further response to Dr. Bellamy's question, the calculated risk of 1-3 deaths per reactor year from core meltdowns, using a probability of 10^{-4} per reactor year, even though perhaps overestimated, is within the range of currently accepted risks and actual deaths from power production, either nuclear or coal. We must accept the fact that some small risks will result from power production.

THOMAS, T.R.: Was the TMI incident considered a serious accident (i.e., one accident per 10,000 reactor years)? If so, there should be no further core meltdowns for at least 150 years. I am afraid that the public perception of risk would rule out future use of nuclear reactors should we have another such incident.

17th DOE NUCLEAR AIR CLEANING CONFERENCE

MATTSON: Of course statistics don't work that way, and the next severe accident could happen tomorrow, even if the probability were one in a million. The industry's job is to see that it doesn't. Clearly, another severe accident close on the heels of the first would place the future of nuclear power in serious jeopardy.

CSILLAG: Concerning the FPC area. I would like to know if there will be any future experimental programs in order to resolve the cesium iodide issue?

MATTSON: The NRC research program on severe accidents is described in a report numbered NUREG-0900, 1982. It includes the accident source term research. The generation and removal mechanisms for CsI are included in that program.

MOELLER: Has the Nuclear Regulatory Commission staff considered specifying a limit on the containment failure rate as a part of their proposed quantitative safety goals?

MATTSON: The staff had proposed to do this, but the Commission has rejected the idea as a policy matter, at this time. The rejection is probably immaterial since the technical work to develop and test a containment performance goal is incomplete and probably will remain so for another year or two.

17th DOE NUCLEAR AIR CLEANING CONFERENCE

POTENTIAL AIR CLEANING PROBLEMS IN FUSION REACTORS*

J. G. Crocker
EG&G Idaho, Inc.
Idaho Falls, Idaho

Abstract

The first generation of fusion reactors is expected to produce energy by fusion of deuterium (D) and tritium (T). This fusion reaction produces helium and a 14.1-Mev neutron as reaction products. Tritium is rare in nature and is produced for fusion reactors by reaction of the 14.1-Mev neutron with lithium in a breeding blanket surrounding the reaction chamber. This neutron may also react with materials surrounding the reaction chamber to produce radioactive isotopes in reactor structural materials, coolant streams or building atmosphere. Thus, the principal air cleaning problems involve removal of the radioactive tritium and activation products that may enter the reactor building as a result of normal operation, maintenance, or an accident. In addition, some fusion reactor designs contain toxic materials that could potentially be released as a result of a severe accident or fire and should be considered in the design of the air-cleaning system. The Department of Energy (DOE) has programs underway to identify sources of air-borne hazards from fusion reactors so that appropriate air-cleaning systems can be designed.

I. Introduction

Nuclear fusion is one of the key technologies under development for future generation of commercial power. The scientific feasibility of fusion is expected to be demonstrated in the mid-1980's, and commercial application is anticipated to begin early in the next century.

The first generation of fusion reactors will produce energy by fusion of deuterium (D) and tritium (T). This reaction produces helium and a 14.1-Mev neutron as reaction products. Deuterium is plentiful and can be economically extracted from seawater to support a fusion economy; however, tritium is rare in nature and must be produced for fusion reactors by reaction of the 14.1-Mev neutron with lithium in a breeding blanket that surrounds the reaction chamber. This high-energy neutron also reacts with materials surrounding the reactor to produce radioactive isotopes, activation products, in structural materials, coolant streams, and the reactor building atmosphere. The specific activation products produced are a function of the materials used in constructing the reactor. Release of tritium or activation products into the reactor building during operation, maintenance or an accident constitute the principal air cleaning problems for D-T burning fusion reactors.

Also, depending upon the specific reactor design certain toxic materials are used in fusion reactors. For example lead or beryllium are used in some designs as a neutron multiplier to improve

* Work supported by the U.S. Department of Energy, Director of Energy Research, Office of Fusion Energy, under DOE Contract No. DE-AC07-76ID01570.

the tritium breeding. Also, if the lithium required for tritium breeding is used in the liquid form, toxic aerosols can be produced in fires that could result from lithium spills. These toxic materials must be considered along with the radioactive isotopes in design of the fusion reactor air-cleaning system.

The Department of Energy has design studies, safety programs, and experiments planned or in progress that will identify potential fusion reactor air-borne hazards and allow development and/or design of appropriate air-cleaning systems prior to operation of commercial fusion reactors.

II. General Description of Fusion Reactors

Energy is produced when certain light nuclei are fused together. To achieve practical power production, a thermonuclear fuel with a sufficiently high density must be contained at very high temperatures long enough for fusion reactions to occur. The nuclear reactions shown in Table I are potentially useful for production of fusion energy. Table I also indicates the energy released in each fusion reaction.

Table I. Fusion reactions and energy released.

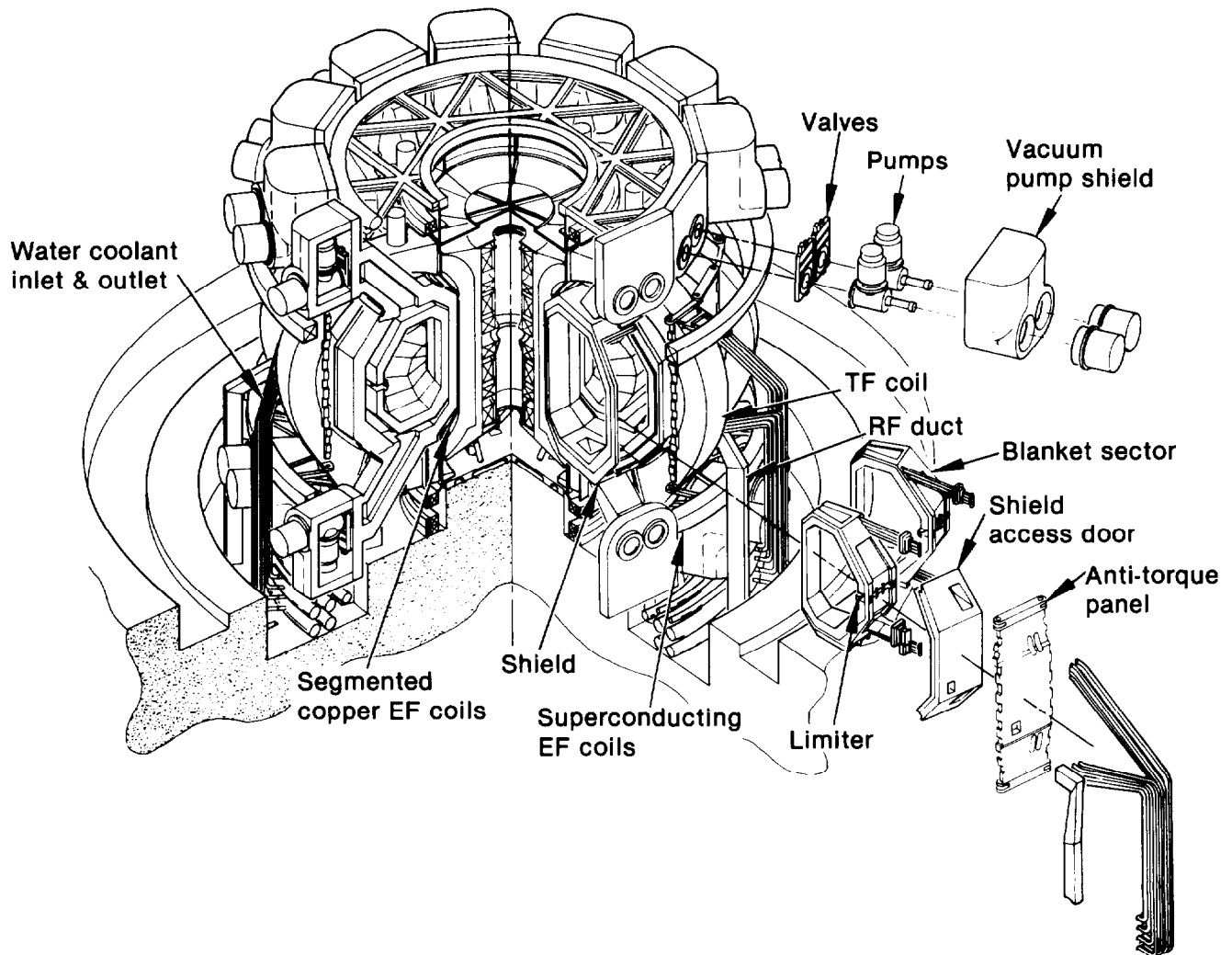
<u>Reactions</u>	<u>Energy (MeV)</u>
$D + T \rightarrow He(4) + n$	17.6
$D + D \rightarrow He(3) + n$	3.3
$\rightarrow T + p$	4.0
$D + He(3) \rightarrow He(4) + p$	18.3
$P + Li(6) \rightarrow He(3) + He(4)$	4.0

Because of the relatively high cross-section for the deuterium-tritium reaction, the first generation of fusion reactors will almost certainly use a mixture of deuterium and tritium as fuel. Although deuterium is abundant in nature and can be economically extracted from water, tritium must be produced in the reactor.

Significant safety advantages could result from burning other fuels in more advanced reactors. Fusion reactors burning pure deuterium or using the proton-lithium fuel cycle would eliminate the requirement for breeding tritium. For pure deuterium fuel in which the reaction products [T and He(3)] are utilized as fuel, the tritium inventory would be about two orders of magnitude lower than for deuterium-tritium fuels. Proton-lithium fuels offer even greater safety advantages since they reduce tritium inventories and the inventory of activation products.⁽¹⁾ The higher temperature required for fusion of advanced fuels will, however, require additional advances in plasma confinement and heating. Recent experimental results in plasma confinement and heating offer promise that pure deuterium fuel or other advanced fuel may eventually be developed.

Two approaches to plasma confinement are currently under development: inertial and magnetic confinement. In the inertial confinement approach, the fuel, in the form of a small pellet, is rapidly compressed to a high density and heated to thermonuclear temperature by a short burst of energy. Either intense lasers or particle beams may be used to provide this pulse of energy. In the magnetic confinement approach, a lower-density fuel at high temperature is contained as a plasma by the magnetic field while the fusion reactions occur. The two leading magnetic confinement schemes are the tokamak and magnetic mirror. Since the tokamak concept is the most advanced in development and reactor designs, most of the discussion in this paper will be based on this concept; however, the information will be applicable in principle to the other fusion approaches as well.

STARFIRE, the tokamak reactor design shown in Figure 1, is the latest in a series of conceptual tokamak designs. This design represents the trend towards more compact reactors with features to



INEL 2 2054

FIGURE 1
STARFIRE REFERENCE DESIGN, ISOMETRIC VIEW

facilitate maintenance and improve safety.⁽²⁾ The large toroidal field (TF) coils produce magnetic fields that contain the plasma. Radio frequency (RF) waves are used to produce a current in the plasma. This current heats the plasma and produces an additional magnetic field that contributes to the plasma confinement. The RF waves also provide additional plasma heating. An austenitic stainless steel first wall is used with a beryllium coating to reduce the quantity of heavy impurities in the plasma. A pumped limiter is used to remove helium ash and other plasma impurities.

The high-energy neutrons produced in the reactions pass through the wall of the plasma chamber (first wall) and deposit their energy in the blanket. The pressurized water blanket cooling system then transfers the energy to the power generating system. The blanket also breeds additional tritium fuel through the reaction of neutrons with lithium. Lithium aluminate is used as the tritium-breeding material for STARFIRE. The primary reason for use of this ceramic compound was to eliminate the lithium fire potential and thereby improve the overall safety of the reactor. Because of the lower lithium atom density in lithium aluminate compared with liquid lithium, a neutron multiplier must be used to obtain adequate tritium breeding. Both beryllium and a lead alloy were proposed for this purpose.

The STARFIRE reactor is contained within a ribbed-box building with a volume of $2.55 \times 10^5 \text{ m}^3$. The maximum accidental pressure from blowdown of the pressurized water cooling system would be approximately 100 kPa (15 psig), so the box-shaped building can be used compared with the conventional cylindrical fission reactor building. The building contains post-accident building isolation and heat removal systems. An atmospheric tritium recovery (ATR) system is provided to clean up tritium releases to the building. The system involves catalytic conversion of tritium gas to tritiated water and collection on molecular sieve. The heating, ventilating, and air conditioning systems contain high efficiency filters followed by two high efficiency particulate air (HEPA) filters.

III. Tritium Cleanup

Fusion reactors will probably contain a tritium inventory in the range from 5 to 40 kg (50 to 400 MCi).^(2,3,4) Figure 2 is a simplified line diagram of a tritium system for a fusion reactor. The majority of circulating tritium will be in the fueling loop indicated by the heavy line in the figure. The largest circulating inventory will be in the vacuum pumps, the tritium processing system and the fuel fabrication injection system. In addition, reactor operation during a shutdown of the breeding system for a few weeks or the fuel processing system for a few days would require on-site storage of a few kilograms of tritium. The breeding system replenishes tritium consumed in the fusion reactor during operation. Limited data on tritium extraction from breeding materials results in large uncertainties in the equilibrium inventory in the breeding blanket. Table II lists the tritium inventories and flows for the NUWMAK and the STARFIRE conceptual designs.^(2,5) The trend, indicated in this table, is towards a lower active inventory (inventory outside the breeding blanket or storage). A lower active inventory would reduce the risks associated with accidental releases.

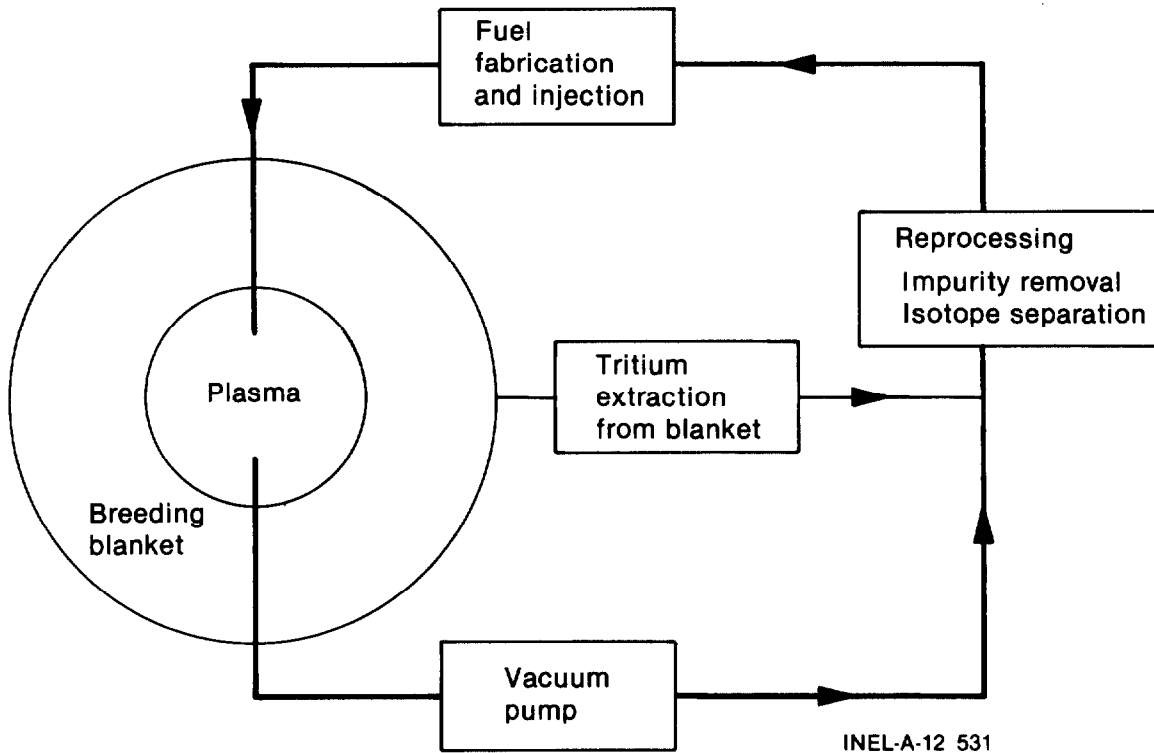


FIGURE 2
TRITIUM FUEL SYSTEM FOR A FUSION REACTOR

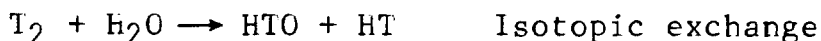
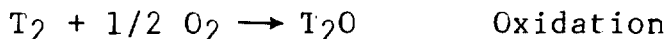
Table II. Tritium inventory and flows in conceptual reactor designs.

	<u>NUWMAK</u>	<u>STARFIRE</u>
Inventory (kg)		
Vacuum pumps	1.6	0.06
Reprocessing	0.35	0.15
Storage	19.4	1.1
Breeding blanket	0.1	~10.0
Tritium recovery	---	0.28
Miscellaneous	---	0.05
Total, active	1.95	0.54
Total, blanket and storage	19.5	~11.1
Flows (kg/day)		
Throughput	19.4	1.3
Burned	0.28	0.54

17th DOE NUCLEAR AIR CLEANING CONFERENCE

As a result of industrial and military applications, techniques for handling tritium have been developed and safety concerns are fairly well understood. Tritium decays with a half-life of 12.3 years, emitting a relatively low energy (less than 18.6 keV) beta particle. Since the penetration of the beta particle in skin is less than 0.01 mm, the primary health hazard results from inhalation and ingestion rather than external radiation. The magnitude of the hazard is dependent on the chemical form of tritium, the oxide form having a biological hazard approximately 2.5×10^4 greater than the elemental gas. Tritiated water can enter the body through the skin and lungs but is only retained in the body with a biological half-life of about 9.5 days, depending on the individual. Unlike some fission products produced in uranium or plutonium fission, tritium is not known to be concentrated in food chains. (6)

In the fusion reactor, tritium in the elemental gas form could be converted to tritiated water during an accidental release. Conversion of tritium results from the following reactions:



These reactions proceed through intermediate steps involving formation of complex ions. Reaction rates are slow at room temperature and catalysis at metal surfaces or by a radiation source is required for a significant conversion rate.

Dilution of tritium gas to nonhazardous levels occurs rapidly in the atmosphere. Experience gained from accidental release of the gas indicates that even large releases may not result in serious consequences. In 1974, an accidental release of nearly 0.5 MCi of tritium gas in the elemental form occurred at the Savannah River Plant. The weather (categorized as Pasquill Type D) was neither strongly favorable nor unfavorable to local deposition. The atmospheric oxidation rate was determined to be under 1% per day, and measured atmospheric concentrations were well under calculated levels. Deposition in surface water and the levels in vegetation, milk, and biological samples did not represent a significant health hazard. (7)

During normal operation, tritium could enter the environment through leakage from gaskets and seals or by permeation through walls and pipes; leakage may be the most significant source of tritium in the primary containment. Tritium levels can be controlled by minimizing the use of gaskets and mechanical seals and by employing multiple containment techniques (double-walled piping and glove boxes) for the more sensitive components.

Accidental releases of tritium to the reactor building could occur from failure of components in the tritium fueling and processing system, the vacuum system, or the tritium breeding system. For example a failure of the breeding blanket cooling system could result in a temperature transient thereby releasing a portion of the tritium that is contained within the lithium or lithium compound breeder. Compartmentalization of systems and components can be used to reduce the quantity of tritium that is vulnerable to release during an accident. For the STARFIRE reactor design, the maximum accidental release to the building was estimated to be 10 g. (2)

17th DOE NUCLEAR AIR CLEANING CONFERENCE

In general, three different kinds of cleanup systems are envisioned to limit and control the quantity of tritium that may be released into the building; these are:

- 1) A coolant cleanup system to limit the buildup of tritium concentration in the primary coolant to an acceptable level.
- 2) Air dryers to remove tritium that enters the reactor building atmosphere from leakage during normal operation or maintenance.
- 3) An emergency tritium cleanup (ETC) system to clean up large accidental spills of tritium into the building.

Tritium will enter the first wall and blanket coolant streams by permeation from the plasma through the first wall, limiter, or divertor. Leakage of the coolant from seals, valves, or during maintenance will allow tritium to enter the reactor building. Thus, a system to remove the tritium from the primary coolant to limit the tritium release to the building to acceptable levels will likely be needed. For example, if the primary coolant system is water, the tritium will likely be in the oxide form and the removal could be by electrolysis and catalytic exchange. Tritium recovered by these means would likely be recycled back into the reactor fueling system.

Systems are likely to be needed to remove tritium that enters the building during normal operation to ease manned access and to reduce contamination of the building and installed components. Air dryers can be used to collect tritium in the oxide form with the resulting tritiated water stream routed through the system used to recover tritium from the primary coolant. For tritium in the isotopic gaseous form, getters such as titanium or aluminum could be used, or catalytic combination to tritium oxide could be used with the oxide form again collected by air dryers. A simplified schematic of such a system to be used at the Tokamak Fusion Test Reactor (TFTR) at the Princeton Plasma Physics Laboratory is shown in Figure 3. The systems typically contain 1) a preheater to heat the tritium-containing gas to 350°C, 2) a palladium catalytic recombiner to convert tritium gas to tritium oxide, 3) an oxygen getter to remove excess oxygen, and 4) two or more molecular sieve beds to collect the tritium oxide. A capability exists to add water vapor to the process following the first molecular sieve bed to increase the efficiency of tritium collection in the second bed. Decontamination factors of 1000 are quoted for the TFTR systems.

High volume emergency tritium cleanup systems will be installed to clean up large accidental spills of tritium. These systems typically work in conjunction with the building heating, ventilating, and air conditioning (HVAC) system to remove tritium oxide. Following a large tritium spill, the reactor building is isolated and the HVAC is put into the recirculation mode. The tritium oxide is collected by condensation or moisture separators and molecular sieve beds. Conversion of the tritium to the oxide form may be accomplished either by catalytic recombination with oxygen and/or water vapor swamping.

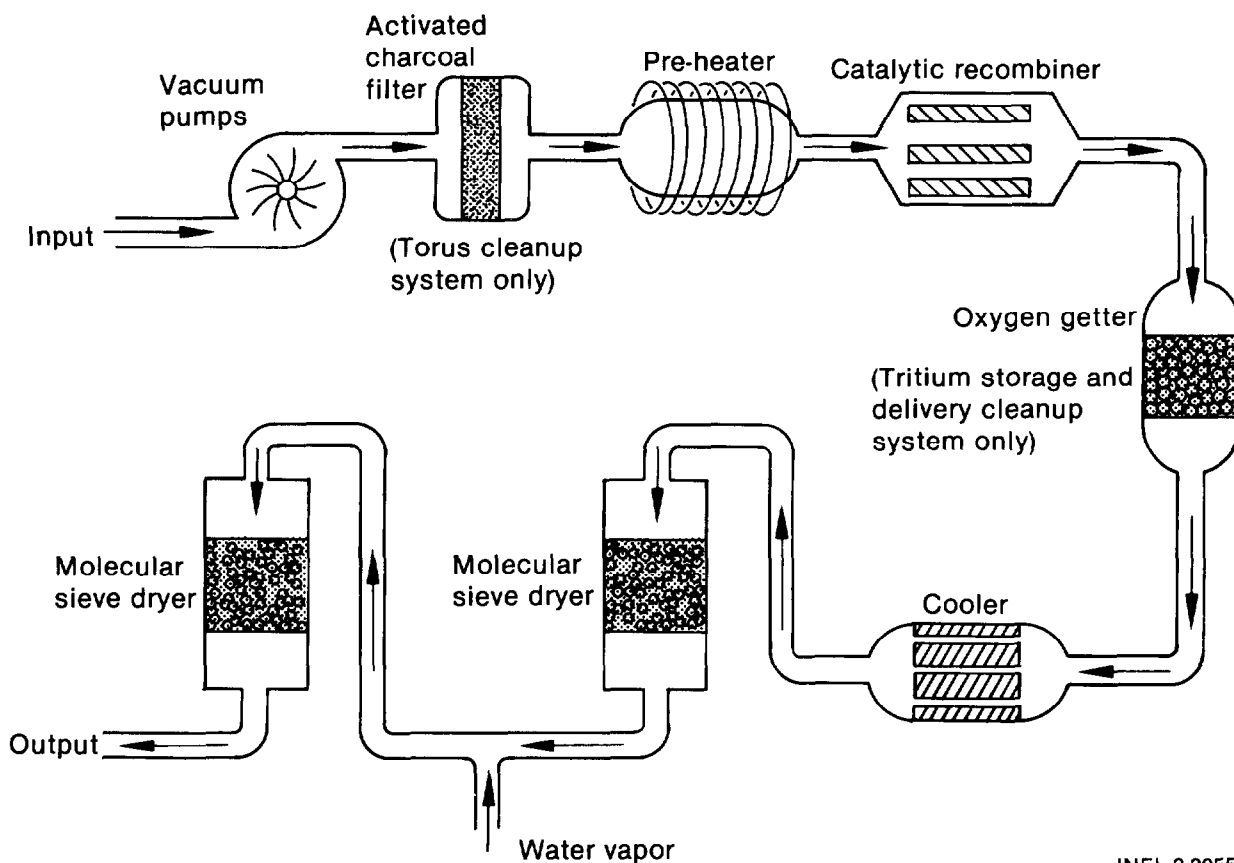


FIGURE 3
TOKAMAK FUSION TEST REACTOR (TFTR) TRITIUM CLEANUP SYSTEM

The Tritium Systems Test Assembly (TSTA) at Los Alamos National Laboratory (LANL) is the flagship of DOE's tritium handling, processing, and safety program for fusion. The facility will simulate tritium flow in a fusion reactor, excluding the breeding system, and will be used to investigate leakage and permeation problems, clean-up and containment techniques, and to develop and test components for future fusion systems. Tritium fueling system response to accident situations will be investigated to allow development of an effective safety system.⁽³⁾ The TSTA will go into operation with tritium in the summer of 1982.

IV. Activation Product Cleanup Considerations

Another source of radioactivity in a fusion reactor is activation products that are generated by interaction of materials with high energy neutrons produced in the deuterium-tritium fusion reaction. The activation products are produced in structural materials, coolant streams, and reactor building gases. Calculations based on conceptual designs have shown that approximately 1 GCi of activity can be produced.⁽⁸⁾ The large majority of these activation products are contained within the materials of the first wall, blanket,

shield, and magnet structures. Materials development programs sponsored by DOE are evaluating alloys that could achieve the high performance required and minimize the production of induced radioactivity.

Activation products are built up rapidly in the structural material of a fusion reactor and a significant fraction of the equilibrium inventory is present in the reactor after only a few days of operation. The inventory and decay characteristics of the activation products are determined by the choice of structural material. Figure 4 shows the activity and decay schemes for several structural materials being considered for fusion reactors.

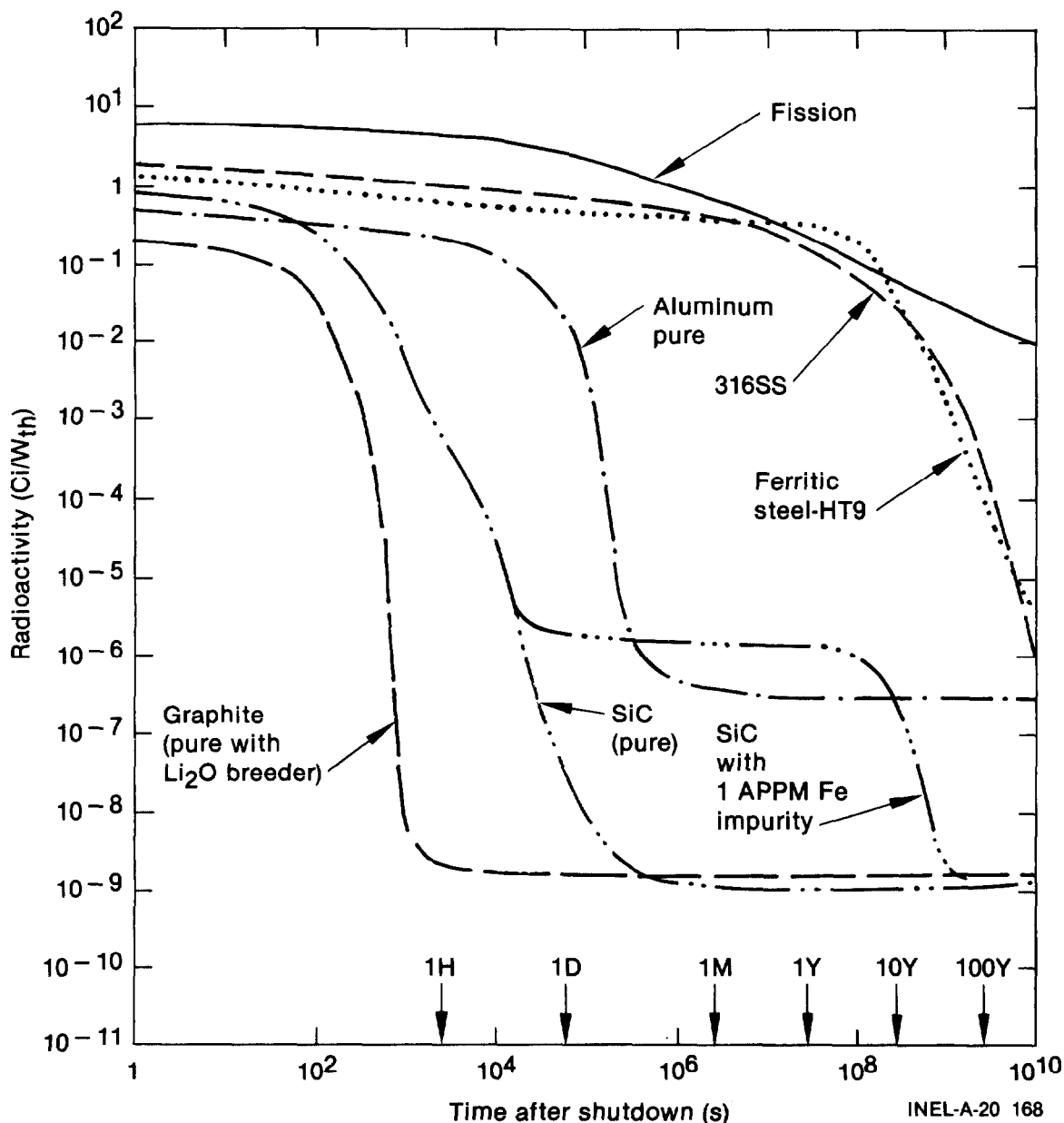


FIGURE 4
RADIOACTIVITY ASSOCIATED WITH TYPICAL 3,000-MW(th) FUSION AND FISSION REACTORS AFTER TWO YEARS OF OPERATION

17th DOE NUCLEAR AIR CLEANING CONFERENCE

Stainless steel, aluminum alloys, vanadium-titanium alloy, and ferritic steel have been proposed for use as first wall and blanket materials. The extensive experience with stainless steel in fission reactors and its ease of fabrication make stainless steel an attractive candidate. However, the relatively long radioactive decay time of stainless steel complicates reactor maintenance and waste management activities. The primary activation products of concern with use of stainless steel are isotopes of iron, nickel, manganese, chromium, molybdenum, and cobalt. For STARFIRE the activation is dominated by ^{55}Fe for times up to 30 years after shutdown, by ^{63}Ni from approximately 30 to 500 years, and by ^{93}Mo for times beyond 1000 years. (2)

Ferritic steel may give a long wall life while reducing the radioactive hazard from the activation products. The effects of large neutron fluences on ferritic steels is not known, however. The rapid decay of the vanadium-titanium alloy and aluminum during the first few weeks may facilitate maintenance operations such as changing the first wall. In addition, the rapid decay for vanadium-titanium may allow early recycle of the material, however, vanadium-titanium alloy is hard to fabricate and there is limited experience in its use. Because of their low melting temperature, aluminum alloys require a lower operating temperature. Other materials, such as ceramics (e.g., SiC), may extend first wall lifetime and produce essentially no activation products. Although material choice may allow a significant reduction in the activation products, factors relating to fabrication, impurities, cost, and supply may limit the flexibility of selection.

Activation products are deposited within the coolant streams of the first wall and blanket by two primary mechanisms, sputtering caused by physical interaction of materials with high energy neutrons and corrosion. For systems with helium coolants, sputtering is the dominant mechanism. For water or liquid metal coolants, corrosion of coolant channel surfaces contributes most to the inventory. The radioactive isotopes are the same as those in the surrounding structural material. By comparison, the inventory of activation products in the coolant streams is approximately five orders of magnitude less than that contained within the solid structural materials. Analysis performed as part of the STARFIRE design showed that 3.2×10^4 Ci of radioactivity was deposited in each of the two primary coolant systems.

The primary release mechanisms for activation products from the structural material involve leakage from the primary coolant system or an energetic thermal accident. Leakage from the primary coolant could occur as a result of minor operational failures, maintenance activities or a severe coolant system accident, e.g., a pipe break. Activation products that are mobilized by such means would be expected to significantly fallout or plate out on reactor building and component surfaces. Those that remain in the reactor building atmosphere would be removed by the high efficiency and HEPA filters of the HVAC. For large releases of radioactivity from the coolant stream, the building would be isolated and the HVAC operated in the recirculation mode.

There are a number of potential thermal accidents that could be postulated to mobilize a portion of the structural activation products. These include fires, hydrogen isotope explosions, magnet system accidents, and coolant and plasma heating system failures. The most consequential of these would be lithium fires in those systems that use lithium in the more reactive forms, liquid lithium or liquid lithium-lead alloys.

Early fusion designs used liquid lithium metal for the breeding material and as a primary coolant. More recently, designs have featured less reactive lithium-lead eutectic or various solid lithium compounds. For example, the STARFIRE design has used LiAlO_2 as the breeding material and water as the blanket coolant. In addition, evacuated containment buildings or buildings with inert atmospheres have received consideration which would effectively eliminate lithium-air reactions.

Both experimental and analytical work are required to evaluate the trade-off between the performance achievable with liquid lithium and the potential safety advantages of less reactive lithium forms. Experimental studies⁽⁹⁾ are underway at the Hanford Engineering Development Laboratory (HEDL) to evaluate the safety aspects of both liquid lithium and alternate lithium forms. Tests have been performed with liquid lithium to determine reaction rates and temperatures during reactions with air, argon, carbon dioxide, and concrete. Fire extinguishment techniques are also being investigated and developed. Results to date show that reaction of 100 kg of lithium with air can lead to approximately 1200 C flame temperatures. Such temperatures can cause rapid oxidization of some of the constituents of stainless steel, which could then be mobilized as aerosols. Radioisotopes of molybdenum and manganese appear susceptible to release by this mechanism. Thus, for fusion systems that use lithium in a reactive form, the air cleaning system must consider removal of activation products in the presence of lithium aerosols at high temperatures. This problem is similar to air cleaning problems in liquid metal fast breeder reactors. Tests at HEDL⁽⁹⁾ have evaluated the effectiveness of filters and scrubbing systems for lithium fires, including various combinations of prefilters, HEPA filters, sand and gravel beds, and aqueous scrubber systems. Based on results from these tests the aqueous scrubber systems appear to offer the best combination of mass loading and filter efficiency of the various systems tested.

If lithium in a reactive form is used in fusion reactors, inherent and engineered safety design can be used to eliminate or mitigate lithium fire accidents. Based on computer modeling, the following design strategies have been shown to be effective:⁽¹⁰⁾ 1) use steel liners for concrete, 2) reduce the lithium inventory per breeding loop, 3) reduce the oxygen concentration in the reactor building, 4) use structural material with high heat removal potential, 5) install a containment atmosphere cooling system, 6) employ a dump tank system below likely spill areas, and 7) employ a pressure relief ventilation system with appropriate filters.

Neutrons that stream through penetrations in the reactor shield can cause production of activation products in the building atmosphere. Reactor building atmospheres that have been considered for fusion include air, nitrogen, carbon dioxide and vacuum.

17th DOE NUCLEAR AIR CLEANING CONFERENCE

If air is used, the short-lived isotopes ^{16}N , ^{13}N , and ^{41}Ar are of primary concern. Proper shield design can limit their production to levels that can be handled by controlled release after an appropriate retention period to allow decay. The long-lived isotope ^{14}C is produced both in air and in nitrogen by the (n, p) reaction with ^{14}N . Again shield design or selective removal of the carbon by activated charcoal filtering would be relied upon to keep the quantities of this isotope to acceptable levels.

For reactors with a CO_2 environment, the primary activation product is ^{16}N formed by the (n, p) reaction with oxygen. Because of the short half life, 7.1 seconds, this isotope causes no particular problems. Some ^{14}C is also formed by neutron reaction with ^{13}C , but the quantities are well within acceptable levels. The STARFIRE reactor used a CO_2 atmosphere to reduce potential air activation problems.

V. Toxic Materials in Fusion Reactors

Fusion reactors, like most complex industrial facilities, will contain a variety of materials and compounds that are considered toxic to humans. In general the relative hazard of these toxic materials is several orders of magnitude less than that of the radioisotope hazards. Nevertheless, consideration should be given to these materials to ensure that they are properly factored into design of the air cleaning system. Probably the most significant of these toxic materials are beryllium, lead, lithium, and copper.

Beryllium may be used in fusion reactors as a neutron multiplier in the blanket, or as a coating on the first wall of the plasma chamber. As a first wall coating, the beryllium is used to limit the quantity of heavy impurities that are sputtered into the plasma. This first wall coating would be subject to erosion from the high flux of neutrons and ions to which it would be subjected. Thus, it could be expected that a significant quantity of beryllium dust could be present in the plasma chamber and vacuum system. Maintenance or a failure of these systems could result in the beryllium dust being dispersed into the reactor building.

Lead has been considered for use as either a neutron multiplier or as part of the reactor shield. In most fusion applications a severe thermal accident would be required to mobilize a significant quantity of the lead. Some designs have featured liquid lithium-lead alloys as the breeding material. These alloys do ignite and burn when exposed to air, so the lead could be dispersed into the reactor building atmosphere by the fire that could ensue from a lithium-lead spill.

As previously discussed, lithium must be used in a D-T burning fusion reactor to breed additional tritium for fuel. The various conceptual designs have featured liquid lithium, lithium-lead, and various solid ceramics such as lithium-silicate, -aluminate, or -oxide. The particular air cleaning requirements will depend on which form is used. If the liquid forms are used, the aqueous scrubber systems appear to be advantageous because of the fire potential following a spill. For the other forms, the high efficiency and HEPA filters are likely adequate.

Large quantities of copper will likely be used in magnetic confinement fusion reactors as stabilizers in the superconducting magnet system. Aluminum is an alternative to copper for this application. Typically the superconducting magnet systems will store 50 to 100 GJ of energy in the magnetic field. Should an arc develop a portion of this energy could be discharged internal to the magnet, and some of the copper could be vaporized; however, it is unlikely that significant quantities of copper could migrate beyond the coil cases or cryogenic dewar.

In general, it appears that the air cleaning systems provided for control of the tritium and activation products would suffice for air cleaning of toxic materials. However, this generality should be examined in detail for each specific fusion reactor design.

VI. Summary and Conclusions

The first generation of commercial fusion reactors will likely produce energy by the fusion of deuterium (D) and tritium (T). Based on current conceptual designs, such reactors will have a tritium inventory of approximately 10^8 Ci, and the high-energy neutrons produced in the D-T fusion process will produce on the order of 10^9 Ci of activation products in surrounding structures, coolants, and the reactor building atmosphere. Potential release of a portion of these radioactive inventories constitute the principal air cleaning problems in fusion reactors.

A multifaceted approach will be required for control of tritium. Tritium systems will employ at least double containment and triple containment where possible. Continuous tritium removal systems will be used to maintain acceptable concentrations of tritium in the reactor coolants and reactor building atmosphere. Also, high volume emergency tritium clean up systems will be employed to collect tritium from large spills. These systems operate by conversion of tritium to tritiated water by catalytic conversion and/or water vapor swamping followed by collection of the tritiated water by condensation and molecular sieve. The U.S. Department of Energy will operate the Tritium Systems Test Assembly at Los Alamos National Laboratory to develop and prove the concepts necessary for processing and control of tritium under normal and accident conditions.

The large majority of the activation products produced are metal alloying constituents of the primary structural materials. These products are bound in solid structural materials and are not readily available for release except during a severe thermal accident. Approximately $10^{-3}\%$ of these structural activation products are deposited in the coolant streams by sputtering or corrosion. A portion of this latter inventory could be released by operational coolant leakage or by coolant system accidents such as a loss-of-coolant accident. The most likely mechanism for release of a significant quantity of activation products from the fusion reactor structural material would be a lithium fire, for those reactors that use liquid lithium or lithium-lead. Thus, one of the most significant concerns for air cleaning is the environmental conditions that accompany the release. For a loss-of-coolant accident in a fusion reactor with a pressurized water coolant, the release would be in a steam environment. Building isolation along with air cleaning by high efficiency

17th DOE NUCLEAR AIR CLEANING CONFERENCE

and HEPA filters should be adequate for this case. For releases that are caused by a lithium fire, the aqueous scrubber systems appear to offer advantages because of the high mass loadings and efficiencies obtainable. Fusion reactor designs are moving toward use of less reactive lithium compounds which should eliminate or greatly reduce the potential for release during fires.

Activation products are produced in the reactor building atmosphere by streaming of neutrons through penetrations in the reactor structure. The isotopes produced are strongly a function of the gas used in the reactor building. The quantity produced is dependent on the effectiveness of the shield design. For the most obvious choice, air, the primary isotopes produced are short-lived ^{16}N , ^{13}N , and ^{41}Ar , along with the long-lived ^{14}C . For a nitrogen atmosphere, ^{14}C is the primary product produced, and for CO_2 , ^{16}N is produced. For the short-lived gases, an HVAC system design with an appropriate delay time to permit radioactive decay prior to exhaust will likely be used. Holdup tanks may be required as part of the delay system. For the ^{14}C , filtration using activated charcoal filters could be used.

Fusion reactors will potentially contain large quantities of toxic materials, including beryllium, lead, lithium, and copper. From a preliminary investigation it appears that the systems provided for removal of structural activation products could be used in the unlikely event that removal of toxic materials from the air is necessary.

In conclusion, fusion reactor design studies and technology development programs established by the DOE for fusion should allow identification and solution of air cleaning problems well before the first commercial fusion reactor is built. The solutions will draw heavily on solution to similar problems in the chemical and fission reactor industries. For the future, use of low activation materials and/or fuel cycles other than the D-T cycle would greatly reduce fusion air cleaning problems.

17th DOE NUCLEAR AIR CLEANING CONFERENCE

VII. References

1. C. C. Baker, et al., "The impact of alternate fuels on fusion reactor technology," ANL/FPP/TM-128, November 1979.
2. "STARFIRE--a commercial fusion tokamak power plant study," ANL/FPP-80-1, September 1980.
3. J. L. Anderson and R. H. Sherman, "Tritium systems test assembly," LA-6855-P, June 1977.
4. V. A. Maroni, "Control of tritium permeation through fusion reactor structural materials," Proceedings of the DOE Environmental Control Symposium, November 1978.
5. "NUWMAK, a tokamak reactor design study," UWEDM-330, March 1979.
6. J. T. Bell, et al., "Tritium permeation through incoloy 800 oxidized in-situ by water vapor," Proceedings of the Third Topical Meeting on the Technology of Controlled Nuclear Fusion, May 1978, CONF-780508, pp. 757-762.
7. W. L. Marter, "Environmental effects of a tritium gas release from the Savannah River Plant, May 2, 1974," DP-1369, November 1974.
8. W. Hafele, et al., "Fusion and fast breeder reactors," RR-77-8, November 1976.
9. L. D. Muhlestein, "Liquid metal reactions under postulated accident conditions for fission and fusion reactors," ANS Topical Meeting on the Technology of Controlled Nuclear Fusion, King of Prussia, October 1980.
10. D. A. Dube and M. S. Kazimi, "Analysis of design strategies for mitigating the consequences of lithium fire within containment of controlled thermonuclear reactors," MITNE-219, July 1978.

17th DOE NUCLEAR AIR CLEANING CONFERENCE

Nuclear Standards and Safety Progress in Nuclear Standards Development

James F. Fish, Chairman, CONAGT
Consultant
Louisville, Kentucky

Two years ago, when I spoke to the 16th Conference about the ASME CONAGT Committee and its assignment, I had hoped that by this time at least part of the new code would be available. Unfortunately, this is not the case. Volunteer organizations, or at least their Chairmen, tend to be over optimistic. I now have every expectation that it will be available in part by early 1983. Certain sections for individual equipment items are complete. The overall structure has been worked out. When this is finally approved, individual equipment sections should fill in quite rapidly.

One item leading to this optimism has been a reorganization of the committee as a result of a study of the committee's work by a task group under Mel First. Their recommendations have been adopted. The effect has been to more nearly equalize the work load under seven Subcommittees.

I have the Code outline as it stands today for Engineered Safety Equipment. It will have four Divisions.

Division I will contain general requirements and common articles covering design, inspection and testing, fabrication, welding and installation, packaging and shipping, QA and nameplates and certification. Individual equipment codes will, in some cases, amplify and add particular requirements in their areas to the common section requirements.

Division II covers ventilation air cleaning and air conditioning.

Division III covers process gas treatment equipment.

Division IV covers field testing to insure quality of performance.

I have every hope and expectation that substantially the whole code will be available to you by the end of 1983.

ORGANIZATION OF THE CODE ON NUCLEAR AIR AND GAS TREATMENT

GENERAL

The ASME Code on Nuclear Air and Gas Treatment consists of Divisions I through IV. All Divisions are broken down into Sections designated by two capital letters. Each Division is made up as follows:

DIVISION I - GENERAL REQUIREMENTS

Section AA - Common Articles

DIVISION II - Ventilation Air Cleaning and Ventilation Air Conditioning

Section BA - Fans and Blowers
Section DA - Dampers and Louvers
Section RA - Refrigeration Equipment
Section CB - Heating and Cooling Coils
Section CC - Humidifiers
Section CD - Electric Heaters
Section FA - Moisture Separators
Section FB - Prefilters and Frames
Section FC - HEPA Filters and Frames
Section FD - Adsorbers and Frames
Section FE - Adsorbent Media
Section IA - Instrumentation and Control
Section SA - Ductwork

DIVISION III - Process Gas Treatment

Section GA - Pressure Vessels, Piping, Heat Exchangers, and Valves
Section GB - Noble Gas Hold-Up Equipment
Section GC - Compressors
Section GD - Other Radionuclide Equipment
Section GE - Hydrogen Recombiners
Section GF - Gas Sampling

DIVISION IV - Testing Procedures

Section TA - Field Testing of Air Treatment Systems
Section TB - Field Testing of Gas Processing Systems
Section TC - Personnel Qualification
Section TD - Laboratory Qualification

17th DOE NUCLEAR AIR CLEANING CONFERENCE

CLOSING REMARKS OF SESSION CHAIRMAN:

Looking back on the opening session there has been a lot of food for thought. Even the welcoming items contained very interesting discussions. Mr. Nicks described the extensive air cleaning activities at Rocky Flats and cited what he considered to be some of our most important research news, e.g., better air cleaning systems, longer lasting systems, systems that are resistant to moisture, corrosion, and acids, etc., and finally he mentioned the need for better detectors to indicate when a given system should be brought on-line. Dr. First, in his welcome, brought out a fact many of us realize, that the US research effort in many areas is lagging behind that in foreign countries, more specifically in air cleaning research. Fortunately, foreign groups are still looking at such things as chemical processing. He also called on us to look at the real problems, not to say that simply better training of people will solve these problems. He said there are better approaches, such as to make it so that it cannot be solved improperly, or cannot be mishandled easily. Roger Mattson, in my opinion, in an excellent keynote address, reviewed, among other things, the NRC's proposed reactor safety goals. These will be qualitative and quantitative. He showed that they will definitely have an impact on air cleaning requirements in the commercial nuclear power plant area. He also pointed out that a thorough research and re-evaluation is now under way on the source term by the NRC staff. Again, the results are going to have repercussions throughout the air cleaning field. He closed with a discussion of the fact that the Nuclear Regulatory Commission has taken a position, as a policy, to encourage a reduction in the volume of low level waste at commercial plants. If this is done by using incinerators, it certainly will have an impact on the air cleaning field.

Finally, Mr. Crocker told us about fusion reactors and some of the air cleaning problems there. To me, it was rather surprising to see how far they have come with their designs in scoping the health problems that may be associated with such facilities. He also pointed out that there are tremendous energy sources within a fusion system and that these, also, must be carefully controlled. He pointed out that there will be problems associated with the tremendous quantities of tritium to be handled. In addition, there will be air cleaning problems with the induced radionuclides from high energy neutrons that result from fusion. He also pointed out that there are many other toxic materials used in fusion reactors, such as beryllium, lead, lithium, and copper. He pointed out that there is much yet to be done with respect to the air cleaning problems associated with tritium. There will be tremendous quantities and, therefore, even low leakage rates can be significant. He also pointed out that some of our present-day cleanup systems, in fact, the principal system which converts tritium from a gas to the oxide, actually increase its toxicity and this has to be looked at. He also discussed induced activity of radionuclides and stated that he thought that conventional air cleaning systems would help in this area. He also pointed out that the amount of induced activity could be modified through the selection of the structural materials used in the fusion reactor and that much attention is being given to that subject today.

17th DOE NUCLEAR AIR CLEANING CONFERENCE

Session 2

FUEL REPROCESSING

TUESDAY: August 3, 1982
Co-CHAIRMEN: J.L. Kovach, NCS
J. Jacox, NCS

BALANCE AND BEHAVIOR OF GASEOUS RADIONUCLIDES RELEASED
DURING INITIAL PWR FUEL REPROCESSING OPERATIONS
A. Leudet, P. Miquel, J.P. Goumondy, G. Charrier

TIME-DEPENDENT ANALYSES OF DISSOLVER OFF-GAS CLEANING
INSTALLATIONS IN A REPROCESSING PLANT
k. Nagel, J. Furrer, G. Becker, W. Obrowski, Y.P. Seghal,
J. Weyman

A MODEL OF IODINE-129 PROCESS DISTRIBUTIONS IN A NUCLEAR
FUEL REPROCESSING PLANT
G.J. McManus, F.A. Duce, S.J. Fernandex, L.P. Murphy

CARBON DIOXIDE-KRYPTON SEPARATION AND RADON REMOVAL FROM
NUCLEAR REPROCESSING OFF-GAS STREAMS
P.M. Hirsch, K.Y. Higuchi, J. Abraham

ADSORPTION OF GASEOUS RuO_4 BY VARIOUS SORBENTS II
Lj. Vujisic, R. Nikolic

TEST RESULTS IN THE TREATMENT OF HTR REPROCESSING OFF-GAS
H. Barnert-Wiemer, B. Bendick, B. Juergens, A. Nafissi,
H. Vygen, W. Krill

SOURCE TERM AND MATERIAL TRANSPORT

SURFACE DEPOSITION OF RADON DECAY PRODUCTS WITH AND WITHOUT
ENHANCED AIR MOTION
S.N. Rudnick, E.F. Maher, W.C. Hinds, M.W. First

FORMATION AND CHARACTERIZATION OF FISSION-PRODUCT AEROSOLS
UNDER POSTULATED HTGR ACCIDENT CONDITIONS
I.N. Tang, H.R. Munkelwitz

17th DOE NUCLEAR AIR CLEANING CONFERENCE

BALANCE AND BEHAVIOR OF GASEOUS RADIONUCLIDES RELEASED DURING INITIAL PWR FUEL REPROCESSING OPERATIONS*

A.Leudet, P.Miquel, P.J.Goumondy, G.Charrier⁺

Commissariat à l'Energie Atomique
Division d'Etudes de Retraitement et des Déchets
et de Chimie Appliquée

⁺ Direction des Essais
France

Abstract

Five fuel pins, taken from a PWR fuel assembly with 32 000 MWD/t burn-up were chopped and dissolved in leak-proof equipment designed for accurate determination of the composition and quantity of gaseous elements released in these operations.

Analytical methods were specially developed to determine directly the noble gases, tritium and gaseous carbon compounds in the gas phase. Volatile iodine was kept as close as possible to the source by cold traps, then transferred to a caustic solution for quantitative analysis.

The quantities and activities of gaseous fission products thus determined were compared with predicted values obtained through computation. Very good agreement was generally observed.

I. Introduction

For a number of years the Commissariat à l'Energie Atomique has devoted a significant part of its R & D activities to the development of gaseous radioactive waste containment and trapping methods / 1 /, with a view to achieve minimal release and in any case, compliance with prevailing regulations.

The design of safe, efficient processes for dissolver off-gas purification in fuel reprocessing plants requires the accurate determination of the quantities of gaseous fission products involved, and their physical and chemical properties. It is important to establish the release process of such products during mechanical and chemical processing, as well as their distribution among the various liquid and gaseous flows.

The information is of special importance because it directly affects the design of equipment and ventilation systems.

It is also important to compare measured quantities and activities with computed data, in order to validate or adjust some of the basic input data used in computations.

For accurate analysis, it is essential to use whole fuel rods with clearly defined characteristics. Hence, the five rods treated were taken from a spent fuel assembly from the Dutch Borssele reactor, which was selected for the following reasons :

* Supported in part by the Commission of the European Communities.

- . the Borssele reactor is a typical pressurized water power reactor
- . the assembly had undergone three irradiation cycles ; burnup was approximately 32 000 MWD/t.
- . initial fuel enrichment was 3.1 %.

Assembly characteristics are therefore very close to those on which reprocessing and safety investigations are based. The results of this work can thus be transposed easily.

II. Gas sampling techniques

The experimental system designed for these investigations essentially consists of a leaktight chopper and dissolver connected to a sampling glove box.

However, since PWR fuel rod length exceeded shear capacity, the rods were first cut in two following recovery of internal gas.

Chopping (Figure 1)

Each half-rod was chopped into 15 mm lengths which were collected in a container used subsequently for dissolving.

After chopping, the released gas was pumped by a cryogenic system into a tubular trap cooled by liquid helium. Three flushing cycles eliminated the last traces of fission gases.

The trap was isolated, heated to 200°C to homogenize its contents, and a gas sample taken for analysis. Since the trap volume was accurately known, the amount of gas was calculated from accurate pressure and temperature readings.

Two - 50°C cold traps were placed between the chopper and the cryogenic pump to retain any iodine present.

Dissolution (Figure 2)

After chopping, the dissolver was connected to a reflux condenser. The gases released during dissolution passed through a - 50°C iodine trap, and to the sampling glove box, where they were homogenized and continuously recycled to the dissolver.

Dissolution occurred without recombination of nitrogen oxides, and only the dioxide was partly crystallized in the cold traps. To prevent any gas leakage, the system pressure was kept slightly below atmospheric by draining excess gas to a collection vessel under vacuum.

On termination of dissolution and gas release the collection vessel was isolated. Boiling is maintained for four hours for maximum iodine desorption from the dissolver liquor. Recycled nitrogen oxide was bubbled through the solution to prevent oxidation of iodine by nitric acid, with the formation of non-volatile compounds.

The quantity of gas released during dissolution was determined on the basis of :

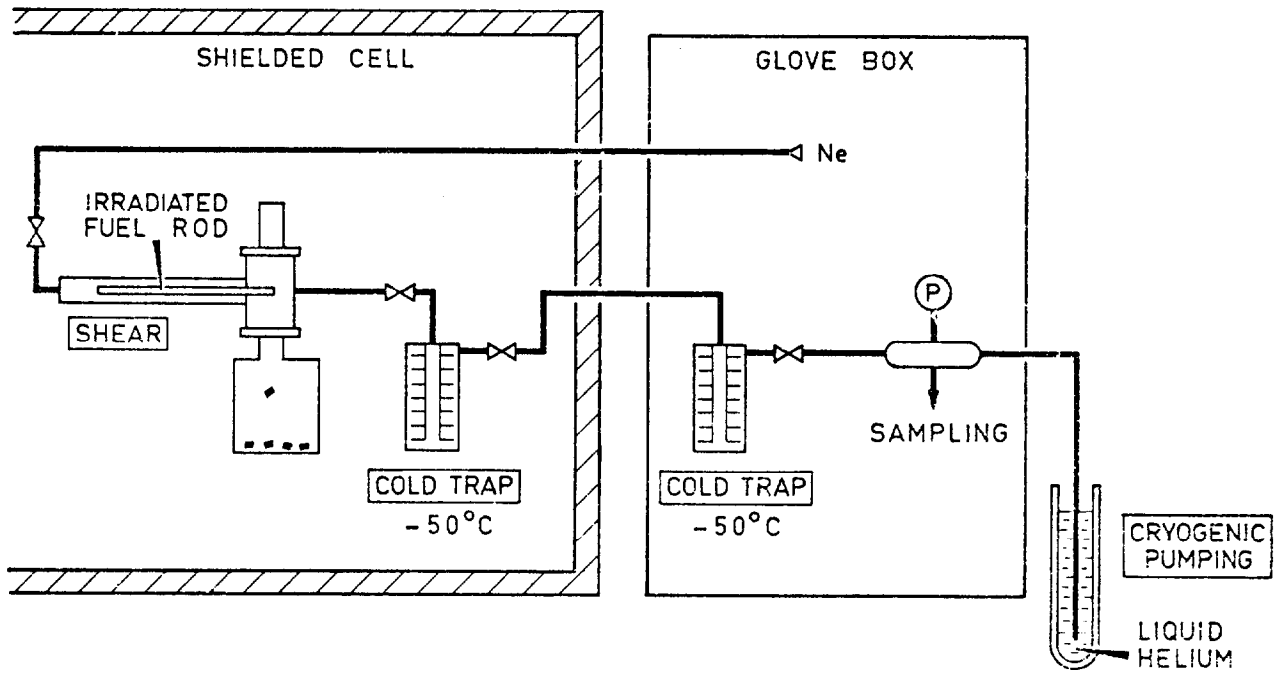


FIG. 1._ SHEARING

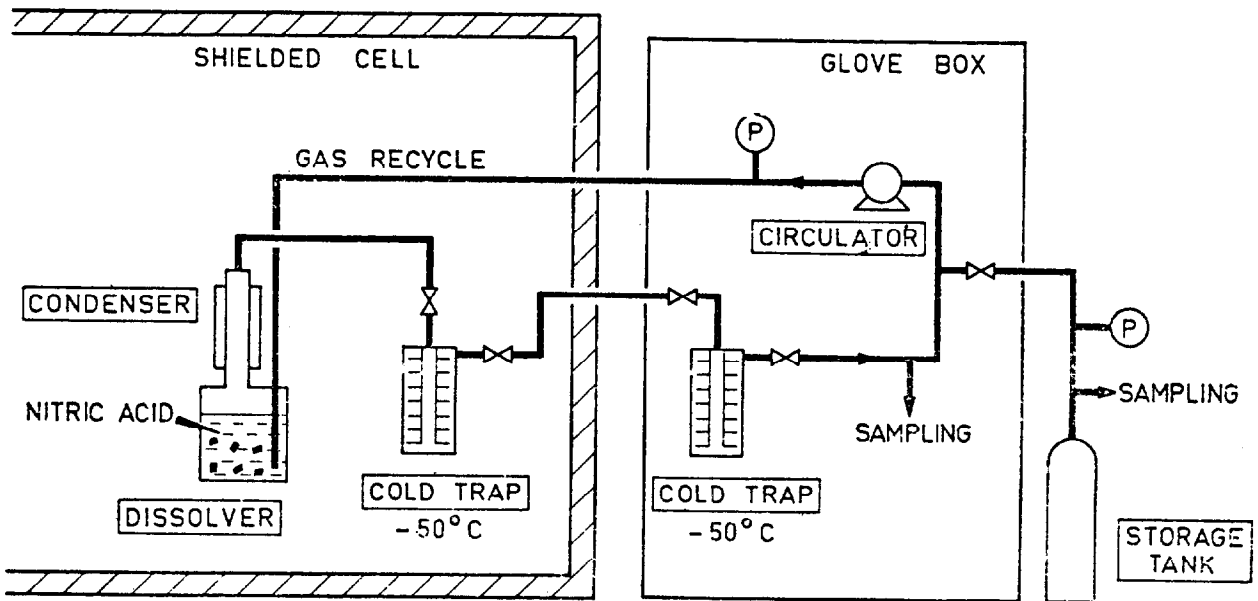


FIG. 2._ DISSOLUTION

- . analysis of gas in the collection vessel
- . analysis of gas remaining in the dissolver system.

In this respect, the presence of a boiling liquid phase and the fact that system temperatures were not accurately known prevented accurate determination of the real gas volume. To overcome this difficulty, an accurately known quantity of carbon-13 and natural isotopes of krypton and xenon was introduced into the dissolver system. The quantities of carbon-14 and noble gases released from the fuel were then readily computed by isotopic analysis.

Finally, the two cold traps were isolated and gradually heated. Nitrogen flushing entrained the iodine to a caustic solution in two absorbers placed in series. A third absorber, filled with methanol, was provided to trap any methyl iodide present.

III. Gas analysis methods

Much work has been devoted to the development of highly sophisticated gas sample analysis methods.

The gas concentration and specific activity of tritium and carbon-14 were measured in a single chromatographic analysis, although the activity of Krypton 85 was higher by a factor of 10^4 to 10^6 (figure 3).

A HP 5880 chromatograph featuring a liquid nitrogen cryogenic system was used. Stable gases were detected by a catharometer and active gases by a Panax type, low background noise circulation counter.

A porapak-Q column was used to separate H_2 , N_2 , Ar, CO and NO at a constant temperature of $-65^\circ C$, and then Kr, CO_2 , N_2O and Xe at programmed temperatures up to $60^\circ C$.

Tritium and ^{14}CO measurements were easy because these gases are eluted before Krypton 85. As for $^{14}CO_2$, thorough krypton decontamination was necessary.

As soon as CO_2 elution began, the gas flow was diverted to a Porapak - N column for good separation of residual krypton 85 and $^{14}CO_2$ which was then easily measured.

During CO_2 analysis, N_2O and Xe were retained in the Porapak - Q configuration. The column was reconnected to the system on completion of CO_2 elution.

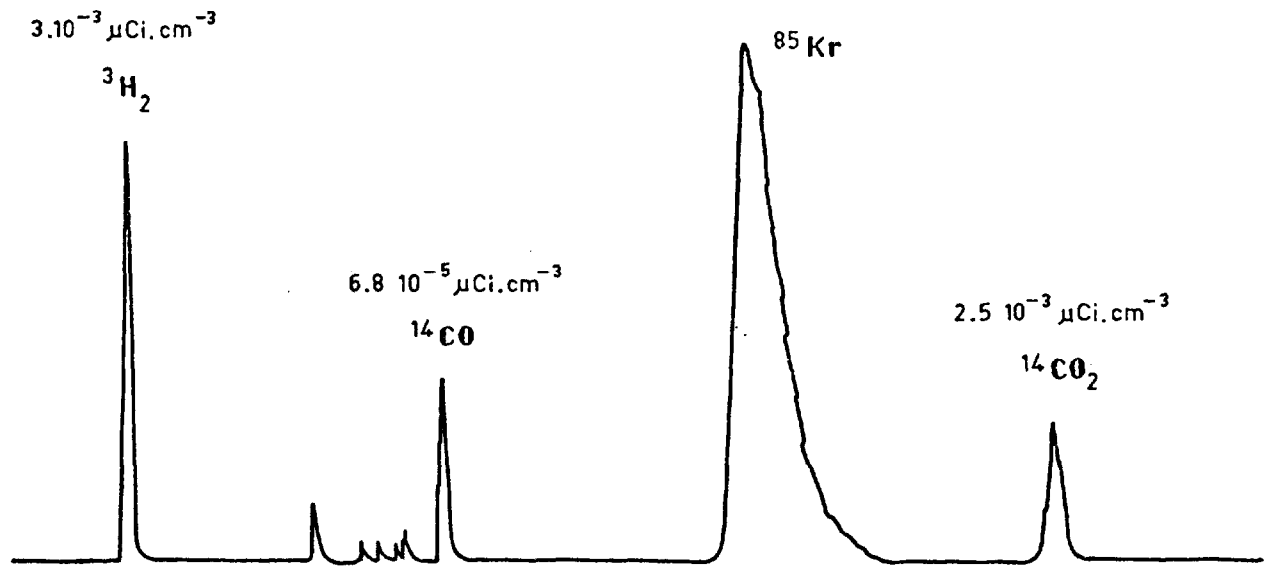
Krypton 85 activity was measured directly by gamma spectrometry, using a Ge-Li detector.

Chromatography was also used for hydrocarbon detection with a flame ionization detector, and also for methyl iodide detection with an electron-capture detector.

The isotopic composition of noble gases was measured by mass spectrometry, a method also frequently used for quantitative analysis of krypton and xenon by isotopic dilution, using a mixture of ^{80}Kr and ^{124}Xe as a tracer.

Complete analysis involved the following steps :

PROPORTIONAL COUNTER



CATHAROMETER

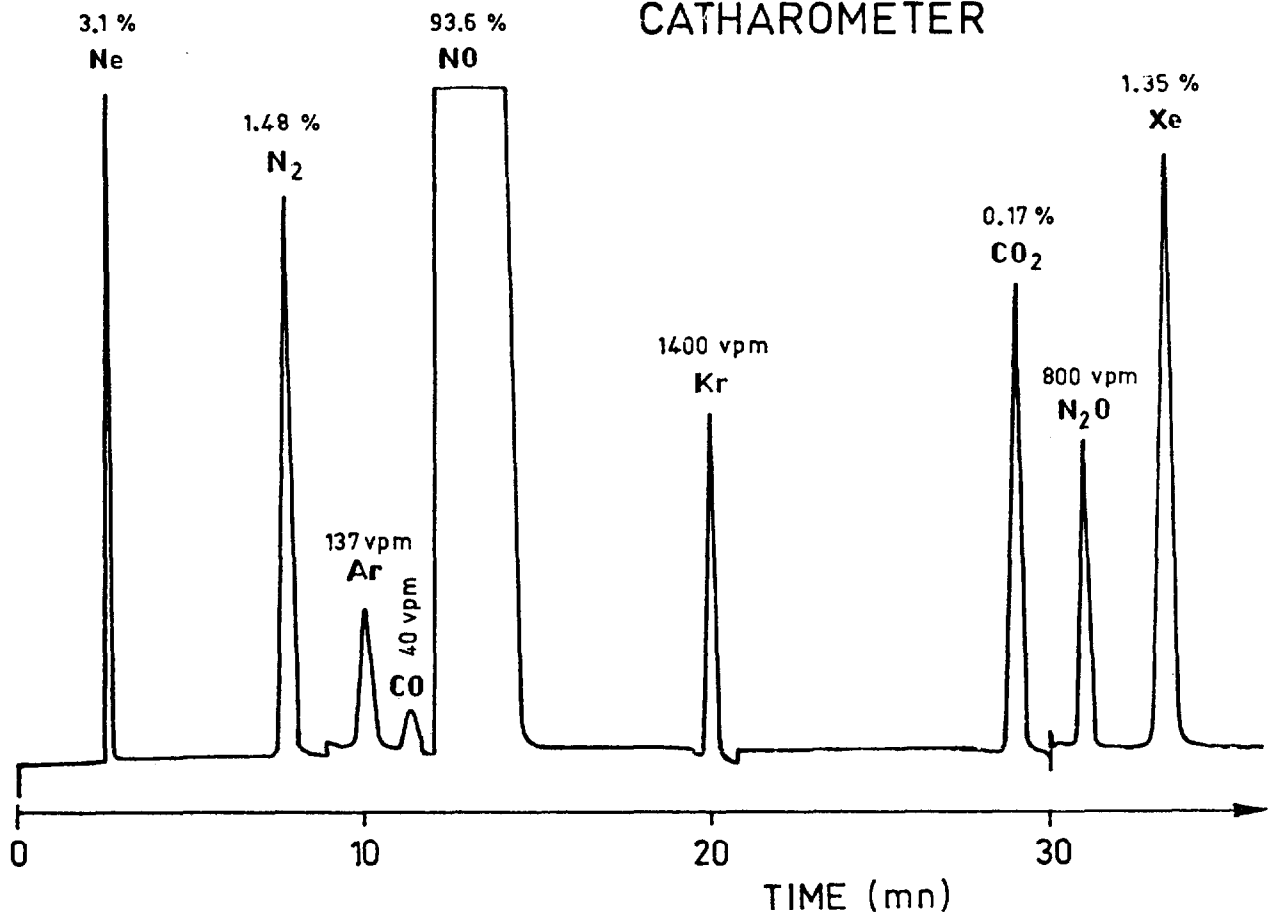


Figure 3 : Typical chromatogram

17th DOE NUCLEAR AIR CLEANING CONFERENCE

- . preparation and analysis of tracer mixture by reverse dilution, using a mixture of natural krypton and xenon.
- . isotopic measurement of the test gas
- . isotopic measurement of the test gas/tracer mixture

Although the procedure may seem complex, the number of manipulations is reduced by using a single tracer mixture. The quantities of krypton and xenon can be readily calculated from measured values of $^{80}\text{Kr}/^{86}\text{Kr}$ and $^{124}\text{Xe}/^{136}\text{Xe}$ isotopic ratios.

This method only requires a few ml of gas, which is an overwhelming advantage in active gas analysis. Mixtures are prepared by a purely barometric method, and all transfers performed using liquid helium. Utilization of a highly accurate pressure sensor (0.1 m bar) yields results with less than 1 % error in a concentration range of a few hundred vpm.

IV. Behavior of gaseous fission products

All the results are given for 1 - year cooling time.

Noble gases

The quantities of gas collected at the various stages of fuel pin processing are given in table I. Krypton and xenon released during chopping respectively account for 4.4. % and 3.8 % of the total quantity collected. A fraction of the gas was measured during the first cut of the clad, and corresponded to the fraction of noble gases present in the gas plenum ; the balance, i.e., 1 % to 2 % of the total, was released during chopping. This operation is relatively ineffective in opening the micropores in which gas remains trapped.

PIN		1	2	3	4	5	MEAN
Kr	SHEARING %	2.6	3.3	5.3	5.8	5.0	4.4
	DISSOLUTION %	97.4	97.6	94.7	94.2	95.0	95.6
Xe	SHEARING %	2.2	2.8	4.6	5.1	4.3	3.8
	DISSOLUTION %	97.8	97.2	95.2	94.9	95.7	96.2

TABLE I.. NOBLE GAS DISTRIBUTION

17th DOE NUCLEAR AIR CLEANING CONFERENCE

BURN-UP Gwd/t _u	KRYPTON		KRYPTON - 85		XENON	
	g/t _u	Adjusted to 33 Gwd/t	Ci/t _u	Adjusted to 33 Gwd/t	g/t _u	Adjusted to 33 Gwd/t
31.0	342	364	8930	9510	5250	5590
31.8	340	353	9030	9370	5240	5440
31.6	333	348	8660	9040	5110	5340
31.5	322	337	8750	9170	4930	5160
31.0	346	368	9250	9850	5300	5640
MEASUREMENTS (MEAN)		354		9390		5430
CALCULATED		370		9150		5430
$\frac{M - C}{C} \%$		- 4.3		+ 2.6		0

TABLE II -- NOBLE GAS CONTENT

The experimentally determined krypton and xenon masses and krypton 85 activities are shown in Table II. Average values show good agreement with computed values, and the maximum discrepancy, found for the mass of krypton was only 4.3 %. The next table gives the average isotopic composition of noble gases.

Kr		Xe	
82	0.2 %	130	0.1 %
83	11.5 %	131	8.2 %
84	30.8 %	132	20.7 %
85	6.3 %	134	28.4 %
86	51.2 %	136	42.6 %

Table III : isotopic composition of noble gases

Iodine

Our procedure permits the detection of volatile iodine from 10^{-4} g, i.e., less than 0.1 % of the mass contained in each half-rod.

Iodine release during chopping was less than this detection limit.

It is well known that fission-generated iodine in oxide fuel combines with the more electro-positive elements, especially cesium, of which a large amount is present. / 2 /.

17th DOE NUCLEAR AIR CLEANING CONFERENCE

Since cesium iodide is not volatile, at least at standard reprocessing temperatures, it seems normal that no iodine is released during shearing.

It is only when the fuel is dissolved that practically all the iodine is released by oxidation of iodides under the combined actions of nitric and nitrous acids in the dissolver solution.

More than 99 % of the iodine can be readily eliminated from the dissolution liquor and carried into the off-gas. Insufficient desorption may be caused by :

- . insufficient oxidation of the iodides due to the lack of nitrous acid. This acid, resulting from NO_2 absorption, shows little stability in a boiling solution.
- . lack of carrier gas, so that molecular iodine cannot be carried into the off-gas.
- . formation of non-volatile compounds such as HI_3 , due to the oxidizing action of boiling concentrated nitric acid. However, these compounds are probably reduced to the elementary form by nitrous acid.

In our experiment, operating conditions were such that the above difficulties were avoided. The analysis of Iodine 129 in the fuel solution confirmed that the residual amount was under 1 %.

Initially an attempt was made to evaluate the amount of methyl iodide present through analysis of Iodine 129 in the ethanol solutions through which the gas stream flowed. Although this compound was not detected, the trapping efficiency remains highly questionable.

An analytical method is currently being developed for the direct determination of organic iodine compounds in the gas. Early results appear to show that only traces of these compounds are present. This, however, is subject to confirmation by further tests.

Nevertheless, the formation of organic iodides seems to be related to the presence of organic impurities in liquid or gaseous reagents. The products used in our experiments were of high purity, which suggests that organic iodides are only formed in very small quantities.

The table IV shows the total quantity of iodine as well as iodine 129 activity. Disregarding one incorrect value due to experimental error, very good agreement is observed with predicted quantities computed using a CEA code.

These results also allow the estimate of the respective proportions of isotopes 127 and 129. Calculations show that Iodine 129 accounts for an average 82 % of total iodine.

Carbon 14

Volatile carbon compounds consist almost entirely of CO_2 . Carbon monoxide CO is only 1 % to 2 % of the amount of dioxide. No traces of light hydrocarbons (to C_6) were detected in the off-gas.

Measured carbon-14 activity was 0.24 Ci.t_U^{-1}

17th DOE NUCLEAR AIR CLEANING CONFERENCE

BURN-UP Gwd/t	TOTAL IODINE		IODINE -129	
	g / t _u	Adjusted to 33 Gwd/t	mCi / t _u	Adjusted to 33 Gwd/t
31.0	201	214	28.2	30.0
31.8	215	223	30.6	31.8
31.6	122*	-	17.9*	-
31.5	204	214	29.5	30.9
31.0	202	215	30.0	31.9
MEASUREMENTS (MEAN)		216		31.2
CALCULATED		223		31.4
$\frac{M - C}{C} \%$		- 3.1		-0.6

* Erroneous measurement (loss of iodine during experiment)

TABLE IV... IODINE CONTENT

Carbon-14 only accounts for 0.1 % of the total carbon measured, in mono-oxide as well as dioxide form.

The amount of CO₂ collected was approximately 80 l STP.t_u⁻¹. The gas released during chopping contained less than 1 % of the total CO₂.

BURN -UP Gwd/t	CARBON -14		TRITIUM	
	mCi/t _u	Adjusted to 33 Gwd/t	Ci / t _u	Adjusted to 33 Gwd/t
31.0	223	237	147	156
31.8	229	238	418	434
31.6	230	240	81	85
31.5	246	258	66	69
31.0	228	243	173	184
MEAN		243		186

TABLE V ... CARBON -14 AND TRITIUM CONTENTS

Tritium

Tritium quantities measured and shown in table V only relate to the fraction contained in the fuel, not including tritium in the zirconium clad.

The fraction of tritium gas released during chopping was very small and variable, representing 10^{-6} to 10^{-4} of the total tritium measured.

During dissolution, more than 99.5 % of the tritium was measured in the dissolution liquor, and 0.2 to 0.4 % was determined in the form of tritiated hydrogen in the gas phase.

Total tritium activity varied widely, from 66 to 420 Ci.t_U⁻¹ (180 Ci.t_U⁻¹ on the average). This spread of results is highly surprising ; it is generally estimated that in LWR fuel, 40 % of the tritium formed remains in the oxide / 3 /. It is also unlikely that such differences in tritium behavior could be accounted for by dissimilarities in thermal conditions affecting different rods in a single fuel assembly.

Experimental error is ruled out by the fact that results are consistent from one half-rod to the other. Furthermore , the tritium in the gas, determined by entirely different methods, shows fluctuations of the same magnitude.

A complete tritium balance will also require determination of tritium trapped in the clad. Attempts are currently being made to achieve tritium desorption by heating the hulls in a sealed oven.

R E F E R E N C E S

- / 1 / A.CHESNE, J.P.GOUMONDY, P.MIQUEL, A.LESEUR
Etat de la Recherche - Développement française dans le domaine du traitement des gaz produits par les usines de retraitement.
CEE Seminar on Radioactive Effluents from Nuclear Fuel Reprocessing Plants, Karlsruhe, 22-25 nov.1977
- / 2 / ANAV, CHESNE, LESEUR, MIQUEL, PASCARD
Brevet français n° 7.730.371 (1977)
- / 3 / E.HENRICH, H.SCHMIEDER, K.H.NEEB
The concentration of tritium in the aqueous and solid waste of LWR fuel reprocessing plants.
International Symposium on the Management of Gaseous Wastes from Nuclear Facilities, Vienna, 18-22 Feb.1980.

DISCUSSION

FURRER: In simulation tests we found that about 99.8 - 99.9% of the iodine was released in the DOG during dissolution. Have you added UI, NO₂ or O₃ to get the whole amount of iodine in the DOG?

LEUDET: No, we didn't require such a complete iodine desorption. Boiling and continuous bubbling of recycled NO_x in the dissolution liquor allowed us to carry out more than 99% of the total iodine into the DOG.

MOELLER: To what degree might the data you have developed be applicable in estimating airborne releases from an accident in a nuclear power plant?

LEUDET: I think that accident conditions in a nuclear power plant would be quite different than our operating conditions and make it impossible to transpose the results of this work.

FERNANDEZ: Could you tell me if the chromatographic conditions for the measurement of methyl iodide were the same as for the noble gases, and if any evidence was found for organic iodides heavier than methyl iodide?

LEUDET: Chromatographic conditions were different for methyl iodide and for noble gas measurements. Concerning the detector, we used an electron-capture detector instead of a catharometer. The material filling the separation column was also different. Up to now, no real evidence has been found for heavier organic iodides.

TIME-DEPENDENT ANALYSES OF DISSOLVER OFF-GAS CLEANING INSTALLATIONS
IN A REPROCESSING PLANT.

K. Nagel, J. Furrer

Kernforschungszentrum Karlsruhe GmbH
Postfach 3640, D-7500 Karlsruhe

G. Becker, W. Obrowski, Y.P. Seghal, J. Weymann

Technische Universität Berlin
Institut für Kerntechnik
D-1000 Berlin 10

Abstract

The iodine- and aerosol-filtering test facility PASSAT of the Nuclear Research Centre in Karlsruhe has been investigated using a method which allows time dependent analyses under accident conditions. This method which is closely related to fault tree analysis needs subdivision in barriers of the system, and their logical combination in a tree. The barriers have binary states: 'defect' and 'intact'. The 'defect' state will be described by a fault tree, whereas the 'intact' state includes dependences of a barrier operation on physical parameters. The 'intact' state enables time dependent calculations.

Calculations have been done for iodine filtering, because the best known entrance data are given. Results demonstrate clearly that the amount of iodine released increases only if both heaters failed, which heat the off-gas from 30° C to 80° C and then to 130° C. Additionally the integrated amount of iodine released depends on time period between the failures of the heaters.

1. Introduction

The dissolver off-gas of a reprocessing plant contains I-129, Kr-85, C-14, and H-3 as gaseous radioactive fission products as well as droplet and solid aerosols. These aerosols may carry along with them toxic fission products such as Ce-144, Cs-134, Cs-137, Sr-90, Ru-106, Sb-124, and the transuranic-elements Np, Pu, Am, Cm. Because of the radiotoxicity of these elements the dissolver off-gas has to be cleaned. At our research centre several independent parts of a planned dissolver off-gas cleaning system have been built in order to accumulate experimental results and experience. The two major parts are called PASSAT and KRETA. PASSAT is to remove aerosols and iodine, KRETA is to retain Kr-85. This paper is focused on PASSAT as a prototype of a filtering facility.

The aim of this work is to analyze the possibilities of failure, to define probabilities and to calculate amounts of radioactivity released under accident conditions. First investigations dealt with the definition of top events and, subsequently, with the construction of fault trees for the independent parts. It means a restriction if one describes the failure behavior of such technical systems by fault

trees. In cooperation with the Technical University of Berlin it was possible to apply an existing software program, which allows performing time-dependent calculations of the amount of toxic fission products released. In the following this work deals with:

2. Operation of PASSAT,
3. The basic method modelling technical facilities,
4. Models of the barriers,
5. Assumptions and results simulating the PASSAT off-gas sytem.

2. Operation of PASSAT

PASSAT is a prototype of a aerosol and iodine filtering facility. This facility was built to investigate the behavior of filter components in a compound system, to get experience in optimal operation conditions and to develop filter vessels which are easy to handle. Based on these different scopes of duties it will be difficult to give a satisfactory description of the system, which met not only the test facility but also the filtering facility of a reprocessing plant. Figure 1 shows the scheme of PASSAT, which is the basis of all investigations in this work. The source at the beginning of the scheme represents essentially dissolver, condensor, NO/NO₂ separation and coarse droplet separator. Source data which have been used in subsequent calculations are given in Table 1.

Tabelle 1 : Source data of PASSAT, which have been used in the calculations.

Aerosol Spectra			
liquid		solid	
size (µm)	mg/std.m ³	size (µm)	mg/std.m ³
5	0.02	0.5	1.2
10	0.2	7.5	0.6
15	0.6	12.5	0.2
20	0.6	15.0	0

Concentration of Aerosols:

liquid: 2mg/std.m³

solid: 2mg/std.m³

Off-gas Temperature: 30°C

Relative Humidity: 100%

Concentration of Iodine: 1g/std.m³

The following fiber packed mist eliminator with flushing capability (Brink filter) retains solid and liquid aerosols. Afterwards the off-gas is heated up to 80°C reducing relative humidity and vaporizing larger aerosol droplets. The heated off-gas flows through a HEPA-filter which separates mainly solid aerosols. Sorption is more effective at higher off-gas temperature. Therefore the heater in front of the first iodine-sorption-filter increases the temperature to 130°C,

which additionally improves the retention factor of the filter by decreasing relative humidity of the off-gas. All filters and heaters are protected against pressure increase by safety valves. The valves carry the off-gas over a safety iodine-sorption-filter to exhaust air. The flow rate of PASSAT is a constant of 150 std.m³/h.

3. Basic Method Modelling Technical Facilities

The fundamental method, which allows time-dependent analyses of failures of technical systems, was elaborated from the Technical University of Berlin /1/. It takes into consideration the dynamic behavior of these systems under accidental conditions, i.e. the functional dependence of components will be covered with respect to time. For this purpose, the determination of the amount of pollutants released which is required for risk analysis was carried out by simulation. On the other hand the probability of events was determined analytically resting largely on conventional methods like evaluation of fault trees.

The mathematical model of the investigated system divides itself into three parts which must be provided by the analyst. These parts are:

- 'release-tree' of the system,
- fault tree of the barriers in defect state,
- 'simulation-models for the behavior of barriers in 'intact' and 'defect' state, further referenced as 'transport cells'.

Firstly, the analysis requires a facility description by means of a so-called 'release-tree'. A 'release-tree' is closely related to a fault tree its top event being the release of toxic fission products. Basic events of a 'release-tree' are barriers of the system taking either 'intact' or 'defect' state. Fig. 2 shows the beginning of the 'release-tree' for PASSAT with essential details. The construction of a 'release-tree' needs simple considerations. The amount of toxic products released depends upon the amount of these arriving in front of the last barrier and on its penetration. The amount of toxic products arriving in front of the last barrier is dependent on the amount of material reaching the next but last barrier and on the amount penetrating it, and so on.

In the second step, fault trees are drawn up by means of conventional methods. They describe conditions under which barriers shift from 'intact state' to 'defect state'. Thirdly, the models of the barriers have to be developed. The models include the time dependent physical behavior of the system components.

Based on the complete 'release-tree' of PASSAT, the software program finds out all possible 'release-paths' of this tree. A 'release-path' corresponds exactly to an accidental state of the system. It contains all barriers which the toxic products have to penetrate in order to reach the atmosphere. The amount released will then be calculated for every 'release-path' by means of simulation. First of all a realisation of all the random events will be carried out using a random-digitgenerator. That means, the time at which barriers go into 'defect state', the duration of this state, actual loading etc. will be chosen randomly. Obviously, those random numbers are not independent of one another, but have to be chosen in such a way, that the combination of

17th DOE NUCLEAR AIR CLEANING CONFERENCE

accidents required for a special path occurs with overlapping intervals. This severely reduces the number of Monte-Carlo-trials required but on the other hand makes it necessary to calculate frequencies for all 'release-paths' analytically before simulation take place. Once the random events are fixed the amounts released can be calculated. The simulation-models then are coupled with one another in the order as described by the 'release-path'. The accident sequence of the coupled system is calculated in small discrete time increments from beginning to end. The amount of toxic substances released from the whole system considered can be calculated under accidental conditions. The simulation trials are repeated as often as necessary to determine the expected value of the amount released with sufficient accuracy.

Frequency of the occurrence of accidents is derived from the fault trees. For this purpose cut-sets are determined and evaluated using the known Vesely-relation.

Total risk of the whole system is calculated in the following manner:

$$R_{\text{system}} = \sum_{I=1}^{NP} (\overline{AM}_I \cdot H_I)$$

NP = Total numbers of 'release-paths'

\overline{AM}_I = Expected value of the amount released by every 'release-path'

H_I = Analytically determined expected value of the frequency of a 'release-path'.

calculations of the amount of products released are based on two assumptions:

- a) the 'release-paths' are independent of one another,
- b) moment and duration of change of a barrier state are independent of the special cut-set causing change of state.

4. Models of the Barriers

The description of the models of the barriers will be followed individually. First of all, in order to have a better understanding of the different criterion for the modelling, the simulation of the barriers will be explained in general. The simulation of the off-gas cleaning installations under normal and accidental conditions has to be carried out with these models. All the process variables which influence the barriers or are being influenced by these must be covered and treated accordingly to these models. Since the process variables are being transferred from one barrier-model to another one, it is urgently needed that each model is in a position to deal with all the present variables even if it does not influence any particular variable and is also not being influenced by it. A list of variables which have been taken into consideration for simulation of the PASSAT off-gas system is shown in Fig. 3. A barrier-model should fit not only in some particular off-gas system but should be as general as possible. As a consequence to this, it should be flexible and easily adaptable with regard to the sets of parameters. With sensible and skilful structuring of the models care is taken of that these can be switched over even to other larger or smaller sets of parameters. At the Institute

17th DOE NUCLEAR AIR CLEANING CONFERENCE

for Nuclear-techniques of the Technical University in Berlin (West Germany), a structure for the models has been developed which matches these requirements closely. The models developed here are in principle not confined to the number and combinations of the process variables. Their application is however restricted because of the fact that the mathematical description of the behavior of the models is valid within certain range. Generally, with a little effort, these can be adapted even to the other ranges of validity by inserting correlations which describe the behavior of these barriers within these ranges. After these initial remarks we shall be describing the modelling of each barrier in detail. The essential barriers of the off-gas system are:

- packed fiber mist eliminator
- HEPA-filter
- iodine-sorption-filter
- heater

A modelling of the behavior of these components under normal and accidental conditions is required in order to assess the behavior of the off-gas system.

4.1 Packed Fiber Mist Eliminator

It removes droplet and solid aerosols from the off-gas. It consists of not vitrified glass fibres with a packing thickness of 5 cm and a packing density of 300 kg/m³. The interesting operating parameters of the separator are the decontamination factor for droplet as well as solid aerosols and the pressure drop over the separator. Experiments have been carried out at Nuclear Research Centre in Karlsruhe (West Germany) to determine these values.

4.1.1 Droplet Aerosols

The separation of the larger drops ($d > 1 \mu\text{m}$) takes place mainly due to hindering and the effects of inertia. The drops strike the fibres and are pressed through the fibre network by the gas. Very small particles are held back mainly by diffusional effects. The liquid which has been held back flows down on the clean gas side of the network and is withdrawn off.

The measurement of the decontamination factors for the droplet aerosols dependent on the diameter of the drops has yielded values as shown in Fig. 4 /2/.

The correlation used for this dependency is as follows:

$$\log DF = 7.4 \log d + 1.11$$

with d = diameter of the aerosols in μm .

As evident from Fig. 5, this correlation describes the real behavior satisfactorily within the range of $1.5 < d < 5 \mu\text{m}$.

The measurements of the decontamination factors were carried out at different volumetric flow rates and temperatures. However there was no evidence that the decontamination factor depends on both parameters within the realistic operational range of the PASSAT off-gas system.

4.1.2 Solid Aersols

The experiments were also carried out to determine the decontamination factor for solid aerosols. The model particles consist of Uranin. The distribution of the particle diameter has been shown in Fig. 6, the most frequent diameter of the particles occurring at 0.12 μm /2/. It was not possible to relate the decontamination factor with the size of the particles, however a total decontamination factor was determined for the given spectrum of the particles in dependence on the volumetric flow rate. The following correlation was used for this purpose.

$$DF = \frac{1289 \cdot 10^{10}}{V^{5.1}} + 1062$$

with V = flow rate in Nm^3/h .

The correlation matches well with the experimental values for the whole range as shown in Fig. 7 /2/.

4.1.3 Determination of the Pressure Drop

Although the pressure drop does not have any influence on the separation efficiency, still it is interesting to know about its value. Complete information is not available for the pressure drop over the separator in the off-gas system. Both the main parameters which influence the pressure drop are flow rate and loading. The pressure drop in dependence on the flow rate is known only for the unloaded filter and is determined with the following correlation:

$$p(v) \text{ mbar} = 0.08 v + 1.6$$

where v = volumetric flow rate in Nm^3/h .

The dependence of the pressure drop on loading is known only at a constant flow of 75 Nm^3/h and is determined by the correlation:

$$p(m) \text{ mbar} = 0.09 m + 8$$

with m = loading in gm.

The pressure drop in dependence on loading and flow rate is determined for the model of this barrier by the following correlation:

$$p(m,v) = (0,09 m + 8) \frac{0.08 \cdot V_{akt} + 1.6}{0.08 \cdot 75 + 1.6}$$

with V_{akt} = actual flow rate in Nm^3/h .

i.e. the pressure drop will be calculated as a function of loading and is corrected with a factor which is given on the basis of deviation from a flow rate of 75 Nm^3/h .

The modelling of the mist eliminator is an example for the description of the behavior of a well known equipment on the basis of the measured quantities. The adjustment to other operational ranges is possible by means of changing the correlations.

4.2 HEPA-Filter

The HEPA-filter cleans the off-gas from aerosols. It consists of folded filter paper with a thickness of 0.4 mm.

The quantities necessary for modelling this filter are mainly the decontamination factor and the pressure drop over the filter.

4.2.1 Pressure Drop

Since the mechanical stability of the thin filter mat is very small, the pressure drop over the filter plays a decisive role in the operation of this component. If the pressure drop over the filter exceeds a certain maximum value the filter mat cannot withstand the force and tears off. This leads not only to a distinct decrease in the decontamination factor but also the filter cake which has already formed on the crude gas side is at least partially washed away and gets on to the clean gas side. Thus, if the filter breaks through, it loses not only its decontamination effect but also acts as a source of aerosols.

The pressure drop in dependence on the loading is shown by Fig. 8. The pressure drop over the filter is given by the Darcy equation:

$$p = K_D \cdot \eta_G \cdot V_a \cdot h_f$$

K_D = filter drag coefficient

η_G = dynamic viscosity of the gas

V_a = flow velocity

h_f = thickness of the filter mat.

The filter drag coefficient for the model is split as:

$$K_D = K_0 + K_{Bel}$$

K_0 = filter constant of the unloaded filter

K_{Bel} = additive corrective term for the loaded filter

The values of K_D and K_{Bel} are determined with the help of the Darcy equation from Fig. 8.

While K_0 is a real constant, K_{Bel} will be determined in each time interval during the simulation.

4.2.2 Decontamination Factor

The values of the decontamination factor depending upon the size of the aerosols are not known for this filter. Therefore a half empirical formula of Friedlander was used which will be explained as follows. There are three main mechanisms which influence the separation of the aerosols on a filter mat. These mechanisms are:

17th DOE NUCLEAR AIR CLEANING CONFERENCE

- influence due to the forces of inertia (the aerosols cannot follow the path of the gas flow between fibres because of inertia)
- diffusion (contact with the particles because of the Brownian movement)
- electrical effects.

For every single effect of separation there are a number of theoretical and half empirical solutions. The total separation efficiency, however, cannot be calculated as a sum of each effect individually and a solution which takes into account all the main three effects is not available. The superposition of the effects due to forces of inertia and diffusion is described by Friedlander as follows /3/:

$$\epsilon_{M_D} = \frac{6 \left[\frac{KT}{3\pi\eta_G} \right]^{2/3}}{v_G^{1/6} \cdot d_f^{1/2} \cdot d_p^{2/3} \cdot v^{1/2}} + 3 \frac{d_p^2 \cdot v^{1/2}}{v_G^{1/2} \cdot d_f^{3/2}}$$

ϵ_{M_D} = separation efficiency of a single fibre due to forces of inertia and diffusion

K = Boltzmann - constant

T = temperature in K

η_G = dynamic viscosity of the gas

v_G = kinematic viscosity of the gas

d_f = diameter of a fibre

d_p = diameter of the particle

v = flow velocity

(all units in cgs-system)

The first term of the equation describes the diffusional effects while the second term takes into account the effects due to the forces of inertia.

The total separation efficiency of the filter network is calculated as follows:

$$\epsilon_g = 1 - e^{-\alpha}$$

with

$$\alpha = \frac{4}{\pi} \epsilon_{M_D} \frac{1-\beta}{\beta} \cdot \frac{h_f}{d_f}$$

β = porosity of the filter network

h_f = thickness of the filter network

This results in a decontamination factor

$$D_f = \frac{1}{1-\epsilon_g} = e^\alpha$$

The decontamination factors determined in this way dependent on particle diameter have been illustrated in Fig. 9.

While simulating aerosol filter, the droplet and solid particles have been treated equally and the swelling of the filter due to dampness thereby resulting in the increase of the pressure drop has not been considered.

If the filter breaks through ($p = 20$ mbar), then it is assumed, that the whole filter cake will be washed away within an hour and gets on to the clean gas side.

4.3 Iodine-Sorption-Filter

A considerable amount of iodine is released during the dissolution of the spent fuel. The off-gas system, therefore, has been provided with an iodine filter. It is a chemisorption filter and consists of silver impregnated silicagel. The decontamination factor for this filter is largely dependent upon the retention time of the gas in the filter and the relative humidity of the gas. The measured decontamination factors dependent on these quantities are illustrated in Fig. 10.

The retention time determined not only by the geometric dimensions of the filter but also by the loading which has already accumulated over the filter. The filter has approximately a capacity of 12 kg of iodine and is exchanged after a loading of nearly 80 %. In order to keep the relative humidity as low as possible, the filter is operated at a temperature of about 130° C.

A distinct decrease in temperature can result in a deterioration of the decontamination factor because the relative humidity of the gas increases with decreasing temperature. Apart from the excessive loading of the filter, this is the single factor affecting the decontamination factor which has been modeled. The resorption processes by which iodine is released from the filter have been neglected. For example, high contents of nitric oxides in the off-gas system may cause resorption.

4.3.1 Modelling of the Separation Efficiency

An eventual break down of the iodine filter has not been provided in the modelling of this filter i.e. its decontamination factor will be calculated in any case from the Fig. 10. However, it is quite possible to obtain a decontamination factor near 1. Such a decontamination factor is never reached because of a sudden failure of this component but always due to relative gradual change of the state of the gas or the loading.

The curves of Fig. 10 have been provided with a raster (10 % relative humidity). The actual values of the decontamination factor are determined by interpolating between the points of the raster in the direction of humidity as well as in the direction of retention time. It was found, that each of the two centre-curves (Fig. 10) could be described as a linear interpolation of the two neighbouring curves with poor results only. The half logarithmic scale of Fig. 10 led to the conclusion, that the logarithm of the decontamination factor should be interpolated rather than the decontamination factor itself. This method was tested with good success against the measured curves and then was used to interpolate for the current values of the remaining retention time and the relative humidity within the raster mentioned above.

Another quantity modeled is the pressure drop over the filter. The values are known for this pressure drop in dependence on flow rate and it can be calculated with the following correlation:

$$p = 0.73 \cdot v^{1.28}$$

with V = flow rate in Nm^3/h .

The dependence of pressure drop on loading is not known.

4.4 Heaters

Two heaters are installed in the PASSAT off-gas system, one in front of the HEPA-filter and the other one in front of the iodine-filter. They heat the off-gas to a temperature of 80°C and 130°C , respectively which is the operating temperature under normal conditions. This helps in keeping the relative humidity to an optimal level for both filters which is a crucial factor in determining the behavior of these components with respect to their decontamination factors. Both heaters have been modeled identically. Although the model has been developed for the PASSAT off-gas system, yet it can be adapted to any other system because of its general nature keeping in mind all the necessary points described already in the previous section of barrier models.

It was observed that once the heater is switched on or off, it attains the new stationary temperature after a transition stage which lasts for an hour. Due to this fact, a model was developed which takes into account the instationary behavior of this component. The following assumptions have been made in the model:

1. The pressure drop over the heater is negligible.
2. The evaporation of water in the liquid phase, for example, when the gas is over saturated, has been neglected.
3. The reduction of droplet aerosols to solid aerosols which can take place due to evaporation of water has not been considered. It will be necessary to account for this effect if the behavior of the system is modeled for droplet aerosols.
4. No attention has been given to the geometric configuration of the heater.

17th DOE NUCLEAR AIR CLEANING CONFERENCE

The time dependent electrical power P_{el} has two effects. Firstly, it heats up the heat capacity of the heater which can also include the capacities of other adjoining components. Secondly, it heats up the gas by convective heat transmission. This is described by a heat conductance αA .

The following balances have been used:

1. Heat output of the heater = heat taken by the gas

$$\alpha A (\delta_h - \delta_M) = c \dot{m} (\delta_2 - \delta_1) \quad (I)$$

2. One part of the electrical energy goes in the heat capacity of the heater while the other part is transmitted to the gas by convection.

$$P_{el} \cdot dt = C_h d\delta_h + \alpha A (\delta_h - \delta_M) dt \quad (II)$$

3. Mean temperature of the gas

$$\delta_M = \frac{\delta_1 + \delta_2}{2} \quad (III)$$

From the above balances one can derive the following equation for the exit temperature δ_2 by eliminating δ_M and δ_h

$$\begin{aligned} \left(\frac{L_{tr}}{\alpha A} + \frac{1}{2}\right) \frac{d\delta_2}{dt} - \left(\frac{L_{tr}}{C_h} + \frac{1}{\alpha A} \cdot \frac{dL_{tr}}{dt}\right) \delta_2 &= \frac{P_{el}}{C_h} + \left(\frac{L_{tr}}{\alpha A} - \frac{1}{2}\right) \frac{d\delta_1}{dt} + \\ &+ \left(\frac{L_{tr}}{C_h} + \frac{1}{\alpha A} \frac{dL_{tr}}{dt}\right) \delta_1 \end{aligned} \quad (IV)$$

with $L_{tr} = c \dot{m}$

The quantity L_{tr} has the unit of a heat conductance and is described as transport conductance. It will be taken as time dependent because a flow control might effect the mass flow rate and heat capacity c depends on the composition of gas which also can vary with time.

Equation (IV) is a linear inhomogenous system with time dependent coefficients. If one neglects the time dependence of the coefficients, the homogenous solution of this equation is as follows:

$$\delta_2 = k e^{-t/T} \quad k \in \mathbb{R} \quad (V)$$

with the time constant as

$$T = C_h \left(\frac{1}{\alpha A} + \frac{1}{2 L_{tr}} \right) \quad (VI)$$

Equation (V) was programmed in discrete form.

The time dependent electrical power P_{el} is treated as follows:

In defect state P_{el} is zero.

In intact state, it will be adjusted during each time interval in such a way that the stationary output temperature becomes equal to the required value, provided P_{e1} does not exceed a maximum value or becomes less than zero.

Symbols used:

A	:	effectiv heat transfer area	$[m^2]$
C_h	:	heat capacity of the heater	$[J/K]$
c	:	specific heat capacity of the gas	$[J/K \cdot kg]$
m	:	mass flow rate	$[kg/s]$
α	:	heat transfer coefficient	$[W/K \cdot m^2]$
δ_1	:	inlet gas temperature	$[^\circ C]$
δ_2	:	exit gas temperature	$[^\circ C]$
δ_h	:	mean temperature of the heat capacity of the heater	$[^\circ C]$

5. Assumptions and Results Simulating the PASSAT Off-gas System

5.1 Feasible States of the Barriers and their Functions

Using the models described earlier the simulation of the off-gas system has been carried out for normal and accidental conditions. The off-gas source parameters have been listed in the chapter 'Operation of PASSAT'. These parameters are kept constant in the evaluation of the simulations, the source of the off-gas system has not been considered so far under accidental conditions. Likewise, the droplet aerosols in the off-gas have been neglected, till now.

The mist eliminator does not go into defect state, it is always to be at disposal. It has a decontamination effect for solid aerosols but not for iodine.

The heaters have no decontamination effect at all. They compensate for the deviations of the required temperature within their range of regulation (range of regulation 0-3 kw, stationary output under operational conditions nearly 2.7 kw). Both the heaters have been modeled identically, they differ only in the range of temperature in which they operate. The heaters can take 'intact' or 'defect' state.

The aerosol filter does not have any decontamination effect for iodine, it retains only aerosols. It can take 'intact' or 'defect' state; it can fail either by chance or if the pressure drop exceeds 20 mbar, then it fails deterministically. The filter cake is washed away completely within an hour.

The iodine filter does not have any stochastic defect state. It can lose its effectiveness only due to excessive loading or because of too high humidity of the off-gas. Irrespective of all the other influences, its decontamination factor is always 2 for aerosols.

Nothing can be said about risk resulting from accidents, because no calculations of failure probabilities have been performed. Those calculations are planned for the future. Till today, only consequences

have been considered.

5.2 Results

With the boundary conditions described earlier, a large number of accidents are possible since each arbitrary combination of different states of the barriers represents an accident. From these numerous combinations, however, only two have significant effects. These are:

- the breakage of the HEPA-filter
- the simultaneous failure of both heaters.

Therefore, these two accidents will be dealt with in the following section.

5.2 Breakage of HEPA-Filter

This accident results in increase of the amount of aerosols released. It does not have decontamination effect any more and beyond that it releases the stock which has already accumulated on it. The release of the stock in this case is more dominant than the loss of decontamination effect. This result can be explained because of the fact that the content of the aerosols in the gas is very low and besides HEPA-filter, the mist eliminator is present which removes aerosols very effectively.

The deterministic breakage of HEPA-filter has in no case taken place while simulating the PASSAT off-gas system i.e. the permissible pressure drop of 20 mbar has never been exceeded. It can be exceeded due to increase in flow rate under accidental conditions. A time dependent model of the source is necessary for the investigation of the real dynamic behavior of the accident 'filter-breakage'. Such a model has been planned in the course of the further work. A flow controller will then also be considered which can take 'intact' or 'defect' state. It will then be possible to take into account the effects of other components on the behavior of the filter.

5.4 Failure of Heaters

The failure of heaters result mainly in the release of iodine. In contrast to filter breakage, this accident is a good example to demonstrate, that the consequences can be highly dependent on the course of accident. The failure of only one heater has no effect on the decontamination factor for iodine.

Fig. 11 shows the progress of the accident when both heaters go out of order almost simultaneously, About 0.7 hr after failure of heater 2, heater 1 goes out of order and the temperature falls down to the entrance temperature of 30° C. About two hours after beginning of the accident, the release-fraction of iodine increases because of the increase in relative humidity of the off-gas and finally reaches nearly 80 %. A similar type of accident is shown in Fig. 12, here heater 1 goes out of order firstly and after about 4.5 hrs the heater 2 fails. When the gas temperature behind heater 2 drops to 40° C, the release-fraction of iodine increases clearly. The time taken to repair the heaters is assumed to be 8 hrs. After repairing heater 1, the release fraction is nearly at once very low again and therefore

17th DOE NUCLEAR AIR CLEANING CONFERENCE

the simulation stops after 8 hrs. The effect of filter-loading has not been shown in both Figures as the iodine filters were almost empty in both simulation-trials. In the third example (Fig. 13) there is a gap of 7 hours between the failures of the two heaters. Thus, after 8 hours, when the repair of the first defect heater is finished, the temperature of the gas has not fallen down to such a level which could have resulted in a severe increase in the release-fraction. After 8 hrs, at the time of the lowest temperature, the release-fraction is still below $10^{-2}\%$ and then becomes less temporarily. By this time, however, the iodine loading of the iodine filter has become excessive and once more the release-fraction increases. That is caused by the strategy decided for the simulation of the behavior of the personnel of the off-gas section. It was assumed that while repairing defect components no maintenance work, for example, change of filter, will be undertaken. The release of iodine varying with the timely sequence of the accident has been shown as follows:

A total number of 37 random trials 'both heaters defect' were carried out. On average 120 gms of iodine were released. The release of iodine in each case is as:

- in 11 trials less than 1 gm
- in 4 trials between 1 and 10 gm
- in 6 trials between 10 and 100 gm
- in 16 trials between 100 and 425 gm.

This finally leads to the conclusion, that the interaction of the components of a multibarrier system can be described adequately by the method of dynamic accident analysis. The insight in the behavior of technical systems under accidental conditions is significantly better than that gained with former (static) methods.

6. R E F E R E N C E S

- /1/ R. Storck: "Eine Methode zur probabilistischen Risikoanalyse unter Verwendung dynamischer Freisetzungsmodelle". Ph. D. thesis, TU Berlin (1979)
- /2/ J. Furrer, R. Kaempffer, A. Linek, A. Maerz: "Results of Cleaning Dissolver Off-gas in the PASSAT Prototype Dissolver Off-gas Filter System". CONF - 801038, p. 566 (1980)
- /3/ S. K. Friedlander: "Theory of Aerosol Filtration". Ind. and eng. Chem. 50 (1958)

17th DOE NUCLEAR AIR CLEANING CONFERENCE

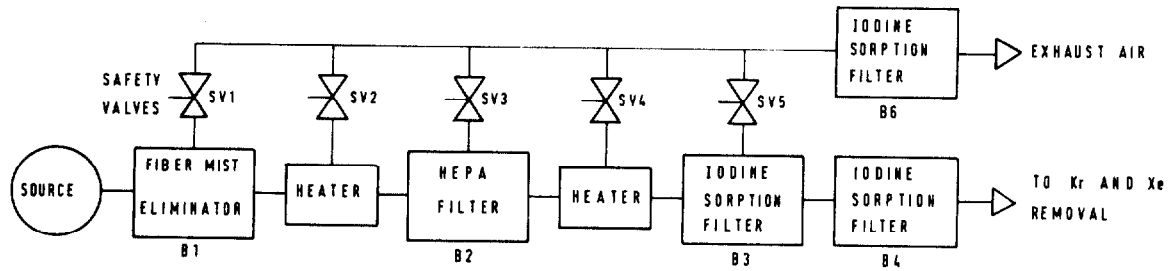


FIG. 1: BLOCKDIAGRAM OF THE AEROSOL- AND IODINE-FILTRATION FACILITY (PASSAT)

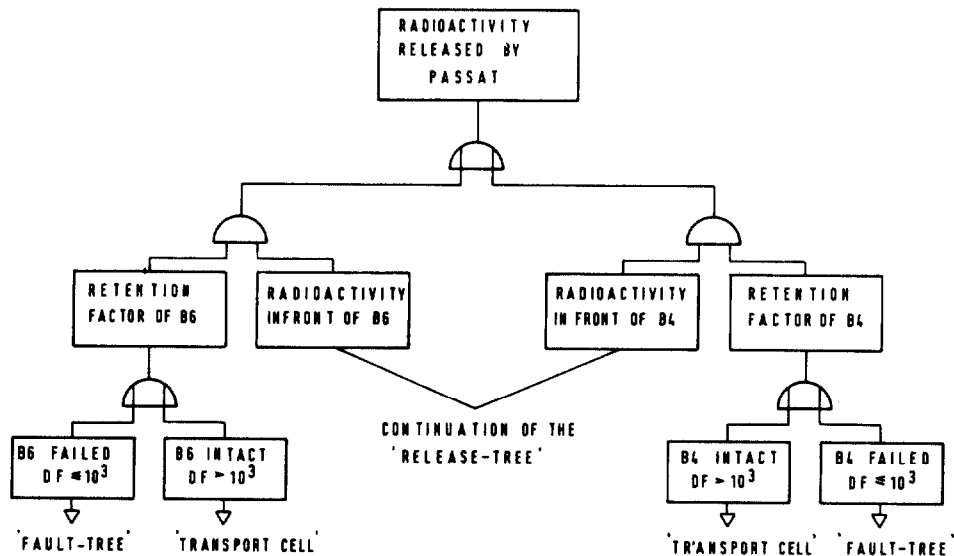


FIG. 2: DETAILS OF THE 'RELEASE-TREE' FOR PASSAT

- 1: VOLUME FLOW RATE (NM³/H)
- 2: AEROSOL-CONCENTRATION (G/NM³)
- 3: IODINE-CONCENTRATION (G/NM³)
- 4: AEROSOL-DIAMETER DISTRIBUTION
(4 CHARACTERISTIC GROUPS)
- 5: GAS TEMPERATURE (°C)
- 6: REL. HUMIDITY (%)
- 7: PRESSURE (MBAR)
- 8: PRESSURE DROP (MBAR)

FIG. 3: LIST OF VARIABLES CONSIDERED

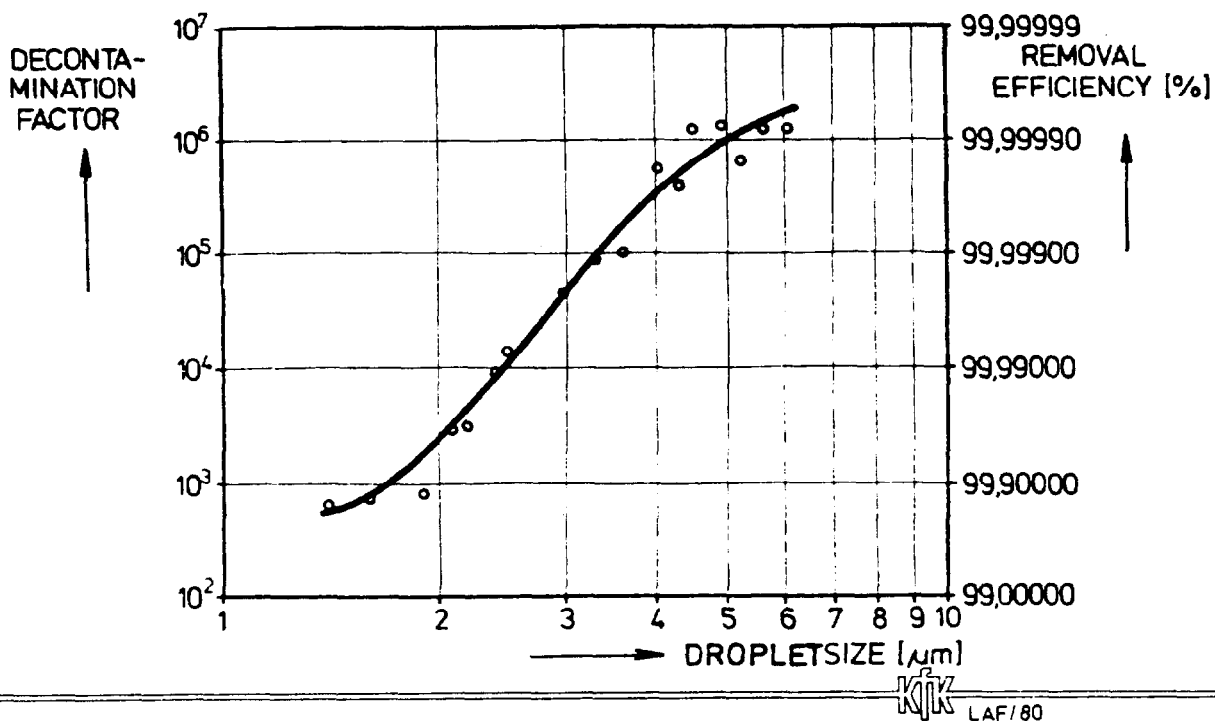
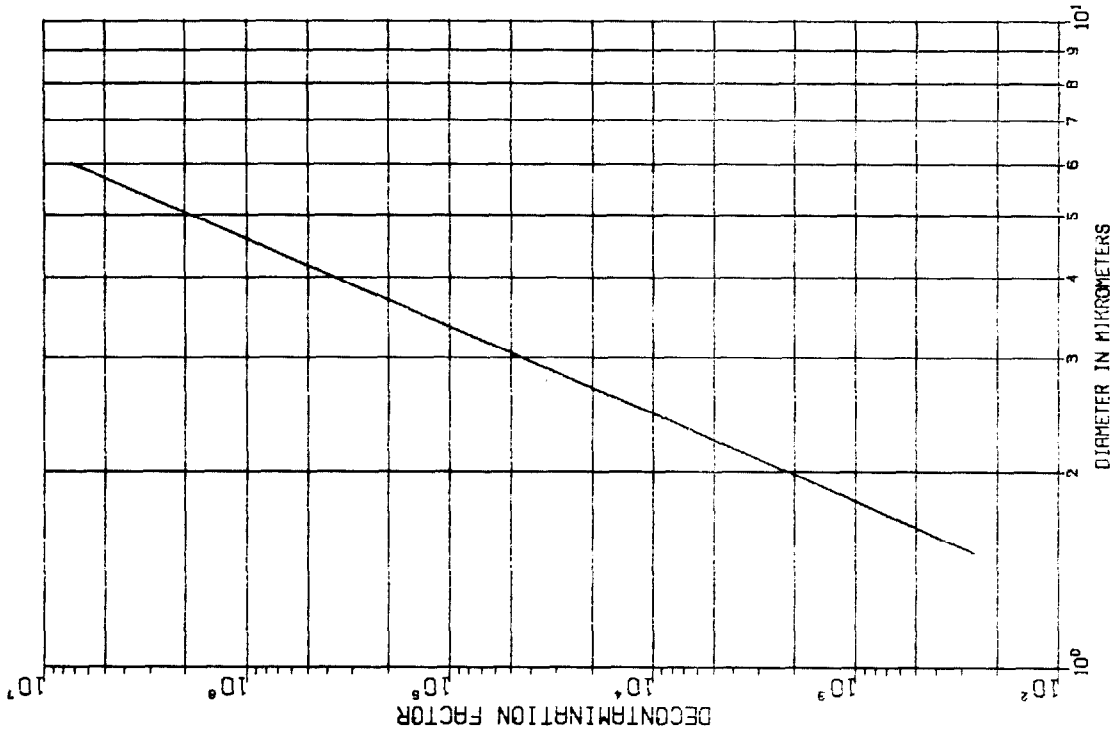
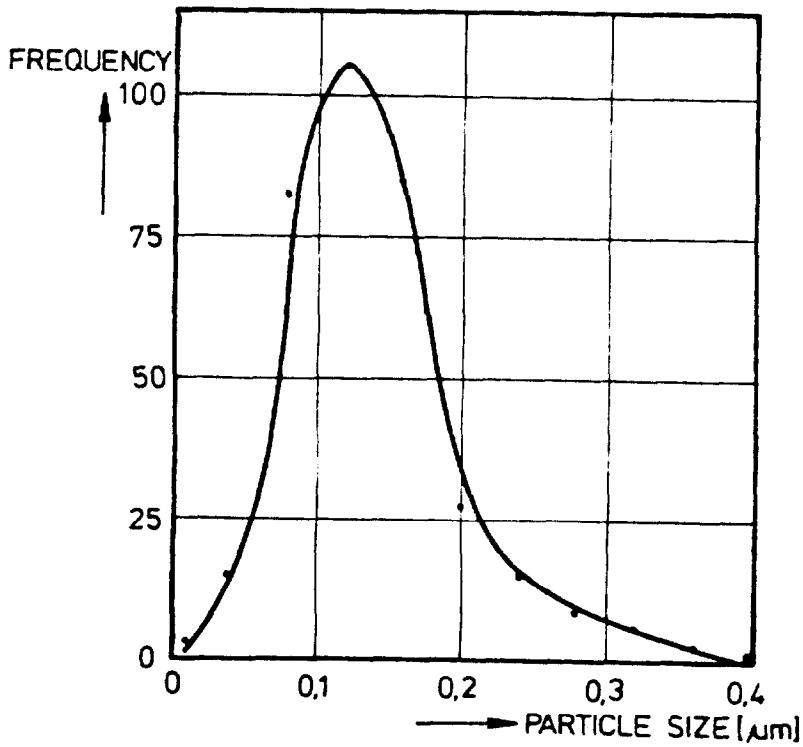


FIG. 4: DECONTAMINATION FACTOR AS A FUNCTION OF DROPLET SIZE (PFME/ 5 cm)



IKT | 08/07/82 | FIBRE MIST ELIMINATOR
DECONTAMINATION FACTOR, DROPLET AEROSOLS

FIG. 5: DECONTAMINATION FACTOR AS A FUNCTION OF PARTICLE DIAMETER



IKT LAF/80

FIG. 6: URANIN PARTICLE SIZE DISTRIBUTION

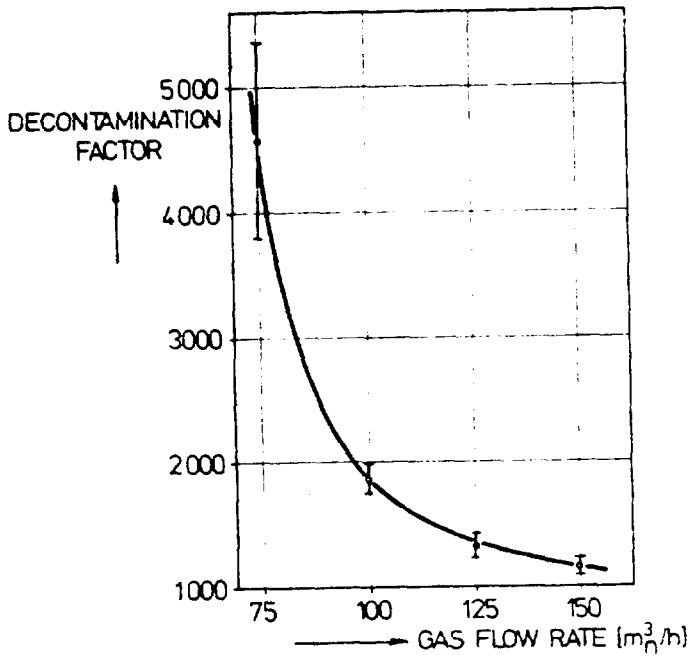


FIG. 7: DECONTAMINATION FACTOR AS A FUNCTION OF FLOWRATE AT PFME (5 cm)

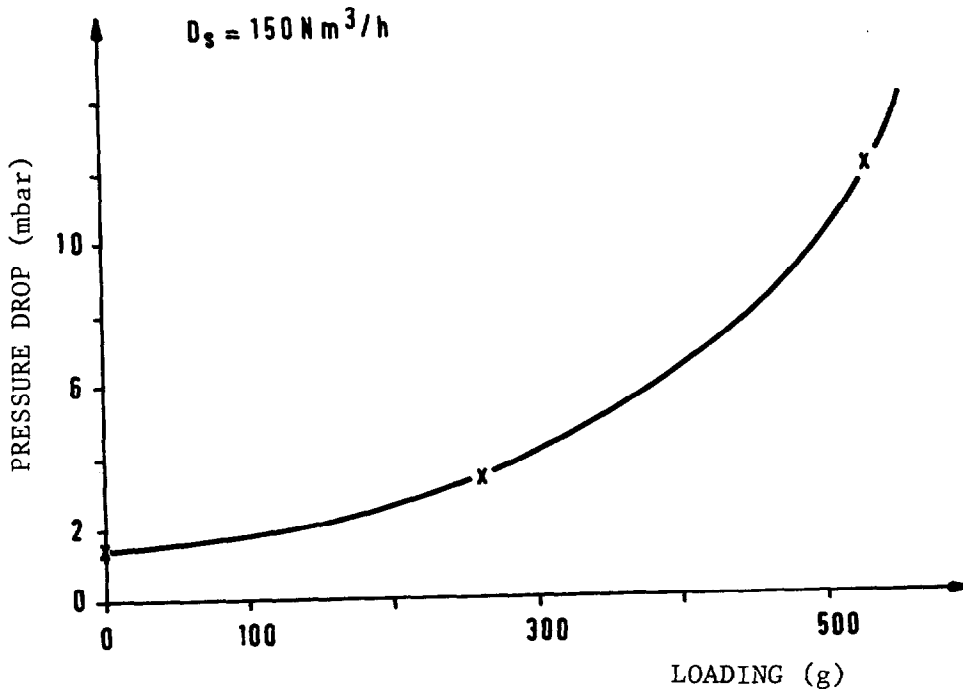


Fig. 8: PRESSURE DROP OF THE HEPA-FILTER AS A FUNCTION OF LOADING

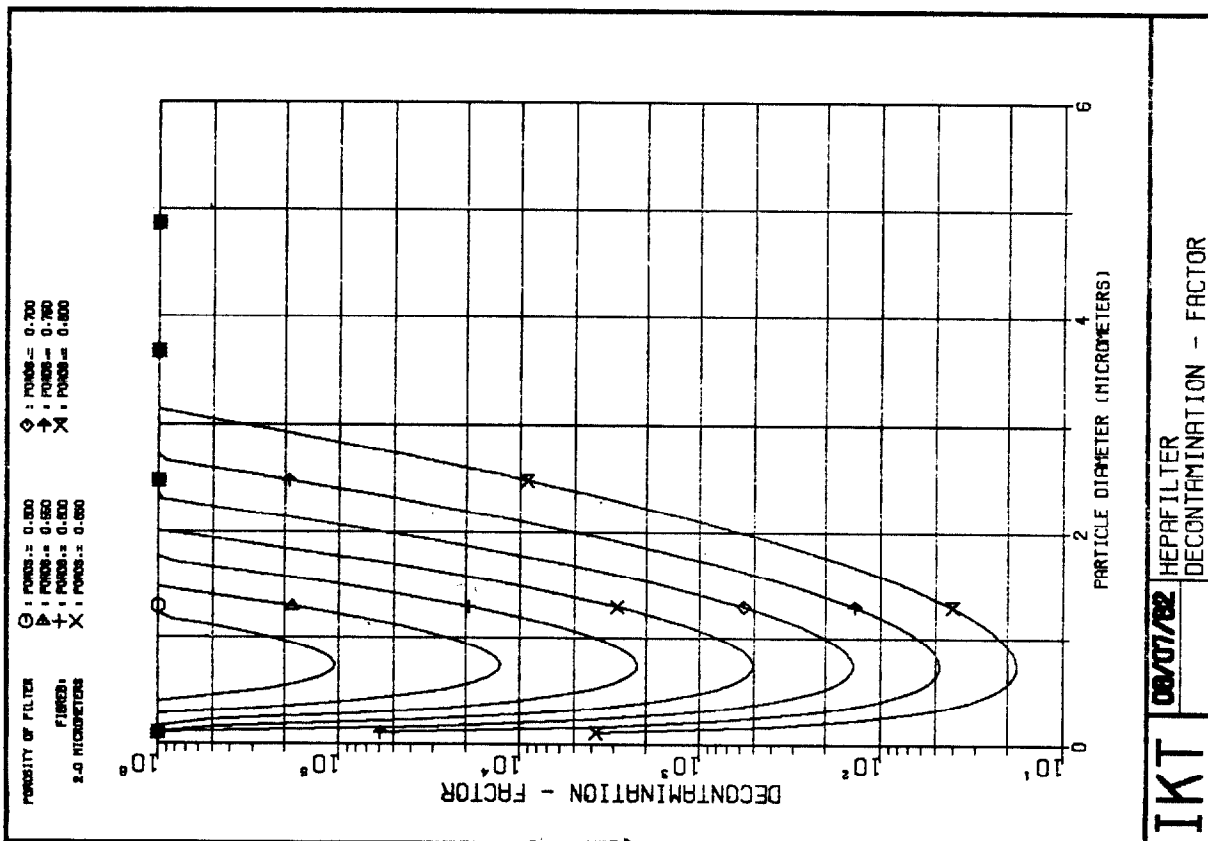
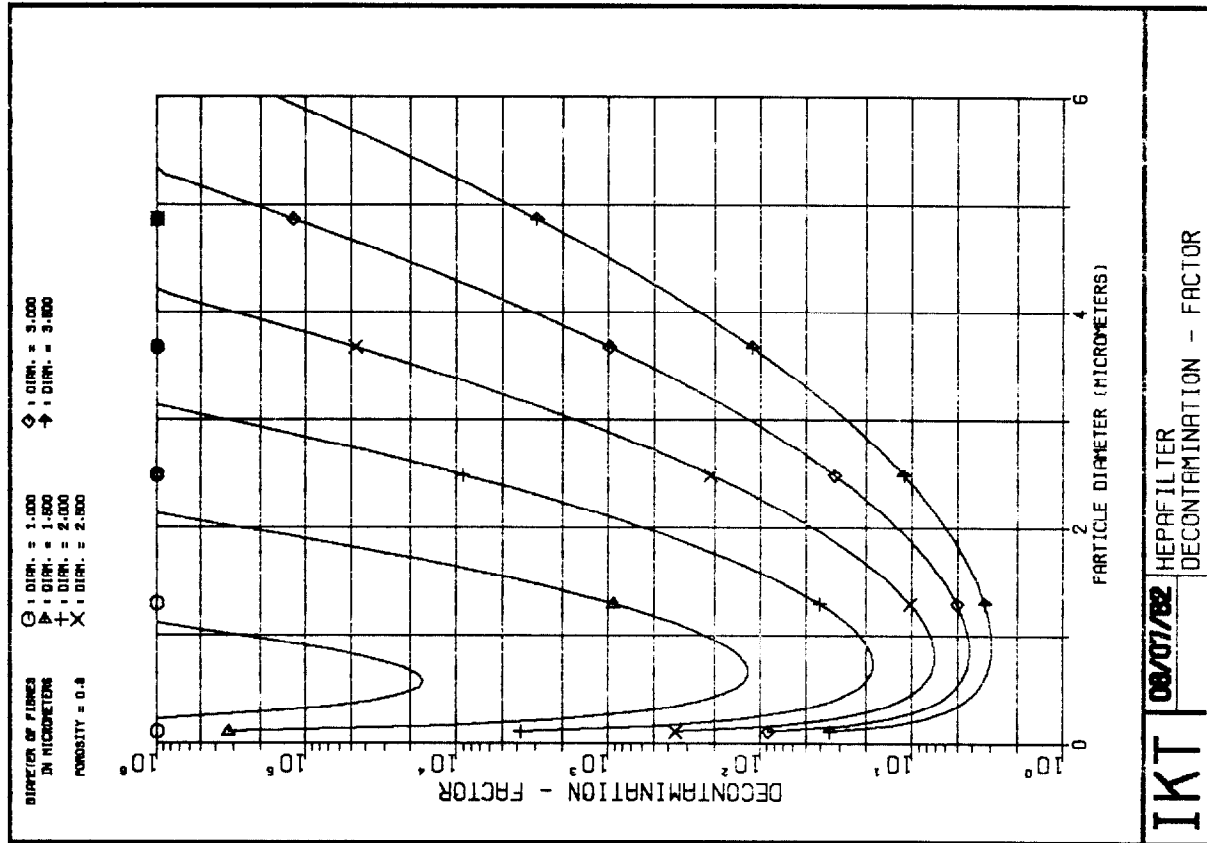


FIG. 9: DECONTAMINATION FACTOR OF THE HEPA-FILTER AS A FUNCTION OF PARTICLE DIAMETER

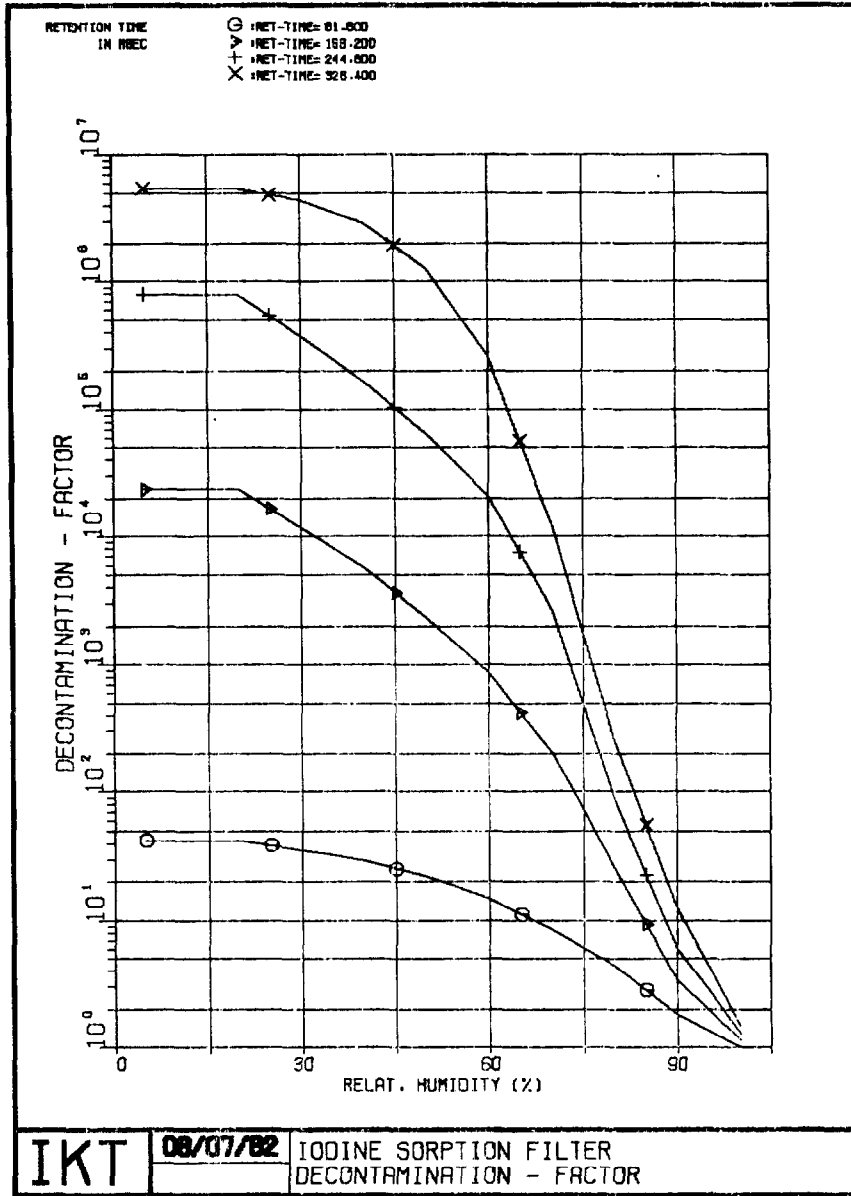


FIG. 10: DECONTAMINATION FACTOR OF THE HEPA-FILTER AS A FUNCTION OF RELATIVE HUMIDITY

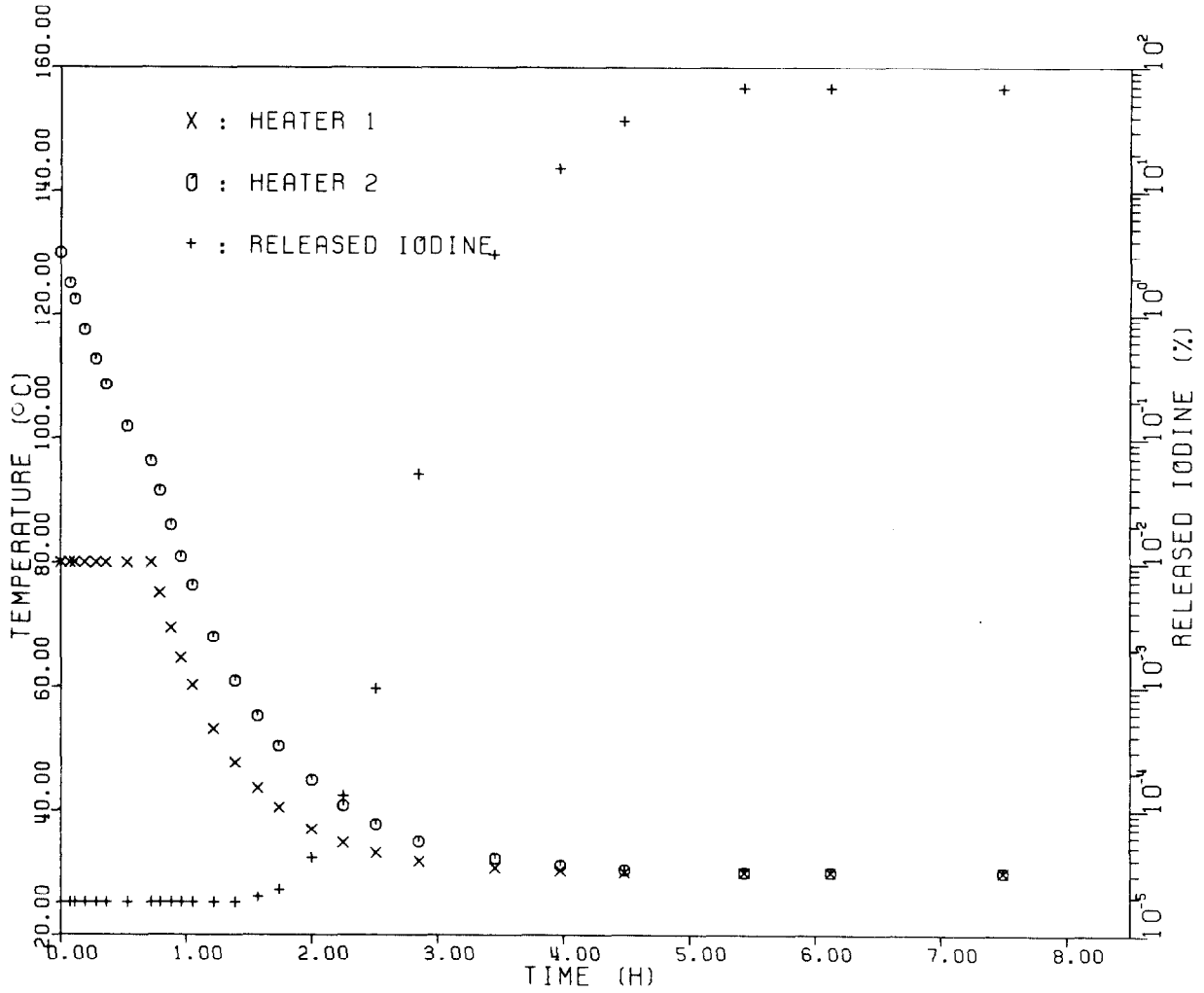


FIG. 11: TIME DEPENDENCE OF THE FAILURE OF BOTH HEATERS WITHIN 8 HOURS AND ACCORDING THE CHANGE OF IODINE RELEASED:

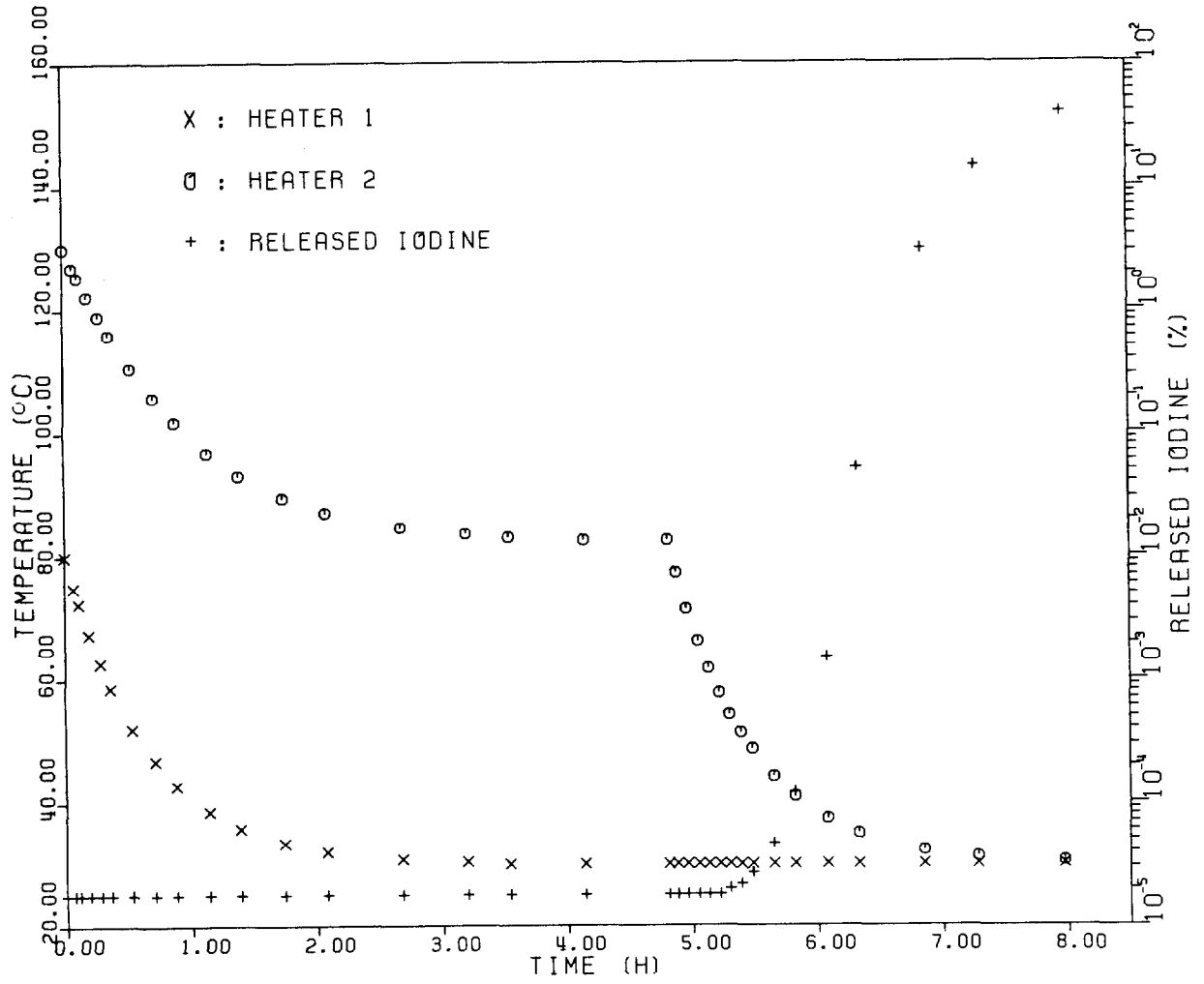


FIG. 12: TIME DEPENDENCE OF THE FAILURE OF BOTH HEATERS WITHIN 8 HOURS AND ACCORDING THE CHANGE OF IODINE RELEASED

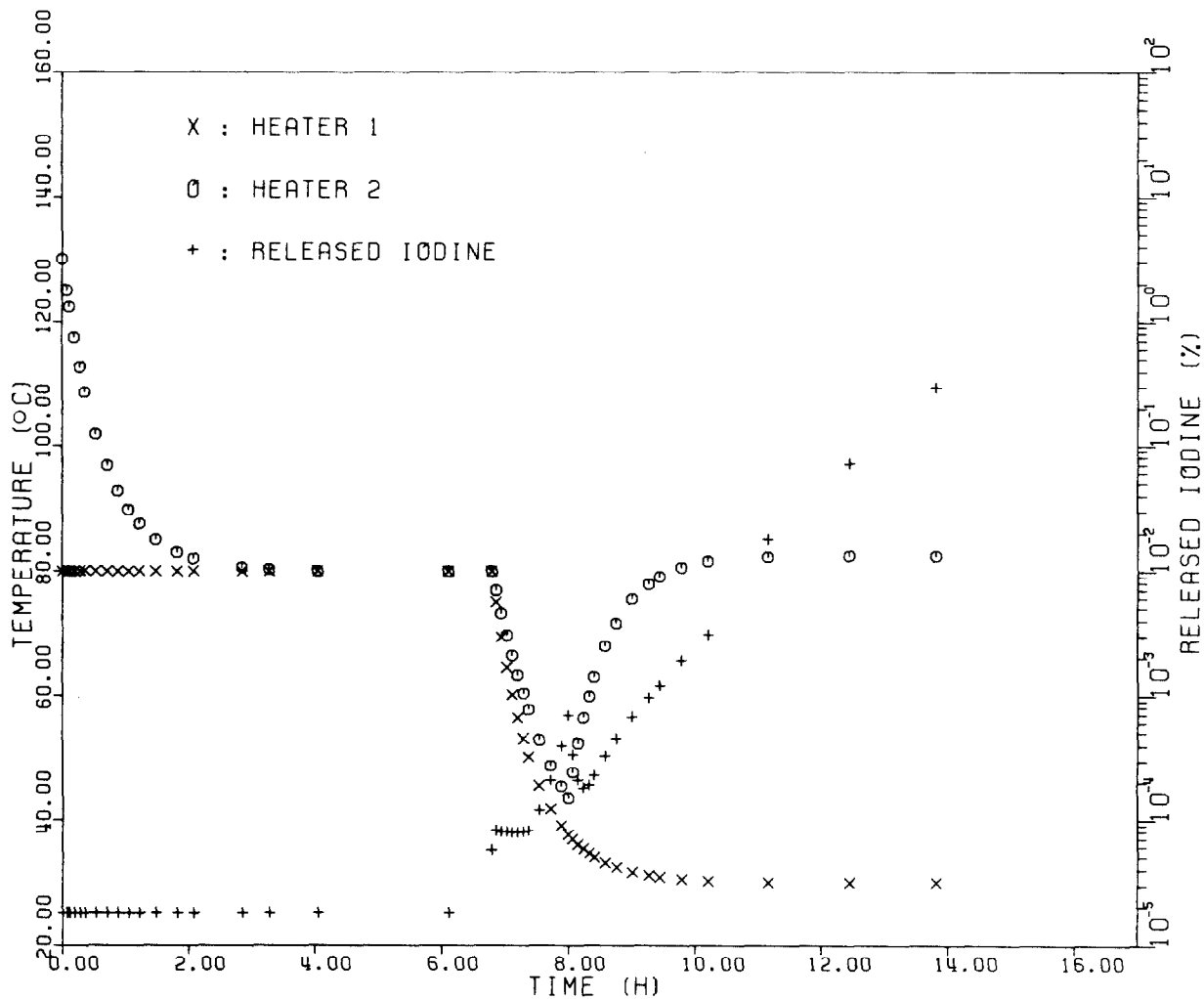


FIG. 13: TIME DEPENDENCE OF THE FAILURE OF BOTH HEATERS WITHIN 8 HOURS AND ACCORDING THE CHANGE OF IODINE RELEASED

DISCUSSION

MOELLER: What quantities of radioactive material would the iodine releases you described represent?

FURRER: If the two heaters were out of operation, which we don't believe would happen, the release of iodine would be some number of Ci. If the PASSAT heater has a failure, we would have a signal from the temperature controller. In a future plant the offgas stream will be switched to a second heater.

Kovach, J.L.: What is the probability of the heater failures that would result in an iodine release?

FURRER: The probability is very low. After three years of experimental work at the PASSAT DOG cleaning facility, we had only one failure at the heater in front of the iodine filter.

A MODEL OF IODINE-129 PROCESS DISTRIBUTIONS
IN A NUCLEAR FUEL REPROCESSING PLANT

G. J. McManus
F. A. Duce
S. J. Fernandez
L. P. Murphy

Exxon Nuclear Idaho Co.
Idaho Falls, Idaho, USA

ABSTRACT

This paper documents the development, demonstration and verification of a model of iodine-129 pathways in a nuclear fuel reprocessing plant. Laboratory experimental results are presented on iodine-129 chemical forms and also on evaporator and solvent extraction behavior. In-plant sampling results for all accessible processes are also reported. A computer program using the developed model is documented. Although the ICPP is somewhat unique in its processes it is believed these results can be applied to other types of fuel reprocessing plants.

I. INTRODUCTION

All fuel reprocessing plants subject to EPA regulations must isolate at least 99.75% of the iodine-129 in the spent fuel from the environment. Therefore, all pathways in a nuclear fuel reprocessing plant containing greater than 0.25% of the original iodine-129 must be identified and characterized. This characterization must include all parameters influencing eventual recovery and fixation of the iodine-129 from process solutions, including ^{129}I concentration, chemical form, and volatility.

Other researchers have attempted to address this problem. Berg and Schottelhopf attempted to close the iodine-129 mass balance around the WAK (Karlsruhe)¹. Yet because greater than 99% of the ^{129}I is volatilized at the WAK into the dissolver off-gas, the partition of the remaining ^{129}I into the downstream off-gas and liquid streams was uncertain due to the small amounts being measured. The release of greater than 99% of the iodine-129 into the dissolver off-gases may not be representative of non-European fuel reprocessing plants. European plants such as the WAK, use high temperature fumeless dissolving where oxygen is added directly to the dissolver solution. This oxygen would subsequently oxidize any iodide to I_2 , which is then sparged from the dissolver into the off-gas.

However, in fuel reprocessing plants not using fumeless dissolution (Purex, electrolytic, etc.) pathways may be considerably different from those found in the European plants. This study was undertaken to measure the iodine-129 pathways in a more typical or "generic" fuel reprocessing plant.

The generic fuel reprocessing plant proposed by Davis⁽²⁾ is shown in Figure 1. In this fuel reprocessing plant, the nuclear fuel is delivered to a head-end step (graphite burner, voloxidizer, etc.); the iodine-129 may be partially released in this step (but much less than 99%). After dissolution, successive steps include solvent extraction, nitric acid recovery, and liquid waste management.

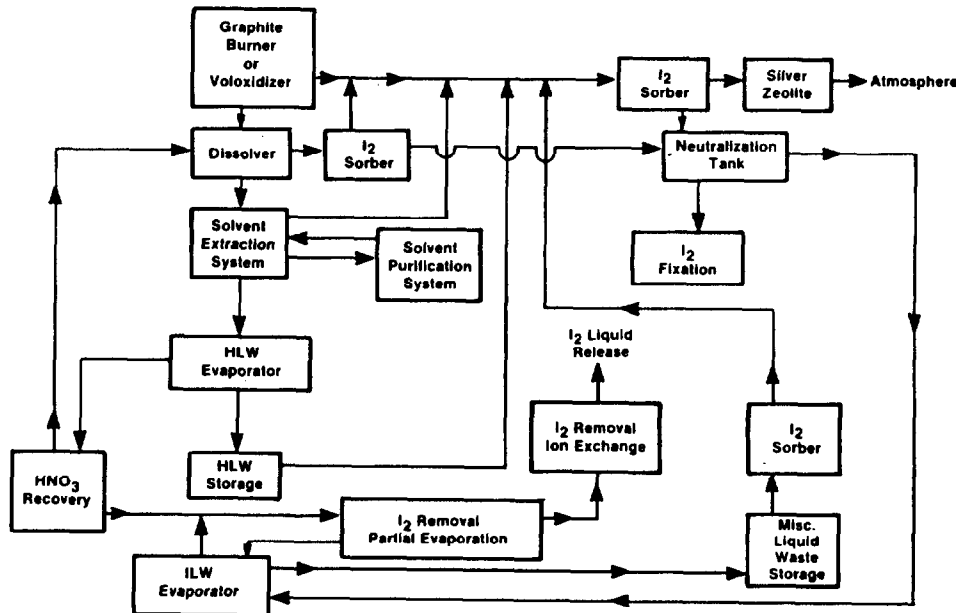


Figure 1. Generic Fuel Reprocessing Plant

ICPP-S-7884

To measure the iodine-129 pathways in a fuel reprocessing plant similar to that shown in Figure 1, a three phase program was undertaken: laboratory evaluation, in-plant sampling, and development of a computer model. The first phase was used to identify those processes most likely to be major pathways and to permit modeling of those unit operations impossible to measure at ICPP. This phase included a laboratory evaluation of the process chemistry, a review of past experience at the Idaho Chemical Processing Plant (ICPP), and simulation of individual process unit operations.

The second phase was the actual in-plant measurement of the iodine-129 pathways. The ICPP was chosen as a suitable site to measure these iodine-129 pathways because it does not use fumeless dissolution and both separation and waste management activities are performed at the same site. A block diagram of possible pathways at the ICPP is shown in Figure 2. All possible pathways identified by Davis⁽²⁾ are present except the head-end step. However, since it is not clear at the present time that a head-end step will be required at future reprocessing plants, this may not be a significant deficiency.

The third phase was the compilation of the pathways analyses into a single computer program. This program must be sufficiently flexible to predict the effect of changes in process conditions on iodine-129 releases. Therefore, a fuel reprocessing plant that differs in some respects from ICPP can still be described by the results presented here.

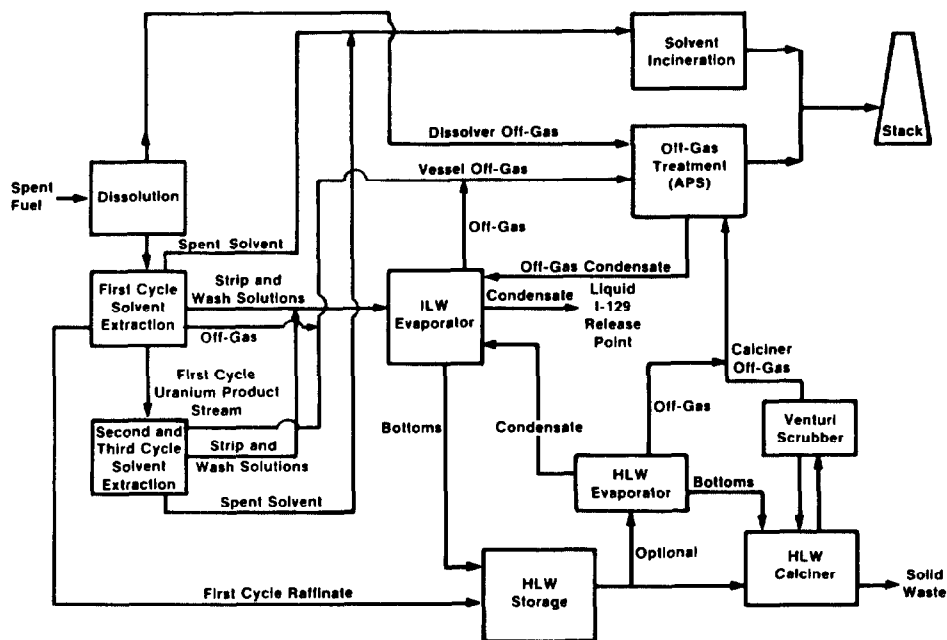


Figure 2. ICPP Pathways Block Diagram

ICPP-S-7882

II. LABORATORY EVALUATION

The purpose of the laboratory evaluation was to identify those processes most likely to be major pathways and to permit modeling of those unit operations impossible to measure *in situ*. To accomplish these goals, the laboratory evaluation was performed in three phases: 1) statistically correlate past off-gas and liquid iodine-129 releases with plant processes to identify the major release points of iodine-129; 2) determine the chemical forms of iodine-129 in the liquid process streams; and 3) determine the chemical and physical behavior of ^{129}I in different plant processes. Each of these phases is discussed in the following sections.

Statistical Correlation of Past Iodine-129 Releases

Liquid iodine-129 discharges for calendar years 1977-1979 and airborne iodine-129 releases for calendar years 1978-1980 were submitted to multivariate analysis to identify the most probable ^{129}I pathways. Multivariate analysis methods, such as factor analysis, can obtain information about a process' contribution to the ^{129}I release based on the radionuclides concentrations in a large number of samples. If one or more radionuclides originate from the same source as does the iodine-129, their variation as a function of time will be similar. By detecting this common variability, sources can be identified.

Multivariate analysis begins with the construction of a correlation matrix. This correlation matrix is constructed by calculating the linear correlation coefficients between each combination (taken two at a time) of nuclides in the data set. Correlation matrices for aqueous ^{129}I discharges were calculated (one each) for the years 1977-1979. Similarly, matrices for airborne iodine-129 releases were calculated (one matrix each) for the years 1978-1980. The eigenvalues of these matrices were

17th DOE NUCLEAR AIR CLEANING CONFERENCE

then calculated. The number of significant sources and their relative contributions were then calculated from these eigenvalues.

The eigenvalues for the airborne iodine-129 releases for the years 1978-1980 indicate only one major source with one or possibly two minor sources. Table I shows the major sources and the amount of the ^{129}I variation attributable to each source. From inspection of the airborne ^{129}I correlation matrices, ^{129}I correlated with ^{14}C , ^3H , ^{125}Sb , ^{154}Eu , and ^{134}Cs in 1980; with ^{14}C , ^{144}Ce , and ^{90}Sr in 1979; and with ^{60}Co in 1978.

The correlation with ^3H , ^{14}C , and ^{125}Sb in 1980 and ^{14}C in 1979 indicates the Waste Calcining Facility (WCF) is the probable release mechanism and represents source 1 in Table I. Two additional facts that suggest source 1 is the WCF (calciner) are the following. First, 50% of all the iodine-129 was released from January to October when only the calciner operated. Secondly, the calciner was the only major process operating in 1979. The minor source (source 2 in Table I) is probably related to dissolution and uranium separation. This would account for the observed correlation of ^{129}I with the fission products ^{144}Ce , ^{134}Cs , and ^{154}Eu since these fission products are associated with dissolution and solvent extraction. Source 3 in Table I probably represents a summation of unaccountable minor sources and random analytical errors.

The eigenvalues for the liquid ^{129}I releases for the years 1977-1979 are similar to the airborne results in that only one significant source is indicated, with one or possibly two minor sources as shown in Table II. Examination of the correlation matrices shows that ^{129}I correlated with ^{106}Ru , ^{238}Pu , and ^{154}Eu in 1977; with ^{90}Sr , ^{137}Cs , ^{238}Pu , and ^{154}Eu in 1978; and with ^{152}Eu and ^{154}Eu in 1979.

TABLE I

MAJOR SOURCES OF AIRBORNE IODINE-129 RELEASES FOR
1978-1980 AND THEIR RELATIVE SIGNIFICANCE

<u>Source</u>	<u>1978 % Variance</u>	<u>1979 % Variance</u>	<u>1980 % Variance</u>
1	37	55	57
2	21	17	21
3	15	13	14

TABLE II

MAJOR SOURCES OF LIQUID IODINE-129 RELEASES FOR
1977-1979 AND THEIR RELATIVE SIGNIFICANCE

<u>Source</u>	<u>1978 % Variance</u>	<u>1979 % Variance</u>	<u>1980 % Variance</u>
1	44	40	47
2	23	18	24
3	33	42	29

The correlation with ^{106}Ru in 1977 and with $^{152}, ^{154}\text{Eu}$ in 1978 and 1979 indicate that some process related to the extraction columns is involved. This conclusion is based on the high distribution coefficients for ruthenium, actinides and lanthanides in TBP (tributyl phosphate). Two additional facts that support this interpretation are the following. First, 90% of the iodine-129 released during 1978 was during July-October. This time period corresponds with the operation of the first-cycle extraction columns. Secondly, evaporator condensate samples were collected on 27 September 1980 (before first-cycle startup) and on 15 October 1980 (after first-cycle operation began). When analyzed for ^{129}I these samples contained $<1 \times 10^{-6} \mu\text{Ci}^{129}\text{I}/\text{mL}$ and $1.2 \times 10^{-4} \mu\text{Ci}^{129}\text{I}/\text{mL}$ respectively. These results indicate that extraction activities were a significant source of iodine-129.

The other minor source (source 2 in Table II) is probably related to calciner operations. The most probable pathway of iodine-129 from the calciner to the aqueous release point would be condensation of iodine-129 from the calciner off-gas. Again, source 3 in Table II probably represents the sum of the contributions from minor, unaccountable sources and random analytical errors.

Iodine-129 Species Distribution

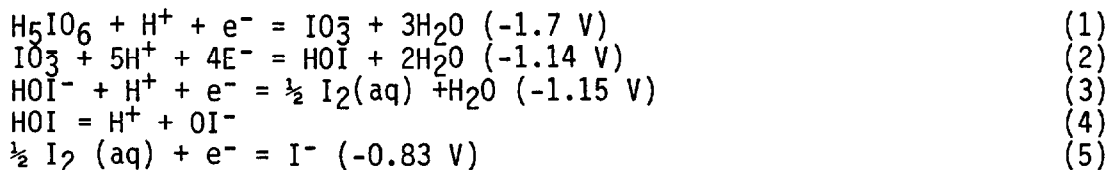
As noted in the previous section, the statistical correlations indicated that the calciner is a significant source of the iodine-129 released to the atmosphere. For this to occur, a substantial amount of iodine-129 must be in the calciner feed. Therefore, experiments were performed to measure total ^{129}I and the chemical species distribution in calciner feed solutions.

Using a previously reported ^{129}I species separation procedure⁽³⁾ five calciner solutions were analyzed. The samples were; (1) and (2) calciner scrub solutions; (3) a 5 to 1 mixture of high-level zirconium fluoride and high sodium concentration waste; (4) high-level zirconium fluoride waste; and (5) a 5 to 1 mixture of zirconium fluoride waste and high sodium concentration waste blended with recycled scrub solution. The scrub solutions were 2M HNO_3 used to scrub the WCF off-gas. The results of these analyses are shown in Table III.

TABLE III
RESULTS OF ^{129}I ANALYSIS OF WASTE CALCINER SOLUTIONS

Sample Number	Reduced ^{129}I (nCi/mL)	Oxidized ^{129}I (nCi/mL)	Percent Reduced ^{129}I
1	1.81+0.20	0.47+0.05	80+12
2	0.89+0.09	0.40+0.04	69+10
3	0.49+0.05	0.34+0.04	59+9
4	Total ^{129}I =	1.53+0.20	
5	1.14+0.20	0.58+0.06	66+5

It appears from these limited data that the iodide/total iodine ratio is a constant (2/3). At this point an attempt was made to develop a thermodynamic model of the calciner feed solution consistent with the determined I⁻/total iodine ratio. The pertinent equilibrium equations and oxidation/reduction potentials are shown below in equations 1-5.



These equilibrium equations were thought to be the most appropriate in the pH range (0 to -0.2) and oxidation-reduction potential (+800 to +850 mV) found in calciner feed solutions.

From equation 1-5 the preponderance area diagram shown in Figure 3 was constructed using well known graphical techniques⁽⁴⁾. The diagram plots logarithmic oxidation-reduction potential versus logarithmic H⁺ activity (i.e., pE vs pH). Each area of the diagram is labeled with the single most predominant species for the pE and pH conditions of that area. Lines between areas graphically represent the pE and pH values at which species adjacent to the lines are in equal concentrations. Equilibrium equations, in logarithmic forms, for the equilibrium lines are also shown in Figure 3. The system pE and pH were measured and are shown on the diagram as a black square.

Solution of equilibrium Equation 2 with these data predicts that 73% of the total iodine is present as iodide ion. This is in excellent agreement with the experimental results obtained by the resin technique of 69 ± 9% iodide ion.

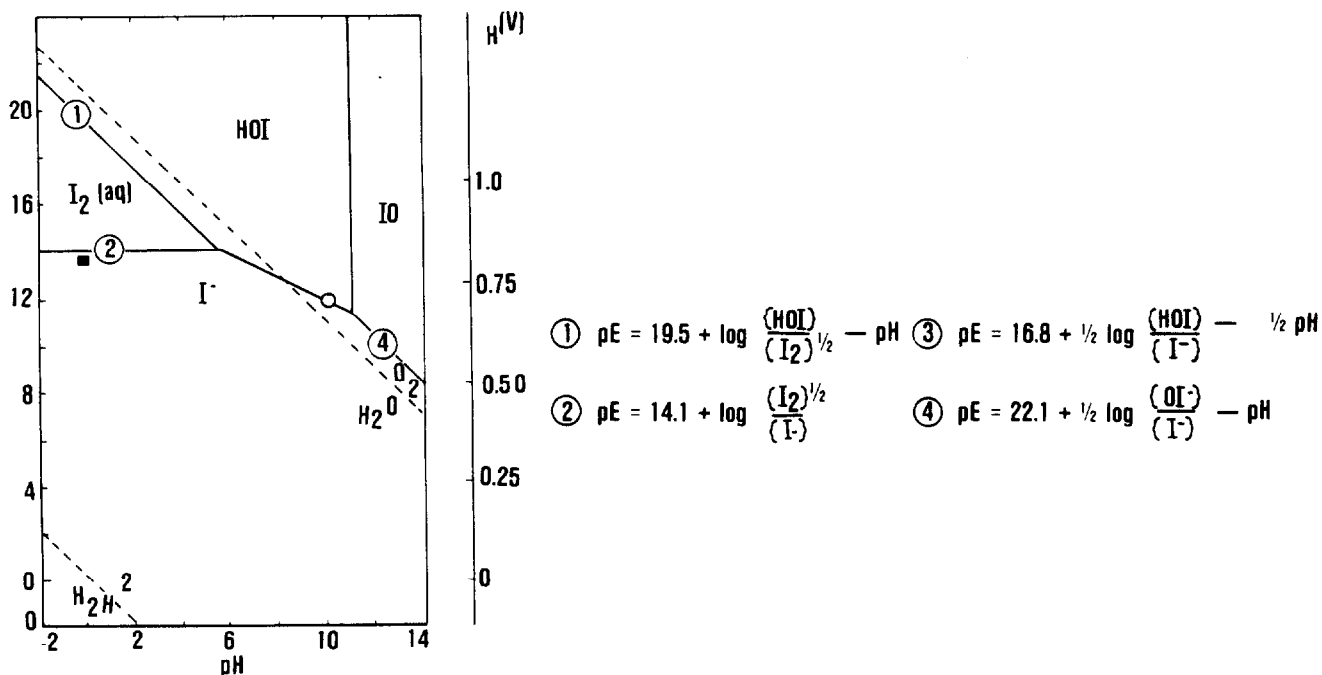


Figure 3. pE vs pH For Iodine System

ICPP-5-4:

Laboratory Simulation of First-Cycle Solvent Extraction Flowsheet

A series of laboratory experiments were performed to better determine the pathways of ^{129}I through a uranium recovery solvent extraction scheme. The experiments simulated the first-cycle extraction flowsheet shown in Figure 4. All tests were done in 250 mL glass separatory funnels with ^{125}I as a tracer. Six extraction tests were performed: three using a simulated coprocessing feed (coprocessing feed is similar to zirconium feed except it contains mercuric nitrate) and three using a simulated zirconium feed. Milligram quantities of stable iodine-127 (added as I^-) were added to one of the zirconium extractions and to two of the coprocessing extractions. The iodine-125 tracer was added to the feed and allowed to equilibrate overnight. Previous work has shown this equilibration time to be sufficient for isotopic exchange.⁽³⁾ Equal amounts of aqueous feed and organic (10% TBP in tetradecane) were then mixed together in the separatory funnel for one to two minutes. After separating, the aqueous and organic phases were drawn off and counted separately on a Low Energy Photon Spectrometer (LEPS) to determine the iodine-125 distribution. Similar tests were done for the other four unit operations. The results of all six tests are presented in Table IV.

TABLE IV

<u>Unit Operation</u>	<u>Aqueous Composition</u>	<u>Distribution Coefficient</u>
Extraction (Zr)	Zr Waste	4
Extraction (coprocessing)	Zr Waste + Hg	4
Scrub	0.7M $\text{Al}(\text{NO}_3)_3$ + 0.3M $\text{NH}_4(\text{OH})$	7.2
First Strip	0.005M HNO_3	<30
Second Strip	0.04M HNO_3	9.2
Carbonate Wash	0.1M Na_2CO_3	9.9

As shown in this table, the majority of the iodine remains in the organic and is not easily stripped. Therefore, there will be an iodine-129 buildup in the organic phase until equilibrium is reached. Based on the distribution coefficients shown in Table IV, equilibrium will be reached after the organic has been cycled 5-10 times. After equilibrium has been reached, 80-90% of the iodine-129 entering the extraction column will exit with the raffinate. The remaining iodine-129 leaving the extraction column is then distributed to second-cycle extraction, to the ILW waste evaporator, and to the solvent burner.

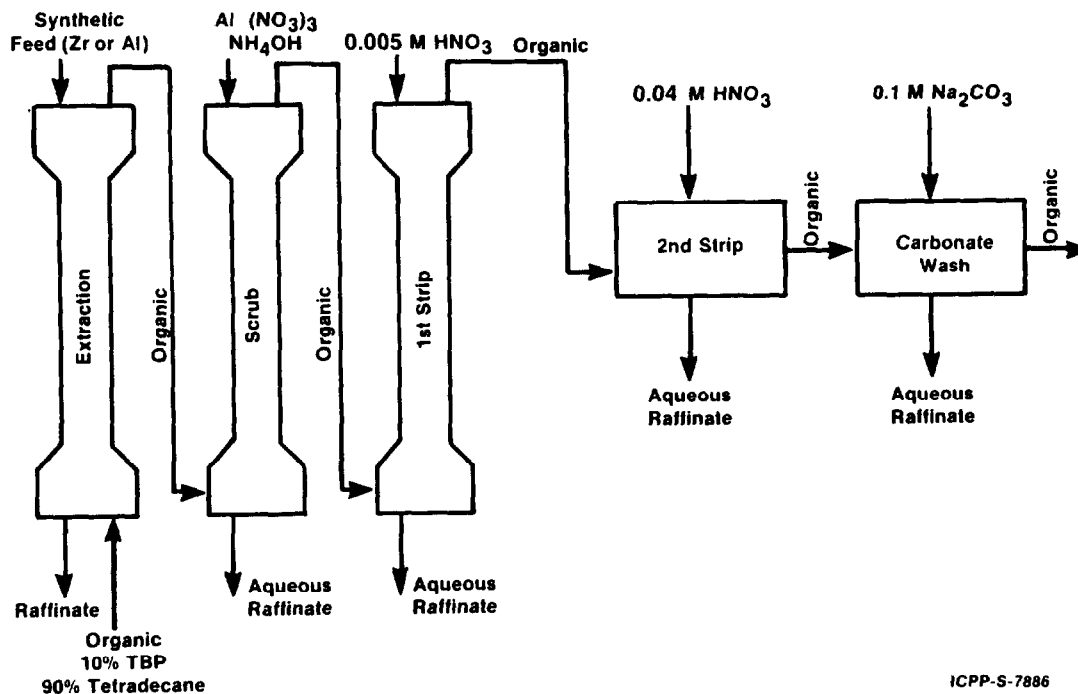


Figure 4. First Cycle Flowsheet

To determine the effect of chemical form on the iodine-129 distribution coefficient, the chemical species distribution before and after extraction was measured by the anion exchange method previously presented. The first cycle distribution coefficient varied from 8.6 for the reduced chemical forms to 0.83 for the oxidized forms. This means either that the iodine species distribution must be known to predict the solvent extraction behavior of iodine-129, or a range of distribution coefficients must be used in the model.

Laboratory Simulation of HLW Evaporator

Since statistical correlations identified the evaporation process as a liquid ^{129}I release pathway, a HLW evaporator was simulated in the laboratory. Using the apparatus shown in Figure 5 two types of HLW, each containing ^{125}I tracer, were investigated. Table V shows the composition of these two wastes.

Each of these two wastes was evaporated with different distillation rates and for each of these rates the iodine-125 in the condensate, bottoms, and off-gas was measured (Table VI). As indicated in Table VI, no more than 4% of the iodine was emitted to the off-gas during evaporation. The fraction of the iodine in the condensate is significantly higher for Type 2 wastes and increases slightly at higher distillation rates. Therefore, the major iodine-129 pathway leaving the HLW evaporator appears to be the condensate waste stream that leads to the ILW evaporator. The high solubility of the volatilized iodine suggests the formation of I_2 during HLW evaporation, but this question was not addressed in these experiments.

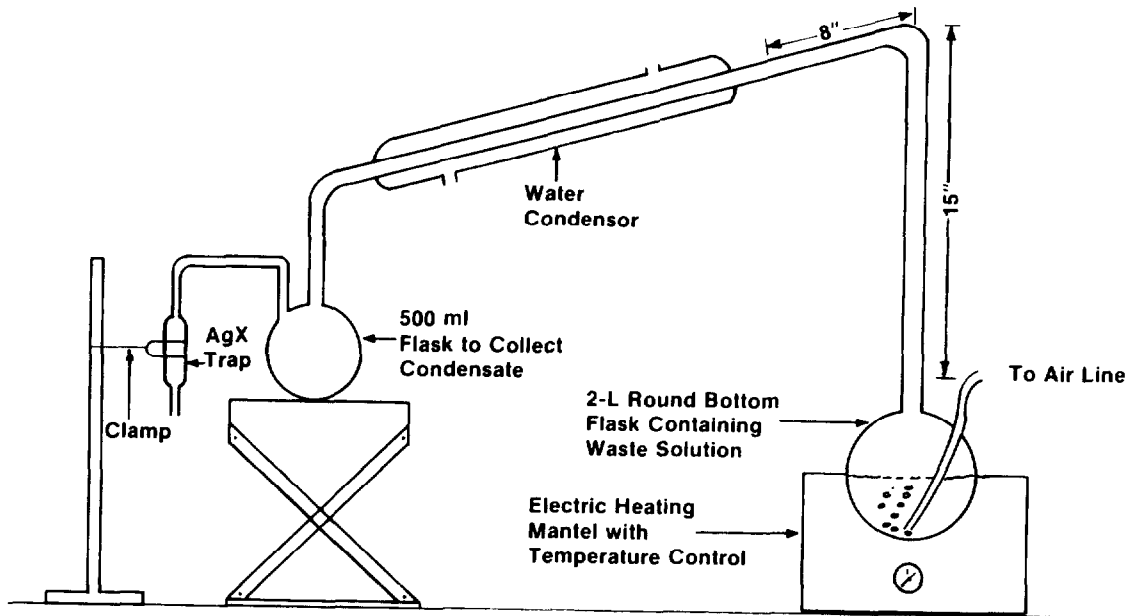


Figure 5. HLW Evaporator Simulation Apparatus

ICPP-S-7887

TABLE V

Species	Waste Type 1 (Molar Concentration)	Waste Type 2 (Molar Concentration)
H ⁺	1.26	1.40
Al ³⁺	0.51	0.65
Fe ^{2+, 3+}	0.064	0.039
F ⁻	0.068	0.016
Cl ⁻	0.0008	0.0073
Na ⁺	0.0222	0.67
NO ₃	3.34	4.40
SO ₄ ²⁻	0.041	0.76

TABLE VI
RESULTS OF HLW EVAPORATOR SIMULATION^a

Feed Type	Distillation Rate (mL/min)	¹²⁵ I In Condensate (%)	¹²⁵ I In Bottoms (%)	¹²⁵ I In Off-Gas (%)
1	1.13	58	16	2
1	1.43	45	39	1
1	2.93	54	23	1
2	1.39	38	23	4
2	1.46	64	24	4
2	2.90	84	19	1

^a Percentages may not add to 100% due to analytical uncertainties

III. IN-PLANT SAMPLING

To verify the data from the laboratory studies, actual plant processes were sampled, including:

- 1) Waste solidification feed solutions, scrub solutions, and off-gas;
- 2) Dissolver off-gas;
- 3) First-cycle raffinates;
- 4) ILW evaporator (Process Equipment Waste or PEW) condensates, bottoms, and off-gas;
- 5) Other process off-gases.

The results of the in-plant sampling are presented in the following sections.

Waste Solidification (WCF) Sampling

From the previous laboratory analysis, it is apparent that more than 80% of the iodine-129 charged to the first-cycle solvent extraction processes remains in the aqueous raffinate and is eventually solidified in the calciner. In addition, the statistical correlations presented previously showed that the calciner is a major airborne release mechanism for iodine-129. Therefore, an iodine-129 mass balance was performed around the calciner to better characterize calciner emissions.

Two sample periods were used to perform the mass balance calculations. The first period was after four months of operation and the second was after one week. Each sample period consisted of raw feed and scrub solution samples and off-gas samples taken at calciner stations 3, 4, 5, and after the Atmospheric Protection System (APS) (Figure 6). The results of mass balance calculations for periods 1 and 2 are shown in Figures 7 and 8, respectively.

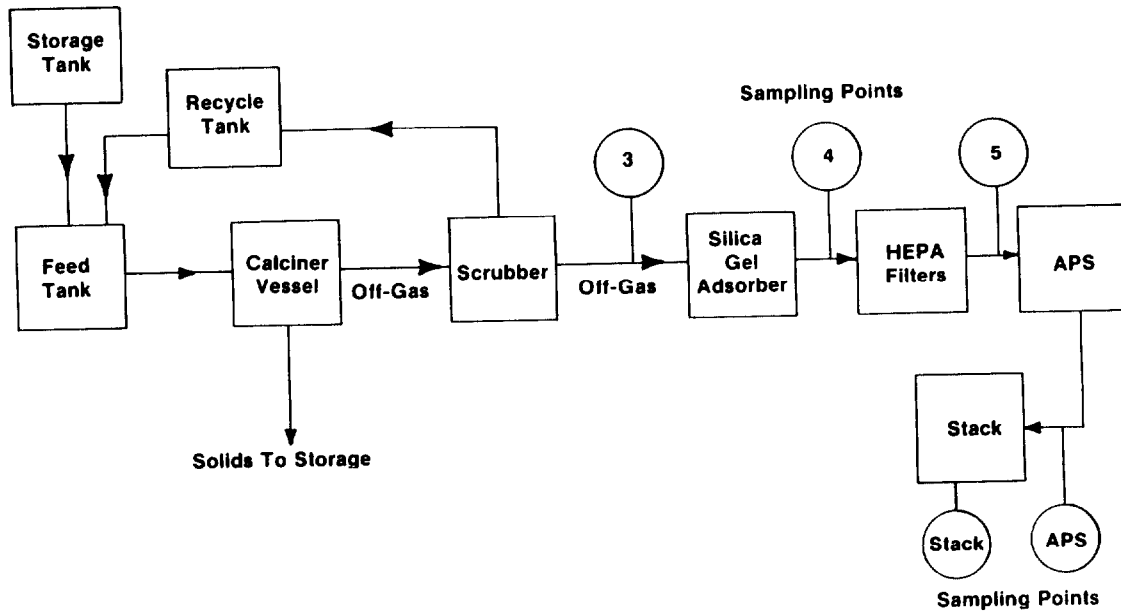


Figure 6. WCF Off-Gas System

ICPP-S-3861

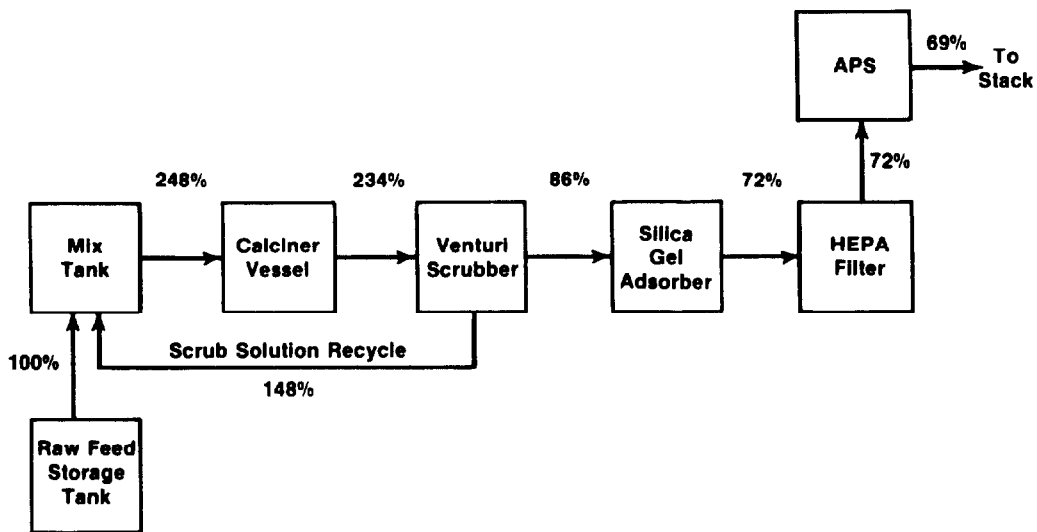


FIGURE 7

WCF MASS BALANCE AFTER 3 MONTHS OPERATION

ICPP-S-8517

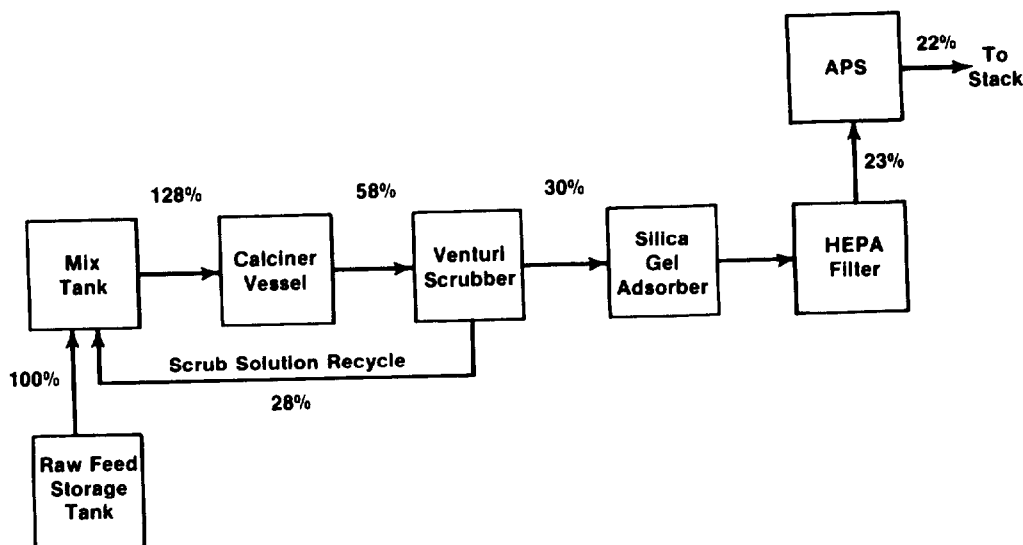


FIGURE 8
WCF MASS BALANCE AFTER 7 DAYS OPERATION

ICPP-S-8511

The following conclusions were drawn from the data presented in Figures 8 and 9.

- 1) Between 14% and 31% of the iodine-129 charged to the calciner as blended feed is released to the atmosphere.
- 2) Iodine-129 builds up in the recycled scrub solution. This is illustrated by the difference in scrub solution concentration between sample period 2 (after one week of operation) and sample period 1 (after four months of operation). This indicates that iodine-129 releases will increase as a calciner run progresses.
- 3) The combined removal efficiency of the silica gel absorbers, HEPA filters and the APS for iodine-129 is less than 30%, and of the three removal systems, the silica gel absorber is the most efficient control device in the off-gas cleanup system. The transmission of iodine-129 through the calciner vessel appears to increase as a calciner run progresses.

In addition to the mass balance performed for total ^{129}I , the chemical forms of the ^{129}I released to the off-gas were measured. The procedure for performing these measurements is described elsewhere⁵⁾. The results of this sampling is shown in Table VII. The significance of the large organic fraction shown in this table is that plateout may be only a minor component of the overall decontamination factor of the off-gas cleanup systems.

TABLE VII

WCF GASEOUS ^{129}I SPECIES DISTRIBUTION

<u>Chemical Form</u>	<u>Fraction Emitted From WCF (%)</u>
I_2	15
HOI	21
Organic	64

Dissolver Off-Gas Sampling

To test the previously presented prediction that the dissolver off-gas was only a minor release point for ^{129}I , in-plant off-gas samples were taken. Both the zirconium fuels dissolution and aluminum fuels dissolution processes were sampled. A diagram of the two off-gas system sampled and the sampler locations are shown in Figure 9.

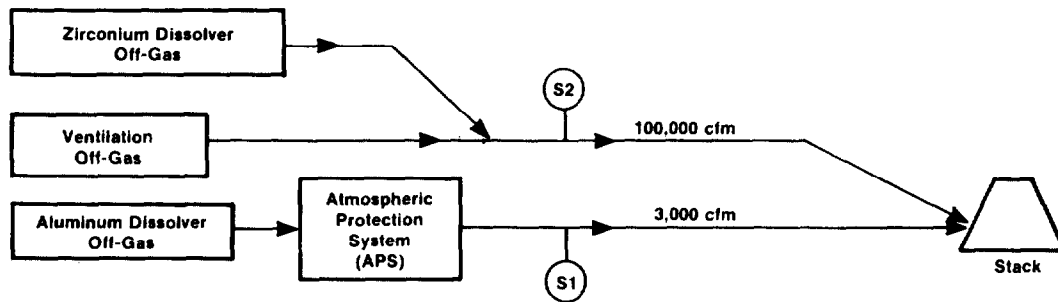


Figure 9. Dissolver Off-Gas Sampling Points

ICPP-S-7885

The location of the aluminum dissolver sampler is shown in Figure 9 as S1. The sampling method has been presented previously⁶. Briefly, two samples were collected on TEDA impregnated charcoal beds with a sample flowrate of 1 L/min. The first sample was taken over a 6.7-hour period; the second sample was collected for 52.8 hours. The average ^{129}I concentration that would be expected if 100% of the ^{129}I was volatilized was calculated and then compared to the amount of iodine-129 found on the charcoal beds. The results are shown in Table VIII. As can be seen from this table, less than 1 percent of the ^{129}I in the spent fuel charged to the aluminum dissolver is volatilized onto the process off-gas.

17th DOE NUCLEAR AIR CLEANING CONFERENCE

TABLE VIII

RESULTS OF ALUMINUM DISSOLVER OFF-GAS SAMPLING FOR ^{129}I

Sample	^{129}I Collected (nCi)	Measured ^{129}I Off-Gas Concentration ($\mu\text{Ci}/\text{cc}$)	Maximum Possible ^{129}I Off-Gas Concentration ($\mu\text{Ci}/\text{cc}$)	Percent ^{129}I Volatilized
1	<0.05	<1.25 x 10 ⁻¹⁰	1.66 x 10 ⁻⁸	<0.75
2	<0.05	<1.58 x 10 ⁻¹¹	1.66 x 10 ⁻⁸	<0.10

A slightly different procedure was used for sampling the zirconium off-gas, indicated as position S2 on Figure 9. Longer sample periods and larger sample volumes were required because of the larger amounts of dilution air at S2 (2000:1 dilution versus 60:1 at S1). In addition to charcoal beds, two samples were subsequently collected using silver zeolite beds in the same sampler configuration. After sampling, the beds were homogenized and the ^{129}I counted directly on a LEPS. As was done with the aluminum off-gas, the average amount of iodine-129 that would be released from the zirconium dissolver if 100% of the ^{129}I was volatilized was calculated and then this amount was compared to that found on the samples (Table IX). As can be seen from Table IX, less than 5% of the iodine-129 charged to the zirconium dissolver is volatilized into the off-gas. Therefore, as the sampling of both aluminum and zirconium dissolution suggests, fuel dissolution is not a major iodine-129 released point to the atmosphere.

TABLE IX

RESULTS OF ZIRCONIUM DISSOLVER OFF-GAS SAMPLING FOR IODINE-129

Sample	Bed Type	Sample Duration (min)	Sample Flowrate (L/min)	Measured Off-Gas Concentration ($\mu\text{Ci}/\text{cc}$)	Maximum Possible Off-Gas Concentration ($\mu\text{Ci}/\text{cc}$)	Percent ^{129}I Volatilized
Back-ground	Charcoal	5640	14.5	2.97 x 10 ⁻¹⁰	----	----
1	Charcoal	4633	11.8	<4 x 10 ⁻¹²	4.44 x 10 ⁻¹⁰	<0.9
2	Charcoal	4420	12.3	<4 x 10 ⁻¹²	2.75 x 10 ⁻¹⁰	<1.5
3	Charcoal	4420	12.6	6.2 x 10 ⁻¹²	3.92 x 10 ⁻¹⁰	1.6
4	Charcoal	6957	11.8	6.3 x 10 ⁻¹²	4.03 x 10 ⁻¹⁰	1.6
5	Silver Zeolite	4320	11.8	2.45 x 10 ⁻¹¹	4.77 x 10 ⁻¹⁰	5.1
6	Silver Zeolite	14130	14.8	4.8 x 10 ⁻¹²	5.30 x 10 ⁻¹⁰	0.9
7	Charcoal	16130	14.8	1.74 x 10 ⁻¹¹	4.06 x 10 ⁻¹⁰	4.3

17th DOE NUCLEAR AIR CLEANING CONFERENCE

Uranium Recovery Process Stream Samples

To verify the laboratory solvent extraction results, actual first-cycle process stream samples were collected. However, due to the high radiation levels only a limited number of streams were sampled. The streams that were sampled and their ^{129}I content are shown in Table X. The two organic feed samples were taken three days apart and indicate that the ^{129}I concentration does reach an equilibrium value. From the organic feed concentration in Table X and the distribution coefficients measured in the laboratory (Table IV), a predicted carbonate wash raffinate concentration of $0.006\mu\text{Ci/L}$ was calculated. This is in reasonable agreement with the measured value of $0.0089\mu\text{Ci/L}$ in Table X. Assuming an average value of $0.016\mu\text{Ci/L}$ for the solvent burner feed solution and an average flowrate of 5L/min , the solvent burner would not release more than 1% of the total ^{129}I processed to the stack.

TABLE X

RESULTS OF THE ^{129}I ANALYSIS FOR FIRST-CYCLE PROCESS STREAMS

<u>Sample Description</u>	<u>Iodine-129 Concentration ($\mu\text{Ci/L}$)</u>
Solvent Burner Feed Solution	0.004
Solvent Burner Feed Solution	0.048
Organic Feed Solution	0.0562
Organic Feed Solution	0.0568
Carbonate Wash Raffinate	0.0089

In-Plant Sampling of ILW Evaporator

Because any aqueous iodine-129 that reaches the environment from the ICPP must pass through the ILW (Process Equipment Waste or PEW) evaporator, a sampling and analysis program around the PEW was performed. Samples of the feed, condensate, and bottoms were analyzed. Two sets of samples were collected: one when only the WCF was operating and one when only the uranium recovery process was operating. The results of both sample periods are summarized in Table XI; the source of iodine-129 to the PEW during each sample period is summarized in Table XII. These tables indicate that when the WCF is in operation the APS condenser accounts for 87% of the iodine-129 sent to the PEW; when the WCF is shut-down it accounts for only 13%. In addition, the amount of iodine-129 sent to the PEW from the APS condenser is an order of magnitude higher during WCF operation than during the uranium recovery process. There-

17th DOE NUCLEAR AIR CLEANING CONFERENCE

fore, during WCF operation, the major aqueous release of iodine-129 is due to condensation of calciner off-gas.

This may also explain why the organic fraction of the ^{129}I released from the WCF is high. The inorganic ^{129}I chemical forms would be preferentially condensed leaving behind the organic ^{129}I . Another plausible explanation is possible reactions with unburned kerosene in the calciner vessel. It is also clear that much more ^{129}I is released from the bottoms by the ILW evaporator than from the HLW evaporator. This may be due to the greater organic content of the PEW feed solutions. This conclusion was supported by the fact that the evaporator iodine off-gas emissions were almost entirely comprised of organic iodides⁽⁵⁾.

TABLE XI

RESULTS OF IODINE-129 ANALYSIS OF
PEW EVAPORATOR FEED SOLUTION,
CONDENSATE, AND BOTTOMS

<u>Operation</u>	<u>Off-Gas (Percent of Total)</u>	<u>Condensate (Percent of Total)</u>	<u>Bottoms (Percent of Total)</u>
WCF	<10	>90	<1
URANIUM PROCESSING	<10	>90	<1

TABLE XII

SOURCES OF IODINE-129 IN PEW

<u>Operation</u>	<u>Fraction ^{129}I from APS Condenser (%)</u>	<u>Fraction ^{129}I from Stored Waste (%)</u>
WCF	87	13
URANIUM PROCESSING	13	87

Other Processes Off-Gas Sampling

In addition to the off-gas sampling already described, three other off-gas streams were sampled; 1) the APS process off-gas during plant shutdown, 2) ventilation off-gas during plant shutdown, and 3) the vessel off-gas (VOG) system. Insignificant amounts of ^{129}I (<0.25% of inventory during processing) were measured in the process off-gas and ventilation off-gas lines during plant shutdown.

17th DOE NUCLEAR AIR CLEANING CONFERENCE

The results of the vessel off-gas sampling showed that the only time detectable quantities of iodine-129 were released was during first-cycle raffinate transfers. This is to be expected because of the atomizing effect of the airlifts used in these transfers. Even though the iodine-129 in the VOG is detectable during transfers (2.9×10^{-12} $\mu\text{Ci/cc}$), the detected ^{129}I accounts for an insignificant fraction of the ^{129}I released from the stack (<0.25%).

IV. COMPUTER MODEL OF IODINE-129 PATHWAYS

Using the data from the laboratory evaluation and in-plant sampling sections of this paper, a computer program that models the ^{129}I pathways was written. The program consists of a series of subroutines based on the major plant processes. These processes include: dissolution and first-cycle extraction, second-cycle extraction, HLW calcination, HLW and ILW evaporation. These subroutines were then combined into the program shown in Appendix I.

Model Verification

To verify the accuracy of the computer program four different operating periods, representative of each major plant process at the ICPP, were selected. These time periods, not used for in-plant sampling were:

- 1) Simultaneous operation of zirconium dissolution, first-cycle extraction, and waste calcination;
- 2) Simultaneous coprocessing dissolution and first-cycle extraction;
- 3) Simultaneous electrolytic dissolution, first-cycle extraction and HLW evaporation;
- 4) Only HLW calcination.

The results shown in Table XIII were obtained using the process flowsheet values for flowrates and flow ratios and the laboratory determined values for the distribution coefficients. These results compare the sum of the calculated gaseous and liquid ^{129}I discharges to the sum of the measured gaseous and liquid ^{129}I discharges. The uncertainty in these releases was also calculated based on the total ^{129}I charged to the plant during these periods. This value is of interest since the EPA regulations are based on the total ^{129}I generated in the nuclear fuel cycle. The least uncertainty was during the period when only the WCF was operating. This may occur because all subroutine parameters were determined by in-plant sampling.

The results obtained when the dissolution/first-cycle subroutine is employed are least accurate, with uncertainties ranging from 12-25%. There are three possible explanations. 1) A conservative 5% of the ^{129}I input to the dissolvers is assumed to be released into the off-gas. Since this 5% represents an upper limit, the off-gas release may be overestimated and the input to the solvent extraction columns may be underestimated. 2) The distribution coefficients for the first-cycle solvent extraction column vary from 0.8 for oxidized iodine species to 8 for re-

TABLE XIII
UNCERTAINTY IN PREDICTED ENVIRONMENTAL RELEASES

Processes Operating	Uncertainty Based on Release (%) ^a	Uncertainty Based on Input (%) ^b
Zr Dissolution	-11.6%	-4.0%
First-Cycle Extraction		
Waste Calcination		
Al + Zr Dissolution	+25%	+3.5%
First-Cycle Extraction		
Electrolytic Dissolution	+8.8%	+3.6%
First-Cycle Extraction		
HLW Evaporation		
Waste Calcination	+0.5%	+0.4%

^a Uncertainty Based = $\frac{\text{Calculated} - \text{Measured}}{\text{Calculated}} \times 100\%$
^b Uncertainty Based = $\frac{\text{Calculated} - \text{Measured}}{\text{Feed to Plant}} \times 100\%$

duced species. Therefore, small changes in the iodine species distribution will cause large changes in the first-cycle distribution coefficients. Best agreement between predicted and measured environmental releases was obtained with distribution coefficients in the range of 3-4, in agreement with the laboratory experiments presented previously. 3) Historically, the solvent extraction process varies significantly from flowsheet values. These deviations from flowsheet values would result in increased uncertainties.

Overall, it appears the computer program (listed in Appendix I) can predict total environmental ¹²⁹I releases within 10-25%.

V. CONCLUSIONS

The following conclusions were reached as a result of the work described here. First, two-thirds of the iodine-129 found in the aqueous waste streams is iodide, with the remaining one-third in higher oxidation states. This species distribution can be explained based on the pH and oxidation-reduction potential of dissolver solutions. Only a small fraction (2-5%) of the iodine-129 entering the plant in the spent fuel elements is released into the off-gas during dissolution. The remaining iodine-129 is distributed through the plant processes with waste solidification being the major atmospheric release point and ILW evaporation being the major liquid release point. Only 14-31% of the ¹²⁹I charged to the HLW calcination process as blended feed is released to the atmosphere. This is due to the recycled scrub solutions that remove 45-65% of the volatilized iodine-129. However, this collected ¹²⁹I is revolatilized when these scrub solutions are solidified.

17th DOE NUCLEAR AIR CLEANING CONFERENCE

A flow diagram of iodine-129 transport through a nuclear fuel reprocessing plant was constructed using the ^{129}I process distribution computer program listed in Appendix I. The results are shown in Figures 10 and 11. Figure 10 illustrates transport without HLW evaporation and Figure 11 illustrates transport with HLW evaporation. Both cases assumed a first-cycle extraction distribution coefficient of 4. From these two figures it can be seen that the HLW evaporation process will determine if the major ^{129}I release point is the off-gas or liquid waste streams.

In conclusion, it appears the computer program listed in Appendix I can accurately predict environmental releases within 10-25%.

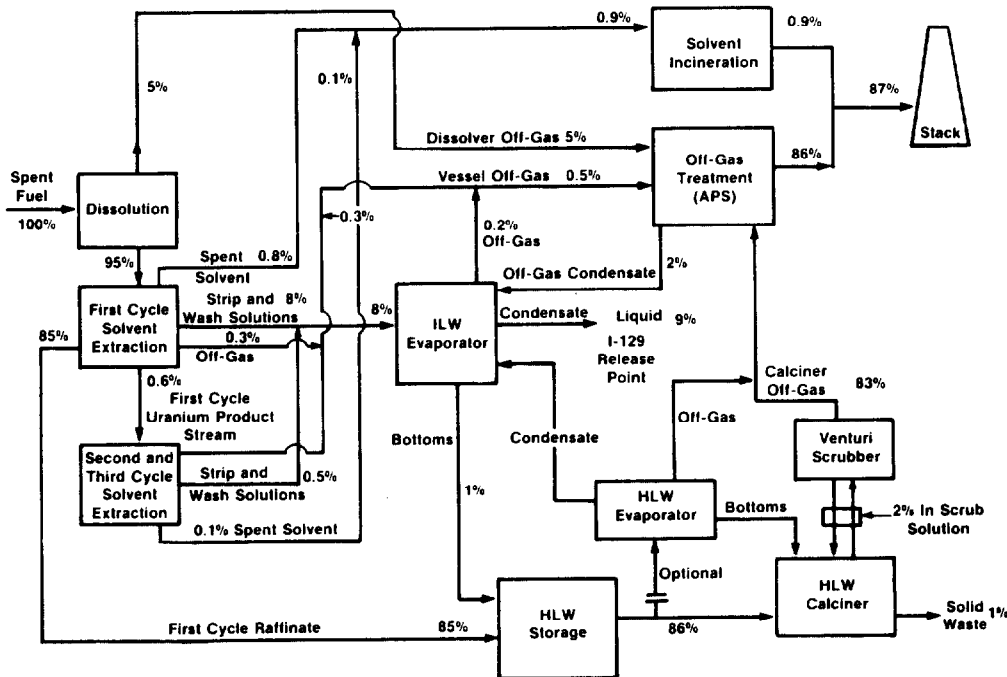


FIGURE 10. ^{129}I TRANSPORT THROUGH FUEL REPROCESSING PLANT WITHOUT HLW EVAPORATION

ICPP A 7936

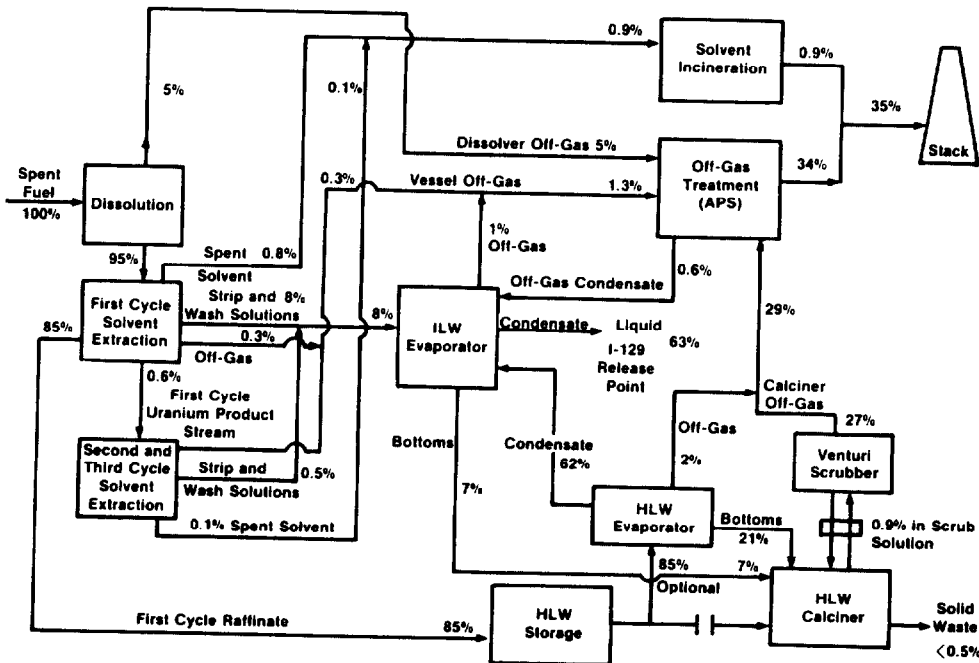


FIGURE 11. ^{129}I TRANSPORT THROUGH FUEL REPROCESSING PLANT WITH HLW EVAPORATION

17th DOE NUCLEAR AIR CLEANING CONFERENCE

VI. REFERENCES

1. R. Berg and H. Schuttlekopf, "Measurement of the Distribution of ^{129}I in and its Discharge from the Karlsruhe Reprocessing Plant", paper presented at a symposium on Radioactive Effluents from Nuclear Fuel Reprocessing Plants", Karlsruhe, W. Ger., November 1977.
2. W. Davis, "A Model of Iodine Transport and Reaction Kinetics in a Nuclear Fuel Reprocessing Plant", ORNL/NUREG 16, May, 1977.
3. G. D. Pierce and S. J. Fernandez, "Anion Exchange Differentiation of Iodine-129 Oxidation States in Waste Solidification Feed Solutions", paper presented at 34th Northwest Regional Meeting of the American Chemical Society, Richland, WA, June 13-15, 1979.
4. L. G. Sillen, "Graphical Presentation of Equilibrium Data", in Treatise on Analytical Chemistry, Part I, Theory and Practice, I. M. Kolthoff and P. J. Elving, Ed., New York: The Interscience Encyclopedia, Inc., 1959.
5. D. C. Hetzer, S. J. Fernandez, B. G. Motes, and L. P. Murphy, "Characterization of the Gaseous Iodine-129 Species in the Process Off-Gas System at the Idaho Chemical Processing Plant", paper presented at 35th Northwest Regional Meeting of the American Chemical Society, Salt Lake City, UT, June 1980.
6. L. P. Murphy, F. A. Duce, and S. J. Fernandez, Continuous Tritium, Carbon-14, Iodine-129, and Krypton-85 Monitor for Nuclear Facility Off-Gas, ENICO-1092, October 1981.

APPENDIX I

```
10 PRINT "INPUT THE FLOWRATE TO THE EXTRACTION COLUMN IN L/HR"  
20 INPUT F9  
30 F9=F9/3.785  
40 PRINT "INPUT THE A/O RATIO FOR THE EXTRACTION COLUMN"  
50 INPUT A1  
60 PRINT "INPUT THE A/O RATIO FOR THE SCRUB COLUMN"  
70 INPUT A2  
80 PRINT "INPUT THE A/O RATIO FOR THE STRIP COLUMN"  
90 INPUT A3  
100 PRINT "INPUT THE A/O RATIO FOR THE SECOND STRIP"  
110 INPUT A4  
120 PRINT "INPUT THE A/O RATIO FOR THE CARBONATE WASH"  
130 INPUT A5  
140 PRINT "INPUT THE DIS. COEF. FOR THE EXTRACTION COLUMN"  
150 INPUT E1  
160 PRINT "INPUT THE DIS. COEF. FOR THE SCRUB COLUMN"  
170 INPUT E2  
180 PRINT "INPUT THE DIS. COEF. FOR THE STRIP COLUMN"  
190 INPUT E3  
200 PRINT "INPUT THE DIS. COEF. FOR THE SECOND STRIP"  
210 INPUT E4  
220 PRINT "INPUT THE DIS. COEF. FOR THE CARBONATE WASH"  
230 INPUT E5  
240 PRINT "INPUT THE # OF  $\mu\text{Ci}$  OF I-129 SENT TO THE DISSOLVER/DAY"  
250 INPUT F  
260 PRINT "INPUT THE # OF OPERATING DAYS"  
270 INPUT D  
280 F1=F/24  
290 N=D*24  
300 Y4=0  
310 S1=0  
320 R1=0
```

17th DOE NUCLEAR AIR CLEANING CONFERENCE

```

330 P=0
340 M9=0
350 F1=0
360 Y3=0
370 K2=0
380 Z9=0
390 Y7=0
400 N=N-1
410 FOR Z=0 TO N
420 S=0.05*F1
430 F2=F1-S
440 F2=F2+Z9
450 R=(F2+Y4)/(E1/A1+1)
460 Y=R*E1/A1
470 Z9=Y*(A2/E2/(1+A2/E2))
480 Y=Y-Z9
490 Y2=Y*(A3/E3/(1+A3/E3))
500 Y1=Y-Y2

510 Y3=Y1*(A4/E4/(1+A4/E4))
520 Y1=Y1-Y3
530 P=Y1*(A5/E5/(1+A5/E5))
540 Y4=Y1-P
550 Y6=Y2+Y3
560 K=0.054*Y6
570 Y5=Y6-K
580 P2=Y5*0.85
590 S2=Y5*0.05
600 Y5=Y5*0.1
610 S1=S+S1+S2
-----
620 R1=R+R1
630 P1=P+F1+P2
640 Y7=Y7+Y5
650 K2=K2+K
-----
660 NEXT Z
670 PRINT " THE AMOUNT OF I-129 SENT TO THE STACK IN ";D;" DAYS"
680 PRINT "IS ";S1;" uCi, THIS CORRESPONDS TO AN AVERAGE"
690 S2=S1*2.45E-13/D
700 PRINT " CONCENTRATION OF ";S2;" uCi/cc"
710 PRINT "THE AMOUNT OF I-129 SENT TO THE PEW IN ";D;" DAYS IS"
720 PRINT P1;" uCi"
730 PRINT "THE AMOUNT SENT OUT IN THE FIRST CYCLE RAFFINATE IN"
740 PRINT D;" DAYS IS ";R1;" uCi, THE TOTAL VOLUME WAS ";F9*24*D;" GALS"
750 PRINT "THE CONCENTRATION OF THE I-129 IN THE RAFFINATE WAS"
760 PRINT R1/(F9*D*24*3.785);" uCi/L"
770 PRINT "THE AMOUNT OF I-129 SENT TO THE SOLVENT BURNER IN ";D;" DAYS"
780 PRINT "WAS ";K2
790 PRINT " THE AMOUNT OF I-129 SENT THE SECOND CYCLE IN ";D;" DAYS"
800 PRINT "IS ";Y7
810 GOSUB 2270
820 GOSUB 2510
830 GOSUB 2640
840 PRINT "IS THE 1ST CYCLE RAFFINATE TO BE CALCINED DIRECTLY 1=Y,2=N"
850 INPUT H
860 GOSUB H OF 960,870
870 PRINT "IS HLLW EVAPORATION DESIRED 1=YES,2=NO"
880 INPUT H
890 GOSUB H OF 1660,910
900 GOSUB 960
910 PRINT "SINCE NO CALCINATION OR HLLW EVAPORATION IS DESIRED THEN"
920 PRINT R1;" uCi OF I-129 FROM THE FIRST CYCLE IS SENT TO THE "
930 PRINT "TANK FARM"
940 GOSUB 2390
950 GOSUB 2610
960 REM -----CALCINER SUBROUTINE-----
970 PRINT "INPUT THE % REMOVAL IN SCRUBBER"
980 INPUT K
990 K=K/100
1000 PRINT "INPUT THE SCRUB FLOWRATE IN GAL/HR"

1010 INPUT D9
1020 IF M9=9 THEN 1070
1030 J=F9
1040 I=R1/(F9*24*D*3.785)
1050 L=D
1060 GO TO 1080
1070 GOSUB 2940

```

17th DOE NUCLEAR AIR CLEANING CONFERENCE

```

1080 R=0
1090 X=0
1100 A=0
1110 E=0
1120 H=0.42
1130 F=0.755
1140 M=L*24/(1400/J)
1150 G=1400/J
1160 B=R1*1000/(D*24*3600)
1170 FOR T=1 TO M
1180 F=3600*B*G
1190 F=F*H
1200 A=F*K+E
1210 C=A*2.642E-7
1220 S=C*D9*1.051
1230 B=I*J+S
1240 E=0.8*A
1250 IF H=>1 THEN 1280
1260 H=H+0.0025
1270 IF H<1 THEN 1290
1280 H=1
1290 N=B-S
1300 N=N*1400*3600/J
1310 P=P+0.071
-----
1320 IF P=>1 THEN 1340
1330 IF P<1 THEN 1350
1340 P=1
1350 O=N*P
1360 Q=O*0.97
1370 Y=O-Q
1380 X=X+Y
1390 R=R+Q
1400 NEXT T
1410 U=R/(L*86400)
1420 V=Q*J*2.0E-7
1430 W=V*2.1186E-8
1440 A=X/(L*86400)
1450 PRINT "AFTER ";L;" DAYS OF OPERATION THE CONCENTRATION OF THE"
1460 PRINT "SCRUB SOLUTION IS ";C;"nCi/mL"
1470 PRINT
1480 PRINT "AND THE SCRUB SOLUTION RECYCLE RATE IS "
1490 PRINT S;"nCi/sec"
1500 PRINT "AFTER ";L;" DAYS OF OPERATION THE AVERAGE I-129 "
1510 PRINT "FLOWRATE OUT THE STACK IS ";U;"nCi/sec"

1520 U=U*1.0E-3*3600*24*L
1530 PRINT "AND THE PRESENT FLOWRATE IS ";U;"nCi/sec"
1540 PRINT
1550 PRINT "ASSUMING AN AVERAGE STACK FLOW OF 100000 CFM THIS RESULTS"
1560 PRINT "IN A I-129 CONCENTRATION OF ";W;"nCi/cc"
1570 PRINT
1580 PRINT "THE AVERAGE AMOUNT OF I-129 SENT TO THE PEW FROM THE APS"
1590 PRINT "DURING THE ";L;" DAYS THE CALCINER WAS OPERATING WAS";
1600 PRINT A;"nCi/sec"
1610 S2=A*1.0E-3*3600*24*L
1620 GOSUB 2380
1630 GOSUB 2590
1640 PRINT
1650 REM-----HLLW EVAPORATOR SUBROUTINE-----
1660 REM C IS I-129 CONCENTRATION IN nCi/L"
1670 C=R1*1000/(F9*D*24)
1680 REM INPUT FLOWRATE OF CONDENSATE F
1690 PRINT "INPUT THE RATE OF DISTILLATION IN GAL/HR"
1700 INPUT F
1710 REM INTIAL VOL CHARGED TO THE EVAPORATOR V
1720 PRI "INPUT THE INTIAL VOLUME OF FEED CHARGED TO THE EVAPORATOR IN"
1730 PRINT "GAL"
1740 INPUT V
1750 REM INPUT HR BETWEEN BATCHS H
1760 PRINT "INPUT THE NUMBER OF HOURS BETWEEN BATCHS"
1770 INPUT H
1780 REM INPUT # OF DAYS OF OPERATION D
1790 PRINT "INPUT THE NUMBER OF BATCHS BETWEEN BOTTOM TRANSFERS"
1800 INPUT N
1810 G=F*H
1820 B9=V-G
1830 REM INPUT # OF DAYS OF OPERATION D
1840 PRINT "INPUT THE # OF DAYS THE EVAPORATOR IS IN OPERATION"

```

17th DOE NUCLEAR AIR CLEANING CONFERENCE

```

1850 INPUT D
1860 V9=B9*D*24/(N*H)
1870 K=0
1880 J=V*K
1890 FOR L=1 TO N
1900 E=0
1910 REM CALCULATES % REMOVAL PER BATCH
1920 FOR T=1 TO H
1930 B=V-T*F
1940 A=F/B
1950 Y=1-EXP(-1.26*A)
1960 E=E+Y
1970 IF E>0.98 THEN 2000
-----
1980 NEXT T
1990 REM CAL I-129 THAT LEFT THE EVAPORATOR IN THE CONDENSATE
2000 I=J*E
2010 REM SUMS AMOUNT I-129 DISTILLED PER BATCH
2020 K=K+I

2030 REM CALCULATES AMOUNT I-129 REMAINING IN THE EVAPORATOR
2040 J=J-I
2050 J=J+G*C
2060 NEXT L
2070 M=H*N
2080 O=D*24/M
2090 REM CALCULATES THE AMOUNT OF I-129 SENT TO THE PEW
2100 P=O*K*1.0E-3
2110 G1=0.02*P
2120 GOSUB 2560
2130 P=P-G1
2140 REM CALCULATES THE AMOUNT OF I-129 SENT TO THE CALCINER
2150 Q=((N-1)*G+V)*C*O*1.0E-3-P-G1
2160 PRINT "THE AMOUNT OF I-129 SENT TO THE PEW IN"
2170 PRINT D;" DAYS WAS ";P;" uCi"
2180 GOSUB 2340
2190 PRINT "THE AMT. OF I-129 SENT TO THE CALCINER IN ";D;" DAYS IS"
2200 PRINT Q;" uCi"
2210 PRINT V9;" GALS OF WASTE ENDED UP IN THE BOTTOMS"
2220 PRINT "THIS CORRESPONDS TO AN AVE. I-129 CONCENTRATION IN THE"
2230 PRINT "BOTTOMS OF ";Q/V9;" uCi/GAL"
2240 M9=9
2250 RETURN
2260 END
2270 REM-----PEW SUBROUTINE-----
2280 REM 1ST CYCLE CONTRIBUTION
2290 D1=P1
2300 RETURN
2310 REM 2ND CYCLE CONTRIBUTION
2320 D1=D1+O2
2330 RETURN
2340 REM HLLW EVAPORATOR CONTRIBUTION
2350 D1=D1+P
2360 RETURN
2370 REM CALCINER CONTRIBUTION
2380 D1=D1+S2
2390 PRINT "INPUT THE AMOUNT OF I-129 THAT GOES TO THE OFF-GAS, COND,"
2400 PRINT "AND THE BOTTOMS"
2410 INPUT G,C,R
2420 G1=G/100
2430 IF H=2 THEN 2560
2440 C1=C/100
2450 R1=R/100
2460 E1=D1*G1
2470 E2=D1*C1
2480 E3=D1*R1
2490 PRINT E2;" uCi OF I-129 WAS SENT TO THE INJECTION WELL"
2500 RETURN
2510 REM-----STACK SUBROUTINE-----
2520 P5=S1+K2+Y4
2530 RETURN

2540 P5=P5+S2
2550 RETURN
2560 P5=P5+G1
2570 IF H=2 THEN 2440
2580 RETURN

```

17th DOE NUCLEAR AIR CLEANING CONFERENCE

```
2590 P5=P5+U
2600 P5=P5+E1
2610 PRINT " THE TOTAL AMOUNT OF I-129 SENT UP THE STACK FROM ALL "
2620 PRINT "PROCESSES WAS ";P5
2630 END
-----2ND-CYCLE SUBROUTINE-----
2640 REM
2650 O2=0
2660 S2=0
2670 PRINT "INPUT THE A/O RATIOS FOR THE IIA,IIB,IIIA,IIIB COLUMNS"
2680 INPUT A2,A3,B2,B3
2690 PRINT "INPUT THE DIS. COEF. FOR THE IIA,IIB,IIIA,IIIB COLUMNS"
2700 INPUT E2,E3,E4,E5
2710 F=Y7
2720 PRINT "INPUT # OF DAYS OF OPERATION"
2730 INPUT N
2740 F1=F/N
2750 N=N-1
2760 FOR Z=0 TO N
2770 R=F1*A2/(A2+E2)
2780 Y2=F1-R
2790 R2=Y2*(A3/E3/(1+A3/E3))
2800 Y3=Y2-R2
2810 R3=R2*B2/(E4+B2)
2820 Y4=E4*Y3
2830 R4=Y4*(B3/E5/(1+B3/E5))
2840 Y5=E5*R4
2850 O2=O2+R+R3+R4
2860 S2=S2+Y3+Y5
2870 NEXT Z
2880 PRINT O2;" uCi OF I-129 WAS SENT TO THE PEW FROM THE 2ND CYCLE"
2890 PRINT S2;" uCi OF I-129 WAS SENT TO THE SOLVENT BURNER FROM THE"
2900 PRINT "THE 2ND CYCLE"
2910 GOSUB 2310
2920 GOSUB 2540
2930 RETURN
-----CALCINATION OF HLLW BOTTOMS-----
2940 REM
2950 PRINT "INPUT THE # OF DAYS THE CALCINER IS RUNNING"
2960 INPUT L
2970 I=Q/U9/3.785
2980 PRINT "INPUT THE RAW FEED FLOWRATE IN GAL/HR"
2990 INPUT J
3000 RETURN
3010 PRINT "INPUT THE RAW FEED FLOWRATE IN GAL/HR"
3020 INPUT J
3030 RETURN
```

DISCUSSION

Anon: Can you tell us the reason for the small release of iodine in the dissolver off-gas?

McManus: You mean versus the high release that has been found in Germany and France? I think it has to do with the temperature of our dissolution process. It is a lower temperature than is used in Europe, and that influences the amount that is released in dissolution.

Anon: What is the temperature?

McManus: Between 40 and 60 degrees.

17th DOE NUCLEAR AIR CLEANING CONFERENCE

CARBON DIOXIDE - KRYPTON SEPARATION AND RADON REMOVAL FROM NUCLEAR FUEL REPROCESSING OFF-GAS STREAMS*

P.M. Hirsch, K.Y. Higuchi, and L. Abraham
General Atomic Company
San Diego, California

Abstract

General Atomic Company (GA) is conducting pilot-plant-scale tests that simulate the treatment of radioactive and other noxious volatile and gaseous constituents of off-gas streams from nuclear reprocessing plants. This paper reports the results of engineering-scale tests performed on the CO₂/krypton separation and radon holdup/decay subsystems of the GA integrated off-gas treatment system.

Separation of CO₂ from krypton-containing gas streams is necessary to facilitate subsequent waste processing and krypton storage. Molecular sieve 5A achieved this separation in dissolver off-gas streams containing relatively low krypton and CO₂ concentrations and in krypton-rich product streams from processes such as the krypton absorption in liquid carbon dioxide (KALC) process.

The CO₂/krypton separation unit is a 30.5-cm-diameter x 1.8-m-long column containing molecular sieve 5A. The loading capacity for CO₂ was determined for gas mixtures containing 250 ppm to 2.2% CO₂ and 170 to 750 ppm krypton in either N₂ or air. Gas streams rich in CO₂ were diluted with N₂ to reduce the temperature rise from the heat of adsorption, which would otherwise affect loading capacity. The effluent CO₂ concentration prior to breakthrough was less than 10 ppm, and the adsorption capacity for krypton was negligible. Krypton was monitored on-line with a time-of-flight mass spectrometer and its concentration determined quantitatively by a method of continuous analysis, i.e., selected-ion monitoring.

Radon-220, a gaseous decay product of the U-232 contaminant in thorium recycle fuels, was treated by holdup and decay on a column of synthetic H-mordenite. The Rn-220 concentration was monitored on-line with flow-through diffused-junction alpha detectors. Single-channel analyzers were utilized to isolate the 6.287-MeV alpha energy band characteristic of Rn-220 decay from energy bands due to daughter products.

The decontamination factor (DF) was determined as a function of bed height for a 34.6-cm-diameter column. The experimental results yielded a mathematical expression to describe the dependence of DF on bed height. A column about 3.66 m (12 ft) long is recommended for achieving the design DF of 1000.

A DF in excess of 1000 was demonstrated in either N₂, air, or CO₂ carrier gas streams. Regeneration of bed material to remove moisture, followed by pretreatment of the adsorbent with carrier gas, significantly improved the performance of the bed. Substantial retention of particulate daughter products of Rn-220 was demonstrated, although those not retained within the bed need to be trapped in a downstream high-efficiency particulate air (HEPA) filter.

*Prepared under contract DE-AT03-76SF71053 for the San Francisco Operations Office of the Department of Energy.

Introduction

Engineering-Scale Off-Gas Treatment System

General Atomic Company (GA) has completed the detailed design and installation of a (radioactively) cold engineering-scale facility for the treatment of off-gas from the reprocessing of spent nuclear fuel. Engineering-scale component tests have been performed to simulate the treatment of fission and decay products and nonradioactive gaseous constituents inherent to nuclear fuel reprocessing.^(1,2,3) The radon removal test results were derived from studies made with the radon holdup/decay subsystem of the GA engineering-scale off-gas treatment system.

The GA off-gas treatment system is designed to process simulated radioactive or other noxious volatile and gaseous constituents in both dissolver off-gas (DOG) and burner off-gas (BOG) streams. Dissolver off-gas is common to several nuclear fuel cycles, e.g., light water reactors (LWRs), high-temperature gas-cooled reactors (HTGRs), and liquid metal fast breeder reactors (LMFBRs), whereas BOG streams are specific to only HTGR fuel reprocessing. Gaseous fission products such as H-3, C-14, Kr-85, I-129, and Rn-220 are released during reprocessing. These fission, activation, or decay products can be removed before the gas effluent is released into the atmosphere. In addition, other gaseous components in the off-gas stream, such as CO, SO₂, and NO_x, can be removed or converted into harmless molecular forms if necessary for environmental and/or process control considerations.

The GA off-gas treatment system is divided into BOG and DOG subsystems. The BOG subsystem includes units for removal of SO₂, HTO, I₂, radon, krypton, and CO₂ and a unit for CO and HT oxidation. The DOG subsystem includes units for removal of NO_x, I₂, H₂O, radon, CO₂, and krypton. The processes used in this engineering-scale system are based on prior laboratory-scale development at various sites under the sponsorship of the U.S. Department of Energy (DOE) or its predecessor agencies. The GA engineering-scale off-gas treatment system is funded under the Consolidated Fuel Reprocessing Program, which is managed by Oak Ridge National Laboratory (ORNL) for DOE.

Carbon Dioxide/Krypton Separation

The off-gas produced during reprocessing of nuclear fuels contains trace amounts of krypton, which can be removed before the off-gas is released into the atmosphere. For LWR, LMFBR, and HTGR fuel, the spent fuel is reprocessed by dissolution in HNO₃. The resulting DOG (for HTGR fuel) contains about 200 ppm Kr-85 (half-life = 10.7 yr) and 250 ppm CO₂, and the balance is air. The air constituent typically contains 1.14 ppm normal isotopic krypton and 330 ppm CO₂. For HTGR fuel, the support structure and moderating graphite material must be burned off prior to dissolution. The BOG contains about 10 to 15 ppm Kr-85, which is initially concentrated by the krypton absorption in liquid carbon dioxide (KALC) process. The resulting off-gas contains about 1.5% krypton, 2.5% xenon, 5% O₂, and 91% CO₂. The CO₂ must be separated from the krypton before storage because the radiolytic interaction of Kr-85 with CO₂ can cause the formation of ozone, creating a potentially explosive gas mixture.

In the cold engineering-scale tests, natural isotopic krypton was separated from CO₂ using an adsorption column filled with molecular sieve 5A (W.R. Grace & Co., Davison Chemical Division). This process was based on prior laboratory-scale studies performed by C.W. Forsberg at ORNL⁽⁴⁾. The separation occurs owing to the different adsorption characteristics of krypton and CO₂ on the molecular sieve material.

17th DOE NUCLEAR AIR CLEANING CONFERENCE

The krypton concentration in the column effluent was monitored on-line by a time-of-flight mass spectrometer and quantitatively analyzed by selected ion monitoring. The krypton breakthrough from the CO₂/krypton separation bed was studied under simulated post-KALC BOG and DOG conditions and the CO₂ decontamination factor (DF) and CO₂ capacity of molecular sieve 5A determined.

Radon Removal by Adsorption/Decay

Radon-220 is a decay product of the U-232 contaminant in recycle fuels originating from thorium-uranium fuel cycles. Radon-220 is a gas with a short half-life at ambient temperature, and it diffuses rapidly, resulting in contamination of the surfaces it touches. Because of the short half-life of Rn-220 (56 s), significant decontamination can be achieved by increasing the Rn-220 residence time in the off-gas treatment system. Laboratory-scale tests conducted by Allied Chemical Corporation at the Idaho National Engineering Laboratory (INEL) have shown that the synthetic molecular sieve H-mordenite is capable of delaying the transport of Rn-220 for several half-lives, thus achieving DFs on the order of 10³.⁽⁵⁾ The success of these experiments has made it desirable to investigate Rn-220 adsorption on a larger scale. Through operation of an engineering-scale system, performance and scale-up design data can be obtained.

In the GA engineering scale studies, Rn-220 was generated from U₃O₈ containing approximately 20 ppm U-232. The radon was transported in a carrier gas stream, which then passed through the radon holdup/decay bed (an adsorber column containing H-mordenite). The Rn-220 concentration was monitored at the inlet and outlet of the adsorber column.

The system chosen for radon analysis is different from that used at INEL. Rather than a batch method of gamma radiation detection, an on-line continuous method of alpha detection was used. The 6.287-MeV alpha particle emitted by Rn-220 was selectively monitored through a system of diffused-junction alpha detectors and sophisticated electronics which discriminate between the Rn-220 alpha particles and the other alphas emitted by daughter products of Rn-220. The solid daughter products resulting from the decay of Rn-220 during holdup on the H-mordenite either adsorb onto the bed material or are removed by the carrier gas. It was unnecessary to determine the absolute Rn-220 concentration levels because only the DF, a relative measurement, was desired. Therefore, identically calibrated alpha detector units possessing equivalent detection efficiencies were utilized to measure the ratio of inlet to outlet Rn-220 concentration, i.e., the DF.

The DF of the radon holdup/decay bed was determined as a function of bed height for a 0.305-m (1-ft) diameter column. The experimental data in concert with a mechanistic analysis of the system yielded a mathematical expression to describe the dependence of DF on bed height. The effects of N₂, air, and CO₂ carrier gas on DF were studied. Regeneration of the bed material to remove moisture and pretreatment of the adsorbent with carrier gas increased the Rn-220 removal efficiency of the bed. The daughter products of Rn-220 were detected in trace quantities in the bed effluent.

PART I: CARBON DIOXIDE - KRYPTON SEPARATION

Experimental Method

Figure 1 is a schematic of the CO₂/krypton separation subsystem of the GA engineering-scale off-gas treatment system. This subsystem is capable of simulating post-KALC BOG streams and DOG streams. The CO₂/krypton separation subsystem, like the other subsystems within the off-gas treatment system, can be isolated to allow

17th DOE NUCLEAR AIR CLEANING CONFERENCE

independent testing. The individual components of the CO₂/krypton separation subsystem are described below.

Separation Vessel Design

The CO₂/krypton separation vessel is fabricated from 316L stainless steel pipe with a 324-mm o.d. and a 5 mm-thick wall (12 in. Sch 10S). The vessel is 1.8 m (71 in.) long and is packed with 8- to 12-mesh 5A molecular sieve adsorbent supported by a 40-mesh 304 stainless steel screen.

Eleven thermocouples are placed 150 mm apart along the bed centerline to measure the CO₂ adsorption temperature gradient. The thermocouples are Chromel-Alumel (K-type) insulated with MgO powder and Inconel 600 sheaths. An expansion compensator (Hyspan Precision Products Incorporated) is located immediately downstream of the vessel to protect the system from stress during adsorbent regeneration. A Rosemount model 1151 DP differential pressure transmitter is provided to measure the pressure drop across the bed. The transmitter range is 0 to 37.4 kPa (0 to 150 in. H₂O), and it has an accuracy of ±0.2% of full scale.

Adsorbent

The adsorbent (Davison 5A molecular sieves) is a crystalline metal aluminosilicate with a three-dimensional interconnecting network structure of silica and alumina tetrahedra. The basic structure of the molecular sieve is represented by the 4A, or sodium, form. The 5A is produced by substituting calcium cations for the sodium cations. The calcium cations, being divalent, will replace two sodium cations and open the structure to apertures of about 5 Å. Most of the adsorption takes place inside the pores. The uniformity of the size of the pores enables large molecules (over 5.5 Å) to be "sieved" out. However, since CO₂, krypton, and N₂ have effective diameters of about 3 Å, the sieving effect is minimal.

The calcium ions induce strong, localized, positive charges in the crystal lattice. Therefore, polar molecules or induced polar molecules will adsorb more than less polar molecules. Since CO₂ has an electric quadrupole moment, whereas the monatomic krypton is nonpolar, the CO₂, and krypton molecules are separated on the basis of polarity.

Simulated Feed Gas Supply

The feed gas supply system is capable of generating either simulated post-KALC BOG or DOG compositions. Figure 1 shows the piping and instrumentation. The BOG N₂ dilution supply is regulated by a Brooks 0-to 50-lpm model 5815 thermal mass flow controller. This controller maintains a preset flow to within ±0.2% and has an accuracy of ±1% of the full-scale reading when the gas is measured at 21.1°C (±5.6°C) and 274 kPa (±104 kPa). The DOG N₂ supply is regulated by a Masoneilan Micro Pak flow control valve in conjunction with a Brooks model 1110 rotameter and model 5522 flow transmitter. The rotameter accuracy is ±1% of full scale.

The BOG and DOG CO₂ supply is regulated by a Brooks 0- to 1000-sccm model 5815 thermal mass flow controller. The BOG krypton supply is regulated by a 0- to 20-sccm Brooks model 5815 thermal mass flow controller and the DOG krypton supply by a 0- to 100-sccm Brooks model 5815 thermal mass flow controller. The DOG O₂ supply is regulated by a Brooks 0- to 100-lpm model 5815 thermal mass flow controller.

Gas Analysis System

The gas analysis system consists of three Beckman model 864 infrared spectrophotometers for CO₂ analysis and a CVC MA-3 time-of-flight mass spectrometer for krypton analysis. This mass spectrometer is intended for use in the mass range 1 to 300 amu with unit resolution greater than 150 and usable resolution to 250.

Carbon Dioxide Analysis. The CO₂ concentration is analyzed at the inlet and outlet of the CO₂/krypton separation bed. The analyzers measure CO₂ in three ranges: 2500 ppm, 2.5%, and 100% full scale, with an accuracy of ±1% of the full-scale value. The analyzers are calibrated with certified standard gas mixtures prepared by Matheson. The sample point locations and specific analyzers are selected by hand valve and solenoid switching.

Krypton Analysis. The krypton concentration is measured on-line at the inlet and outlet of the CO₂/krypton separation bed with a time-of-flight mass spectrometer using a select-ion method of analysis. With the time-of-flight principle, a sheet of positive ions of various mass-to-charge (m/e) ratios is accelerated to a high level of kinetic energy and directed through a field-free drift tube toward an ion detector. The positive ions are formed by bombarding the sample gas with a stream of electrons created by thermionic emission of a heated filament. Because all the ions receive equal energy, their drift velocities depend on the m/e ratio; i.e., the lighter ions travel to the ion detector faster than the heavier ions. Because all the ions leave the starting position almost simultaneously and all drift the same distance to reach the detector, those of equal mass separate into sheets displaced from other masses. As each sheet of ions strikes the detector, the ions dislodge secondary electrons, which are directed into a multiplier, where gains of up to 10⁷ can be achieved. This process takes place 30,000 times/s. The resultant peak heights that are observed are linearly related to ion abundance and hence to relative species concentration in the sample gas.

Process Control and Data Acquisition

The N₂ and CO₂ gas flow rates are regulated by a Diogenes (Rosemount, Incorporated) process controller. The output signals from the flow indicators, CO₂ analyzers, mass spectrometer, thermocouples, and pressure sensors are monitored by a Hewlett Packard data acquisition system that continuously scans and displays the test data on a cathode ray tube (CRT). The data can also be printed and/or stored in a floppy disc file at specified time intervals.

Results

The first series of runs was carried out to study the adsorption characteristics of krypton and CO₂ under simulated post-KALC BOG conditions. The heat of adsorption of CO₂ on molecular sieve 5A is high, and its adsorption capacity is significantly reduced at elevated temperatures. Therefore, the temperature rise was limited to 25°C by diluting the krypton/CO₂ flow with N₂ to achieve a total flow rate of about 47 slpm. This flow rate represents an N₂ dilution factor greater than 70. The krypton breakthrough curve for this simulated diluted BOG stream is shown in Fig 2. The krypton broke through in about 34 min and attained a steady-state outlet concentration equal to the inlet concentration of 410 ppm. The CO₂ was essentially fully adsorbed onto the bed at a feed stream composition of 1.2%. The CO₂ concentration in the adsorber effluent was less than 10 ppm. The maximum bed temperature rise was approximately 20°C, which is in agreement with the CO₂ heat of adsorption data supplied by the manufacturer of molecular sieve 5A.

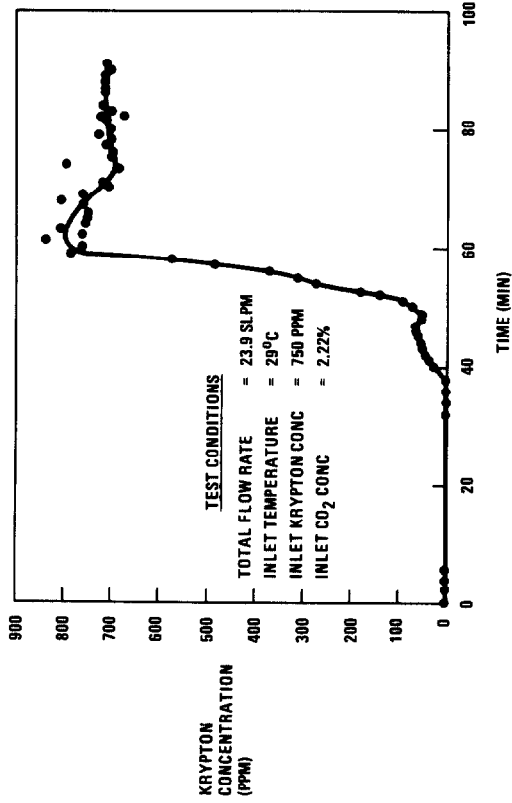


Figure 3. Nitrogen-diluted KALC effluent; krypton breakthrough on molecular sieve 5A.

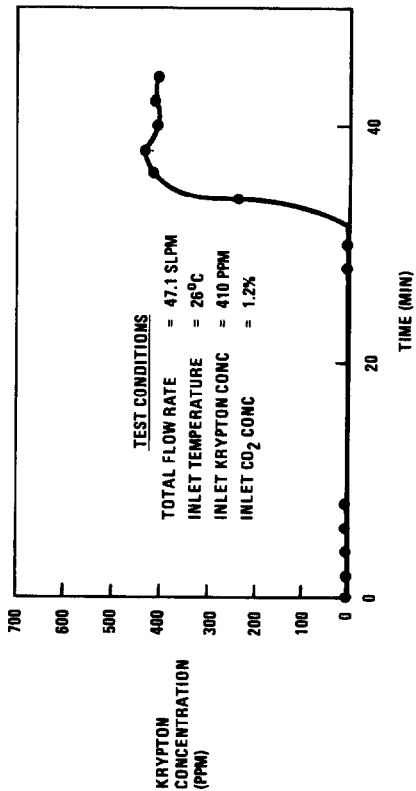


Figure 2. Nitrogen-diluted KALC effluent; CO₂/krypton separation on molecular sieve 5A.

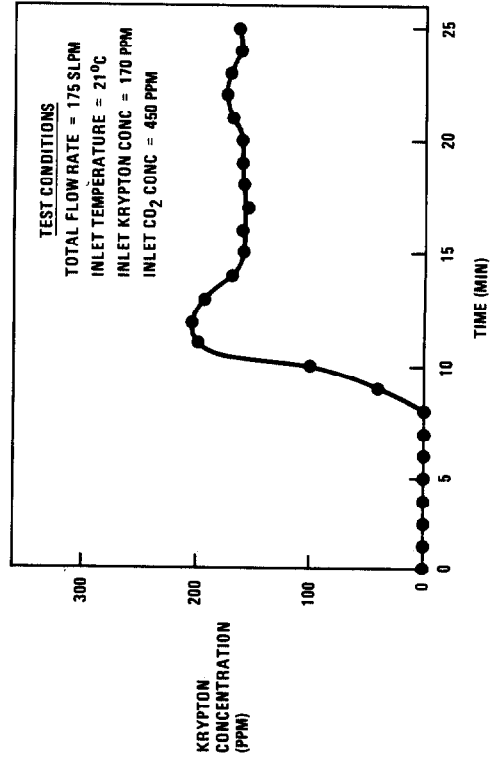


Figure 5. Simulated dissolver off-gas; krypton breakthrough on molecular sieve 5A.

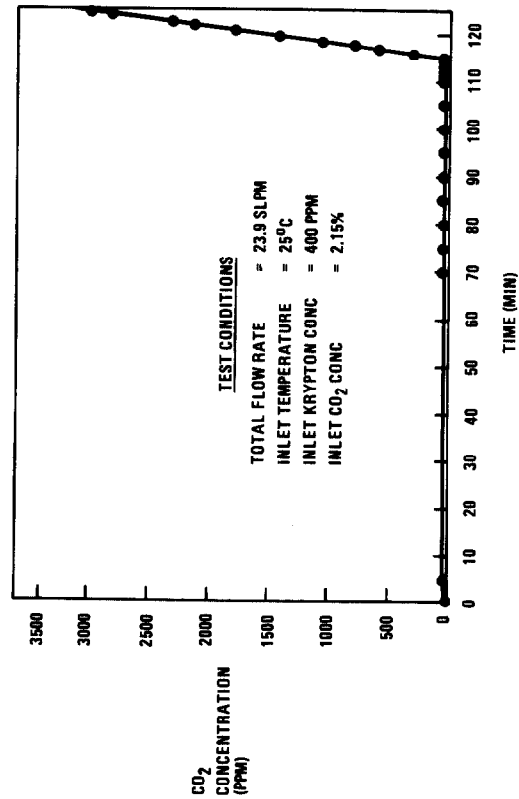


Figure 4. Nitrogen-diluted KALC effluent; CO₂ breakthrough on molecular sieve 5A.

17th DOE NUCLEAR AIR CLEANING CONFERENCE

An additional run was carried out with the N₂ gas flow rate reduced in half to study its effect on krypton breakthrough (Fig 3). (Prior to this and all succeeding runs, the CO₂/krypton separation bed was regenerated at 200°C with N₂ back-purge gas until the effluent CO₂ concentration was less than 10 ppm.) Krypton breakthrough started after 45 min, and a bed temperature rise of 35°C due to CO₂ adsorption was observed. Even at the higher CO₂ concentration of 2.22%, the concentration in the bed effluent was less than 10 ppm.

A CO₂ breakthrough run was carried out to determine the CO₂ adsorption capacity of molecular sieve 5A under simulated post-KALC conditions. The CO₂ breakthrough began after 116 h, as shown in Fig 4. After 122.5 h, a power failure occurred which terminated the run. It was not possible to repeat this run; however, by extrapolating the initial breakthrough curve to 2.15% CO₂, an estimate of the CO₂ adsorption capacity was made. The value obtained was 0.0968 g CO₂/g molecular sieve 5A, which is in excellent agreement with the manufacturer's data of 0.098 g CO₂/g molecular sieve 5A.

The DOG run series was carried out at a total flow rate of 250 lpm, compared with 47.1 lpm for the simulated N₂-diluted BOG runs. As expected, the krypton breakthrough occurred very rapidly owing to the relatively high flow rate. Both N₂ and air carrier gas were studied to simulate probable dissolver operating conditions. Figure 5 shows a typical DOG krypton breakthrough. The time to krypton breakthrough was 9 min, which was average for the DOG runs. The CO₂ concentration in the effluent from the CO₂/krypton separation bed was less than 10 ppm. The CO₂ adsorption capacity is expected to be the same as that obtained under simulated N₂-diluted BOG conditions, because the CO₂ concentrations in the feed are about equal.

Conclusions and Recommendations

Molecular sieve 5A was an effective adsorbent for separating CO₂ from simulated post-KALC BOG streams and DOG streams containing krypton. The CO₂ adsorption capacity of the molecular sieve material was approximately 0.097 g CO₂/g molecular sieve 5A, which is in agreement with the manufacturer's data. The effluent from the CO₂/krypton separation bed contained less than 10 ppm CO₂ for more than 100 h prior to breakthrough for an inlet CO₂ concentration of 2.2%.

The resultant krypton-rich N₂ effluent needs to be separated in another type of adsorption column for further concentration of krypton prior to krypton waste storage. A Canadian study⁽⁶⁾ has shown that removal of krypton from N₂ gas streams by selective adsorption is technically feasible.

As an alternate engineering scale-up approach, the amount of N₂ dilution to post-KALC BOG streams can be reduced by redesigning the separation column to incorporate in-vessel cooling by an extended-surface internal heat exchanger. In this configuration, the heat generated by CO₂ adsorption can be more effectively removed from the column material, thus reducing the necessary N₂ dilution rate in addition to increasing the adsorption capacity for CO₂ owing to its increased partial pressure.

PART II: RADON REMOVAL

Experimental Method

Figure 6 shows a schematic of the radon holdup/decay subsystem of the GA engineering-scale off-gas treatment system. This subsystem, like all others within

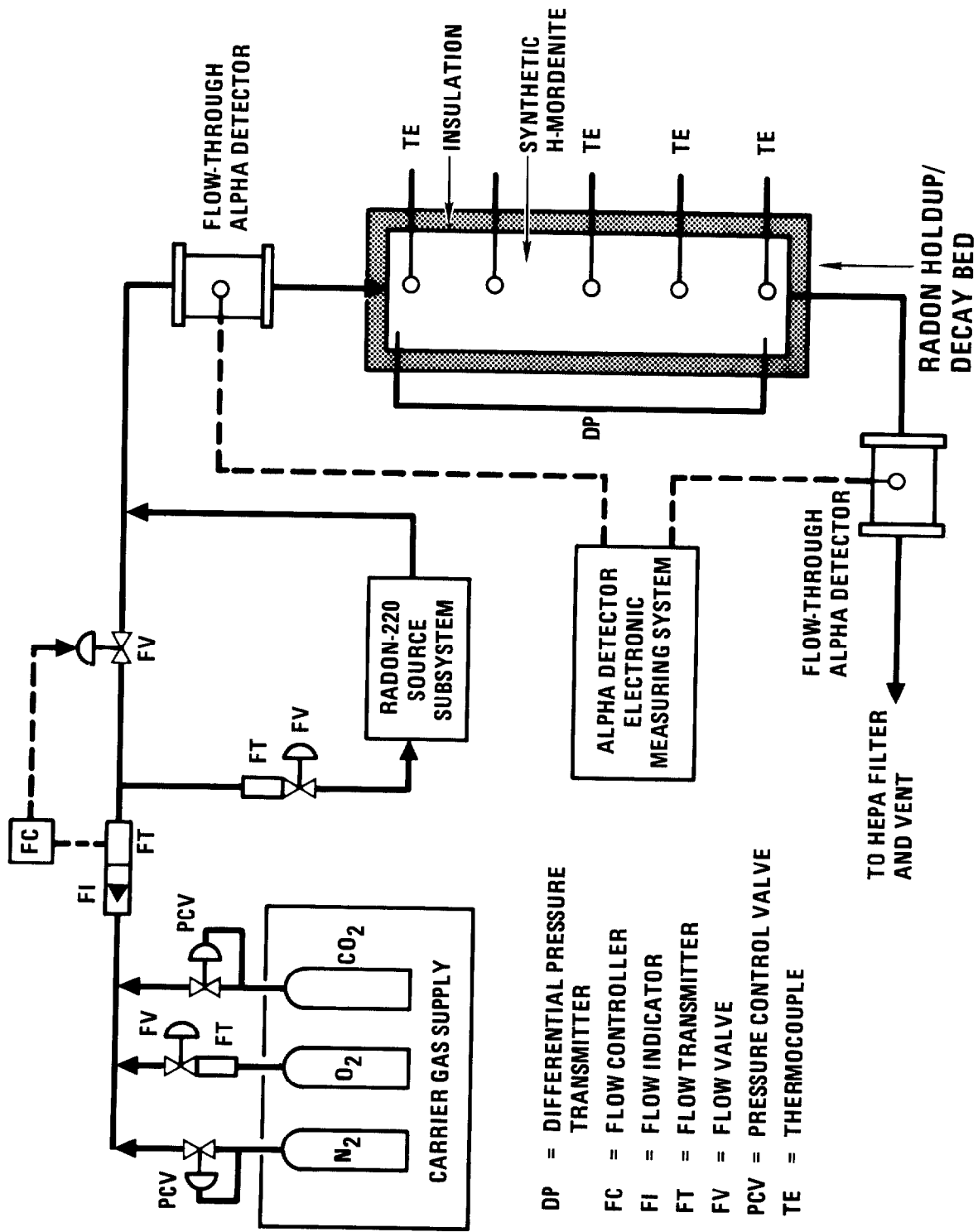


Figure 6. Schematic of the Rn-220 holdup/decay subsystem.

17th DOE NUCLEAR AIR CLEANING CONFERENCE

the off-gas treatment system, is capable of being isolated from the integrated system to allow independent testing. The individual components of the radon removal subsystem are described below.

Radon Holdup/Decay Vessel Design

The radon holdup/decay vessel is fabricated from 356-mm-o.d., 4.8-mm-thick (14-in. Sch 10S) 316L stainless steel pipe and is rated at 500°C at 50 psig. The vessel accepts a variable-depth adsorption bed of 3 m (118 in.) maximum length. The adsorbent is supported by a 40-mesh 304 stainless steel wire screen. A port is provided at the top of the vessel for vacuum removal of the contaminated bed material.

Five thermocouples are evenly distributed along the bed centerline for measuring the temperature gradient. The thermocouples are Chromel-Alumel (K-type), insulated with MgO powder and Inconel 600 sheaths. An expansion compensator (Hyspan Precision Products Incorporated) is located immediately downstream of the vessel to protect the system from stress during adsorbent regeneration. A Rosemount model 1151 DP differential pressure transmitter is provided to measure the pressure drop across the bed. The transmitter range is 0 to 7.5 kPa (0 to 30 in. H₂O) with an accuracy of ±0.2% of full scale.

Adsorbent

The adsorbent (Zeolon 900H) is a hydrogen-substituted synthetic mordenite manufactured by Norton Company. Zeolon 900H is an aluminosilicate characterized by a system of parallel channels with uniform diameters of about 10 Å. This material is highly acid resistant and has a silica-to-alumina ratio of 10:1. The adsorbent is a 3.2-mm (1/8-in.) diameter extrudate and is 4.8 to 7.9 mm (3/16 to 5/16 in.) in length.

Carrier Gas Supply

The carrier gas is either pure N₂, simulated air (80% N₂, 20% O₂), or pure CO₂. The total carrier gas flow rate is regulated at 10 scfm by a Fisher model 513 microflute flow control valve in conjunction with a Brooks model 1110 rotameter and model 5522 flow transmitter. The rotameter accuracy is ±1% of full scale. The oxygen supply is regulated by a Brooks model 5815 thermal mass flow controller. This controller maintains a preset flow to within ±0.2% with an accuracy of ±1% of the full-scale reading when the gas is measured at 21.1°C (±5.6°C) and 274 kPa (±104 kPa).

A side stream is diverted from the main carrier gas stream to the radon source subsystem, where it acts as a sweep gas to carry radon to the holdup/decay column. The side stream is maintained at 2 scfm by a Brooks model 5815 thermal mass flow controller. The side stream is adequate for transporting the relatively small amount of Rn-220 released from the source material. The radon-containing stream is rejoined with the main carrier gas downstream of the Fisher flow control valve. The flow control valve compensates for the pressure differential between the main carrier gas line and the sidestream passing through the radon source subsystem. The column effluent is conducted into a vent line and passed through an absolute filter bank for removal of particulates. The filtered carrier gas stream is then diluted with ventilation air supplied by a 6000-scfm blower prior to discharge through the pilot plant stack.

Rn-220 Source Subsystem

The radon source subsystem consists of the radon source material and auxiliaries required for safe containment of the radioactive materials within the system. A description of the components shown in Fig. 7 is given below.

Encapsulated Uranium Disc Assembly. The primary containment for the Rn-220 source material was designed and fabricated by Mott Metallurgical Corporation. The encapsulated uranium disc assembly is designed to provide safety in handling of the U_3O_8 sample during assembly and disassembly of the radon generator. The U_3O_8 was enclosed within a cavity (5.08 cm in diameter by 7.92 mm deep) formed between two porous 316 stainless steel discs. The discs were 2- μ sintered metal filters (5.40-cm o.d. by 2.38 mm thick). The bottom disc was welded to a stainless steel retainer flange, forming a cavity for the U_3O_8 . The uranium sample was transferred to the cavity in a glove box. The cavity was then sealed by press-fitting the upper disc so that it rested on a small ledge machined into the flange.

Rn-220 Source Material. The Rn-220 source material consists of 2.097 g U_3O_8 containing 1.733 g uranium. The material is in the form of a black, loose, granular powder containing some fines. The uranium composition on a weight basis is given below:

U-234 =	95.938%
U-238 =	3.91%
U-235 =	0.1040%
U-236 =	0.048%
U-232 =	19.7 ppm (alpha pulse height analysis performed on 9/7/78).

The activities of the U-234 and U-232 are about 10.2 and 0.73 mCi, respectively.

Isolation, Shielding, and Safety Interlocks. The encapsulated uranium disc assembly is sealed between two 2-in. welding neck flanges by two gaskets (Flexitall Gasket Company). Two manually operated ball valves are welded onto the upstream and downstream flanges. The entire assembly is radially shielded by 2 in. of lead and axially shielded by 1/2 in. of lead.

Upstream of the inlet ball valve and downstream of the outlet ball valve are high-efficiency particulate air (HEPA) filters that capture any particulates that escape from the uranium disc assembly. The HEPA filters are Gelman polysulfyn cartridge model 12791, which have better than 99.97% retention for 0.3- μ m particles. On the upstream and downstream sides of the absolute filters are solenoid-operated, fail-close stainless steel block valves (ASCO model 8210 C88). The solenoid valves are interfaced with the motor control center so that they automatically close upon failure of the pilot plant stack blower. The operator is alerted to this condition by a red-light visual alarm. The solenoid valves also automatically close upon power failure, thereby isolating the Rn-220 from the main system.

Radon Detection System

Theoretical Background. Figure 8 shows the decay chain for U-232 and Th-232. In converting thorium to uranium, uranium isotopes are produced in various abundances. Table I gives the five principal isotopes and their typical mass fractions. Alpha emission is predominant in the decay scheme of each of these isotopes and spans a broad energy range. It is assumed, however, that only Rn-220 and its decay products can enter the transport lines. Radon is a gas at ambient temperature, whereas its precursors are nonvolatile solids.

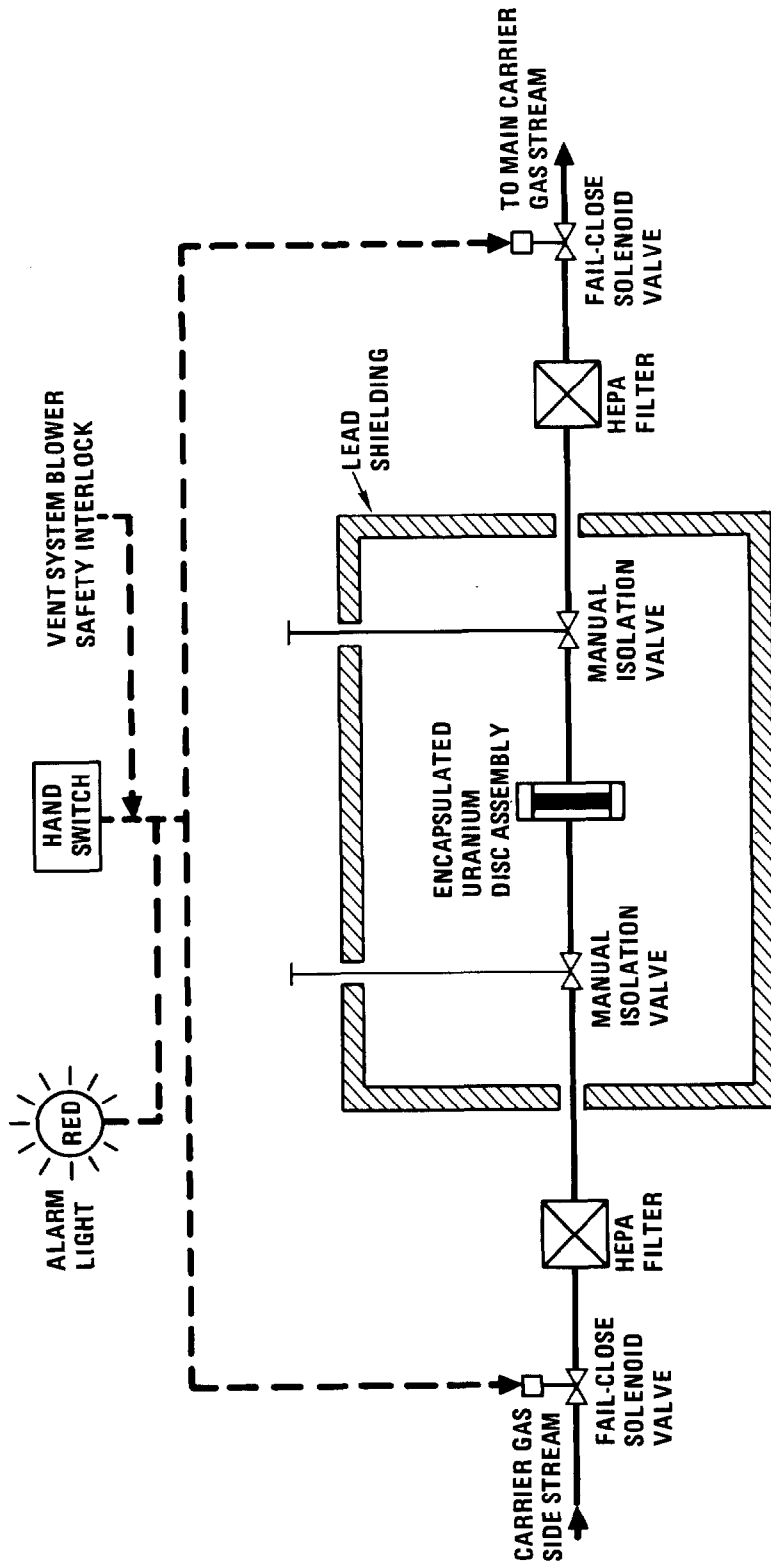


Figure 7. Schematic of the Rn-220 source subsystem.

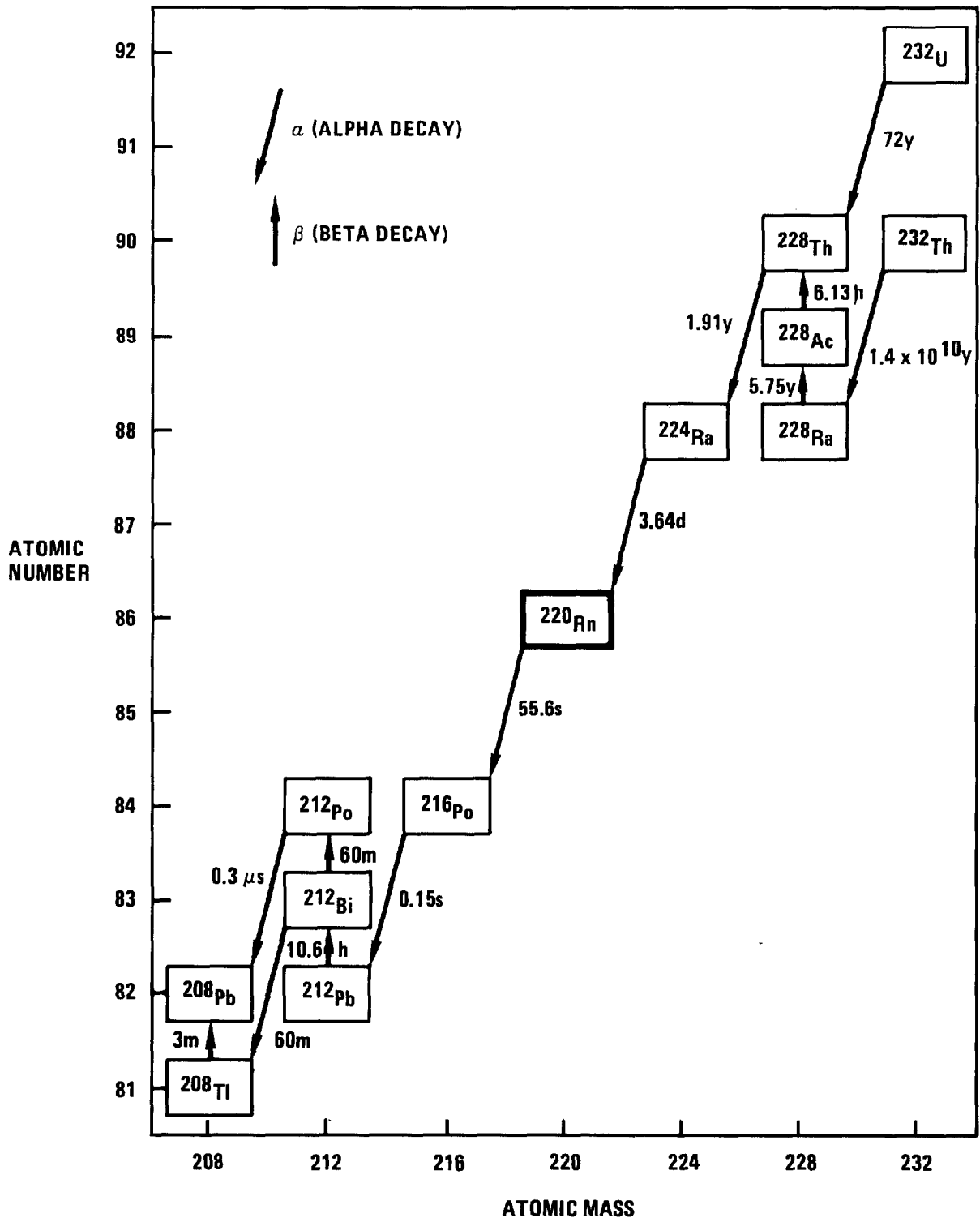


Figure 8. U-232 and Th-232 decay chain. (5)

Table I. Mass fractions of the principal uranium isotopes^(7,8).

<u>Isotope</u>	<u>Typical Mass Fraction</u>
U-232	0.00038
U-233	0.83
U-234	0.14
U-235	0.025
U-236	0.003

Table II. The alpha spectrum of Rn-220 and its daughter products⁽⁹⁾.

<u>Nuclide</u>	<u>Alpha Energy (MeV)</u>	<u>Alpha Intensity (%)</u>
Rn-220	6.287	~99.7
	5.747	0.3
Po-216	6.78	100
Bi-212	6.049	25
	6.088	10
Po-212	8.78	100

17th DOE NUCLEAR AIR CLEANING CONFERENCE

Table II lists the alpha spectra for Rn-220 and its daughter products. The 6.287-MeV alpha particle accompanies the decay of Rn-220 approximately 99.7% of the time. It is possible, therefore, to distinguish Rn-220 from its daughter products by using an electronic system capable of discriminating alpha particles of varying energies. This may be achieved with an alpha detector in series with a single-channel analyzer tuned to the 6.287-MeV alpha energy band emitted by Rn-220. In addition to alpha particles, beta and gamma radiation is also present. The use of an electronic discriminator makes certain that the beta and gamma radiation and all alpha particles whose energy is less than 6.287 MeV are not counted. Similarly, ignoring all particles whose alpha energy exceeds that produced by Rn-220 excludes nuclides emitting more energetic alpha particles from the count. Figure 9 illustrates these concepts.

Flow-Through Alpha Detectors. The flow-through alpha detector assemblies and associated electronics were designed and supplied by Harshaw Chemical Company, Crystal and Electronics Product Department. Figure 10 shows a block diagram of the alpha detector. The detector assembly consists of a flanged, stainless steel chamber fitted with an array of four silicon, diffused-junction, alpha particle detectors. The flow channel contains a series of baffles arranged to maximize the spectral resolution in the analysis.

A diffused-junction detector can be thought of as an ionization chamber in which the gas has been replaced with a semiconducting solid. The semiconductor is a partially depleted, phosphorous-diffused, p-type silicon nuclear radiation detector. Discrimination between alpha particles is based upon the differences in the specific ionization of the particles. The number of ions collected determines the height of the electronic pulse, as illustrated in Fig. 9.

Detector Electronics. The small output signal generated by the diffused-junction detectors requires sophisticated electronics, as shown in Fig. 10. The individual components are as follows:

1. Preamplifier. A low-noise, charge-sensitive preamplifier (Harshaw model NB-25) intended for use with silicon detectors. The charge created in the detectors by radiation energy is converted to an amplified voltage. The preamplifier is located near the flow-through alpha detector assemblies to minimize external electrical interference.
2. Mercury switch pulse generator. A pulse generator (Harshaw model NP-10A) designed to closely simulate the output pulse characteristics of nuclear radiation detectors. It is primarily used for calibrating and testing the associated pulse-handling instruments, i.e., amplifier, single-channel analyzer, scaler, and linear rate meter.
3. Detector bias supply. A high-voltage power supply (Harshaw model NV-30) that provides up to ± 300 V dc for operation of solid-state detectors.
4. Amplifier. A research-grade linear amplifier (Harshaw model NA-25) for accepting the output signal from the preamplifier.
5. Single-channel analyzer. A single-channel pulse height analyzer (Harshaw model NC-22) for discriminating the output pulses from the linear amplifier. The energy threshold and band width can be selected to allow measurement of the 6.287-MeV Rn-220 alpha particles.

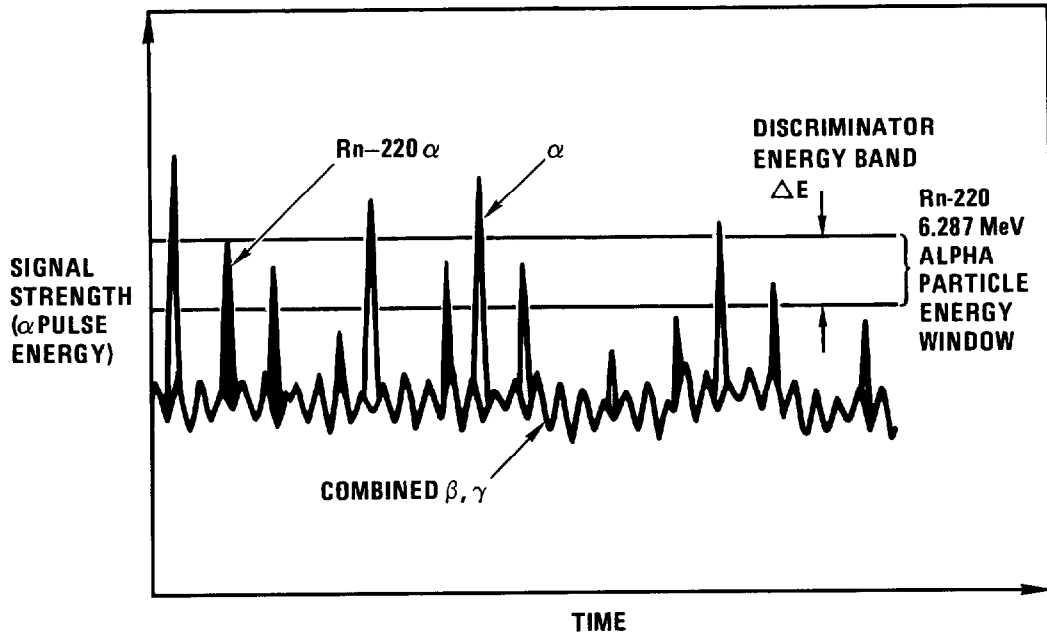


Figure 9. Rn-220 alpha pulse, energy discrimination.

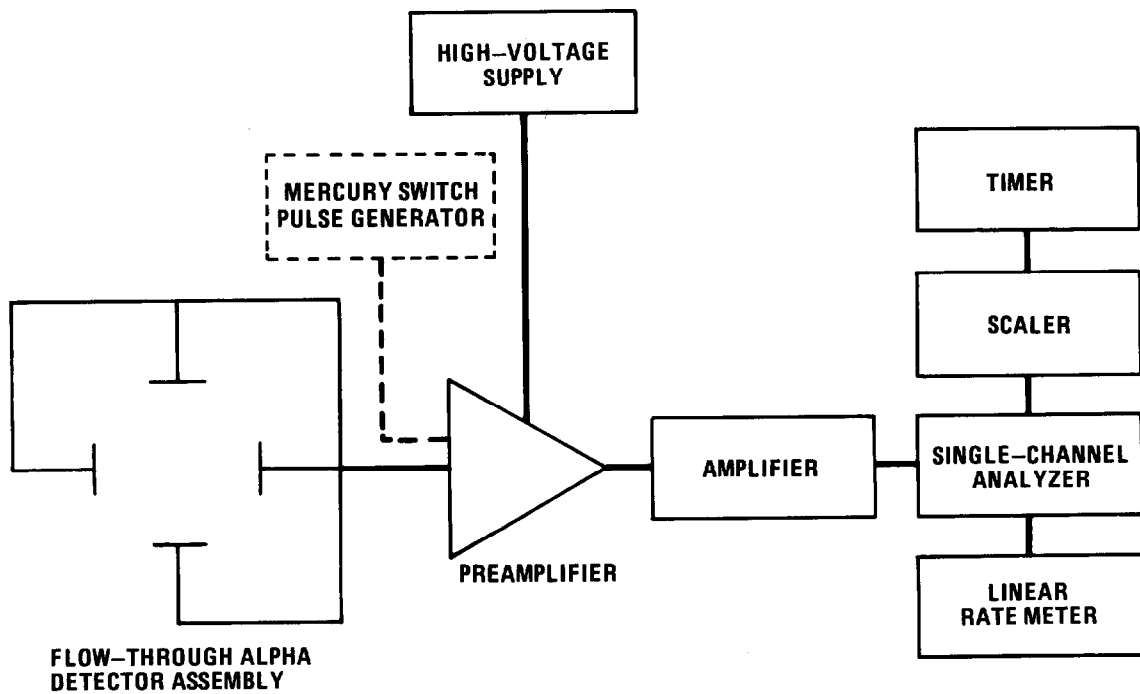


Figure 10. Block diagram of the alpha particle electronic measuring system.

17th DOE NUCLEAR AIR CLEANING CONFERENCE

6. Linear rate meter. A linear rate meter (Harshaw model NR-30) driven by the single-channel analyzer. It is capable of measuring alpha count rates from 10 to 10^5 cps in twenty ranges.
7. Scaler. A high-rate pulse counter (Harshaw model NS-12) capable of a maximum continuous count rate of 20 MHz with a resolution of 50 ns. The maximum count capacity is 10^6 with reset capability.
8. Timer. A digital preset timer (Harshaw model NT-27) for control of the scaler. Timing is from 0.1 s to 990 min in 1% increments.

Process Control and Data Acquisition

The main carrier gas and side-stream flow rates are regulated by a Diogenes (Rosemount, Incorporated) process controller. The output signals from the flow indicators, linear rate meter, thermocouples, and pressure sensors are monitored by a Hewlett Packard data acquisition system that continuously scans and displays the test data on a CRT. The data can also be printed and/or stored in a floppy disc file at specified time intervals.

Results

The goals of the radon holdup/decay test series were as follows: (1) to empirically determine the H-mordenite bed length necessary to achieve the design criterion DF of 10^3 ; (2) to determine the effects of N₂, air, and CO₂ carrier gas on DF at a fixed bed length; (3) to determine the effects of bed regeneration and pretreatment with carrier gas on radon removal efficiency; and (4) to determine whether particulate daughter products of Rn-220 are effectively trapped within the H-mordenite bed.

The first series of runs was carried out to determine the effect of holdup/decay bed length on removal efficiency. Nitrogen carrier gas was chosen because it does not adsorb on H-mordenite. The H-mordenite was used as received; i.e., it was neither regenerated nor pretreated with N₂. The total carrier gas flow rate was 17 Nm³/h (10 scfm) at a face velocity of 3 m/min through the bed. A 3.4-Nm³/h (2-scfm) side stream was bypassed through the radon generator subsystem, as shown in Fig. 6.

The column lengths studied were 1.07 m (3.5 ft), 1.52 m (5.0 ft), 2.29 m (7.5 ft), and 3.05 m (10.0 ft). Table III presents the test conditions for runs 1 through 4. The diffused-junction detectors were cleaned with absolute ethanol and dried with high-purity nitrogen before each run. A background noise count was taken at the inlet and the outlet of the radon holdup/decay bed immediately prior to introducing radon into the carrier gas. At the completion of each run, a background count was taken to account for any daughter products that accumulated on the diffused-junction detectors. The average value of these two alpha count rates was used to correct the data obtained during actual radon measurement for background noise and detector contamination. Immediately after introducing radon into the system, a Rn-220 alpha energy spectrum was measured at the bed inlet to set the detection band so that overlapping daughter peaks such as Bi-212 and Po-212 could be discriminated. This procedure was carried out before each run.

Figures 11 through 14 plot the total adjusted inlet and outlet Rn-220 alpha counts versus time. The accuracy of the alpha detectors was severely affected by electrical interference introduced by other pilot plant activities. Therefore, the runs were carried out after normal working hours, limiting their duration. The Rn-220 removal efficiency is expected to decrease slowly during a long-term run owing to adsorption of Rn-220 daughter products and small quantities of moisture onto the

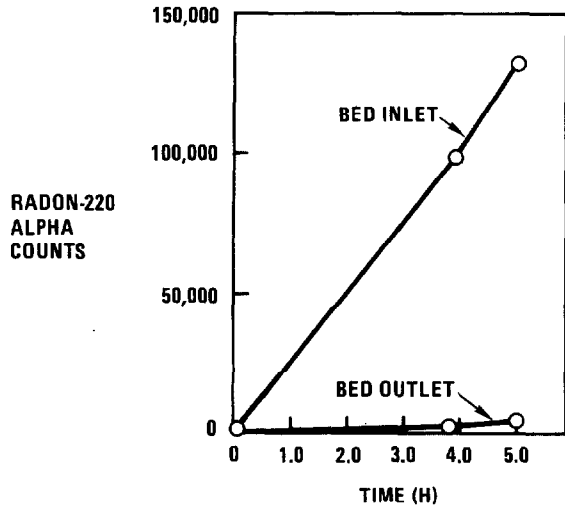


Figure 11. Cumulative Rn-220 alpha counts for the inlet and outlet of a 1.07-m (3.5-ft) holdup/decay bed

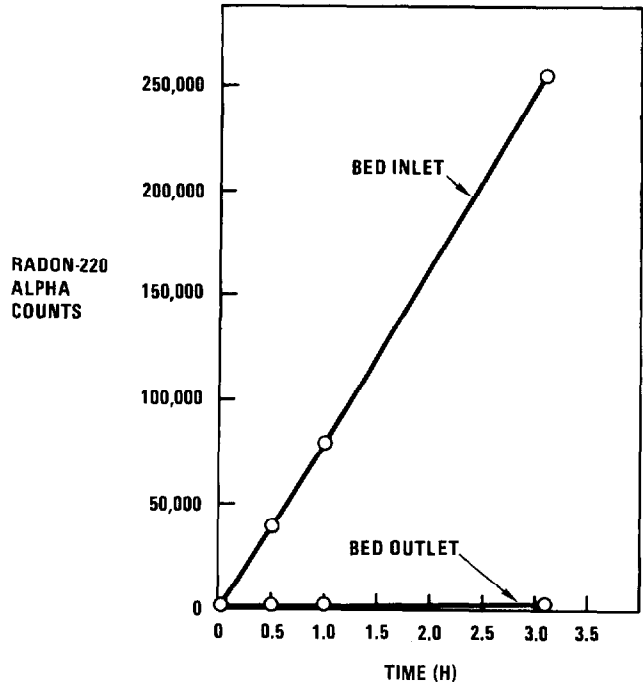


Figure 12. Cumulative Rn-220 alpha counts for the inlet and outlet of a 1.52-m (5.0-ft) holdup/decay bed.

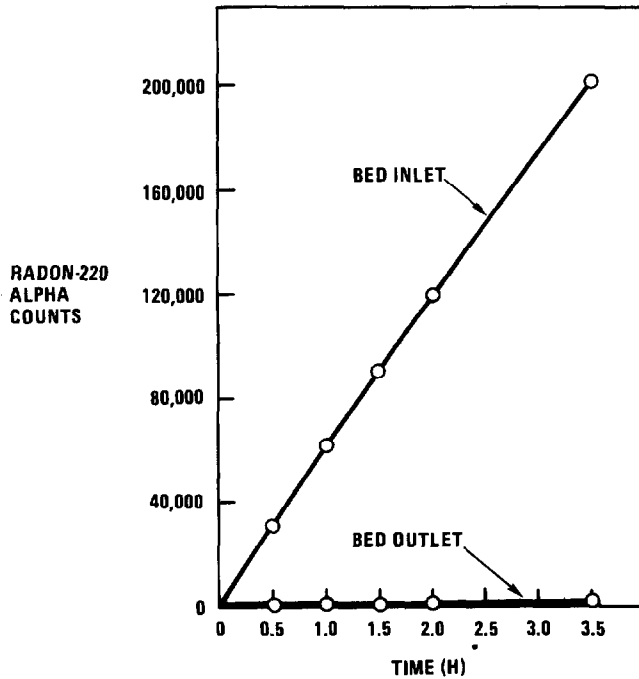


Figure 13. Cumulative Rn-220 alpha counts for the inlet and outlet of a 2.29-m (7.5-ft) holdup/decay bed.

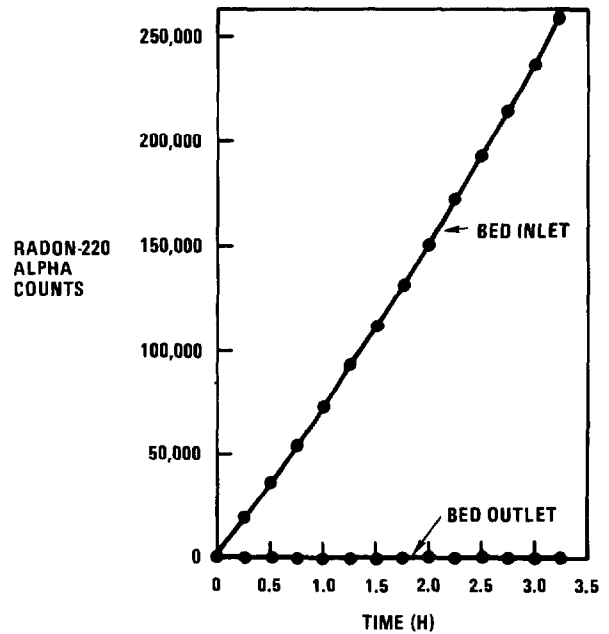


Figure 14. Cumulative Rn-220 alpha counts for the inlet and outlet of a 3.05-m (12-ft) holdup/decay bed.

17th DOE NUCLEAR AIR CLEANING CONFERENCE

bed material. The cumulative DFs, i.e., the total inlet Rn-220 alpha counts divided by the total outlet Rn-220 alpha counts over the duration of the run, are presented in Table III and shown graphically in Fig. 15 for the bed lengths studied.

A mechanistic analysis of the removal of short-lived isotopes by holdup and decay in an adsorbent bed yields a general equation which takes into account three mechanisms of mass transport: (1) molecular diffusion in the gaseous phase; (2) eddy diffusion; and (3) intraparticle mass transfer resistance⁽¹⁰⁾. The equation at steady-state is:

$$\frac{C}{C_0} = \exp \left\{ - \frac{LV_s}{2D} \left[\left(1 + \frac{4D\rho K\lambda}{V_s^2} \right)^{1/2} - 1 \right] \right\}, \quad (1)$$

where C_0 = concentration of the radioactive isotope in the feed to the adsorption bed,
 C = concentration of the radioactive isotope in the effluent from the adsorption bed,
 D = effective diffusion coefficient,
 K = effective adsorption coefficient,
 L = length of adsorption bed,
 V_s = superficial carrier gas velocity,
 λ = decay constant for the radioactive isotope,
 ρ = bulk density of the adsorbent.

Combining constant terms, Eq. 1 can be rewritten as:

$$DF = \exp (k'L) = k^L, \quad (2)$$

where

$$DF = C_0/C, \quad (3)$$

and

$$k' = \frac{V_s}{2D} \left[\left(1 + \frac{4D\rho K\lambda}{V_s^2} \right)^{1/2} - 1 \right] \quad (4)$$

is a constant for the fixed run conditions.

This simple expression can be used to fit the data given in Table IV. Figure 16 shows a plot of log DF versus L. A least-squares analysis yields a value of 2.15 for the constant k when L is measured in feet. Figure 15 shows the curve determined by the least-squares analysis. This curve predicts a 2.74-m (9-ft) bed length to achieve a DF of 10^3 , which is in good agreement with the results found for CO₂ carrier gas in previous laboratory-scale experiments.⁽⁵⁾

The DOG at the inlet to the radon holdup/decay bed is primarily air, whereas the BOG at the radon holdup/decay bed inlet is primarily CO₂. It was therefore necessary to determine the DF of Rn-220 in both air and CO₂ carrier gas so that the results could be applied to the design of a full-scale facility.

The carrier gas can have an effect on the adsorption properties of Rn-220 owing to competition with Rn-220 for adsorption sites. Nitrogen and oxygen do not have a

Table III. Rn-220 holdup/decay test conditions and results.

Run No.	Bed Length [m (ft)]	Carrier Gas	Total Flow Rate [Nm ³ /h (scfm)]	Radon Source Subsystem Flow Rate [Nm ³ /h (scfm)]	Holdup/Decay Bed ΔP [kPa (in. H ₂ O)]	Cumulative Rn-220 DF
1	1.07 (3.5)	N ₂	17.5 (10.3)	3.4 (2.0)	0.069 (0.3)	31
2	1.52 (5.0)	N ₂	7.7 (10.4)	3.4 (2.0)	0.49 (1.9)	180
3	2.29 (7.5)	N ₂	17.5 (10.3)	3.4 (2.0)	0.90 (3.6)	290
4	3.05 (10.0)	N ₂	17.4 (10.2)	3.4 (2.0)	1.4 (5.5)	830
5	3.05 (10.0)	CO ₂	16.8 (9.91)	3.4 (2.0)	1.4 (5.5)	>1000
6	3.05 (10.0)	Air	17.5 (10.3)	3.4 (2.0)	1.4 (5.5)	>3800

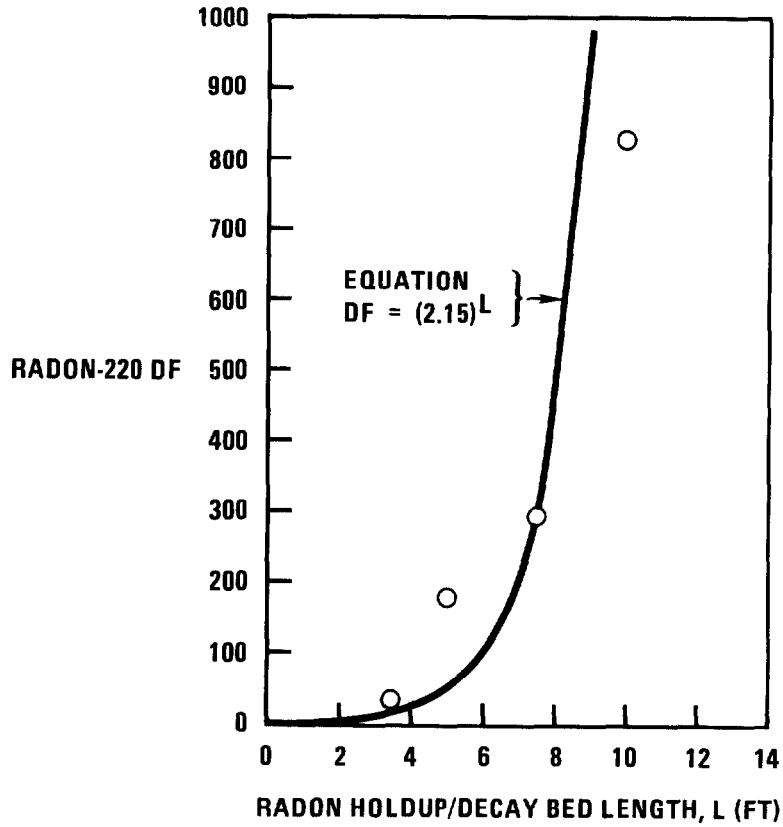


Figure 15. Rn-220 decontamination factor versus radon holdup/decay bed length.

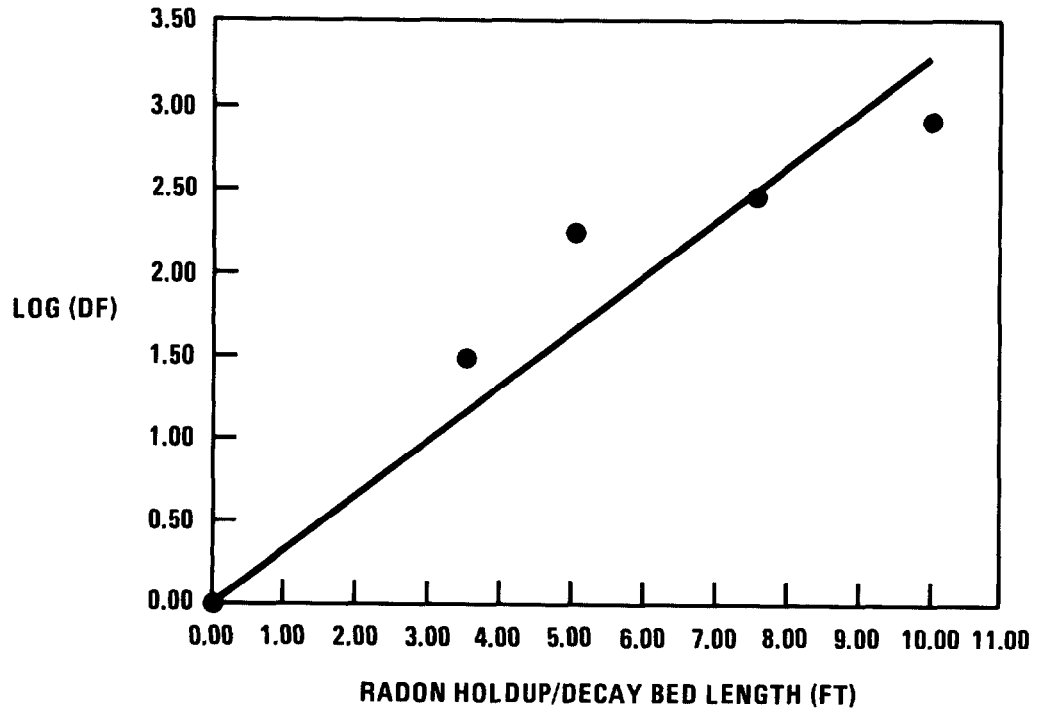


Figure 16. Plot of log DF versus radon holdup/decay bed length.

17th DOE NUCLEAR AIR CLEANING CONFERENCE

significant affinity for H-mordenite, and Rn-220 should have the same adsorption behavior in each of these carrier gases. Carbon dioxide, however, adsorbs strongly on H-mordenite, and the behavior of Rn-220 in this gas may differ from that in N₂ and air.

Table III shows the test conditions for runs 5 and 6. Prior to each run, the 3.05-m (10-ft) holdup/decay bed was regenerated with dry N₂ at 200°C for about 24 h. For run 5, the H-mordenite was pretreated with a steady 17-Nm³/h (10-scfm) flow of CO₂ for 48 h before introducing Rn-220 into the feed. A 55°C bed temperature gradient was observed, indicating that CO₂ was being strongly adsorbed. Pretreatment was considered complete when the H-mordenite regained ambient temperature. Radon-220 was introduced into the carrier gas and measured at the inlet and the outlet of the radon holdup/decay bed for 4 h. No measurable Rn-220 was detected at the outlet of the bed over the duration of the run after adjusting for background counts. The maximum measurable DF, based on the background counts at the outlet alpha detector, was slightly greater than 1000. Therefore, the actual DF for a 3.05-m (10-ft) bed with CO₂ as the carrier gas was at least 1000.

Prior to run 6, the H-mordenite was pretreated with a 17-Nm³/h (10-scfm) flow of dry simulated air (80% N₂, 20% O₂) for 3 h before introducing Rn-220 into the feed stream. The Rn-220 concentration was measured at the bed inlet and the outlet for 3 h. No measurable Rn-220 was detected at the outlet of the bed over the duration of the run after adjusting the measured counts for background noise. The maximum measurable DF, based on the background counts at the outlet alpha detector, was about 3800. Therefore, the actual DF for a 3.05-m (10-ft) bed with air as the carrier gas was at least 3800.

During the air and CO₂ carrier gas studies, trace amounts of Rn-220 daughter products were detected in the radon holdup/decay bed effluent. These particulates can be removed from the off-gas stream by installing a HEPA filter at the outlet of the bed.

Conclusions and Recommendations

A series of Rn-220 removal tests was carried out with the radon holdup/decay subsystem of the GA engineering-scale off-gas treatment system. The removal efficiency was studied in N₂, air, and CO₂ carrier gas streams to simulate dissolver and burner off-gas compositions.

In N₂ carrier gas, the Rn-220 DF obeyed the relation $DF = (2.15)^L$, where L is the length of the holdup/decay bed in feet. Although this expression represents a statistical fit of a small number of data points, it is in good agreement with the results found for CO₂ carrier gas in previous laboratory-scale experiments⁽⁵⁾.

A DF in excess of 1000 was demonstrated in air and CO₂ carrier gas streams for a bed length of 3.5 m (10 ft). However, a 3.66-m (12-ft) bed is recommended to ensure that the design DF of 1000 is attained.

The H-mordenite adsorbent for Rn-220 removal must be regenerated prior to its use, because adsorbed water reduces its effective radon removal efficiency.⁽⁵⁾ For BOG streams, the adsorbent must be pretreated with CO₂ to protect against the initial flow perturbation and heat generation caused by the adsorption of CO₂.

Trace amounts of Rn-220 daughter products in the bed effluent can be removed from the off-gas stream. Installation of a HEPA filter at the outlet of the bed is recommended to trap these particulates.

17th DOE NUCLEAR AIR CLEANING CONFERENCE

Acknowledgment

The authors extend their appreciation to John W. McLean for his technical support in conducting the experiments and maintaining the equipment.

References

1. Abraham, L., and P.M. Hirsch, "Consolidated fuel reprocessing program interim development report: off-gas treatment system," DOE Report GA-A16292 (June 1981).
2. Hirsch, P.M., "Consolidated fuel reprocessing program: off-gas treatment system NO_x converter component tests," DOE Report GA-16559 (January 1982).
3. Hirsch, P.M., "Selected conversion of NO_x by catalytic reduction with ammonia," Environ. Prog. 1, 24-29 (February 1982).
4. Forsberg, C.W., "Separation of radioactive krypton from carbon dioxide and oxygen with molecular sieves," Oak Ridge National Laboratory Report ORNL/TM-5826 (October 1977).
5. Hohorst, F.A., "Containment of Rn-220 via adsorption on molecular sieves for HTGR-OGCS," Idaho National Engineering Laboratory Report ICP-1114 (May 1977).
6. Ruthven, D.M., J.S. Devgun, and F.H. Tezel, "Removal of Kr from N₂ by selective adsorption," in Proceedings of the Sixteenth DOE Nuclear Air Cleaning Conference, Vol. 1, p. 177 (February 1981), CONF-801038.
7. Hamilton, C.J., et al., "HTGR spent fuel composition and fuel element block flow," DOE Report GA-A13886, Vol. II (July 1976).
8. Zane, G., et al., "Large high-temperature gas-cooled reactor medium-enriched uranium spent fuel element definitions and block flows," DOE Report GA-A14980, Vol. II (August 1978).
9. Weast, R.C. (ed.), Handbook of Chemistry and Physics, The Chemical Rubber Company, Cleveland (1967).
10. Underhill, D.W., "A mechanistic analysis of fission-gas hold-up beds," Nucl. Appl. 6, 544 (1969).

DISCUSSION

HOHORST: What absolute concentrations of ^{220}Rn were used in, for example, curies·meter⁻³?

HIRSCH: The U_3O_8 sample that was used for these tests contained approximately 20 ppm U-232. This was the only such source available in the USA for Rn-220 generation. The actual Rn-220 release from the U_3O_8 sample depends on Rn-220 generation, diffusion, and decay within the U_3O_8 particles. The actual release from these particles is indeterminable. Therefore, we did not obtain absolute Rn-220 concentrations, but rather measured the relative concentration at the bed inlet and outlet to calculate the DF. Since the amount of Rn-220 produced by a reprocessing plant on a yearly basis is extremely small, (in the mg range) the large size of the Rn holdup/decay bed is more than adequate to treat all the Rn-220.

LITTLE: CO_2 removal using 5A sieves appears effective. However, the use of N_2 for dilution to prevent heat buildup is counter productive. How does this dilution affect the final collection of the Kr product?

HIRSCH: Alternatives to nitrogen dilution may consist of either modifying the CO_2/Kr separation bed by installation of internal heat exchangers or by operating the CO_2/Kr separation bed at much colder temperatures to counteract the heat generation by CO_2 adsorption. The effectiveness of these processes has yet to be determined. With respect to nitrogen dilution, the resultant Kr-rich N_2 effluent needs to be separated in another process for further concentration of Krypton prior to Krypton waste storage. A Canadian study given in reference 6 has shown that removal of krypton from N_2 gas streams by selective adsorption is technically feasible.

RINGEL: Will it be technically feasible to separate a larger amount of CO_2 from a smaller amount of Kr by adsorption of the CO_2 ?

HIRSCH: The Kr concentration in KALC overhead product is high enough to allow separation of Kr from CO_2 with a relatively larger concentration by adsorption. The flow rate from KALC is about 0.5 LPM. It will not require much bed material to capture the CO_2 for long periods of time. In addition, the separation bed can be regenerated and re-used.

ADSORPTION OF GASEOUS RuO_4 BY VARIOUS SORBENTS. II

Lj. Vujisić and R. Nikolić

Department of Chemistry

Boris Kidrič Institute of Nuclear Sciences-Vinča

Belgrade, Yugoslavia

Abstract

Sorption of gaseous RuO_4 on impregnated Alcoa Alumina H-151 impregnated charcoal, silica gel and HEPA filter was investigated. The results obtained on various sorbents are compared and discussed in connection with possibilities to use chosen material in air cleaning systems.

I. Introduction

Ruthenium, in nuclear facilities, transforms to volatile compounds rather easily and because of its elusive and variable chemical and gamma-ray spectral characteristics it is rarely detected in waste gases. However, Ru-103 and Ru-106 have generally been observed among the principal radionuclides precipitated by rainfall and pollen⁽¹⁾.

Among volatile radioactive species removal of ruthenium tetroxide from waste gases is greatest problem. In the last years large number of papers have been published concerning its adsorption. Unfortunately, many investigators seem to have avoided purification of RuO_4 from other volatile compounds during its generation. Because of usually unknown RuO_4 initial concentration it is impossible to make complete balance of RuO_4 in adsorption experiments. That is one of the reasons why decontamination factor and adsorption characteristics for the same materials differ in various papers concerning RuO_4 adsorption.

Among many investigated materials for RuO_4 adsorption the best results were obtained with silica gel. However, there is dis-

agreement in results obtained on silica gel as adsorbent for RuO_4 given by different authors. Discrepancies in the results may be caused by different characteristics of silica gel and by different experimental conditions. Most experiments were done at high temperature and long residence time which are not normal operating conditions of filtration systems.

In this paper special attention was paid to generate very pure RuO_4 of known concentration and to find suitable adsorption material for RuO_4 under normal ventilation conditions (25°C , residence time 0.3 sec). Adsorption materials investigated in the present work were blue silica gel (Merck), Alcoa Alumina H-151 and Alcoa Alumina H-151 impregnated with: CrCl_3 , $\text{K}_2\text{Cr}_2\text{O}_7$, Na_2CrO_4 , CoCl_2 and $\text{Co}(\text{NO}_3)_2$.

II. Experimental

Anhydrous ruthenium tetroxide was prepared from ruthenium chloride by following procedure. First, ruthenium chloride was fumed with concentrated sulfuric acid to remove the chlorides. Solution of $^{106}\text{RuCl}$ (product of Amersham) was also treated with sulfuric acid and the chlorides were removed by repeated evaporation of sulfuric acid solution. Aliquots of ruthenium sulfate solutions labelled with ^{106}Ru were added to the solutions of inactive ruthenium sulfates in 50% sulfuric acid and heated to 60°C in an all glass apparatus. Solid sodium bismuthate was added to oxidize ruthenium to ruthenium tetroxide and slow stream of dry nitrogen was passed through the apparatus. Ruthenium tetroxide vapor, carried by the stream of nitrogen, was dried with anhydrous magnesium perchlorate and collected in an U shaped glass tube, which was immersed into a trap containing solid carbon dioxide.

In order to obtain certain concentration of ruthenium tetroxide in the gas stream for adsorption experiments the U shaped tube was immersed in NaCl-ice bath and stream of dry nitrogen was passed through it. Temperature of the bath and flow rate of nitrogen were determined in preliminary experiments for several desired RuO_4 concentrations. Concentration and purity of ruthenium tetroxide were determined spectrophotometrically. For spectrophotometric measurements ruthenium tetroxide was collected in dilute perchloric acid and spectra of these solutions were registered immediately after the gas

17th DOE NUCLEAR AIR CLEANING CONFERENCE

generation. The spectra were typical for ruthenium tetroxide solutions in perchloric acid⁽²⁾.

Adsorption of ruthenium tetroxide was followed by measurements of gamma radioactivity of sorbent samples on a scintillation counter. Concentration of ruthenium tetroxide in the gas stream and concentration of ruthenium species retained with sorbents were calculated from known initial specific radioactivity of generated ruthenium tetroxide. Therefore in order to calculate ruthenium concentration in this way, in adsorption experiments, it is necessary to obtain very pure ruthenium tetroxide, labelled with ¹⁰⁶Ru isotope.

Adsorption of ruthenium tetroxide by various sorbents was first investigated under nearly stationary conditions. Ruthenium tetroxide was carried by a very slow stream of dry nitrogen (0.2 dm³/h) through a series of glass tubes containing various sorbents which are normally used in filtration systems of nuclear facilities. From these experiments the most convenient sorbents for ruthenium tetroxide were chosen for further investigation. Sorbents for investigation of ruthenium tetroxide adsorption were placed in a glass column with 5 cm inner diameter. Apparatus for investigation of ruthenium tetroxide adsorption is schematically presented in the Figure 1.

The column was filled with three separate beds of various sorbents. The first bed was the test bed followed by the two safety beds. Two separate safety columns were also placed after the adsorption column.

Ruthenium tetroxide of desired concentration was passed through the adsorption column with air stream of 360 dm³/h flow rate. Residence time was, in all experiments, 0.3 sec. Relative humidity of the air was 60±5% and the temperature of the air stream and the test bed was 22-25°C.

III. Results and Discussion

In preliminary experiments of ruthenium tetroxide adsorption by various sorbents⁽³⁾ it was shown that silica gel is promising material for adsorption of ruthenium tetroxide in filtration system of nuclear facilities, when the adsorption is carried out under normal filtration conditions (25°C, 60% R.H., residence time

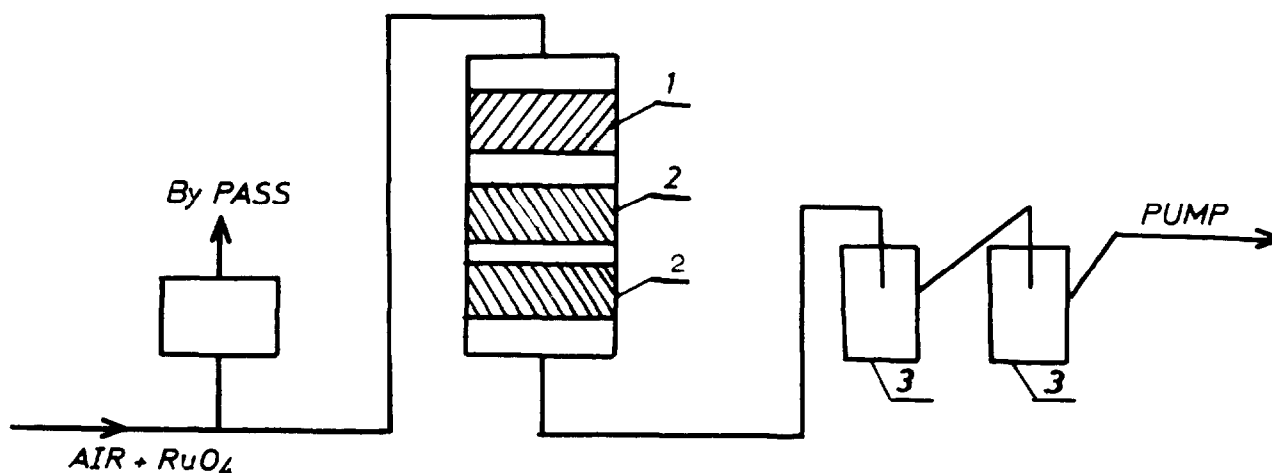


Figure 1. Schematic diagram of the apparatus for investigation of adsorption of RuO_4 ; (1) test bed, (2) safety beds, (3) safety columns.

0.3 sec.).

For investigation of ruthenium tetroxide adsorption blue silica gel, produced by Merck, grain size 1-1.6 mm containing 2% of moisture was chosen. Chemical analysis of the silica gel, used in these experiments, show that it contains iron, cobalt, nickel and chromium. During adsorption of ruthenium tetroxide on this silica gel from the wet air stream black deposit on silica gel have been formed immediately. Retention of ruthenium tetroxide in these experiments was better than 99.8%. Detailed information about experimental conditions and results of ruthenium tetroxide sorption on blue silica gel are given in previous paper⁽³⁾.

There are some assumptions⁽⁴⁾ that ruthenium tetroxide is physically adsorbed on silica gel. If that is the case one could expect adsorbed ruthenium species to be eluted from silica gel by water or acids. However, if Merck's blue silica gel after adsorption of ruthenium tetroxide is immersed in 50% H_2SO_4 only less than 0.1% of adsorbed ruthenium is dissolved. Therefore, it can be assumed that ruthenium tetroxide is chemically adsorbed on silica gel. Probable mechanism of adsorption is gradual reduction of ruthenium tetroxide by

17th DOE NUCLEAR AIR CLEANING CONFERENCE

polyvalent metal ions, contained in silica gel, into a stable RuO_2 . If this conclusion is correct than good adsorption of ruthenium tetroxide by other sorbents which are impregnated or contain polyvalent metal ions can be expected. It is known⁽⁵⁾ that iron wool and Fe_2O_3 powder are also fairly good sorbents for RuO_4 , but from some practical reasons they are not convenient for use in an off gas filtration systems (filling and refilling of adsorption columns). To avoid failure due to indefinite grain size of iron materials Alcoa Alumina H-151, which contains 0.1% of Fe_2O_3 and have definite grain size was chosen as a base material for sorption of RuO_4 .

Alcoa Alumina H-151 is inexpensive, chemically stable and inflammable. It also may have advantage in comparison with silica gel because it adsorbs water poorly while capacity of silica gel for RuO_4 is reduced by significant water adsorption.

Sorption of RuO_4 was investigated on Alcoa Alumina H-151 without further treatment and Alcoa Alumina H-151 impregnated with: 0.1M CrCl_3 , 0.1M $\text{K}_2\text{Cr}_2\text{O}_7$, 0.1M Na_2CrO_4 , 0.1M CoCl_2 and 0.1M $\text{Co}(\text{NO}_3)_2$. The residence time in all the experiments was 0.3 sec, temperature of the air stream and the test bed was 22-25°C, and relative humidity of the air stream was 60 \pm 5%. The results obtained on these sorbents are presented in Table I. In the same table the results for sorption of RuO_4 on silica gel⁽³⁾ under the same condition are given for comparison.

From the Table I it can be seen that unimpregnated Alcoa Alumina H-151 adsorbs RuO_4 very poorly although it was expected that it would be very good adsorber since it contains 0.1% of Fe_2O_3 . In addition to it, safety beds with Merck's silica gel and the safety columns did not retain ruthenium species after they passed the Alcoa Alumina H-151 bed. Similar effect was observed earlier with other sorbents⁽⁶⁾.

From Table I it can also be seen that all the sorbents investigated retain RuO_4 to some extent. With exception of silica gel and Alcoa Alumina H-151 impregnated with $\text{Co}(\text{NO}_3)_2$ significant losses of ruthenium from the system are observed with all the sorbents. A tentative explanation for this behavior might be that with strong reducing agents RuO_4 is directly reduced to RuO_2 with evolution of oxygen which prevents further reduction of RuO_4 in the gas stream. Similar behavior was observed with activated charcoal and HEPA

17th DOE NUCLEAR AIR CLEANING CONFERENCE

Table I. Results of RuO_4 adsorption on various sorbents; temperature 22-25°C, relative humidity 60±5%, residence time 0.3 sec.

impregnant	C(mg/m ³)	Q _o (mg)	R(%)	Q ₁ (mg)
A l c o a A l u m i n a H - 151				
	6.0	1.67	1.20	1.61
CrCl ₃	7.2	2.66	44.4	1.46
K ₂ Cr ₂ O ₇	10.2	3.04	21.8	2.34
Na ₂ CrO ₄	4.0	1.85	22.3	1.38
CoCl ₂	2.8	1.04	39.6	0.58
Co(NO ₃) ₂	0.9	0.34	99.9	0.0

B l u e S i l i c a G e l (3)				
	10.0	0.50	99.9	0.0
	9.7	0.97	99.9	0.0
	9.7	1.45	98.5	0.0
	9.4	1.65	98.2	0.0
	10.2	2.04	98.0	0.0
	10.0	2.92	97.3	0.0

C - concentration of RuO_4 in the air stream,
 Q_o - generated amount of RuO_4 ,
 R - retention of RuO_4 by the test bed,
 Q₁ - nonadsorbed amount of RuO_4 in the system.

filters^(3,6). Difference between sorption properties of Alcoa Alumina H-151 impregnated with $Co(NO_3)_2$ and $CoCl_2$ may be explained by oxidative properties of NO_3 ions and possibilities of various complex formation between ruthenium and nitrates⁽⁷⁾.

IV. Conclusion

Results of RuO_4 adsorption on charcoal, silica gel and Alcoa Alumin H-151 unimpregnated and impregnated by chromium and cobalt salts show that probably the most important fact is the way

17th DOE NUCLEAR AIR CLEANING CONFERENCE

of reduction of RuO_4 . If reduction of RuO_4 goes directly to RuO_2 or metal ruthenium than oxygen is evolved. Hence, oxidative atmosphere is formed which prevents further reduction of RuO_4 . Oxidative atmosphere might also be formed **when** other oxidative substances are present in the gas stream. For instance, in nuclear power plants, various iodine species which are present in the waste gases stream may also interact with ruthenium volatile species causing losses of ruthenium in filtration systems and difficulties in detection of ruthenium species on the filters.

Satisfactory adsorption material for ruthenium tetroxide can only be a sorbent on which reduction of ruthenium tetroxide goes slowly and gradually through formation of ruthenium compounds in which ruthenium is in various lower oxidation states.

Acknowledgements: Performed under contract of Serbian Fund for Scientific Activities.

References

1. G.G.Eichholz, Prog.Nucl.Energy, 2, 29 (1978).
2. R.E.Connec, C.R.Hurley, J.Am.Chem.Soc., 74, 5012 (1952).
3. R.Nikolić, Lj.Vujisić, Jahrestagung Kerntechnik, Düsseldorf, 1981, p.323
4. M.Klein, C.Weyers, W.R.A.Goossens, IAEA-SR-72/03, 1982.
5. A.Donato, W.Bocola, Energ.Nucl. (Milan), 18, 353 (1971).
6. R.Nikolić, Lj.Vujisić, unpublished data.
7. F.A.Cotton, G.Wilkinson, Advanced Inorganic Chemistry, Interscience Publishers, 1962., p.820.

DISCUSSION

KLEIN, M.: Do you think the difference in the trapping mechanism for Ru could be: (1) in the case of silica gel, RuO₄ is first adsorbed and then reduced so that the Ru remains on the bed (2) in the case of impregnated Alcoa alumina, RuO₄ is reduced in the gas phase into aerogels of Ru oxides which are not efficiently trapped by either a silica gel bed or an Alcoa alumina bed?

Vujisic: The mechanism of RuO₄ adsorption on silica gel is slow and gradual reduction occurs on it. But in the case of Alcoa alumina 4-151 (either unimpregnated or impregnated with Cr and Co salts, except Co (NO₃)₂) it reduces directly and a lot of oxygen is liberated. So, this oxidative atmosphere prevents further reduction of RuO₄ on the sorbent material.

17th DOE NUCLEAR AIR CLEANING CONFERENCE

TEST RESULTS IN THE TREATMENT OF HTR REPROCESSING OFF-GAS

H. Barnert-Wiemer
B. Bendick
B. Juergens
A. Nafissi
H. Vygen

Kernforschungsanlage Juelich GmbH,
Juelich, Fed. Rep. of Germany
W. Krill

Nukem GmbH, Hanau, Fed. Rep. of Germany

Abstract

The AKUT II-facility (throughput 10 m³/h, STP) for the clean up of the burner off-gas has been tested with synthetic off-gas and with off-gas from cold burner tests. The results are reported.

During dissolution of the burner ash in nitric acid an off-gas is formed whose main component is air and which, besides the gaseous fission products, contains NO_x. Before the separation of the gaseous fission products NO_x and/or O₂ are removed by reaction with H₂ or NH₃. For these reactions catalysts were used. Because of the known disadvantages of catalytic systems, like reduction in efficiency by poisoning or thermal influence, the alternative method of thermal, flameless reduction was tested.

The reactions were carried out in a stainless steel and a quartz reactor. Throughput, reaction temperature, O₂-, NO_x-, H₂-, and NH₃-concentrations respectively were varied. The goal of these tests was to remove O₂ and NO_x to below 1 ppm behind the reactor and NH₃ to below the detection limit of 50 ppm.

It was found that at a reaction temperature of 750°C in the stainless steel reactor these goals can be reached for both H₂ and NH₃ as reducing agents. In the quartz reactor only the O₂-H₂-reaction takes place. Obviously stainless steel acts as a catalyst for all other reactions.

I. Burner Off-Gas

The composition of the burner off-gas

The burner off-gas consists mainly of CO₂ with varying amounts of CO and impurities in the ppm-range (Table I), of which I₂, Xe, Cs, and part of the Kr are fission products. The water vapor contains also 10⁻² ppm fission product T in the form of tritiated water. The rest of the impurities stems from the oxygen used for burning and from the graphite. O₂ should not be present in the off-gas in the percent range except for burner disturbances. When the O₂ concentration reaches 5 % the burner is shut down automatically.

CO ₂	85 Vol %
CO	15 Vol %
(O ₂	< 5 Vol %)
H ₂ O	1000 ppm
Xe	42 ppm
Kr	18 ppm
J ₂	1 ppm
Cs-Aerosols	50 mg/m ³
N ₂	50 ppm
Ar	550 ppm
CH ₄	30 ppm
C _m H _n	30 ppm
SO ₂	6 ppm
Cl ₂	2 ppm
NO _x	1 ppm
NH ₃	0,5 ppm

Table I: Typical Composition of the Burner Off-Gas

The AKUT II-facility

To clean up the burner off-gas the AKUT II-facility (1,2) has been built. The facility is operated with synthetic off-gas and with off-gas from the JUPITER facility (3).

The AKUT II-facility with a nominal throughput of 10 m³/h [STP] is divided into a low pressure section ($p \leq 1,5$ bar) for the removal of impurities other than Kr and a high pressure section ($p \leq 100$ bar) for the enrichment and separation of Kr (Figure 1).

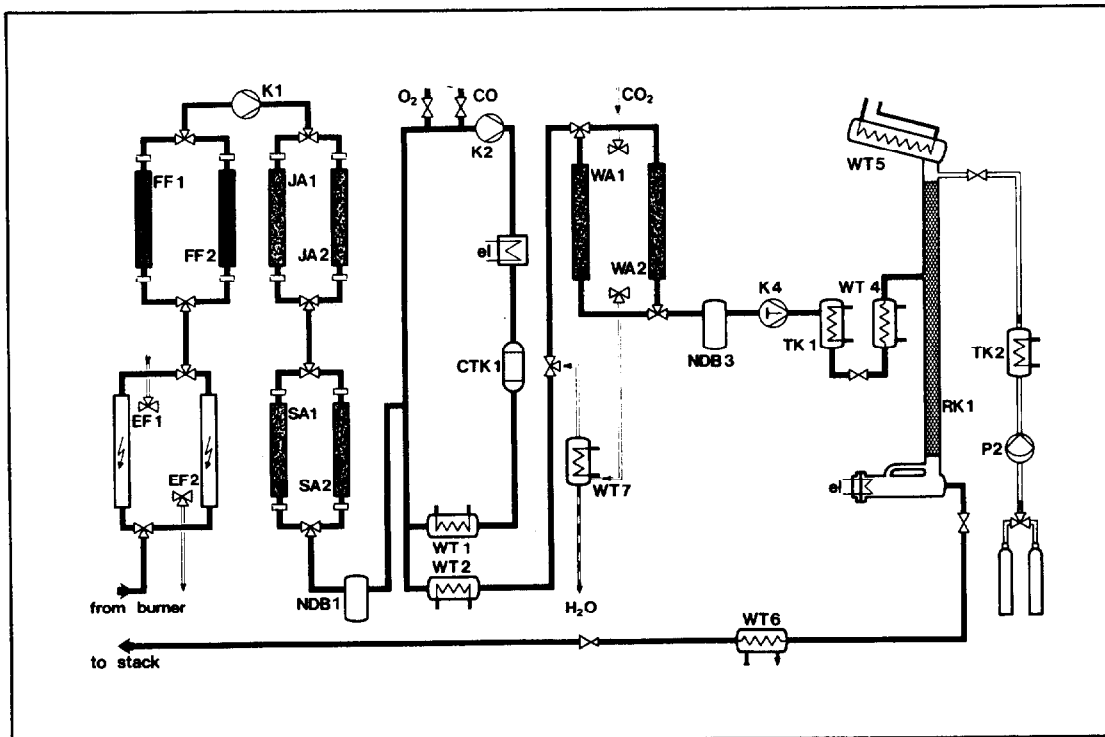


Figure 1: Schematic Flowsheet of the AKUT II-Facility

17th DOE NUCLEAR AIR CLEANING CONFERENCE

The low pressure section comprises electrostatic precipitators (EF 1+2), HEPA-filters (FF 1+2), adsorption beds for I₂ and Cl₂ (IA 1+2), SO₂ (SA 1+2), and H₂O (WA 1+2) and a recycle system with a catalytic oxidizer (CTK 1) for the conversion of CO and O₂ to CO₂ (Table II).

AKUT II Component	Bed		Material		Operation			Regeneration		
	Volume [l]	Height [mm]	Name	Manufacturer	Pressure [bar abs.]	Temperature [°C]	Nominal Gas Velocity [m/s]	Pressure [bar abs.]	Temperature [°C]	Gas Velocity [m/s]
I ₂ -Adsorber (IA 1 + 2)	6.5	650	AC 6120	Süd-Chemie, München	1.4	25	0.21	-	-	-
SO ₂ -Adsorber (SA 1 + 2)	6.5	650	Zeolon 900 Na	Norton, Wesseling	1.3	25	0.23	1.1	250	0.24
Oxidizer (CTK 1)	12	2 x 40	1922 K (0.15 % Pd)	Kali-Chemie, Hannover	1.2	250-650	Space Velocity: 12.5 m ³ (STP)/lh	-	-	-
H ₂ O-Adsorber (WA 1 + 2)	6.5	650	3 A Molecular Sieve	Merck, Darmstadt	1.2	25	0.25	1.1	350	0.28

Table II: AKUT II, Adsorption and Catalyst Beds

For the enrichment of Kr the gas is compressed (K 4), liquefied (TK 1 and WT 4), and fed into the distillation column (RK 1).

The two sections have been operated separately. The following analyzers were used for monitoring concentrations:

Halogens: Oxidant Monitor Type 924-9 by Mast Co., Davenport, Iowa

SO₂: Model 953 by Beckman, Munich, and a model 299 by Perkin-Elmer, Überlingen, with a 20 m gas cell

H₂O: AQUANAL by K. Gerhard, Blankenbach

CO: URAS by Hartmann und Braun, Frankfurt and a model 299 by Perkin-Elmer, Überlingen, with a 20 m gas cell

O₂: MAGNOS by Hartmann und Braun, Frankfurt, and a Type OA 137 by Servomex, Ratingen

Test results

Three test phases can be distinguished: first the components were tested separately. Then the low pressure section was tested as a whole before it was connected to the JUPITER facility.* In table III the tested flows and concentrations in the feed and the

*With JUPITER off-gas 5 test runs were made with a duration between 4,5 and 7 hours

resulting effluent concentrations are listed.

	Synthetic Off-Gas		JUPITER Off-Gas	
	Feed	Effluent	Feed	Effluent
Flow	5 – 10 m ³ /h (STP)		3.5 – 9.5 m ³ /h (STP)	
Concentrations:				
CO ₂	82.5 – 97.5 %	~ 100 %	40 – 99 %	~ 100 %
CO	2.5 – 17.5 %	< 20 ppm	0 – 60 %	< 100 ppm
O ₂	–	0.35 %	0 – 1.5 %	0.3 – 1.5 %
H ₂ O	775 – 2500 ppm	2 ppm	600 – 2500 ppm	3 ppm
SO ₂	7 – 19 ppm	0.1 ppm	0.05 – 5 ppm	0.02 ppm

Table III: AKUT II, Test Conditions

The I₂-adsorber tests were not completed because the iodine analyzer broke down. They will have to be repeated after repair of the analyzer, but no surprises are expected because the material AC 6120 has been tested sufficiently at other institutions (4).

The SO₂ adsorption material Zeolon 900 Na has been tested at General Atomic Company (5) and has been put into the AKUT II-facility for intermediate use. During the tests it reached the expected decontamination factors (Table III). For two reasons laboratory tests are under way to find a chemical rather than a physical adsorbent:

- a) on physical adsorbents other components such as water vapor (containing tritiated water vapor) are coadsorbed, which are released to the stack during regeneration of the adsorbent. Besides Zeolon 900 Na has a rather low dynamic adsorption capacity for SO₂ (30 mg/g at a face velocity of 0.08 m/s) (5)
- b) the radioactive isotope S 36 with a lifetime of 88 days is formed during irradiation from the chlorine present in the graphite. It might be necessary to store SO₂ till this isotope has decayed.

Table IV contains the preliminary data of the chemical adsorbents tested so far. The tests were made with a high SO₂ concentration of 2300 ppm to shorten the run time. In previous tests with 18 ppm SO₂ in the feed with all adsorbents less than 0.1 ppm SO₂ in the effluent were reached at ambient temperature. A rise of temperature up to 400°C produced no significant improvement. The utilisation of the active component has been a few percent at best so far but tests for optimisation are going on.

The next component downstream of the SO₂-adsorbers is the catalytic oxidizer (Table II). The catalyst (0.15 wt.-% Pd on Al₂O₃) can be operated as low as 200°C, but since the CO-O₂ reaction

Adsorption Material	Active Comp.	Percentage of Act. Comp. wt-%	Bulk Packing Density kg/l	Cost DM/kg	Time till Breakthrough min
Merck Nr. 5953	MnO ₂	40-60	0.91	432.-	155
Kali-Chemie Br 1601	MnO ₂	8	0.9	26.-	50
Kali-Chemie Br 1598	MnO ₂	8	0.48	23.-	18
Süd-Chemie G-72 D	ZnO	90	1.05	10.20	35
Süd-Chemie G-3	Fe ₂ O ₃ /Cr ₂ O ₃	80/9	1.0	9.40	32
Süd-Chemie ODL-N-140	CuO	22	0.75-1.0	35.-	35

Table IV: Chemisorption of SO₂

Bed volume: 136 ml
 Bed height: 150 mm
 Gas flow: 100 l/h [STP]

Superficial face velocity: 0.03 m/s
 SO₂ concentration: 2300 ppm SO₂ in CO₂
 Temperature: 20°C

breaks down completely between 190°C and 200°C it is advisable to keep a safety margin. We do not operate lower than 250°C.

The gas recycle of the oxidizer system, which dilutes the off-gas to a concentration far below the CO-O₂ explosion limit, was operated at 150 ± 20 m³/h [STP].

The CO concentration behind the catalyst is < 20 ppm (detection limit of the Perkin Elmer IR-analyzer model 299 with 20 m gas cell) and independent of the CO feed concentration when the O₂ surplus is ≥ 0.33 %. During the JUPITER tests the Perkin Elmer IR-analyzer was not available, so that a less sensitive analyzer was used where the detection limit was 100 ppm CO.

The JUPITER off-gas shows a fluctuation of flow, O₂ and CO concentration even at steady state conditions. The typical variation would be between 10 and 11 m³/h [STP], 10 and 13 % CO, and 0 - 0.2 O₂ in a 3 minute rhythm (corresponding to the feed of crushed fuel elements into the burner). The CO fluctuations were controlled well in the oxidizer system, but sudden CO increases > 5 % caused O₂ surplusses up to 1.5 %. Work is under way to improve the control system and also to reduce the pressure drop across the connecting

ducts, because the AKUT II blower (K 1) could only suck 9,5 m³/h [STP] due to a too high pressure drop.

If in the off-gas hydrocarbons are present these are reduced in the oxidizer to H₂O and CO₂.

Water vapor is removed in the H₂O-adsorbers (WA 1+2). In the laboratory 3 A, 4 A, and 5 A molecular sieves have been tested. No difference was detected in capacity, breakthrough curve or decontamination factor. The 3 A molecular sieve was chosen for AKUT II. Figure 2 shows the breakthrough curves for identical molecular sieves and identical loading conditions for the laboratory adsorber of 34 mm diameter and the AKUT II adsorber of 113 mm diameter. Rather unexpectedly the breakthrough time and with it the length of the mass transfer zone were much longer for the adsorber with 113 mm diameter compared to the adsorber with 34 mm diameter.

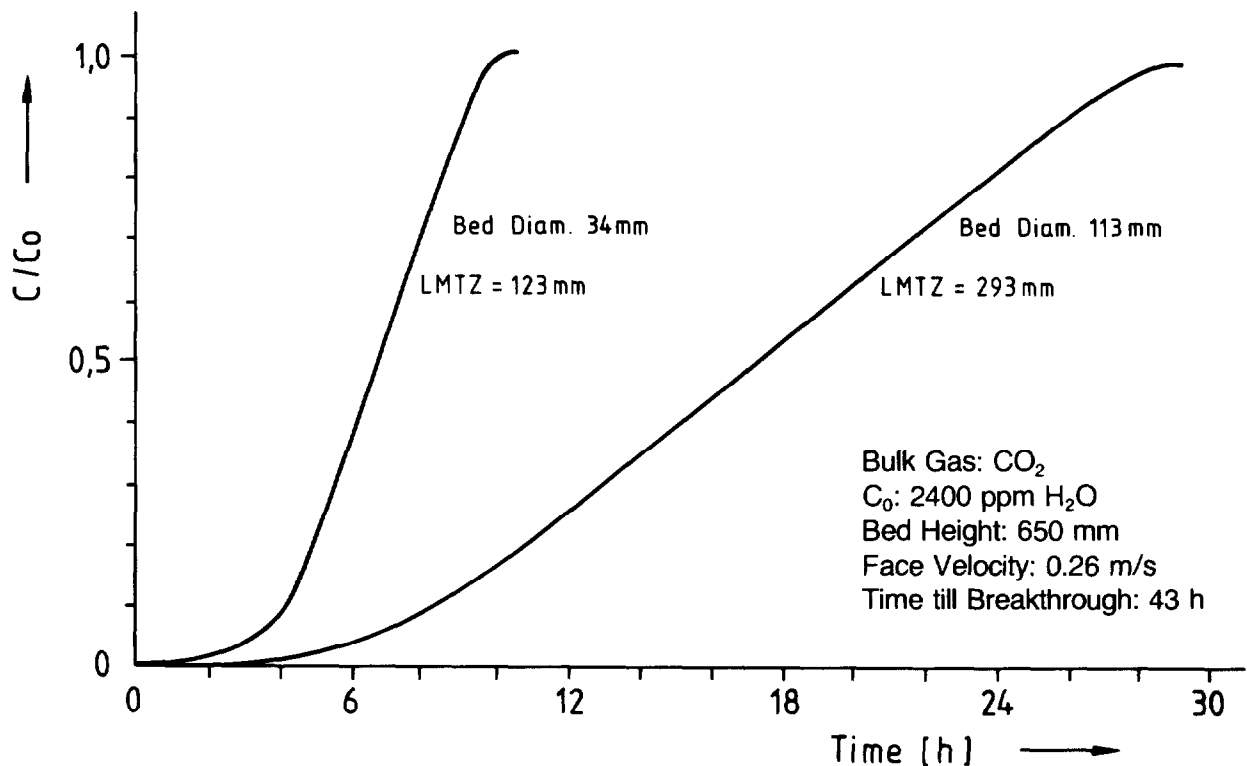


Figure 2: Adsorption of H₂O on 3 A Molecular sieve (Merck), ratio of effluent concentration c and feed concentration c_0 versus time

The H₂O effluent concentration was 2 - 3 ppm and in the tested range independent of the feed concentration (Table III). The capacity of 190 g H₂O/kg MS corresponds to the data given in literature (6).

Behind the water adsorbers the off-gas was released into the hot cell off-gas ducts.

17th DOE NUCLEAR AIR CLEANING CONFERENCE

The distillation column RK 1 has been tested separately with pure CO₂ to gain the flooding curves.

The overall length of the column is 5.8 m and the inner diameter is 40 mm. The total height of the packing (wire spirals 5 x 5 mm) is 4.7 m. It is divided into four parts with liquid distributors between them.

The diameter of the column was designed such that the vapor velocity at nominal throughput was 50 % of the flooding velocity. The flooding velocities were calculated with the empirical equation given in Perry's Handbook (7)

$$\frac{U_t^2 a_p \rho_g}{g \epsilon^3 \rho_l} \mu_l^{0.2} = \text{function} \left[\frac{L}{G} \sqrt{\frac{\rho_g}{\rho_l}} \right] \quad (1)$$

- U_t = superficial gas velocity, ft./sec.
- a_p = total area of packing, sq. ft./cu. ft. bed
- ϵ = fractional voids in dry packing
- g = gravitational constant, 32.2 ft./sec.²
- ρ_l, ρ_g = gas and liquid densities, lb./cu. ft.
- L = liquid-mass rate, lb./(sec.)(sq. ft.)
- G = gas-mass rate, lb./(sec.)(sq. ft.)
- μ_l = liquid viscosity, centipoise

For comparison the flooding curves were also calculated with the equation given by Sawistowski (8)

$$\ln \frac{U_F^2 a \rho_G}{g \epsilon^3 \rho_L} \left(\frac{\mu_L}{\mu_W} \right)^{0.2} = -4 \left(\frac{L}{G} \right)^{1/4} \left(\frac{\rho_G}{\rho_L} \right)^{1/8} \quad (2)$$

- where
- U_F = flooding velocity of the gas phase based on total column cross-section
 - a = surface area of packing per unit volume of column
 - g = acceleration due to gravity
 - ϵ = void fraction of the packing
 - ρ_L = density of the liquid
 - ρ_G = density of the gas
 - μ_L = viscosity of the liquid
 - μ_W = viscosity of water at 20°C (approx. 1 centipoise)
 - G = mass rate of flow of the gas phase
 - L = mass rate of flow of the liquid phase

In Figure 3 the vapor velocities at flooding points for L/V = 1, i.e. for total reflux, at temperatures between - 10°C and + 20°C are shown. The calculated curves are based on equation (1) (dot - dash - line) and equation (2) (dashed line). The diagram also contains our data (solid line). The difference between the vapor velocities calculated by equation (1) and our data is only between 8 % at 12°C and 1 % at - 10°C. This is very satisfactory, considering the fact that equation (1) was derived from data on air-water-systems where e.g. the ρ_L/ρ_G ratio is 1000 compared to the CO₂ system where $\rho_L/\rho_G = 6.5$ at 10°C.

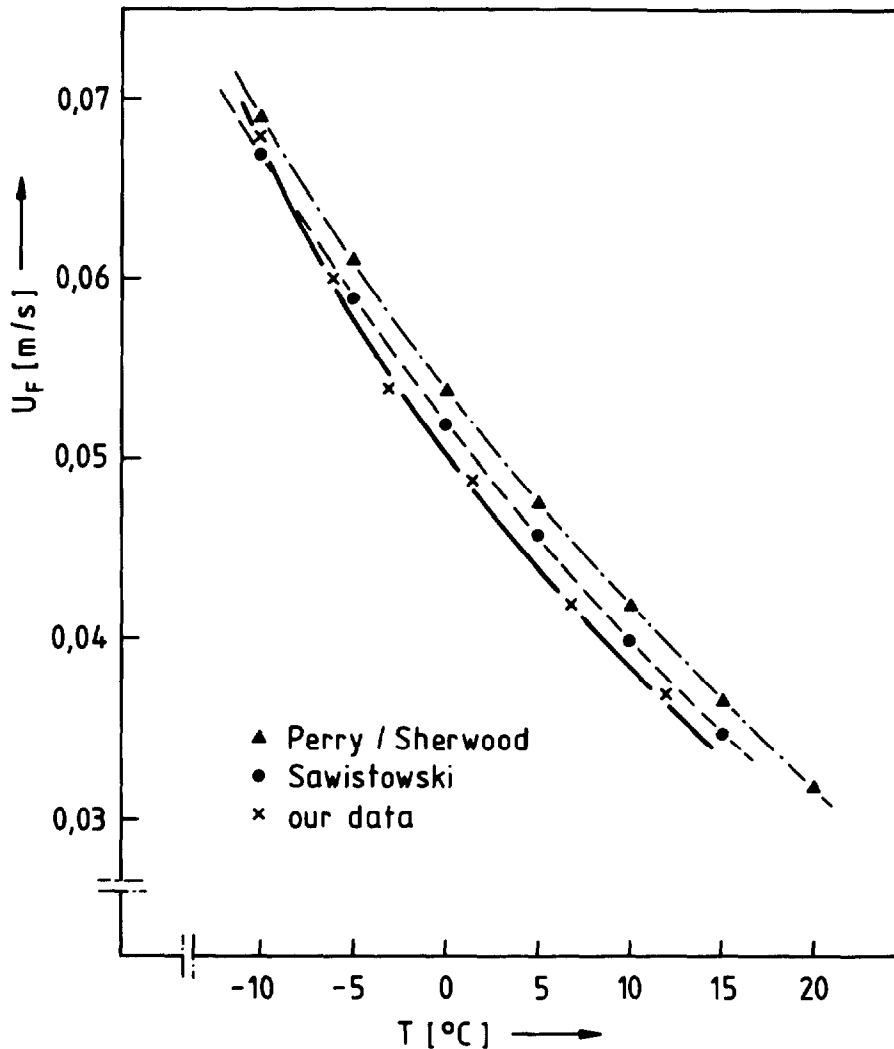


Figure 3: Vapor velocities at flooding points versus temperature for $L/V = 1$

The pressure drop (Δp) through the column is plotted versus the vapor velocity (U_D) for several temperatures in Figure 4. The curves show the typical lower break at the loading velocity and the typical upper break at the flooding velocity.

The values for the vapor velocity and the pressure drop at the flooding points (U_F and Δp_F) at various temperatures (T) are inserted in the diagram. (U_F was plotted versus T in Figure 3.)

Work planned for the AKUT II-facility in near future is

- to get the low pressure section ready for the next JUPITER campaign, planned for september
- to run the distillation column at L/V ratios other than 1 and to determine the efficiency of the column for CO_2-N_2 , CO_2-O_2 , and CO_2-Kr systems.

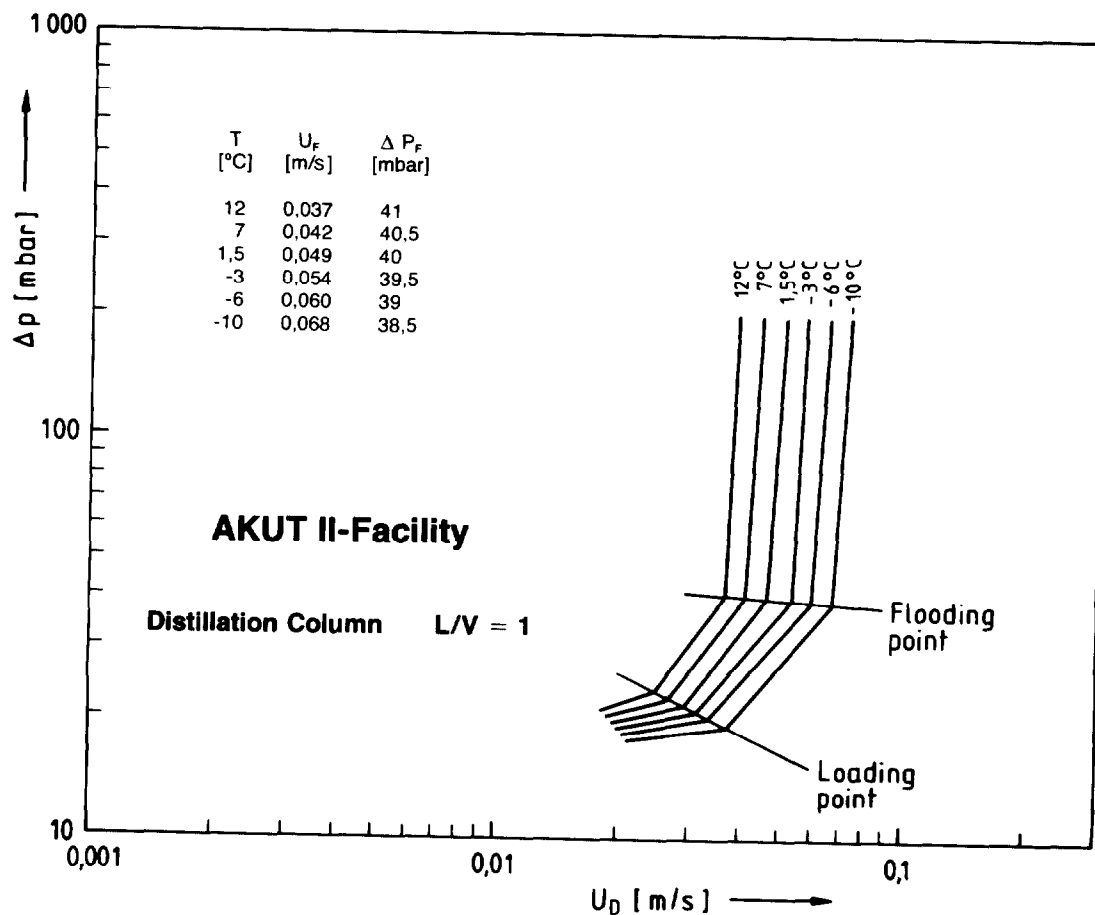


Figure 4: The Pressure Drop Δp through the Distillation Column versus Vapor Velocity U_D at Various Temperatures

II. Dissolver Off-Gas

Introduction

During dissolution of nuclear fuel in concentrated nitric acid nitrogen oxides are formed which are released into the process off-gas system together with the gaseous fission products. A typical composition of the dissolver off-gas is shown in table V.

N ₂	75.4	Vol. %
O ₂	20.3	Vol. %
H ₂ O	1.5	Vol. %
Xe	1.06	Vol. %
Ar	0.9	Vol. %
NO _x	0.5	Vol. %
Kr	0.16	Vol. %
H ₂ , J ₂ , CO ₂ , C _n H _m	< 0.1	Vol. %

Table V: Typical Composition of the Dissolver Off-Gas

17th DOE NUCLEAR AIR CLEANING CONFERENCE

The goal of the experiments reported herein was the removal of O₂ and NO_x from the dissolver off-gas to below 1 ppm to protect the cryogenic Krypton-separation unit following downstream.

The main work on removal of O₂ and/or NO_x has been done on catalytic reduction:

O₂ and NO_x together have been reacted with H₂ over noble metal catalysts [9,10]. To remove NO_x alone, it was reduced with NH₃ over mordenite [11,12].

Since the use of catalysts includes some drawbacks like poisoning and dust formation, it was decided to check the possibilities of thermal reduction. As reducing agents both H₂ and NH₃ were tested [13].

The reaction equations for the O₂-NO_x-H₂ and the O₂-NO_x-NH₃ systems are listed in table VI. The stoichiometric amount of H₂ was determined by equations I and II and of NH₃ by equations VI and VII. The NH₃, which is formed according to equation III and the NH₃

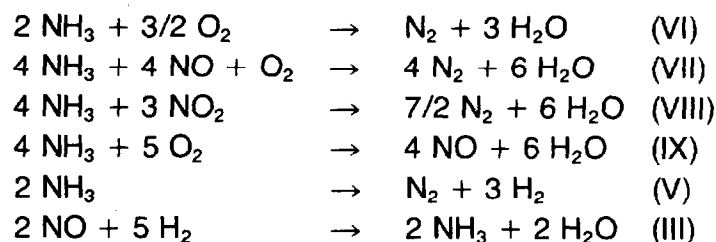
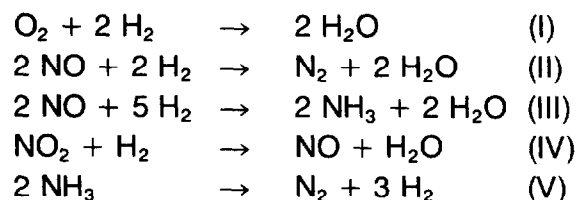


Table VI: Reaction Equations for the O₂-NO_x-H₂ and the O₂-NO_x-NH₃ Systems

surplus in the O₂-NO_x-NH₃ system dissociate according to equation V into N₂ and H₂. This leads to the second goal of our tests besides the removal of O₂ and NO_x below 1 ppm: to introduce no NH₃ into the off-gas.

Table VII contains the different gas mixtures, the various gas streams and concentration ranges, and the reactor materials that were tested successively.

Tested Gas Mixtures

N_2 - O_2 - H_2
 N_2 - NO - H_2
 N_2 - O_2 - NO - H_2
 N_2 - O_2 - NO - H_2 - H_2O
 N_2 - O_2 - NO - H_2 - I_2

 N_2 - O_2 - NO - NH_3
 N_2 - O_2 - NO - NH_3 - H_2O

Tested Gas Compositions

N_2 : 600, 800, 1000 l/h (20°C, 1.1 bar)
 O_2 : 0.5, 1 %
NO : 750, 1500 ppm
 H_2O : 0, 10000 ppm
 H_2 : 23 to 140 % surplus
 NH_3 : - 40 to + 60 % surplus
 I_2 : 0 to 3000 ppm

Tested Reactor Materials

Stainless Steel Nr. 1.4571 (DIN)
Quartz

Table VII: Tested Gas Mixtures, Gas Compositions, and Reactor Materials

Test Equipment

Figure 5 shows the design of the thermal reactor fabricated from stainless steel Nr. 1.4571 (DIN). Five thermocouples in protective tubes are located at various heights. Three resistance heater jackets were controlled independently to establish a fairly even temperature profile throughout the reactor.

The quartz reactor had the same dimensions as the metal reactor, but was equipped with only 2 thermocouples, T 2 and T 6.

Figure 6 shows the test assembly. the gases were supplied from gas cylinders, with the exception of iodide and water vapor. Iodine was liberated from a sodium iodide solution by reaction with ammonium ferro sulfate. Water vapor was added by directing part of

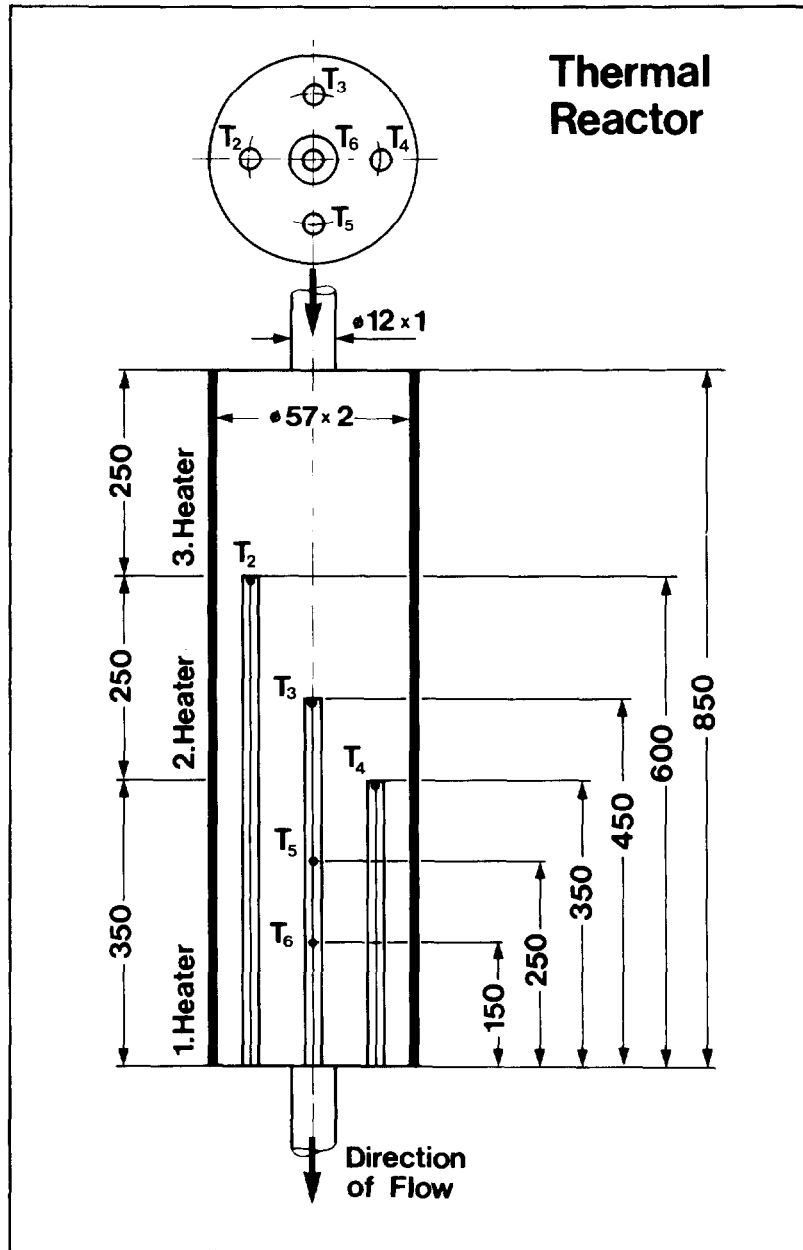


Figure 5: Design of the Thermal Reactor

the N_2 stream through a water tank. Entrained water aerosols were separated in a demister. All gases were blended upstream of reactant gas supplies. Before the gas entered the reactor it was heated in a preheater wrapped with a heating tape. The gas entered the reactor in all tests with a temperature of 420°C . The reactor temperature was varied between 420°C and 750°C . Behind the reactor the gas was cooled to ambient temperature in a water cooled heat exchanger, where part of the water vapor condensed.

The gas was analysed for iodine and ammonia discontinuously, all other analyses were continuous. For O_2 concentrations above 1000 ppm a MAGNOS (Hartmann & Braun), for O_2 concentrations below 1000 ppm an ELCOFLUX C5 (Dr. Thiedig & Co) were used. H_2 was measured with CALDOS analyzers by Hartmann & Braun, and NO_x with a

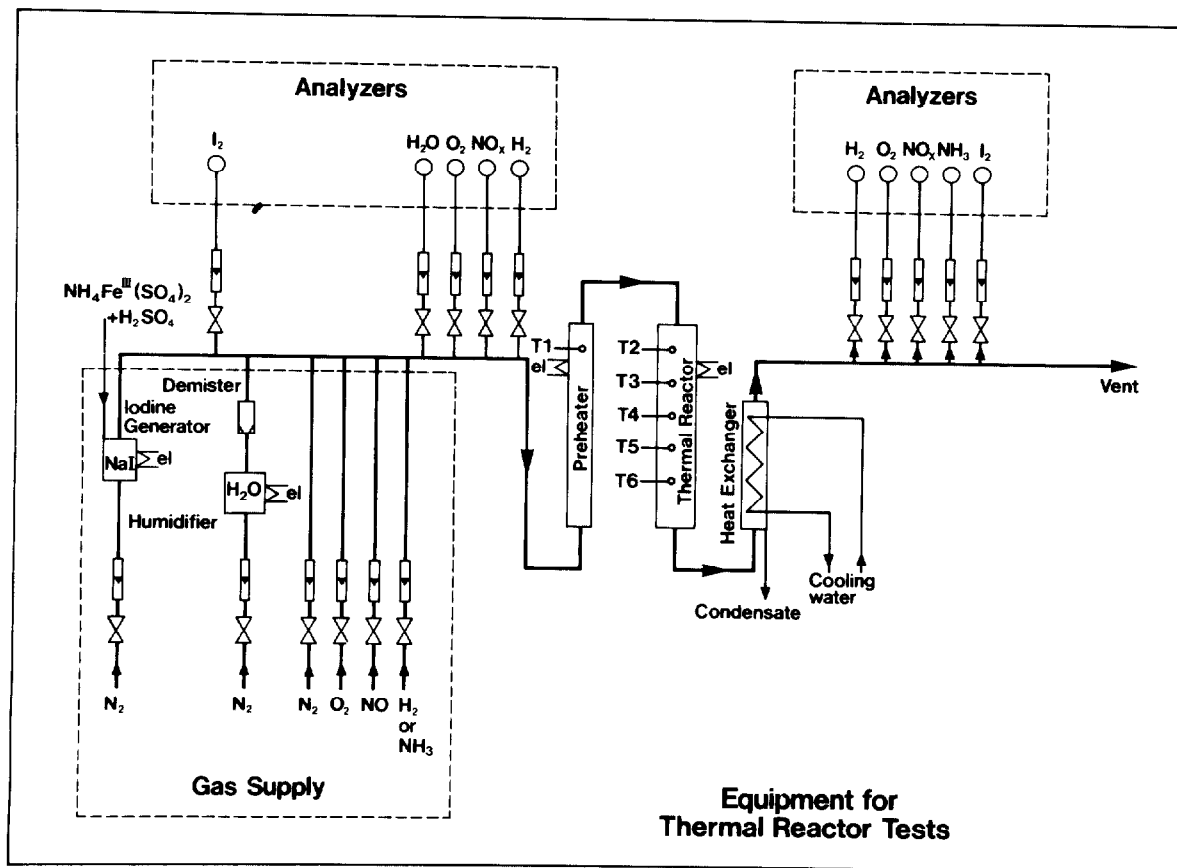


Figure 6: Test Assembly

LUMINOX 201 by BOC and a model 951 by Beckman. For water analysis an AQUANAL by K. Gerhard KG was used. NH_3 was absorbed in boric acid and titrated. I_2 was absorbed in an aqueous potassium carbonate solution, reduced to iodide with sodium sulfate and then determined with an ion selective electrode.

Reduction tests with the metal reactor

H_2 as reducing agent

The first reaction to be tested was the O_2 - H_2 reaction. Figure 7 shows the complete reduction of O_2 with H_2 as a function of reactor temperature and throughput. The higher the throughput, that means the lower the residence time, the higher the temperatures that are necessary for complete removal of O_2 . For the higher H_2 surplus (curves a and c) the reaction temperature can be lower than for the lower surplus (curves b and d). It is interesting to note that for the lower O_2 concentration tested (0,5 %) for the highest throughput of 1000 l/h [STP] higher reaction temperatures were measured (curves c and d).

In the next test series with NO and H_2 the NH_3 formation and the reaction temperature were checked.

Figure 8 shows the results for a feed of 1500 ppm NO . The numbers in the curves give the H_2 concentration in the reactor

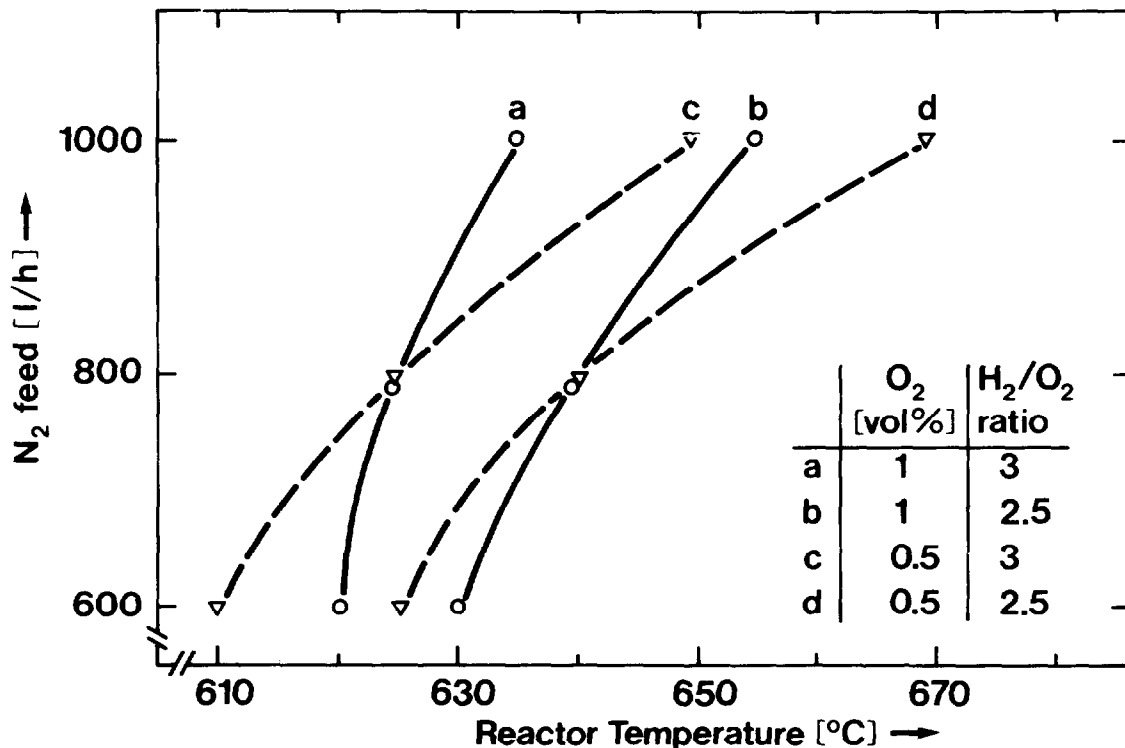


Figure 7: Complete Reduction of O₂ with H₂ as a Function of Reactor Temperature and Throughput

effluent. Below 500°C NO is reduced and NH₃ formed. It can be seen that for higher H₂ surplus NO is reduced at a lower temperature and that the formation of NH₃ depends on the amount of H₂ present. For 1,5 % H₂ in the effluent all NO is reduced to NH₃. The NH₃ dissociates at temperatures above 450°C, and at 630°C the NH₃ concentration is below the detection limit of 50 ppm.

In the diagram no throughput was entered as parameter because the curves are identical for the three tested throughputs of 600, 800 and 1000 l/h [STP]. For a feed of 750 ppm NO the curves are similar in shape and do not render any different results.

From the tests described so far it can be seen that both NO and O₂ can be removed completely by reaction with H₂. The next step was to test the simultaneous reduction of NO and O₂ with H₂. Again the N₂-feed of 600, 800 and 1000 l/h [STP], O₂ feed concentrations of 0.5 % and 1 %, NO feed concentrations of 750 and 1500 ppm, and H₂ concentrations in the effluent of 0.5 %, 1 % and 1.5 % (corresponding to stoichiometric surplusses between 23 % and 140 %) were tested.

Figure 9 shows the results of one of these tests with a feed of 0.5 % O₂, 750 ppm NO, and 2 % H₂ (which corresponds to 93 % stoichiometric surplus).

For the specific gas composition shown in Figure 9 O₂ is removed completely for a N₂ feed of 600 l/h [STP] at 520°C, for a N₂ feed of 800 l/h [STP] at 630°C. For a N₂ feed of 1000 l/h [STP] 3 ppm O₂ remain, even at 740°C. For NO_x the temperature is always

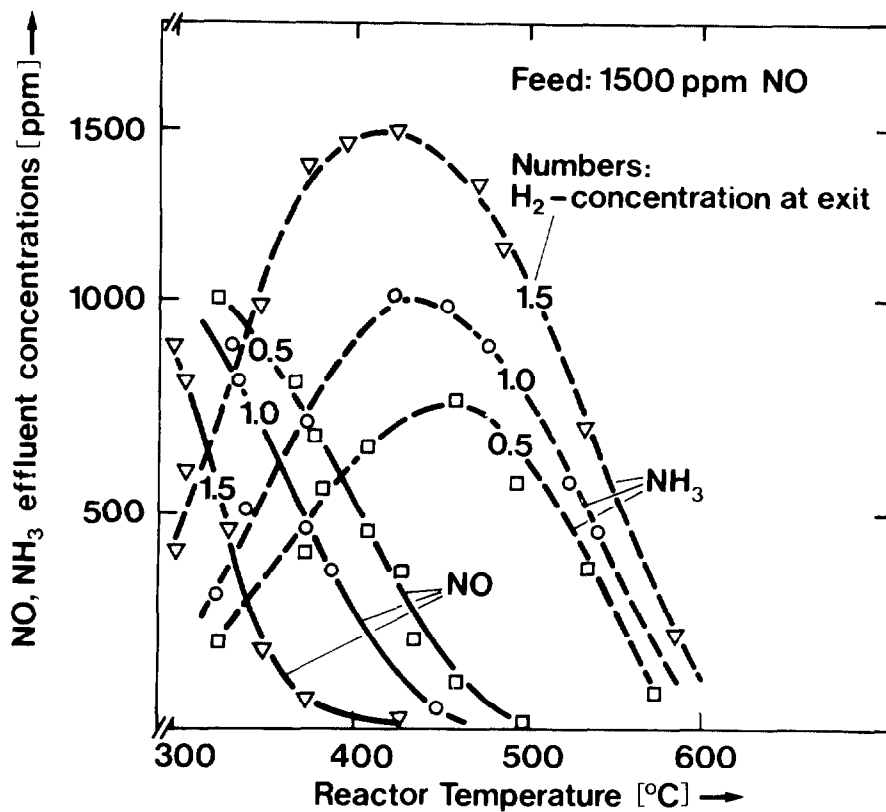


Figure 8: NO and NH₃ Effluent Concentrations vs. Reactor Temperature
 lower than for O₂. NH₃ in all cases needs 730°C to 750°C for complete dissociation.

Summing up the different runs with N₂-O₂-NO_x-H₂-gas mixtures it can be said that

- in all tests on the reduction of O₂ and NO_x with H₂ NH₃ was formed. The NH₃ formation depends mainly on the NO_x concentration, the H₂ concentration, and to a lesser degree on the throughput, with the lowest concentration at a N₂ feed of 800 l/h [STP] and the highest at 600 l/h [STP],
- for a N₂ feed of 600 l/h [STP] (corresponding to a residence time of 3,5 s) for all tested O₂ and NO_x concentrations and independent of the H₂ surplus no O₂, NO_x or NH₃ can be detected behind the reactor for a reactor temperature of 730°C ± 20°C,
- for a N₂ feed of 1000 l/h [STP] (corresponding to a residence time of 2,1 s) for all tested mixtures traces of O₂ and NO_x ≤ 10 ppm and also traces of NH₃ ≤ 160 ppm were found in the effluent.

This means that if a mean reactor temperature of 730°C + 20°C is maintained and the residence time is > 3,5 s than for all tested gas mixtures no O₂, NO_x or NH₃ is found in the reactor effluent.

Since the dissolver off-gas is saturated with water vapor, its influence was tested by adding 10.000 ppm water vapor to the gas

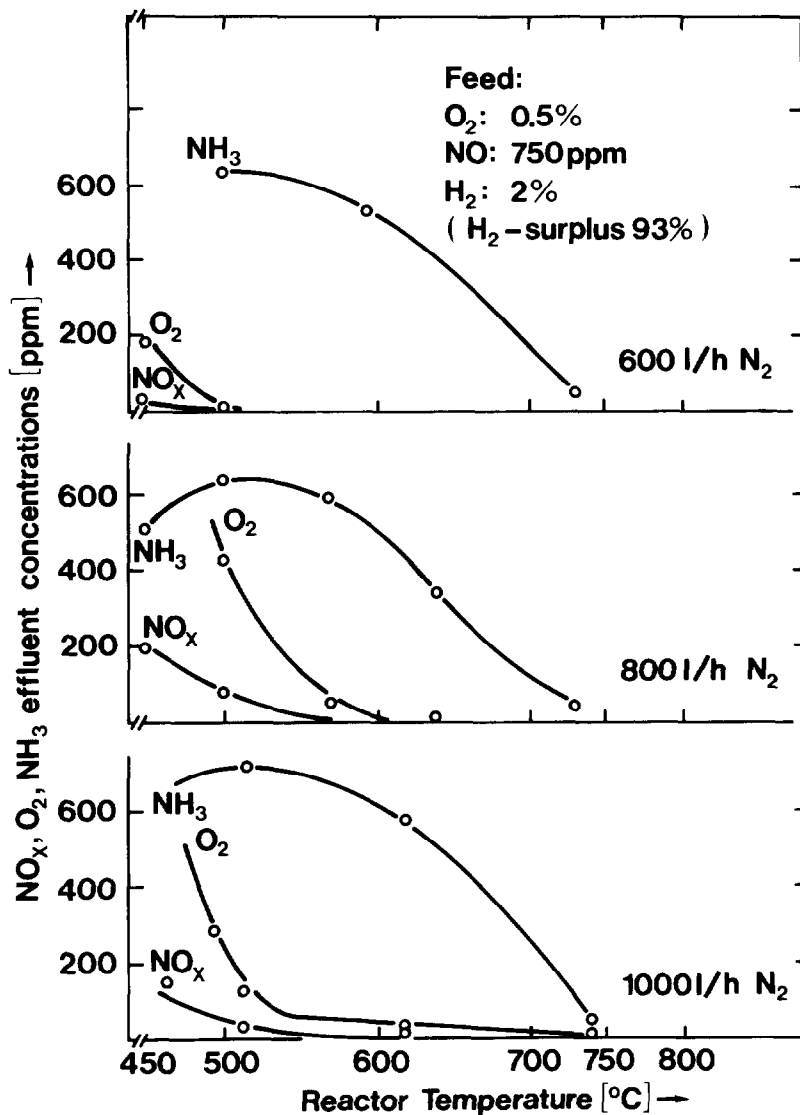


Figure 9: O₂, NO_x, NH₃ Concentrations in Effluent vs. Reactor Temperature and Throughput

mixture. Generally speaking it can be stated that by the presence of water the reaction temperatures for O₂ and NO_x were lowered and the NH₃ formation was enhanced. But at the temperature of 730°C ± 20°C all NH₃ had dissociated so that in the end no difference was noticeable.

NH₃ as reducing agent

In the following test series NH₃ was used as reducing agent. Again a N₂ feed of 600, 800 and 1000 l/h [STP], O₂ concentrations of 0.5 and 1 %, but only one NO concentration of 1500 ppm were tested. NH₃ was varied between -40 and +60 % of the stoichiometric amount. Figure 10 shows the results of varying amounts of NH₃ on the O₂ and NO_x concentrations in the effluent. O₂ is reduced to NO for under-stoichiometric NH₃ supply and only at ~40 % overstoichiometric supply no NO_x is detectable in the effluent. Furtheron it can be seen that only for the lowest N₂ feed stream of 600 l/h [STP] all O₂ is reduced. For the two higher throughputs even at 40 % over-

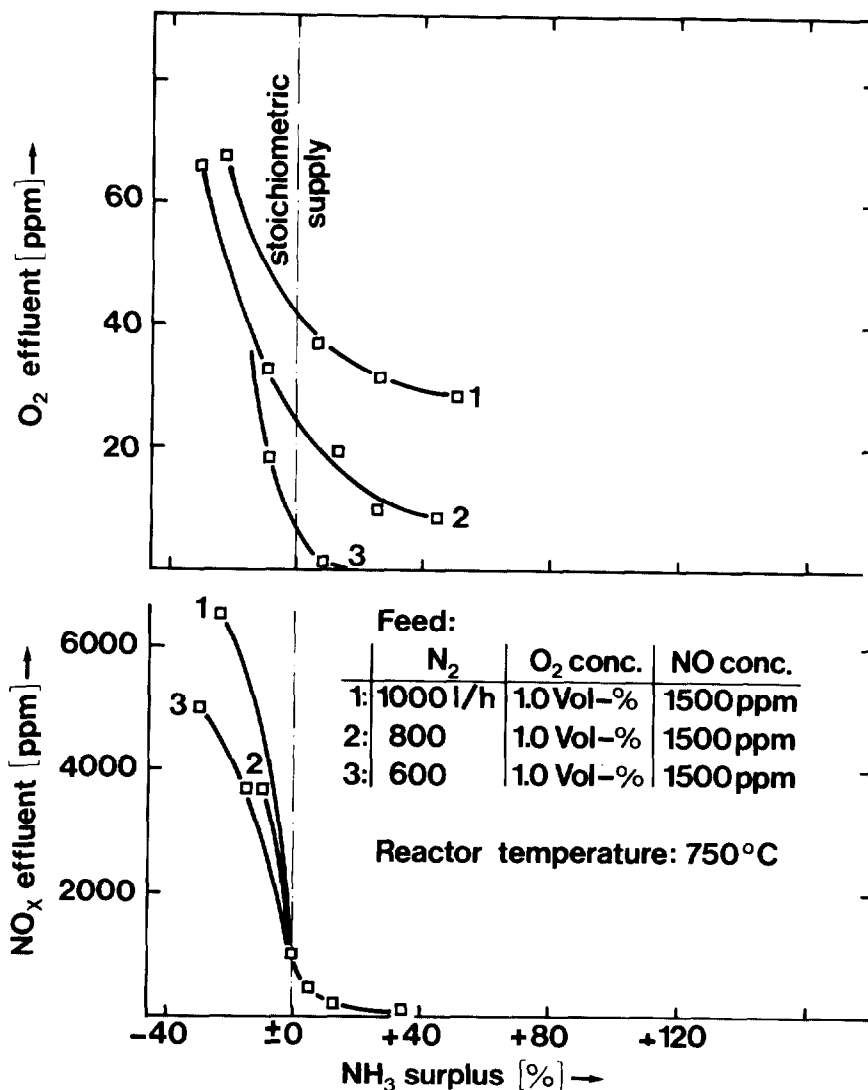


Figure 10: O₂ and NO_x Concentrations in Effluent for NH₃ as Reducing Agent

stoichiometric NH₃ supply 10 to 30 ppm O₂ are detectable in the effluent.

In Figure 11 the O₂, NO_x, and NH₃ concentrations in the reactor effluent versus the feed stream are shown. Only for the N₂ feed of 600 l/h [STP] O₂ and NO_x are removed below 1 ppm. But even for the lowest throughput NH₃ is found in the effluent: NH₃ concentration is 170 ppm and 320 ppm for a feed of 0.5 % O₂ and 1 % O₂ respectively. That means that a longer residence time than the one tested is necessary to remove NH₃ completely.

Introduction of 10.000 ppm H₂O did not influence the results.

Reduction tests with the quartz reactor

To clarify the question whether the reactor material influences the described reactions, part of the tests were repeated in a quartz reactor of the same dimensions as the stainless steel reactor.

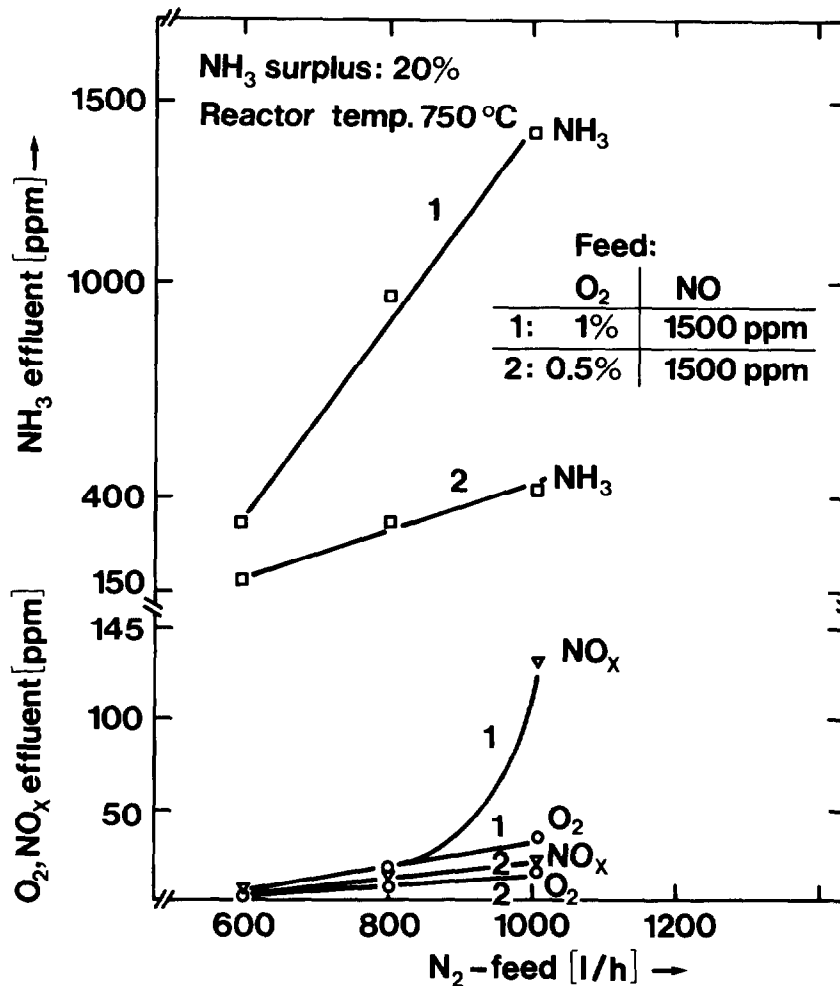


Figure 11: O₂ and NO_x Reduction with NH₃

The tests were made with a N₂ feed of 600 l/h [STP], an O₂ feed concentration of 1 %, a NO feed concentration of 1500 ppm, and a reactor temperature of 750°C.

In the O₂-H₂ reaction O₂ was removed completely at a stoichiometric H₂ surplus of only 1 %. The NO-H₂ reaction did not take place.

The tests were repeated with NH₃ as reducing agent. And again no reaction took place.

When a few pieces of the stainless steel reactor material were put into the quartz reactor all reactions rendered the same results as in the stainless steel reactor. It is obvious that the NO_x-H₂- and the O₂-NO_x-NH₃ reactions are catalyzed by stainless steel. Since the steel Nr. 1.4571 (DIN) which we used is not the right material for a reactor with a prolonged life time, and the recommended material for temperatures around 750°C which is not susceptible to embrittlement by N₂ is Incoloy 800, it would be advisable to check the influence of this material on the reactions.

Influence of iodine on the reactions

The last test series was made to determine the effect of iodine

17th DOE NUCLEAR AIR CLEANING CONFERENCE

on the described reactions. The tests were made in the metal reactor at 740°C and a N₂ feed of 600 l/h [STP]. Summing up the data, it can be stated that below 25 ppm I₂ in the gas no influence was noted. More than 25 ppm I₂ led to traces of O₂ and NO_x (≤ 10 ppm) in the effluent. An I₂ excursion of 3000 ppm caused the complete breakdown of all reactions. If the I₂ influx is stopped and the reactor flushed for a few minutes with a N₂-H₂ mixture the reactor recovers and the reactions take place again.

In the quartz reactor only the O₂-H₂ reaction was tested, since other reactions do not take place as mentioned above. At an I₂ concentration of 140 ppm the H₂-O₂ reaction broke down completely.

It is assumed that iodine atoms interrupt the H₂-O₂ chain reaction with the consequence that the reaction rate drops and the gas needs a longer residence time for complete reaction. It is also possible that the catalytic centers of the metal are poisoned by the iodine and the NO_x-H₂ reaction is impaired. To clear this point more experiments would be necessary.

Summary

Summing up the tests with thermal reactors it can be said, that

- O₂ and NO_x can be reduced with H₂ at 730 ± 20°C. No O₂, NO_x, or NH₃ is detected in the effluent if the residence time is ≥ 3.5 s.
- O₂ and NO_x can also be reduced with NH₃, but a longer residence time than for H₂ is needed, because more intermediate reactions are involved.
- The reactions are catalysed by stainless steel.
- Traces of iodine ≥ 25 ppm impair the reactions.
- Saturation of the gas with water vapor does not increase the reaction temperature or the residence time.

III. References

- (1) H. Barnert-Wiemer, M. Heidendael, H. Kirchner, E. Merz, G. Schröder, H. Vygen:
Burner and Dissolver Off-Gas Treatment in HTR Fuel Reprocessing
Proc. of the 15th DOE Nuclear Air Cleaning Conference, Boston, Massachusetts, 7-10 Aug. 1978
- (2) H. Barnert-Wiemer, E. Merz:
Abgasbehandlung bei der Wiederaufarbeitung von Brennelementen des Hochtemperaturreaktors (HTR)
Jahrestreffen der Verfahrensingenieure, Straßburg 1.-3.10.1980
- (3) U. Brinkmann, W. Heid, H. Huschka, G. Kaiser, W. Theymann:
Research and Development Work in HTR Fuel Fabrication, Fuel Performance, Spent Fuel Treatment in the FRG
Conf. on Gascooled Reactors Today, Bristol, 20-24 Sept. 1982

17th DOE NUCLEAR AIR CLEANING CONFERENCE

- (4) J.G. Wilhelm, J. Furrer:
Jodabscheidung in Wiederaufarbeitungsanlagen
Tagungsbericht V/2266/78 der Kommission der Europäischen
Gemeinschaft, Luxemburg, Febr. 1978
- (5) L. Abraham, P.M. Hirsch:
Consolidated Fuel Reprocessing Program, Interim Development
Report: Off-Gas Treatment System
GA-A16292 (June 1981)
- (6) W. Kast:
Adsorptive Trocknungsverfahren für Gase
Haus der Technik, Essen, Vortragsveröffentlichungen 404 (1977)
- (7) R.H. Perry, C.H. Chilton:
Chemical Engineers' Handbook
Mc Graw Hill, 5th Edition
- (8) H. Sawistowski:
Chem. Engng. Science, Vol. 6, pp 138/140 (1957)
- (9) R. v. Ammon et al.:
Die katalytische Reduktion von Sauerstoff und Stickoxiden mit
Wasserstoff im Abgas von Wiederaufarbeitungsanlagen
Laborversuche zum Katalysatorverhalten
KFK 2437 (1977)
- (10) H. Barnert-Wiemer, B. Bendick:
Untersuchungen an Katalysatoren zur Reduktion von Stickoxiden
und Sauerstoff mit Wasserstoff
Jül-1677 (1980)
- (11) T.R. Thomas, D.H. Munger:
An Evaluation of NO_x Abatement by NH₃ over Hydrogen Mordenite
for Nuclear Fuel Reprocessing Plants
ICP-1133 (1978)
- (12) P.M. Hirsch:
Off-Gas Treatment System NO_x Converter Component Tests
GA-A 16559 (1982)
- (13) B. Bendick:
Verfahren zur Abtrennung von Sauerstoff und Stickoxiden aus dem
Auflöserabgas einer Wiederaufarbeitungsanlage für HTR-Brenn-
elemente
Jül-1759 (1982)

17th DOE NUCLEAR AIR CLEANING CONFERENCE

SURFACE DEPOSITION OF RADON DECAY PRODUCTS WITH AND WITHOUT ENHANCED AIR MOTION

S.N. Rudnick, E.F. Maher, W.C. Hinds, and M.W. First
Harvard Air Cleaning Laboratory
Boston, MA 02115

Abstract

The effectiveness of fan-induced air motion in reducing airborne activity of short-lived radon decay products was evaluated in a 78-m³ chamber. Observed reductions were as high as 50% for RaA (²¹⁸Po), 79% for RaB (²¹⁴Pb), and 86% for RaC (²¹⁴Bi). Activity Measurements of these nuclides on chamber and fan surfaces, along with airborne activity, were used to calculate material balances. Greater than about 90% of deposited activity was found on chamber surfaces, although areal activity density was higher on fan surfaces. Deposition velocity and diffusional boundary thickness were also determined. When no fans were used, boundary layer thickness was estimated to be 25 times the recoil distance of a RaB atom and, with fans, about 4 times the recoil distance, suggesting that recoiling RaB atoms probably do not play a significant role in the relationship between surface and airborne activity. The results of this study have relevance for all habitable spaces having excessive radon concentration.

Introduction

Engineering strategies to control short-lived radon decay products in buildings or mines can be divided into three types: 1) prevention of radon entry (e.g., sealants, ventilated crawl spaces, and judicious selection of building materials); 2) dilution with outside air directly or through heat exchangers; 3) removal of radon or its decay products from the indoor airspace by various air treatments. Historically, air dilution has been most effective, although not employed for this specific purpose. Recently, it has become less acceptable because of high energy costs for heating and air conditioning dilution air. Research conducted in the present study was directed to a subdivision of strategy 3, removal of radon decay products due to air motion produced by fans.

Fans remove radon decay products from the airspace by causing surface deposition, which is often termed plateout. The primary mechanism causing plateout by fans is diffusion, and although this mechanism is also active when no fans are in use, fan-induced air motion can enhance its importance greatly. Because partitioning of radon decay products between the airspace and surfaces is fundamental to understanding the health hazards associated with radon, experimental data on plateout, as well as on the fate of all radon decay products, are necessary for formulation and verification of a mathematical model.

Plateout due to fan-induced air motion has been reported previously by several investigators.^(1,2,3) Wrenn⁽¹⁾ observed reductions in working level of up to 90% in two uranium mines due to air motion caused by air recirculation rates between 20 and 60/h, far in excess of that which would be used in buildings. Holub⁽²⁾ reported working level reductions of 41% in an experimental chamber when a mixing fan was used. His tests indicated that this reduction was the result of radon decay product deposition on the fan rather than on chamber surfaces. Abu-Jarad⁽³⁾ reported a 28% reduction in working level for an experimental chamber when a mixing fan was operating. Using plastic track etch α -detectors, he compared activities on fan blades and chamber surfaces, before and after treatment, and found that fan deposition accounted for about 2% of activity lost from the airspace. He concluded that enhanced deposition on chamber surfaces was responsible for most of the working level

reduction.

Experimental Methods

Experimental studies were designed to simulate closely conditions occurring in a residence or building. Nonetheless, transient effects, such as time-dependent variations in air infiltration rate or radon intrusion rate, were not studied because experimental results would have been too difficult to analyze. Consequently, all measurements were made after steady-state experimental conditions were attained.

Apparatus

Experiments were made in a chamber having a volume of 78-m³ and surface area of 122 m². This chamber was unfurnished and had a linoleum floor, painted metal walls, and five sealed windows. Air infiltration rates were established by exhausting the requisite airflow through a calibrated venturi flowmeter. Although air was forced to infiltrate through cracks and pores in chamber surfaces, pressure in the chamber was less than barometric pressure by at most 3 mm of mercury. Aerosol particles in the chamber entered with air that infiltrated from adjacent air-conditioned laboratory spaces. Aerosol concentration ranged from 12 to 83 μg/m³ during the experimental program.⁽⁴⁾

Radon (²²²Rn) was generated by bubbling 0.2 L/min of humidified air through a 100-μCi ²²⁶Ra solution. Gas exiting the bubbler passed through a droplet trap and a filter and, then, flowed to a distribution manifold on the floor of the chamber. This arrangement simulated seepage of radon through the floor.

Sampling ports were located in the exhaust duct and in one wall of the chamber. Both ports accepted 50-mm diameter open-faced filter holders, which minimized aerosol sampling losses. Tests made with carbon monoxide released in the chamber as a tracer gas showed that these locations gave representative samples of concentrations in the chamber and confirmed that the chamber air was well mixed.⁽⁴⁾ Air samples for radon were taken from the exhaust duct through a filter into an evacuated 100-cm³ Lucas flask.⁽⁵⁾

Measurement of Radon Decay Product Concentration

Radon decay product concentrations were determined from a 5-minute air sample collected on a Millipore AA membrane filter, which was counted by alpha scintillation after the filter was placed in direct contact with the Ag-activated ZnS-phosphor-coated side of a disposable mylar film (W.B. Johnson and Associates, Montville, N.J.). The mylar film was touching the window of a photomultiplier tube in a light-tight enclosure during the counting period, which started 2 minutes after the end of the sampling period and continued for 30 minutes. Working level and concentrations of RaA, RaB, and RaC were calculated from the counts in three time intervals using the modified Tsivoglou method.⁽⁶⁾

Measurement of Radon Decay Product Surface Activities

Different equipment and procedures were used to measure surface activities of radon decay products on chamber surfaces and on fan parts.

On Chamber Surfaces. Steady-state radon decay product activities on chamber surfaces were measured in the following manner: 47-mm diameter paper or aluminum-foil disks were affixed to various locations on ceiling, floor, and walls and allowed to remain in the chamber for a sufficient time to establish steady-state activities of RaA, RaB, and RaC. The disks were removed one at a time from the chamber; by comparing activities of

successive samples at the same location, we determined that our entry into the chamber had no effect on plateout measurements. The disks were counted under vacuum by alpha-particle spectrometry using a 12.6-cm² silicon surface-barrier detector. Total number of counts under the RaA and the RaC' (²¹⁴Po) alpha peaks during one time interval and total number of counts under the RaC' alpha peak for a later time interval were determined for 4 or more disks removed from various locations. From these 3 counts, the steady-state activities of RaA, RaB, and RaC on the surfaces were estimated using a computer program written for radon decay product airborne concentration⁽⁷⁾ and modified for calculation of surface activity.⁽⁴⁾ No significant differences in areal density were observed when using aluminum-foil or paper disks at the same location, although peak resolution was considerably better with foil. This resolution difference results from higher energy loss of an α particle when escaping the rougher paper surface on its way to the detector, an observation reported by previous investigators.^(8,9)

On Fan Blades and Housing. Steady-state activities on fan blades and fan housing were measured using 6 identical, 75-cm², Ag-activated-ZnS scintillation detectors. Each detector was provided with a protective rigid grill to permit direct contact with surfaces and a 1-mg/cm² aluminized mylar film to shield the photomultiplier tube from room light (model 43-1, Ludlum Measurements, Sweetwater, TX).

Activities on front and back fan blade surfaces and fan housing were measured simultaneously with as many detectors as could be positioned within the first 2 minutes after removing the fan from the chamber. The modified Tsivoglou method,⁽⁶⁾ adapted for calculation of surface activity,⁽⁴⁾ was used to back-calculate steady-state radon decay product activities to the instant when the fans were removed from the chamber.

When measuring deposition on the 51-cm box fan, usually 4 detectors were placed on front and back surfaces of 2 blades out of a total of 14 and another 2 detectors on 2 inside locations of the housing. Three detectors per blade side were used to characterize average activity on 1 of the 4 blades of the 130-cm ceiling fan. Deposition was not uniform with distance along the blade, as shown in Table I.

Table I Relative areal activity density on blade of 130-cm ceiling fan.

Air infiltration rate	Relative areal activity density					
	0.23/h			0.52/h		
Decay product	RaA	RaB	RaC	RaA	RaB	RaC
Position on blade						
Inner third	1.00	1.00	1.00	1.00	1.00	1.00
Middle third	1.30	1.85	1.78	1.20	1.65	1.60
Outer third	1.74	2.30	2.53	1.20	2.00	2.48

Surfaces near the blade tip were found to have up to 2.5 times the areal activity density as those near the inner part of the blades. Similar trends were noted for top and bottom blade surfaces, but as expected, no differences in areal density with position were found when the fan blades were still. The higher activity areal density at the tips of the fan blades was probably due to the thinner boundary layer thickness and to the larger air volume per blade area swept out by the faster moving surface.

Results

The importance of radon decay product plateout was quantified from activity measurements in the air, on chamber surfaces, and on fan parts. These measurements were also used to calculate individual material balances and estimate plateout rates, deposition

velocities, and diffusion boundary layer thicknesses for RaA, RaB, and RaC.

Plateout

Plateout of radon decay products will always occur to some extent. Its importance can be greatly enhanced through air mixing caused by fans.

Without Fans. Measurements of working level (WL) and airborne concentrations of RaA, RaB, and RaC at various air infiltration rates are given in Figure 1. Theoretical curves, shown also in Figure 1 and based on the assumptions of no plateout, spatially uniform steady-state concentrations, and infiltration air free of radon and its decay products, were plotted from Equations 1, 2, 3, and 4⁽⁴⁾:

$$WL = \frac{S\lambda_r}{(\lambda_r+I)(\lambda_a+I)} \left[k_1 + \frac{k_2\lambda_a}{\lambda_b+I} \left(1 + \frac{\lambda_b}{\lambda_c+I} \right) \right] \quad (1)$$

$$C_a = \frac{S\lambda_r\lambda_a}{133.2(\lambda_r+I)(\lambda_a+I)} \quad (2)$$

$$C_b = \frac{C_a\lambda_b}{\lambda_b+I} \quad (3)$$

$$C_c = \frac{C_b\lambda_c}{\lambda_c+I} \quad (4)$$

where

WL = working level (i.e., any combination of RaA, RaB, RaC, and RaC' atoms in one liter of air that will, on decay to Pb-210, release 130,000 MeV of alpha-particle energy), WL

C = radon decay product concentration, pCi/L

S = radon intrusion rate per chamber volume, atoms/(h·L)

I = air infiltration rate (i.e., volumetric flow rate of infiltrating air divided by chamber volume), 1/h

λ = radioactive decay constant ($\lambda_r = 0.00758$, $\lambda_a = 13.7$, $\lambda_b = 1.55$, and $\lambda_c = 2.11$), 1/h

k = dimensional conversion factor ($k_1 = 1.052 \times 10^{-4}$ and $k_2 = 5.908 \times 10^{-5}$), $WL \cdot L/\text{atom}$

r, a, b , and c are subscripts indicating radon, RaA, RaB, and RaC, respectively.

In all cases, the measured concentrations were less than the theoretical curves, a result of plateout on chamber surfaces. Differences, which varied from 8.4 to 26% for WL , 11 to 26% for RaA, 9.1 to 25% for RaB, and 7.4 to 26% for RaC, were larger at lower air infiltration rates, suggesting that longer residence times at lower infiltration rates had a greater effect on plateout than the diffusional boundary layer thickness, which would be expected to be thicker at lower infiltration rates.

With Fans. Reduction in radon decay product concentration resulting from increasing plateout by air mixing was studied using a ceiling fan and a portable box fan. Manufacturer's specifications for these fans are given in Table II.

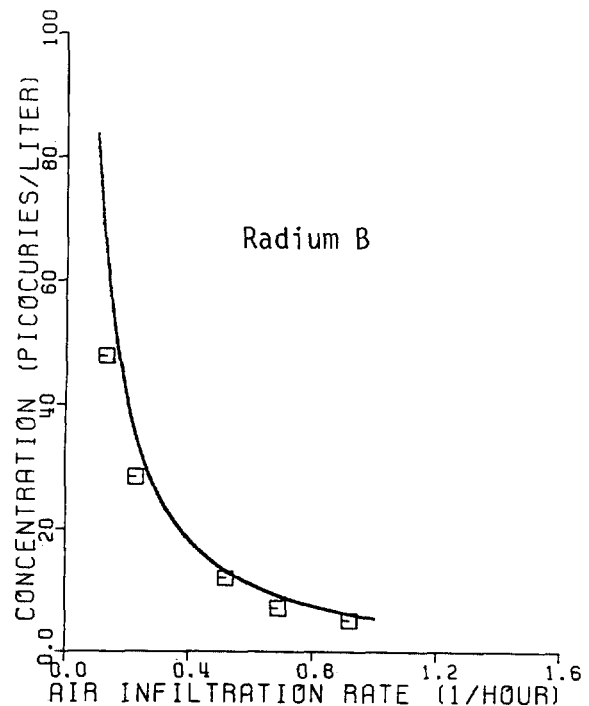
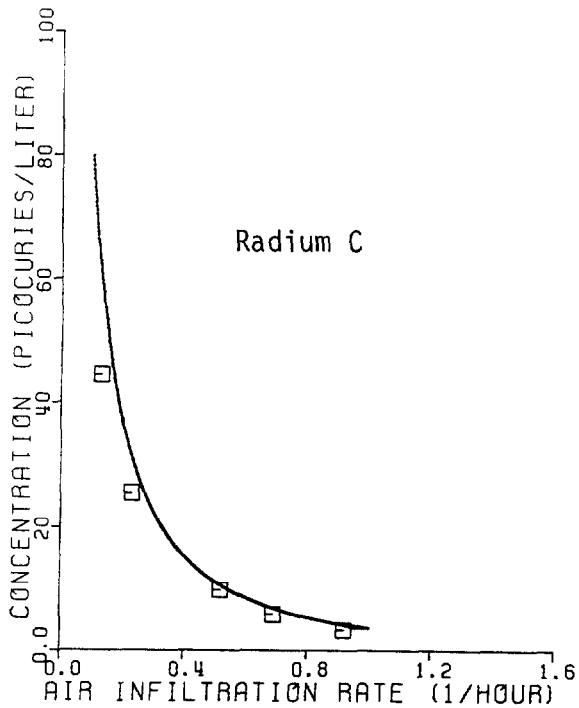
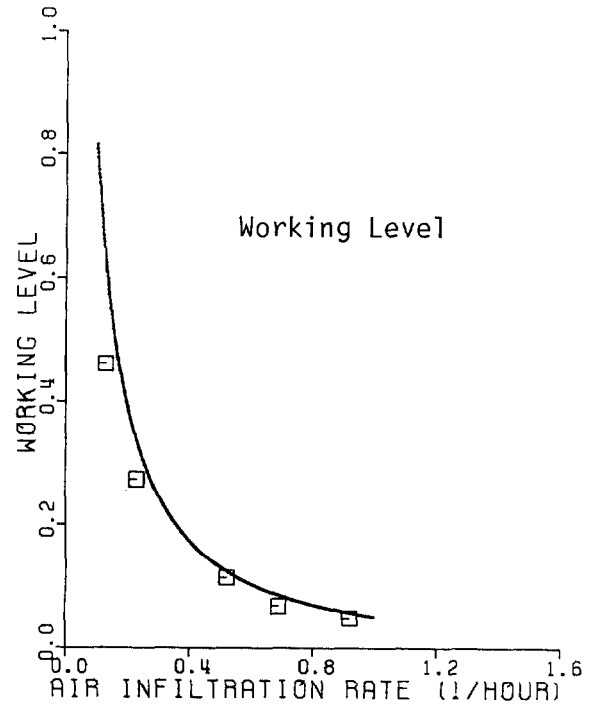
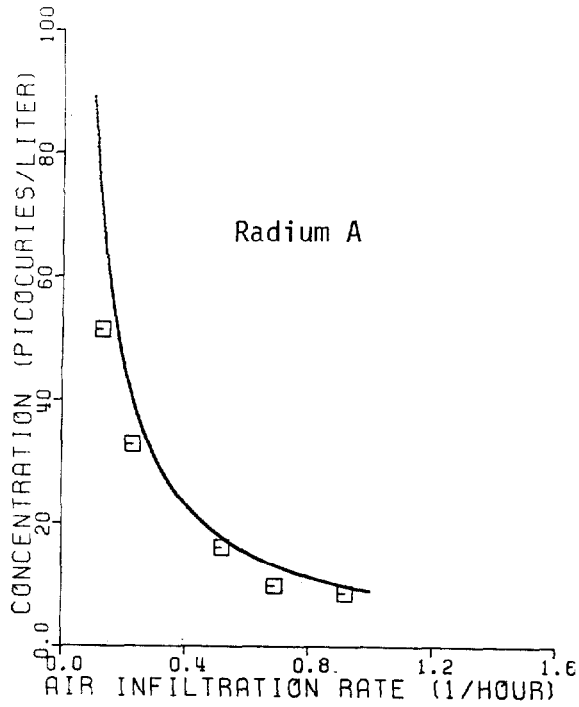


Figure 1 Effect of air infiltration rate on radon decay product concentration with no fans in use. (Square symbols denote experimental data; solid lines denote theoretical curves based on the assumptions of no plateout, spatially uniform steady-state concentrations resulting from decay of 100- μ Ci Ra-226 into 78- m^3 chamber, and radon- and radon-decay-product-free infiltrating air.)

17th DOE NUCLEAR AIR CLEANING CONFERENCE

Table II Manufacturer's fan specifications.

Fan type	51-cm box fan			130-cm ceiling fan	
	11077*			22306-7J*	
Model number					
Setting	High	Medium	Low	High	Low
Airflow rate, m ³ /min**	156	147	136	198	113
Fan speed, rev/min	1000	930	750	200	115
Power consumption, W	185	150	100	155	80

*Hunter Comfort Conditioning Division, Robbins & Myers, Inc., Memphis, TN 38114.

**NEMA method

Figure 2 shows the ratio of radon decay product concentration with a fan to the concentration without a fan versus air infiltration rate. Use of box fans reduced WL by 43 to 76% and concentrations of RaA by 32 to 50%, RaB by 45 to 79%, and RaC by 43 to 86%.

Material Balance Calculations

Steady-state material balance equations for radon, RaA, RaB, and RaC in terms of atoms per unit time are given by Equations 5 through 8. The left side of these equations accounts for entry of radon and its decay products into the chamber, including its airspace and surfaces, and the right side for their exit in the exhausted air and elimination by decay.

For radon,

$$SV + n_r^i VI = n_r VI + N_r \lambda_r \tag{5}$$

where

V = chamber volume (i.e., its airspace volume), L

n_r^i = radon concentration in infiltrating air, atoms/L

N_r = number of airborne radon atoms in the chamber

n_r = radon concentration in exiting air, atoms/L

We assumed that radon adsorption on chamber surfaces was negligible.

Similarly, for RaA, RaB, and RaC,

$$N_r \lambda_r + n_a^i VI = n_a VI + N_a \lambda_a + W_a \lambda_a \tag{6}$$

$$N_a \lambda_a + W_a \lambda_a + n_b^i VI = n_b VI + N_b \lambda_b + W_b \lambda_b \tag{7}$$

$$N_b \lambda_b + W_b \lambda_b + n_c^i VI = n_c VI + N_c \lambda_c + W_c \lambda_c \tag{8}$$

where

n^i = radon decay product concentration in infiltrating air, atoms/L

n = radon decay product concentration in exiting air, atoms/L

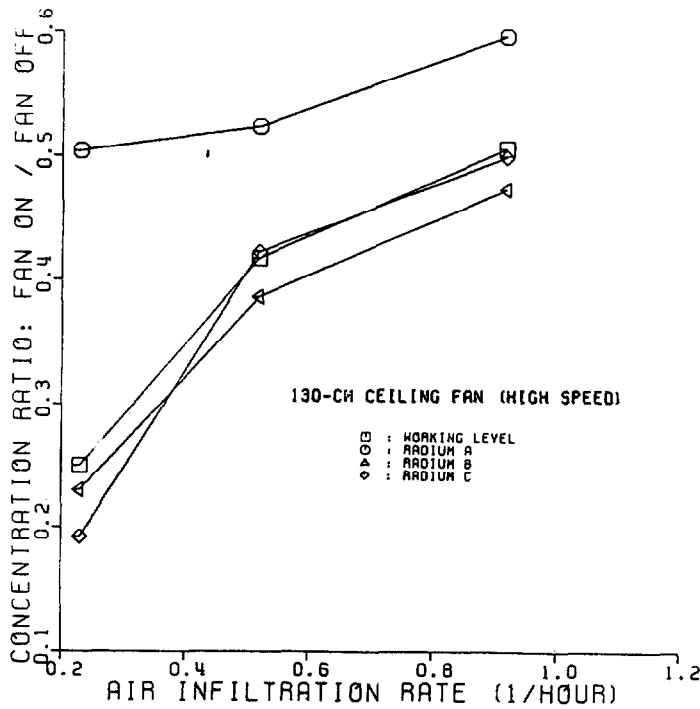
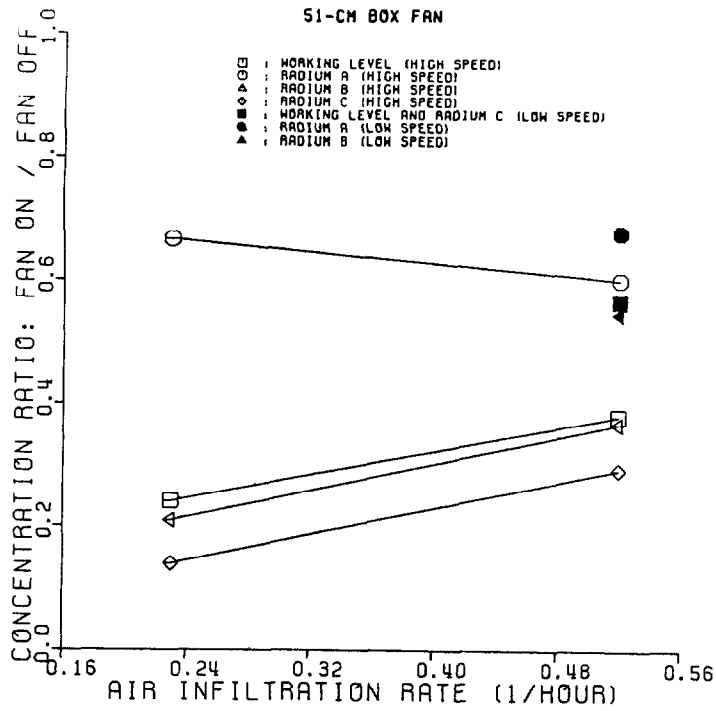


Figure 2 Effect of mixing fans on radon decay product concentration.

17th DOE NUCLEAR AIR CLEANING CONFERENCE

N = number of airborne radon decay product atoms in the chamber

W = number of radon decay product atoms on chamber surfaces

Measurements indicated that infiltration air was free of radon and its decay products (i.e., $n_r^i \approx n_a^i \approx n_b^i \approx n_c^i \approx 0$) and that point-to-point concentrations were fairly uniform and not much different from exhaust concentrations⁽⁴⁾ (i.e., $n \approx N/V$ for radon and its decay products).

Applying these approximations to Equations 5 through 8 and rearranging gives surface activities (i.e., disintegrations per unit time) of each decay product:

$$W_a \lambda_a = SV\lambda_r / (I + \lambda_r) - n_a V(I + \lambda_a) \quad (9)$$

$$W_b \lambda_b = SV\lambda_r / (I + \lambda_r) - n_b V(I + \lambda_b) - n_a VI \quad (10)$$

$$W_c \lambda_c = SV\lambda_r / (I + \lambda_r) - n_c V(I + \lambda_c) - (n_a + n_b) VI \quad (11)$$

The amount of radon decay products on chamber surfaces can also be expressed in terms of potential alpha energy in MeV (\overline{PAE}); i.e.,

$$\overline{PAE} = E_a W_a + E_c (W_a + W_b + W_c) \quad (12)$$

where

E_a = energy of alpha particle from RaA = 6.00 MeV

E_c = energy of alpha particle from RaC' = 7.68 MeV

Inserting Equations 9 through 11 into Equation 12 and rearranging yields

$$\begin{aligned} \overline{PAE} = & [E_a \lambda_a^{-1} + E_c (\lambda_a^{-1} + \lambda_b^{-1} + \lambda_c^{-1})] SV\lambda_r / (I + \lambda_r) \\ & - [n_a + n_b + n_c + n_a I (\lambda_a^{-1} + \lambda_b^{-1} + \lambda_c^{-1}) \\ & + n_b I (\lambda_b^{-1} + \lambda_c^{-1}) + n_c I / \lambda_c] VE_c - (1 + I / \lambda_a) n_a VE_a \end{aligned} \quad (13)$$

The right side of Equations 9, 10, 11, and 13 can be used to calculate activities of radon decay products and potential alpha energy on chamber surfaces. The measured parameters required are air infiltration rates, airspace volume, airborne concentrations of RaA, RaB, and RaC, and radon intrusion rate. If these calculated values are in agreement with measured values of RaA, RaB, and RaC activities and potential alpha energy on chamber surfaces, and the fate of all radon decay products has been confirmed.

Material balance results for 5 tests in which surface measurements were made are shown in Table III for radon decay products and Table IV for potential alpha energy. The amount of radon decay products on chamber surfaces and fan parts are given in Table V. As shown in Table III, measured activity of RaA on all surfaces ranged from 46% to 86% of calculated activities based on Equation 9. The range was 46% to 114% for RaB and 56% to 250% for RaC based on Equations 10 and 11, respectively. Measured potential alpha energy on surfaces, shown in Table IV, ranged from 52% to 116% of calculated amounts based on Equation 13. If the test with two box fans are ignored, this range would narrow to 94% to 116%.

Table III Material balance based on radon decay product activities.

Air Treatment	Air Infiltration Rate, h ⁻¹	Radon Decay Product	Radon Decay Product Activities, μCi (Coef. var. *)		Total Measured	Calculated from Eq. 9-11	Total Measured / Calculated	p-value
			Total Measured	Calculated				
None	0.23	RaA	0.459 (10.7%)	0.536 (36.9%)	0.459	0.536	0.855	0.704
		RaB	0.746 (14.7%)	0.700 (9.73%)	0.746	0.700	1.064	0.726
		RaC	0.826 (8.30%)	0.855 (8.56%)	0.826	0.855	0.965	0.772
None	0.52	RaA	0.132 (30.5%)	0.287 (46.9%)	0.132	0.287	0.459	0.271
		RaB	0.119 (73.7%)	0.172 (31.1%)	0.119	0.172	0.689	0.630
		RaC	0.267 (19.3%)	0.106 (52.1%)	0.267	0.106	2.500	0.035
130-cm ceiling fan (high speed)	0.23	RaA	1.35 (7.60%)	1.81 (5.75%)	1.35	1.81	0.742	<0.003
		RaB	2.40 (9.30%)	2.54 (1.40%)	2.40	2.54	0.943	0.529
		RaC	2.57 (6.20%)	2.63 (1.42%)	2.57	2.63	0.976	0.704
130-cm ceiling fan (high speed)	0.52	RaA	0.528 (12.0%)	0.716 (12.8%)	0.528	0.716	0.736	0.093
		RaB	1.03 (14.7%)	0.900 (3.98%)	1.03	0.900	1.143	0.407
		RaC	1.09 (8.60%)	0.857 (4.35%)	1.09	0.857	1.270	0.021
Two 51-cm box fans (high speed)	0.52	RaA	0.494 (15.3%)	0.693 (13.1%)	0.494	0.693	0.712	0.093
		RaB	0.466 (28.3%)	1.01 (3.63%)	0.466	1.01	0.458	<0.003
		RaC	0.570 (13.5%)	1.01 (3.61%)	0.570	1.01	0.561	<0.003

* Coefficient of variation for counting error in percent is given parenthetically.

Table IV Material balance based on potential alpha energy.

Air Treatment	Air Infiltration Rate, h ⁻¹	Potential Alpha Energy MeV (Coef. var.*)		Total Measured / Calculated	p-value
		Total Measured	Calculated from Eq. 13		
None	0.23	9.53x10 ⁸ (8.37%)	9.49x10 ⁸ (6.65%)	1.005	0.960
None	0.52	2.25x10 ⁸ (28.0%)	2.03x10 ⁸ (23.6%)	1.105	0.787
130-cm ceiling fan (high speed)	0.23	3.00x10 ⁹ (5.54%)	3.19x10 ⁹ (1.02%)	0.941	0.271
130-cm ceiling fan (high speed)	0.52	1.27x10 ⁹ (8.61%)	1.10x10 ⁹ (2.90%)	1.156	0.134
Two 51-cm box fans (high speed)	0.52	6.49x10 ⁸ (14.6%)	1.25x10 ⁹ (2.59%)	0.517	<0.001

* Coefficient of variation for counting error in percent is given parenthetically.

Table V Distribution of radon decay products between chamber surfaces and fan.

Air Treatment	Air Infiltration Rate, h ⁻¹	Radon Decay Product	Deposition on Chamber Surfaces μCi (% of total) ^a	Deposition on Fan Blades μCi (% of total) ^a	Deposition on Fan Box Housing μCi (% of total) ^a	Total Deposition μCi
None	0.23	RaA	0.453 (98.7%)	0.00575 (1.3%) ^b	-	0.459
		RaB	0.739 (99.0%)	0.00723 (1.0%) ^b	-	0.746
		RaC	0.820 (99.2%)	0.00624 (0.8%) ^b	-	0.826
None	0.52	RaA	0.131 (99.4%)	0.000786 (0.6%) ^b	-	0.132
		RaB	0.118 (99.5%)	0.000531 (0.5%) ^b	-	0.119
		RaC	0.226 (99.6%)	0.00116 (0.4%) ^b	-	0.267
130-cm Ceiling Fan (high speed)	0.23	RaA	1.30 (96.6%)	0.0459 (3.4%)	-	1.35
		RaB	2.32 (96.7%)	0.0802 (3.3%)	-	2.40
		RaC	2.48 (96.5%)	0.0902 (3.5%)	-	2.57
130-cm Ceiling Fan (high speed)	0.52	RaA	0.515 (97.6%)	0.0128 (2.4%)	-	0.528
		RaB	0.100 (97.2%)	0.0290 (2.8%)	-	1.03
		RaC	0.105 (96.5%)	0.0380 (3.5%)	-	1.09
Two 51-cm Box Fans (high speed)	0.52	RaA	0.442 (89.4%)	0.0228 (4.6%)	0.0294 (6.0%)	0.494
		RaB	0.414 (88.8%)	0.0296 (6.4%)	0.0224 (4.8%)	0.466
		RaC	0.513 (90.0%)	0.0383 (6.7%)	0.0182 (3.2%)	0.570

^a Percentage of total deposition is given parenthetically

^b Deposited on stationary blades of 130-cm ceiling fan

Measured and calculated values of activities and potential alpha energy on surfaces had an error attributable to counting. Counting error associated with calculated activities and potential alpha energy was traceable to measurements of airborne radon decay product concentrations used in Equations 9, 10, 11, and 13. We assumed that the number of counts measured followed a Poisson distribution and that counting error could be estimated using the standard error propagation equation.

To determine whether differences between measured and calculated values could be explained solely by counting errors, we tested the null hypothesis that the difference is zero. We assumed that the difference was distributed normally with a variance equal to the sum of the counting-related variances of measured and calculated values. Counting-related variances are given in Tables III and IV in terms of the coefficient of variation. Entries in the last column of these tables are p-values, the probability of erroneously rejecting the null hypothesis. Values of p less than 0.05 indicate significance at the 95% confidence level; i.e., the difference between measured and calculated values of activity or potential alpha energy cannot be explained solely by counting errors. Alternative explanations for material balance discrepancies (i.e., $p < 0.05$), other than counting error, are uncertainties in radon source activity, air infiltration rate, sampling rate, and detector efficiency, as well as nonuniform airborne concentrations in the chamber (i.e., deviations from a well-mixed model) and nonuniform radon decay product deposition on chamber surfaces. Because activity measurements were made on only a small fraction of the surface area of the chamber, nonuniform deposition is probably the primary cause for material balance discrepancies.

For 15 material balances shown in Table III, counting error can account solely for the differences between measured and calculated values in 10 cases. For 5 material balances shown in Table IV, 4 of the differences can be explained by counting error.

Plateout Parameters for Radon Decay Products

Various parameters, such as plateout rate, deposition velocity, and boundary layer thickness, can be used to quantify plateout of radon decay products. These parameters are useful for mathematical modeling and for comparison purposes.

Plateout Rates. The plateout rate of RaA, P_a , is defined as the number of equivalent chamber volumes of RaA that are completely deposited on chamber surfaces per unit time. An equivalent chamber volume of RaA is equal to N_a , the number of RaA atoms airborne in the chamber, whether attached to particles or not. Thus, the number of atoms of RaA plating out per unit time is equal to $P_a N_a$. At steady state, $P_a N_a$ is also equal to the number of atoms of RaA on chamber surfaces that decay per unit time (i.e., surface activity of RaA). Thus,

$$P_a = W_a \lambda_a / N_a \quad (14)$$

As shown schematically in Figure 3, evaluation of the plateout rate for RaB is more complicated than for RaA because of two reasons: (1) when atoms of RaA on chamber surfaces decay, they become RaB atoms; and (2) they also recoil when the alpha particle is emitted and may therefore become resuspended. The steady-state material balance for RaB on chamber surfaces is given by Equation 15:

$$P_b N_b + W_a \lambda_a = W_b \lambda_b + W_a \lambda_a R \quad (15)$$

where R is the fraction of RaA atoms on chamber surfaces that, upon decay to RaB, become resuspended into the chamber airspace, which is assumed to be well mixed. Evaluation of R requires experiments that we did not conduct, and as far as we know, R has never been measured for conditions resembling a building or a mine. To overcome this deficiency, we defined P'_b as a net plateout rate of RaB; i.e.,

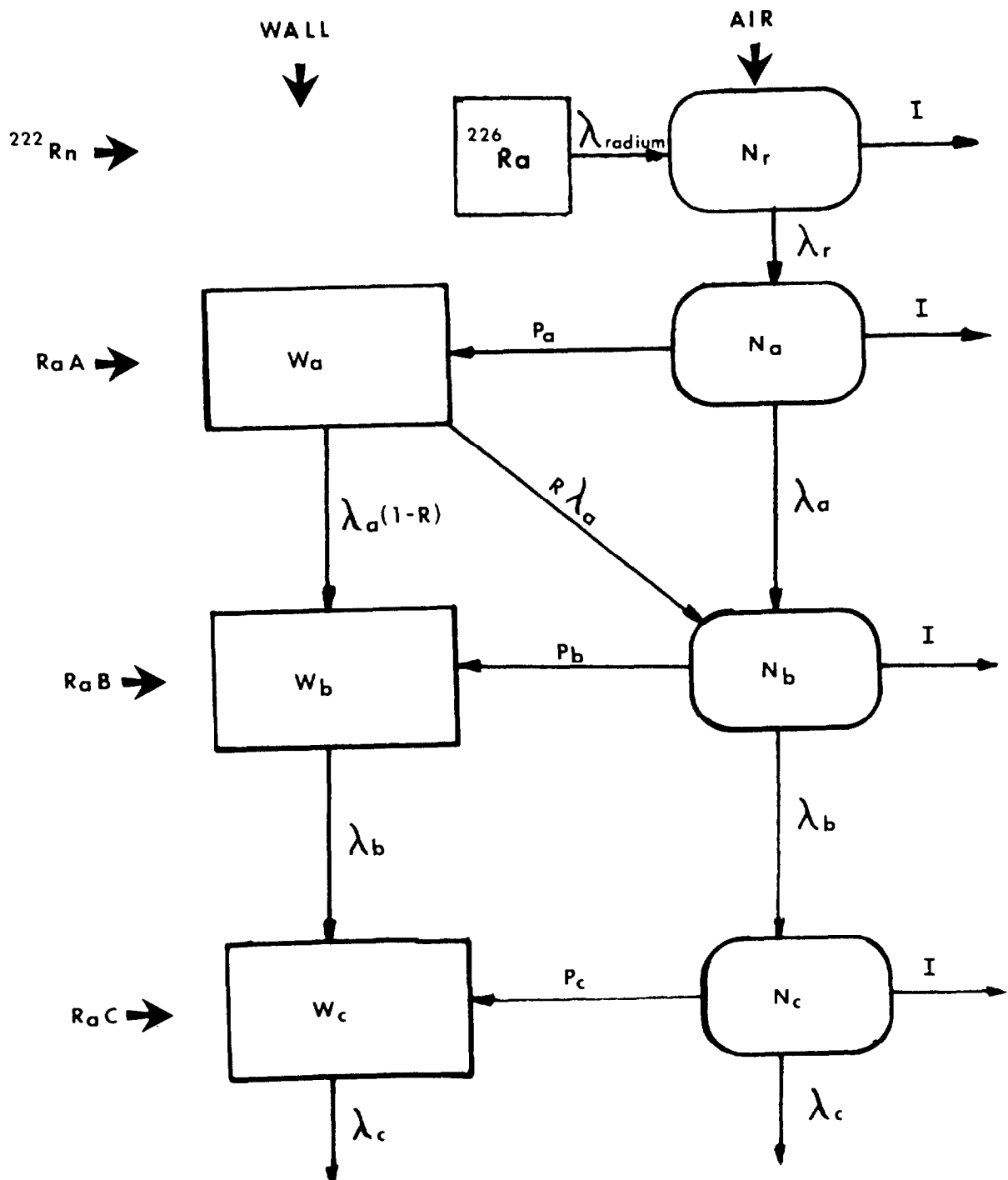


Figure 3 Schematic chart showing model for fate of radon decay products.

$$P'_b = (P_b N_b - W_a \lambda_a R) / N_b \quad (16)$$

Thus,

$$P'_b = (W_b \lambda_b - W_a \lambda_a) / N_b \quad (17)$$

One expects R to take on values between 0 and 0.5 because half the atoms recoil into the surface. When $R = 0$, $P'_b = P_b$ and when $R = 0.5$, $P'_b = P_b - 0.5 W_a \lambda_a / N_a$. The plateout rate for RaC can also be obtained from a material balance:

$$P_c = (W_c \lambda_c - W_b \lambda_b) / N_c \quad (18)$$

Beta recoil from decay of RaB to RaC and RaC to RaC' was assumed to be unlikely.⁽¹⁵⁾

Using Equations 14 through 18, we calculated plateout rates, which are summarized in Table VI. For W_a , W_b , and W_c , we used the average of measured and calculated values given in Table III; although this is somewhat arbitrary, the average should be a good estimate of true surface activities because material balances must be satisfied. The plateout rate of RaB (P_b) was calculated assuming $R = 0$ or $R = 0.5$; the correct value for P_b should lie somewhere between these two calculated values. Coefficients of variation due to counting errors are also given in Table VI. Coefficients of variations for RaB and RaC tend to be much larger than for RaA, reflecting the statistical penalty incurred when two large numbers are subtracted and the difference is small. For this reason, measured plateout rates for RaA are probably more accurate than for RaB and RaC. P_a can be more accurately determined also because it is larger than P_b or P_c inasmuch as more RaA is unattached to particles than RaB or RaC and most of the plateout is attributable to unattached species. By the same reasoning, P_b should be greater than P_c . With the exception of the no-air-treatment test at an infiltration rate of 0.52/h, $P_a > P_b > P_c$, as expected.

Deposition Velocities. Deposition velocity is defined as the flux of atoms to the chamber surfaces, i.e., atoms per unit time per unit area, divided by the concentration in the chamber airspace, which is assumed to be well mixed. Inasmuch as deposition velocity is a measure of how rapidly these atoms move from the well-mixed airspace to chamber surfaces, different deposition velocities would be obtained for atoms attached and unattached to particles. Because unattached atoms have a deposition velocity that is about 500 greater than attached atoms⁽¹⁰⁾, we assumed that only the former play a significant role in plateout. Thus,

$$v_a = P_a V / A f_a \quad (19)$$

where

v_a = deposition velocity of unattached RaA atoms, m/s

A = area of chamber surfaces

f_a = unattached RaA atoms/total RaA atoms

Measurements using a diffusion battery indicated that $f_a \approx 1/3$ in our experimental chamber.⁽⁴⁾ Approximate deposition velocities for unattached RaA atoms were calculated from Equation 19 and are given in Table VII.

Boundary Layer Thickness. In a very simplistic model for the distribution of radon decay products in a chamber, concentrations are assumed to be spatially uniform except in a very thin boundary layer in which they decrease linearly to zero at the surface. If plateout of unattached RaA atoms is a molecular diffusion process, then in the boundary layer

Table VI Calculation of plateau rate.

AIR TREATMENT	AIR INFILTRATION RATE, h^{-1}	RaA	RaB		RaC
			R=0.5 ^b	R=0 ^b	
NONE	0.23	2.57 (21.8%)	0.346 (17.5%)	0.166 (53.4%)	0.141 (70.1%)
NONE	0.52	2.61 (35.6%)	0.0680 (15.3%)	-0.109 (135%)	0.130 (155%)
130-cm ceiling fan (high speed)	0.23	16.1 (8.9%)	4.91 (9.2%)	2.61 (16.2%)	0.690 (107%)
130-cm ceiling fan (high speed)	0.52	12.4 (15.6%)	2.69 (14.5%)	1.40 (28.6%)	0.000401 (1.321%)
Two 51-cm box fans (high speed)	0.52	11.4 (15.8%)	2.38 (19.3%)	0.780 (63.1%)	0.00351 (1.58%)

^aCoefficient of variation for counting error is given parenthetically

^bResuspension fraction R is unknown, but is between 0.0 and 0.5

Table VII Deposition velocity and boundary layer thickness for RaA.

Air Treatment	Air Infiltration rate, h^{-1}	Deposition Velocity (cm/s)	Diffusion Boundary Layer Thickness (mm)
None	0.23	0.14	3.6
None	0.52	0.14	3.6
130-cm Ceiling Fan (High Speed)	0.23	0.86	0.58
130-cm Ceiling Fan (High Speed)	0.52	0.66	0.75
Two 51-cm Box Fans (High Speed)	0.52	0.61	0.82

Fick's first law will be obeyed, i.e.,

$$J = -D_a \frac{\partial C_a}{\partial l} \quad (20)$$

where

J = flux of unattached RaA atoms to chamber surfaces, atoms/(s·m²)

D_a = diffusion coefficient for unattached RaA atoms, m²/s

C_a = concentration of unattached RaA atoms, atoms/m³

l = distance from the surface, m

Combining Equations 19 and 20 and incorporating the assumptions yields

$$L_a = D_a / V_a \quad (21)$$

where L_a is the diffusion boundary layer thickness for unattached RaA atoms.

Boundary layer thicknesses for RaA, based on $D_a = 0.05$ cm²/s,⁽¹¹⁾ are summarized in Table VII. Boundary layer thicknesses for RaB and RaC were not calculated because their measured plateout rates are not believed to be accurate. Deposition velocity and diffusion boundary layer thickness for unattached RaB and RaC, however, would be expected to be approximately equal to those for RaA.

Conclusions and Summary

In a 78-m³ chamber, observed reductions in airborne activity caused by air motion induced by a 130-cm ceiling fan were as high as 50% for RaA, 77% for RaB, 81% for RaC, and 75% for *WL*; with a 51-cm box fan, reductions were 40% for RaA, 79% for RaB, 86% for RaC, and 76% for *WL*. Although these reductions are roughly comparable, the ceiling fan has significant advantages: it consumes less energy than the box fan, is considerably quieter, is probably better designed to operate continuously for many years, and produces less noticeable air motion. The manufacturer claimed that the ceiling fan can be used profitably all year round; i.e., by altering the direction of rotation or pitch of the blades, it can be used to "reduce air conditioning cost during the cooling season and reduce wasteful heat stratification during the heating season."⁽¹²⁾ Use of ceiling fans in the winter, however, tends to make a residence feel colder except possibly for buildings using local heat sources or having very high ceilings.⁽¹³⁾

To determine the fate of radon decay products, a material balance was calculated based on measurements of decay product activities on chamber surfaces, on the fan, in the airspace, and in exiting air. Less than 7% of the surface deposition of radon decay products took place on fan blades or fan housing, as shown in Table V. Holub et al.⁽²⁾ found deposition on a fan, but none on walls, when conducting similar experiments. The reason for these contradictory results can be explained as follows: the surface area of a fan is significantly less than that of walls, and, therefore, areal activity density on a fan could be many times higher. Thus, the relative external activity on the fan measured by the beta-gamma detection system of Holub et al. may have been in a measurable range with their equipment, whereas the wall activity was not. Holub⁽¹⁴⁾ found no activity on the fan when he replaced his nichrome-wire condensation nuclei generator with a different type of generator. He suggested that the activity he measured on the fan in his original experiments was due to the charged state of the condensation nuclei.⁽¹⁴⁾

17th DOE NUCLEAR AIR CLEANING CONFERENCE

Deposition velocities for unattached radon decay products were found to be 0.14 cm/s when no fans were used and between 0.61 and 0.86 cm/s with fans; boundary layer thicknesses for unattached decay products were 3.6 mm without fans and between 0.58 and 0.82 mm with fans. The likelihood of recoil-caused resuspension of a radon decay product atom into the well-mixed airspace can be estimated by comparing the boundary layer thickness and the stopping distance of a recoiling RaB atom. When the boundary layer thickness is much larger than the stopping distance, recoil can be neglected, whereas if the opposite is true, resuspension must be taken into account. When they are about the same, the importance of recoil is less clear. The stopping distance in air of a recoiling RaB atom has been reported to be equal to about 0.1 mm.^(8,15) This is about one quarter the boundary layer thickness calculated for those tests in which fans were used and about one twenty-fifth the boundary layer thickness when no fans were in operation. Thus, recoil probably did not play a significant role in the interaction of airborne and surface activity of RaB under the conditions of our experiments, although special tests are necessary to validate this speculation.

Acknowledgement

This work was supported in part by the United States Environmental Protection Agency Contract No. 68-01-6250, Ronald Bruno, project officer.

References

1. Wrenn M.E., Eisenbud M. and Costa-Ribeiro C., "Reduction of radon daughter concentrations in mines by rapid mixing without makeup air," *Health Phys.* 17:405 (1969).
2. Holub R.F., Drouillard R.F., Ho W., Hopke P.K., Parsley R. and Stukel J.J., "The reduction of airborne radon daughter concentration by plateout on an air mixing fan," *Health Phys.* 36:497 (1979).
3. Abu-Jarad F. and Fremlin J.H., "The effect of a fan in reducing the concentration of the radon daughters inside a room by plate-out to the surface of the wall using plastic α -detectors," *Health Phys.* 42:82 (1982).
4. Rudnick S.N., Hinds W.C., Maher E.F., Price J.M., Fujimoto K., Gu F. and First M.W., "Effect of indoor air circulation systems on radon decay product concentration," Final Report for U.S.E.P.A. Contract No. 68-01-6050, Harvard University School of Public Health, Boston, MA (25 February 1982).
5. Lucas H.F., "Improved low-level alpha-scintillation counter for radon," *Rev. Sci. Instrum.* 28:680 (1957).
6. Thomas J.W., "Measurement of radon daughters in air," *Health Phys.* 23:783 (1972).
7. Kerr G.D., "Measurement of radon progeny concentrations in air by alpha-particle spectrometry," Oak Ridge ORNL-TM-4924 (1975).
8. Busigin A., van der Vooren A.W. and Philips C.R., "Collection of radon daughters on filter media," *Envir. Sci. Technol.* 14:533 (1980).
9. Shreve J.D., Jr. and Cleveland J.E., "Effects of depressing attachment ration of radon daughters in uranium mine atmosphere," *Amer. Ind. Hyg. Assoc. J.* 33:304 (1972).

17th DOE NUCLEAR AIR CLEANING CONFERENCE

10. Porstendorfer J., Wicke A. and Schraub A., "The influence of exhalation, ventilation and deposition processes upon the concentration of radon (^{222}Rn), Thoron (^{220}Th) and their decay products in room air," *Health Phys.* 34:465 (1978).
11. Raabe O.G., "Concerning the interactions that occur between radon decay products and aerosols," *Health Phys.* 17:177 (1969).
12. Robbins & Myers, Inc., Hunter Division, Manufacturer's literature provided to retailers, Memphis, TN (1981).
13. Consumer's Union, "Summer cooling," *Consumer Reports*, 47:350 (July 1982).
14. Holub R.F., private communication to S. Rudnick at EPA International Meeting on Radon and Radon Progeny Measurement, Montgomery, AL (27-28 August 1981).
15. Jonassen N. and McLaughlin J.P., "The effect of RaB recoil losses on radon daughter measurements," *Health Phys.* 80:234 (1976).

DISCUSSION

YOUNG: Has the use of aerosol additions with subsequent filtration with high efficiency filters been used to selectively remove radon and daughter products from process streams or ventilation systems:

FIRST: We also included that aspect in our studies. I did not report on that today because it is going to be published in Health Physics in an issue devoted exclusively to radon and decay products. We did find, of course, that decay products seek any surface. Once you put in aerosols, or allow aerosols to come in, you get a large fraction attached to particles. We performed studies using diffusion batteries whereby we could remove the unattached radon decay products and get the attached out the other end in pretty pure form. We related the results to particle size and to particle numbers and ended up by having a rather serious disagreement among ourselves as to whether it was better to have more particles or whether it was worse from the standpoint of health. We looked at where the radon decay products would deposit if they were unattached. Some think they may go deep into the lungs. My impression from the diffusion constants that we worked with is that they probably would not get very far down before they would deposit by diffusio-phoresis, whereas small particles would go down deep into the alveola spaces. Which is worse from the standpoint of lung cancer is a matter of some debate in the literature. I think it is still up in the air.

YOUNG: I wasn't thinking primarily in terms of stripping decay products from the air in homes or business buildings. I was thinking more about process systems, or where you want to remove radon selectively. It seems like the utilization of aerosols or downstream filters might be one technique of doing it.

FIRST: We also did filter studies. A HEPA filter strips unattached radon daughter products out of the air at 100% efficiency with one passage but you end up with the remaining radon in the air.

ROUYER: According to your study, what do you recommend as the most effective means to decrease working level in insulated buildings? Is it to put fans and increase plateout, or is it to increase the ventilation rate?

FIRST: The easiest and simplest thing to do is to increase the ventilation rate. Almost everywhere, it was never a problem in buildings and residences until we started conserving energy and tightened up the buildings so that there was little natural or mechanical air exchange. Proposals have been made to use heat exchangers so that one can continue to ventilate buildings, but recover some of the heat (or some of the air conditioning) in the exhausted air. That is a very inefficient way of recovering heat because the temperature differential will be very small and one does not get much heat recovery for the large amount of equipment that must be purchased and installed. In addition, you have to expend energy for blowers, motors, and so on. We were looking for simple ways that wouldn't cost anything, wouldn't take up any space, and wouldn't require any

17th DOE NUCLEAR AIR CLEANING CONFERENCE

maintenance. One of the ways you can do that, for example, is to greatly increase the surface area in a room, but this is very awkward. However, if you have a hot air heating system, you can fill the ducts with egg crate separators and this will impose almost no added resistance, but will give a many-fold surface area increase and you can strip out decay products by diffusion very nicely. That was another of the things we looked at but did not report on in this paper.

FORMATION AND CHARACTERIZATION OF FISSION-PRODUCT AEROSOLS
UNDER POSTULATED HTGR ACCIDENT CONDITIONS

I. N. Tang and H. R. Munkelwitz
Brookhaven National Laboratory
Upton, N. Y. 11973

Abstract

The paper presents the results of an experimental investigation on the formation mechanism and physical characterization of simulated nuclear aerosols that could likely be released during an HTGR core heat-up accident. Experiments were carried out in a high-temperature flow system consisting essentially of an inductively heated release source, a vapor deposition tube, and a filter assembly for collecting particulate matter. Simulated fission products Sr and Ba as oxides are separately impregnated in H451 graphite wafers and released at elevated temperatures into a dry helium flow. In the presence of graphite, the oxides are quantitatively reduced to metals, which subsequently vaporize at temperatures much lower than required for the oxides alone to vaporize in the absence of graphite. A substantial fraction of the released material is associated with particulate matter, which is collected on filters located downstream at ambient temperature. The release and transport of simulated fission product Ag as metal are also investigated. Electron microscopic examinations of the collected Sr and Ag aerosols show large agglomerates composed of primary particles roughly 0.1 μm in diameter.

I. Introduction

The potential evolution of substantial amounts of radioactive aerosols as a consequence of high-temperature vaporization of nuclear materials during a reactor accident is a major consideration in reactor safety analysis. In an earlier study (1), the rate and extent of aerosol formation were reported for HTGR core graphite heated up to 1600°C in either a dry or moist helium. It was shown that particles in the Aitken nuclei size range were formed with initial concentrations as high as 10^7 particles per cm^3 . Since airborne particles at high concentrations readily serve as condensation or adsorption sites for gaseous species, it would be expected that, under appropriate conditions, the presence of aerosol particles could greatly facilitate the gas-phase transport of vaporized fission products.

In the present paper, we report the results of an investigation concerning the release and transport of simulated fission products Ag, Sr and Ba as particulate matter. Although extensive research efforts have been expended during the past fifteen years or so, both in the United States and abroad, on the formation and characterization of radioactive aerosols pertaining to LWR and LMFBR safety (2,3), only meager consideration has been given to the potential aerosol problems in HTGR safety (4). The results of the present study show that fission product transport via aerosols is an important safety problem to be seriously considered in HTGR accident analyses.

II. Experimental Procedure

A high-temperature flow apparatus, shown schematically in Figure 1, was constructed. Basically, it consisted of a quartz tube inside which a graphite sample was heated inductively in flowing dry helium. A filter assembly was located some distance downstream from the heated release source. The quartz tube had an enlarged section (8 cm dia. x 40 cm length) immediately above the heated sample region for effective deposition of condensable vapor species on the walls. Fission products

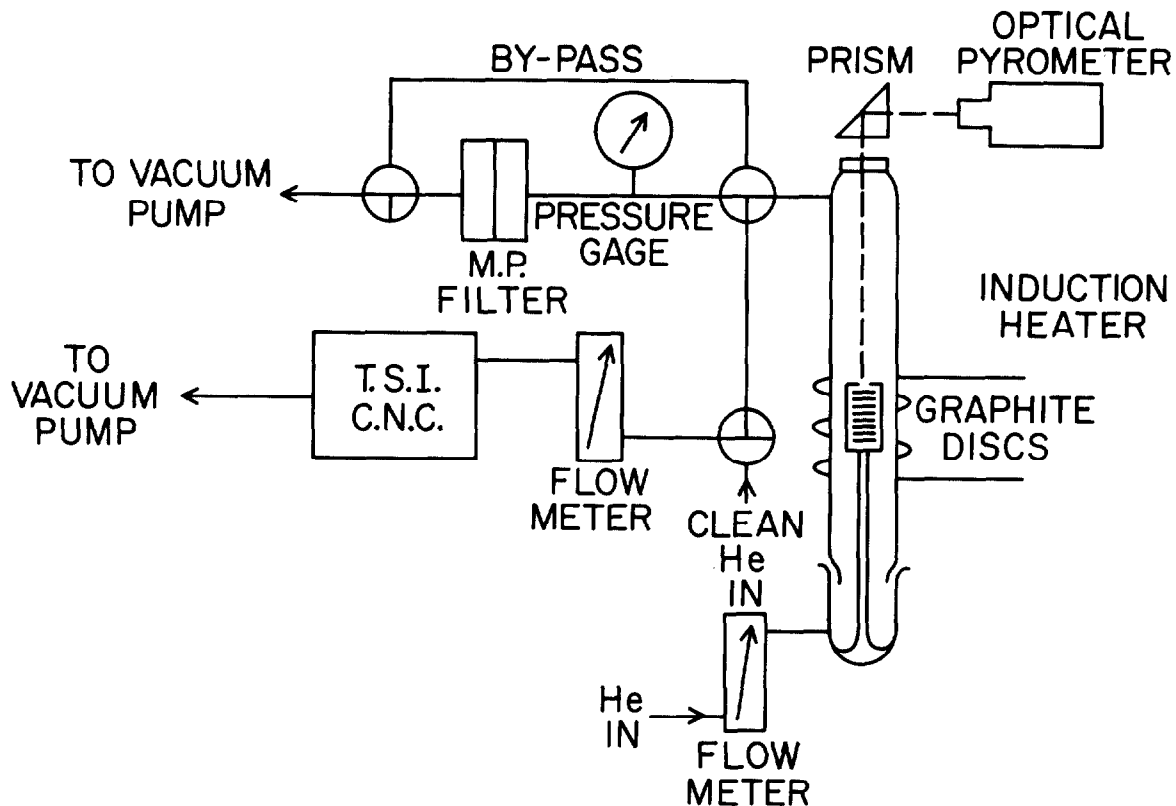


Figure 1. Schematic Diagram of Fission Product Transport Apparatus

associated with particles passed through the vapor deposition section and were subsequently collected on a $0.2\ \mu\text{m}$ filter (Fluoropore or Nucleopore) placed in the filter assembly. The quantity of the collected material was analyzed by atomic absorption.

The simulated fission products Sr and Ba were initially in the form of nitrate, whereas metallic Ag, except otherwise indicated, was used in the experiments. A typical experiment with Sr was conducted in the following manner. Thin wafers (2 mm thickness x 2 cm diameter) of H451 graphite were first dried at 150°C in a vacuum oven to a constant weight. The preweighed wafers were then placed in a glass vessel, which was evacuated and back-filled with an aqueous $\text{Sr}(\text{NO}_3)_2$ solution of predetermined concentration. After an overnight soak, the wafers were removed from the vessel and dried in the vacuum oven to a constant weight. The final weights were noted. The amount of $\text{Sr}(\text{NO}_3)_2$ salt absorbed in the pore structure of the graphite was then calculated from the weights before and after impregnation for each wafer.

The $\text{Sr}(\text{NO}_3)_2$ impregnated wafers were then enclosed in an H451 graphite crucible having a 3 mm-diameter sight hole on its cover for temperature monitoring. The optical path (sight glass and prism) and pyrometer were calibrated together for temperature measurement using foils of gold, silver, palladium, nickel and platinum, whose melting points are accurately known. In later experiments, however, the wafers were simply stacked together and mounted on a graphite pedestal.

The assembled source was then heated inductively in flowing helium, with the filter assembly bypassed, to a temperature of about 1100°C at which $\text{Sr}(\text{NO}_3)_2$ is converted to SrO according to the following reaction:



After allowing a sufficient time for conversion (usually 30 min.), the filter was valved back to the gas stream. The sample temperature was then increased to a pre-determined level and held constant during a sampling period. At the conclusion of the sampling period, the exposed filter was removed and immediately replaced with a new filter before the temperature was raised again. Occasionally, the filter assembly was left in the gas stream during the initial heating period to ascertain whether or not Sr was released during the conversion process. In no instance was a significant amount of Sr found. When desired, a small flow (100 cc/min.) could be diverted into a continuous-flow condensation nuclei counter for monitoring the particle concentrations of the gas stream.

III. Results and Discussion

Vaporization Mechanism for Ag, Sr and Ba

Both $\text{Sr}(\text{NO}_3)_2$ and $\text{Ba}(\text{NO}_3)_2$ decompose at $\sim 1100^\circ\text{C}$ to form respective oxides, which are stable refractory material having a high melting point and low vapor pressures at moderate temperatures. Electron probe microanalysis (5) has shown that fission product Sr and Ba form ceramic oxides in irradiated oxide fuel kernels. Fission product Ag, on the other hand, is present in the fuel kernels as metal since it is not stable in its oxide form at temperatures as low as 300°C . Some of the relevant physical properties are given in Table I for Ag, SrO, and BaO, along with the approximate release temperatures observed for each species in the presence of graphite.

Table I

Selected Physical Properties

<u>F.P.</u>	<u>m.p., °C</u>	<u>b.p., °C</u>	<u>Observed* Release Temp., °C</u>	<u>Vapor Pressure at Release Temp, torr</u>
Ag	961	2212	~1100	~0.04
SrO	2430	~3000	~1250	~ 1.3×10^{-7}
BaO	1923	~2000	~1500	~ 1×10^{-3}

* In presence of graphite

The release temperatures given in Table I for Ag, SrO and BaO were derived from a series of experiments in which the simulated fission products were each released from a heated H451 graphite source into dry helium flowing at 2.5 l/min. The material collected on filter at each temperature was analyzed and the amount was converted into percent of the initial fission product loading as element. A summary of the results is shown in Figure 2, where cumulative percentage of the material collected as particulate matter in each experiment was plotted vs. release temperatures. The steepest portion of the release curve was taken as a rough estimation of the release temperature for the fission product under investigation.

The vapor pressures of the two oxides at the release temperatures, as shown in the last column of Table I, are rather low for vaporization to take place significantly. Thermodynamic considerations, however, indicate that chemical reactions of the oxides with graphite could proceed to reduce the oxides to the metallic state, which would then vaporize at relatively low temperatures. In the case of SrO, for example, the overall reaction could be as follows:

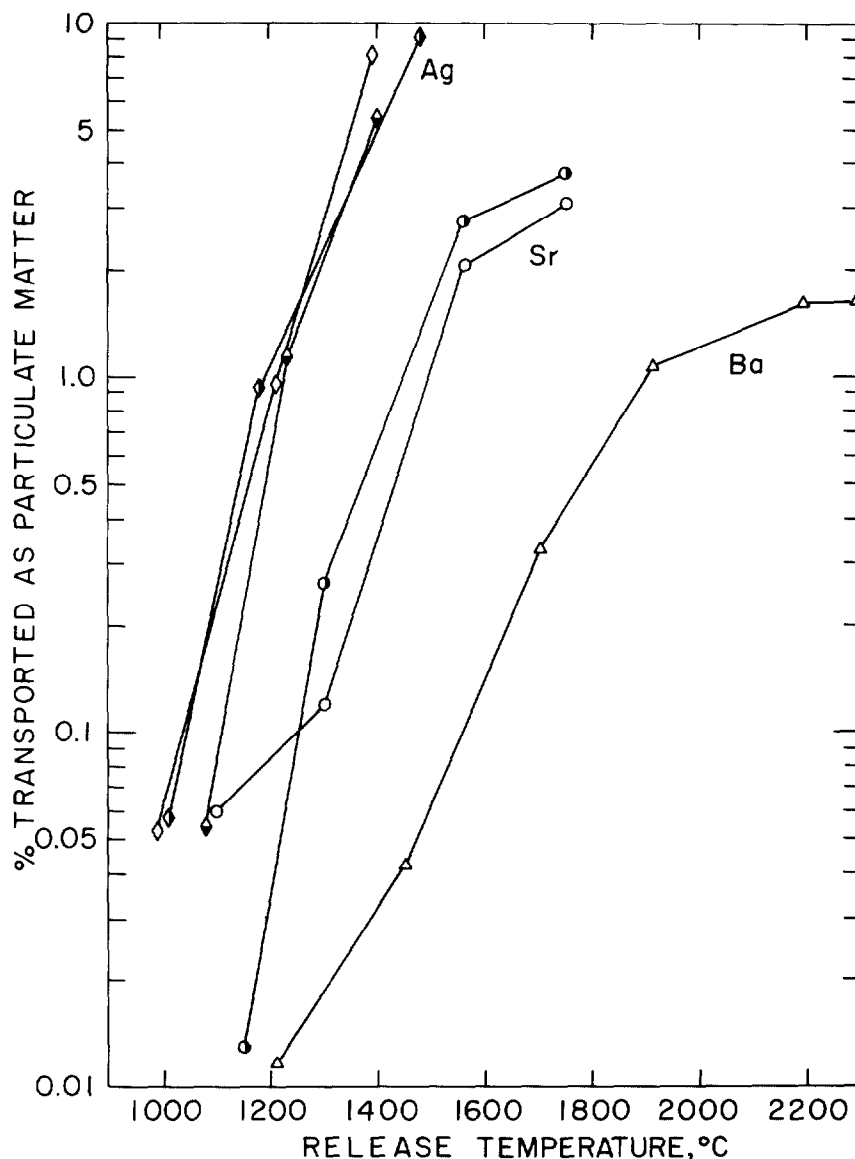


Figure 2. Particulate Transport as a Function of Source Temperature



where the letter in the parenthesis indicates the state of substance being either solid or gas. The thermodynamic equilibrium of Reaction (2) may be represented by

$$P_{\text{CO}} \cdot P_{\text{Sr}} = K_p = e^{-\Delta G^\circ / RT} \quad (3)$$

where the activity of a solid substance is taken as unity, K_p is the equilibrium constant, ΔG° is the Gibb's free energy of reaction, and R is the gas-law constant. A computation of the equilibrium partial pressure for metallic Sr at $T = 1500^\circ\text{K}$ yields a value of 0.14 torr for P_{Sr} , as compared to the vapor pressure of the oxide, $P_{\text{SrO}} = 1.2 \times 10^{-7}$ torr at the same temperature. The above calculation clearly indicates that, in the presence of graphite, fission product strontium would vaporize as metal rather than as oxide. In order to further confirm this hypothesis, another experiment was carried out, in which SrO was placed in a

tungsten crucible and heated in the absence of graphite. The results from this experiment were compared with those of an earlier experiment performed in the presence of graphite. As shown in Figure 3, SrO was not vaporized appreciably in the absence of graphite, even at temperatures as high as 1760°C.

Physical Characterization of Sr and Ag Aerosols

The color of the freshly collected Sr aerosol on Fluoropore filters usually varied from light brown to black, depending upon the thickness of the deposit. Upon exposure to room air, the deposit always lost its color, indicating the conversion of elemental Sr to the oxide, and eventually to the hydroxide form.

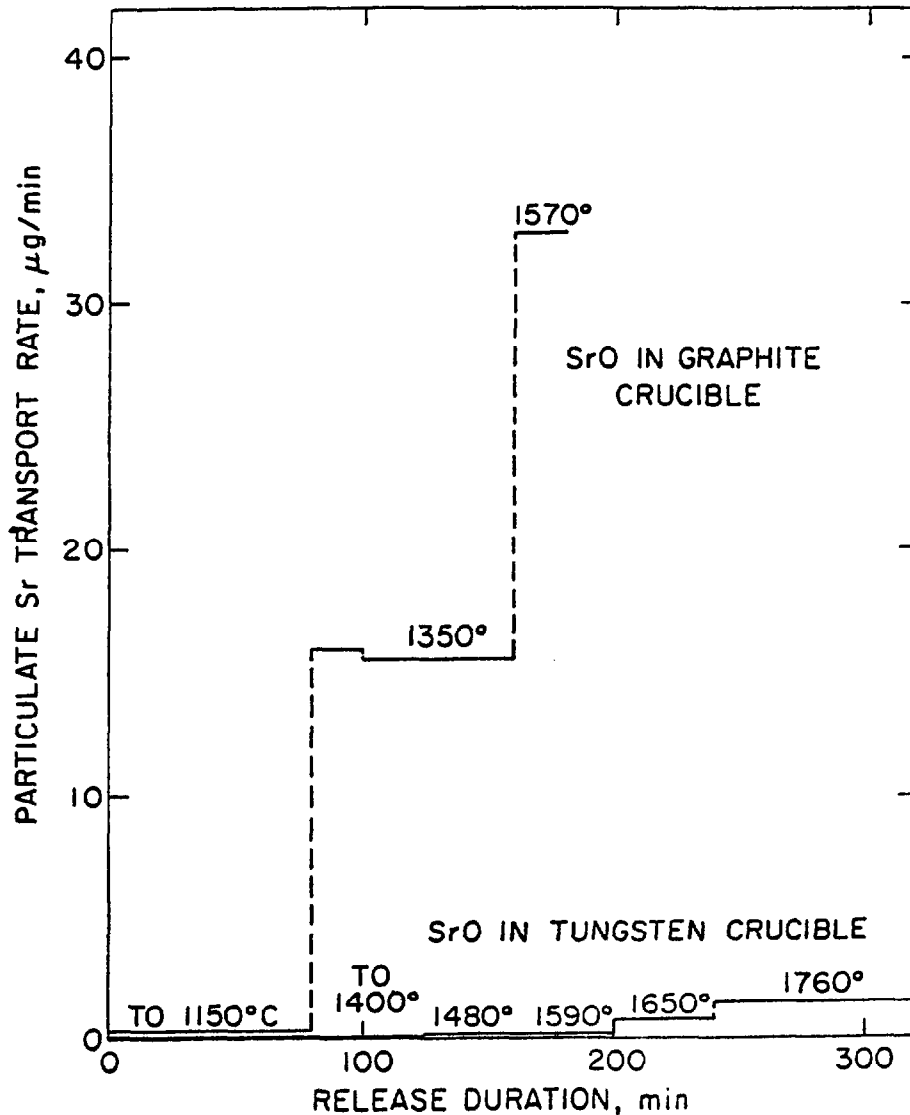


Figure 3. Effect of Graphite on SrO Vaporization

In an effort to study the particle size and morphology of the Sr deposit, electron microscope samples were prepared in experiments where the filters were exposed only briefly to the aerosol stream. At 1 liter/min flow rate, filter samples with aerosol collection times of 120, 60, 30 and 10 sec were obtained. These samples were kept under inert atmosphere before electron microscopic examinations. It turned out that with even the shortest collection time the aerosol deposit on filter was very heavy. A picture at 42000X magnification is shown in the upper insert of Figure 4, together with the Sr elemental analysis result (lower insert) by the x-ray fluorescence microprobe method. Although the electron micrograph is not in very sharp focus the picture shows essentially agglomerates with primary particles roughly 0.1 μm in diameter, which were most likely formed by vapor-phase nucleation.

Figure 5 shows a composite of electron micrographic pictures of Ag aerosols at four different magnifications. These Ag aerosols, produced from a AgNO_3 impregnated graphite source in the same manner as Sr and Ba aerosols, were collected on Nucleopore filters for better examination. Unlike Sr and Ba aerosols which are chemically reactive in ambient air, Ag aerosols are stable in air and, therefore, they provide a good means for studying the morphology of fission product aerosols. Such information is needed to understand the aerosol formation mechanism. In this particular case, agglomerates composed of primary particles almost uniform in size ($d_g = 0.098 \mu\text{m}$, $\sigma_g = 1.20$) are clearly revealed, indicating the condensational nature of the particles, as opposed to fission product adsorption on existing particles.

Sr Transport vs. Initial Loading in Graphite

The experiments reported in the present study were all made with simulated fission products impregnated in the graphite matrix with concentrations between approximately 1 mg to 10 mg of Sr, for example, per g of graphite. A legitimate question then arises as to whether or not the extent of aerosol formation depends on the initial loading of fission products in the graphite matrix. To answer this question, we present in Figure 6 the results from six experiments made under identical conditions. Here, the % Sr collected on filter is plotted vs. initial Sr loading in the graphite samples. In addition, the concentration corresponding to one monolayer coverage on graphite was calculated for Sr on the basis of an estimated graphite surface area of 1 m^2/g . As shown in Figure 6, the extent of aerosol formation in terms of percentage collected on filter as particulate matter is independent of the initial loading for concentrations down to approximately one monolayer coverage of Sr in H451 graphite. Work is in progress to reduce the initial Sr concentration further down to below one monolayer coverage.

IV. Conclusion

The experimental results of our investigation to date have clearly demonstrated that the formation of nuclear aerosols under certain HTGR accident conditions could be an important mechanism by which vaporized fission products such as Ag, Sr and Ba are transported in the gas phase. Electron microscopic examinations of the collected Sr and Ag aerosols have revealed large agglomerates composed of primary particles roughly 0.1 μm in diameter. These primary particles are most likely formed by vapor phase nucleation. The percentage of aerosol formation is independent of the initial loading in the graphite matrix for concentrations down to one monolayer coverage, as demonstrated for the case of Sr.

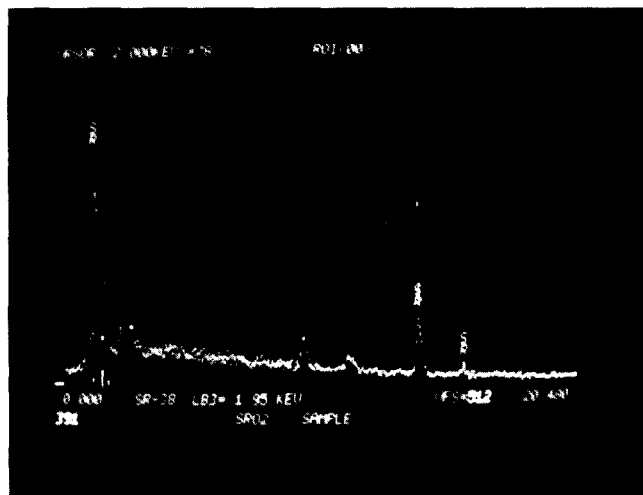
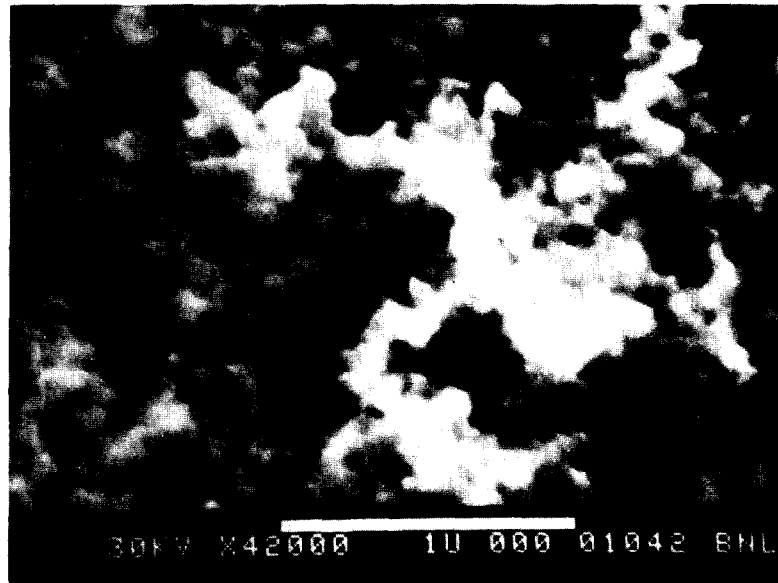


Figure 4. Sr Aerosol Deposit on Fluoropore Filter

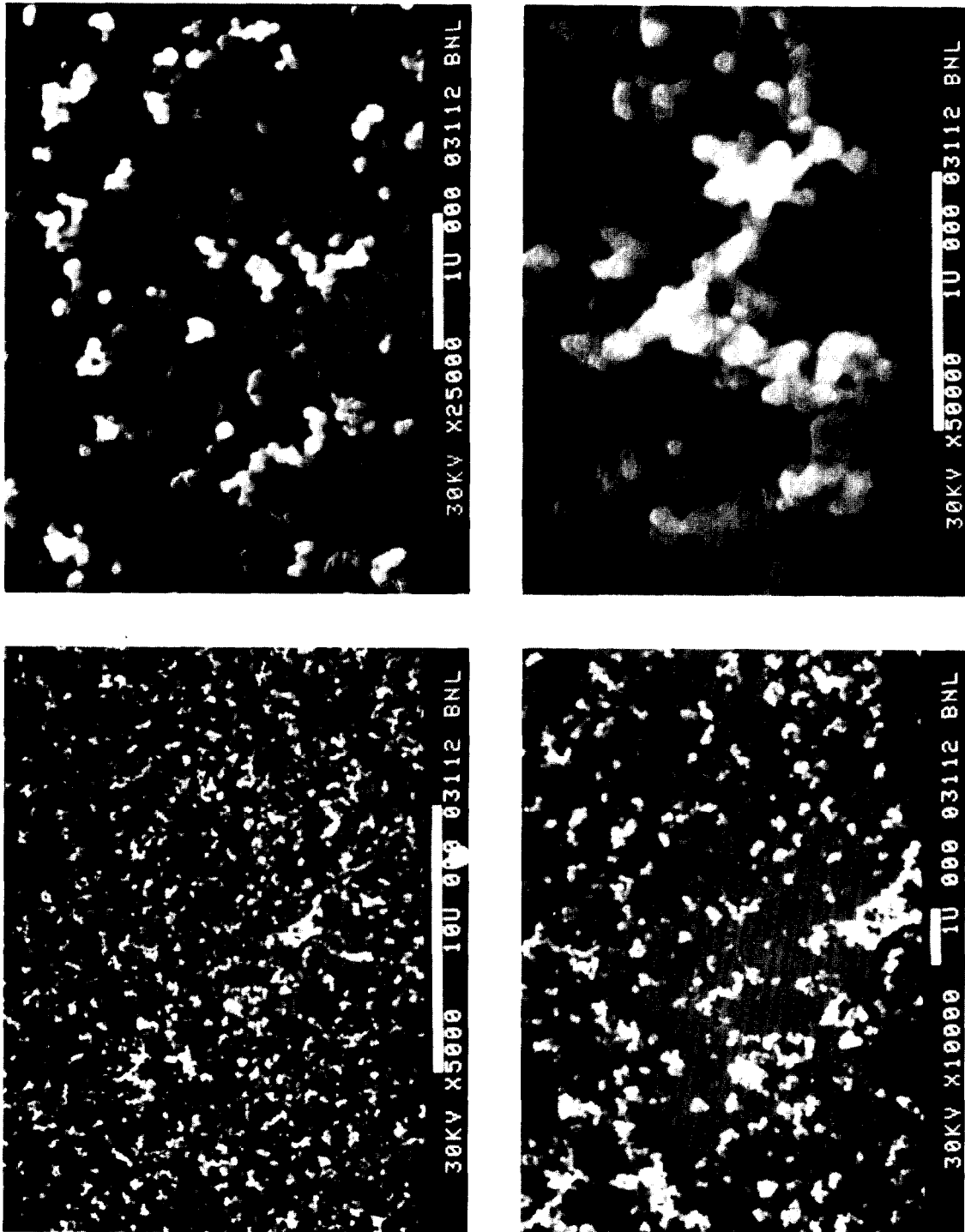


Figure 5. Ag Aerosol Deposit on Nucleopore Filter

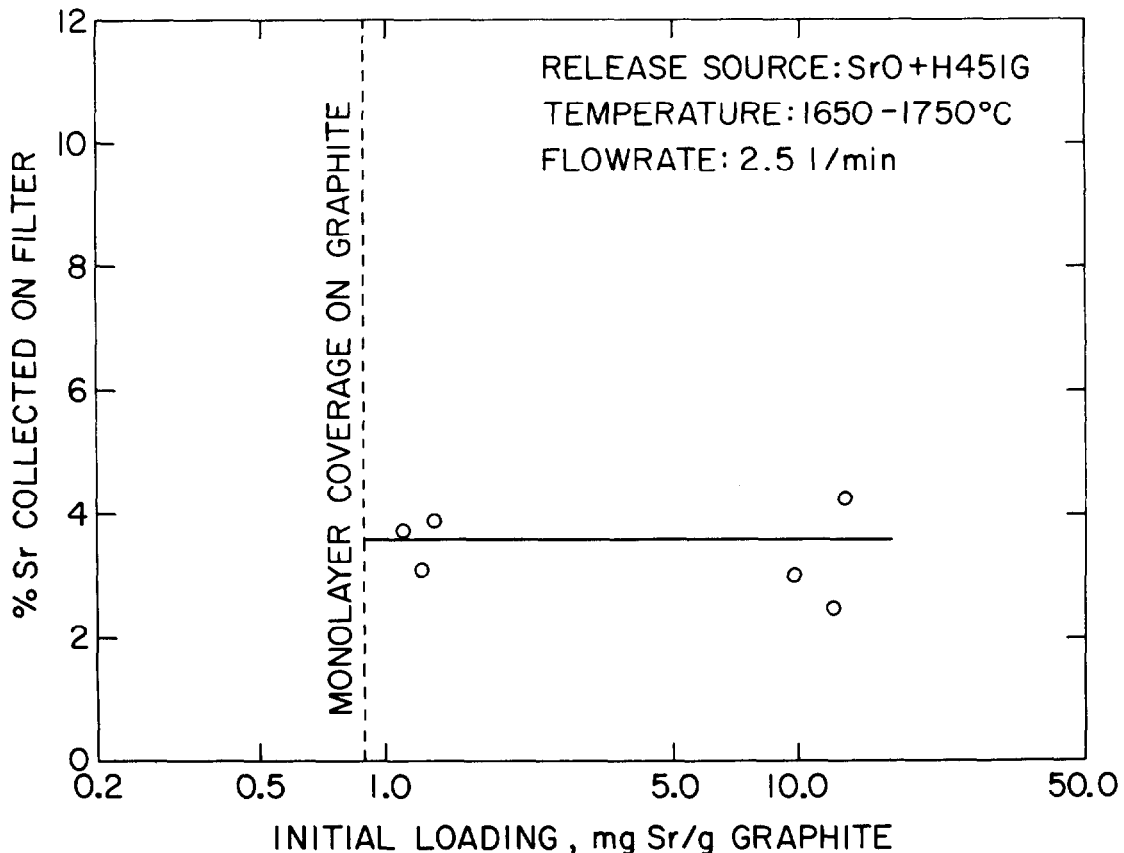


Figure 6. Effect of Initial Sr Loading on Particulate Transport

V. Acknowledgement

This work was performed under the auspices of the U. S. Nuclear Regulatory Commission.

The authors would like to thank George S. Smith and Judson G. Davis for assistance in performing the experiments, Robert Wilson for filter sample analyses, and John B. Warren for the electron microscopic work. The guidance of C. A. Sastre and D. G. Schweitzer of the HTGR Safety Division at BNL is greatly appreciated.

VI. References

1. I. N. Tang, H. R. Munkelwitz and S. L. Nicolosi, "Aerosol formation from core graphite heated in dry and moist helium." Brookhaven National Laboratory, BNL-NUREG-25330, 1980.
2. Nuclear Aerosols in Reactor Safety, CSNLI/SOAR No. 1, Nuclear Energy Agency, June 1979.
3. J. A. Gieseke, R. C. Behn, A. C. Chace and L. D. Reed, "Analytical studies of aerosol behavior predictions for fast reactor safety," BMLI-1932, Battelle Columbus Laboratory, Columbus, Ohio, 1975.
4. See, for example, General Atomic Standard Safety Analysis Report (GASSAR).
5. H. Kleykamp, "Mikrosondenuntersuchungen zum Verhalten der spaltprodukte in hoch abgebrannten HTR-brennstoffen," KFK 2213, Karlsruhe, 1975.

17th DOE NUCLEAR AIR CLEANING CONFERENCE

CONCLUDING REMARKS OF SESSION CHAIRMAN:

Summarizing, most of the papers on fuel reprocessing were from overseas. We hope that this ratio will change in the future. We have had both experimental data and modeling papers presented and I think the conclusion is that we still need additional experimental data to confirm the design of off-gas cleanup systems, to evaluate potential failures of these cleanup systems, and to assure that we have safe fuel reprocessing facilities. We certainly appreciate the contribution by our foreign visitors to this technology and we hope that this will fill in some of the gaps that we in the U.S. have not had a chance to work on the past few years. I want to thank all the authors for their work and for their presentations. I would also like to apologize for some of the equipment failures we had. When we had two simultaneous failures in our audiovisual system just in one session, I am wondering if we are justified in looking at single failures even in nuclear applications. The number of components here is much smaller than in a nuclear power plant, if we tried to apply statistics. I think we had better look at multiple failures and make sure we can protect our systems from them.

Session 3

RADIOIODINE

TUESDAY: August 3, 1982

Co-CHAIRMEN: T.R. Thomas, Exxon Nuclear
Idaho Co.

J.D. Christian, Exxon Nuclear
Idaho Co.

ORGANIC IODINE REMOVAL FROM SIMULATED DISSOLVER OFF-GAS
STREAMS USING PARTIALLY EXCHANGED SILVER MORDENITE

R.T. Jubin

A PARAMETRIC STUDY ON REMOVAL EFFICIENCY OF IMPREGNATED
ACTIVATED CHARCOAL AND SILVER ZEOLITE FOR RADIOACTIVE
METHYL IODIDE

H. Shiomi, Y. Yuasa, A. Tani, M. Ohki, T. Nakagawa

DATA ANALYSIS OF IN PLACE TESTS OF IODINE FILTERS IN THE
FRENCH NUCLEAR FACILITIES

P. Mulcey, L. Trehen, J.L. Rouyer

IODINE FILTERING FOR FRENCH REPROCESSING PLANTS

G. Bruzzone, J.L. Rouyer, Ph. Mulcey, A. Vaudano

RETENTION OF ELEMENTAL RADIOIODINE BY DEEP BED CARBON FILTERS
UNDER ACCIDENT CONDITIONS

H. Deuber, J.G. Wilhelm

EXPERIENCES WITH A CHARCOAL GUARD BED IN A NUCLEAR POWER
PLANT

L.C. Scholten

DEPOSITION OF AIRBORNE RADIOIODINE SPECIES ON SURFACES OF
METALS AND PLASTICS

M.J. Kabat

Consolidated Fuel Reprocessing Program

ORGANIC IODINE REMOVAL FROM SIMULATED DISSOLVER
OFF-GAS STREAMS USING PARTIALLY EXCHANGED SILVER MORDENITE*

R. T. Jubin, Fuel Recycle Division
Oak Ridge National Laboratory
Oak Ridge, Tennessee 37830

ABSTRACT

The removal of methyl iodide by adsorption onto silver mordenite was studied using a simulated off-gas from the fuel dissolution step of a nuclear fuel reprocessing plant. The methyl iodide adsorption of partially exchanged silver mordenite was examined for the effects of NO_x , humidity, filter temperature, and degree of silver exchange. Partially exchanged silver mordenite, in general, achieved significantly higher silver utilizations than the fully exchanged material. Silver utilizations of $>95\%$ were achieved, assuming the formation of AgI. The experimental results indicate that CH_3I loadings increase proportionally with silver loading up to 5 wt % silver and then appear to level off. Tests conducted to determine the effect of temperature on the loading showed higher loadings at 200°C than at either 150 or 250°C . The presence of NO , NO_2 , and H_2O vapor showed negligible effects on the loading of CH_3I . In contrast to iodine loaded onto fully exchanged silver mordenite, the iodine loaded onto the partially exchanged silver mordenite could not be stripped by either 4.5% hydrogen or 100% hydrogen at temperatures up to 500°C .

A study of the regeneration characteristics of fully exchanged silver mordenite indicates a decreased adsorbent capacity after complete removal of the iodine with 4.5% hydrogen in the regeneration gas stream at 500°C . The loss of adsorbent capacity was much higher for silver mordenite regenerated in a stainless steel filter housing than in a glass filter housing.

A cost evaluation for the use of the partially exchanged silver mordenite shows that the cost of the silver mordenite on a once-through basis is $<\$10/\text{h}$ of operation for a 0.5-t/d reprocessing plant.

1. Introduction

Iodine-129 is produced by both natural and man-made sources. The natural sources include the spontaneous fission of uranium and the interaction of cosmic rays with xenon in the atmosphere. The annual production through these natural paths is ~ 10 mg/year. With its long half-life (1.6×10^7 years), ^{129}I tends to accumulate worldwide. As of 1940, the estimated accumulation has been reported to be 2×10^5 g.¹ A light-water reactor (LWR) will produce 234 g of ^{129}I per ton of fuel based on a uranium burnup of 30 000 MWd/t.² In handling the spent fuel, a single 5-t/d nuclear fuel reprocessing plant would have to process 3.2×10^5 g/year of ^{129}I . In addition to ^{129}I , various amounts of other short half-life iodine isotopes are also produced; however, none of these appear in significant amounts after long (200-d) decay times.

*Research sponsored by the Office of Spent Fuel Management and Reprocessing Systems, U.S. Department of Energy, under Contract No. W-7405-eng-26 with Union Carbide Corporation.

17th DOE NUCLEAR AIR CLEANING CONFERENCE

During the past two decades, various systems have been studied to reduce the iodine released to the environment. Two liquid scrubber systems are currently available: the Iodex system and the mercuric nitrate-nitric acid (Mercurex) system. Solid sorbents have also been studied, either as secondary systems to provide final filtering following use of either the Iodex or Mercurex system or as primary systems to replace the liquid based methods. These solid sorbents include silver faujasite, silver mordenite, alumina silicates, and macroporous resins. Activated carbon has also been examined as a reference material; however, this material cannot be considered as a primary sorbent for treating reprocessing plant off-gas because of its low ignition temperature and its adverse reactions with nitrogen oxide (which could lead to the formation of explosive compounds and to poisoning by organic contaminants in the off-gas).

If high decontamination factors (DF's) are required, one of the more promising systems for primary iodine removal is the Iodex system; otherwise, solid sorbent-based processes tend to be favored. The Iodex system has already been tested on an engineering scale and has demonstrated good capabilities and operability. Decontamination factors in excess of 10^6 have been obtained. There are, however, concerns about the long-term integrity of the materials of construction that come in contact with the 20 to 23 M HNO₃ scrub solution.

Silver-impregnated solid sorbents offer a simpler iodine removal scheme in comparison to liquid systems. In this case, however, iodine DF's are limited to about 10^3 , and high operating costs can be expected, particularly if the silver is not recovered. In the past few years, regenerable adsorbents have received considerable attention.

At the 14th ERDA Air Cleaning Conference,³ it was reported that silver-exchanged faujasite (AgX) loaded with elemental iodine could be regenerated in situ with a pure hydrogen stream at 500°C; however, a 50% loss in loading capacity was observed after five loading cycles. Silver-exchanged faujasite is capable of adsorbing iodine at temperatures as high as 500°C; and like most other sorbents, it is adversely affected by water vapor, especially when condensation occurs. Faujasite is also adversely affected by acid vapor found in the dissolver off-gas system. Average I₂ loadings were 100 to 200 mg I₂ per g AgX or 23 to 47% utilization of the available silver.

A silver-containing alumina silicate, AC-6120, also showed potential on a once-through basis. Silver utilizations of ~59% have been reported with AC-6120.

Similar studies with silver mordenite (AgZ) showed only a negligible reduction in loading capacity after eight cycles.⁴ Average I₂ loadings were 100 to 130 mg I₂ per g AgZ or 42 to 55% utilization of the available silver. However, these tests were limited to elemental iodine loading.

The high cost of silver, the lack of an available AC-6120 regeneration scheme plus limited regeneration potential, and the lack of acid resistance of the AgX make these materials less attractive than AgZ for large-scale use.

Previous work on AgZ at the Oak Ridge National Laboratory was reported at the 16th DOE Air Cleaning Conference.⁵ This work demonstrated the increased loading of CH₃I following hydrogen pre-treatment of the AgZ. Hydrogen stripping of the iodine loaded bed was also demonstrated; however, the regeneration procedure caused a dramatic loss in the iodine loading capacity of the bed.

The objectives of the solid sorbent studies reported here were to evaluate:

1. the suitability of silver-exchanged mordenite as a back-up or secondary iodine removal system to the Iodex process in nuclear fuel reprocessing plants;
2. the removal capabilities of silver-exchanged mordenite for organic iodides;
3. the use of low silver content mordenite for iodine removal; and
4. the regeneration potential of both fully and partially exchanged silver mordenite.

2. Experimental Procedure

Silver-exchanged mordenite (AgZ) was prepared by ion exchange with 0.16-cm-diam extrudates of the sodium form of Norton Zeolon 900; silver-exchanged faujasite (AgX) and lead-exchanged faujasite (PbX) were prepared from 0.16-cm-diam extrudates of the type 13X Linde molecular sieve. Fully exchanged AgZ or PbX was prepared by placing 1500 g of the unexchanged zeolite into an ion exchange column and batch contacting with 3 L of 1 M silver nitrate or lead nitrate solution at 40°C. The spent solution was replaced at regular intervals with fresh solution until no change in silver or lead concentration was detected. The solution was drained, and the exchanged zeolite was air dried at 60°C for 24 h. Fully exchanged silver mordenite was also purchased from the Ionex Corporation under the trade name of Ionex Ag-900. Partially exchanged silver mordenite (LAgZ) was prepared by contacting unexchanged mordenite in a stirred tank reactor with a limited amount of silver nitrate solution and air dried at 60°C. During this exchange, virtually all of the silver from the solution is substituted for sodium in the zeolite structure. Thus, the degree of exchange is easily controlled by limiting the quantity of silver available. The AgZ beds were pretreated *in situ* prior to sorbent tests by heating to 200°C and purging with 4.5% H₂-95.5% Ar at a flow rate of 5 L/min for 24 h. The beds were then isolated and brought to the operating temperature. The same procedure was used to pretreat the LAgZ beds. The hydrogen pretreated condition of AgZ and LAgZ is denoted by Ag₂Z and LAg₂Z respectively.

Methyl iodide loading tests were conducted using an apparatus similar to that used in previously reported work.⁵ A schematic of the equipment is presented in Fig. 1. Heated air streams containing the

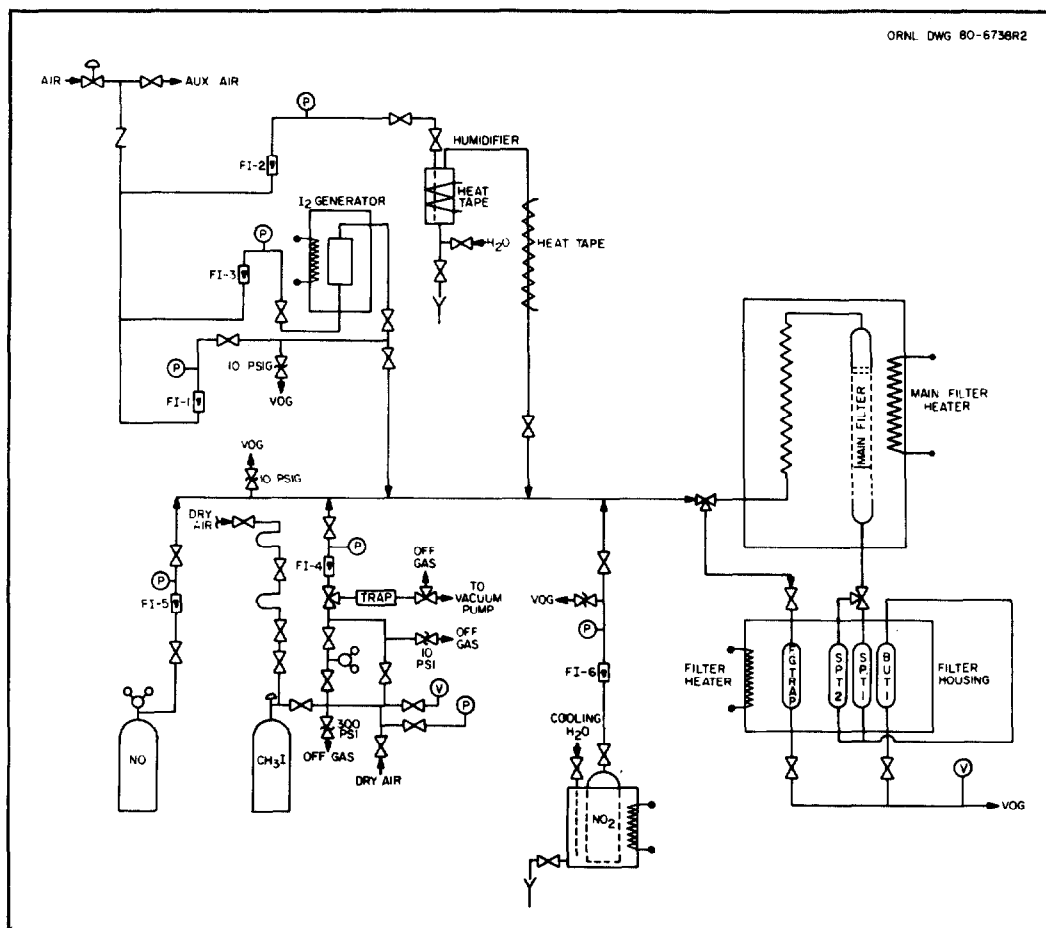


Fig. 1. Test apparatus for methyl iodide loading studies.

desired amount of NO, NO₂, CH₃¹²⁷I tagged with CH₃¹³¹I, and water vapor were passed through the segmented filter bed located in the heated main filter enclosure. Initial studies were conducted using a glass filter casing. A stainless steel filter divided into six segments (Fig. 2) was used in later experiments. The breakthrough of the bed was monitored by collecting the CH₃I, leaving the main filter on AgX. At regular intervals, this trap was removed and counted for ¹³¹I. Normally, when >0.1% of the iodine in the feed gas stream was found to be passing through the main filter, the run was stopped. The bed segments were counted for ¹³¹I using a sodium iodide detector and a single channel analyzer set on the 364-keV gamma-ray peak of 8-d half-life ¹³¹I. Using a 100-keV window, the gross count over a 1-min period (corrected for background) was used as a measure of the iodine content of the bed. The total amount of CH₃I loaded on the test bed was then calculated from the known ratio of ¹²⁷I to ¹³¹I.

ORNL DWG. 80-15046R

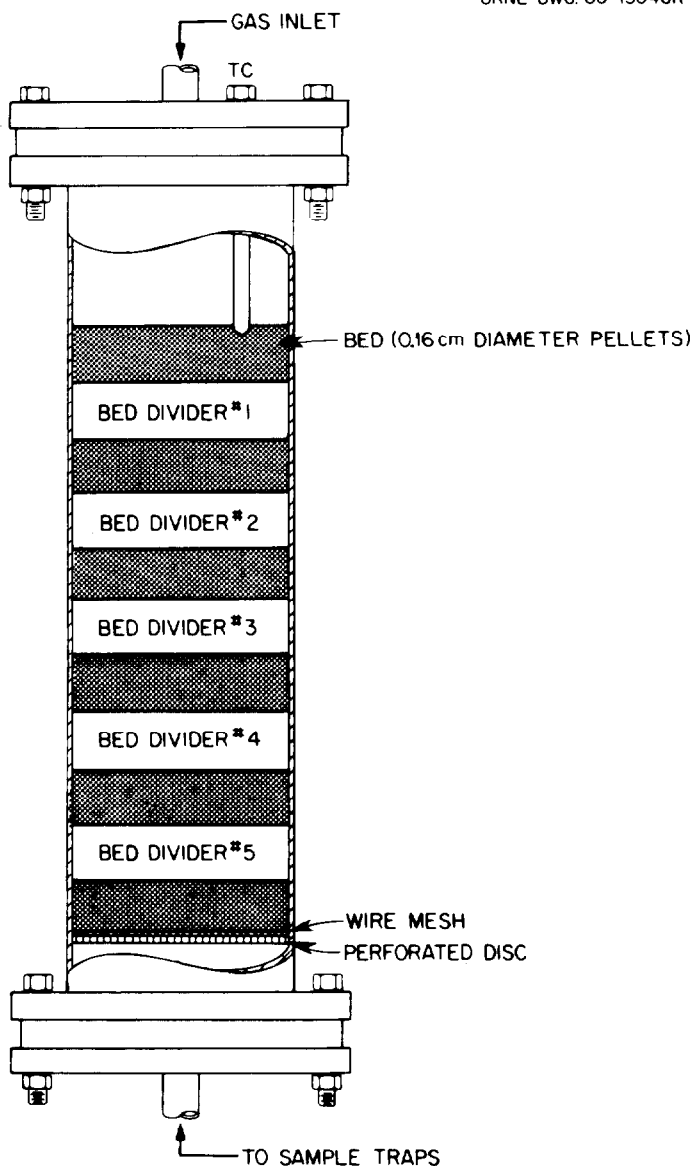


Fig. 2. Stainless steel main filter.

3. Experimental Results

3.1 Temperature and Humidity Effects on AgZ

The effects of NO, NO₂, humidity, pretreatment conditions, operating temperature, and CH₃I concentration on the loading capacity of AgZ were evaluated using an eight-run fractional 2ⁿ factorial-designed experiment.⁵

Analysis of those data indicated that (1) pretreatment with 4.5% H₂–95.5% Ar at 200°C for 24 h improved loadings; (2) loadings were improved at higher operating temperatures; (3) loadings were improved in moist air conditions; and (4) the other variables, NO, NO₂, and CH₃I concentration, produced variations in loadings that were less than the response error.

A follow-on study was conducted to examine the effects of temperature and humidity on AgZ. An air stream containing 1000 mg of CH₃I per m³ and a dewpoint of either approximately –54°C or approximately +35°C was passed across four hydrogen pretreated beds operated in series at temperatures of 100, 125, 150, 175, 200, or 225°C. The CH₃I loading on the first of four 2.54-cm-thick beds at breakthrough is shown in Fig. 3 as a function of temperature. Breakthrough, for this study, is the point where the DF across the main test beds drops below 10³.

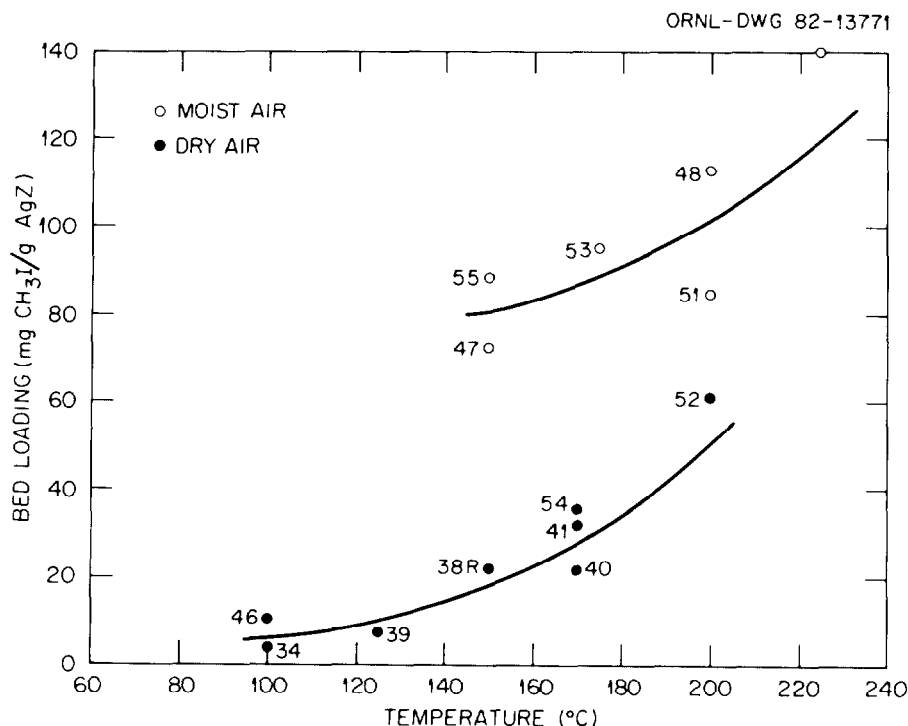


Fig. 3. CH₃I loading at breakthrough on the first of four 2.54-cm-deep beds as a function of temperature.

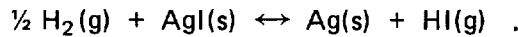
As indicated by the original scoping study, the presence of water in the system resulted in higher CH₃I loadings. As the operating temperature increases, loadings also increase, and the mass transfer zones (MTZ) are also increased. At 150°C, the MTZ for both the humidified bed and the dry bed is 5 to 7.5 cm in length. At 200°C, the MTZ is over 10 cm. As a result, the entire MTZ was not contained within the four test beds. Hence, even higher bed loadings should be expected prior to breakthrough on longer beds. This, in fact, was demonstrated during one experiment at 200°C with moist air. The run was continued past breakthrough and was terminated at a first bed loading of 139.5 mg CH₃I/g AgZ. Tests at 225°C with

moist air have shown first bed loadings of 141.5 mg CH₃I per gram of AgZ at breakthrough of the last bed. Higher loadings could possibly be achieved since, in both cases, the first bed was not saturated under the given conditions.

Improved loading was also observed in a run that was stopped at breakthrough, that is, a DF < 1000, which was allowed to remain at its operating temperature (150°C) overnight. When loading was reinitiated 18 h later, the DF across the bed remained above 1000 for 2 h, allowing the additional loading of ~20 mg/g on the first bed before breakthrough occurred again. During the heat soaking period, the iodine apparently distributed into the Ag₂Z pellet thus freeing some of the more accessible silver sites for the second loading period. The elevated temperatures probably facilitate similar movement of the iodine into the more inaccessible silver sites, thus increasing the overall silver utilization.

3.2 Regeneration Test of AgZ

Loaded Ag₂Z beds were regenerated with the equipment shown in Fig. 4, using both 4.5% H₂–95.5% Ar and pure H₂. Both gas streams satisfactorily remove the chemisorbed iodine. The assumed reaction is:



Equilibrium vapor pressures of HI at an operating temperature of 500°C are 26.5 and 119.1 Pa for 5 and 100% H₂ respectively.

ORNL DWG. 80-15053

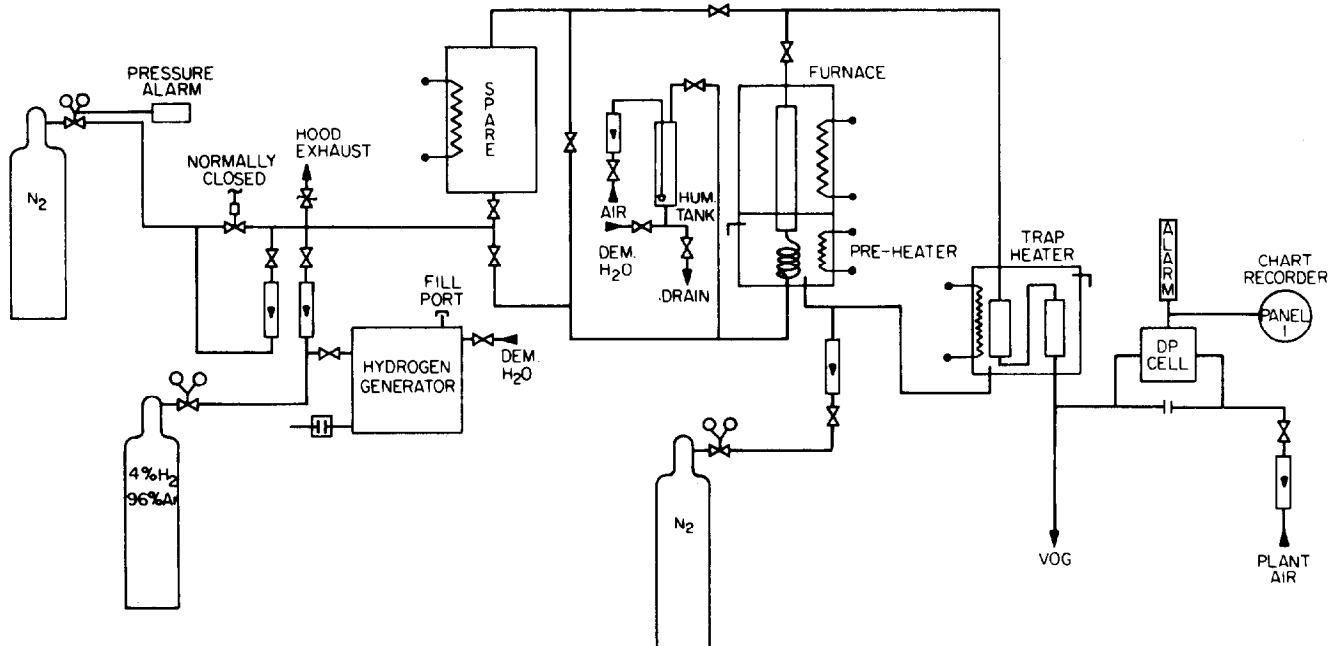


Fig. 4. Hydrogen regeneration flowsheet for silver mordenite.

The hydrogen flow was countercurrent to the original iodine flow. The iodine in the form of HI was then trapped on the PbX bed. During 24 h of regeneration with an H₂ flow of 0.5 SLPM,* >50% of the I₂ is removed in 6 h and >98% in 24 h. The second loading of the regenerated bed using the same feed conditions as the initial loading resulted in significantly lower loadings than the original loading. The addition of water vapor to the feed gas improved loads to approximately one-third of the original loadings at 150°C.⁵ This loading is significantly lower than the post-regeneration loadings reported by Thomas et al.⁴

*Standard liters per minute.

An examination of the AgZ by x-ray diffraction and scanning electron microscopy showed:

1. the presence of free silver following 4.5% H₂ pretreatment at 200°C,
2. the formation of small (<2000 Å) nodules of silver during 4.5% H₂ at 200°C pretreatment,
3. no free silver or silver nodules on air-pretreated AgZ, and
4. large (>8000 Å) nodules of silver following regeneration at 500°C with 4.5% H₂.

To determine the effects of temperature and time on the formation of the silver nodules and subsequent CH₃I loading on the AgZ, a series of beds was treated with 100% H₂ for 24 or 48 h at temperatures of 200, 400, or 500°C. Following this treatment, the beds were loaded with CH₃I in dry air. The results of the bed loadings are shown in Table 1.

Table 1. CH₃I loadings of 100% hydrogen-treated AgZ in dry air

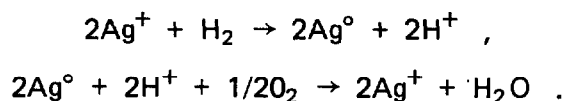
Run	Temperature (°C)	Time (h)	Loading (mg/g)
57	200	24	35.6
58	200	48	12.3
59	400	24	11.0
61	400	48	8.0
60	500	48	0.26

Loadings showed decreased retention capacity for CH₃I as exposure time to H₂ increased and as temperature of exposure increased. Photomicrographs showed small increases in the nodule size from 200 to 400°C and a significant increase in nodule size at 500°C. It is the migration of the silver to these nodules that is believed to (at least partially) account for the decrease in CH₃I loadings. The migration of silver in the presence of hydrogen was also noted by Yates in 1965.⁶ Yates reported that silver crystallites of 170 Å formed in the presence of H₂ at 250°C. These temperatures of interest are well below the melting point of silver (961°C). The vapor pressure of silver is correspondingly low (10⁻⁵-mm Hg at 757°C).

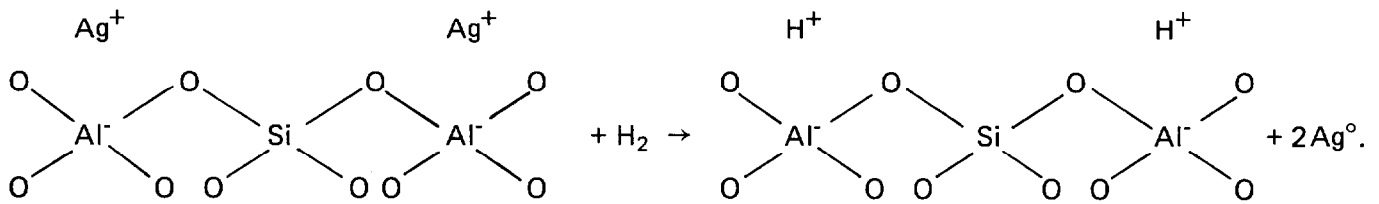
Work by Scheele et al.⁷ using glass housings for the AgZ did not show the same large nodules following a hydrogen pretreatment at 500°C nor was the loading as low. A series of tests was conducted using a 5.08-cm-diam glass column to explore the possible effects of filter housing material. AgZ was placed in this column and treated with 100% H₂ at 500°C for 24 h. The bed was then loaded with CH₃I to 54 mg/g at 200°C in moist air. This is approximately half the loading observed for AgZ under the same loading conditions but treated with 4.5% H₂ at 200°C and 10 times higher than loadings following hydrogen treatment at 500°C in stainless steel.

Beyer and Jacobs⁸ have also reported on the roles temperature and iron impurities play in the hydrogen reduction and reoxidation of AgZ. At increasing reduction temperatures, the intensity of the (111) diffraction of crystalline silver external to the zeolite increases and the particle size of the silver crystallites also increases. They also report that upon oxidation at sufficiently high temperatures, the external silver phase disappears. After a second redox cycle at 653 K, a small amount of the silver remains located between the zeolite crystallites, indicating a slight irreversibility of the system.

The proposed stoichiometry appears straightforward for both reduction and oxidation:



A second, and possibly clearer, representation of the reduction reaction showing the role of the mordenite is given by Tszuri and Takahashi:⁹



Beyer and Jacobs also indicated that the reduction is a catalyzed process where hydrogen is probably activated on iron impurities within the zeolite structure of the material they used. It was shown that rate of reduction strongly depends on the iron content. In fact, using partially deironized material, the rate of reduction of silver ions showed a fivefold decrease, whereas the reduction mechanism remained unchanged as deduced from the slope of the Arrhenius plots.

This "activation" of the hydrogen by iron would account for the rapid formation of large silver nodules when treating AgZ in the stainless steel housing at high temperatures and the much slower formation of nodules in the glass housing. These reactions must be taken into account when designing actual plant off-gas systems using silver zeolites since it appears that only a very limited amount of CH₃I can be adsorbed onto AgZ in which the silver has formed large metal agglomerates.

3.3 Scoping Tests on Partially Exchanged Silver Mordenite

Tests on fully exchanged AgZ indicate the iodine probably first chemisorbs at the easily accessible silver sites. Experience in exchanging the sodium for silver has also shown that the last 25% of the exchange is more difficult to accomplish. With this in mind, the CH₃I loading characteristics of partially exchanged silver mordenite (LA₀AgZ) were examined using a fractional factorial designed experiment. The experiment examined the effects of NO, NO₂, humidity, bed temperature, dilute hydrogen, and silver content on the loading capacity. The dilute hydrogen stream was added in an attempt to maintain the silver in the reduced state during the loading phase. Although hydrogen was also used for regeneration of the loaded AgZ beds, the loading operation was conducted at a significantly lower temperature than the regeneration step. Experimental conditions are presented in Table 2. The eight-run design, along with the loading on the first bed, and the effects of each variable are shown in Tables 3 through 7.

Response errors for a designed experiment can be estimated using the dummy variable.¹⁰ Using this technique, values of 2.16, 6.86, 3.98, 0.14, and 1.96 mg/g were obtained for Tables 3 through 7 respectively. However, this method probably overestimates the response errors since some degree of interaction between the measured variables is likely. A response error has also been calculated using replicate runs. This method indicates the response error to be on the order of 0.5 mg/g. The response error is, however, controlled somewhat by how closely breakthrough can be determined and how quickly the run can be stopped. If the entire mass transfer zone is contained within the test beds, then the effect of not stopping the run at the exact moment of breakthrough is not critical since the first bed is no longer playing an active role in iodine removal. Under certain conditions, the mass transfer zone becomes longer than the 15-cm bed length. The first bed is therefore still loading at the time of shutdown, hence more variation in its loading would be expected.

Analysis of the scoping studies indicated that:

1. Increased CH₃I loadings occur with increasing silver content. This increase in loading appears to stabilize above the 3% Ag content.

17th DOE NUCLEAR AIR CLEANING CONFERENCE

2. An operating temperature of 200°C is favored over either 150 or 250°C. The difference between 200°C loadings and 250°C loadings appears to decrease as the silver content increases. This corresponds to the bed loading versus temperature response observed for the fully exchanged material.
3. NO and NO₂ produced small and varied positive and negative effects.
4. The effects of water vapor also produced mixed results.
5. The addition of 1 vol % hydrogen to the inlet stream resulted in increased bed loadings at the lower silver contents. This is probably the result of maintaining more of the limited amount of silver in the reduced state.

Table 2. Experimental conditions for scoping studies

Variable	Value
Bed weight, g	~40
Bed diameter, cm	5.08
Bed thickness, cm	2.54
Number of beds	6
Carrier gas	Air
Superficial velocity, m/min at STP	10.0
CH ₃ I concentration mg/m ³ at STP	1000
NO concentration, %	0 or 3.0
NO ₂ concentration, %	0 or 3.0
Relative humidity (dewpoint), °C	-54 or ~35
Pretreatment	4.5% H ₂ in argon for 24 h
Bed temperature, °C	150, 200, or 250
Hydrogen, %	0 or 1.0
Silver content, wt %	1.5, 3.0, 5.0, or 9.0

Table 3. Summary of screening runs for 1.5–3.0% LAgZ^a

Run	Bed 1 loading ^b (mg/g)	NO	NO ₂	Dew point (°C)	Temperature ^c	Ag (wt %) in AgZ	4% H ₂	Dummy
1	17.74	-	-	-	-	-	-	+
2	21.63	+	-	-	+	+	-	-
3	11.13	-	+	-	+	-	+	-
4	30.10	+	+	-	-	+	+	+
5	37.44	-	-	+	-	+	+	-
6	7.48	+	-	+	+	-	+	-
7	22.95	-	+	+	+	+	-	+
8	14.18	+	+	+	-	-	-	-
		-=0 %	-=0%	-=-54°C	-=200°C	-=1.5% Ag	-=0 LPM	
		+ =3%	+ =3%	+ = 35°C	+ =250°C	+ =3.0% Ag	+ =5 LPM	
Effect		-3.968	-1.483	0.363	-9.068	15.398	2.413	-1.528

^a Run conditions: six beds each, 2.54-cm-thick, 5.08 cm in diameter, gas rate 20 SLPM; pretreated 24 h at 200°C with dry 4.5% H₂-95.5% Ar; average decontamination factor >10³.

^b Loadings are based on a dry density of 0.78 g/cm.

^c Bed temperature.

17th DOE NUCLEAR AIR CLEANING CONFERENCE

Table 4. Summary of screening runs for 1.5–3.0% LAgZ^a

Run	Bed 1 loading ^b (mg/g)	NO	NO ₂	Dew point (°C)	Temperature ^c	Ag (wt %) in AgZ	4% H ₂	Dummy
1	17.74	—	—	—	—	—	—	+
2	26.05	+	—	—	+	+	—	—
3	16.23	—	+	—	+	—	+	—
4	30.10	+	+	—	—	+	+	+
5	37.44	—	—	+	—	+	+	—
6	10.04	+	—	+	+	—	+	+
7	16.32	—	+	+	+	+	—	+
8	14.18	+	+	+	—	—	—	—
		—=0 %	—=0%	—=–54°C	—=200°C	—=1.5% Ag	—=0 LPM	
		+ =3%	+ =3%	+ = 35°C	+ =150°C	+ =3.0% Ag	+ =5 LPM	
Effect		–1.840	–3.610	–3.035	–7.705	12.930	4.880	–4.925

^a Run conditions: six beds each, 2.54-cm-thick, 5.08 cm in diameter, gas rate 20 SLPM; pretreated 24 h at 200°C with dry 4.5% H₂–95.5% Ar; average decontamination factor >10³.

^b Loadings are based on a dry density of 0.78 g/cm.

^c Bed temperature.

Table 5. Summary of screening runs for 3.0–5.0% LAgZ^a

Run	Bed 1 loading ^b (mg/g)	NO	NO ₂	Dew point (°C)	Temperature ^c	Ag (wt %) in AgZ	4% H ₂	Dummy
1	21.48	—	—	—	—	—	—	+
2	21.63	+	—	—	+	+	—	—
3	20.99	—	+	—	+	—	+	—
4	30.10	+	+	—	—	+	+	+
5	37.44	—	—	+	—	+	+	—
6	23.60	+	—	+	+	—	+	+
7	22.95	—	+	+	+	+	—	+
8	29.33	+	+	+	—	—	—	—
		—=0 %	—=0%	—=–54°C	—=200°C	—=5.0% Ag	—=0 LPM	
		+ =3%	+ =3%	+ = 35°C	+ =250°C	+ =3.0% Ag	+ =5 LPM	
Effect		0.450	0.195	4.780	–7.295	4.180	4.185	–2.815

^a Run conditions: six beds each, 2.54-cm-thick, 5.08 cm in diameter, gas rate 20 SLPM; pretreated 24 h at 200°C with dry 4.5% H₂–95.5% Ar; average decontamination factor >10³.

^b Loadings are based on a dry density of 0.78 g/cm.

^c Bed temperature.

17th DOE NUCLEAR AIR CLEANING CONFERENCE

Table 6. Summary of screening runs for 1.5–9% LAgZ^a

Run	Bed 1 loading ^b (mg/g)	NO	NO ₂	Dew point (°C)	Temperature ^c	Ag (wt %) in AgZ	4% H ₂	Dummy
1	21.48	–	–	–	–	–	–	+
2	28.45	+	–	–	+	+	–	–
3	20.99	–	+	–	+	–	+	–
4	27.60	+	+	–	–	+	+	+
5	22.51	–	–	+	–	+	+	–
6	23.60	+	–	+	+	–	+	+
7	28.99	–	+	+	+	+	–	+
8	29.33	+	+	+	–	–	–	–
		–=0 %	–=0%	–=–54°C	–=200°C	–=1.5% Ag	–=0 LPM	
		+ =3%	+ =3%	+ = 35°C	+ =250°C	+ =9.0% Ag	+ =5 LPM	
Effect		0.665	1.450	–2.940	–1.495	14.255	–5.160	1.385

^aRun conditions: six beds each, 2.54-cm-thick, 5.08 cm in diameter, gas rate 20 SLPM; pretreated 24 h at 200°C with dry 4.5% H₂–95.5% Ar; average decontamination factor >10³.

^bLoadings are based on a dry density of 0.78 g/cm.

^cBed temperature.

Table 7. Summary of screening runs for 5–9% LAgZ^a

Run	Bed 1 loading ^b (mg/g)	NO	NO ₂	Dew point (°C)	Temperature ^c	Ag (wt %) in AgZ	4% H ₂	Dummy
1	17.74	–	–	–	–	–	–	+
2	28.45	+	–	–	+	+	–	–
3	11.13	–	+	–	+	–	+	–
4	27.60	+	+	–	–	+	+	+
5	22.51	–	–	+	–	+	+	–
6	7.48	+	–	+	+	–	+	+
7	28.99	–	+	+	+	+	–	+
8	14.18	+	+	+	–	–	–	–
		–=0 %	–=0%	–=–54°C	–=200°C	–=5.0% Ag	–=0 LPM	
		+ =3%	+ =3%	+ = 35°C	+ =250°C	+ =9.0% Ag	+ =5 LPM	
Effect		3.752	2.717	1.477	0.278	3.038	–3.388	0.097

^aRun conditions: six beds each, 2.54-cm-thick, 5.08 cm in diameter, gas rate 20 SLPM; pretreated 24 h at 200°C with dry 4.5% H₂–95.5% Ar; average decontamination factor >10³.

^bLoadings are based on a dry density of 0.78 g/cm.

^cBed temperature.

Silver utilization averaged 72% for both 1.5 and the 3% LA $\overset{\circ}{\text{g}}$ Z, whereas silver utilizations of over 50% were rare with Ag $\overset{\circ}{\text{Z}}$; the highest silver utilization on Ag $\overset{\circ}{\text{Z}}$ seen to date is 64%. One hundred percent silver utilization on three percent LA $\overset{\circ}{\text{g}}$ Z was seen in run 5 of the first LAgZ scoping study (Table 3).

For both 5 and 9% LAgZ, the silver utilization and the associated CH₃I appears low. The maximum silver utilization for the 9% LAgZ was 27%. This may be the result of a changing batch of sodium mordenite. In the period between the two purchases of NaZ, the Norton Company changed production sites of the Zeolon-900 from Stow, Ohio to Brian, Texas.¹¹ An effort to determine the difference in the process and/or material used has been undertaken by both Norton and ORNL. This change in base material could have an impact on future solid sorbent work. Should the difference result from impurities in the water used in processing, treatment steps could be taken to produce material of similar quality to that obtained from the Ohio plant. On the other hand, if the difference occurs as a result of using locally available raw materials, it may be much more difficult, if not impossible, to produce the same product as before. An initial response from Norton indicated that the new NaZ was from the first batch of product from the Texas plant and may not have been properly washed prior to final firing thus leaving impurities inside the mordenite pellet.

Similar problems were encountered by Holland et al.¹¹ with 3A molecular sieves from Linde. In this case, an eightfold change in iodine retention apparently resulted from a change in the binder.

Prior to the 5 and 9% scoping studies, several intermediate silver loading studies were conducted using the early batch of substrate. Silver loadings of 12 wt % yielded CH₃I loadings between 86 and 118 mg of CH₃I per gram AgZ depending on the run conditions. These loadings correspond to silver utilizations of 61 to 84%. In addition to this evidence, two batches of 3% Ag made from the new NaZ have consistently produced CH₃I loadings and silver utilization of approximately half the loadings and silver utilizations observed for the four batches of 3% AgZ made from original NaZ.

3.4 Regeneration of LAgZ

Regeneration studies of the LA $\overset{\circ}{\text{g}}$ Z indicate that the use of 4.5% H₂ in argon at 500°C does not perform in the same manner as it does with fully exchanged silver mordenite. Very little (<5% in 24 h) of the iodine loaded onto the LA $\overset{\circ}{\text{g}}$ Z is removed by the 4.5% H₂ treatment at temperatures up to 500°C, and only limited iodine removal (~13%) was achieved using pure hydrogen at 500°C for 48 h. Although air purges at temperatures up to 250°C are also ineffective for removing iodine, air at 500°C will remove >90% of the iodine in 24 h. The regenerated material has been reloaded with CH₃I to ~90% of the original iodine loading and regenerated three times with similar results. During the air regenerations at 500°C, 30 to 40% of the iodine is removed in the first hour and an additional 30 to 35% is removed during the second hour of regeneration.

Additional tests of LA $\overset{\circ}{\text{g}}$ Z regeneration were conducted using pure O₂ at 500°C and pure N₂ at 500°C. In both tests <1% of the iodine loaded on the bed was removed by the pure gas stream. Use of a combined 20% O₂–80% N₂ gas stream produced results similar to those observed for an air stream. The negative response for either pure stream indicates a probable reaction between the O₂ and N₂, possibly forming an NO_x. However, this behavior is not fully understood and is currently under investigation.

A second unexplained, but possibly useful, phenomenon was the inability to remove the iodine from the loaded LA $\overset{\circ}{\text{g}}$ Z beds with hydrogen. It is suspected that the hydrogen gas stream may facilitate a transfer of iodine from silver sites to sodium sites within the pellets. Similar removal, or lack of removal, characteristics were noted by Thomas¹² using a mixed bed of AgZ and NaZ. During the regeneration mode, the iodine was not removed from the bed with hydrogen at 500°C as had been demonstrated for AgZ beds. Interpellet iodine transfer for LA $\overset{\circ}{\text{g}}$ Z was examined during four transfer and reloading cycles. A cycle consists of the transfer of iodine from one site within the pellet to another by passing a 4.5% H₂ stream across the beds.

17th DOE NUCLEAR AIR CLEANING CONFERENCE

This was tried, followed by a reloading of CH_3I onto the beds until breakthrough occurred. The total bed loadings for each step in the four cycles are shown in Table 8. This procedure appears to allow at least a doubling in iodine capacity on the bed.

**Table 8. Total bed loadings during interpellet iodine transfer studies
loading on bed in mg $\text{CH}_3\text{I/g}$ LAgZ**

Cycle	Bed number					
	1	2	3	4	5	6
Initial loading	37.4	37.2	22.7	11.5	1.90	0.03
1st transfer	23.6	22.4	22.0	11.0	2.36	0.048
2nd loading	37.7	41.7	42.4	10.1	14.8	6.99
2nd transfer	26.9	22.6	23.5	23.8	5.42	8.08
3rd loading	44.3	42.0	41.8	39.6	28.8	10.8
3rd transfer	32.7	24.0	28.2	22.2	25.2	21.3
4th loading	43.0	35.1	37.9	32.7	24.8	23.7
4th transfer	43.7	33.4	21.0	25.5	19.0	22.1
5th loading	58.9	51.7	35.6	33.8	21.0	23.1

3.5 LAgZ Potential as Main Filter Material

The high degree of silver utilization achieved by LAgZ makes this material attractive for use in a main filter. Of concern during early studies was the high cost associated with the use of silver-substituted zeolites; however, the cost associated with LAgZ is quite low. For example, assuming the following: (1) 3% silver loading by weight; (2) 95% silver utilization; (3) \$10 per troy oz. of silver (\$6.70 per troy oz. of silver on May 21, 1982); and (4) \$11 per kg for 1/16-in.-diam Norton Zeolon 900, a 0.5-t/d nuclear fuel reprocessing plant would require 7.5 kg/d of sorbent to remove the 0.25 kg/d of halogens present in the plant off-gas. The cost of the sorbent amounts to ~\$82 for the substrate and \$76 for silver per day or a total cost of \$6.60/h of operation. The total volume of waste generated would be approximately 0.01 m³/d.

Future work with the partially exchanged silver mordenites will be directed to optimize the degree of silver loading to reduce the total cost and more importantly, the waste volume. The use of interpellet iodine transfer may also play a role in reducing the waste volume.

4. Conclusions

The following conclusions can be made from the experimental results and interpretation of the data:

1. Loadings of ~142 mg of CH_3I per g of AgZ can be obtained. This represents a silver utilization of ~60%.
2. Increased bed temperature has a positive effect on the loading capacity of the AgZ and AgZ.
3. Water vapor content up to a dewpoint of 35°C has a positive effect on the CH_3I loadings on AgZ.
4. Nodules of free silver are formed in AgZ during hydrogen exposure. The size of the nodule appears to be a function of the temperature more than the exposure time. Nodules ~2000 Å in diameter are formed in beds up to 400°C. At 500°C, nodules 10 to 20 times as large are formed.
5. CH_3I loading decreases with hydrogen exposure at increasing temperature.

17th DOE NUCLEAR AIR CLEANING CONFERENCE

6. Higher loadings are achieved using glass filter housings than when using stainless steel when high temperature hydrogen for regeneration is employed.
7. Iron plays a key role in the migration of silver in the mordenite.
8. High silver utilizations (>95%) can be achieved for LA $\overset{\circ}{\text{g}}$ Z.
9. A bed temperature of 200°C produces higher CH₃I loadings on LA $\overset{\circ}{\text{g}}$ Z than temperatures of 150 or 250°C.
10. LA $\overset{\circ}{\text{g}}$ Z cannot be regenerated using hydrogen at 500°C as can A $\overset{\circ}{\text{g}}$ Z.
11. Interpellet iodine transfer can be used to extend LA $\overset{\circ}{\text{g}}$ Z capacity.
12. Air at 500°C can strip iodine from LA $\overset{\circ}{\text{g}}$ Z.
13. LAgZ produced from newly acquired NaZ resulted in lower iodine capacity. This may be the result of incomplete washing of the NaZ prior to final firing at the manufacture.

Future plans include:

1. Further examine the effects of stainless steel on A $\overset{\circ}{\text{g}}$ Z regeneration and nodule formation.
2. Examine the effect of operating conditions on the length of the mass transfer zone.
3. Determine the optimum silver loading on A $\overset{\circ}{\text{g}}$ Z to minimize waste volume and maximize silver utilization.
4. Investigate the mechanisms involved in CH₃I loads on A $\overset{\circ}{\text{g}}$ Z and LA $\overset{\circ}{\text{g}}$ Z.
5. Study mixed I₂ and CH₃I loadings on LAgZ.
6. Determine differences between the two batches of NaZ.
7. Explore air stripping mechanisms for LA $\overset{\circ}{\text{g}}$ Z.
8. Examine interpellet transfer in LA $\overset{\circ}{\text{g}}$ Z.

5. References

1. D. T. Pence and B. A. Staples, "Solid adsorbents for collection and storage of iodine-129 from reprocessing plants," *Proc. 13th AEC Air Cleaning Conf.*, CONF-740807, p. 758 (August 1974).
2. L. L. Burger, "Storage of unprocessed fuel," *Nuclear Waste Management Quarterly Progress Report April Through June 1977*, ed. by A. M. Platt, Pacific Northwest Laboratories, BNWL-2377-2 (November 1977).
3. B. A. Staples, L. P. Murphy, and T. R. Thomas, "Airborne elemental iodine loading capacities of metal zeolites and a dry method for recycling silver zeolite," *Proc. 14th ERDA Air Cleaning Conf.*, CONF-760822, p. 363 (August 1976).
4. T. R. Thomas, B. A. Staples, and L. P. Murphy, "The development of A $\overset{\circ}{\text{g}}$ Z for bulk ¹²⁹I removal from nuclear fuel reprocessing plants and PbX for ¹²⁹I storage," *Proc. 15th DOE Air Cleaning Conf.*, CONF-780819, p. 394 (August 1978).
5. R. T. Jubin, "Organic iodine removal from simulated dissolver off-gas streams using silver-exchanged mordenite," *Proc. 16th DOE Air Cleaning Conf.*, CONF-801038, p. 519 (October 1980).
6. D. J. C. Yates, "The stability of metallic cations in zeolites," *J. Phys. Chem.* **69**, 1676 (1965).
7. L. L. Burger, "Iodine-129 fixation," *Nuclear Waste Management Quarterly Progress Report April Through June 1981*, ed. by Judy Powell, Pacific Northwest Laboratories (in publication).

17th DOE NUCLEAR AIR CLEANING CONFERENCE

8. H. K. Beyer and P. A. Jacobs, "Reduction and Reoxidation of Silver Mordenites," *Molecular Sieves-II*, ed. by James R. Katzer, ACS Symposium Series No. 40, American Chemical Society, Washington, D.C. (1977).
9. K. Tsutsumi and H. Takahashi, "The formation of metallic silver in silver form zeolites," *Bull. Chem. Soc. Jpn.* 45(8), 2332-2337 (1977).
10. T. D. Murphy, Jr., "Design and analysis of industrial experiments," *Chem. Eng.* 84, 168-82 (1977).
11. B. Horan, Norton Chemical Process Products Division, Akron, Ohio, personal communication.
12. W. D. Holland, A. H. Shaw, A. F. Kaiser, J. C. McGee, *Experimental Studies Concerning the Drying of Voloxidizer Off-Gases*, ORNL/Sub-7164/1 (July 1981).
13. T. R. Thomas, personal communication.

DISCUSSION

VIKIS: How do you rationalize your observation that air releases the sorbed iodine at 500°C, but N₂ or O₂ individually would not? What happens to the organic part of CH₃I, does it stay on the sorbent or does it go through?

JUBIN: We currently suspect the formation of small quantities of NO_x from the N₂ and O₂ as the gas stream passes across the silver mordenite bed. We have been able to strip the loaded iodine from the bed using streams of NO or NO₂. The formation of NO_x is presently under investigation at ORNL. The organic portion passes through the bed.

PORREY: Do you intend to investigate the differences in early and later base mordenite material? What does Norton believe is the problem? Have x-ray diffraction studies been done to determine differences?

JUBIN: We are presently investigating the differences between the two batches of sodium zeolite. No significant differences were observed using x-ray diffraction. A quantitative analysis of both batches also showed no major differences in the major and minor components. Norton believes the problem lies with inadequate washing of the zeolite prior to its final firing. This resulted in some additional material being trapped within the micro- and macropore structure. This possibility is supported by a pore size distribution measurement of both batches which showed a reduced pore size in the material from the Brian, TX facility.

THOMAS, T.R.: Are you getting better CH₃I loading capacities with Ag₂O or Ag⁰Z (pretreated with H₂)? Is it the Fe⁰ impurities in the Ag⁰Z or the Fe⁰ from the S.S. reactor that is responsible for low CH₃I loadings after regeneration?

JUBIN: We get better loading capacities for CH₃I using Ag⁰Z (pretreated with H₂ at 200°C for 24 hours). Loading capacities drop as time and, more critically, temperature is increased. We believe the major factor is the Fe⁰ in the reactor vessel itself since only small losses in capacity are noted following regeneration in a glass housing.

17th DOE NUCLEAR AIR CLEANING CONFERENCE

THOMAS, T.R.: From your paper, I estimate it would cost about \$700,000/yr. (based on 300 days) for the AgOZ (3% - 5% by wt exchanged) for a 5t/d FRP. Is that correct?

JUBIN: Yes, assuming a throwaway bed. However, over half of the cost is the substrate itself. If higher silver loadings perform as well as the 3% LAgZ, the total cost and waste volume can be reduced by 25% and 50% by using 6% LAgZ. The performance characterization of the 5-6 LAgZ and 9% LAgZ will be completed as soon as the problems encountered with the new NaZ are resolved.

A PARAMETRIC STUDY ON REMOVAL EFFICIENCY OF
IMPREGNATED ACTIVATED CHARCOAL AND SILVER ZEOLITE
FOR RADIOACTIVE METHYL IODIDE

H. Shiomi, Y. Yuasa and A. Tani
Nippon Atomic Industry Group Co., Ltd.
Kawasaki, Japan

M. Ohki and T. Nakagawa
Toshiba Corporation
Yokohama, Japan

The Tokyo Electric Power Co., Inc.
The Tohoku Electric Power Co., Inc.
The Chubu Electric Power Co., Inc.
The Hokuriku Electric Power Co., Inc.
The Chugoku Electric Power Co., Inc.
The Japan Atomic Power Co., Ltd.

Abstract

The removal efficiency of impregnated activated charcoal and silver zeolite for radioactive methyl iodide is influenced by various parameters such as temperature, relative humidity, face velocity and packing density. This study is to evaluate the dependency of the removal efficiency on each parameter and these combined parameters, quantitatively. Four types of adsorbents, BC-727, AgX, CHC-50 and SS 208C 5KI₃, were tested. From experimental data and mass transfer theory, an experimental equation for evaluating the removal efficiency of adsorbents was derived under a series of experiments for radioactive methyl iodide-131. It was concluded that the removal efficiency calculated from the experimental equation agreed well with the experimental value. Effects of experimental specific parameters, such as Pre-flow time, methyl iodide injection time and After-flow time, on the removal efficiency of adsorbent are also described.

I. Introduction

Impregnated activated charcoal and silver zeolite are being utilized at Nuclear Power Facility and Radioactive Isotope Facility, in order to remove radioactive iodine from gaseous effluents of those facilities. The trapping efficiency of these adsorbents for radioactive iodine is affected by such parameters as bed length, packing density, temperature, relative humidity and face velocity. The dependency of the trapping efficiency on each parameter is important to design a radioactive iodine removal system and to evaluate reliability of the system under accident conditions.

Influence of individual parameters has been reported^{(1), (2), (3)}, but the quantitative evaluation on influence of these combined parameters has hardly been discussed. It is desirable, however, to evaluate quantitatively the influence of combined parameters from above mentioned reasons. From the point of view, authors have tried to conduct a series of experiments in order to derive and check an experimental equation which can evaluate the influence of combined

parameters.

II. Experimental

Apparatus and Experimental Procedure. The experimental apparatus consisted of methyl iodide generator, humidifier and adsorbent bed installed in a thermostated oven as shown in Figure 1. Figure 2 shows the construction of the bed and the stainless steel filter elements which were assembled into the bed. The filter element have internal dimensions of 60mm diameter by 10mm long and both sides are covered with a stainless steel screen 50mm in diameter. Each filter element was packed with the adsorbents shown in Table I.

Table I. Impregnated Adsorbents under Investigation

Adsorbents	Base Material	Nominal Size	Apparent Density	Impregnation
BC-727	Coconut	8 x 16	0.50g/cm ³	KI+I ₂ , 5 w/o
AgX*	Molecular Sieve Type X	10 x 16	1.1 g/cm ³	Ag(Exchanged metal cation)
CHC-50**	Coconut	28 x 60	0.60g/cm ³	TEDA, 10 w/o
SS 208C 5KI ₃ ***	Coconut	8 x 16	0.50g/cm ³	KI+I ₂ , 5 w/o

* CTI-NUCLEAR silver zeolite, Type III

** Toyo Roshi (Toyo Filter Paper) Co., Ltd.

*** Sutcliffe Speakman & Co., Ltd.

The experiments were conducted according to the order of pre-flow step, methyl iodide injection step and after-flow step.

Pre-flow step: Air with controlled relative humidity was run through the bed until the adsorbents reached equilibrium. The Ueshima-Brooks mass flowmeter measured and controlled flow rate of dry air. The mass flowmeter has a rated accuracy of ± 2 percent. Relative humidity can be controlled in the range of 0 ~ 95 percent with accuracy of ± 1 percent and temperature of the adsorbent bed in the thermostated oven can be controlled in the range of 20 ~ 90°C within ± 0.5 °C.

Methyl iodide injection step: After the pre-flow step, Nitrogen gas which contained methyl iodide tagged with ¹³¹I was being injected into humid air flow during from 0.25 hours to 2 hours. The injection flow rate was monitored with a NaI(Tl) scintillation detector.

After-flow step: Following the methyl iodide injection step, humid air was passed through the bed at the same condition as in the pre-flow step for 0.1 ~ 15 hours.

After these steps, the piping and the bed were swept with dry air, and then the bed was disassembled to the filter elements. Radioactivity collected in each filter element was measured with a

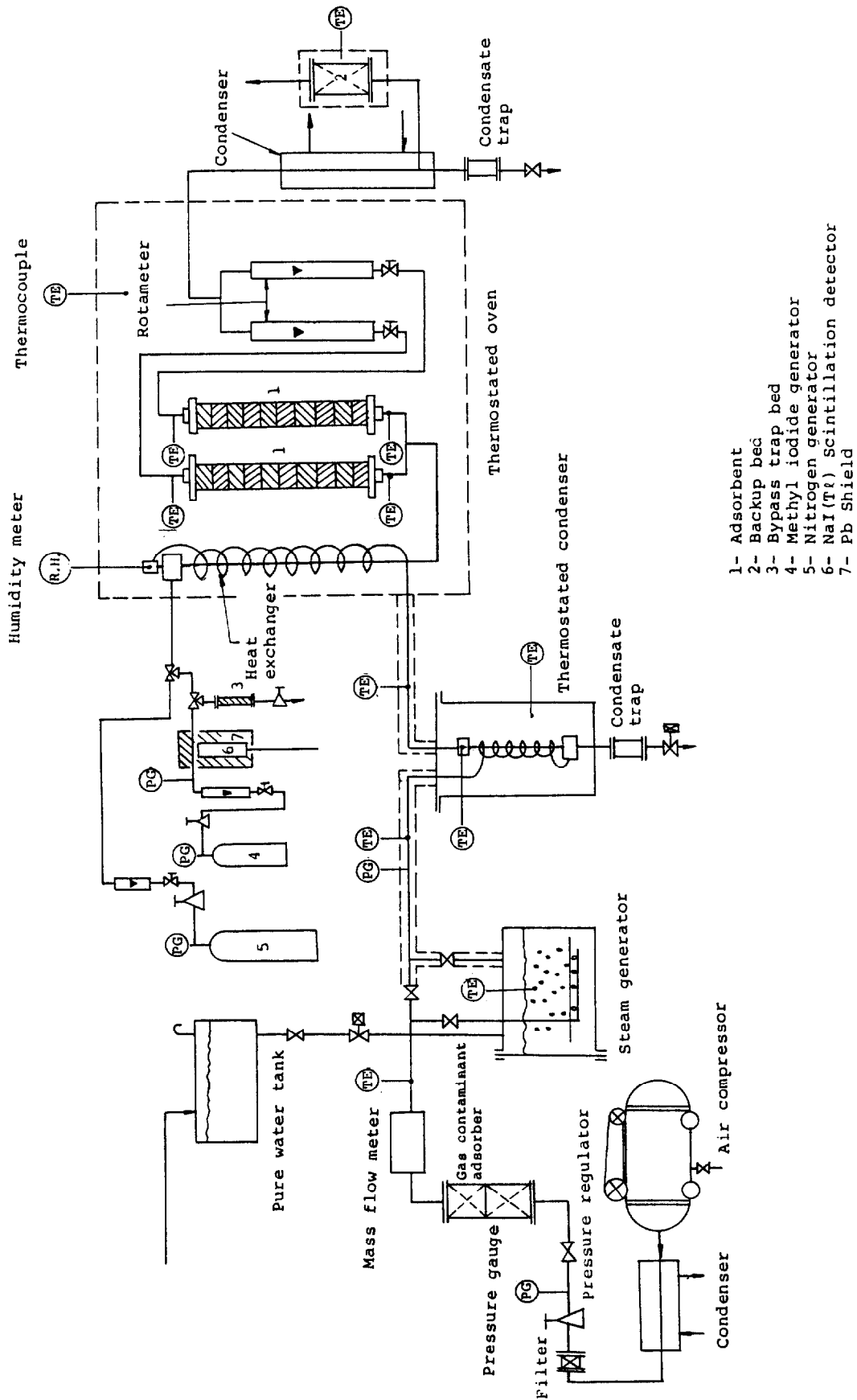
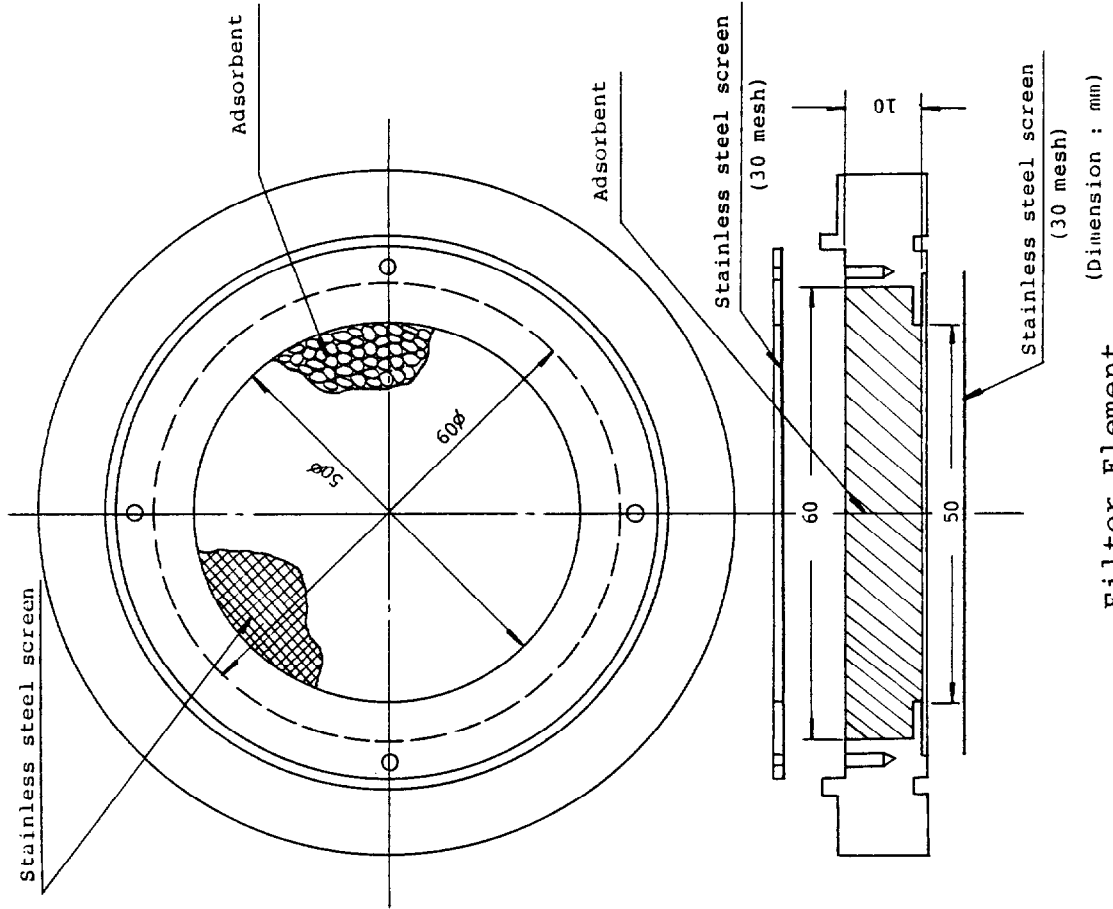


Fig. 1 Schematic Diagram of Experimental Apparatus



Filter Element

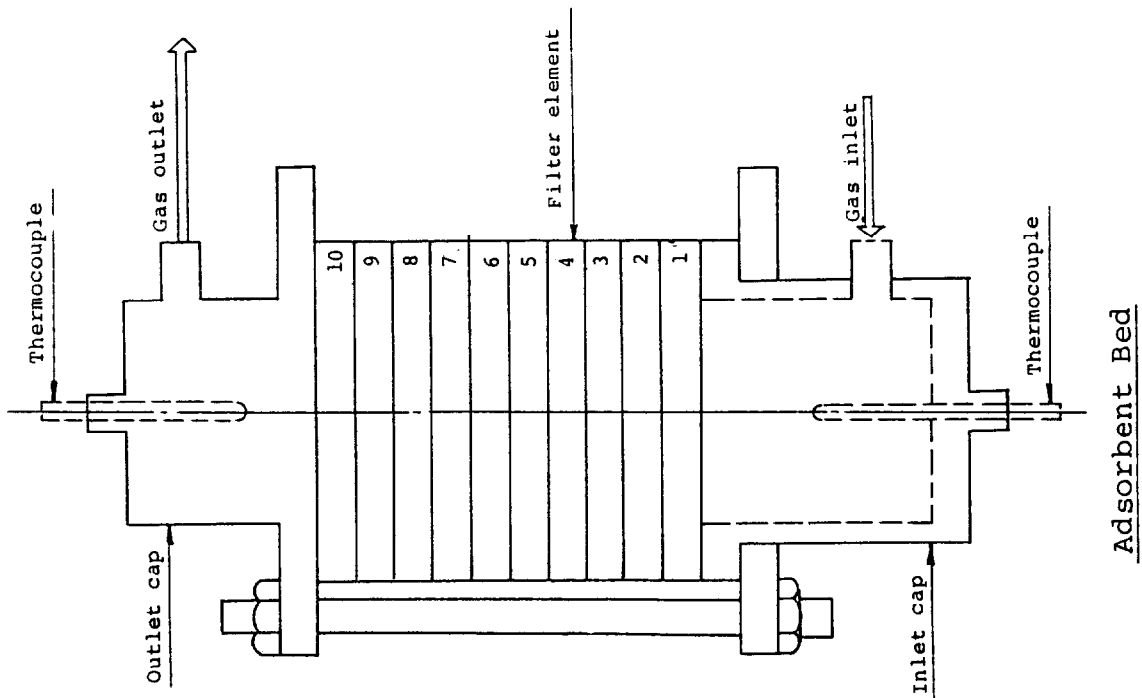


Fig.2 Filter Element and Filter Bed Assembly

Ge(Li) detector.

Experimental Conditions. Table I shows the properties of adsorbents which were used in experiment. Removal efficiency of the adsorbents for methyl iodide-131 is affected by such parameters as temperature, relative humidity, face velocity, packing density, pre-flow time, methyl iodide injection time and after-flow time.

Experiments were done under such conditions as shown in Table II.

Table II. Experimental Conditions

Parameter	Adsorbent	Experimental Range
Temperature (°C)	BC-727	25 ~ 80
	AgX	30 ~ 85
	CHC-50	30 ~ 80
	SS 208C 5KI ₃	20 ~ 65
Relative Humidity (%)	BC-727	30 ~ 95
	AgX	0 ~ 95
	CHC-50	30 ~ 85
Face Velocity(cm/sec)	BC-727	10 ~ 25
	AgX	5 ~ 35
Packing Density (g/cm ³)	BC-727	0.38 ~ 0.60
	AgX	1.05 ~ 1.30
Pre-flow (hours)	BC-727	0 ~ 22
Injection (hours)	BC-727	0.25 ~ 2
After-flow (hours)	BC-727	0.1 ~ 10

Each experiment was done under the condition that one parameter was varied over the range shown in Table II and the other parameters were fixed. Each value of the fixed parameters is following,

Temperature: 66°C
 Relative Humidity: 70%
 Face Velocity: 20cm/sec
 Packing Density: approximately Apparent Density
 Pre-flow Time: 20 hours
 CH₃I-injection Time: 1 hour
 After-flow Time: 1 hour
 CH₃I-131+CH₃I-127 Concentration: 0.10±0.03mg/m³
 Bed Depth: 1cm x 10

Calculation Method of Removal Efficiency. It is well known that radioactive intensity of the filter elements is to be inversely exponential with bed depth. The typical profile which was shown in Figure 3 was expressed with the following equation,

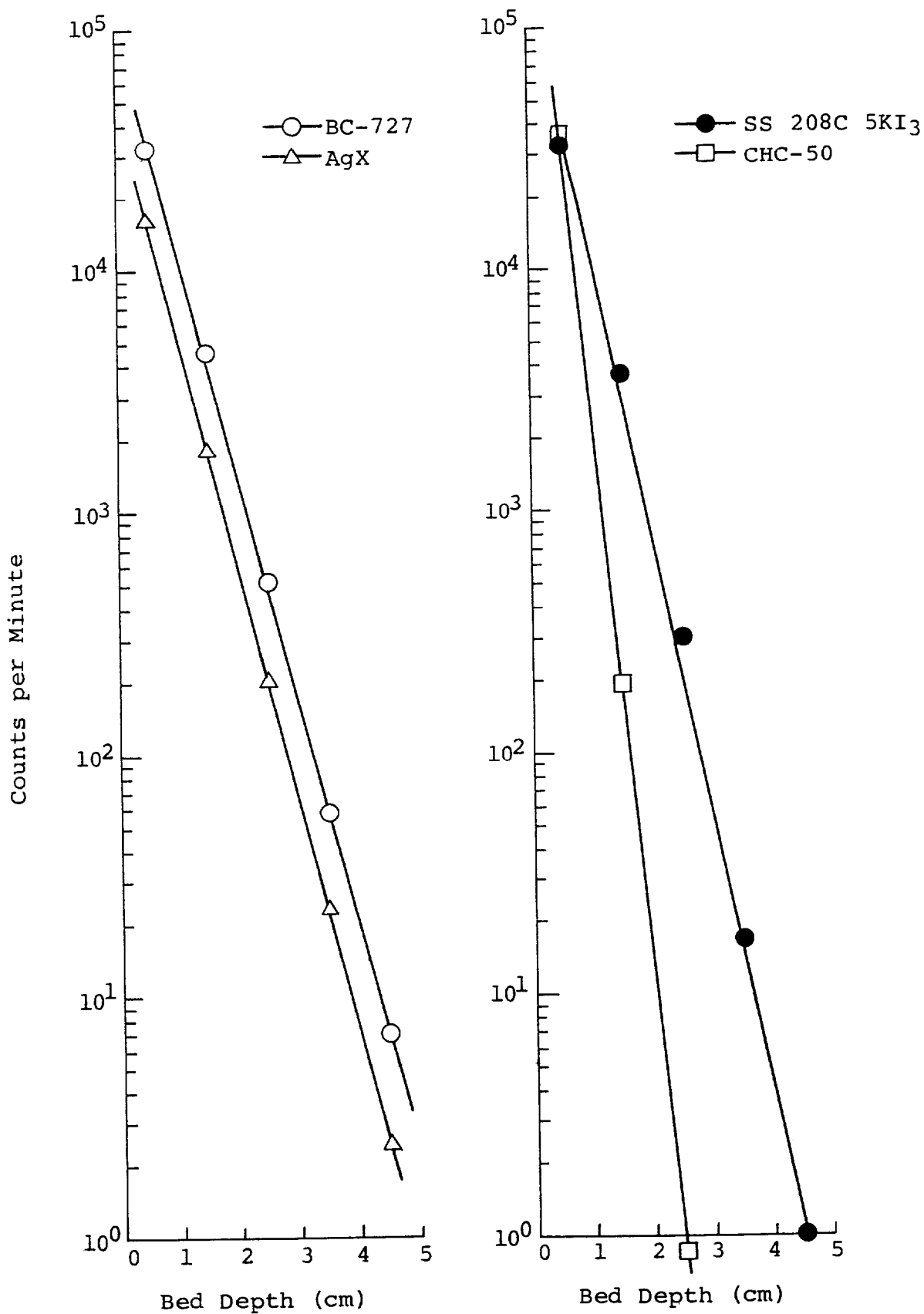


Fig. 3 Experimental Depth Profile of CH₃I-131 with New Adsorbent in Five One-Centimeter Layers

$$Q_i \propto e^{-\mu L_i} \quad (1)$$

where

- Q_i : radioactive intensity of the i th filter element
- L_i : distance of the i th filter element from inlet of the bed
- i : number of filter element ($i = 1 \sim 10$)
- μ : removal coefficient

The equation (1) is obtained by mass balance in the bed and external fluid phase diffusion model on outer surface of the adsorbent as shown in Appendix, and the removal coefficient μ is presented by the equation,

$$\mu = \frac{k_g a_v}{V_g} \quad (2)$$

Trapping efficiency η is defined with the following equation,

$$\eta = 1 - \frac{C^*}{C_0} \quad (3)$$

where

- C^* : concentration of CH_3I^* in gaseous phase
- C_0 : inlet concentration of CH_3I^* in gaseous phase

From Appendix, equation (3) is transformed into the equation,

$$\eta = 1 - e^{-\mu L} \quad (4)$$

where L : bed length

Influence of each parameter was evaluated by calculating the removal coefficient from the profile of the radioactive iodine-131 intensity obtained by experiments.

III. Results and Discussion

Effect of Temperature. Figure 4 illustrates results obtained from experiments which were conducted to investigate the effect of temperature on the removal efficiency for such adsorbents as BC-727, AgX, CHC-50 and SS 208C $5KI_3$, and it reflects the well-known effect of increasing removal efficiency with increasing temperature on a new adsorbent (4).

From Figure 4, the removal efficiency was approximated by the following equation,

$$\mu \propto \exp(aT) \quad (5)$$

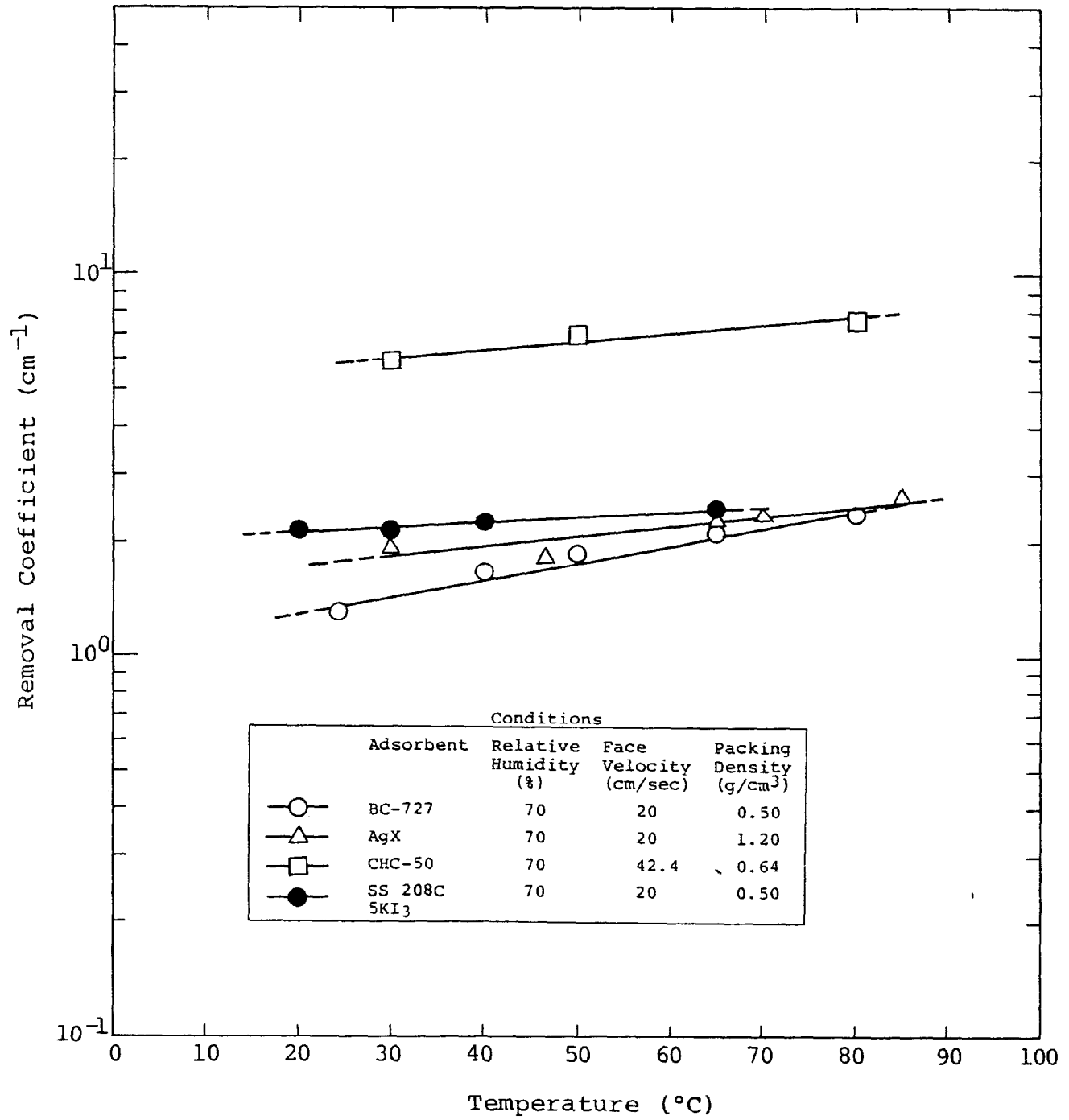


Fig.4 Effect of Temperature

17th DOE NUCLEAR AIR CLEANING CONFERENCE

where μ : removal coefficient (cm^{-1})
T: Temperature ($^{\circ}\text{C}$)
a: constant (temperature factor)

The constant "a" is shown in Table III, calculated from the equation (5) and the experimental results for each adsorbent.

Values of the constant "a" in Table III appear the following tendency,

- 1) The effect of temperature on BC-727 and SS 208C 5KI₃ is different, in spite of the same removal mechanism, isotopic exchange mechanism, for methyl iodide-131,
- 2) The methyl iodide removal mechanism on AgX and CHC-50 is chemical adsorption, and both adsorbents have the same value of the temperature factor "a".

Effect of Relative Humidity. Figure 5 illustrates results of experiments conducted to investigate the effect of relative humidity on the removal efficiency for such adsorbents as BC-727, AgX and CHC-50. The results appear the well-known tendency of decreasing removal efficiency with increasing relative humidity. This decrease of the removal efficiency is associated with the increase of the amount of water adsorption, because adsorbed water interferes with the interaction of methyl iodide and the adsorbent to an extent depending on the amount of adsorbed water ⁽⁵⁾.

From Figure 5, the effect of relative humidity on the removal efficiency was made an approximation with the equation,

$$\mu \propto \exp (-bH) \quad (6)$$

where μ : removal coefficient (cm^{-1})
H: relative humidity (%)
b: constant (relative humidity factor)

The relative humidity factor "b" for each adsorbent was calculated from the equation (6) and the experimental results, and was shown in Table III.

The relative humidity factor "b" of AgX shown in Table III hold to a fairly good approximation in the wide region of dry \sim 95% relative humidity. In case of BC-727, the relative humidity factor "b" in Table III can be applied in the region of 60 \sim 95% relative humidity, that is, the factor "b" for dry \sim 40% relative humidity is different from the above mentioned value, because amount of adsorbed water on the adsorbent decrease suddenly in comparison with amount of adsorbed water in the former region.

From values of the relative humidity factor "b" shown in Table III, the followings were derived,

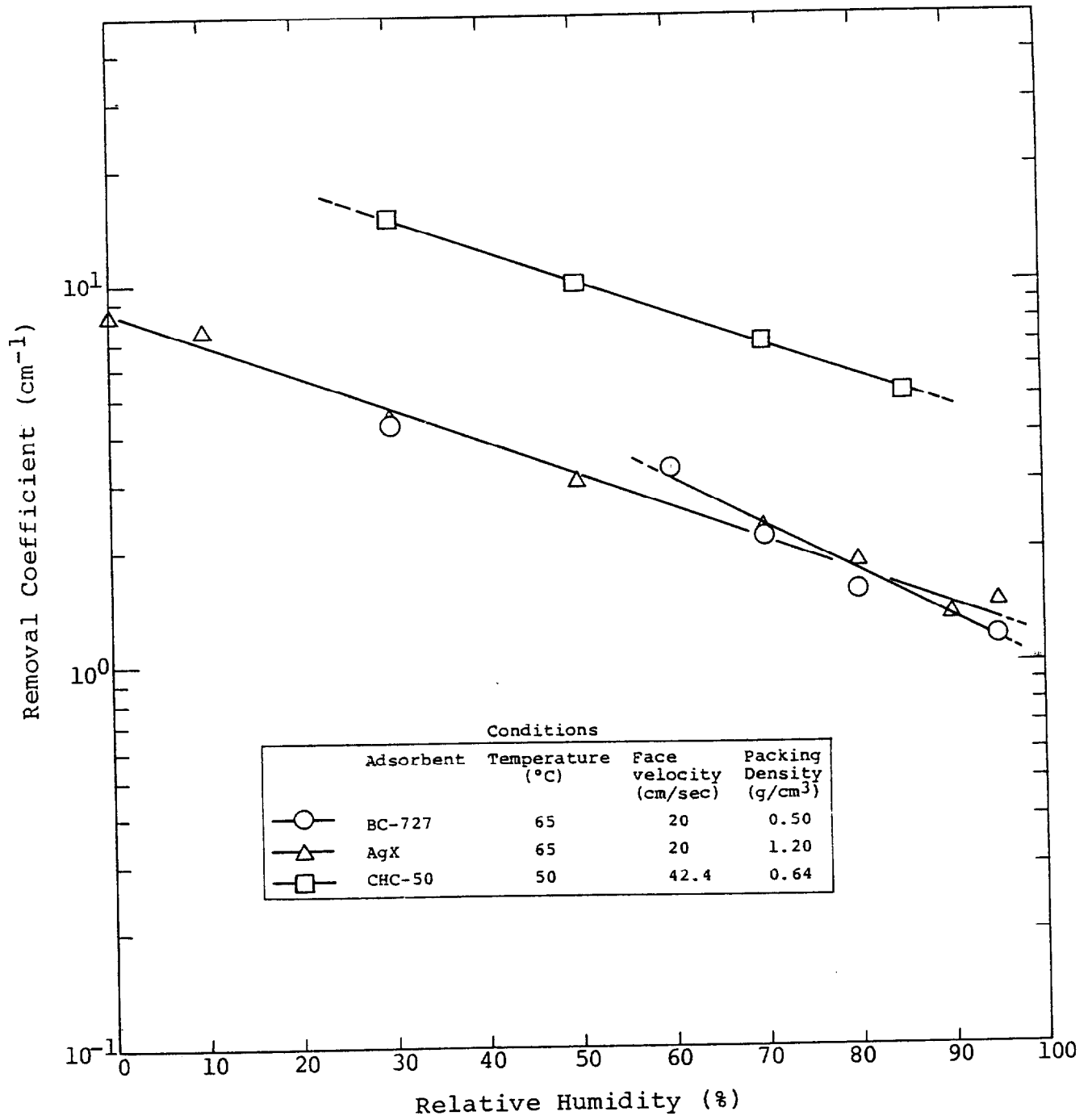


Fig.5 Effect of Relative Humidity

- 1) The effect of relative humidity on AgX is the same as that of CHC-50,
- 2) BC-727 is apt to be influenced by the high relative humidity, compared with other adsorbents.

Effect of Face Velocity. Some papers have been reported on the influence of face velocity on methyl iodide-131 removal with various adsorbents ⁽⁶⁾, ⁽⁷⁾. In most of these reports, however, the influence has been discussed from a combination of the stay time of the feed gas in the bed and the decontamination factor of methyl iodide-131, and has been little discussed from the standpoint of transfer phenomenon of methyl iodide-131 in the bed.

Authors investigated the effect of the face velocity on the methyl iodide-131 removal efficiency from mass transfer theory in order to express the effect by mathematics.

From Appendix, the removal coefficient " μ " of methyl iodide-131 can be expressed by the following equation,

$$\mu = \frac{k_g a_v}{V_g} \quad (2)$$

where

k_g : mass transfer coefficient

a_v : surface area per unit volume of the adsorbent

V_g : face velocity

Mass transfer coefficient " k_g " can be calculated from the experimental equation (Appendix equation) given by Chu et al ⁽⁸⁾. Reynolds Number in the present experiments is from 1 to 30, therefore, the methyl iodide-131 removal coefficient is expressed by following equation,

$$\mu = 34.2(1-\theta) \left\{ \frac{d_p V_g \rho_g}{\eta(1-\theta)} \right\}^{-0.78} \left(\frac{\eta}{\rho_g D_g} \right)^{-2/3} \quad (7)$$

where

μ : removal coefficient

θ : void fraction

d_p : particle diameter

V_g : face velocity

ρ_g : fluid density

η : fluid viscosity

D_g : diffusion constant

From the equation (7), the ratio of the methyl iodide-131 removal coefficient under face velocity V_{g1} to that under face velocity V_{g2} is presented as follows,

$$\frac{\mu_1}{\mu_2} = \left(\frac{V_{g1}}{V_{g2}} \right)^{-0.78} \quad (8)$$

17th DOE NUCLEAR AIR CLEANING CONFERENCE

Figure 6 shows the influence of face velocity on the methyl iodide-131 removal efficiency for BC-727 and AgX. From the equation (8), data points in Figure 6 were fit by the following equation,

$$\mu \propto V_g^{-f} \quad (9)$$

where μ : removal coefficient
 V_g : face velocity
 f : constant (face velocity factor)

The fitting results for the face velocity factor "f" are shown in Table III.

Obtained value of the factor "f" is about 0.8 for both adsorbents, and almost agree with the value in the equation (8). Accordingly, the controlling mechanism of methyl iodide-131 mass transfer in the bed would be external fluid phase diffusion as mentioned in Appendix.

Table III. Summary of Constants of Experimental Equations

Parameter	Experimental Equation	Adsorbent	Constant
Temperature (T)	Equation (5) $\mu \propto \exp(aT)$	BC-727	a = 0.010±0.001
		AgX	a = 0.006±0.002
		CHC-50	a = 0.005±0.001
		SS 208C 5KI ₃	a = 0.003±0.001
Relative Humidity (H)	Equation (6) $\mu \propto \exp(-bH)$	BC-727	b = 0.028±0.004
		AgX	b = 0.020±0.001
		CHC-50	b = 0.020±0.002
Face Velocity (V _g)	Equation (10) $\mu \propto V_g^{-f}$	BC-727	f = 0.822±0.011
		AgX	f = 0.797±0.020

Effect of Packing Density. Figure 7 shows the influence of packing density on the methyl iodide-131 removal efficiency for BC-727 and AgX.

The methyl iodide-131 removal coefficient is expressed by the above mentioned equation (7). Such parameters as d_p , V_g , ρ_g , η and D_g in the equation (7) are independent of void fraction, therefore, the methyl iodide-131 removal coefficient ratio under the different void fraction are appeared as follows,

$$\frac{\mu_1}{\mu_2} = \frac{1 - \theta_1}{1 - \theta_2} = \frac{\gamma_1}{\gamma_2} \quad (10)$$

where μ : removal coefficient

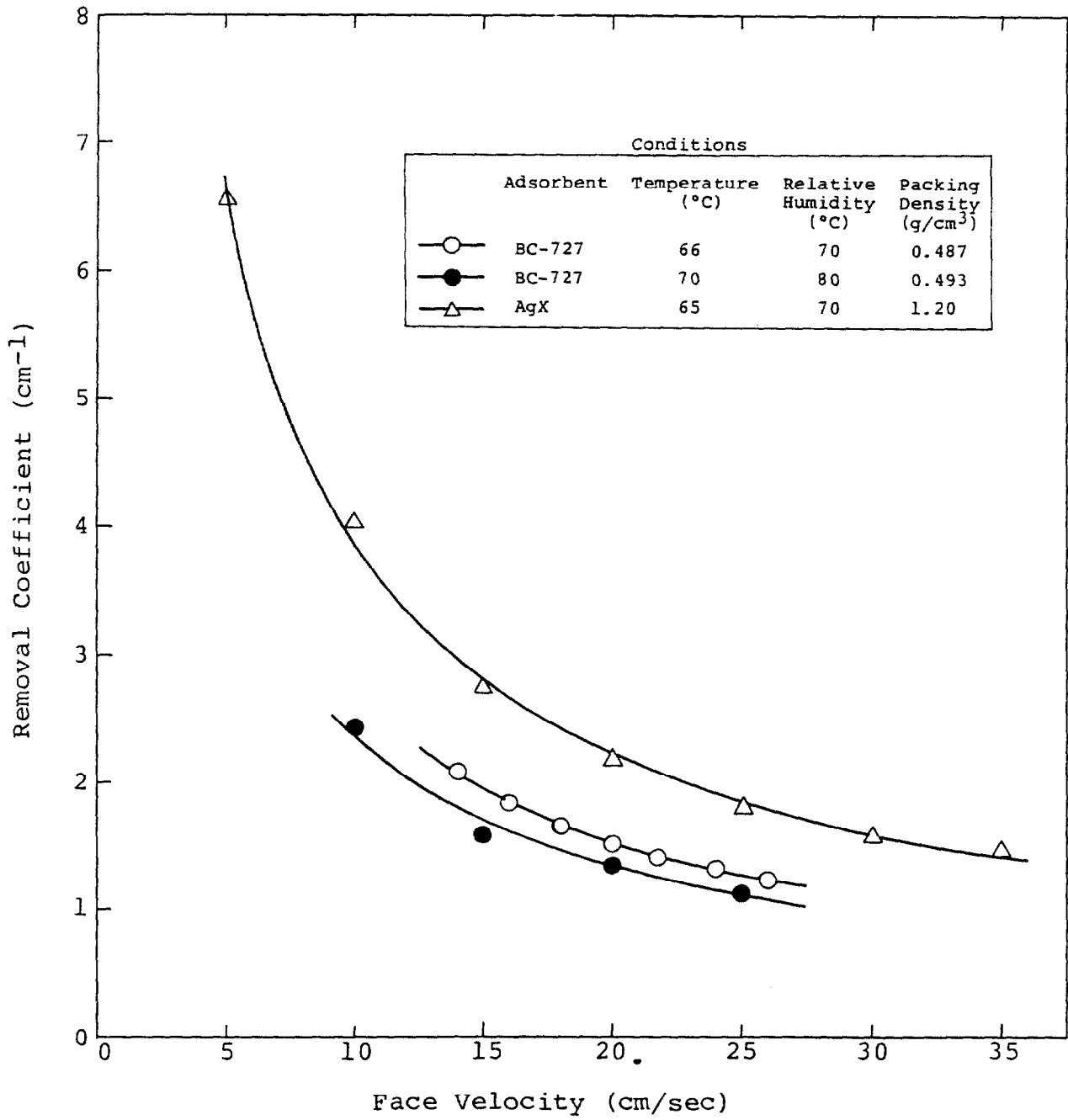


Fig.6 Effect of Face Velocity

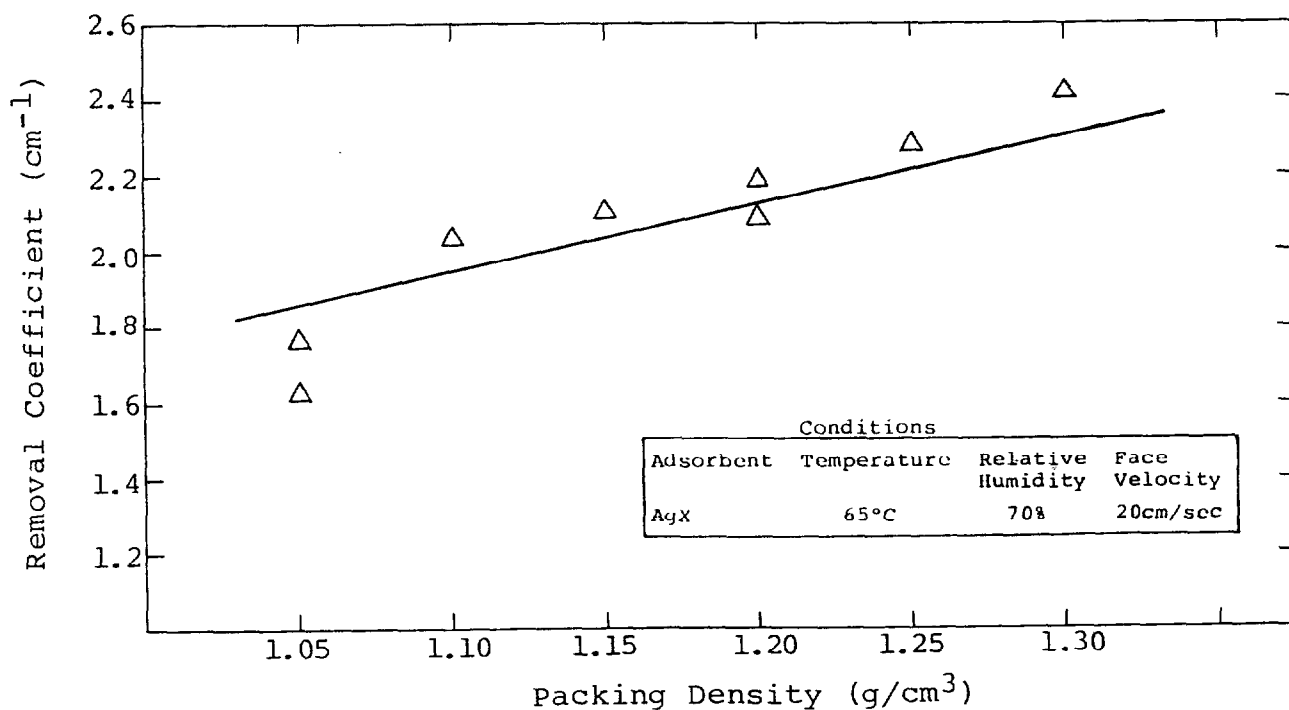
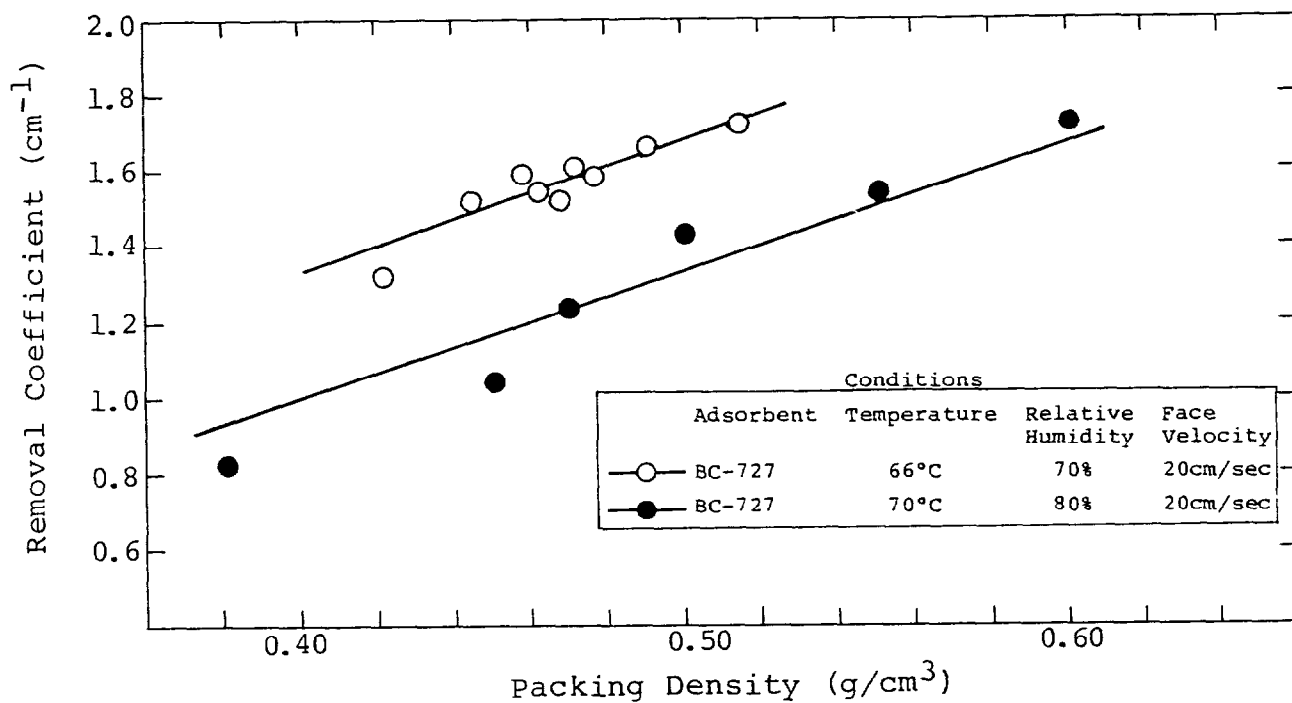


Fig.7 Effect of Packing Density

θ : void fraction

γ : packing density

It is thought that the experimental data in Figure 7 follow the equation (10), and some scatter of the data from the straight line calculated by equation (10) is caused by a variation of adsorbent particle diameter.

Effect of Pre-flow Time. A series of experiments were conducted in order to investigate the effect of the pre-flow time on the methyl iodide removal efficiency.

The results are shown in Figure 8. It is seen that the methyl iodide removal efficiency decreases as the pre-flow time increases in early time, and its efficiency reaches a constant when it reaches a certain value and it will not decrease any more even if the pre-flow time increases.

Figure 9 shows the change of gas temperature at the inlet and the outlet of the bed during the pre-flow time. The inlet and outlet gas has the same temperature before the pre-flow, but outlet gas temperature increases suddenly at the start of the pre-flow and decreases gradually as the pre-flow time increases. The increase of the outlet gas temperature would be caused by heats of water adsorption on adsorbents. In case of the present experimental conditions, water adsorption reaches the equilibrium after the pre-flow time of about 8 hours and temperature of the inlet gas corresponds to that of the outlet gas, as shown in Figure 9.

Changes of the removal efficiency for the methyl iodide seen in Figure 8 would be brought by such distribution of temperature in the bed that was presumed from the change of gas temperature at the outlet shown in Figure 9. Accordingly, the pre-flow time should be taken until the outlet gas temperature became stable.

Effect of Methyl Iodide Injection Time. Figure 10 shows the results of the experiments which were done to investigate the effect of methyl iodide injection time on the methyl iodide removal efficiency. It is seen from Figure 10 that the methyl iodide removal efficiency is not affected by the injection time in the region of 0.25 ~ 2.0 hours.

Effect of After-flow Time. It is well known that the after-flow is performed after methyl iodide injection in order to evaluate the ability of the adsorbent to hold the methyl iodide once it is captured.

It was confirmed that the methyl iodide removal efficiency was not affected by the after-flow time in the region of 0.1 ~ 10 hours as shown in Figure 11.

Evaluation of experimental equation. The methyl iodide trapping efficiency " η " on the adsorbent bed is expressed by the equation (11), as described previously in Calculation Method of Removal Efficiency.

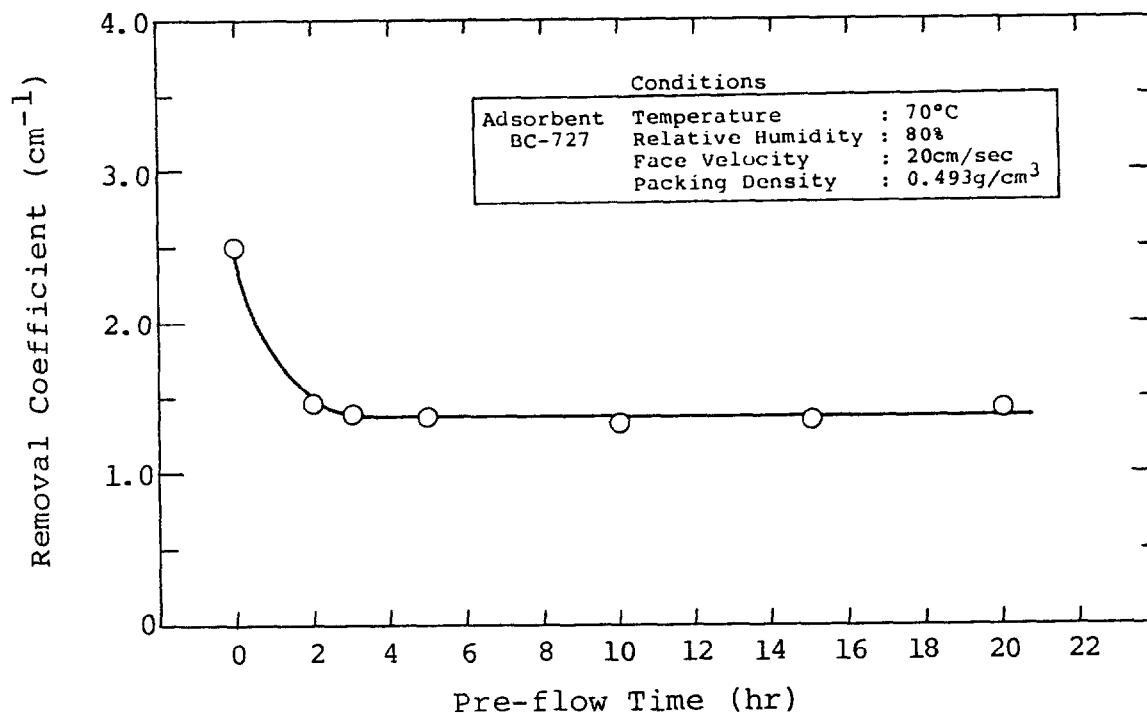


Fig. 8 Effect of Pre-Flow Time

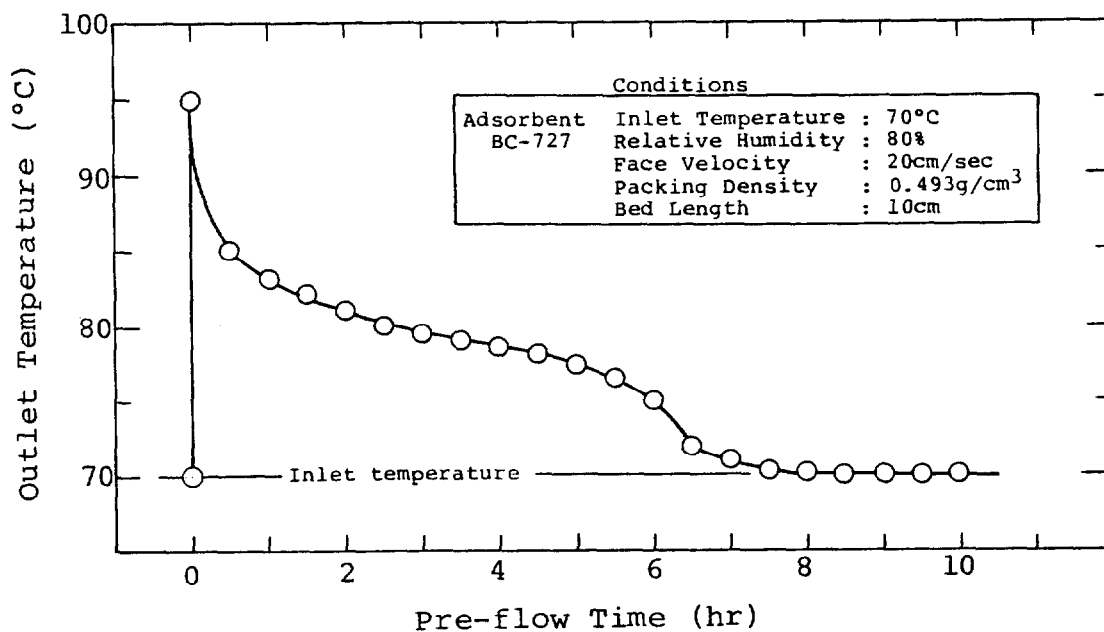


Fig. 9 Change of Outlet Temperature during Pre-flow

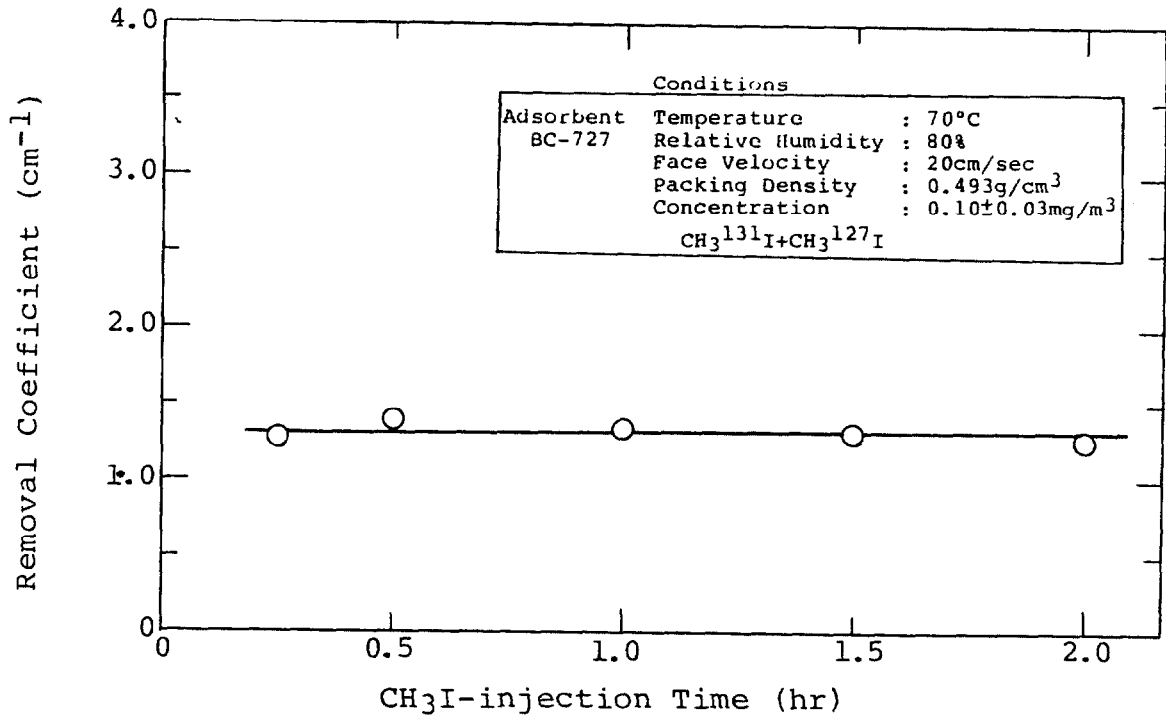


Fig.10 Effect of CH₃I-injection Time

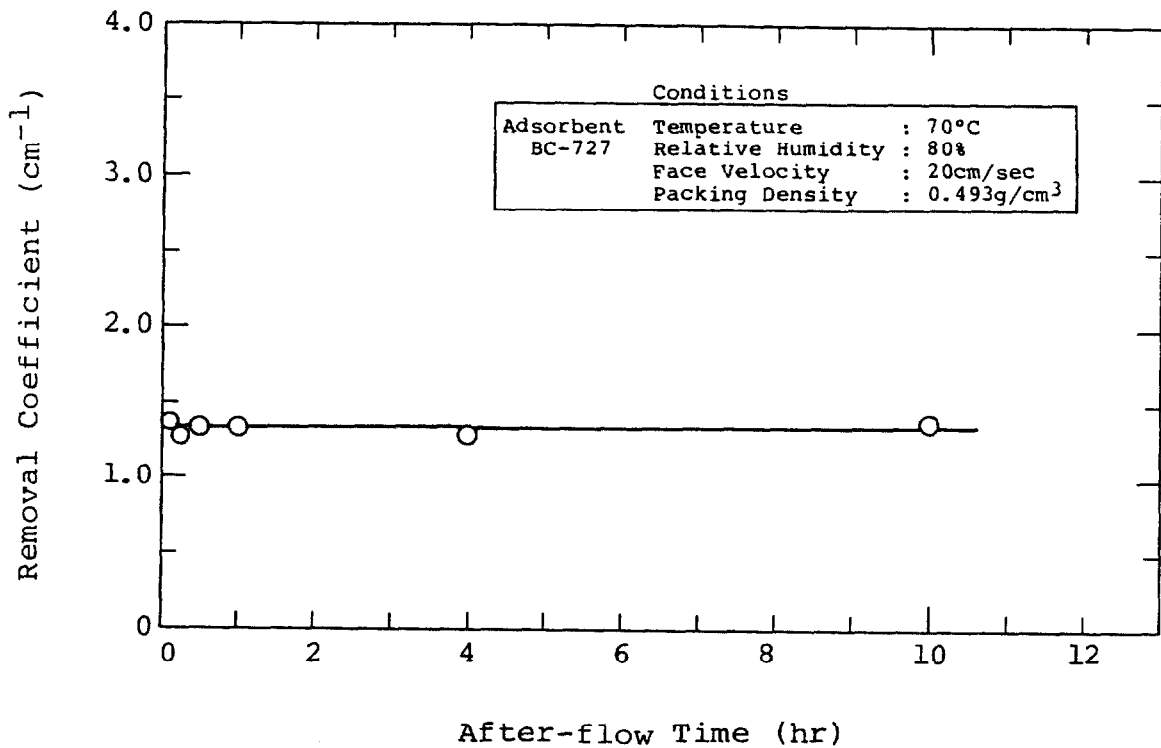


Fig.11 Effect of After-flow Time

17th DOE NUCLEAR AIR CLEANING CONFERENCE

$$\eta = 1 - \frac{C^*}{C_0} = F(L, T, H, V_g, \gamma) = 1 - e^{-\mu L} \quad (11)$$

$$\mu = G(T, H, V_g, \gamma) \quad (12)$$

where

- C*: concentration of CH₃I* in gaseous phase
- C₀: inlet concentration of CH₃I* in gaseous phase
- L : bed length (cm)
- T : temperature (°C)
- H : relative humidity(%)
- V_g: face velocity (cm/sec)
- γ : packing density (g/cm³)
- μ : removal coefficient (cm⁻¹)

Authors derived the equation (13) by combining mass transfer model described in Appendix and individual experimental equations (5), (6) and (9) for each parameters.

$$\mu = A \cdot \gamma \cdot V_g^{-f} \cdot \exp(aT - bH) \quad (13)$$

where

- μ : removal coefficient (cm⁻¹)
- γ : packing density (g/cm³)
- V_g: face velocity (cm/sec)
- T : temperature (°C)
- H : relative humidity (%)
- A : constant
- a : constant (temperature factor)
- b : constant (relative humidity factor)
- f : constant (face velocity factor)

In order to check applicability of the above equation, a series of experiments were conducted. Table IV shows the experimental conditions. Standard conditions in Table IV were used to obtain the constant "A" in the equation (13).

17th DOE NUCLEAR AIR CLEANING CONFERENCE

Table IV. Experimental Conditions for Checking The Experimental Equation

Parameter	Standard Condition	Experimental Range
Temperature (°C)	66	63 ~ 69
Relative Humidity (%)	70	55 ~ 85
Face Velocity (cm/sec)	20	14 ~ 26
Packing Density (g/cm ³)	0.468 *	0.421 ~ 0.515
	0.487 **	0.438 ~ 0.536

* Adsorbent: BC-727, Lot No. M-2767

** Adsorbent: BC-727, Lot No. M-3000

The experimental results are shown in Figure 12. The calculated value of the methyl iodide removal efficiency agreed with the experimental results within ±20%, as shown in Figure 12.

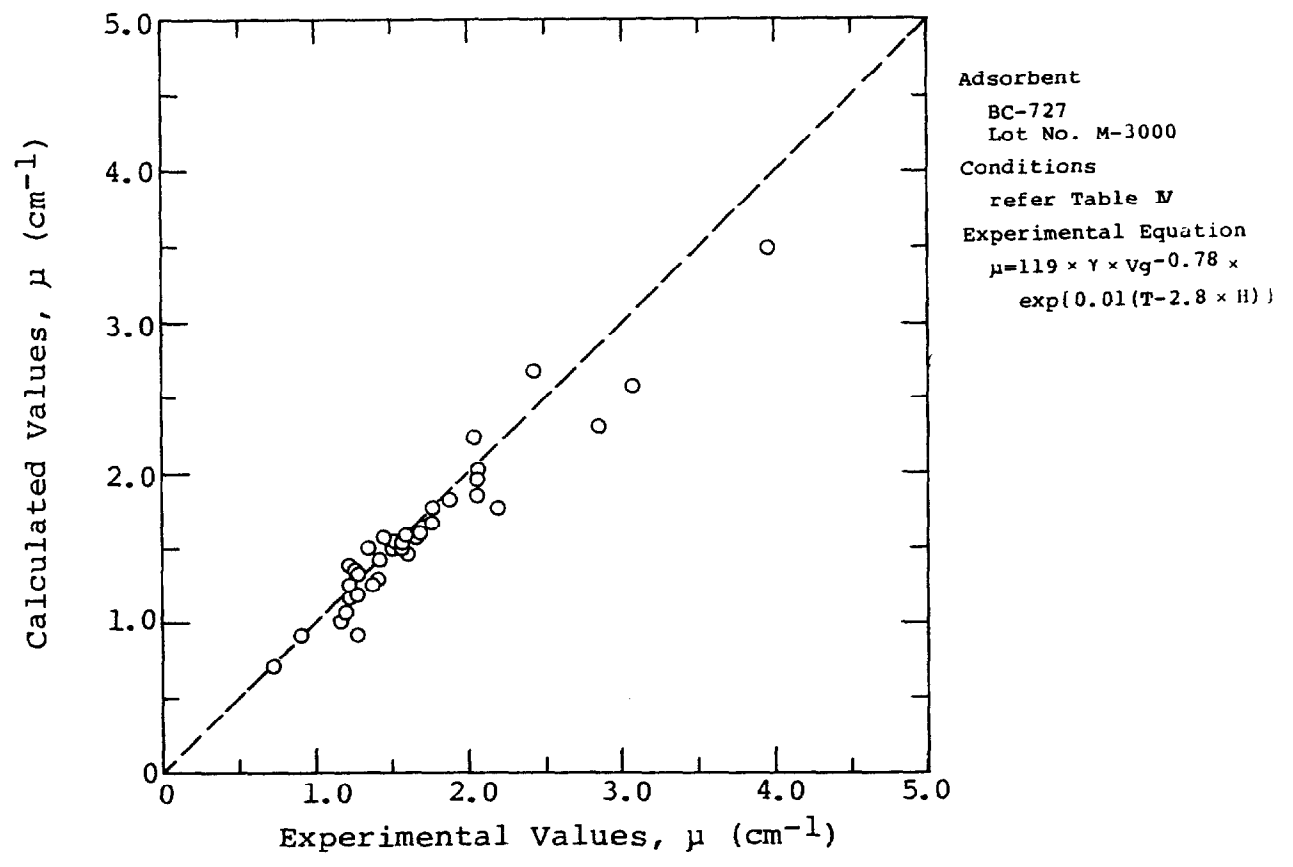
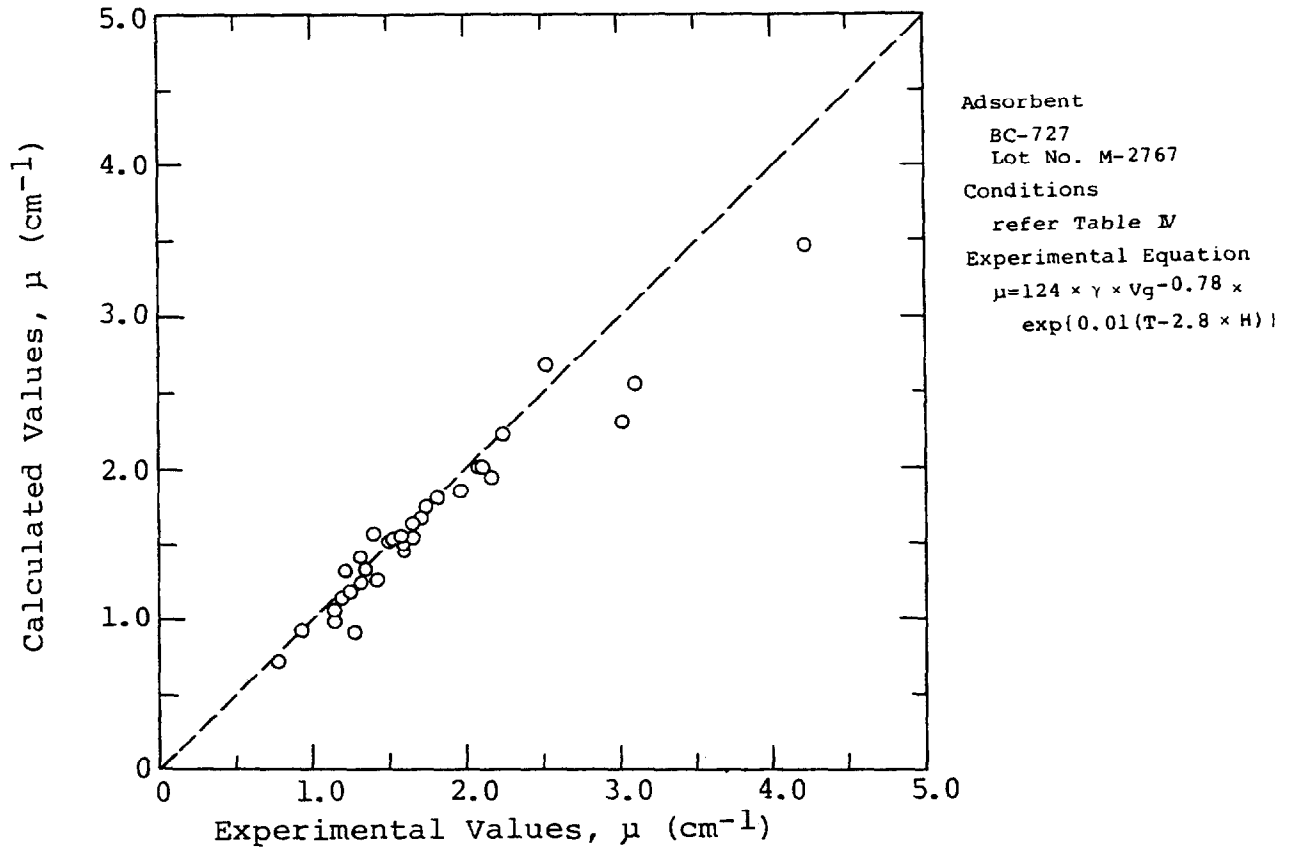


Fig.12 Comparison of The Experimental Results with Calculated Results

IV. Conclusion

The experimental equation for evaluating the methyl iodide removal efficiency of adsorbents was derived from a series of experiments. It was concluded that the removal efficiency calculated from the present equation agreed well with the experimental value.

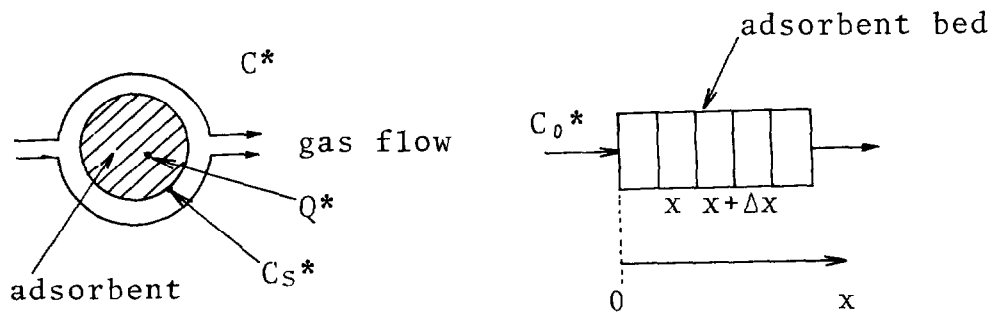
References

1. D. A. Collings, L. R. Taylor, and R. Taylor, "Development of Impregnated Charcoals for Trapping Methyl Iodide at High Humidity", AEC Report CONF-660904, (1966)
2. G. W. Parker, G. E. Cheek, and A. Ferreli, "Retention of Methyl Iodide by Impregnated Carbons Under Ambient Conditions", AEC Report CONF-660904, (1966)
3. D. T. Pence, F. A. Duce, and W. J. Maeck, "Developments in the Removal of Airborne Iodine Species with Metal-Substituted Zeolites", AEC Report CONF-740807, (1974)
4. J. R. Hunt, L. Rankovic, R. Lubbers, and J. L. Kovach, "Iodine Removal Adsorbent Histories, Aging and Regeneration", ERDA Report CONF-760822, (1976)
5. R. D. Ackley, R. E. Adams, and W. E. Browning, Jr., "Removal of Radioactive Methyl Iodide from Steam Air Systems", USAEC Report ORNL-4040, (1967)
6. V. R. Dietz, C. H. Blachly, and L. A. Jones, "Dependence of Gas Penetration of Charcoal Beds on Residence Time and Linear Velocity", ERDA Report CONF-760822, (1976)
7. D. A. Collins, L. R. Taylor, and R. Taylor, "The Development of Impregnated Charcoals for Trapping Methyl Iodide at High Humidity", British TRC Report 1300(W), (1967)
8. Ju Chin Chu, James Kalil, and William A. Wetteroth, "Mass Transfer in a Fluidized Bed", Chemical Engineering Progress, Vol. 49, No.3, p. 141 ~ 149, (1953)

Appendix

Mass Transfer Model of Methyl Iodide

The following model for mass transfer model of methyl iodide was presumed.



*: radioactive

- C^* : concentration of CH_3I^* in gaseous phase (mol/cm^3)
- C_S^* : concentration of CH_3I^* on adsorbent external phase (mol/cm^3)
- C_0^* : inlet concentration of CH_3I^* in gaseous phase (mol/cm^3)
- Q^* : concentration of I^* on the adsorbent (mol/g)
- V_g : face velocity (cm/sec)
- γ : packing density (g/cm^3)
- t : time (sec)
- x : axial distance (cm)

Mass Balance

$$-V_g \frac{\partial C^*}{\partial x} + \frac{\partial Q^*}{\partial t} = 0 \quad (14)$$

(Gas diffusion was neglected.)

External Fluid Phase Diffusion

$$\gamma \frac{\partial C^*}{\partial x} = k_g a_v (C^* - C_S^*) \cong k_g a_v C^* \quad (15)$$

- where
- k_g : mass transfer coefficient
 - a_v : surface area per unit volume of the bed (cm^2/cm^3)

From the equations (14) and (15), the next equations can be obtained.

17th DOE NUCLEAR AIR CLEANING CONFERENCE

$$C^*(x) = C_0 * \exp \left(- \frac{k_g a_v}{V_g} x \right) \quad (16)$$

$$Q^*(x,t) = \frac{k_g a_v}{\gamma} C_0 * t \exp \left(- \frac{k_g a_v}{V_g} x \right) \quad (17)$$

Consequently, the methyl iodide removal coefficient " μ " which was defined by the equation (1) described in Calculation Method of Removal Efficiency is expressed by the equation (2),

$$\mu = \frac{k_g a_v}{V_g} \quad (2)$$

Mass transfer coefficient " k_g " can be calculated the following equations (18), (19), (20) and (21) given by Chu et al⁽⁸⁾.

$$10000 > Re' > 30, \quad J = 1.77 (Re')^{-0.44} \quad (18)$$

$$30 > Re' > 1, \quad J = 5.7 (Re')^{-0.78} \quad (19)$$

$$Re' = \frac{d_p V_g \rho_g}{\eta (1-\theta)} = (N_{Re'}) \quad (20)$$

$$J = \frac{k_g}{V_g} \left(\frac{\eta}{\rho_g D_g} \right)^{2/3} = \frac{k_g}{V_g} (N_{Sc})^{2/3} \quad (21)$$

where

- $N_{Re'}$: modifide reynolds number
- N_{Sc} : schmidt number
- d_p : particle diameter
- ρ_g : fluid density
- η : fluid viscosity
- θ : void fraction
- D_g : diffusion constant

Surface area per unit volume of the bed " a_v " can be calculated by the equation (22), assuming the adsorbent to be a sphere.

$$a_v = \frac{6 (1-\theta)}{d_p} \quad (22)$$

DISCUSSION

CSILLAG: I would like to know if the equation holds for 100% relative humidity?

SHIOMI: No, because we can not obtain reliable experimental data under 100% relative humidity conditions.

BELLAMY: Is it true that the only carbons tested were new virgin carbons?

SHIOMI: Yes.

BELLAMY: Was your equation checked against data from another laboratory?

SHIOMI: No, but this would be a good idea. We want to evaluate our equation for used adsorbents.

DEUBER: I would like to draw attention to the fact that retention increases with increasing residence time. To investigate the effect of face velocity, one should compare it at the same residence time?

SHIOMI: Thank you. I think so.

DEUBER: Did you do some tests on the influence of concentration? I ask this because in the past some have found an increase and some a decrease with changing concentration.

SHIOMI: We have not tested that relationship so far.

17th DOE NUCLEAR AIR CLEANING CONFERENCE

DATA ANALYSIS OF IN PLACE TESTS OF IODINE FILTERS IN THE FRENCH NUCLEAR FACILITIES

P. Mulcey, L. Trehen and J.L. Rouyer
Institut de Protection et de Sûreté Nucléaire
Commissariat à l'Energie Atomique - France

Abstract

The first part of the paper is devoted to the characteristics of the iodine adsorbers which equip French air cleaning systems and to their operating conditions.

The analysis of the data obtained with in place testing of iodine filters is developed further on. Data already available and new complementary data to be obtained are examined.

An analysis of the results of in place tests will give an idea of the rejection level observed for acceptance tests and will show the possible influence of several parameters (air velocity, relative humidity, ageing) upon the measured decontamination factors.

Finally, an assessment is made of the evolution of French cleaning systems during the last few years and of the complementary measurements to be carried out in the frame of the standardized test method.

I. Introduction

French legislation on the inspection of ventilation systems in nuclear facilities⁽¹⁾⁽²⁾ states that the efficiency of their gaseous effluent cleaning systems must be measured at least once a year.

Moreover because of the TMI₂ accident the Permanent Group in charge of Nuclear Reactors⁽³⁾ has decided to bring the inspection frequency to three months in the case of ventilation systems where the iodine adsorbers are in service permanently.

The method adopted in France for many years is now covered by and AFNOR Experimental Standard⁽⁴⁾.

The technique, consisting of an in placetest on the air cleaning system as a whole by the use of a radioactive tracer (iodine 131 - labelled I₂ or ICH₃), is the only method used so far on all iodine filters fitted.

17th DOE NUCLEAR AIR CLEANING CONFERENCE

It gives the overall efficiency of the air cleaning unit at the moment of testing, for working conditions as close as possible to those for which the trap was designed.

The results obtained in this way on certain air cleaning systems have been analysed with a dual purpose :

- to examine the data available now and the new data required to improve the analysis and management of the filters to maximum advantage ;
- to show up any correlations between the decontamination factor and certain parameters affecting its measurement (air velocity, relative humidity, weathering).

In our opinion the method used in France, and more generally in Europe, to measure the decontamination factor of iodine traps must on no account be questioned or fundamentally changed, since no other available method can evaluate the efficiency of the system as a whole for working conditions close to those found in normal operation or in the event of accident.

However from the results obtained by this method it is often difficult to estimate the relative contributions of the leakage rate and the intrinsic efficiency of the active charcoal in the overall decontamination factor, especially when this is small.

For other technical reasons examined below, other measurements, besides the present one, are needed to enrich the data used for calculating the efficiency at the time of inspection and estimating its variation in the time interval between two decontamination factor measurements.

The test method has already been published(5), (6) and will therefore not be described again here.

General remarks

1. Characteristics of iodine adsorber units

All power reactor systems and most laboratory and experimental reactor air cleaning units are equipped with standard 610 x 610 x 292 mm cells, installed either in bag-in bag-out housings or on honeycombed metal frames (filtering walls).

These cells contain about 35 kg of active charcoal impregnated to 1 % with potassium iodide. Coal base charcoal 8-16 mesh ASTM, has usually been used in preference to coconut base charcoal because of its better efficiency at high relative humidity but the fitting of preheaters on new facilities could eventually lead to a review of this choice.

17th DOE NUCLEAR AIR CLEANING CONFERENCE

The charcoal bed is 5 cm deep ; at the nominal flow rate of 1200 m³/h for 25 cm/s the residence time averages 0.2 s.

A sample of this active charcoal is checked in the laboratory beforehand (2-ton batches). To be accepted the sample must have a K factor(8) greater than 8 for a 25 cm/s air velocity and a 90 % relative humidity.

It is practically impossible to correlate the efficiency of the samples with that of the adsorbers these generally being equipped with cells from different active charcoal batches.

2. Working conditions

a) Air velocity

The gas velocity through the active charcoal, too fast on the earliest ventilation systems, has gradually been brought to a value of around 25 cm/s and even less in certain cases.

b) Active charcoal bed depth

For new reactors, especially the 1300 MW(electric) type the bed depth has been increased to 10 cm.

c) Relative humidity

To improve the efficiency of the adsorbers the systems are being equipped more and more with preheaters, which guarantee a relative air humidity below 40 %.

d) Degree of use

A few circuits are ventilated permanently and the efficiency of the adsorbers deteriorates fairly quickly as a result. In all other cases the adsorber is by-passed in normal operation. The insulating dampers must be particularly well made to avoid by-pass leaks. On new ventilation systems the increasing tendency is to use double dampers with the inner part under pressure.

e) Charcoal conditioning

Pneumatically rechargeable carbon adsorbers have been developed over the last few years and are being fitted on certain circuits.

The use of these devices is likely to modify the test procedures.

This point will be examined below.

II. Analysis of data concerning iodine adsorbers

1. Available data

These data are obtained either at the time of testing of during the working period between tests.

a) Data supplied by the test

The first information is obtained by visual inspection of the trap when faults can be detected on the cells themselves (active charcoal leaks; poor air-tightness assembly). During this inspection the ventilation flow sheet is also checked for testing purposes.

The measurements carried out next concern :

- the flow rate through the iodine adsorbers. Whenever possible the pressure drop of the adsorber is measured and checked for consistency with the flow rate determined in the duct ;

- the relative humidity at which the test is performed, to check that the preheaters are working properly ;

- the overall efficiency of the system, obtained from estimates of the iodine 131 activity fixed on the charcoal samples taken.

b) Operational data

In most cases the only working data available are those obtained from periodic flow rate measurements and pressure drop readings for traps on continuously operating circuits.

2. Supplementary data

Certain additional information is necessary to improve the evaluation of iodine traps.

a) Acceptance tests

These should be supplemented by a sampling qualification measurement applicable to each new kind of circuit or facility . This would be especially useful for older types of circuit where requirements for sampling points have not always been foreseen at the design stage.

b) Periodic tests

It is becoming more and more necessary to have a fast and accurate means of estimating leakage of the facility (assembly, by-pass dampers,...) so that in certain cases, when the measured overall efficiency falls below the required level, repairs can be made without changing the cells.

17th DOE NUCLEAR AIR CLEANING CONFERENCE

c) Operation

- For circuits which in normal operation are normally by passed and brought into play only on special occasions (refuelling operations, gaseous effluent handling line...) it would be possible, knowing the number of hours in service, to estimate the probable ageing of the traps and to inform the operator of the risks involved in working with an air cleaning system of efficiency below safety standards.

- It would also be advisable to generalise the periodicity of flow rate measurements on circuits in permanent use, since any operational or configurational anomalies would then be detected.

III. Analysis of results

The results were analysed from two viewpoints : 1 - the rejection level observed at reception of air cleaning units before start up of the facility ; 2 - possible correlations between the measured efficiencies and the different parameters involved (air velocity, relative humidity and weathering of the charcoal).

1. Rejection levels observed on reception

The analysis was carried out on twelve 900 PWR type reactors distributed over 3 different sites.

The results are given in the table below :

Table. Rejection ratio
Expressed in percentage of the total number of tests performed

Site	Number of absorbers per site	Rejection ratio		
		Acceptance test	First routine test	Second routine test
A	34	0	30	0
B	35	2.9	38.5	33.3
C	37	8.1	50	44.4
TOTAL	106	3.8	39.5	25.9

17th DOE NUCLEAR AIR CLEANING CONFERENCE

In most cases of below standard efficiency the causes are not known exactly. For one circuit the poor measured value was due to a fault in the filter housing design which was remedied on the spot. In the other cases failure can be attributed to defective assembly of the elements or to paintwork carried out after the adsorbers were fitted. Once the filter elements had been changed the values were up to standard.

2. Influence of the air velocity and relative humidity

Attempts were made to correlate the efficiencies measured on reception with the air velocity and relative humidity.

The analysis was performed on all the air cleaning systems of the containment buildings for the 12 reactors mentioned above.

The nominal flow rate of these systems, which work in close circuit, corresponds to an air velocity of 26.1 cm/s and a 0.19 s. apparent residence time in the charcoal.

For this series of tests the relative humidity of the air passing through the adsorbers ranged from 15 to 40 %.

a) Influence of the air velocity

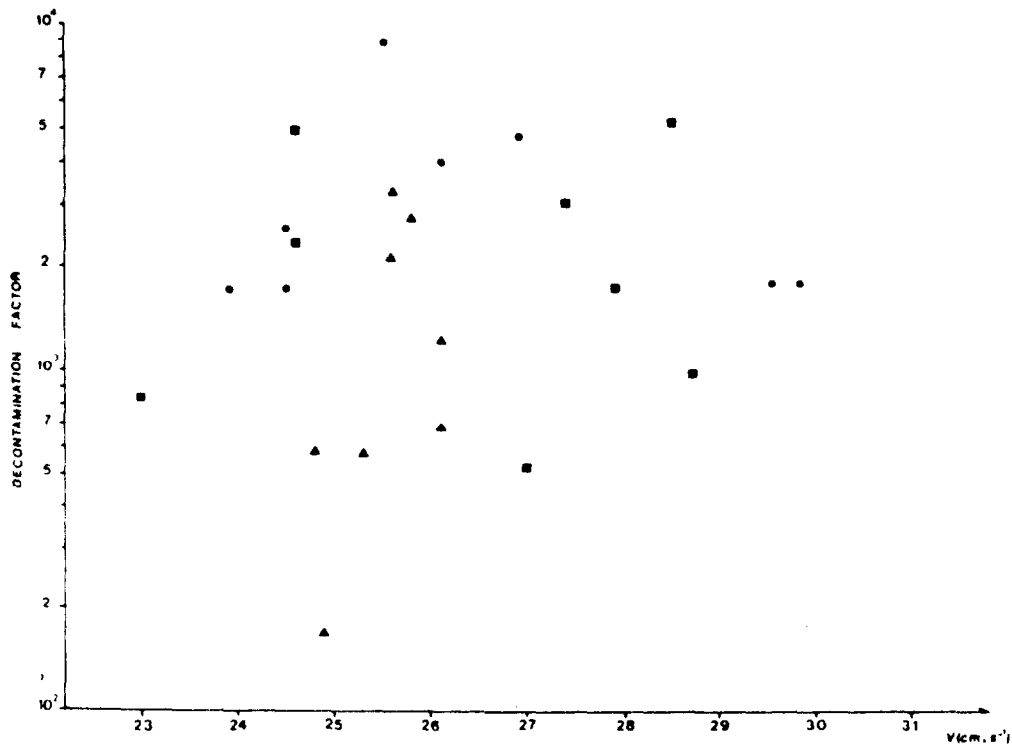
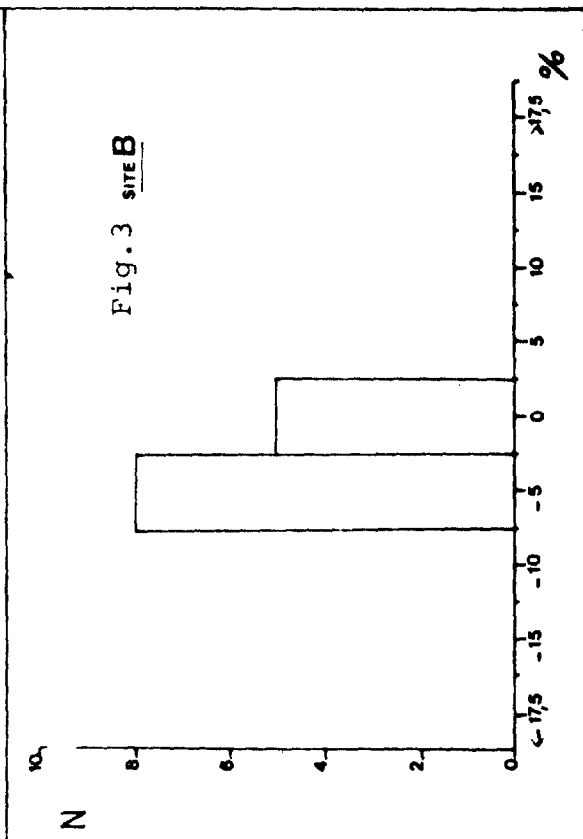
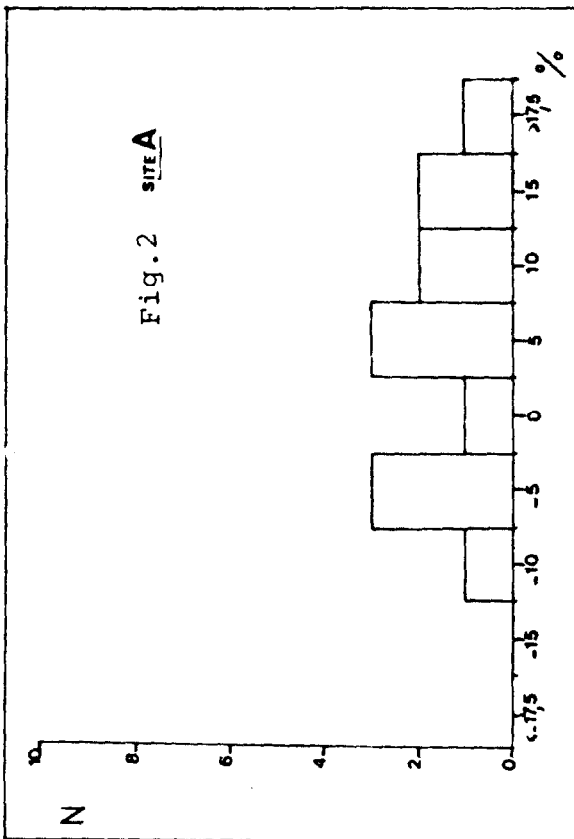
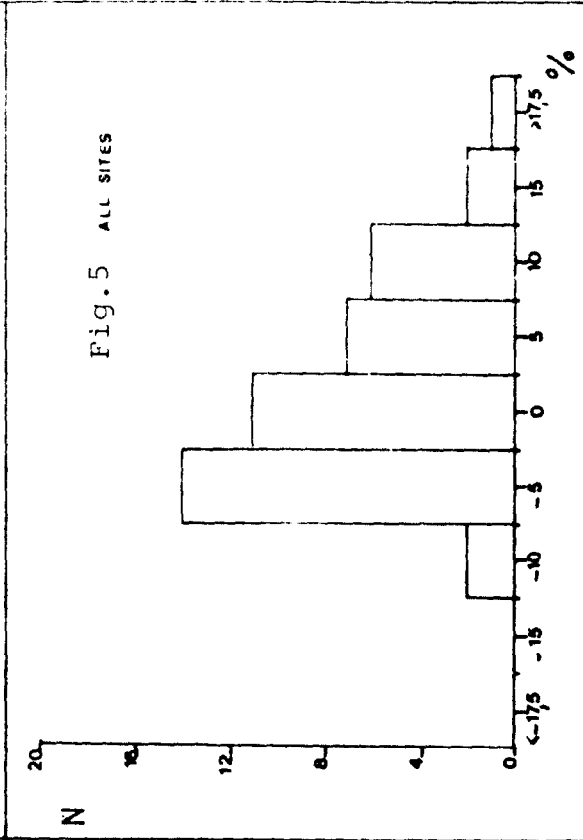
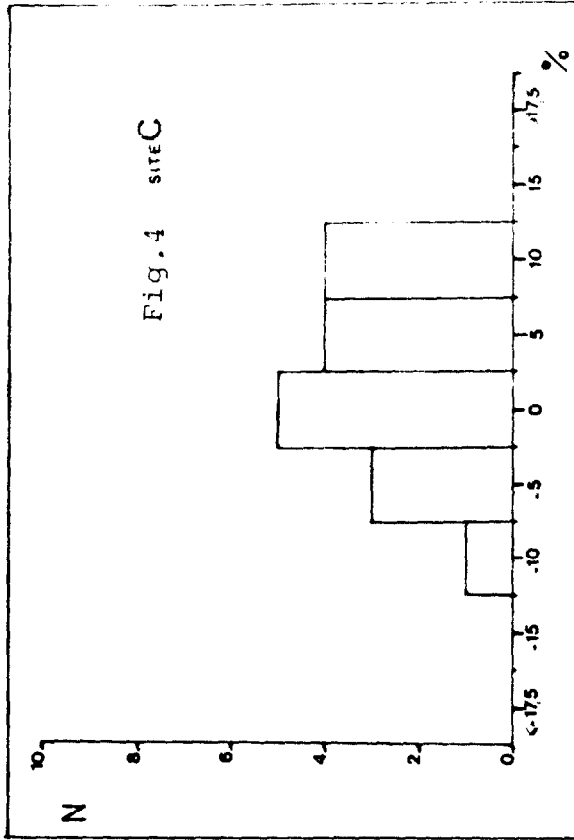


Fig.1



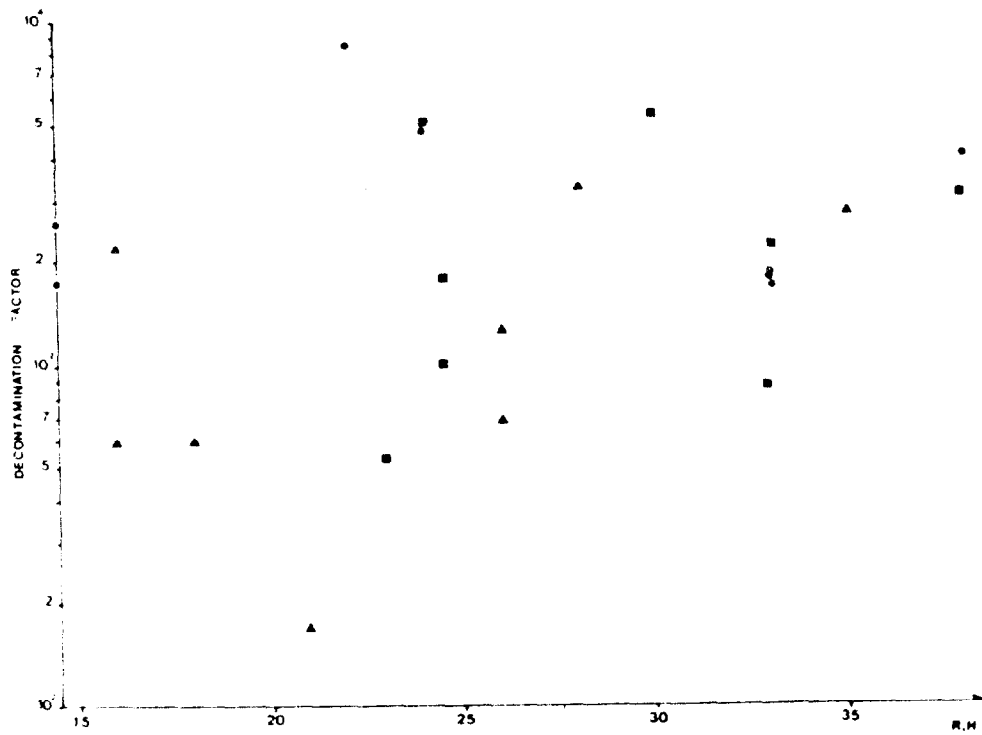


Fig.6

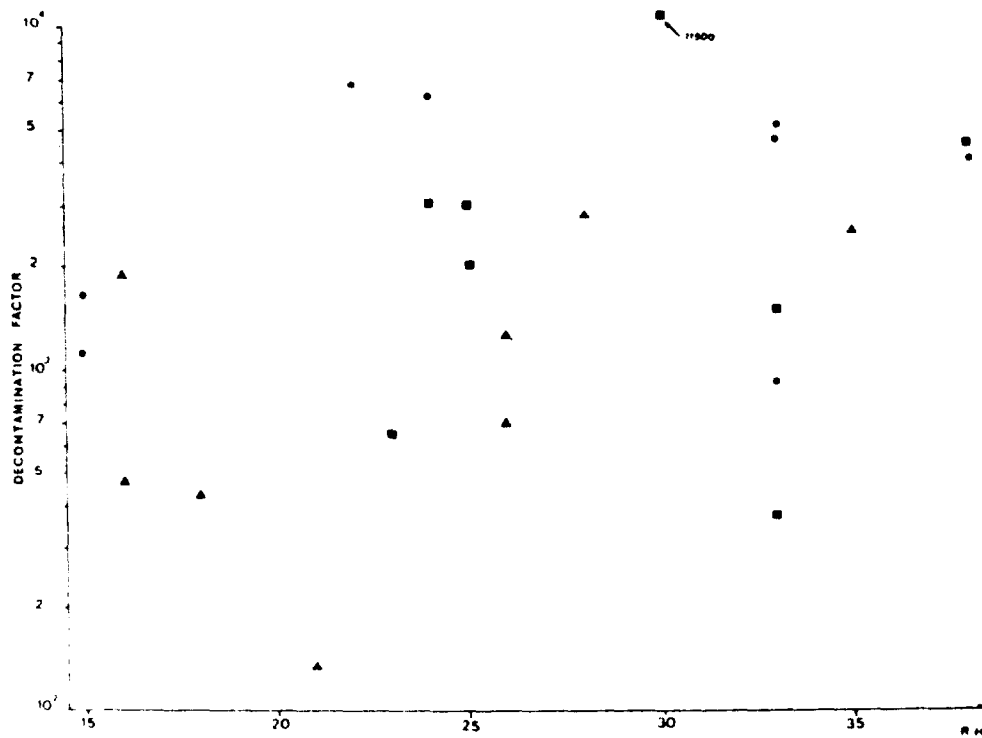


Fig.7

17th DOE NUCLEAR AIR CLEANING CONFERENCE

The results, given on figure 1, show no correlation between the measured efficiency and the air velocity in the range 23 to 30 cm/s.

Figures 2 to 5 show the air velocity distribution expressed in percentage deviation from the design flow rate for the systems at the 3 sites taken separately and together.

b) Influence of relative humidity

The results are shown on figures 6 and 7.

Figure 6 corresponds to the measured efficiency and figure 7 to the efficiency reduced to the design flow rate by a logarithmic correction. Again no correlation can be established.

This analysis of results, which should be extended to all air cleaning units, suggests that the efficiency of the air cleaning system is limited by the quality of the system, the assembly tightness and the leak rate of the units installed (usually around 1 to 2 x 10⁻⁴) and is independent of air velocity and relative humidity (below 40 %) for a rather large range about the nominal operating conditions.

3. Influence of weathering

The weathering effect on iodine adsorbers in permanent operation has been studied on a system fitted with 4 charcoal filter trains working in parallel at an air flow rate of about 40.000 m³/h each.

The efficiency of each train was tested at 3 monthly intervals, the lifetime of the traps being about 6 months.

The results, given on figures 8 and 9, correspond to tests carried out on the same system at different times and are expressed by the apparent K factor of the adsorber ($K = \frac{\log E}{\tau}$, with E the measured efficiency and τ the average air residence time in the charcoal,

It is observed that :

- the initial efficiency of train D is systematically below average, showing a fault in the ventilation design ;

- since weathering is more pronounced during the second six month period the initial efficiency is limited by design and assembly defects ;

- weathering varies from one train to another, showing that their flow rates must be more carefully balanced after the test.

17th DOE NUCLEAR AIR CLEANING CONFERENCE

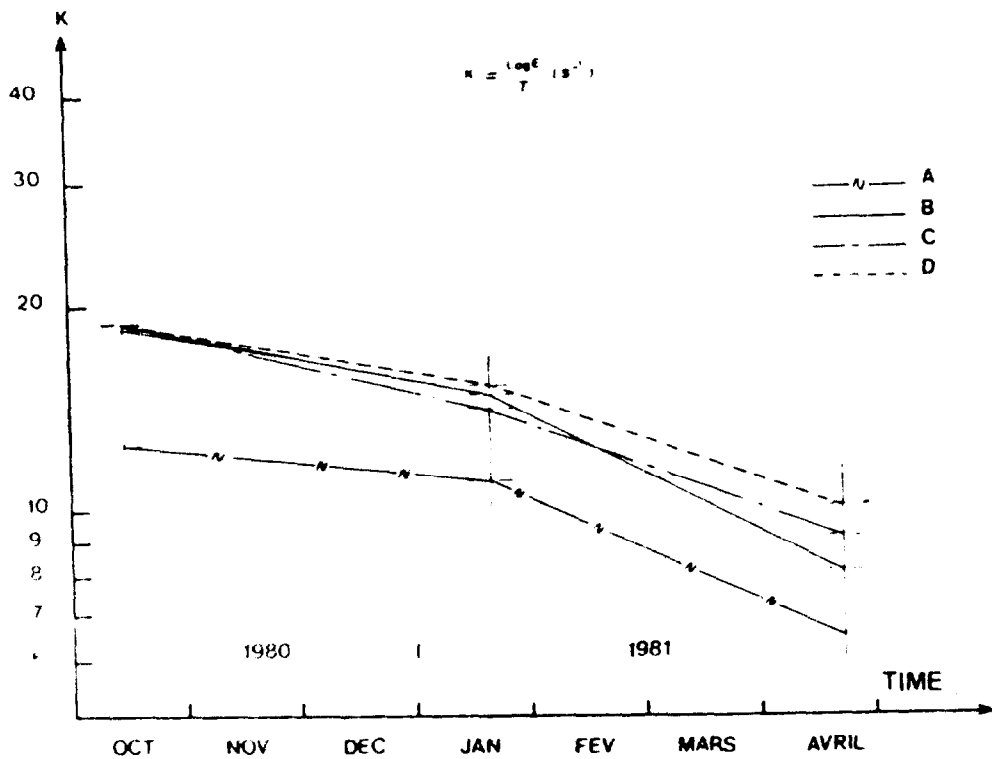


Fig. 8

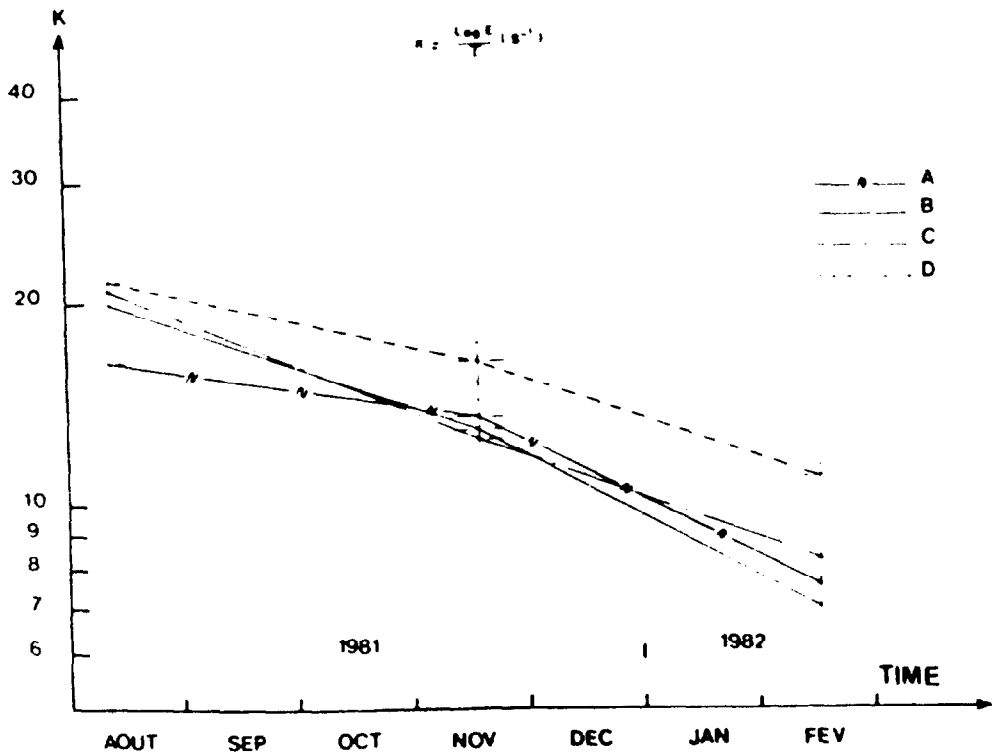


Fig. 9

17th DOE NUCLEAR AIR CLEANING CONFERENCE

Lack of attention to this flow rate equilibrium factor is troublesome for two reasons :

- the train taking the greatest flow rate ages more quickly (proportionately, in a first approximation, to the volume of air passing through) ;

- its efficiency is lowered, all other things being equal, by the higher air velocity.

In the event of an accident the efficiency of the set-up may in fact be unnecessarily reduced.

IV. Development of equipment and means of inspection

1. Development of equipment

The main improvements made to iodine adsorbers over the last few years (9) (10) concern :

- systematic by passing of iodine filters wherever possible ;
- fitting of new facilities with preheaters to lower the relative humidity and improve efficiency, especially for methyl iodine trapping ;
- use of rechargeable carbon adsorbers, accompanied by a systematic increase to 10 cm in the bed depth.

2. Development of inspection methods

a) Needs

An inactive testing method to supplement the normalised inspection should be developed for the following reasons ;

- Qualification of sampling points

A conventional tracer method must be used here so that the representativity of sampling points specific to iodine tests may be determined and if necessary their position changed, or if this is impossible a correction factor applied to the measured activity. This application is intended above all for circuits of an older design where the configuration cannot always guarantee the homogeneity of the tracer at the sampling points or at the trap itself. This application refers to a standard tracer method.

- Leak measurements on ventilation systems under pressure

On a few circuits the air cleaning units are placed downstream from the blower and are hence under higher pressure than the surrounding premises.

17th DOE NUCLEAR AIR CLEANING CONFERENCE

In such cases a leak measurement is necessary in order to detect any anomaly liable to cause radioactive contamination of personnel or premises when the adsorber is tested. There again a standard tracer method is fitted for use.

- Leak rate evaluation

The leak rate of iodine adsorbers is determined at present by means of a double injection of molecular iodine then methyl iodide. Comparison of the results obtained generally shows whether the efficiency is limited by leakage. However the method is long, costly and ill-suited to adsorbers containing weathered charcoal.

The use of rechargeable carbon adsorbers has led EDF to propose a test procedure based on reference samples measured every 6 months. A standardized radioactive efficiency test would be carried out on reception and after each active charcoal replacement (maximum lifetime : 4 years).

If this procedure were to be adopted, assuming the results obtained could be correlated with the findings of in-place tests, a yearly or twice-yearly check on the leak rate of the facility would be necessary in our opinion, the initial measured value being difficult to guarantee for 4 years.

For this last application a specific method must be used in keeping with the behaviour of the active charcoal.

b) Characteristics of the method

The method to be developed must meet the above 3 requirements and possess the following characteristics :

- Tracer gas. This must :
 - . be non radioactive,
 - . non inflammable,
 - . non toxic,
 - . non corrosive,
 - . non degradable,
 - . easily injectable,
 - . not affect the sorption properties of the charcoal and be quickly eliminated,
 - . stay in the active charcoal for a time consistent with leak rate measurements,
 - . not interfere with any other gases present in the effluent cleaned up.

17th DOE NUCLEAR AIR CLEANING CONFERENCE

- Detector. This must be :
 - . small and light-weight,
 - . robust,
 - . autonomous for electricity supply and gas intake (at least 10h),
 - . highly sensitive and if possible specific for the gas injected,
 - . capable of continuous tracer gas measurement,
 - . able to give a direct and rapid response.

The "tracer gas plus detector" pair must be able to measure leak rates $> 10^{-4}$ for the general working conditions of the systems tested (flow-rate, temperature, air relative humidity, moisture content of the charcoal, etc...). Such an apparatus is being studied in our laboratories.

V. Conclusions

Analysis of the results of in place tests on French facilities is not yet perfect, but certain facts emerge :

- The method used at present to measure the decontamination factor of iodine adsorbers, the only one of its kind to be covered by statutory rules, should be supplemented when necessary by other techniques allowing the leak rate of the facility in particular cases to be determined ;

- Certain additional information is necessary to improve the analysis and gain better control of the efficiency changes taking place with time in systems used only occasionally in normal operation (repairs, fuel handling, gaseous effluents treatments) ;

- No correlation has been observed, within the range of variation of these parameters, between the efficiency of iodine traps, as measured on reception and the air velocity or relative humidity ;

- Special attention must be paid to the balancing of flow-rates on systems in permanent operation and equipped with several charcoal filter trains working in parallel, otherwise the efficiency of the whole is undermined.

17th DOE NUCLEAR AIR CLEANING CONFERENCE

VI. References

1. Décret n°75.306 relatif à la Protection des Travailleurs contre les Dangers des Rayonnements Ionisants dans l'Industrie Nucléaire (1975)
2. Arrêté fixant la Périodicité des Contrôles des Installations de Ventilation (1977)
3. Premiers enseignements tirés de l'analyse de l'accident de Three Miles Island - Groupe Permanent chargé des Réacteurs Nucléaires - Ministère de l'Industrie (1979).
4. "Méthode de contrôle du coefficient d'épuration des pièges à iode"
Norme Expérimentale AFNOR NF.M.62.206 (1982)
5. Sigli P. and Trehen L.
"Contrôle des pièges à iode des centrales nucléaires"
CEC Seminar on Iodine Filter Testing - Karlsruhe (1973)
6. Deckers B., Sigli P. and Tréhen L.
"Operating experience with the testing of iodine adsorbers on the air clean up systems of the Belgian PWR power plants"
14th ERDA Air Cleaning Conference CONF. 76.0822 (1976)
7. Taylor L.R. and Taylor R.
"The ageing of impregnated charcoals"
CEC Seminar on Iodine Filter Testing - Karlsruhe (1973)
8. Decoursière P.
"Evolution de la filtration des iodes dans les centrales nucléaires"
CEC Seminar on Iodine Removal from Gaseous Effluents in the Nuclear Industry - Mol (1981) - To be published
9. Madoz J.P. and Decoursière P.
"Principes de conception retenus pour assurer la fonction "piégeage des iodes" des systèmes de ventilation des réacteurs à eau légère du palier 1300 MWe"
IAEA Seminar on the Testing and Operating of Off Gas Cleaning Systems at Nuclear Facilities - Karlsruhe (1982)
To be published.

DISCUSSION

DEITZ: Does the relative humidity reach a higher value than 40 % during weathering? What is the activity of the test gas? What are the atmospheric contaminants in weathering?

MULCEY: Relative humidity can reach higher values than 40 % for the circuits which are not equipped with preheaters. Nevertheless, for the corresponding adsorbers, the humidity control performed before testing (after the 16 hours service needed for equilibrium in case of stand-by adsorbers) very rarely shows relative humidities greater than 60 %. The activity of the test gas during the injection is of the order of 10^{-7} Ci per m^3 with a maximum of about 10^{-6} Ci per m^3 in the case of deep-bed adsorbers. The injection technique used (in-place production of the radioactive tracer) does not allow the test gas activity to be constant during the injection time. The concentration of the atmospheric contaminants, partly responsible for the weathering of the charcoal (SO_2 for example) mainly depends on the industrial surroundings of the nuclear site. These contaminants have not been measured in France. For the site studied here, the values measured every 3 months show a rather good agreement with the weathering formula proposed by Taylor.

THOMAS: Do you wish to supplement the tracer method with a leak test similar to the Freon test used in the U.S.? Is 6 months the typical service life of your charcoal adsorbers? Are you required to do in-situ tracer analysis every 3 months by French law?

MULCEY: To answer your first question, I can say that this method will be similar in its principle to the U.S. one, but that the tracer gas and the detector to be used could be somewhat different. A study is starting now in our laboratory and I should be able to bring more informations in a few months. Regarding your second question, 6 months is the typical service life for continuously operating 5 cm bed depth charcoal adsorbers. As was said before, this service life is in accordance with what can be expected using Taylor's formula. French law only requires a yearly test of each ventilation system (Reference 2 of the paper). As a consequence of the T.M.I. 2 accident, safety authorities have required the licensee to perform an in-place test of the continuously operating charcoal adsorbers every 3 months. This decision only concerns some circuits of the 6 first 900 Mwe PWR'S.

DEUBER: Could you elaborate on the drawbacks of using I_2 for in-site leak testing?

MULCEY: The technique uses the well known fact that the decontamination factor of a given impregnated charcoal bed is higher for molecular iodine than for methyl iodide (generally by one order of magnitude). For new carbon, the efficiency of the adsorber is mainly governed by the leak rate of the system and a comparison between the D.F. for I_2 and ICH_3 can easily indicate a leak rate, the D.F. for I_2 being then a good estimation of the maximum leak rate of the system. For aged carbon, the overall

17th DOE NUCLEAR AIR CLEANING CONFERENCE

efficiency is also governed by the intrinsic efficiency of the carbon which can be greatly affected by ageing and weathering. Then, the leak rate estimation using the D.F. obtained for I_2 is no longer valid. This technique (rather expensive and time consuming) is then used only when a significant leak rate is anticipated from an anomalously low value obtained in a ICH_3 acceptance test.

WILHELM: The important parameter with respect to the influence of wet air is the water adsorbed on the carbon. So, a correlation between the relative humidity of the air to be filtered and the removal efficiency will only, under operational conditions during the test, give meaningful numbers when the adsorption-desorption equilibrium is reached for the water on the carbon surface.

MULCEY: I fully agree with your comment. It is the reason that we ensure that for each test performed the preconditioning time under all operational conditions (flow-rate, heating, etc...) is at least 16 hours.

17th DOE NUCLEAR AIR CLEANING CONFERENCE

IODINE FILTERING FOR FRENCH REPROCESSING PLANTS

G. Bruzzone*, J.L. Rouyer*, Ph. Mulcey*, A. Vaudano**

* Commissariat à l'Energie Atomique, IPSN/DPr/STEP/SPT, B.P. n° 6,
92260 FONTENAY AUX ROSES, France

** Commissariat à l'Energie Atomique, DERDCA/DGR/SEP, B.P. n° 6,
92260 FONTENAY AUX ROSES, France

Abstract

This paper describes the study of iodine trapping performed on a test rig called "SIRROCO" on a scale 1 cartridge filled with adsorbent AC 6120 and the tests on samples done in parallel to compare the removal efficiencies of the industrial filter with those of the sorbent. Influence of the major parameters encountered in French operating conditions are discussed. The sorbent tests have to be further pursued, particularly those concerning influence of No.

I. Introduction

Recommendations made in France for gaseous releases coming from fuel reprocessing facilities require that iodine 129 is filtered in two stages. The first stage of the removal consists of chemical primary trapping in a soda scrubber. Cleaning is finalized with secondary trapping by adsorption on a specific silver impregnated sorbent.

The requirement for this second barrier on new reprocessing plants has necessitated the selection of a feed material and the test of a filter at one-one scale in representative conditions of operation.

This paper describes the study performed on a test rig called "SIROCCO" and the tests on samples done in parallel to compare the removal efficiencies of the industrial filter with those of the sorbent and to evaluate the influence of the major parameters in French operating conditions.

II. Study on "SIROCCO" rig

II.1. Description of the experimental installations

Test were made on a cartridge filled with adsorbent AC 6120 which has been chosen because of the good removal performances described by the team of J.G. WILHELM.

Characteristics of the rig as well as of the cartridge are given in table I and figure 1.

II.2. Preparation of the experiment

To start the experiment, it has been necessary to :

- verify the representativity of upstream and downstream sample points as well as airflow measurements, by helium tracing,
- design and realize several systems with new sampling tubes in glass and teflon for the injection of iodine 127 and 131.

Table. I

FEATURES OF THE "SIROCCO" TESTING INSTALLATION

TESTING RIG

Nominal Flow rate	200 N m ³ /h
Temperature	150°C ± 5°C
Volumetric Flow rate	310 m ³ /h

ABSORBENT CARTRIDGE

- Geometrical parameters

. Shape	coaxial cylindrical
. Inside radius	15,65 cm
. Outside radius	28,15 cm
. Total height	56 cm
. Useful height	43,5 cm
. Absorbent bed depth	12,5 cm
. Inside useful area	0,43 m ²
. Outside useful area	0,77 m ²

- Dynamical parametersGas velocity

. Inside face	20,1 cm/s
. Outside face	11,2 cm/s

Average stay time

0,8 s

AC 6120 SORPTION MATERIAL

- Nature: impregnated amorphous silica	Ag NO ₃
- Silver mass rate	12%
- Apparent bulk density	0,70
- Total volume	96,3 dm ³
- Total mass	67,4 kg

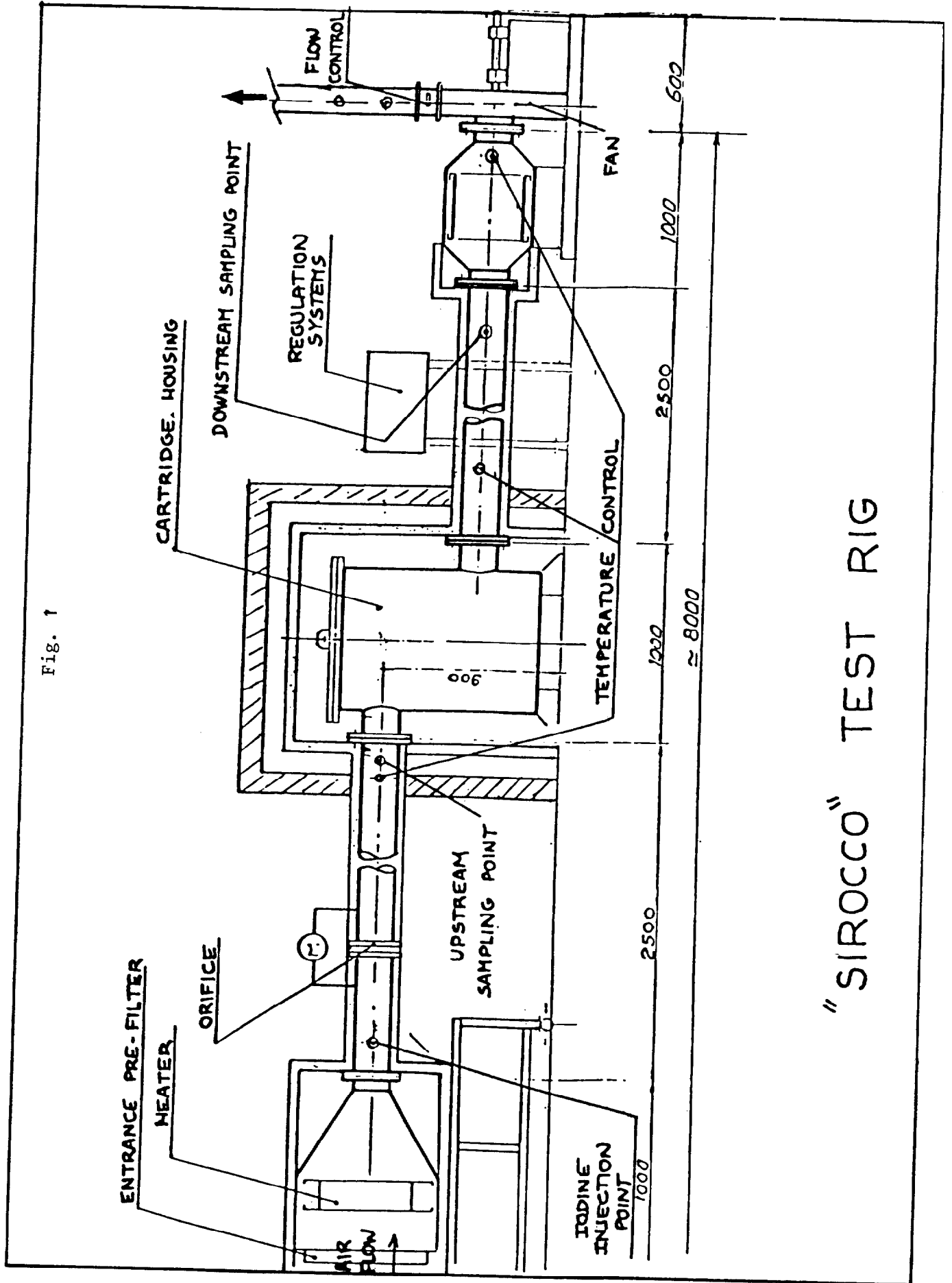


Fig. 1

"SIROCCO" TEST RIG

17th DOE NUCLEAR AIR CLEANING CONFERENCE

II.3. Tests

The housing containing the cartridge is placed in an air stream at 150°C and is permanently loaded with iodine 127 vapour.

Weekly injections of molecular and methyl iodine labelled with iodine 131 were made to measure decontamination factors and follow their time-dependant evolution.

II.4. Results

- The test rig has been continuously operated for 7 560 hours with a iodine 127 loading time of 5 300 hours.

- Figures 2 and 3 show DF evolution for ICH_3 and I_2 as a function of the cartridge saturation.

Trapping efficiency of AC 6120 falls rapidly for ICH_3 above a saturation level of about 80 mg/g. For I_2 , figure 3 shows a DF decrease at a saturation level above 100 mg/g.

Two reasons could explain this apparent better behaviour of AC 6120 for molecular iodine :

- . a partial adsorption of I_2 on duct walls between the cartridge outlet and the downstream sample point (which would increase DF value in decreasing downstream activity),
- . other trapping mechanisms than those for ICH_3 .

- Data gathered for elution confirm, for ICH_3 as well as for I_2 , the degradation of cartridge removal efficiencies over a saturation level of about 85 mg/g.

II.5. Conclusion

The study realized on SIROCCO rig with AC 6120 sorbent has allowed us to :

- determine the useful parameters for filter design
- confirm the removal efficiencies at high temperature in the absence of NO_x
- obtain the values of DF which would indicate the necessity for replacement of the sorbent.

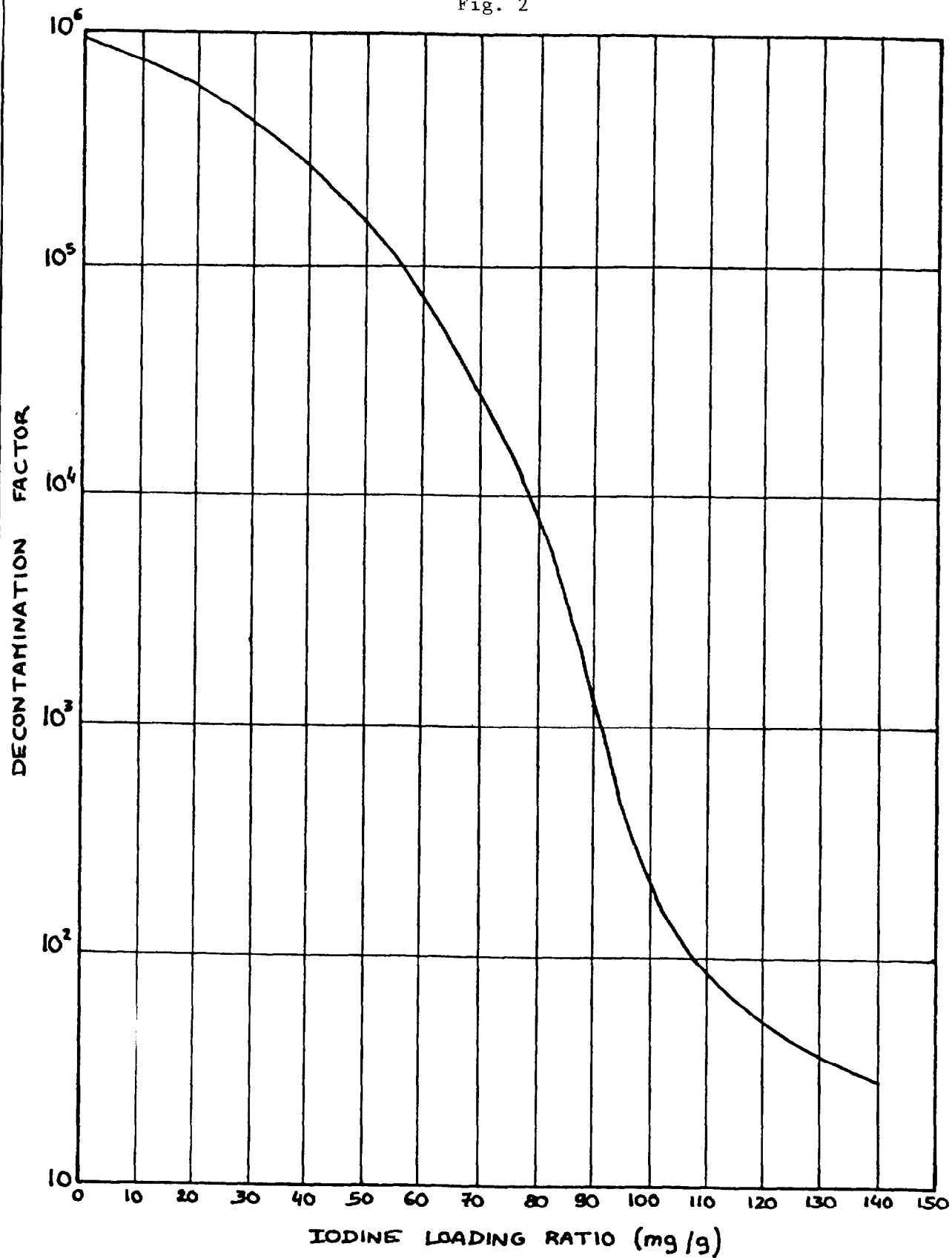
These results achieved on an industrial type installation, had to be fulfilled by laboratory tests on sorbent under all conditions representative of new French reprocessing plants.

III. Tests on sorbent samples.

The tests performed on AC 6120 samples had the following objectives :

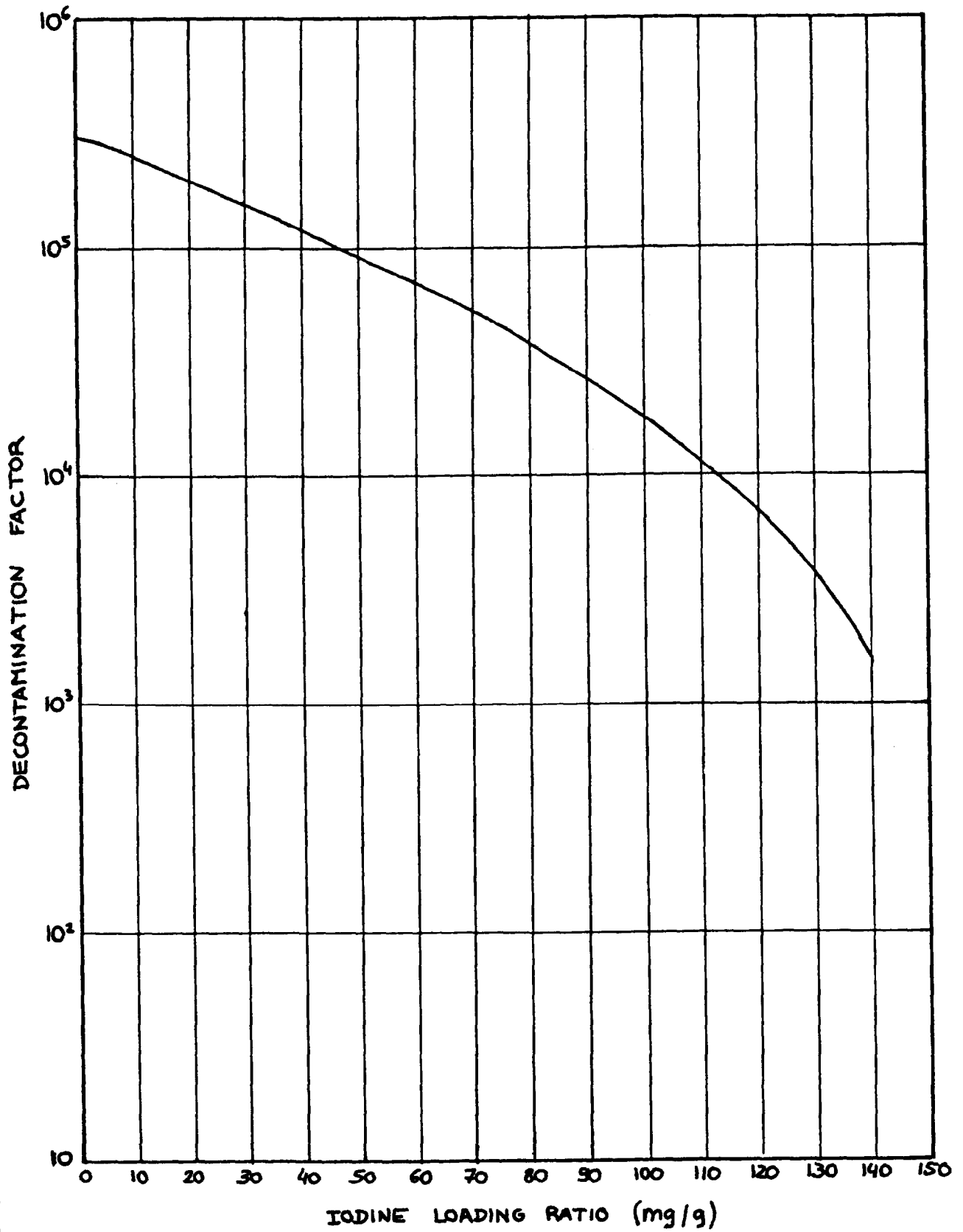
- to reveal an eventual isotopic exchange of iodine 131 or iodine 123 with iodine 127. This exchange could occur on the rig while it cannot occur in the reprocessing plant, since the isotopic ratio between active and inactive iodine is 5 on the plant, whereas it is $5 \cdot 10^{-9}$ on the rig for iodine 131,
- to compare the saturation curve obtained for samples with the ones obtained on SIROCCO, which might indicate leakages from the filter,
- to measure the sorbent removal efficiency as a function of gas velocity,
- to study the influence of nitrogen oxides.

Fig. 2



VARIATION OF DF WITH ¹²⁷IODINE LOADING FOR ¹³¹I-ICH₃

Fig. 3



VARIATION OF DF FOR ¹³¹I₂ WITH ¹²⁷I IODINE LOADING

17th DOE NUCLEAR AIR CLEANING CONFERENCE

III.1. Estimation of isotopic exchange

The method of estimating isotopic exchange consists in DF measurement of two AC 6120 beds presaturated in molecular iodine.

This DF can be attributed to several phenomena i.e. trapping by some non saturated residual silver, iodine physical adsorption on sorbent and isotopic exchange.

The measured DF gives then an estimation at the upper limit of the isotopic exchange.

The DF values obtained and given in table II, are low : 4,5 average for molecular iodine and 1,2 average for methyl iodine.

They indicate that if it occurs, isotopic exchange is very slight. Utilization of iodine 123 or iodine 131 as a radioactive tracer is then justified.

TABLE II - Estimation of isotopic exchange

Test conditions

Sweep gas : air at 150°C, dew point : 30°C, velocity : 25 cm/s

Loading : 2 beds of AC 6120, 2.5 cm deep
 Equilibrium time of the beds : 2 h
 injection < 200 mg of I₂ or ICH₃ traced with I 123
 (~1 m Ci) during 1 h.
 air flow continued for 2 h.

Tests with molecular iodine

Test	Overall DF		Individual DF	
	1st bed	2nd bed	1st bed	2nd bed
1	4,8	26,4	4,8	5,5
2	3,7	15,6	3,7	4,2

Tests with methyl iodine

Test	Overall DF		Individual DF	
	1st bed	2nd bed	1st bed	2nd bed
3	1,2	1,5	1,2	1,2
4	1,2	1,4	1,2	1,2

17th DOE NUCLEAR AIR CLEANING CONFERENCE

III.2. Comparison of sorbent and filter removal efficiencies

Removal efficiencies for the cartridge of "SIROCCO" and those of sorbents with equivalent depth are comparable : efficiencies are about as high and DF drops, registered over 80 mg/g, correspond approximately to 56 % of silver consumption by iodine.

These comparable performances of the filter and the samples indicate that leakages from the filter are very low.

III.3. Removal efficiencies as a function of gas velocity

For safety of the environment, it is necessary to know the variations of removal efficiencies around normal operating conditions.

The results for several velocities are given in table III, which shows that velocities around the nominal value for the industrial trap are acceptable.

TABLE III - Removal efficiency as a function of gas velocity

Test conditions

Temperature : 150°C
 Due point : 30°C
 Air velocity : 10 to 50 cm/s
 Equilibrium time of the beds : 3 h
 Injection \leq 20 mg of ICH_3 traced with I123 (\sim /mCi)
 Air flow continued for 3^h
 5 beds of AC 6120 of 2.5 cm depth.

Results

Test	Air velocity (cm/s)	Overall DF			Individual DF			
		Bed number	1st	2nd	3rd	1st	2nd	3rd
		depth (cm)	2,5	5	7,5	2,5	5	7,5
1	10		1 900	-	-	1 900	-	-
2	25		210	59 000	-	210	280	-
3	50		20	580	-	20	29	28

III.4. Influence of nitrogen oxide

The influence of NO_2 has been extensively studied by the team of J.G. WILHELM, but information concerning NO is rather scarce. This is of concern for French reprocessing because NO/NO_2 ratio at the level of the filter is quite high.

17th DOE NUCLEAR AIR CLEANING CONFERENCE

It is possible that NO reduces impregnated silver nitrate, and thus reduces removal efficiency.

Initial tests have been carried out but the results have to be confirmed by other tests.

IV. Conclusions

The study performed on an industrial iodine filter have allowed approval for the secondary trapping for new French reprocessing plants.

To optimise the operating conditions, the study had to be completed with sorbent tests. These have to be further pursued, particularly those concerning influence of NO. A new test rig called "TEAM" will be utilized. This rig has been described in reference (2).

The placement of such a cleaning system is meant to complete the removal of iodine 129 in the gaseous effluents of reprocessing plants. This involves the development of monitors able to control periodically the removal efficiency and operate the sorbent management to obtain the best possible conditions.

V. Références

(1) G. BRUZZONE, Ph. MULCEY, J.L. ROUYER, Essais de qualification d'un dispositif de piégeage de l'iode à haute température, Séminaire sur la rétention de l'iode dans les effluents gazeux de l'industrie nucléaire, Mol, Belgique (1981)

(2) G. BRUZZONE, Ph. MULCEY, Un testeur d'échantillons d'adsorbants, Séminaire sur la rétention de l'iode dans les effluents gazeux de l'industrie nucléaire, MOL, Belgique (1981)

(3) J. FURRER, R. KAEMPFER, J.G. WILHELM, Entwicklung von abluzifiltern für Wiederaufarbeitungsanlagen, KFK 2262

DISCUSSION

THOMAS, T.R.: Are you testing AC 6120 adsorbent in the dissolver offgas of a fuel reprocessing plant? If not, when do you plan to install it in a French facility?

ROUYER: No, we made the tests under simulated conditions. UP3, the next French reprocessing facility where our iodine trap will be installed, will be started in 1987.

RETENTION OF ELEMENTAL RADIOIODINE BY DEEP BED CARBON FILTERS
UNDER ACCIDENT CONDITIONS

H. Deuber, J. G. Wilhelm
Laboratorium für Aerosolphysik und Filtertechnik
Kernforschungszentrum Karlsruhe GmbH
Postfach 3640, D-7500 Karlsruhe 1
Federal Republic of Germany

Abstract

New German guidelines require a minimum retention of elemental radioiodine of 99.99 % by the filters used to vent the annulus of pressurized water reactors in the case of a design basis accident (LOCA). On the basis of an analysis of the results from various laboratory investigations on the retention of elemental radioiodine by activated carbons it is concluded that this requirement will be met with the deep bed annulus exhaust air filters. Taking into account that the radioiodine penetrating a deep bed iodine filter is in a nonelemental form, as shown in our investigations, there even seems to be a wide safety margin.

1. Introduction

German pressurized water reactors are provided with iodine filters to vent the annulus in an accident (1). According to new guidelines the minimum retention to be achieved with these filters in a design basis accident (LOCA) is 99.99 % for elemental radioiodine (2). The corresponding value for organic radioiodine (which has not been raised) is 99 %.

We have concluded that in the event of a LOCA this new requirement will be met with the deep bed annulus exhaust air filters, both with respect to the performance of the activated carbon and the leaktightness. That the leaktightness of the filters is sufficient can be inferred from surveillance tests (3,4). That also the performance of the activated carbon contained in the filters suffices can be concluded from an evaluation of the results of laboratory investigations on the retention of elemental radioiodine by activated carbons. In this paper we present this evaluation in which both results of studies described in the literature and of studies recently performed in our laboratory have been taken into account.

2. Design and operation of accident filters

As already indicated, in German PWRs annulus exhaust air filters containing activated carbon are installed to mitigate the consequences of an accident. Mostly the activated carbon 207B, 8 - 12 mesh, impregnated with KI, is used. Bed depth and face velocity are about 50 cm and 50 cm/s, respectively (residence time: ≈ 1 s) (3,4).

During normal situations the filters have to be in the stand-by mode. During an accident the filters can be challenged by leakage of steam and radioactivity as well as transfer of heat through the inner containment shell. However, during a LOCA the effect of leakage can be neglected even if the design basis leakage (0.25 %/d) is exceeded to a certain extent.

Therefore, in a LOCA temperatures and relative humidities of < 150 °C and < 10 %, respectively, have to be anticipated in the annulus during the major part of the first phase of the accident in which a pressure differential across the inner containment shell exists. The length of this phase may be of the order of 10 h. Afterwards, temperatures and relative humidities near to 30 °C and 100 %, respectively, have to be envisaged. Filter operation under these conditions could last up to two months.

As regards the iodine concentration in the inlet air of the annulus exhaust air filters and the iodine loading of the carbon, values of < 1 mg I/m³ and < 1 mg I/g carbon, respectively, have to be reckoned with.

From data pertaining to serious accidents (5) it can be concluded that, if the integrity of the inner containment shell were maintained, in serious accidents the challenge of the annulus exhaust air filters would not be much more serious than that outlined above.

3. Results of previous investigations

This chapter contains results which various experimenters obtained in investigations on the retention of elemental radioiodine by activated carbons. To a certain extent these results have already been reviewed a few years ago (1,6).

In these investigations a small bed depth or residence time was used in general (2.5 to 5 cm and 0.1 to 0.2 s, respectively). In addition, the purging time was often short (several h). The retention test according to ASTM D3803 (7) is a typical example. In this test, performed at 180 °C, the bed depth and residence time are about 2.5 cm and 0.13 s, respectively; the purging time is 4 h. It seems that attempts to establish the chemical form of penetrating radioiodine have rarely been made.

In this review both the influence of various parameters on the retention of radioiodine and the chemical form of penetrating radioiodine are dealt with. Emphasis is placed on studies performed under conditions which are of importance in the present context.

3.1 Influence of various parameters on the retention of elemental radioiodine

Base material

It was observed by Caron et al. (8) that up to some 150 °C the base material exerts no significant influence. The decontamination factors (DF's) found with coconut and coal carbon were 10^5 to 10^6 (impregnant: none, KI or TEDA; dry air; residence time: 0.17s; purging time: several h). However, at higher temperatures, coconut carbon was ascertained to perform best in general (9,8,10,11). This finding has been attributed to the high potassium content and high basicity of coconut carbon. It has been concluded that, in addition to physical adsorption, formation of KI is of importance in the retention of elemental iodine by carbons (11).

Particle size

The retention of I_2 decreases with increasing particle size of the carbon. This may be explained by longer diffusion time with higher particle size. We have observed a decrease of DF from between 10^5 and 10^6 to 10^4 with increase of particle size from 8 - 12 to 5 - 10 mesh (207B (KI); 30 °C; 98 - 100 % R. H.; residence time: 0.1 s; purging time: 2 h). In other experiments the particle size was varied from 16 - 32 to 2 - 4 mesh (12). The DF's always exceeded the maximum measurable value of 10^4 (BC727 (KI); 25 °C; 25 % R. H.; residence time: \approx 0.13 s; purging time: \approx 3 h).

Impregnant

Up to some 150 °C the influence of the impregnant is not significant in dry air as can be seen from the DF's of between 10^5 to 10^6 found by Caron et al. (8) for carbons impregnated with KI, TEDA or not impregnated, under the conditions mentioned above. In these experiments the same was observed for humid air at ambient temperature except for a low DF for carbons without impregnants. The last finding can be attributed to poorer retention of organic iodine species formed from I_2 . We have obtained similar results in humid air at 30 °C (13). At temperatures higher than 150 °C both insignificant and significant (detrimental) influence of impregnants have been noticed (8,10).

Service life

Various authors have reported on the decline of DF due to aging (14-18,4). We have observed a decrease of DF by two orders of magnitude due to aging in a nuclear power station for one year (wood carbon impregnated with KI₃; 30 °C; 40 % R. H.; residence time: 0.1 s, purging time: 2 h or 2 weeks) (4). By purging for two weeks the DF of the aged carbon was diminished to between 10^3 and 10^4 . A similar decrease of DF was observed in other

cases for the same length of aging (18). The DF fell to between 10^2 and 10^3 over one year of service (coconut carbons impregnated with KI and TEDA, 180 °C, dry air, residence time: ~ 0.1 s; purging time: 4 h). In these cases the decrease of DF could be correlated to the decrease of pH of the water extract of the carbon.

I₂ concentration

With a rise of the I₂ concentration to values much higher than 1 mg/m³ a fall of DF has been observed (19,20). This can be attributed to exceeding of the loading capacity which is approximately 1 mg I/g carbon. However, the DF may also drop if the I₂ concentration declines to values much lower than 1 mg/m³ (21,19,20). This performance has not to be expected from theoretical considerations (22). It may therefore be assumed that the effect is caused by the formation of more penetrating iodine species whose proportions increase with decreasing I₂ concentration.

Temperature

Because a high temperature is not favorable for physical adsorption a decrease of DF with increase of temperature has to be expected. This effect has been found to be very dependent on the purging time. At a purging time of several hours, Caron et al. (8) found no significant influence up to a temperature of some 150 °C (carbon: coconut or coal; impregnant: KI, TEDA or none; dry air; residence time: 0.17 s). However, at a purging time of approximately one week, the DF dropped from between 10^5 and 10^6 to between 10^3 and 10^4 at the same conditions. Insignificant influence of temperature up to nearly 150 °C in dry and humid air has been noticed by various investigators when the purging time was kept short (23,21,24,25,19,8).

Relative humidity

With impregnated carbons ordinarily little influence of the relative humidity on the retention of I₂ has been observed (25,19,8,26,27). Even with water-clogged carbon a good retention was noticed (25,19). However, with unimpregnated carbons a decrease of DF with increase of relative humidity was found (21,8,27). This may be attributed to the formation of other iodine species which are difficult to trap with unimpregnated carbons in humid air.

Face velocity

At the same residence time the influence of the face velocity appears to be negligible in a wide range. We have found the same DF's of between 10^5 and 10^6 at 25 and 50 cm/s (carbon: 207B; impregnant: KI or TEDA; 30 °C, 98 - 100 % R. H.; residence time: 0.1s; purging time: 2 h).

Residence time

In accord with expectation, an increase of DF with increase of residence time has been found (21,28,1,3,4,13). However, when the residence time becomes longer than about 0.1 s, the increase usually becomes relatively small. This has to be ascribed to the

formation of more penetrating iodine species whose influence becomes evident when the bulk of elemental iodine has been removed. With aged carbons this may occur at a residence time much higher than 0.1 s (3).

Purging time

With extended purging iodine may desorb from the carbon. This effect depends strongly on temperature. With impregnated carbons usually little influence has been noticed at ambient temperature in dry and humid air (8,27). However, with a certain carbon (wood carbon impregnated with KI_3) we observed a marked effect even at a low temperature (4). If the temperature approaches 150 °C the effect becomes very pronounced. In the experiments of Caron et al. (8) the DF was mostly lower than 10^4 at 150 °C at a purging time of approximately one week (carbon: coconut or coal; impregnant: KI, TEDA or none; dry air; residence time: 0.17 s).

Radiation

Intense gamma radiation may significantly influence the DF. In a radiation field of about 10^7 rad/h, Evans (10) mostly found DF's of between 10^3 and 10^4 , compared with DF's of greater than or equal to 10^5 with no radiation at all (various impregnated carbons; 80 °C; 75 % R. H.; residence time: \approx 0.1 s; purging time: 4h). These values translate to a desorption rate of the order of 10^{-4} %/h. With no impregnation desorption was even stronger. The influence of radiation was due to generation of organics (see Sec. 3.2). Lorenz (29,30) investigated the influence of radiation (and heat) by loading highly radioactive iodine on carbon (up to about 10^3 Ci ^{130}I equivalent to about 10^8 rad/h). The desorption rate of radioiodine was of the order of 10^{-4} to 10^{-3} %/h.

The influence of the various parameters on the retention of elemental radioiodine by impregnated activated carbons, in the range of interest in the present context, is summarized in Table I. It is obvious that the critical parameters are service life, temperature, purging time and radiation. With unfavorable values of these parameters, in the range of interest here, there is a potential that a DF of 10^4 is not achieved if the residence time is in the range of 0.1 to 0.2 s only.

3.2 Chemical form of penetrating radioiodine

Because only small amounts of radioiodine usually desorb from carbons it is not easy to determine the chemical iodine species involved.

Evans (10) succeeded in identifying four organic iodine species which desorbed from the carbon when an intense radiation field was applied. These were methyl iodide, methylene iodide, ethyl iodide and vinyl iodide.

Other investigators have tried to distinguish elemental and organic iodine by passing the desorbing iodine through samplers with components for selective retention. Lorenz et al. (29,30)

employed silver plated honeycombs to selectively trap I_2 desorbing from the carbon loaded with highly radioactive iodine. Mostly they found small percentages of I_2 only, particularly in the experiments with humid air.

Caron et al. (8) collected I_2 with copper screens. Often they observed an abundance of I_2 in their desorption tests (carbon: coconut and coal; impregnant: KI, TEDA, none; 200 °C; dry air; residence time: \approx 0.17 s; purging time: up to about 1 week).

We usually trap I_2 on a specific sorbent (DSM11; see appendix). In desorption tests we did not find measurable percentages of I_2 (carbon: wood; impregnant: KI₃; 30 °C; 40 % R. H.; residence time (total): 0.35 s; purging time: 2 weeks) (4).

4. Results of recent investigations

In this chapter results are given which we obtained in recent investigations on the retention of elemental radioiodine by activated carbons. The aim of these studies was to more realistically determine the retention of elemental radioiodine to be expected with the deep bed annulus exhaust air filters of a PWR in the case of a LOCA. In particular, these studies aimed at assessing the safety margin to be anticipated.

Investigations with four activated carbons are dealt with here. Data on these carbons are given in Table II. As can be seen, carbons of different base materials and different impregnants were used. The first two carbons (207B (KI) and 207B (TEDA)) have been on the market for several years. The other two carbons (Kiteg II and Radshield 25) have been developed in recent years.

Other relevant experimental data are presented in Table III and in the appendix. As can be seen from Table III two combinations of temperature and relative humidity were employed: (a) 30 °C and 98 to 100 % R. H. and (b) 130 °C and 2 % R. H.. The second combination may be regarded to conservatively represent the conditions in the annulus of a PWR during the first phase of a LOCA and the first combination the conditions thereafter (see Sec. 2.).

Total test bed depth and residence time (25 cm and 0.5 s, respectively) were shorter than those mostly used in the annulus exhaust air filters (50 cm and 1.0 s, respectively). The test bed was sectioned to establish retention or penetration as a function of bed depth or residence time and to facilitate analysis of the iodine species involved.

Purging time (after end of loading) was 2 h or 1 week (168 h).

In the following sections first the influence of various parameters on retention of elemental radioiodine, than the chemical form of penetrating radioiodine are covered.

4.1 Influence of various parameters on the retention of elemental radioiodine

The results are presented in terms of retention in Tables IV to VII and in terms of penetration in Figs. 1 to 8. The following discussion will be mainly based on Figs. 1 to 8. It should be borne in mind that in these penetration profiles the steep part has to be ascribed to elemental iodine and the flat part to more penetrating iodine species present as impurities or formed in the test bed.

The penetration of the carbon 207B impregnated with KI by ^{131}I loaded as I_2 at different purging times and at different temperatures is given in Figs. 1 and 2. As regards the penetration at 30 °C (Fig. 1), at a purging time of 2 h there is a strong decrease with increasing bed depth. The detection limit corresponding to a penetration of $10^{-5}\%$ is reached at a bed depth of 7.5 cm (residence time of 0.15 s). At a purging time of 168 h there is practically the same decrease of penetration up to a bed depth of 3.75 cm. Then the penetration curve levels off. A penetration of about $10^{-4}\%$ is reached at a bed depth of 25 cm (residence time of 0.5 s).

At 130 °C the penetration of 207B (KI) is as follows (Fig. 2): At a purging time of 2 h the penetration is similar to the corresponding penetration at 30 °C. However, at a purging time of 168 h the penetration is much higher at short bed depths. There is a difference of partly more than one order of magnitude compared with the corresponding penetration at 30 °C. For the long purging time the penetration found at larger bed depths is little different from the corresponding penetration at 30 °C.

The penetration of 207B (TEDA) is shown in Figs. 3 and 4. At 30 °C (Fig. 3) there is little difference in the values obtained for different purging times. Both penetration curves, initially very steep, level off at a bed depth of 3.75 cm. At a bed depth of 25 cm the penetration is equal to or less than $10^{-4}\%$.

At 130 °C the penetration of 207B (TEDA) can be described as follows (Fig. 4): It is similar to the corresponding penetration at 30 °C in the case of the short purging time. However, in the case of the long purging time the penetration is much higher, both at small and large bed depths. There is a difference of up to two orders of magnitude compared with the corresponding penetration at 30 °C.

The penetration profiles found with Kiteg II (Figs. 5 and 6) are rather similar to those found with 207B (KI), both qualitatively and quantitatively. A notable difference is the relatively small slope of the penetration curve at higher bed depths in the case of the low temperature and the low purging time.

As regards the penetration profiles obtained with Radshield 25 (Fig. 7 and 8), they are also rather similar to those obtained with 207B (KI). The slope of the penetration curve at higher bed depths in the case of the low temperature and the low purging time is relatively small, similar to that observed with Kiteg II.

A summary of the penetration values for the four carbons investigated is given in Table VIII. Values for bed depths of 5 cm and 25 cm are presented. The former may be largely attributed to elemental iodine, the latter to more penetrating iodine species.

As regards the penetration values for a bed depth of 5 cm, at 30 °C they are similar for all carbons at the same purging time. However, the influence of purging is minimal at this temperature. (This is more obvious if values for bed depths of smaller than 5 cm are compared.) At 130 °C there is a wide scatter of the values at the same purging time. However, those for 207B (KI), Kiteg II and Radshield 25 are relatively similar compared with those for 207B (TEDA). The latter are at least one order of magnitude higher than the former. The influence of purging is pronounced with all carbons at 130 °C. The penetration increases by roughly two orders of magnitude over one week of purging.

The penetration values for a bed depth of 5 cm show also that at the small purging time there is little influence of the temperature (and relative humidity). Except for 207B (TEDA), even somewhat smaller values have been found at the higher temperature.

As regards the penetration values for a bed depth of 25 cm, those for 207B (KI), Kiteg II and Radshield 25 are similar and generally much lower than those for 207B (TEDA).

Our data show that the performance of 207B (TEDA) is relatively poor with respect to retention of elemental iodine at elevated temperature and extended purging. It appears that this peculiar behavior, attributable to the TEDA impregnant, has not been reported in the literature.

207B (TEDA) exempted, our data compare favorably with literature data if retention of elemental radioiodine by new activated carbons in the same range of parameters is considered (see Table I):

- (a) There is no significant influence of the type of carbon (base material, impregnant).
- (b) Temperature and purging time exert a detrimental influence if they are raised simultaneously.

Our results also confirm that even with new activated carbons there is a potential that under unfavorable conditions, in the range of interest in this context, a DF of 10^4 for elemental radioiodine is not achieved if the residence time is in the range of 0.1 to 0.2 s only. However, our results demonstrate that at a higher residence time there is no such a potential with suitable new activated carbons.

The influence of aging is being assessed in supplementary studies although no dramatic effect is anticipated with a high residence time.

4.2 Chemical form of penetrating radioiodine

As described in the appendix, in the tests with long purging the normal back-up beds (207B (KI)) were preceded by other components to determine the percentages of particulates (particulate filter), of I₂ (sorbent DSM11) and of organic species relatively easy to trap such as CH₃I (sorbent AC 6120).

The distribution of ¹³¹I among test and back-up beds in the long purging runs is displayed in Figs. 9 to 12. The particulate filters have not been indicated because in no case was any ¹³¹I detected on these components.

The ¹³¹I distribution found in the long purging runs in which 207B (KI) was tested is shown in Fig. 9. As regards the back-up beds, at 30 °C ¹³¹I was found on the first AC 6120 bed, at 130 °C on both AC 6120 beds. No ¹³¹I was detected on the other back-up beds.

The ¹³¹I distribution in the tests with 207B (TEDA) is shown in Fig. 10. At 30 °C the distribution in the back up beds was similar to that in the corresponding test with 207B (KI). Only the first AC 6120 bed contained ¹³¹I. However, at 130 °C the distribution was very different. ¹³¹I was found on all the back-up beds, except for DSM11.

The ¹³¹I distribution in the tests with Kiteg II and Radshield 25 is given in Figs. 11 and 12. The distribution in the back-up beds was largely similar to that in the tests with 207B (KI).

From the fact that no ¹³¹I was detected on the back-up component DSM11 in any of the tests, it has to be concluded that only nonelemental ¹³¹I penetrated the carbon beds. This is in agreement with the penetration profiles shown in Figs. 1 to 8. The nonelemental ¹³¹I was mostly easy to retain on AC 6120. However, in the high temperature test with 207B (TEDA) it was highly penetrating.

The above results on the chemical form of iodine desorbing from the test beds are in agreement with the results of our previous investigations (4) described in Sec. 3.2. They differ from the results of Caron et al. (8) who found high portions of I₂ desorbing from the test beds as mentioned in Sec. 3.2. This difference may be attributed to the fact that in the tests of Caron et al. the temperature was higher and the residence time shorter.

5. Summary

New German guidelines require a minimum retention of elemental radioiodine of 99.99 % by the filters used to vent the annulus of pressurized water reactors in the case of a design basis accident (LOCA).

17th DOE NUCLEAR AIR CLEANING CONFERENCE

Studies of various experimenters on the retention of elemental radioiodine by activated carbons, performed mostly with a residence time of between 0.1 and 0.2 s, reveal that with shallow beds there is a potential that a retention of 99.99 % is not achieved in the range of conditions of interest in this context (Table I). However, our investigations demonstrate that at a higher residence time there is no such a potential with suitable new activated carbons (Table VIII). We are conducting supplementary studies on the influence of aging although we do not expect a dramatic effect with a high residence time.

On the basis of the results so far available on the retention of elemental radioiodine by activated carbons it is therefore concluded that the requirement mentioned above will be met with the deep bed annulus exhaust air filters. Taking into account that the radioiodine penetrating a deep bed iodine filter is in a non-elemental form, there even seems to be a wide safety margin.

The work was supported by the Minister of the Interior of the Federal Republic of Germany.

K. Bleier, W. Sellien, S. Winkler, H. Fischer and A. Ladanyi participated in the performance and evaluation of the tests.

17th DOE NUCLEAR AIR CLEANING CONFERENCE

6. References

- (1) Wilhelm, J. G.,
"Iodine filters in nuclear power stations,"
KFK 2449 (1977)
- (2) Reaktor-Sicherheitskommission,
"RSK-Leitlinien für Druckwasserreaktoren"(1981)
- (3) Wilhelm, J. G. et al.,
"Behavior of gasketless deep bed charcoal filters
for radioiodine removal in LWR power plants,"
16th DOE Nuclear Air Cleaning Conference,
CONF - 801 038, p. 465
- (4) Wilhelm, J. G. et al.,
"Operational experience with iodine filters at German LWRs,"
CEC Seminar on Iodine Removal from Gaseous Effluents
in the Nuclear Industry, Mol, 21 - 24 Sept. 1981
- (5) Dillmann, H.-G., Pasler, H.,
"Theoretical and experimental investigations into the
filtration of the atmosphere within the containments of
pressurized water reactors after serious reactor accidents,"
16th DOE Nuclear Air Cleaning Conference,
CONF - 801 038, p. 373
- (6) Holladay, D. W.,
"A literature survey: methods for the removal of iodine
species from off-gases and liquid waste streams of nuclear
power and nuclear fuel reprocessing plants, with emphasis
on solid sorbents,"
ORNL/TM - 6350 (1979)
- (7) American Society for Testing and Materials,
"Standard test methods for radioiodine testing
of nuclear-grade gas-phase adsorbents,"
ASTM D3803 (1979)
- (8) Caron, J. et al.,
"Piégeage de l'iode et de l'iodure de méthyle
a temperature élevée,"
Congrès international sur la diffusion des produits
de fission, Saclay, 4 - 6 Nov. 1969, p. 285
- (9) Lingjaerde, R. O., Podo, L.,
"A study on the trapping of iodine at high temperatures
on activated charcoal,"
DP - 213 (1963)

17th DOE NUCLEAR AIR CLEANING CONFERENCE

- (10) Evans, A. G.,
"Effect of intense gamma radiation on radioiodine retention by activated carbon,"
12th AEC Air Cleaning Conference,
CONF - 720 823, p. 401
- (11) Evans, A. G.,
"Effect of alkali metal content of carbon on retention of iodine at high temperatures,"
13th AEC Air Cleaning Conference,
CONF - 740 807, p. 743
- (12) Bellamy, R. R.,
"Elemental iodine and methyl iodide adsorption on activated charcoal at low concentrations,"
13th AEC Air Cleaning Conference,
CONF - 740 807, p. 683
- (13) Deuber, H.,
"Aspects of retention and differentiation of gaseous radioiodine species,"
Paper presented at the Boris Kidrič Institute of Nuclear Sciences,
Belgrade, 1981
- (14) Milham, R. C.,
"High temperature properties of activated carbon:
Part I: Desorption of iodine;
Part II: Standard method for ignition temperature measurement,"
IAEA Symposium on Treatment of Airborne Radioactive Wastes,
New York, 26 - 30 Aug. 1968,
STI/PUB/195, p. 417
- (15) Milham, R. C.,
"Charcoal post treatment; heat degradation and service life,"
10th AEC Air Cleaning Conference,
CONF - 680 821, p. 167
- (16) Evans, A. G.,
"Effect of service on retention of iodine by activated carbon,"
11th AEC Air Cleaning Conference,
CONF - 700 816, p. 539
- (17) Bennet, E. C., Strege, D. E.,
"Evaluation of weathered impregnated charcoals for retention of iodine and methyl iodide,"
UNI - 39 (1973)

17th DOE NUCLEAR AIR CLEANING CONFERENCE

- (18) Evans, A. G.,
"Effect of service aging on iodine retention of
activated charcoals,"
14th ERDA Air Cleaning Conference,
CONF - 760 822, p. 251
- (19) Adams, R. E. et al.,
"Application of impregnated charcoals for removing
radioiodine from flowing air at high relative humidity,"
IAEA Symposium on Treatment of Airborne Radioactive Wastes,
New York, 26 - 30 Aug. 1968, STI/PUB/195, p. 387
- (20) Adams, R. E. et al.,
"Trapping of radioactive iodine and methyl iodide
by impregnated charcoals,"
Nuclear Safety Program Annual Progress Report for
Period Ending December 31, 1968,
ORNL - 4374 (1969), p. 93
- (21) Billard, F. et al.,
"The influence of physical parameters on the adsorption
of iodine 131 by activated charcoals,"
International Symposium on Fission Product Release
and Transport, Oak Ridge, 5 - 7 April 1965,
CONF - 650 407, p. 814
- (22) Ritzman, R. L., Genco, J. M.,
"Evaluation of data regarding the efficiency of
activated charcoal adsorbers at low gas phase
iodine concentration,"
WASH - 1231 (1972)
- (23) Adams, R. E., Browning, W. E.,
"Removal of iodine from gas streams,"
7th AEC Air Cleaning Conference, TID - 7627, p. 242
- (24) Adams, R. E. et al.,
"Removal of radioactive methyl iodide from steam air systems,"
ORNL - 4040 (1967)
- (25) Adams, R. E., Ackley, R. D.,
"Removal of elemental radioiodine from flowing
humid air by iodized charcoals,"
ORNL - TM - 2040 (1967)
- (26) Ludwick, J. D.,
" The iodine collection efficiency of activated
charcoal from Hanford reactor confinement systems:
methyl iodide retention by activated charcoal,"
BNWL - 1046 (1969)

17th DOE NUCLEAR AIR CLEANING CONFERENCE

- (27) Davis, R. J., Ackley, R. D.,
"Long-term effects on radioiodine trapping by charcoal,"
12th AEC Air Cleaning Conference,
CONF - 720 823, p. 469
- (28) Kovach, J. L., Newton, R. G.,
"Deep bed activated carbon for liquid, solid,
aerosol and gaseous filters,"
11th AEC Air Cleaning Conference,
CONF - 700 816, p. 738
- (29) Lorenz, R. A. et al.,
"The behavior of highly radioactive iodine on charcoal,"
13th AEC Air Cleaning Conference,
CONF - 740 807, p. 707
- (30) Lorenz, R. A. et al.,
"The behavior of highly radioactive iodine on
charcoal in moist air,"
14th ERDA Air Cleaning Conference,
CONF - 760 822, p. 323
- (31) Deuber, H., Wilhelm, J. G.,
"Determination of the physico-chemical ^{131}I species
in the exhausts and stack effluent of a PWR power plant,"
15th DOE Nuclear Air Cleaning Conference,
CONF - 780 819, p. 446
- (32) Deuber, H., Wilhelm, J. G.,
"Occurrence of penetrating iodine species in the
exhaust air of PWR power plants,"
16th DOE Nuclear Air Cleaning Conference,
CONF - 801 038, p. 1354
- (33) Wilhelm, J. G.,
"Testing iodine filters for nuclear installations,"
IAEA Symposium on Treatment of Airborne Radioactive Wastes,
New York, 26 - 30 Aug. 1968,
STI/PUB/195, p. 403.

7. Appendix: Experimental

Relevant experimental data of our investigations on the retention of elemental radioiodine by activated carbons are given in Table III. The reasons for the choice of the parameters are dealt with in the text.

As indicated in Table III, ten successive test beds of a depth of 2.5 cm each were used the first two of which consisted of sections of a depth of 1.25 cm each.

As regards the back-up beds, in the tests with long purging the normal back-up beds (207B (KI)) were preceded by other components to allow differentiation of the iodine species penetrating the test beds. These components were (in direction of flow):

- 1 particulate filter;
- 2 beds of sorbent DSM11 for retention of I_2 ;
- 2 beds of sorbent AC 6120 for retention of organic species that are relatively easy to trap, such as CH_3I .

Details on the performance of these sorbents have been reported in the literature (31,32).

All the back-up beds were maintained at a temperature which was favorable for trapping the iodine species (80 °C). All the back-up beds had a depth of 2.5 cm corresponding to a residence time of 0.05 s.

(33,1) The investigations were performed with our standard test rig. The elemental iodine was tagged with ^{131}I . The detection limit for ^{131}I , measured with a NaI(Tl) detector, was 10^{-11} Ci per bed (100 % error at the 3σ confidence level). Total activities of greater than or equal to 10^{-4} Ci ^{131}I were used. These values correspond to a minimum detectable penetration of 10^{-5} %.

Table I Influence of various parameters on the retention of I_2 by impregnated activated carbons according to literature (temperature ≤ 150 °C)

Parameter	Change of DF with change or increase of parameter	Remarks a)
Base material	Not significant	
Particle size	Decrease	DF $\approx 10^4$ reported
Impregnant	Not significant	
Service life	Decrease	DF $< 10^4$ reported
I_2 concentration	Possibly significant	Formation of other I species; exceeding of loading capacity
Temperature	Decrease	At long ₄ purging time; DF $< 10^4$ reported
Rel. humidity	Not significant	
Face velocity	Not significant	
Residence time	Increase	At same residence time
Purging time	Decrease	At high ₄ temperature; DF $< 10^4$ reported
Radiation	Decrease	Formation of other I species; DF $< 10^4$ reported

a) DF's: minimum values at residence times of between 0.1 and 0.2 s

17th DOE NUCLEAR AIR CLEANING CONFERENCE

Table II Activated carbons investigated

Designation	Base material	Particle size (mesh)	Impreg-nant	Supplier
207B (KI)	coal	8 - 12 ^{a)}	KI	Sutcliffe Speakman, U.K.
207B (TEDA)	coal	8 - 12 ^{a)}	TEDA	Sutcliffe Speakman, U.K.
Kiteg II	coconut shell	8 - 16 ^{b)}	KI, tertiary amine ^{c)}	Nuclear Consulting Services, U.S.A.
Radshield 25	coconut shell	8 - 16 ^{b)}	tertiary amine	Charcoal Engineering, U.S.A.

a) BSS 410

b) ASTM D2862

c) additionally buffer and antioxidant

Table III Values of test parameters

Parameter	Unit	Value
Carrier concentration	mg/m ³	1
Temperature	°C	30 or 130
Relative humidity ^{a)}	%	98 - 100 or 2
Face velocity	cm/s	50
Pressure (absolute)	bar	1
Bed depth ^{b)}	cm	2.5
Residence time per bed	s	0.05
Preconditioning time ^{c)}	h	≥ 16 or 1
Injection time	h	1
Purging time	h	2 or 168

a) 98 - 100 % at 30 °C; 2 % at 130 °C (dew point : 30 °C)

b) Ten successive test beds of depth 2.5 cm were used. The first two test beds consisted of sections of depth 1.25 cm. Details of the back-up beds are given in the appendix. (Diameter of all beds: 2.5 cm)

c) ≥ 16 h at 30 °C; 1 h at 130 °C.

Table IV Retention of ¹³¹I loaded as I₂ by 207B (KI) a)

Bed depth (cm)	Residence time (s)	Retention (%)		
		30 °C, 98 - 100 % R. H.		130 °C, 2 % R. H.
		2 h b),c)	168 h b)	2 h b),c) 168 h b)
2.5	0.05	99.930	99.971	99.9908 99.42
5.0	0.10	99.99935	99.9973	99.99985 99.9970
7.5	0.15	99.99999	99.99911	99.99997 99.99900
10.0	0.20	-	99.99957	- 99.99946
12.5	0.25	-	99.99972	- 99.99958
15.0	0.30	-	99.99977	- 99.99964
17.5	0.35	-	99.99981	- 99.99971
20.0	0.40	-	99.99984	- 99.99976
22.5	0.45	-	99.99986	- 99.99978
25.0	0.50	-	99.99988	- 99.99981

a) Values of additional parameters: see Table III

b) Purging time

c) - : Retention higher than maximum detectable retention (99.99999 %)

Table V Retention of ¹³¹I loaded as I₂ by 207B (TEDA) a)

Bed depth (cm)	Residence time (s)	Retention (%)		
		30 °C, 98 - 100 % R. H.		130 °C, 2 % R. H.
		2 h b)	168 h b)	2 h b)
2.5	0.05	99.925	99.933	99.942
5.0	0.10	99.99948	99.9985	99.9982
7.5	0.15	99.99969	99.99931	99.99952
10.0	0.20	99.99977	99.99955	99.99965
12.5	0.25	99.99982	99.99966	99.99973
15.0	0.30	99.99987	99.99973	99.99978
17.5	0.35	99.99990	99.99979	99.99982
20.0	0.40	99.99993	99.99983	99.99985
22.5	0.45	99.99995	99.99986	99.99987
25.0	0.50	99.99996	99.99988	99.99988
				168 h b)
				96.0
				99.62
				99.979
				99.9918
				99.9938
				99.9947
				99.9953
				99.9957
				99.9960
				99.9963

a) Values of additional parameters: see Table III

b) Purging time

Table VI Retention of ^{131}I loaded as I_2 by Kiteg II a)

Bed depth (cm)	Residence time (s)	Retention (%)		
		30 °C, 98 - 100 % R. H.		130 °C, 2 % R. H.
		2 h b), c)	168 h b)	2 h b), c) 168 h b)
2.5	0.05	99.988	99.976	99.969 98.9
5.0	0.10	99.99977	99.9976	99.99993 99.957
7.5	0.15	99.99989	99.9985	- 99.9981
10.0	0.20	99.99994	99.99905	- 99.9988
12.5	0.25	99.99996	99.99935	- 99.99909
15.0	0.30	99.99996	99.99953	- 99.99924
17.5	0.35	99.99998	99.99965	- 99.99935
20.0	0.40	-	99.99972	- 99.99944
22.5	0.45	-	99.99977	- 99.99950
25.0	0.50	-	99.99981	- 99.99956

a) Values of additional parameters: see Table III

b) Purging time

c) - : Retention higher than maximum detectable retention (99.99999%)

Table VII Retention of ^{131}I loaded as I_2 by Radshield 25 a)

Bed depth (cm)	Residence time (s)	Retention (%)		
		30 °C, 98 - 100 % R. H.		130 °C, 2 % R. H.
		2 h b), c)	168 h b)	2 h b), c) 168 h b)
2.5	0.05	99.967	99.989	99.987
5.0	0.10	99.99979	99.9989	99.99997
7.5	0.15	99.99991	99.99952	-
10.0	0.20	99.99996	99.99976	-
12.5	0.25	99.99998	99.99985	-
15.0	0.30	99.99999	99.99990	-
17.5	0.35	-	99.99993	-
20.0	0.40	-	99.99995	-
22.5	0.45	-	99.99996	-
25.0	0.50	-	99.99997	-

a) Values of additional parameters: see Table III

b) Purging time

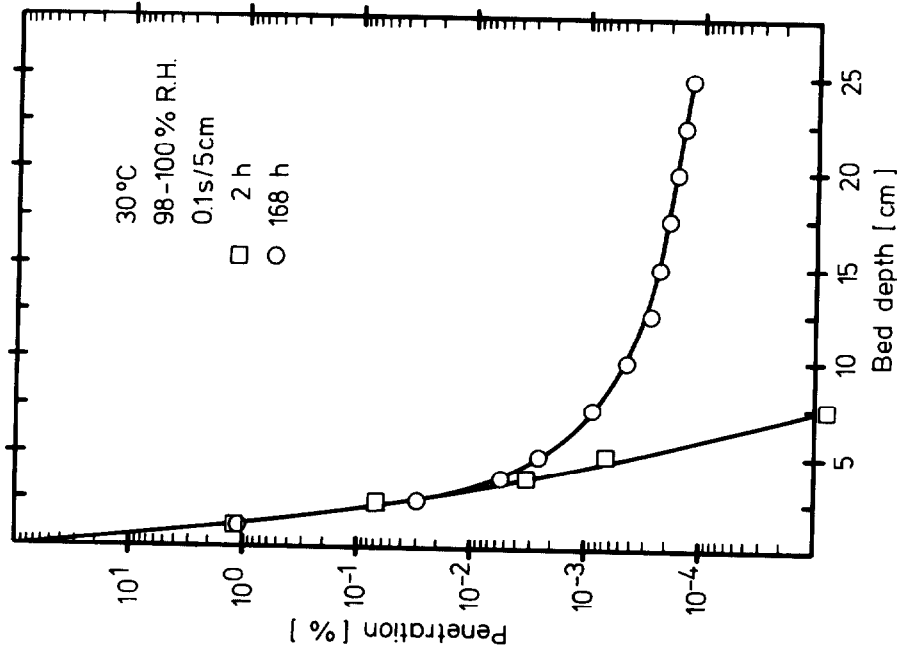
c) - : Retention higher than maximum detectable retention (99.99999 %)

Table VIII Penetration of various activated carbons by ¹³¹I loaded as I₂ a)

Carbon	Bed depth (cm)	Residence time (s)	Penetration (%)		
			30 °C, 98 - 100 % R. H.		130 °C, 2 % R. H.
			2 h b)	168 h b)	2 h b)
207B (KI)	5	0.1	$6.5 \cdot 10^{-4}$	$2.7 \cdot 10^{-3}$	$1.5 \cdot 10^{-4}$
	25	0.5	$< 1.0 \cdot 10^{-5}$	$1.2 \cdot 10^{-4}$	$< 1.0 \cdot 10^{-5}$
207B (TEDA)	5	0.1	$5.2 \cdot 10^{-4}$	$1.5 \cdot 10^{-3}$	$1.8 \cdot 10^{-3}$
	25	0.5	$3.8 \cdot 10^{-5}$	$1.2 \cdot 10^{-4}$	$1.2 \cdot 10^{-4}$
Kiteg II	5	0.1	$2.3 \cdot 10^{-4}$	$2.4 \cdot 10^{-3}$	$7.3 \cdot 10^{-5}$
	25	0.5	$< 1.0 \cdot 10^{-5}$	$1.9 \cdot 10^{-4}$	$< 1.0 \cdot 10^{-5}$
Radshield 25	5	0.1	$2.1 \cdot 10^{-4}$	$1.1 \cdot 10^{-3}$	$3.0 \cdot 10^{-5}$
	25	0.5	$< 1.0 \cdot 10^{-5}$	$3.0 \cdot 10^{-5}$	$< 1.0 \cdot 10^{-5}$
					168 h b)
					$3.0 \cdot 10^{-3}$
					$1.9 \cdot 10^{-4}$
					$3.8 \cdot 10^{-1}$
					$3.7 \cdot 10^{-3}$
					$4.3 \cdot 10^{-2}$
					$4.4 \cdot 10^{-4}$
					$5.2 \cdot 10^{-3}$
					$3.5 \cdot 10^{-4}$

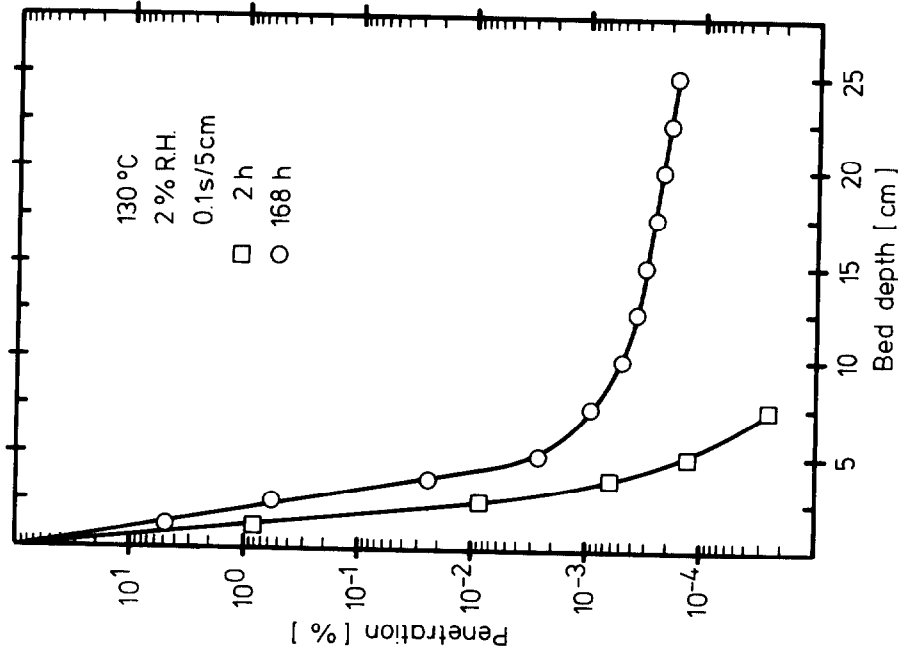
a) Values of additional parameters: see Table III

b) Purging time



Penetration of 207B (KI) by ^{131}I loaded as I_2 ,
at different purging times

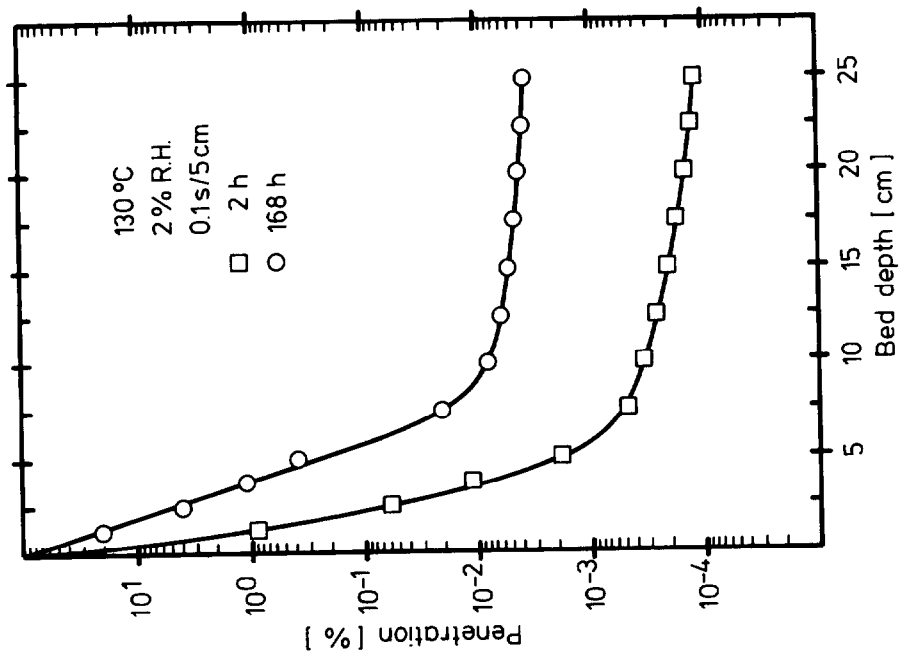
Fig. 1 a)



Penetration of 207B (KI) by ^{131}I loaded as I_2 ,
at different purging times

Fig. 2 a)

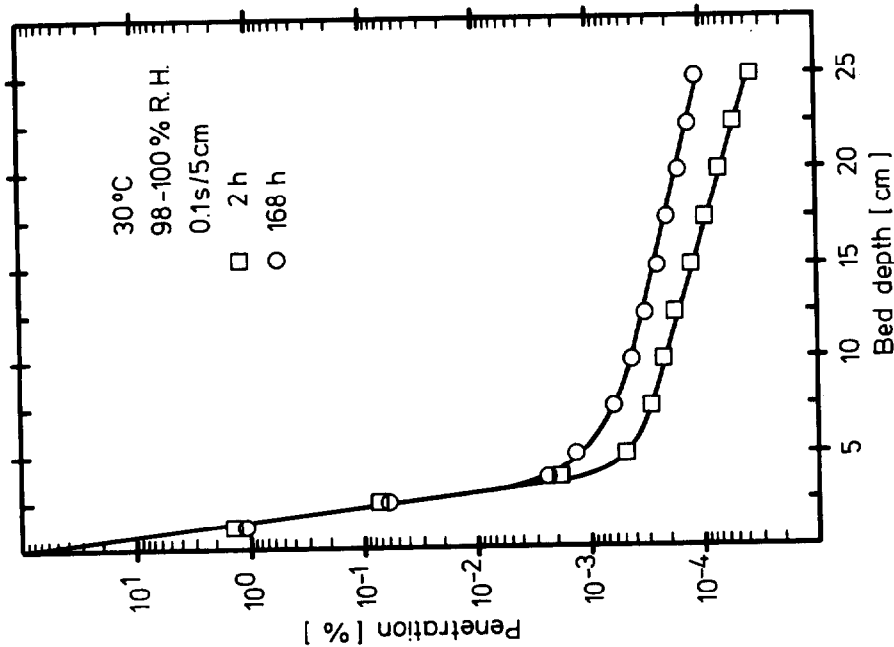
a) The values of the test parameters are indicated in Table III.
The corresponding retention is given in the respective tables.



LAF II D8230E

Penetration of 207B (TEDA) by ¹³¹I loaded as I₂ at different purging times

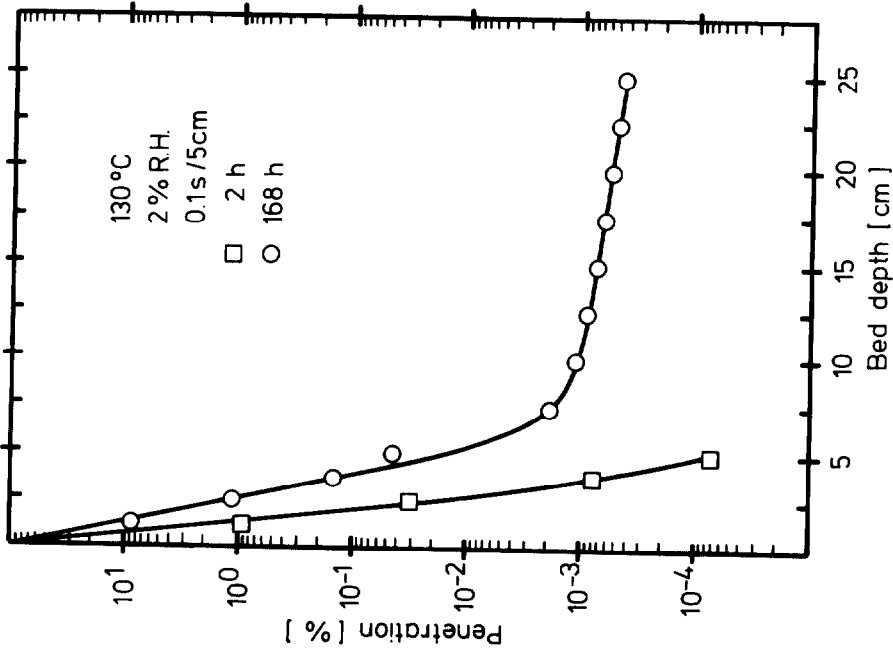
Fig. 4



LAF II D8229E

Penetration of 207B (TEDA) by ¹³¹I loaded as I₂ at different purging times

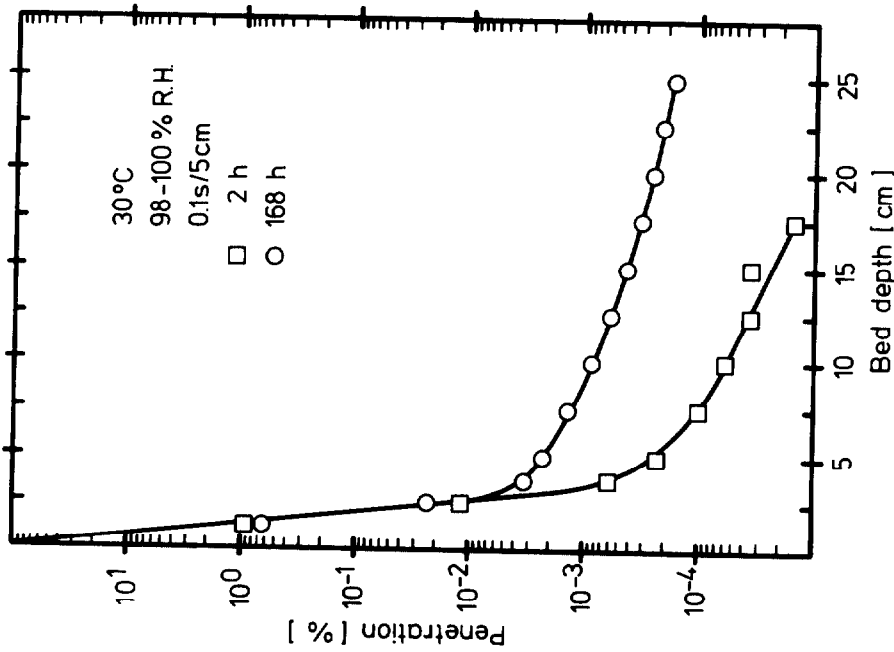
Fig. 3



ORNL
LAF II DB232E

Penetration of Kiteg II by ¹³¹I loaded as I₂ at different purging times

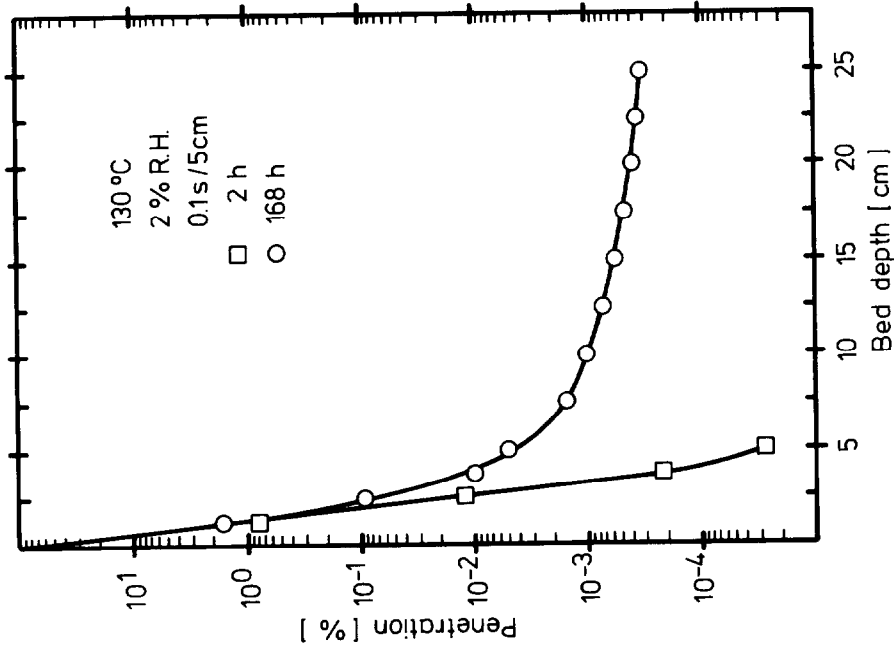
Fig. 6



ORNL
LAF II DB231E

Penetration of Kiteg II by ¹³¹I loaded as I₂ at different purging times

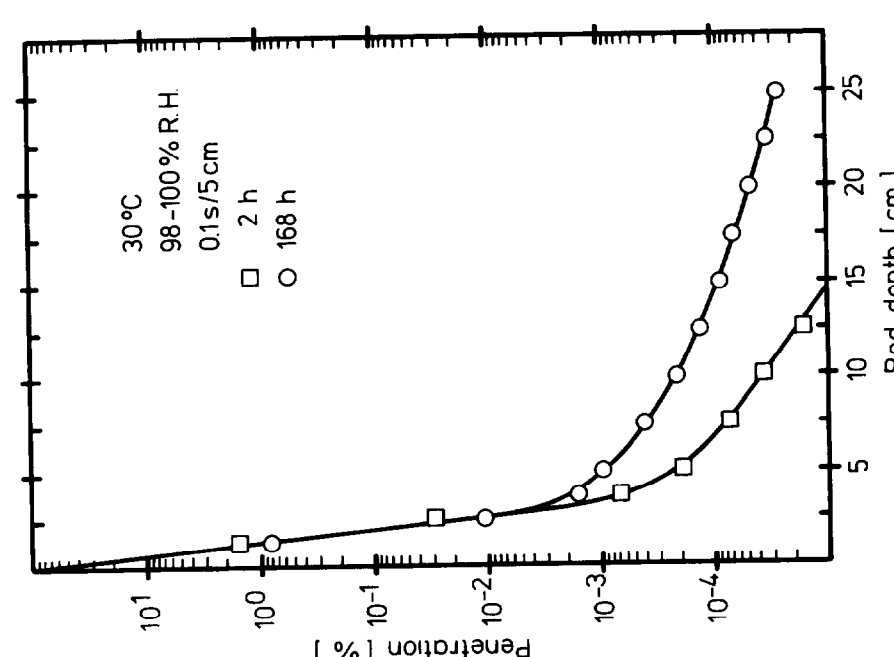
Fig. 5



K
LAF II DR234E

Penetration of Radshield 25 by ¹³¹I loaded as I₂ at different purging times

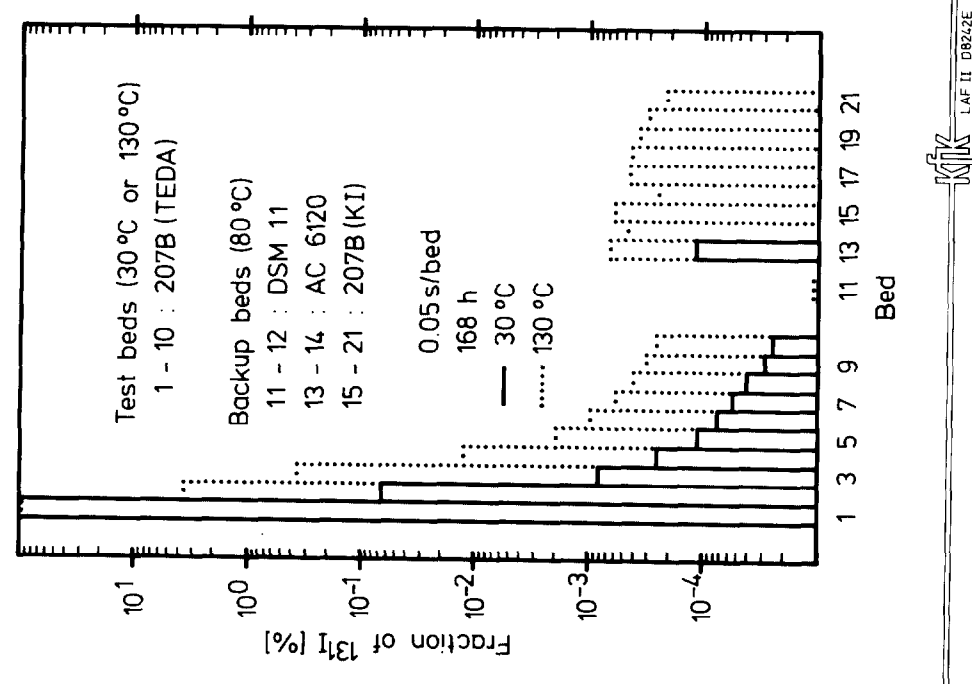
Fig. 8



K
LAF II DR238E

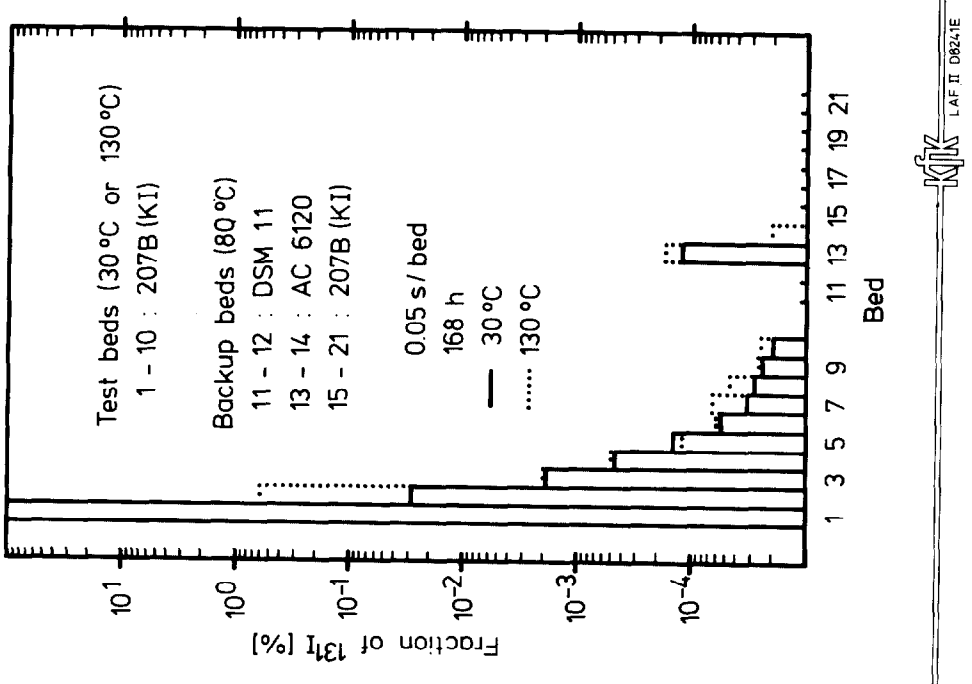
Penetration of Radshield 25 by ¹³¹I loaded as I₂ at different purging times

Fig. 7



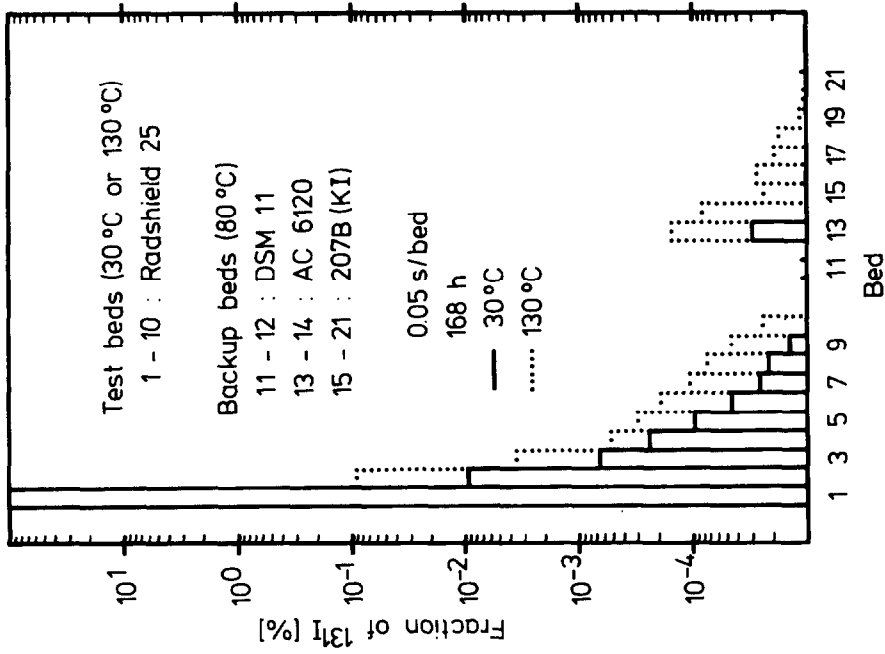
Distribution of ^{131}I among test and backup beds
(^{131}I loaded as I_2)

Fig. 10



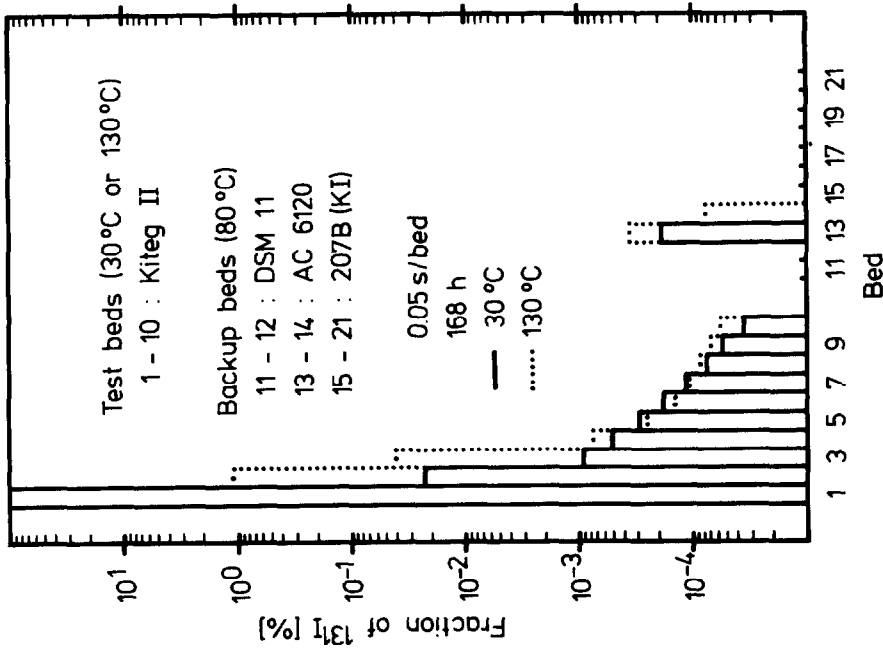
Distribution of ^{131}I among test and backup beds
(^{131}I loaded as I_2)

Fig. 9



Distribution of ^{131}I among test and backup beds (^{131}I loaded as I_2)

Fig. 12



Distribution of ^{131}I among test and backup beds (^{131}I loaded as I_2)

Fig. 11

DISCUSSION

DEITZ: Do your results apply to weathered carbons?

DEUBER: The results of this paper apply to new carbons only. The effect of aging is being investigated.

WILHELM: Regarding the question of Dr. Deitz, I would like to add that the desorption experiments will be continued on carbon samples aged in reactor stations. The results are not yet available. We may get the results of the weathered carbons in time for the next Air Cleaning Conference. You have to keep in mind that the real bed is double that shown here. If we used the real bed depth for these studies it would not be possible to detect activity on the downstream side as the decrease would be six orders of magnitude or more. With the real filter we are sure we meet the German standard.

DEUBER: I would like to add that what is coming out of the adsorber is not elemental iodine. This, of course, increases the safety margin.

BURCHSTED: The tests reported were all impregnated carbons. Did you make comparative tests with unimpregnated carbons, and if so, what were the results for elemental iodine?

DEUBER: We made some tests with unimpregnated carbons at 30°C. As regards penetration of I₂ (steep part of the penetration curve), no significant difference was found compared with impregnated carbons.

BANGART: Why was it necessary to increase the removal efficiency guidelines and are you required to meet the same guidelines regardless of differences in facility design or siting factors, such as differences in the distance to the nearest offsite residents?

DEUBER: The minimum I₂ retention to be achieved with accident filters of PWRs was raised in the new guidelines because otherwise unacceptably high doses would be calculated. The dose calculation requirements have been changed. The new guidelines apply to all new PWRs.

17th DOE NUCLEAR AIR CLEANING CONFERENCE

EXPERIENCES WITH A CHARCOAL GUARD BED IN A NUCLEAR POWER PLANT

L.C. Scholten
Environmental Research Department
N.V. KEMA
Joint laboratories of the electric utilities in The Netherlands
Arnhem, The Netherlands

Abstract

Deterioration of the charcoal in an iodine filter is a well-known problem. At a Dutch nuclear power plant the life-time of the charcoal was less than 3 months, at continuous service. A simple guard bed filled with unimpregnated charcoal was placed in front of the main bed. Now the life-time is several years. Results are shown of laboratory tests on charcoal from test canisters.

I. Introduction

The quality of impregnated charcoal in iodine filters at nuclear power plants decreases during service. The static and dynamic ageing can be more or less predicted ⁽¹⁾, but poisoning causes more often a much faster decrease. This problem has been distinguished for a long time ⁽²⁾. Several countermeasures are suggested. M.W. First has pleaded for guard beds in which organic vapours are prefiltered ⁽³⁾. A concept for prefiltering is given by Ohlmeyer ⁽⁴⁾ which uses the old charcoal from the main bed as prefilter material in a multi-way sorption bed. Wilhelm has pleaded for organizational measures and the use of overdimensioned filters ⁽⁵⁾.

Soon after the start-up of a Dutch nuclear power plant a severe deterioration of the charcoal in an iodine filter was detected and the charcoal had to be rejected immediately. The cause of the deterioration was a poisoning by aromatics as was predicted by Wilhelm ⁽⁶⁾. The problem had to be solved at short notice and a simple guard bed was constructed. The bed proved to be a good solution for this particular plant. The construction of the bed and experimental results are given below.

II. Description of the system

The reactor involved is of standard German design with a nominal power of 450 MWe. It is situated at an estuary and in the vicinity are an oil refinery and an aluminium foundry, so poisoning of the charcoal by air-pollutants from outside the plant is not unlikely. The containment consists of a spherical inner containment and a cylindrical outer containment. The inner containment is divided in two parts. The upper part has service rooms and is normally accessible. In the

lower part the primary loops are situated with all the greater components as reactor vessel, steam generators and so on. The air in the equipment room is internally recirculated, partly over an absolute-charcoal-absolute filter installation. The equipment room is kept at underpressure in respect of the service room by sucking off over a deep-bed charcoal filter direct to the stack. A simplified ventilation scheme of the plant is given in Figure 1. The secondary containment is normally ventilated over absolute filters and will only be sucked over a charcoal filter after an accident.

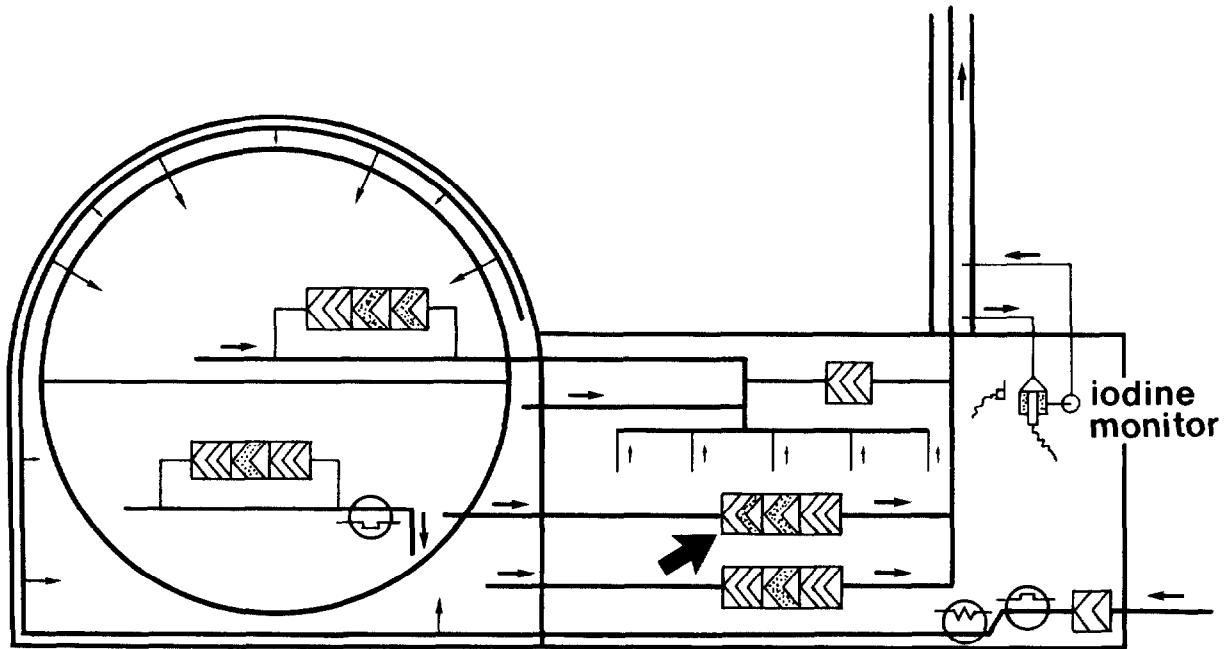


Figure 1 Simplified ventilation scheme of a PWR

The filter installation for the suck-off of the equipment room originally contained two 100% redundant absolute-charcoal-absolute filters. Therefore, only one of the filters is in continuous service. In the licensing of the plant it is stated that these filters should have an efficiency for methyl iodide of at least 99%, at a relative humidity of near 100% at 30°C. The charcoal filter consists of a vessel filter with a bed-depth of 50 cm and a nominal staytime of 1 second. In front of and behind the charcoal bed a HEPA filter is provided with the standard dimensions of 610 x 610 x 292 mm. Parallel to the main bed are two control filters with the same bed-depth.

17th DOE NUCLEAR AIR CLEANING CONFERENCE

By regulatory demand the quality of the charcoal from the control filters must be tested yearly at the laboratory, and in-situ tests must be executed every 2 years and after each refill. The same figures are applicable for the emergency filter of the secondary containment exhaust. So far the service-time of this filter has only been for trial.

III. Performance of the charcoal

The charcoal for the first initial filling of the beds was previously tested with CH_3I and showed a K-factor of $4,5 \text{ s}^{-1}$ at the specified conditions. The required K-factor is $\geq 2 \text{ s}^{-1}$. Also the in-situ test was satisfactory. After a year, in which the reactor was started up, the charcoal from the control filters was submitted to the first periodical test. The test was done at our laboratory installation, as described earlier (7). The test conditions are given in Table I. The charcoal was rejected. The beds were refilled with charcoal from stock and tested in-situ. After half a year the charcoal from the control filters was tested for security. Again the charcoal was rejected. This batch had a content of aromatics of 14 mg.g^{-1} . From interpolation the life-time was estimated at 4 to 5 months.

Table I Test conditions

Challenge gas	CH_3I	
Loading	20	$\mu\text{g.g}^{-1}$
Bed diameter	25	mm
Bed length	50	cm
Superficial velocity	50	cm.s^{-1}
Staytime	1.0	s
Relative humidity	≥ 99	%
Temperature	30	$^{\circ}\text{C}$
Preconditioning time	16	h
Sweep time	1	h
Post sweep time	2x2	h

A quick solution was desired. Therefore, a simple guard bed was constructed (Figure 2). The content is 50 dm^3 , which is about 10% of the main bed. It is filled with pure, unimpregnated charcoal of $\phi 4 \text{ mm}$ bars. A simple prefilter mat is placed in front of the bed. The casing dimensions are equal to a standard HEPA filter of $1800 \text{ m}^3.\text{h}^{-1}$. So it could be placed in front of the main bed instead of the projected HEPA filter.

No reconstructions of the filter housing were necessary. No time was available to measure the type and quantity of the air-pollution, neither their influence on charcoal. So the performance could not be calculated exactly. From the content of organic solvents on the rejected charcoal from

17th DOE NUCLEAR AIR CLEANING CONFERENCE

the main bed, and some general adsorption figures of aromatics on pure charcoal, a life-time for the guard bed was estimated of at least 3 months. A procedure was set up whereby every 3 months the charcoal in the guard bed was replaced. Thereby no retesting or a costly in-situ test is required.

Figure 3 shows the performance of the main bed after the installation of the guard bed. In the beginning the charcoal was tested every 3 months, but later on the frequency was decreased to once every year. As can be seen from the figure, a life-time of many years may be expected, any how much better than those few months without the guard bed.

IV. Discussion

The deterioration of the charcoal in the main bed was due to organic vapours. For this particular plant a simple guard bed placed in front is already adequate to protect the main bed against vapours. The low-volatile organic components in the air are captured in the guard bed. The high-volatile components will pass the guard bed, but consequently also the main bed. In our laboratory tests we use a preconditioning time of 16 hours. So we do not measure the influence of the high-volatiles. But for those components which are blown away during preconditioning, the material balance on the charcoal will be low in actual practice. So their effect on the quality of the charcoal will also be low.

We had to make the design of the guard bed in a hurry. The results, however, are very satisfactory. The cost of one filling is about \$ 50. The pressure drop is 10-15 mm WG. We believe that this simple design can be used satisfactorily at more plants, at low operational costs, especially because the frequency of costly tests can be reduced. Due to its standard dimensions it can often be installed without additional costs for rebuilding.

V. References

- 1 Collins, R.D. et al., "The ageing of charcoal used to trap radioiodine"; Proc. IAEA-symp. on the Management of gaseous Wastes from Nuclear Facilities. Paper no. SM-245/17 Vienna (18-22 February 1980).
- 2 Ackley, R.D. and Adams, R.E., "Ageing and weathering of impregnated charcoals used for trapping radioiodine (an interim report)"; Proc. Tenth AEC Air Cleaning Conference, NTIS, Springfield, VA (p. 170) (1968).
- 3 First, M.W., "Trends in the design and operation of off-gas cleaning systems in nuclear facilities"; Proc. IAEA-symp. on the Management of gaseous Wastes from Nuclear Facilities. Paper no. SM-245/62 Vienna (18-22 February 1980).

17th DOE NUCLEAR AIR CLEANING CONFERENCE

- 4 Ohlmeyer, M. and Benzel, M., "Higher safety and saving of filter material with multi-way sorption filters"; Kerntechnik 20 no. 2 p. 86-93 (1978).
- 5 Wilhelm, J.G., "Iodine filters in nuclear power plants"; CEC-document V/1531/76-E, Luxembourg (1976).
- 6 Wilhelm, J.G. and Gerlach, K., "Ergebnisse und Erfahrungen aus der Untersuchung von Jodfiltern"; Proc. Seminar on Iodine filter testing, Karlsruhe, 4-6 Dezember 1973; CEC-document V/559/74, Luxembourg (1974).
- 7 Lugt, van der G. and Scholten, L.C., "Methods used at KEMA for measuring iodine adsorption on charcoal and experiences with charcoal filters installed at a nuclear power plant"; Proc. Seminar on Iodine filter testing, Karlsruhe, 4-6 Dezember 1973; CEC-document V/559/74, Luxembourg (1974).
- 8 Scholten, L.C. and Landman, E.B., "In-situ testing of charcoal filters in the Dutch nuclear power plants"; Proc. Seminar on Iodine removal from gaseous effluents in the nuclear industry, Mol, 21-24 September 1981; CEC-document V/5283/82, Luxembourg (1982).

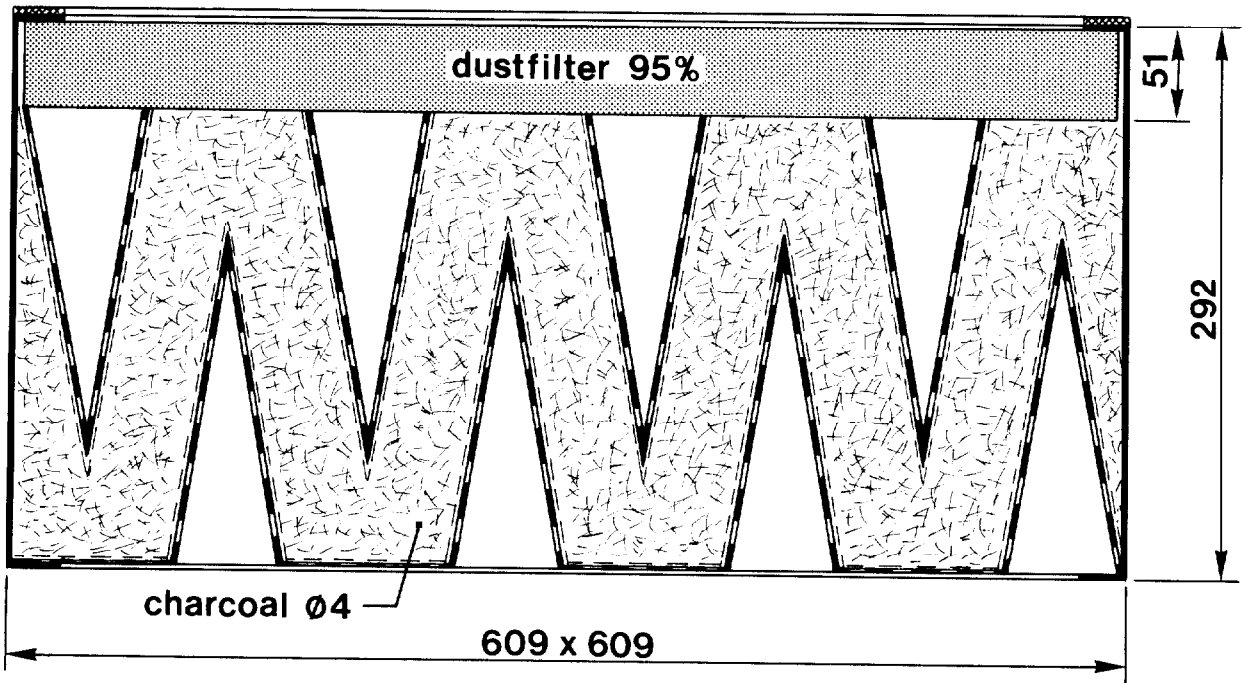


Figure 2 Charcoal guard bed

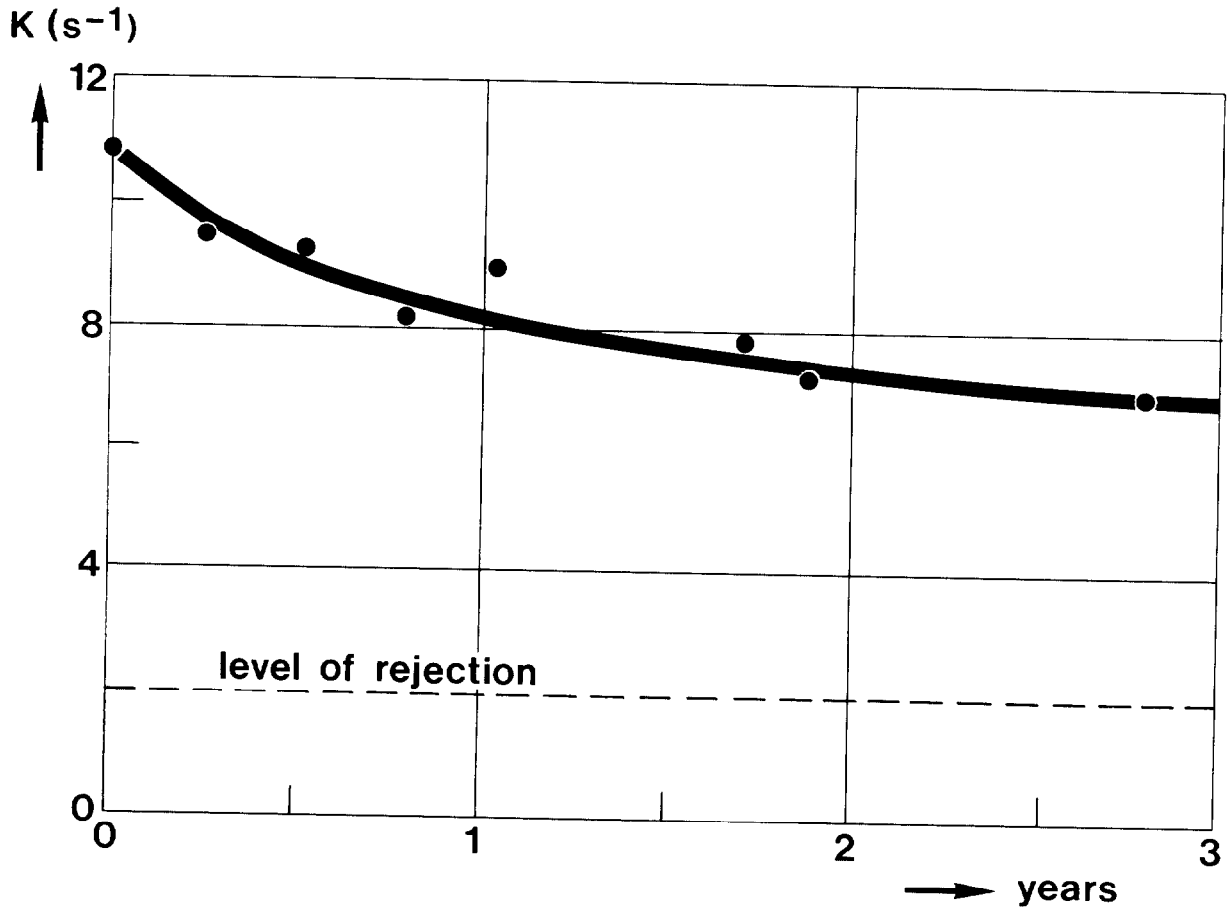


Figure 3 Decrease of charcoal quality with use of a guard bed

DISCUSSION

DEUBER: Do the K values shown in Figure 3 apply to carbon samples from by-pass cartridges?

SCHOLTEN: Yes, the figures are from samples tested in our laboratory installation.

BELLAMY: Please define your term, "K-factor".

SCHOLTEN: It is the logarithm of the decontamination factor divided by the stay-time. It is a very useful figure to compare the removal efficiencies of different batches of carbon.

DEPOSITION OF AIRBORNE RADIOIODINE SPECIES
ON SURFACES OF METALS AND PLASTICS

M.J. Kabat
Ontario Hydro
Health and Safety Division
P.O. Box 160
Pickering, Ontario
Canada

Abstract

In this study the deposition velocity of gaseous radioiodine species I_2 , HOI and CH_3I on several materials, which are commonly used in nuclear industry, was experimentally evaluated. Materials were identified which cause minimal deposition loss of airborne radioiodine sample in remote sampling systems. It was found that carbon steel and stainless steel, both extensively used in the construction of sampling lines, have high affinity for elemental iodine vapour. This causes significant loss of iodine sample due to wall deposition, particularly at high humidities which prevail under emergency release conditions. Aluminum, polyethylene and teflon cause minimal loss of iodine sample in remote sampling applications under both normal and emergency release conditions in nuclear power plants.

I. Introduction

It has been generally recognized that high chemical affinity of iodine can lead to significant sampling errors due to its wall deposition in sampling lines. For this reason it has been recommended in the ANSI N 13.1 standard (1) that "Materials to be avoided for sampling iodine are rubber, copper and some plastics". However, while all essential requirements for airborne particles sampling were clearly specified, no actual values and limits on iodine sample loss, due to deposition, were found in this standard and other available literature.

Practical experience from our experimental investigation on the behaviour of gaseous iodine species indicated that significant deposition of airborne inorganic iodine species occurs also on other metals and plastics, commonly used in the construction of lines for remote sampling of airborne radioiodine from operational areas and gaseous effluents of nuclear facilities. To correctly define and minimize experimental errors involved in gaseous radioiodine monitoring, an experimental study was performed on the deposition of its airborne species on sampling line internal surfaces under most common sampling conditions. The experimental setup and procedures are further described and results discussed.

II. General Requirements on Remote Sampling of Iodine

Accuracy requirements for gaseous effluent monitoring have not been officially established. A simplified assumption was made in this experimental study that the overall error, which is the total of sampling and detection, experimental and statistical errors, should not exceed $\pm 40\%$. Then, if the detection system performs with an accuracy as high as $\pm 15\%$ and the air sample in the sampling nozzle is perfectly representative, only $\pm 25\%$ is allowed for sample loss error due to the combination of:

1. Iodine deposition in sampling line.
2. Gaseous iodine absorption in particulate sample collector.
3. Iodine penetration through the iodine sample collector.
4. Air sample bypassing the collector.
5. Ambient air in-leak into the collection system.

The above factors are variable and can reach significant values under typical operating conditions. All of them cause negative errors, some of which can result in unacceptable underestimates of iodine levels in monitored areas or gaseous effluents.

Iodine loss in particulate collectors can be minimized with the use of suitable (pure glass fibre) filter which does not chemically react with elemental iodine vapour and hypoiodous acid.

The identification of sample loss, from the above factors 3, 4 and 5, was described in publication (2). The experimental determination of iodine sample loss due to wall deposition is further described.

III. Theoretical Aspects of Iodine Deposition

For field applications it is not possible to accurately define, or control operational conditions and state of materials which are associated with iodine deposition on internal surface of sampling lines. Therefore, only essential theoretical aspects of iodine deposition were evaluated, which were relevant to this experimental project.

The rate of gaseous iodine species deposition on surfaces is comprised of two components:

- the rate of iodine molecule diffusion through a carrier gas to surfaces
- the rate of chemical reaction of the surface materials with molecules of iodine species

17th DOE NUCLEAR AIR CLEANING CONFERENCE

From experimental data in publication (3) it is evident that suppression effect of the diffusion process can be neglected when surfaces are exposed to rapidly exchanging, turbulent challenge gas in small diameter sampling tubes. Therefore, chemisorption controls the rate of iodine deposition.

Furthermore, it can be assumed, even for emergency release conditions, that the airborne concentration of airborne species in sample stream is very low (< 10 µg/l). Therefore, surface saturation with iodine reaction products does not occur through reasonably long sampling periods.

Under the above conditions, the rate of iodine deposition dI/dt is proportional to the deposition velocity constant V_g , the exposed surface area A (m^2) and airborne iodine concentration I_C ($Bq \cdot m^{-3}$)

$$\frac{dI}{dt} = V_g \times A \times I_C \quad (Bq \cdot s^{-1})$$

V_g is proportional to the reaction rate of iodine with a specific element or chemical compound under defined reaction conditions:

$$V_g = \frac{I_s}{I_C \times t} \quad (m \cdot s^{-1})$$

I_s = iodine deposited per unit of exposed surface ($Bq \cdot m^{-2}$)

t = exposure period (s)

Then the deposition of iodine D_u per unit length of the sampling line is:

$$D_u = \frac{V_g \times A_u \times R_u}{V_u} \quad (m^{-1})$$

A_u = internal surface area per unit of length

R_u = residence time per unit of length

V_u = internal volume per unit of length

and the fraction of iodine, D_L , deposited from air sample at any length L of the sampling line, is:

$$D_L = 1 - e^{-D_u \times L}$$

Since the iodine deposition mechanism is based on its chemisorption, it can be assumed that impurities, oxidation products and air humidity have significant influence on the deposition rates. The value of V_g is also affected by mass transfer conditions. For example slow transfer is provided by pure diffusion in large volumes of steady air, while more rapid mass transfer occurs in laminar flow or turbulent flow conditions in small diameter sampling lines.

IV. Materials Tested

The iodine deposition velocity values were evaluated with copper, carbon steel, stainless steel, aluminum, polyvinylchloride, polyethylene and teflon. Test strips of the above materials were cut out of sheets 0.5 - 1 mm thick and tested "as received" with an original surface, established during long-term storage in clean atmosphere.

Since various solvents or solutions are used in some facilities to decontaminate or remove corrosion products from sampling lines, iodine deposition on clean metal surfaces was also evaluated. For this purpose the tested metals were initially rinsed in methanol. Then copper, carbon and stainless steel were etched in 1% HCL solution, and aluminum in 1% NaOH. The metals were then washed in distilled water and rinsed with methanol.

V. Experimental System

Method Description

The deposition velocity of elemental iodine vapour and gaseous HOI and CH_3I , on surfaces of above listed materials, was evaluated under both laminar and turbulent flow conditions. Well defined samples of tested material were exposed to continuously passing air, containing single, almost pure, chemical species of iodine. Sufficiently high air flow was applied to minimize the effect of iodine depletion from challenge gas, passing the exposure chamber. A species selective iodine samplers collected iodine, downstream of the tested material. The airborne concentration of the iodine species was determined from iodine activity, measured in each section of the sampler and total volume of air that was passed through the chamber during the test period. Radioiodine deposited on the tested material was also measured and V_g calculated from the equation given in paragraph 2.

17th DOE NUCLEAR AIR CLEANING CONFERENCE

Selective samplers containing Cu screens, HOI absorbent and TEDA charcoal, described in publication (4), were applied for the analysis of gaseous iodine species.

Testing Parameters

The deposition experiments were performed under the following conditions:

Physical Conditions:

Temperature Range	20 to 24°C
Relative Humidity	5 and 97 ± 3% RH
Challenge Gas	laboratory air, containing specific iodine forms
Pressure	atmospheric
Concentrations	I ₂ ; 10 µg/l ± 30%
	HOI; 0.01 - 0.05 µg/l
	CH ₃ I; 1 µg/l ± 20%
Flow	0.1 lpm through each test line

Tested Materials:

- Copper, carbon steel, stainless steel and aluminum (tested with both original and chemically cleaned surfaces).
- Polyvinylchloride, polyethylene, teflon, rubber (tested only with original surfaces).

Surface Areas:

- single strips, 560 mm² each, in type 1 exposure chambers
- eight plates, 1600 mm² each, in type 2 exposure chamber

Equipment and Procedure

The experimental setup, used for the evaluation of iodine deposition under laminar flow conditions is illustrated in Figures 1 and 2.

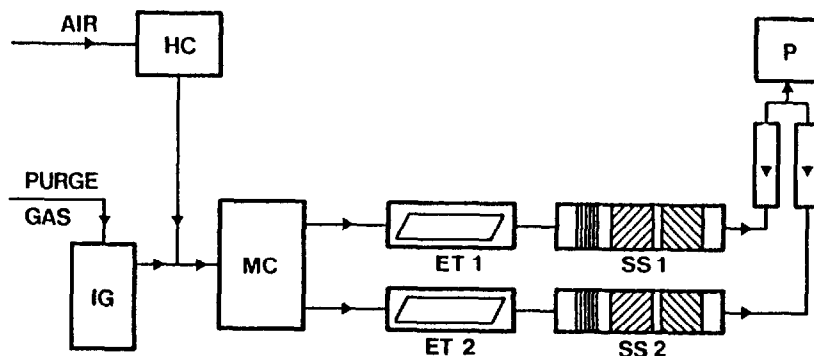


Figure 1
Diagram of iodine deposition test system

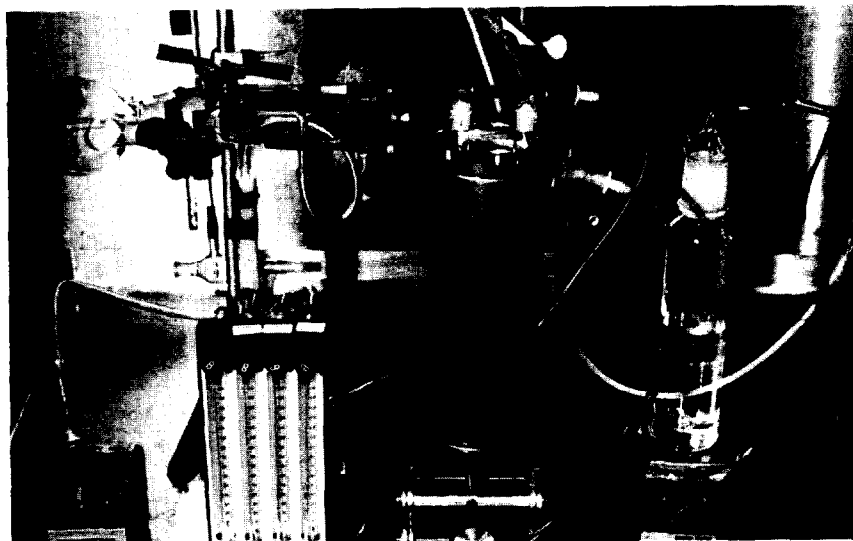


Figure 2
Experimental setup, used for the evaluation of iodine species deposition

Individual chemical forms of gaseous radioiodine (I_2 , HOI and CH_3I), formed in the generator IG, were mixed with air conditioned to the required humidity level in HC, and carried into the mixing chamber MC. Two samples of tested material were installed in glass exposure tubes ET and simultaneously exposed to passing challenge gas. Subsequently, iodine species were collected with selective samplers SS. Two samples of each tested metal, "as received" and "chemically cleaned", were simultaneously exposed to identical challenge gas to evaluate the effect of surface protection, impurities and corrosion products on their surface.

The exposure tubes, illustrated as a part of experimental setup in Figures 1 and 2, contain single strips (40 x 7 mm) of tested material in glass tubes (9 mm ID) to present laminar flow conditions in a sampling line. The "type 2" exposure chamber, illustrated in Figure 3, containing up to eight samples (40 x 40 mm each) was used to evaluate the difference between laminar and turbulent flow conditions. The first set of plates was exposed to laminar flow in the chamber while the second set was installed across the flow direction, to develop turbulent conditions. Only a single exposure chamber of the second type was tested at a time.



Figure 3

"Type 2" chamber, containing eight samples, used for the testing of iodine deposition in laminar and turbulent flow.

Elemental iodine vapour was generated from chilled, $5 \times 10^{-5}M$ solution of elemental iodine in distilled water, hypoiodous acid was purged from $5 \times 10^{-8}M$ solution of elemental iodine in distilled water and methyl iodide released from a pressure cylinder.

VI. Discussion of ResultsIodine Deposition on Metal Surfaces

The experimentally determined values of the deposition velocity, V_g , are listed in Table 1. Each value of V_g was confirmed by at least two measurements.

Table I

Measured velocity values of iodine species deposition on metal surfaces

Exposure Conditions			Deposition Velocity V_g . ($m \cdot s^{-1}$)			
Iodine Form	Relative Humidity % (#3%)	Surface	Copper	Carbon Steel	Stainl. Steel	Aluminum
I_2	5	N.Cl.	2.0(-3)	3.4(-4)	1.8(-4)	8.4(-5)
		Ch.Cl.	2.3(-3)	1.1(-3)	8.7(-4)	1.7(-4)
	97	N.Cl.	2.1(-3)	1.3(-3)	1.6(-3)	8.0(-4)
		Ch.Cl.	2.3(-3)	2.5(-3)	2.0(-3)	1.8(-3)
HOI	5	N.Cl.	1.0(-5)	1.4(-5)	4.0(-6)	1.9(-6)
		Ch.Cl.	1.4(-4)	8.0(-6)	3.3(-5)	2.5(-5)
	97	N.Cl.	2.2(-4)	2.0(-5)	1.8(-5)	1.2(-5)
		Ch.Cl.	2.7(-4)	3.8(-5)	4.4(-5)	5.6(-5)
CH_3I	5	N.Cl.	2(-8)	8(-8)	1(-7)	8(-8)
		Ch.Cl.	1(-7)	8(-8)	7(-8)	1(-7)
	97	N.Cl.	7(-8)	4(-8)	8(-8)	4(-8)
		Ch.Cl.	7(-8)	4(-8)	8(-8)	1(-6)

V_g = deposition velocity (exp)

N.Cl. = non-cleaned surface

Ch Cl = chemically cleaned surface

For easier comparison of iodine loss, D_L values in 30 m length of 12.5 mm ID sampling line, at 100 lpm sampling flow, were calculated for all tested materials. The D_L values for tested metals are listed in Table II.

17th DOE NUCLEAR AIR CLEANING CONFERENCE

Table II

Loss of iodine sample D_L due to wall deposition in a 30 m long, 12.5 m diameter sampling line, at 100 lpm sampling flow

Exposure Conditions			Deposition Loss D (%)			
Iodine Form	Relative Humidity % (±3%)	Surface	L			
			Copper	Carbon Steel	Stainl. Steel	Aluminum
I ₂	5	N.Cl.	76.2	21.7	12.1	5.9
		Ch.Cl.	80.8	54.6	46.5	11.5
	97	N.Cl.	77.9	60.7	68.3	43.7
		Ch.Cl.	80.8	83.4	76.7	72.5
HOI	5	N.Cl.	0.7	1.0	0.3	0.1
		Ch.Cl.	9.6	0.6	2.3	1.8
	97	N.Cl.	14.6	1.4	1.3	0.7
		Ch.Cl.	17.6	2.7	3.1	3.9
CH ₃ I	5	N.Cl.	0.001	0.006	0.007	0.006
		Ch.Cl.	0.007	0.006	0.005	0.01
	97	N.Cl.	0.005	0.003	0.006	0.003
		Ch.Cl.	0.005	0.003	0.006	0.10

The measured deposition velocities of airborne I₂, HOI and CH₃I on metal surfaces followed the expected pattern:

$$I_2 > HOI > CH_3I$$

It has been confirmed that the reactive forms of airborne iodine, I₂ and HOI, are more rapidly absorbed on chemically cleaned metal surfaces than on original non-cleaned surfaces. Apparently, surface protection films, eventually oxides, have lower affinity for the reactive forms of airborne iodine. Slightly higher V_g, for HOI absorption on non-cleaned surface of carbon steel at low humidity, was confirmed by repeated measurements. This effect was probably caused by the presence of organic, surface protection components.

Further, it was found that the deposition loss of both I₂ and HOI rapidly increases at high humidity. The rate of copper reaction with HOI was accelerated with high humidity more than the reaction of other tested metals, while no significant change was found on the reaction of copper with elemental iodine vapour. Apparently the above effects result from different redox mechanisms and/or different degree of their involvement in the reaction of the tested metals with airborne I₂ and HOI.

17th DOE NUCLEAR AIR CLEANING CONFERENCE

The results of elemental iodine deposition tests, performed in a "type 2" exposure chamber, were not sufficiently conclusive, because I₂ depletion within the chamber was too rapid. More satisfactory results were obtained from HOI tests, which did not show any significant difference between deposition rates measured under laminar and turbulent flow conditions.

Iodine Deposition on Plastic Surfaces

The values of both measured deposition velocity and calculated deposition losses, are listed in Table III.

Table III

Measured deposition velocity values V_g and sample loss D_L from iodine deposition in a 30m long, 12.5 mm ID sampling line, at 100 lpm flow

Exposure Conditions			Tested Plastics							
Iodine Form	Relative Humidity % (±3%)	Surface	Polyvinylchlor.		Polyethylene		Teflon		"Buna N"	
			V _g -1 m.s	D _L %						
I ₂	5	NC1	1.0(-3)	51.2	4.0(-5)	2.8	3.5(-4)	22.2	2.0(-3)	76.2
	97	NC1	2.7(-3)	85.6	1.5(-4)	10.2	2.0(-4)	13.4	2.7(-3)	85.6
HOI	5	NC1	1.2(-3)	57.8	3.3(-4)	21.1	2.5(-6)	0.2	1.5(-3)	65.9
	97	NC1	1.3(-3)	60.7	2.2(-4)	14.6	9.5(-6)	0.7	1.6(-3)	68.3
CH ₃ I	5	NC1	3.4(-6)	0.24	1.0(-6)	0.07	3.4(-7)	0.02	1.9(-6)	0.14
	97	NC1	6.0(-6)	0.43	3.2(-7)	0.02	2.5(-7)	0.02	4.5(-6)	0.32

The measured deposition velocities also followed the pattern:

$$I_2 > HOI > CH_3I$$

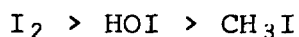
The deposition of HOI was much more efficient on plastic than metal surfaces. Polyvinylchloride and rubber have significantly higher affinity for I₂, HOI and CH₃I than the affinity of teflon and polyethylene. However, I₂ and HOI react with teflon and polyethylene in rather interesting ways:

The deposition of I₂ is more rapid on teflon than on polyethylene. On the contrary, HOI has much higher affinity for polyethylene. Also the sorption of both I₂ on teflon and HOI on polyethylene is more efficient under low humidity conditions. Apparently physical adsorption contributes, to some degree, to iodine species deposition on plastic materials.

VII. Conclusions

The following conclusions have been made from the results of this experimental study:

- Deposition rates of I_2 , HOI and CH_3I on raw surfaces of tested metals are in the following order:



Copper > Carbon Steel > Stainless Steel > Aluminum

Aluminum is the optimal metal for the construction of sampling lines.

- Significant loss of elemental iodine, due to its wall deposition, occurs in carbon steel and stainless steel sampling lines, > 10 m long, under typical sampling conditions.
- High humidity significantly increases deposition loss of I_2 on tested metals, with the exception of copper.
- The deposition loss of HOI in 30 m long sampling lines, made of aluminum, stainless steel or carbon steel, are within acceptable limits.
- Practically no CH_3I loss occurs in sampling lines from wall deposition on tested metals.
- Gaskets and other components, made of polyvinylchloride or rubber are to be avoided in iodine sampling systems.
- The use of polyethylene will minimize deposition loss of elemental iodine.
- Teflon is the optimal material for systems, sampling airborne radioiodines in which HOI is the major component.
- The deposition loss of CH_3I on plastic materials can also be neglected.

Maximal loss of iodine samples occurs under accidental release conditions, when I_2 and HOI are the major iodine forms and high humidity is present in the effluent stream, particularly during initial stages of the accident. Graphical comparison of three optimal materials is made in Figure 4, which illustrates the fraction F of elemental iodine, and HOI reaching a sample collector, for any sampling line length up to 30 m, diameter 12.5 mm, at sample flow of 100 lpm and 97% RH.

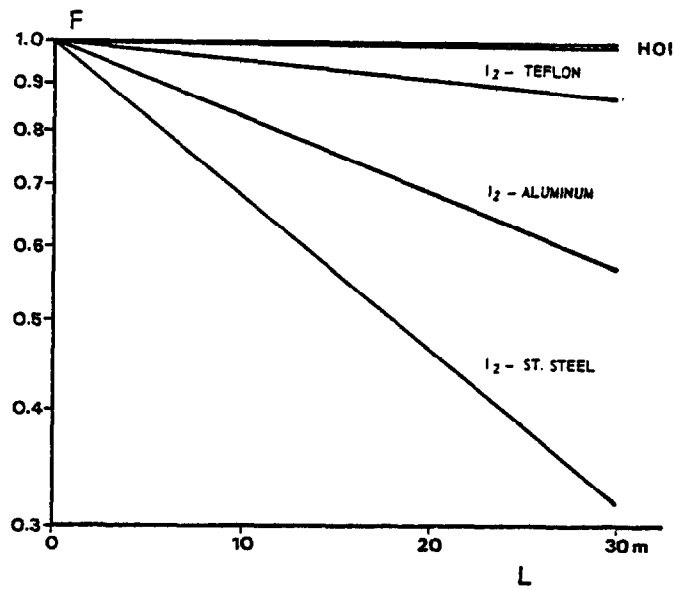


Figure 4

Fraction (F) of elemental iodine, reaching sample collectors through sampling lines up to 30 m long, at 12.7 mm diameter, 100 lpm flow.

It is evident from this graph that under the above conditions, minimal deposition loss of iodine sample would happen in teflon lined aluminum sampling line. It is logical that both length and internal diameter of the sampling line should be minimized to obtain sample with the least possible loss.

17th DOE NUCLEAR AIR CLEANING CONFERENCE

REFERENCES

1. ANSI N13.1-1969, Guide to Sampling Airborne Radioactive Materials in Nuclear Facilities.
2. M.J. Kabat, Recent Developments in Gaseous Effluent Monitoring in Ontario Hydro. IAEA Symposium "Monitoring of Radioactive Effluents from Nuclear Facilities". pp. 261-276, Portoroz, Yugoslavia, 1978.
3. P.J. Barry, Sampling for Airborne Radioiodine by Copper Screens. Health Physics, 15, pp. 243-250, 1968.
4. M.J. Kabat, Selective Sampling of Hypoiodous Acid. 14th ERDA Air Cleaning Conference, Sun Valley, Idaho, August 1976, Proceed. pp 490-506.

DISCUSSION

DEITZ: How were the tubing samples cleaned before the test?

KABAT: Copper, carbon steel and stainless steel were etched in HCl, and aluminum in NaOH solutions. The procedure is briefly described in paragraph IV of this paper.

WILHELM: I wish to point out that the adsorption of radioiodine species will be much affected by impurities and dust, which will plateout on the walls of the sampling tubes. Under accident conditions, condensation of water is to be expected and should be avoided by heating. Short length of sampling tube, large tube diameter, and high air velocity are important for reliable results.

KABAT: Yes, condensed moisture, oil, and dust deposits will have significant effect on deposition loss of iodine species. Most materials will increase the loss of elemental iodine. Oil and most other organic deposits will increase the loss of HOI. Therefore, I have recommended that sampling lines be flushed with chemically inert solvents at intervals determined from the rate of deposition of impurities. I am not aware of any experimental data on the effect of tracer heating on the loss of iodine species. I suspect that iodine chemisorption and the rate of corrosion of internal surfaces would be accelerated with increased temperature.

DEUBER: It might be worthwhile to mention that we have found negligible deposition of I₂ in sampling lines of polyethylene (lengths greater than 10 m) used in nuclear power stations for several years.

KABAT: This observation is in good agreement with our results, listed in Table III.

17th DOE NUCLEAR AIR CLEANING CONFERENCE

BURCHSTED: Jesse Thomas gave a discussion on sizing sampling lines in the 9th or 10th Air Cleaning Conference, and his information, including equations for calculating size, was summarized in The Nuclear Air Cleaning Handbook. Mr. Wilhelm's comment reiterates Thomas' conclusions, which were to keep sampling lines large, short, and as near vertical as possible.

KABAT: Almost all previous work on airborne activity sampling lines was related to particulate samples. When designing delivery lines for both particles and radioiodine, it must be considered that some recommendations for particulate sampling line sizing and materials and for sample collectors might contradict recommendations for optimal sampling of airborne radioiodine species. For example, the use of equation ($Q = 150$) for the optimal size of

sampling lines would cause unacceptable loss of iodine samples. Deposition loss of I_2 in a stainless steel line of 12.5 mm dia., 1 m long, would increase from 3.7 to 33.5% under conditions in Table II of this paper. Under the same conditions, more than 90% sample loss of I_2 would occur in a 7 m long sampling line. Further, we have recommended sole use of pure glass fiber filters as a particulate collector, when installed upstream of iodine sample collectors. We found that filters based on cellulose, synthetic fibers, and metallic fibers retained significant portions of gaseous I_2 and HOI.

BANGART: Please comment on the influence of sample flow velocity on iodine deposition. Some plants in the U.S. are planning to sample at a velocity of approximately 0.06 cfm over sample line lengths of tens of meters in order to minimize buildup of activity on the cartridges.

KABAT: An "as high as practical" flow should be applied to minimize the residence time of iodine in a sampling line. There are certain contradictions in optimizing for particulate and iodine sampline, which were discussed in my answer to the previous comment. Therefore, sampling lines should be optimized for the more critical component i.e., for radioiodine or for larger particles. From Table I, it can be derived that sample velocity of 0.06 cfm would result in an unacceptable deposition loss of elemental iodine in lines ≥ 0.5 in. diameter, ≥ 10 m long.

BURCHSTEAD: There has been much speculation about the existance of HOI over several air cleaning conferences. Is this HOI really a serious consideration?

KABAT: I cannot comment on the significance of HOI in U.S. nuclear power stations because I do not have experimental data on airborne radioiodines in light water reactors. However, HOI was identified to be the major airborne iodine species in Candu nuclear power stations. The results of our field measurements were summarized in a paper presented at the IAEA Seminar "The Testing and Operation of Off-gas Cleaning Systems at Nuclear Facilities", held in Karlsruhe in May 1982. The title of this paper is "Canadian Nuclear Air Cleaning Standards and their Application in Ontario Hydro".

17th DOE NUCLEAR AIR CLEANING CONFERENCE

KOVACH, J.L.: In all other investigative studies, it was found that HOI was an artifact of the adsorbent used and both ORNL and AECL studies show that HOI does not exist in the vapor phase. How do you justify identifying products as HOI and, is the existence of HOI a formal position of Ontario Hydro, or is its existence your personal opinion?

KABAT: The challenge is quite clear. However, its basis is somewhat inaccurate. I shall try to rectify the major points.

1. I have never seen a published statement that "HOI was an artifact of the adsorbent used." In the past, some doubts were expressed about the existence of HOI as a result of preliminary theoretical considerations. However, no conclusion was made in the recent ORNL and AECL studies on iodine chemistry, that "HOI does not exist in the vapour phase." On the contrary, I quote R. Lemire (AECL): "Based on currently available thermodynamic data, the predominant chemical form of iodine in the gas phase is predicted to be HOI except under moderately oxidizing conditions where I_2 and HOI would be present in roughly equal concentrations."

2. The reaction of pure elemental iodine with distilled water is generally recognized to be hydrolysis, resulting in the formation of HI and HOI, as primary products. Since we have experimentally established that gaseous species released from dilute aqueous solutions of elemental iodine are not iodine vapour or HI, we consider the presence of HOI to be sufficiently evident from the above elementary facts. (HOI might also occur in clustered or hydrated forms under certain conditions.) Most results of our experimental studies on the chemical behaviour of this volatile product of iodine hydrolysis have substantiated this interpretation. Further, absorption characteristics of the major airborne radioiodine species, which we have identified in Candu power stations, are identical with the properties of HOI generated in a laboratory under controlled conditions from diluted aqueous solutions of elemental iodine.

3. The answer is, no. The existence of HOI is not just my personal opinion. The requirements for testing charcoals for HOI removal efficiency have been included in the CSA N288.3 Standard. Many technical comments and recommendations had been received from AECL, Ontario Hydro, AECB, and other organizations before the standard was approved. However, no negative comment was received and no doubt was expressed on the existence of HOI and on its inclusion into charcoal testing requirements.

Several experts in U.S.A. (particularly at Science Applications, Inc.) have measured and reported the occurrence of airborne HOI in U.S. nuclear power stations. Amazingly, charcoal samples from TMI-2 were also evaluated by NUCON for its HOI removal efficiency.

17th DOE NUCLEAR AIR CLEANING CONFERENCE

To summarize my position:

From our developmental work on the chemistry of airborne radioiodines and from field applications we introduced and systematically performed during the last ten years, we have learned that (1) much practical experience in "low concentration iodine chemistry", (2) a very thorough and systematic experimental approach, and primarily (3) the availability of a dependable species selective monitoring system are essential for successful generation, isolation, and determination of airborne HOI. It is a highly reactive compound and it is unstable at concentrations which would be detectable with classical physico-chemical methods. Several attempts were made in some laboratories to determine airborne HOI, which did not meet with much success. Therefore, several investigators have taken a reserved position on its existence. However, good portions of data can be found which support the claim of the existence of airborne HOI in nuclear power stations, operational areas, and gaseous effluents.

Even at very low concentrations, HO¹³¹I presents a very significant radiobiological hazard (1 ppb $\sim 10^8$ MPC_a occupational). No business or personal interest has ever been involved in our investigations and its existence is not for us a matter of academic discussions. We are directly responsible for the protection of our occupational personnel and the public. We cannot admit any superficiality or major omissions in the control of airborne radioiodine hazard. Therefore, our effort still continues, to improve the understanding of its properties and to develop optimal methods for its efficient control, monitoring, and personal protection. The possibility of this product being identified as another chemical compound of iodine is very remote because no other realistic alternative has ever been suggested. However, even if this ever happens, its behaviour will be reasonably understood and its hazard well under control.

CLOSING REMARKS OF SESSION CHAIRMAN:

I would like to wrap up the session with a brief summary. We had seven papers and a lot of new information. R. T. Jubin studied the use of silver mordenite adsorbents for the recover of methyl iodide and found that the pickup of methyl iodide is comparable to elemental iodine. This is new information because four years ago we weren't sure that these materials would work for organic iodide. Operating temperature is about 200°C. Water vapor has a positive effect, NO_x has no effect, and now he is looking at the use of partial exchanged silver zeolites, 5-10% by weight, to maximize the use of silver. He has done some preliminary cost estimations and it looks to be between \$500,000 and \$700,000/y for a full size reprocessing plant.

Mr. Shiomi studied the removal efficiencies of methyl iodide on charcoal and silver exchange zeolites as a function of five variables—bed length, packing density, temperature, relative humidity, and face velocity. The important thing is that it was done with new adsorbents in the absence of contaminants. We are all aware that weathering and contamination drastically change the performance of a bed. He did a semi-empirical fit of data to an equation that has four constants and five variables. My concern would be that the four constants would change each time there is a new batch of material or there are contaminants on the adsorbent or agent. This remains a problem.

Mr. Mulcey gave a paper on in situ testing and performance of iodine adsorbents in French nuclear facilities and their pressurized water reactor. French law requires an annual check, and in some cases a three month check, on beds in continuous use. They use a tracer method with elemental iodine or methyl iodide. They believe this gives them the actual performance of the adsorbent in situ, rather than a leak test, such as is used in the U.S. They have found the following problems: (1) The lifetime of some of the traps is less than six months, a very short time. (2) It is difficult to get equal flow through parallel beds. We have the same problem in this country. (3) Defective assembly construction means leakage around the frame. A comparable problem here. They believe that the tracer method is costly and difficult and would like to partially supplement it with a leak test in between the initial installation test and retests every two years using the radioactive tracer technique. They found no correlation between efficiency and face velocity or relative humidity in the in situ test.

Mr. Rouyer has been doing laboratory testing of iodine adsorbents in French facilities using a German material, AC 6120, which has been thoroughly demonstrated in their reprocessing facilities by both hot and cold testing. The French are planning to install this adsorbent in their French nuclear reprocessing facilities by the end of 1986. This, I might add, is the only silver exchange adsorbent of silver nitrate on silicic acid that has been tested in hot service, in actual plant dissolver offgas.

17th DOE NUCLEAR AIR CLEANING CONFERENCE

Dr. Deuber gave a review paper on iodine adsorbents to see if they would meet the new German guidelines of September 4th that require iodine efficiency of 99.9%. In the case of the design basis accident, or a loss of coolant type accident, these adsorbents would have to survive and operate at temperatures as high as 150° C and relative humidity less than 10% for ten hours, and then, perhaps, drop down to 30° C and relative humidity of 100% for two months. So the question is, would they provide the kind of efficiency under these conditions. Dr. Deuber looked at about ten variables i.e., base material, particle size, impregnant service life, radiation field, iodine concentration, iodine species, temperature, relative humidity, face velocity, residence time, and purging time. Can you imagine an equation which describes all the parameters at once? It is very complicated. It was concluded that deep beds of potassium iodide impregnated charcoals would provide the necessary decontamination factors.

Dr. Scholten has been testing the performance of charcoal adsorbents in the Netherlands nuclear power plant. I believe it is a PWR. Initially, they found problems in that the material would last less than three months and they would have to pull out the whole bed containing several tons of charcoal. They were aware of repeated advice by Dr. Melvin First, for example, that they should have had a guard bed. Dr. Wilhelm has indicated that they should use a bigger bed. To solve this problem, they installed a guard bed in front, 1/10th the size of their iodine adsorbent bed, and changed it every three months instead of the adsorbent bed. At least, they have 1/10th the waste they would have had otherwise, so I would say that is a pretty good technique although they still don't get away from the problem that they have organic contaminants in the atmosphere that have to be removed.

Dr. Kabat studied the deposition of gaseous radioiodine species in sampling lines and I think this information will be very useful for up-dating ACN 13.1 for sampling methodology. He found that the deposition rates followed a trend where elemental iodine is the worst (something we have always known), that HOI is next, and methyl iodide is the least problem. He looked at four different metals and found that aluminum is the best metal, i.e., has the least deposition. He recommends that we avoid polyvinyl chloride and rubber type materials. Polyethylene is the best for elemental iodine and Teflon is best for HOI. He has attempted to calculate the deposition rate to determine the fraction that might be lost.

Session 4

WASTE PROCESSING

TUESDAY: August 3, 1982
Co-CHAIRMEN: M.J. Kabat, Ontario Hydro
C.H. Cheh, Ontario Hydro

OFF-Gas CHARACTERISTICS OF LIQUID-FED JOULE-HEATED CERAMIC MELTERS

R.W. Goles, G.J. Sevigny

IMMOBILIZATION OF KRYPTON-85 IN ZEOLITE 5A⁺

A.B. Christensen, J.A. DelDebbio, D.A. Knecht, J.E. Tanner, S.C. Cossel

THE LONG-TERM STORAGE OF RADIOACTIVE KRYPTON BY FIXATION IN ZEOLITE 5A⁺

R.D. Penzhorn, H. Leitzig, K. Gunther, P. Schuster, H.E. Noppel

VOLATILIZATION AND TRAPPING OF RUTHENIUM IN HIGH TEMPERATURE PROCESSES

M. Klein, C. Weyers, W.R.A. Goossens

RADIOCARBON TREATMENT SYSTEMS

PLANT FOR RETENTION OF ¹⁴C IN REPROCESSING PLANTS FOR LWR FUEL ELEMENTS

H. Braun, H. Gutowski, H. Bonka, D. Gundler

MECHANISM OF THE CO₂-Ca(OH)₂ REACTION

V.S. Chew, C.H. Cheh, R.W. Glass

¹⁴C RELEASE AT LIGHT WATER REACTORS

C. Kunz

CARBON-14 IMMOBILIZATION VIA THE Ba(OH)₂·8H₂O PROCESS

G.L. Haag, J.W. Nehls, Jr., G.C. Young

17th DOE NUCLEAR AIR CLEANING CONFERENCE

OPENING REMARKS OF SESSION CHAIRMAN:

Welcome to Session 4 of the 17th DOE Nuclear Air Cleaning Conference. Eight papers will be presented on radioactive waste processing and radiocarbon treatment systems. We are aware of the possibility that long-lived, volatile fission and activation products could cause in the future an increase in ambient radiation levels on a global scale, if they are allowed to accumulate in the biosphere. Their global impact has not been clearly established; however, to comply with the ALARA policy, their release from fuel cycle operations should be maintained at minimal achievable levels. Requirements for their removal should be based on realistic cost-benefit analysis.

Four radionuclides represent this class: Carbon-14, Krypton-85, Tritium and Iodine-129. There is no significant hazard from ^{129}I liberated from fuel cycle operations because its efficient effluent control has been well established. The removal of ^{14}C complies with cost-benefit criteria because it is based on relatively simple and inexpensive processes. The high proportion of presentations on ^{14}C at this session indicates that this task has been given proper attention. However, systems for the immobilization of ^{85}Kr and its long term storage are also being developed and the volatilization and trapping of other radiobiologically significant radionuclides is also being investigated.

Let us hear from experts about recent developments in this area.

17th DOE NUCLEAR AIR CLEANING CONFERENCE

OFF-GAS CHARACTERISTICS OF LIQUID-FED JOULE-HEATED CERAMIC MELTERS*

R. W. Goles and G. J. Sevigny
Pacific Northwest Laboratory
Richland, Washington 99352

Abstract

The off-gas characteristics of liquid-fed, joule-heated ceramic melters have been investigated as a function of melter operational conditions and simulated waste feed composition. The results of these studies have established the identity and behavioral patterns of gaseous emissions, the characteristics of melter-generated aerosols, the nature and magnitude of melter effluent losses and the factors affecting melter operational performance.

I. Introduction

Liquid-fed, joule-heated ceramic melters are to form the basis of the planned Defense-Waste Processing Facility (DWPF) to be constructed at the Savannah River Plant (SRP). The purpose of this facility (DWPF) is to isolate and immobilize defense-related nuclear waste as a borosilicate glass. The Pacific Northwest Laboratory (PNL) is assisting the Savannah River Laboratory (SRL) in establishing the design criteria for the DWPF by providing a technology transfer and all necessary liquid-fed ceramic melter research and development.

Off-gas characterization studies have been established as part of the SRL-DWPF melter development program being conducted at PNL. The objective of these studies is to establish the off-gas properties of liquid-fed, joule-heated melters as a function of melter operational parameters and feed composition.

The scope of these studies is quite broad and covers all aspects of off-gas concern including: 1) effluent characterization, 2) emission abatement, 3) flow rate behavior, and 4) corrosion effects. This paper will discuss the results obtained from each of these areas after a brief description of the liquid-fed melter process.

II. Liquid-Fed Melter Processing System

The following is a brief description of the liquid-fed melter processing system which was developed at PNL in support of the SRP-DWPF. A much more detailed account of the liquid-fed melting process can be obtained from Reference 1.

Melter

Several processes for solidifying and immobilizing high-level (radioactive) liquid waste as a stable borosilicate glass have been and are currently being evaluated at PNL.⁽²⁾ The process being

* Work performed for the Office of Nuclear Waste Management under U.S. Department of Energy contract TDO-954 (AR-05-15-10).

evaluated in this study utilizes a joule-heated ceramic-lined melter which is directly fed a uniform slurry composed of glass formers and simulated liquid radioactive waste. Upon entry into the melter, the waste components of the slurry are oxidized and melted with the glass formers present in the feed to form a molten borosilicate glass. The power required to maintain this continuous glass production process is supplied by resistive ac heating of the melter glass pool. In addition to the primary source of power, auxiliary radiant heaters located in the melter plenum above the glass melt surface have also been employed to increase or "boost" feeding and glass production rates. Limited use has also been made of plasma and propane combustion torches to supply supplemental heating to the melter plenum. Figure 1 schematically illustrates the liquid-fed melting process.

Two different joule-heated ceramic melters were used in these developmental studies and are referred to as the Liquid-Fed Ceramic Melter (LFCM), which has a melting surface area of 1.05 m², and the Pilot-Scale Ceramic Melter (PSCM), which possesses a 0.73 m² surface area. The maximum glass production rates associated with

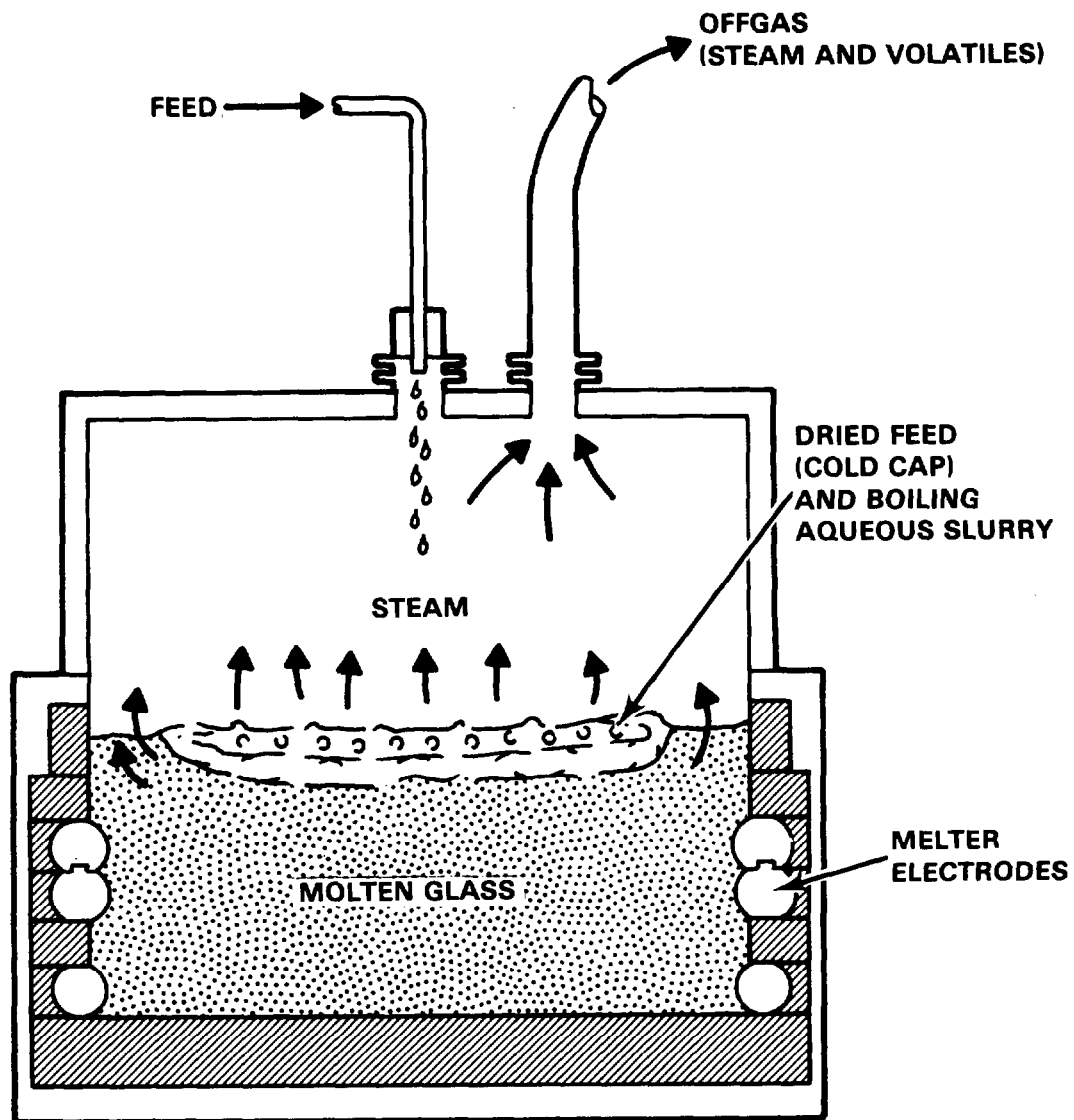


Figure 1. Liquid-fed, joule-heated ceramic melter system.

17th DOE NUCLEAR AIR CLEANING CONFERENCE

these melters are nominally 40 kg/h-m² for unboosted operation, and 60 kg/h-m² when auxiliary plenum heaters are employed. Table I summarizes all important operational parameters associated with liquid-fed melter tests involving the LFCM and PSCM melters. These melter tests, which are arranged chronologically in Table I, form the bases of the experimental off-gas studies which are discussed below.

Melter Off-Gas System

Both melters being studied in this report share a common 0.1-m (4-in.) stainless steel off-gas system consisting of an ejector venturi, a downdraft condenser, a packed scrubbing tower and a final absolute filter, physically arranged in the order listed. In addition to these common off-gas elements, both melters are equipped with a close-coupled HEPA filter receptacle and a total (condensable and noncondensable) off-gas flowmeter. Since the purpose of the DWPF off-gas support studies was to establish melter off-gas characteristics, the performance of the generic off-gas processing equipment present in the common melter off-gas system was of little programmatic interest and consequently will not be discussed here.

Feed Composition

The liquid slurry feed used in the SRL-DWPF melter development program is a uniform mixture of simulated defense waste sludge and glass formers (frit). The composition of this slurry as equivalent oxides is detailed in Table II. The actual waste loading of the slurry is 29 wt% of the total oxides present. In addition to the major elemental constituents listed in Table II, SRL simulated waste also contains stable elemental substitutes for all volatile and semi-volatile isotopes which are present in typical defense waste and which are of radiological concern. The trace elemental composition of the SRL feed slurry is presented in Table III.

Although the waste composition of the liquid feed remained essentially constant throughout the period of testing covered in this report (see Table II), the rheology of the feed was dramatically affected with the addition of formic acid to the DWPF waste stream flowsheet. Initial experiments were conducted with an alkaline (pH 11 to 12) slurry having the physical characteristics of a Bingham plastic fluid. Acidification (pH 5 to 6) of the liquid waste stream with formic acid resulted in slurries which behaved more like an ideal Newtonian fluid. The presence of formic acid in melter feed slurries not only changed the fluidic properties of the feed, it also dramatically influenced the off-gas emission properties of the liquid-fed melter.

III. Melter Effluent Characterization

One of the major tasks involved in the DWPF off-gas studies was that of determining melter emission characteristics. The nature and extent of melter-generated effluents had to be established before off-gas system criteria could be finalized for the DWPF melters. Consequently, an off-gas sampling system was developed to provide this basic off-gas design data.

Table I. Liquid-fed melter operational parameters.

Operational Parameters	Experiment									
	<u>PSCM-1</u>	<u>LFCM-4</u>	<u>PSCM-2</u>	<u>LFCM-6</u>	<u>PSCM-3</u>	<u>LFCM-7</u>	<u>PSCM-4</u>	<u>PSCM-5</u>	<u>PSCM-6</u>	<u>PSCM-7</u>
Feed Type	Basic	Basic	Basic	Basic	Acidic	Acidic	Acidic	Acidic	Acidic	Acidic
Feed Rate, L/h-m ²	45	90	110	100	62	121	83	100	122	68
Glass prod. Rate, kg/h-m ²	22	41	50	45	28	57	39	50	60	43
Plenum Temp., °C	400	600	400-800	600	300	500	400	520	850	300
Boosting Type	None	Elec. Lid Heat	Propane Combustion	Elec. Lid & Plasma Torch	None	Elec. Lid Heat	None	Elec. Lid Heat	Elec. Lid Heat	None
Boosting Power, kW	--	30	35	40	--	15	--	36	55	--
Off-Gas Temp., °C	375	375	375	400	250	300	275	375	400	270
Off-Gas Cooling, L/h	0	8	23	24	0	Vari-able	0	23	23	0
Experiment Duration, h	120	120	120	120	125	111	107	99	138	115

Table II. Simulated waste slurry and glass compositions.

Waste Slurry Composition		Acid Waste	
Alkaline Waste Conc., g/L	Compound	Compound	Conc., g/L
338.0	Frit-131	Frit-131	341.3
14.7	Zeolite	Zeolite	9.9
3.30	Anth. Coal	HCHO ₂	>18.0
90.9	Fe(OH) ₃	Fe(OH) ₃	81.2
21.0	Al(OH) ₃	Al(OH) ₃	34.2
19.5	MnO ₂	Mn(CHO ₂) ₂	28.2
10.4	Ni(OH) ₂	Ni(CHO ₂) ₂	8.3
8.90	CaCO ₃	Ca(CHO ₂) ₂	16.7
5.84	SiO ₂	SiO ₂	15.6
4.93	NaOH	NaCHO ₂	8.42
2.01	NaNO ₃	NaNO ₃	2.01
0.73	Na ₂ SO ₄	Na ₂ SO ₄	0.72

Typical Slurry and Glass Oxide Composition*					
Oxide	Waste Sludge	Frit-131†	Zeolite††	Total	Final Glass Composition, Wt. %
Fe ₂ O ₃	60.7			60.7	12.7
Al ₂ O ₃	22.3		1.9	24.2	5.1
MnO	13.8			13.8	2.9
NiO	4.1			4.1	0.8
CaO	7.2		1.1	8.3	1.7
SiO ₂	15.6	197.6	4.7	219.9	45.6
Na ₂ O	4.6	60.4	0.2	65.2	13.6
Na ₂ SO ₄	0.7			0.7	0.1
B ₂ O ₃		50.2		50.2	10.5
Li ₂ O		19.4		19.4	4.1
MgO		6.8		6.8	1.4
TiO ₂		3.4		3.4	0.7
La ₂ O ₃		1.7		1.7	0.4
ZrO ₂		1.7		1.7	0.4
TOTAL	129.0	341.2	7.9	480.1	100.0

* Feed slurry glass content = 0.48 kg/L.

(†) Frit-131 Composition (-200 mesh).

(††) Zeolite Composition (Linde Ionsiv IE-95)

Oxide	Wt%
SiO ₂	57.9
B ₂ O ₃	14.7
Na ₂ O	17.7
Li ₂ O	5.7
MgO	2.0
TiO ₂	1.0
La ₂ O ₃	0.5
ZrO ₂	0.5
TOTAL	100.0

Component	Wt%
CaAl ₂ Si ₄ O ₁₂ 6H ₂ O	80
Na ₄ Ca _{1.5} Al ₃ Si ₈ O ₂₄ 8H ₂ O	20
TOTAL	100

Assumed Oxide Forms	Wt%
CaO	10.6
Al ₂ O ₃	19.2
SiO ₂	47.7
Na ₂ O	2.5
H ₂ O	20.0
TOTAL	100.0

17th DOE NUCLEAR AIR CLEANING CONFERENCE

Table III. Concentration of trace melter feed additives.

Trace Additives	Concentration, g/L	
	Oxides	Elemental
Cs ₂ O	0.25	0.24
SrO	0.098	0.083
Sb ₂ O ₃	0.16	0.060
SeO ₂	0.04	0.029
CdO	0.38	0.033
TeO ₂	0.05	0.036
RuO ₂	0.085	0.064

Melter Off-Gas Sampling Network

The sampling network, which was developed in support of melter emission characterization studies, is schematically illustrated in Figure 2. The components making up this network were designed to determine the composition of melter exhaust with regard to the effluents listed below.

- Gases: H₂
- N₂
- O₂
- CO
- CO₂
- SO₂
- Semivolatiles: Cs
- Sb
- Se
- Te
- Mn (Tc)
- Ru
- Cd (Cm)
- Sr
- Halogens
- Others
- Particulates

The gaseous composition of melter off-gas emissions was established using a gas chromatograph (GC) and real-time gas analyzers. The gas sample stream used for this purpose is extracted prior to any off-gas processing. This hot, water-laden gas stream is first passed through a tube and shell condenser, which reduces the water loading of the gas while minimizing the gaseous interactions with condensed-phase water. The quenched gas stream is subsequently passed through a filter and a permeation dryer and is finally distributed to the individual gas analyzers using a stainless steel bellows pump.

The GC used in these studies is programmed to sample and analyze the composition of the continuously-flowing gas stream every 30 min. The gaseous components, which are routinely quantified by this instrument, include O₂, N₂, CO and CO₂. In addition, the GC pro-

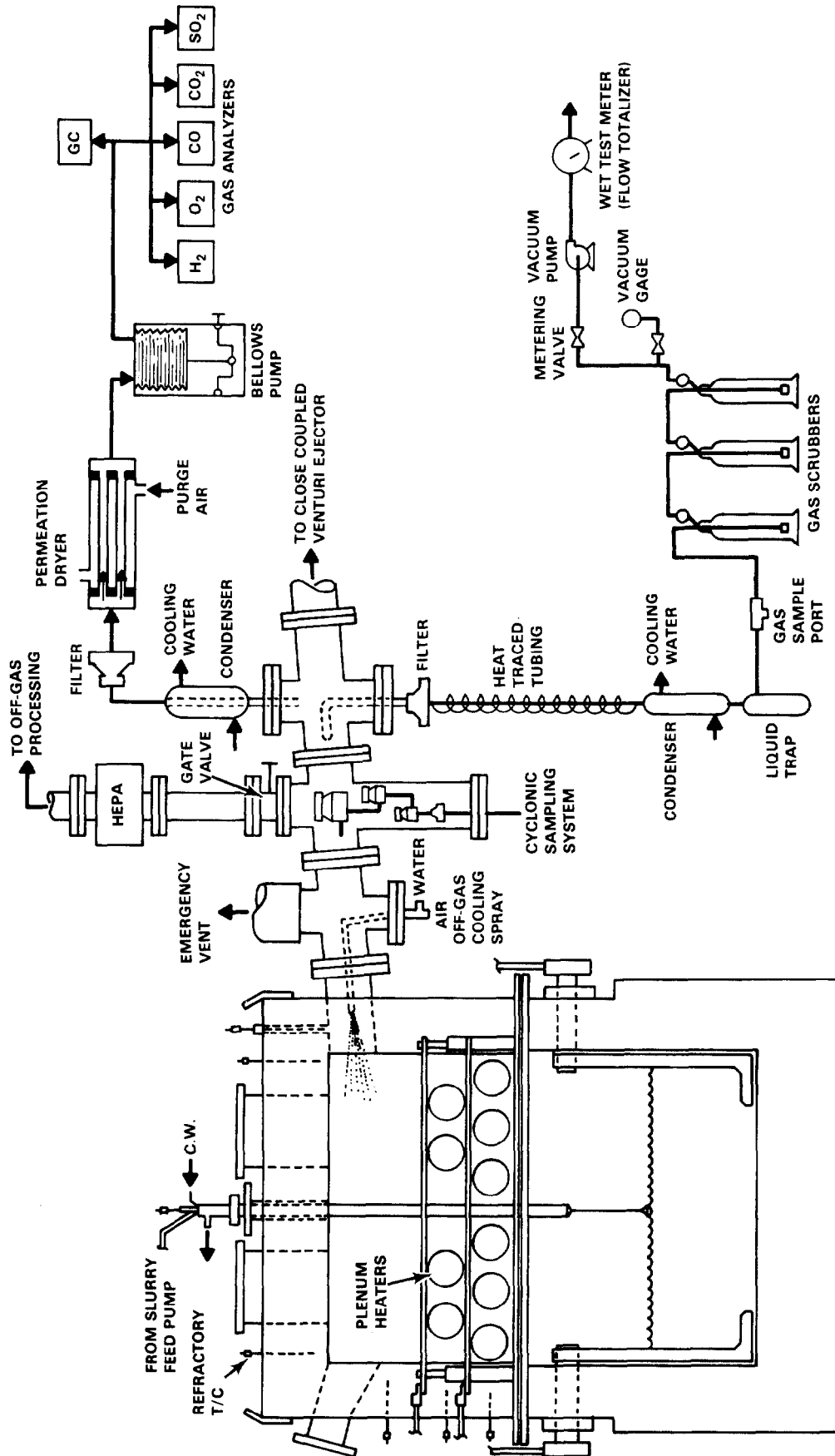


Figure 2. Melter off-gas sampling network.

17th DOE NUCLEAR AIR CLEANING CONFERENCE

vides semi-quantitative information with regard to gaseous concentrations of H_2 , SO_2 and NO_x .

Real-time measurements of melter off-gas concentrations were initiated during the latter part of this study with the installation of five continuous gas monitors. These instruments have provided continuous compositional off-gas data with regard to H_2 , O_2 , CO , CO_2 and SO_2 for all melter tests following the PSCM-4 experiment.

Characterization of the pathways and magnitudes of melter-generated semivolatile emissions were assessed using a differential sampling system composed of a filter, a heat-traced sampling line, a condenser and a series arrangement of three gas scrubbing units (Figure 2). The distribution of semivolatiles across the five discrete sample fractions generated by the system were analytically determined using emission spectrometry (ICP), atomic absorption (AA), ion chromatography (IC) and x-ray fluorescence techniques. All semivolatile studies conducted have been exclusively concerned with characterizing the unquenched melter exhaust composition.

Melter-generated aerosols were characterized with regard to concentration, size and composition. Total off-gas particulate loading was most directly established, gravimetrically, by HEPA filtration of the entire melter off-gas stream (Figure 2). Particle size information is obtained from a cyclonic sampling system consisting of a series arrangement of three cyclones and a final absolute filter. The cut points of the cyclones employed are $16\ \mu m$, $6\ \mu m$ and $1\ \mu m$ at 18 actual L/m. The final absolute filter is designed to collect submicron fines which are able to pass through all three preceding cyclones. The elemental composition of the particulate matter collected by these sampling devices is established using ICP, AA and IC analytical techniques.

Melter Exhaust Composition

The noncondensable ($20^\circ C$) gases generated by liquid-fed melters are functionally dependent upon the slurry feed composition as well as melter operating conditions. The alkaline waste feed used during the initial stages of this study possessed very low concentrations of organic matter. Consequently, the gross melter off-gas composition was essentially CO_2 -enriched inleakage. The emission rates of the combustible gas CO during all of the alkaline feed tests were always less than 1/10 the rate associated with CO_2 . Table IV summarized the average gross compositional data associated with alkaline-feed melter exhausts. The dramatic difference existing between the PSCM-2 data and that of all other experiments listed in Table IV is due to the method of boosting used in that test. During PSCM-2, a propane torch was used to supply supplemental heat to the melter plenum in order to facilitate increased feeding rates. Consequently, the major source of off-gas combustion products was the boosting torch and not the melter. Figure 3 illustrates the time-correlated behavior of the gross composition of the melter exhaust during the PSCM-2 test. The relationships illustrated are consistent with the propane combustion process.

The composition of melter-generated, noncondensable gases was dramatically affected when formic acid was added to the simulated

Table IV. Melter noncondensable off-gas composition (basic waste).

Experiment	Melter Inleakage, scfm	Molar %											
		CO ₂			CO			O ₂			N ₂		
		Hi	Avg	Lo	Hi	Avg	Lo	Hi	Avg	Lo	Hi	Avg	Lo
PSCM-1	5-10	6.4	3.4	1.8	<0.01	--	--	20	14.0	7.1	89	81	73
LFCM-4	32	1.1	0.58	0.40	0.03	0.02	0.001	21	20.5	20.0	78	78	78
PSCM-2	45	8.6	4.6	0.20	3.0	0.50	0.001	21	14.0	8.0	82	80	79
LFCM-6	29	0.87	0.54	0.13	0.07	0.02	<0.001	20	20.0	18.0	80	79	78

Table V. Melter generated off-gas components (acid waste).

Experiment	Melter Inleakage, scfm	Molar %											
		CO ₂			CO			H ₂					
		Hi	Avg	Lo	Hi	Avg	Lo	Hi	Avg	Lo			
PSCM-3*	20	2.9	1.3	0.26	1.3	0.40	0.04	1.11	NA	0.17			
LFCM-7	90	2.2	0.74	0.03	0.44	0.13	0.002	0.63	0.54	0.40			
PSCM-4	20	4.4	2.9	1.5	0.75	0.44	0.20	1.3	1.1	0.94			
PSCM-5	30	6.5	2.8	2.0	0.90	0.35	0.10	1.8	0.80	<0.10			
PSCM-6	30	6.5	4.1	2.0	0.60	0.09	<0.005	1.2	NA	<0.05			
PSCM-7	12**	8.0	5.0	1.5	1.2	0.75	0.10	3.5	1.9	0.30			

* Sample stream diluted ~2.5 times.

** Off-gas dilution was used.

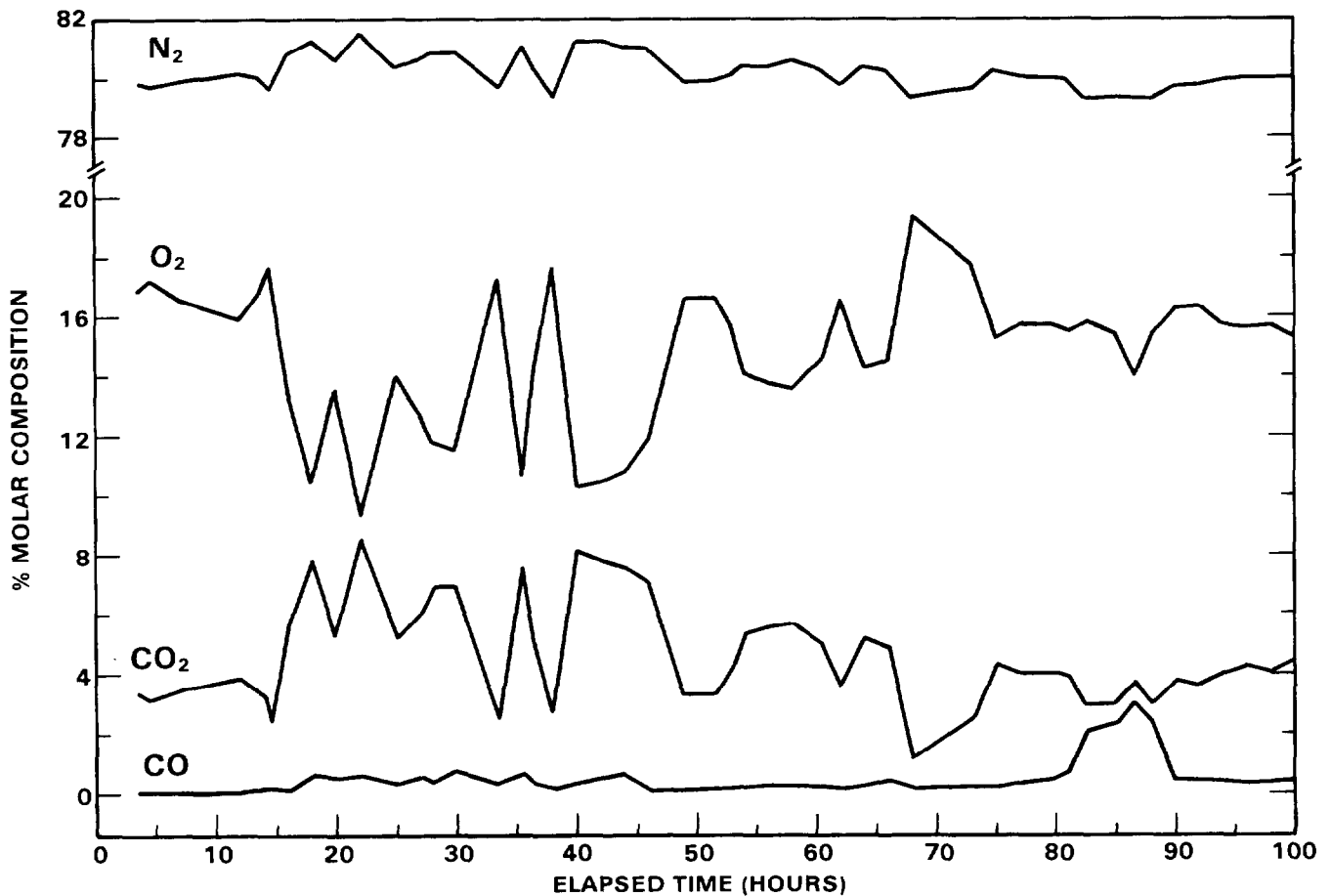


Figure 3. Combustion boosted melter exhaust composition.

melter feed. This compositional alteration increased the organic loading in the melter feed by approximately an order of magnitude. Consequently, melter exhaust gases were of particular interest during these acidified feed tests due to the possibility of generating H_2 and CO (water gas) in sufficient quantities to present a flammability hazard after off-gas quenching. Figure 4 illustrates the time-related behavior of gross melter exhaust gases during a 120-h melter test which employed 100 h of radiant lid heat boosting followed by 20 h of unboosted operation. The presence of plenum heaters during liquid feeding clearly reduces melter emissions of the combustible gases H_2 and CO. With the termination of lid heating, the melter plenum cooled, reducing the oxidation rates of these gases sufficiently to allow significant quantities of each gas to escape the plenum through the off-gas system. This result is quite reproducible; however, virtual elimination of combustible gas emissions during boosting, as is illustrated in Figure 4, may not always be achievable. Similarly, the concentration of combustibles leaving an unboosted melter may be significantly higher than is indicated in Figure 4 since they are slurry composition-, temperature-, feed and inleakage rate-dependent variables. Indeed, dilution air was required during the unboosted PSCM-7 test to reduce H_2 in the quenched off-gas stream to below 70% of its lower inflammability limit ($\sim 4\%$). A summary of the gaseous concentrations of organic

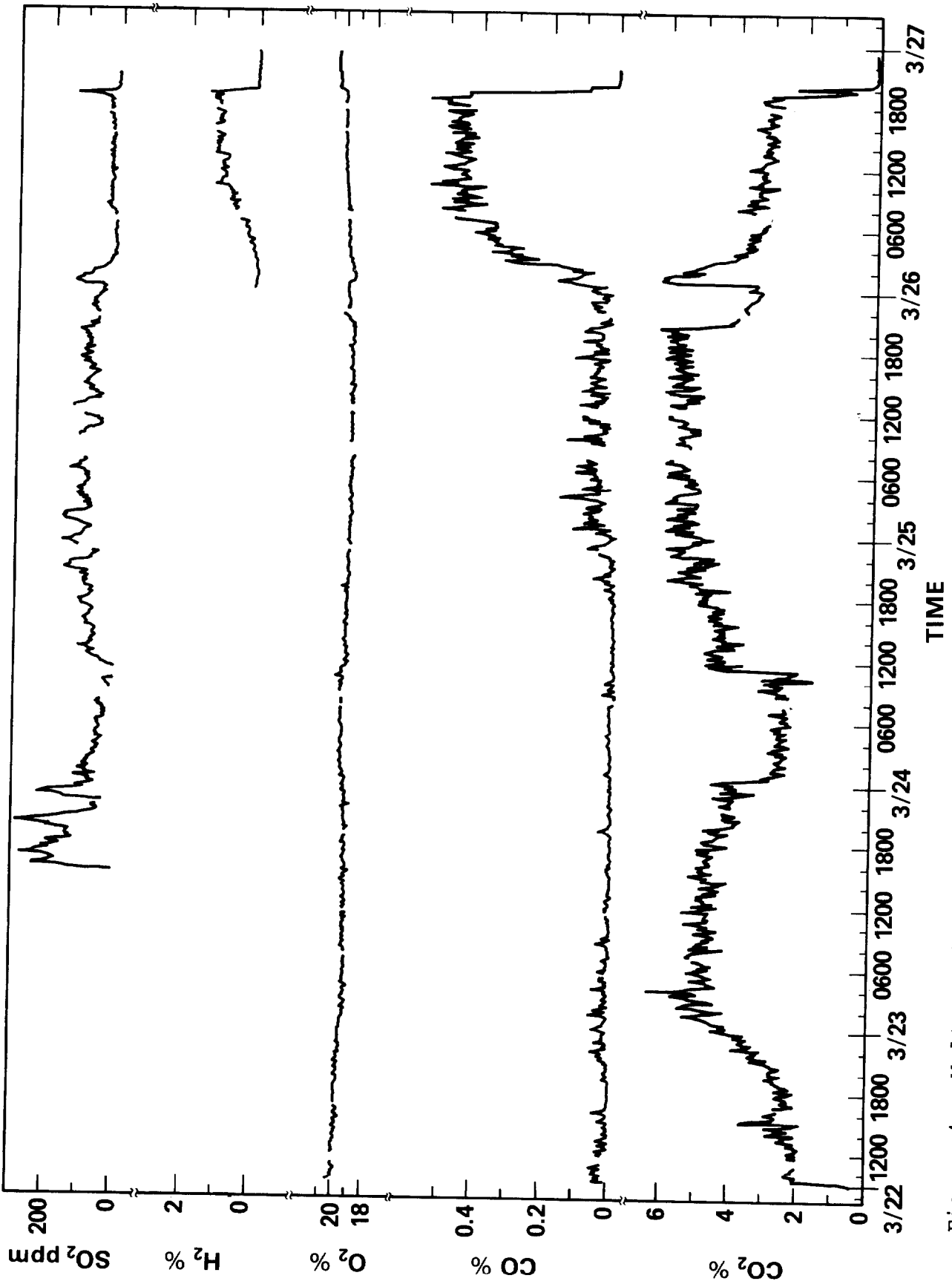


Figure 4. Melter exhaust gas composition of a 100-h boosted, 20-h unboosted test.

17th DOE NUCLEAR AIR CLEANING CONFERENCE

decomposition and reaction products generated during all formate feed melter testing is presented in Table V, along with average melter inleakage rates.

The off-gas data presented in Figure 4 clearly illustrates that melter generated emissions are not smooth and continuous functions even under the most controlled operational conditions. This behavior is due to the erratic, nonuniform way in which melter feed is dried, oxidized and melted during the liquid feeding process. Large excursions in melter gas generation rates usually occur when dammed up liquid feed lying atop an insulating layer of dry feed (the cold cap) abruptly flows out upon a hot glass surface. The liquid quickly flashes off this hot surface, producing a flow pulse composed of steam and volatile organic reaction products. Figure 5 illustrates the behavior of some of the more important melter-generated gases accompanying flow surging events. The frequency and magnitude of these surging events are positive indicators of melter system instabilities which are most often associated with erratic or overfeeding conditions.

The ability of melter-generated gases to accompany steam flow surges suggests that the evolution of combustible gases from the melter cold cap is quite prompt. Figure 6 portrays the time-dependent compositional behavior of the melter exhaust stream upon feed interruption or termination. With the exception of SO_2 , none of the melter-generated gases increase in concentration when feeding was terminated. This fact implies that volatile decomposition and reaction products generated from the melter feed are formed soon after introduction of the feed into the melter environment. Consequently, significant accumulations of chemically-reactive organic feed components within the melter cold cap apparently do not occur under stable steady-state feeding conditions.

On the other hand, the increase in terminal SO_2 exhaust concentration (illustrated in Figure 6) suggests sulfur, as Na_2SO_4 , may be accumulating within the melter as a molten salt. This was indeed found to be the case, as post-run inspection of the idling melter glass surface later proved. This observation stimulated speculation that accumulations of Na_2SO_4 could be responsible for changes in the melting capacity of liquid-fed melters that occur during the initial ~24 hours of liquid feeding (the startup phase). Melter emission characteristics of SO_2 further support this notion, as is shown in Figure 7. During the initial startup phase, when the melter's ability to handle feed is limited, feed-rate normalized SO_2 emission rates are uncharacteristically low, indicating that accumulation of Na_2SO_4 is probably occurring. As processing continues at a fixed feeding rate, SO_2 emission rates gradually increase along with the melting capacity of the liquid-fed melter. It is known⁽³⁾ that the presence of a molten Na_2SO_4 phase within a ceramic melter will increase the heat transfer rate between the molten glass and the feed, thereby boosting melting capacity. All of the above-mentioned liquid-fed melter characteristics are consistent with this fact.

Although Figure 7 suggests that SO_2 evolution is an important mechanism responsible for sulfur melter feed losses, this is true only for boosted experiments where plenum temperatures are greater

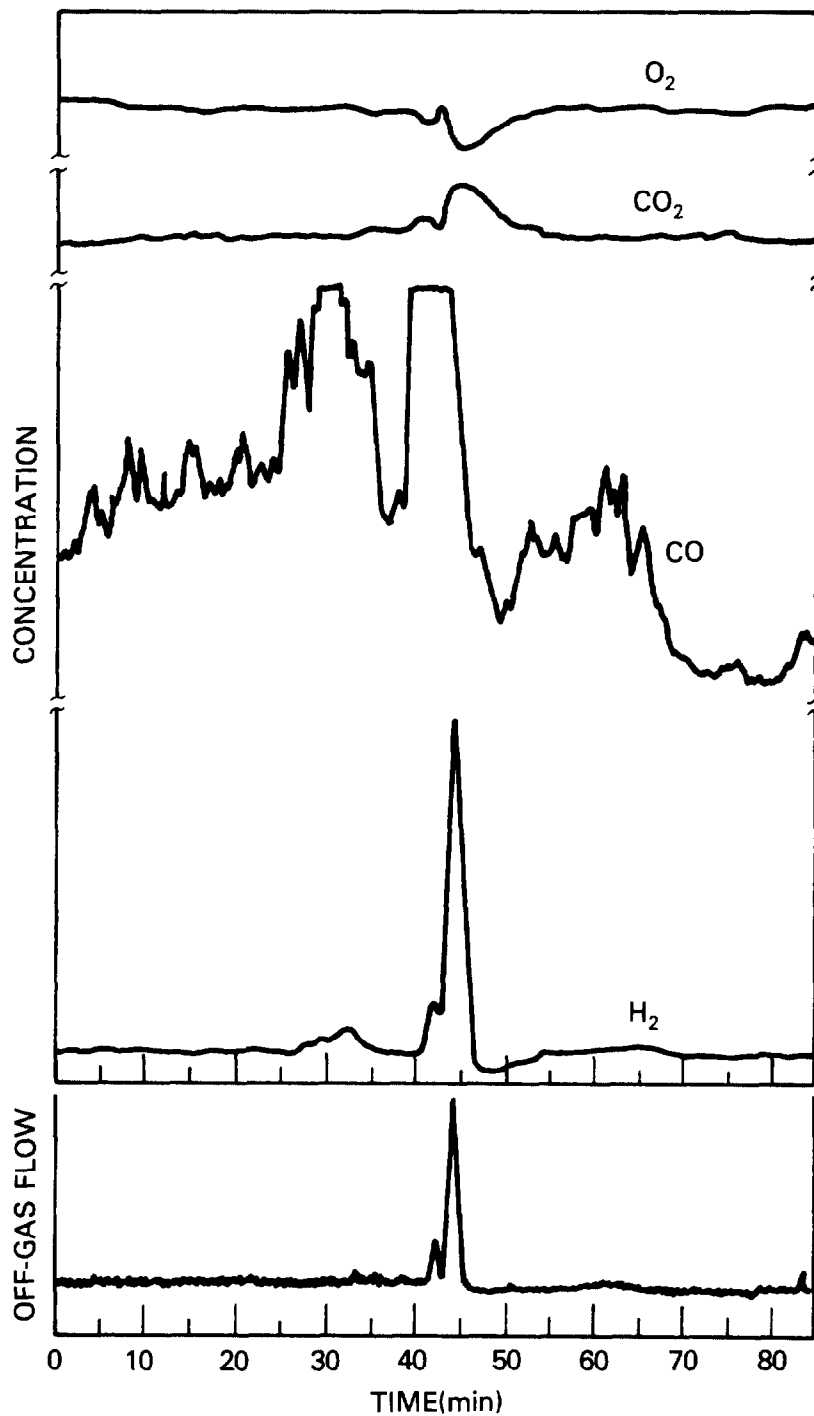


Figure 5. Compositional behavior of noncondensable melter exhaust gases accompanying a flow surge. (Maximum extent of the surge event: flow-3X; $H_2 < 3.5\%$; $CO \gg 0.5\%$; $CO_2-15\%$; $O_2-17\%$.)

than 700°C . Emission rates of SO_2 during unboosted runs are at least an order of magnitude lower than when boosting techniques are employed. However, total melter losses of sulfur are found to be more or less independent of boosting, indicating the presence of other volatile chemical channels of escape (SO_3). Filtered gas-scrubbing techniques have further verified that significant

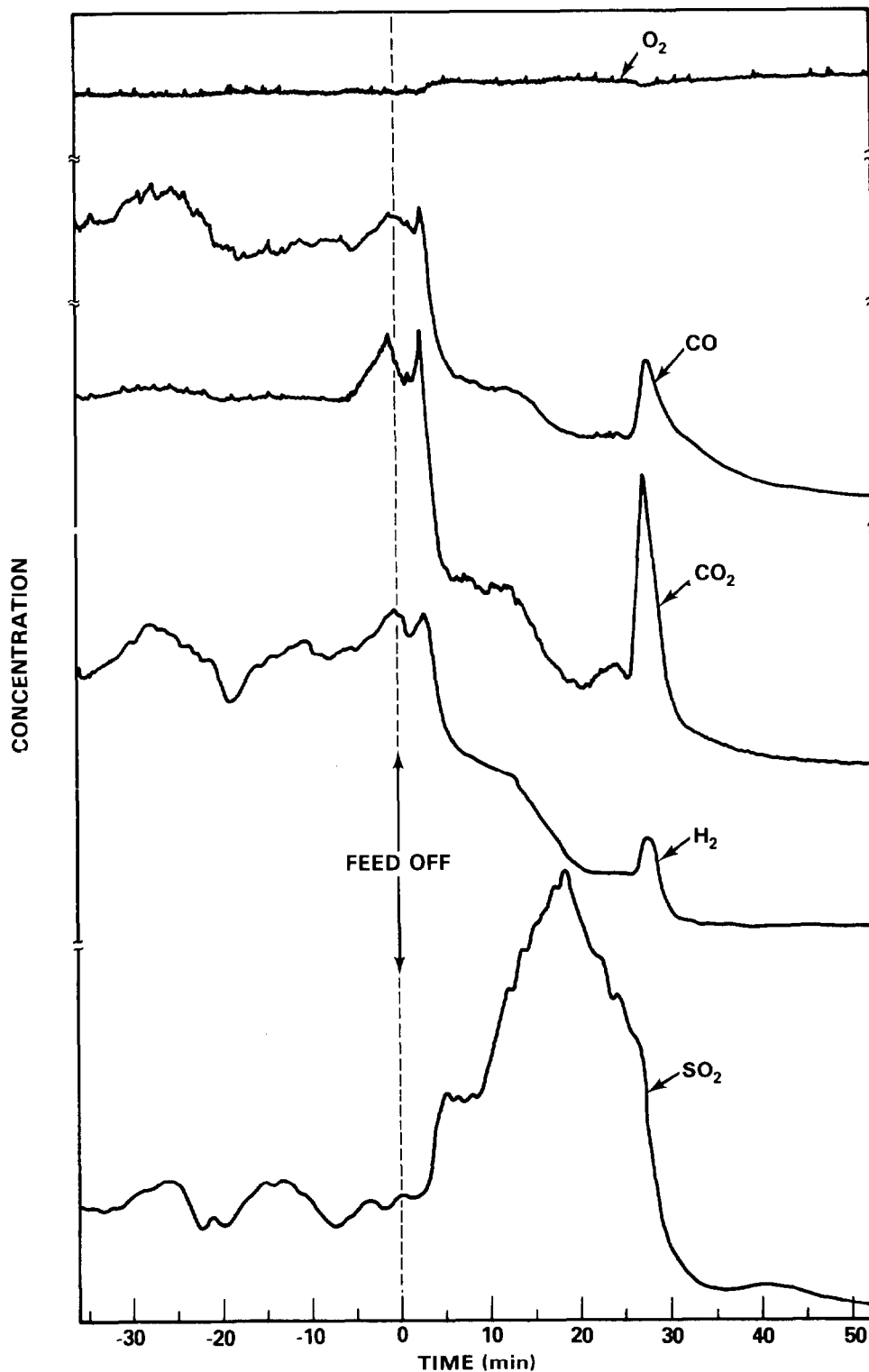


Figure 6. Melter off-gas compositional behavior associated with feed termination. (The $t = 30$ min compositional spike is due to the injection of a small quantity of liquid feed.)

concentrations of acidic volatile gases of sulfur as well as the halogens always exist in unquenched melter exhaust streams independent of any and all melter operating conditions. This subject will be further developed in discussions that follow.

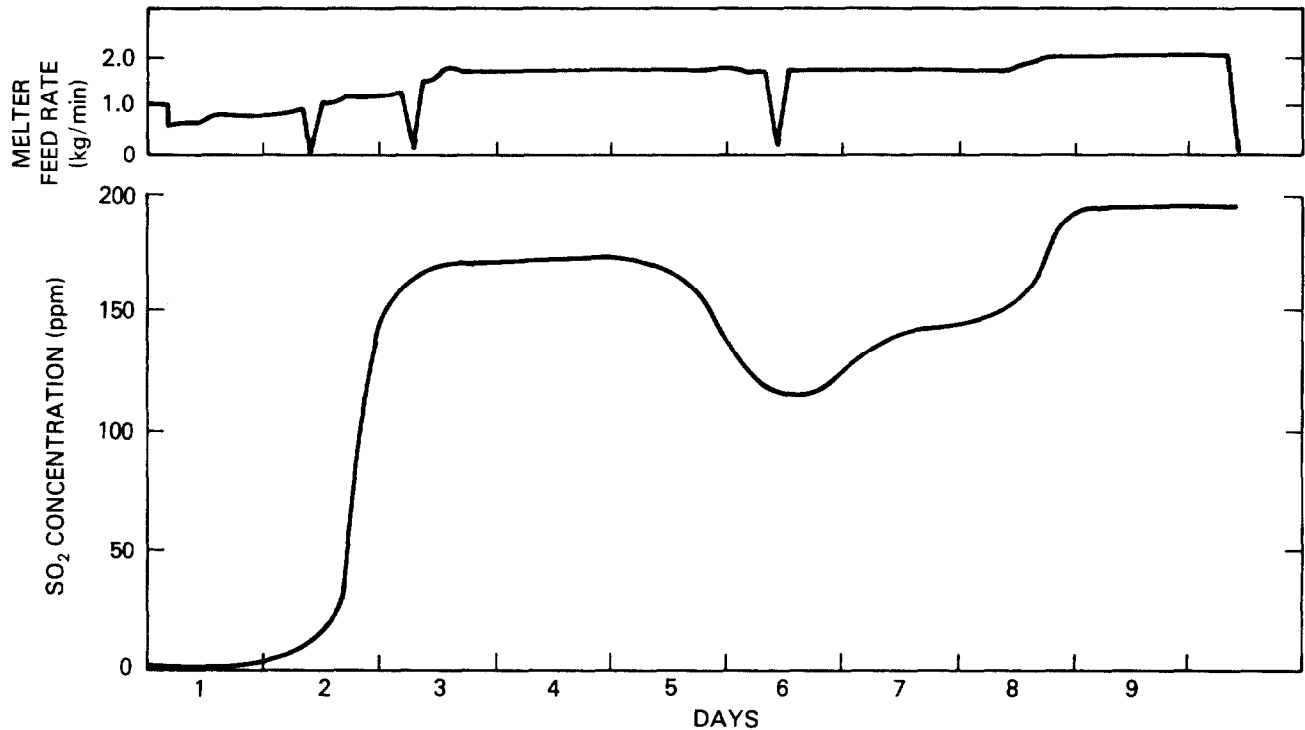


Figure 7. Melter SO₂ emission characteristics accompanying a ~240-h test.

Nature of Melter Feed Component Losses

In order to characterize the pathways and magnitudes of melter feed component losses, a differential sampling system composed of an aerosol filter, condenser and a series arrangement of three gas-scrubbing units was employed. The manner in which any given element is distributed across the five discrete sampling fractions of this device is indicative of the physical state or states assumed by the effluent. Typical data generated with this differential sampling system during a formate-feed melter test is summarized in Table VI. The DF values listed in this table are melter decontamination factors, which are ratios of the rate at which feed components enter the melter to the rate at which they are evolved. Particulate DFs are partial DFs relating to only a single loss mechanism: aerosol emission. The data presented in this abridged table clearly shows that melter gas-phase losses to the off-gas system are only significant for Cl, S and B, which readily form volatile acid gases previously referred to. This is not to say that melter-induced volatilization has no influence upon melter losses of other feed component elements. On the contrary; the low DFs associated with the semivolatile elements Cd, Cs and Te, as well as Se and Sb, clearly underscore the importance of this volatilization process. What is being said is that apart from the mechanisms responsible for producing airborne effluents, particulate transport through the off-gas system is the predominant loss mechanism associated with liquid-fed melter operation.

17th DOE NUCLEAR AIR CLEANING CONFERENCE

Table VI. PSCM-6 particulate and total feed component DFs.

<u>Element</u>	<u>Average DF</u>	
	<u>Particulate</u>	<u>Total</u>
Al	27,000	22,000
B	6,800	100
Cd	9.9	9.9
Cl	21	2.9
Cs	14	14
Fe	1,900	1,800
La	2,100	2,100
Mn	1,800	1,800
Na	300	300
S	11	5.5
Sr	1,800	1,800
Te	3.0	3.0
Zr	22,000	22,000

Characteristics of Melter Aerosols

Since most melter off-gas system losses are associated with aerosol emission, establishing the characteristics of these aerosols was of particular engineering interest. The size distribution of melter-generated aerosols was established using a cyclonic particle-size analysis system, which was described earlier. Table VII details the manner in which melter particulate matter was distributed across the cyclonic sample fractions as a function of melter experiment. All melter tests, with the exception of PSCM-4, exhibited aerosol-size distributions which were definitely bimodal in nature. This suggests that the overall aerosol distribution may be comprised of two independent components, each having its own characteristic size distribution. Gross compositional dissimilarities between the discrete cyclonic size fractions illustrated in Table VIII strongly reinforce this argument. Moreover, since the submicron size fraction detailed in this table (LFCM-7) contains only 12% of the total sample mass, but possesses essentially all the semivolatile matter of the sample, the mechanism responsible for the small diameter component of the overall distribution is probably a volatilization/condensation process that occurs within the melter plenum. The composition of the large cyclonic size fractions are very similar to that of the slurry feed as shown in Table IX. Consequently, the large component of the bimodal distribution must almost certainly be associated with a gross entrainment mechanism.

Since the major melter loss mechanism associated with the radiologically important semivolatiles is associated with submicron aerosol emission, the elemental makeup of this size fraction is of particular interest. Table X presents representative submicron compositional data collected during the PSCM-4 experiment. If one attempts to conduct a material balance for this submicron matter by assuming an oxide form for all elements except for a stoichiometric quantity of Na, which is associated with the Cl in the sample, one can account for 99% of the matter present. It should be noted that while the submicron sample fraction is quite rich in semivolatiles, it is essentially salt (83 wt% NaCl).

17th DOE NUCLEAR AIR CLEANING CONFERENCE

Table VII. Size distribution of melter aerosols.

Experiment	Average wt% Versus Cut Point			
	16 μm	6 μm	1 μm	<1 μm
LFCM-7	76.7	2.8	8.5	11.9
PSCM-4	--	0.9	3.6	95.6
PSCM-5	13.5	3.9	20.2	62.2
PSCM-6	46.1	0.5	12.7	40.7
PSCM-7	7.5	3.2	9.4	79.9

Table VIII. Elemental distribution across cyclonic sampling system.

Element	Elemental Distribution, %			
	16 μm	6 μm	1 μm	<1 μm
Al	96.2	0.9	2.5	0.4
B	87.8	1.8	7.8	2.6
Ba	83.7	5.8	10.5	0
Ca	77.7	2.7	15.2	4.4
Cd	10.7	0.8	7.3	81.2
Ce	92.1	0	7.9	0
Cr	46.4	21.7	23.3	8.6
Cs	7.5	0	5.4	87.1
Cu	82.6	4.9	4.2	8.3
Fe	77.3	2.6	17.0	3.1
La	91.9	1.5	6.1	0.5
Li	83.2	1.5	5.3	10.0
Mg	91.5	1.6	5.8	1.1
Mn	89.4	6.4	3.6	0.6
Mo	77.5	5.6	9.8	7.1
Na	68.8	1.7	5.6	23.9
Nd	93.4	0	6.6	0
Sb	100.0	0	0	0
Se	56.9	1.9	11.4	29.8
Si	92.0	1.8	5.6	0.6
Sr	77.6	2.8	19.6	0
Te	5.5	0.4	3.2	90.9
Ti	91.2	1.8	6.0	1.0
Zr	91.6	1.6	5.6	1.2

Melter Emission Performance

Melter performance with regard to effluent emission is commonly expressed in terms of a unitless decontamination factor or DF. By definition, a melter feed component DF is the ratio of the rate at which that particular feed component enters the melter to the rate at which it is evolved from it. Consequently, melter DFs are related to the liquid-fed melter process efficiencies for converting feed components into a borosilicate glass. Table XI presents experimental feed component DFs for all pertinent DWPF melter tests conducted at PNL. The entries in this table are grouped according to feed type and each group is ordered with respect to the experimental melter employed. This ordering has significance with regard to the interpretation of the data. The initial melter tests conducted with

17th DOE NUCLEAR AIR CLEANING CONFERENCE

Table IX. Composition of 16 μ m cyclonic sample fraction.

Compound	Wt%	
	16 μ m	Feed
Al ₂ O ₃	3.4	5.1
B ₂ O ₃	9.0	10.5
CaO	1.6	1.7
Fe ₂ O ₃	14.4	12.7
La ₂ O ₃	0.3	0.4
LiO ₂	3.5	4.1
MgO	1.1	1.4
MnO	3.2	2.9
Na ₂ O	13.0	13.6
SiO ₂	38.0	45.6
TiO ₂	0.7	0.7
ZrO ₂	0.3	0.4

alkaline feed were, with one exception, all boosted experiments (see Table I). Consequently, a major goal of all of these tests was to establish maximum melter feeding rates under a variety of plenum heating conditions. To complicate matters, an evolving slurry feed system being developed during this same period was often responsible for inconsistent feed delivery to the melter. As a result, stable steady-state operating conditions during these early melter scoping tests were rarely, if ever, achieved. The spread in melter emission performance data during this initial testing phase is in large part a reflection of the unequilibrated conditions that existed when this data was collected. The average DFs listed for the alkaline feed components should, however, provide a fairly representative description of the ceramic melter effluent emission behavior that occurred during this initial development period.

With the exception of the LFCM-7 test (melter capacity scoping study), all acid feed melter experiments sought to establish operational stability under a variety of running conditions. Table XII presents partial melter DFs associated with off-gas aerosol emission for the PSCM-5 and PSCM-6 experiments. The data associated with each of these tests were collected over several days of stable, steady-state melter operation using three independent sampling devices. The internal agreement between results obtained in each test is, without question, indicative of the stability associated with each of these experiments. Consequently, effluent results of individual acid feed experiments should be more representative of average melter behavior than were those associated with the alkaline feed.

A comparison of melter DFs achieved with alkaline and acidic waste slurries reveals that, with only a single exception, higher effective emission rates (lower DFs) were observed for the

17th DOE NUCLEAR AIR CLEANING CONFERENCE

Table X. Submicron particulate composition.

<u>Element</u>	<u>Elemental Wt%</u>	<u>Assumed Form</u>	<u>Compound Wt%</u>	<u>Feed Composition, %</u>
Al	0.04	Al ₂ O ₃	0.08	4.95
B	0.07	B ₂ O ₃	0.24	9.86
Ca	0.14	CaO	0.20	1.66
Cd	0.55	CdO	0.63	0.006
Cs	2.1	Cs ₂ O	2.2	0.044
Cu	0.06	CuO	0.09	--
Fe	0.29	Fe ₂ O ₃	0.41	13.69
K	0.36	K ₂ O	0.43	--
Li	1.1	Li ₂ O	2.4	3.98
Mg	0.02	MgO	0.03	1.29
Mn	0.08	MnO ₂	0.13	3.25
Na	33.7	} NaCl Na ₂ O	83.0	--
			6.7	13.88
Ni	0.03	NiO	0.04	0.76
Pb	0.04	PbO	0.05	--
Si	0.66	SiO ₂	1.4	44.47
Te	0.56	TeO ₂	0.71	0.006
Zn	0.02	ZnO	0.02	--
Cl	55.0	--	--	0.4
TOTAL			98.8	

radiologically important semivolatiles when acidified melter waste was employed. The reducing power of the formic acid feed component apparently promotes volatilization in the plenum and thereby produces greater effective off-gas losses of these elements.

Ruthenium is an exception to the above statement. Ever since melter experiments with a formate feed formulation began, no significant airborne ruthenium has been detected in melter exhaust streams, except for the very atypical LFCM-7 test. Feed and glass sample analyses, on the other hand, indicate significant ruthenium melter losses (DF = 2), and yet no specific sink has been conclusively identified to account for these losses. In all probability, ruthenium is being reduced by the formic acid to its elemental state, whereupon it is lost to the melter floor as slag. A surface plate-out mechanism is a possible, but less likely, explanation for these losses; however, no evidence of off-gas line plating has ever been found. A thorough examination of the melter and its plenum is planned to establish the nature of the observed ruthenium losses.

The effect of feed-boosting techniques upon overall melter emission performance has been studied under controlled conditions. If

Table XII. Steady state aerosol emission performance

PSCM-5 Boosted Test				PSCM-6 Boosted/Unboosted Test			
Sample Type*	Feed Rate, L/h	Particulate		Sample Type*	Feed Rate, L/h	Particulate	
		Loading, mg/L	DF			Loading, mg/L	DF
C	51	0.55	470	S	68	0.29	820
S	72	0.49	460	HEPA	68	--	810
S	79	0.44	510	C	67	0.37	840
C	81	0.61	440	S	74	0.25	910
HEPA	81	--	370	C	90	0.41	700
S	86	0.48	492	S	91	0.28	840
C	93	0.78	440	HEPA	90	--	720
HEPA	93	--	670	S	58**	0.32	870
ALL			480	C	58**	0.54	660
				ALL			800

* C = cyclone; S = differential samples; HEPA = absolute filtration.
 ** Unboosted operation.

the previous melter stability comments are neglected, Table XI strongly suggests that melter DFs are dramatically reduced when boosting is employed. However, tests designed to illustrate this effect have failed to show any significant relationships between feeding rates and melter emission performance. Table XII presents gross aerosol DF values associated with the boosted PSCM-5 and PSCM-6 tests. Clearly, this data shows no correlation between feeding rates and DF. Moreover, the boosted PSCM-6 experiment did not utilize electric radiant lid heaters for the entire melter test, yet no significant differences in melter emission performance were observed throughout the experiment. Consequently, this data suggests that electric radiant plenum heaters can be employed to boost liquid feeding rates of ceramic melters without significantly deteriorating melter emission performance.

The implementation of feed-boosting techniques, however, are not without operational difficulties. The high exhaust stream temperatures ($>600^{\circ}\text{C}$) resulting from the auxiliary plenum heaters present various off-gas problems associated with the formation of fused off-gas-line deposits and accelerated material corrosion rates. A cooling spray (see Figure 1) has been successfully used to control exiting melter exhaust gas temperatures to 400°C or less. However, the spray nozzle itself acts to collect entrained feed. These feed deposits ultimately grow to form a local obstruction to melter off-gas flow. Although these deposits are soft and easily removed, the current cooling spray configuration clearly compromises melter off-gas system design.

IV. Melter Idling Test

Because of the high ($\sim 1000^{\circ}\text{C}$) plenum temperatures associated with idling (unfed) joule-heated ceramic melters, volatilization losses of radiologically important glass components sustained during these periods could overwhelmingly influence the overall melter source term. The composition of typical melter idling emission deposits, which appears in Table XIII, verifies the importance of this loss mechanism for the semivolatiles. In order to determine the overall importance of this melter loss mechanism, emission rates of semivolatile elements were investigated as a function of plenum temperature and, consequently, melter surface glass viscosity. Temperature control was maintained through use of plenum water sprays, which cooled but did not disturb the surface of the melter glass pool.

This study was immediately initiated upon completion of a 120-h liquid-fed melter test (PSCM-5). With a 42 L/h water spraying rate and the melter under automatic resistance control, the melter glass surface was cooled to the point that it formed a continuous nonconvective layer above the bulk melter glass pool (plenum 280°C). At a 27 L/h spray rate, the surface viscosity decreased significantly. Convective mixing opened vents in the glass surface that migrated at random across the melter glass pool. However, plenum temperatures were not high enough to melt feed deposits formed upon the melter walls and lid during the preceding PSCM-5 experiment. Finally, the cooling spray was terminated and the melter was allowed to idle at a fixed current rate, which slowly brought the melter plenum up to 850°C . Samples were collected from the plenum during all phases of this study.

17th DOE NUCLEAR AIR CLEANING CONFERENCE

Table XIII. Melter idling deposit

Elements As Oxides	Weight Percent		
	Gray Deposits	White Deposits	Glass
Al ₂ O ₃	1.2	0.11	3.7
B ₂ O ₃	14.2	1.6	10.0
CaO	0.22	0.46	1.2
CdO	0.02	0.02	0.009
Cr ₂ O ₃	0.57	0.58	0.02
Cs ₂ O	3.7	8.3	0.05
Fe ₂ O ₃	0.10	0.17	14.8
K ₂ O	0.79	0.85	*
Li ₂ O	1.92	2.6	4.4
MgO	<0.05	<0.05	1.4
MnO ₂	0.05	0.05	3.9
Na ₂ O	31.0	31.0	15.7
NiO	0.25	<0.02	1.2
RuO ₂	0.82	2.1	0.01
Sb ₂ O ₃	<0.01	<0.01	0.02
SiO ₂	<0.02	0.47	45.1
SrO	<0.005	<0.005	0.02
TeO ₂	0.70	0.70	0.002
TiO	<0.01	<0.01	0.8
ZnO	0.02	0.02	0.008

* Used in sample preparation.

The results obtained from these plenum samples are graphically summarized in Figure 8, which characterizes the emission rates of the semivolatile elements under various idling conditions (temperature) employed during this test. These data indicate that emission rates of all semivolatile elements decreased as a function of time after the completion of PSCM-5 under the influence of a 42 L/h water-spraying rate. Reducing the cooling spray rate to 27 L/h caused measurable increases in both plenum temperature and semivolatile emission rates; however, an equilibrated plenum temperature was not achieved during the brief period (24 h) of reduced spraying.

Termination of the water-cooling spray caused the plenum temperature to increase steadily to the point where plenum surface deposits formed during PSCM-5 began to melt and "burn" away. This period was responsible for the dramatic peaking of emission rates of the semivolatile elements. The fact that all semivolatiles do not form maxima at the same point in time is most probably due to temperature,

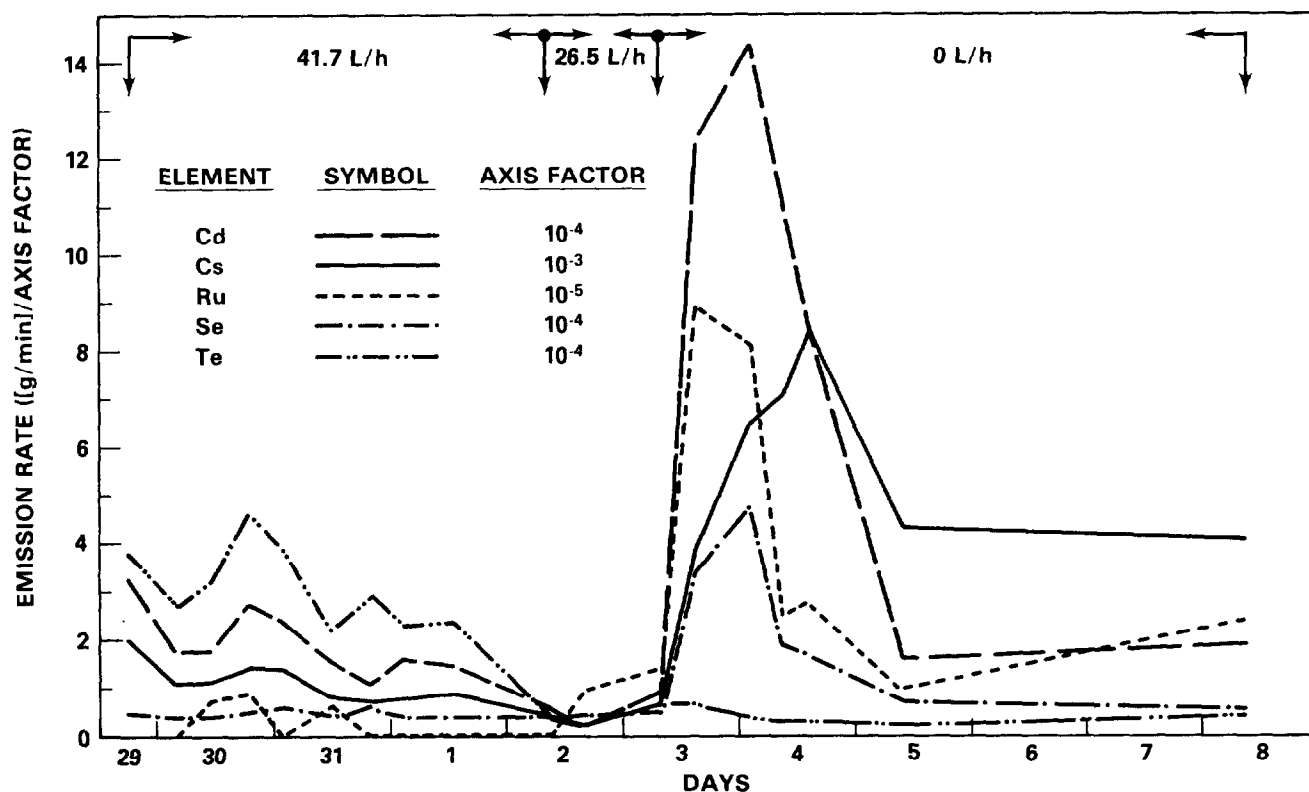


Figure 8. Melter idling emission rates of semivolatile elements.

which was steadily increasing throughout the interval over which these maxima occurred.

The plenum temperature during the last two sampling periods was $\sim 850^{\circ}\text{C}$, and all plenum surfaces appeared clean. The emission rates occurring during these periods are, with the exception of Se and Te, significantly greater than the minimum emission rates exhibited by these elements during full 42 L/h spray cooling. However, these elevated idling emission rates are still significantly below those rates observed during moderate liquid feeding conditions. Specifically, the Cs emission rate expected from the PSCM for a liquid feeding rate of 50 L/h (1.1 kg/min) would be of the order of 10 mg/min. This is more than twice the value observed during the hot melter idling conditions. Consequently, it appears that the plenum cooling approach, although capable of reducing emission rates of most semi-volatiles (by a factor of ~ 10 for Cs), is of little practical value in reducing the overall melter off-gas radiological burden.

It should be noted that the effect of directly feeding water onto the surface of an idling melter has also been investigated as an alternative method for reducing idling emissions. On a qualitative as well as a quantitative basis, this approach was a less satisfactory means of cooling the plenum and melter glass surface than was the plenum spray approach. The water feeding technique produced a high degree of entrainment and aerosol carryover into the off-gas system. Moreover, at the water feeding rates used (45 L/h), convective mixing was actually exacerbated, although total melter surface

17th DOE NUCLEAR AIR CLEANING CONFERENCE

flooding was never attempted. On the other hand, the water plenum spray initiated no observed entrainment and minimized or eliminated convective surface mixing.

V. Melter Flow Rates

The off-gas flow rate behavior of the two liquid-fed melters has been examined over the past year as part of the SRL-DWPF melter development program. During this period of study, two separate feed formulations have been used and a variety of melter operational running conditions have been employed. The results of these studies have shown that both feed composition and melter feeding rates have a preponderant influence upon the stability of melter off-gas flow rate.

The effect of feed composition upon melter flow rate behavior is related to the physical ability of the feed components to form a structurally sound insulating layer (cold cap) between the incoming liquid feed and the hot glass surface. As portions of the insulating cold cap become calcined, structural collapse occurs, bringing dammed up liquid feed into contact with the extremely hot glass surface. This results in the flashing off of the water component (and volatile reaction products) of the feed, producing a flow pulse or an off-gas surge. The magnitude and extent of these surges are naturally dependent upon the amount of liquid feed present on the cold cap that is delivered to the hot glass surface. Consequently, an erratic melter exhaust flow rate is often indicative of an unstable, overfed operational condition. Exhaust flow rate patterns associated with stable and unstable melter operating conditions are illustrated in Figure 9.

The two melter feed formulations used in these studies exhibited significantly different melter off-gas properties. The alkaline waste formulation produced a noisy, erratic melter flow rate with surges as high as seven times that of the average flow. The acid feed, on the other hand, possessed a very compliant, nonbridging cold cap, which reduced the frequency and magnitude of off-gas surging events. Average melter flow characteristics associated with each of these feed formulations are summarized in Table XIV. These data clearly show the stabilizing influence of the formic acid feed component upon melter flow rate behavior.

Due to the conservative, stable manner in which most PSCM runs were conducted, PSCM flow rate data associated with acidified feed are probably more representative of average melter behavior than are the values associated with the LFCM. The LFCM data, on the other hand, can be used in assessing the effects of heavy melter feeding conditions.

VI. Corrosion

Extensive metal corrosion has been observed in liquid-fed melter plenums and in associated melter off-gas lines and processing equipment. The nature of the corrosion observed suggests acidic chemical attack by volatile halogens and sulfur compounds. In order to identify suitably corrosive-resistant melter off-gas materials, corrosion coupons representing different groups of alloys were exposed to the plenum environment of liquid-fed melters during processing (300°C to

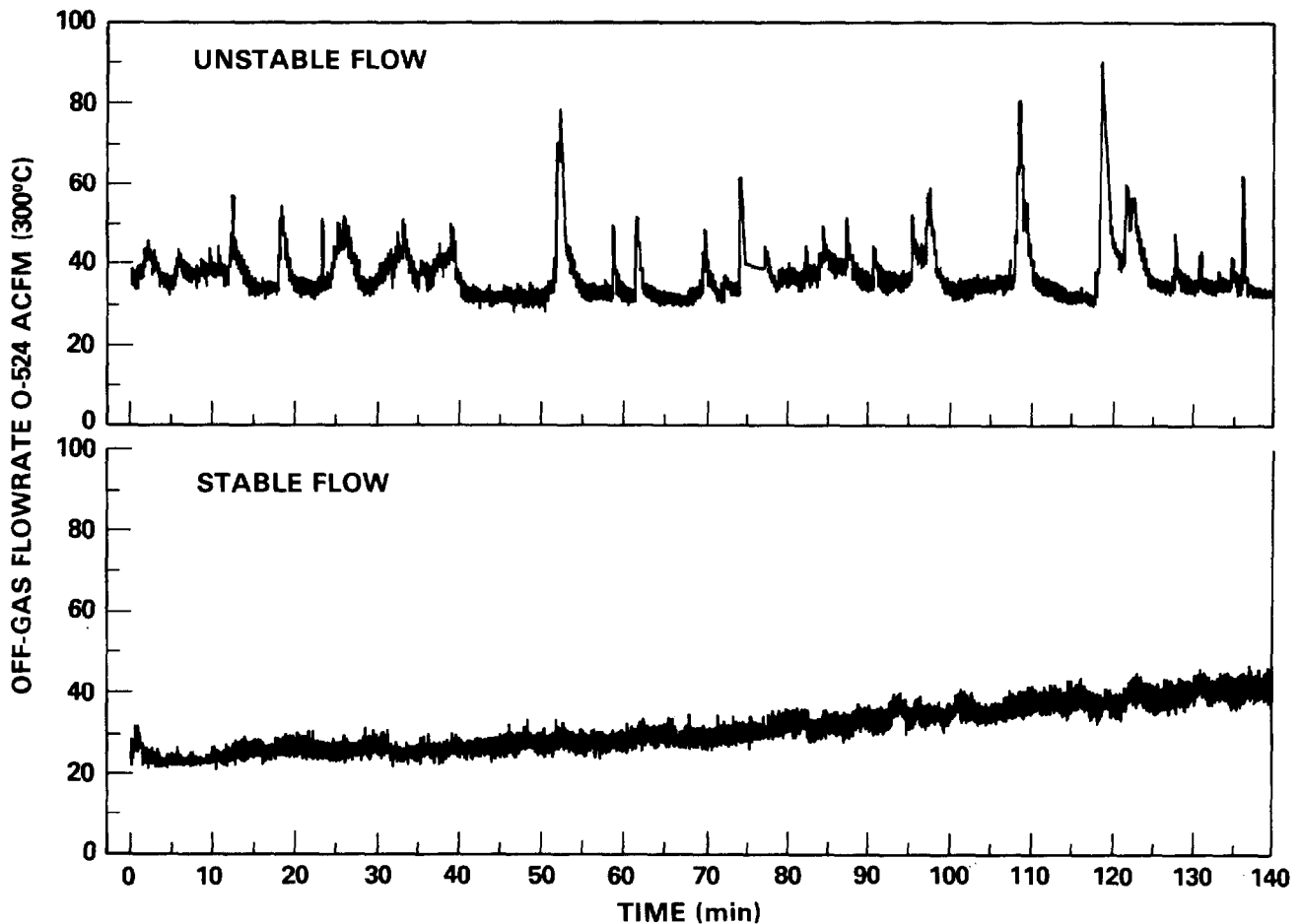


Figure 9. Typical off-gas flow rate behavioral patterns associated with liquid-fed melters.

Table XIV. Liquid-fed melter flow rate behavior.

<u>Experiment</u>	<u>Feed</u>	<u>Average, Flow, scfm</u>	<u>Maximum Surge, scfm</u>	<u>Average Surge Duration, min</u>
LFCM-4	Alkaline	90	620	3
LFCM-6	Alkaline	90	470	3
PSCM-3	Acid	70	220	3
LFCM-7	Acid	240	710	3
PSCM-4	Acid	70	300	4
PSCM-5	Acid	80	230	3
PSCM-6	Acid	80	190	3

500°C) and idling (850°C) conditions. The extent of corrosion as a function of operating conditions was established gravimetrically through coupon weight loss. The results of these studies, which are summarized in Table XV, indicate that the corrosion rates occurring during actual liquid feeding are much greater than those occurring during hot idling, although temperature cycling between feeding and idling conditions has been found to accelerate overall corrosion rates. In addition, titanium, tantalum and all alloys having high iron concentrations were found to be quite unsuitable for liquid-fed

Table XV. Corrosion sample results.

Material	Exposure, h		Weight Change g/cm ²	Cor. Rate, cm/y	Spalling	Observations		Cr	Approximate Composition, Wt%				
	Idling	Operating				Deposits*	Color**		Co	Fe	Ni	Mo	W
Inconel®-690	1134	214	-0.025	0.020	Light	Light	Blk-Silver	30	--	9.5	60	--	--
	198	214	-0.014	0.074	Light	None	Black						
	1256	214	-0.036	0.023	Light	Light	Multi						
	320	330	-0.011	0.015	Light	Light	Black						
Inconel®-625	1134	214	+0.015		None	Heavy	Brown	21.5	--	2.5	61	9	--
	198	214	+0.007		None	Heavy	Brn-Silver						
	1256	330	+0.013		None	Heavy	Brn-Black						
	320	330	+0.012		None	Heavy	Brn-Silver						
Inconel®-617	122	116	-0.004	0.008	Med-Pits	Medium	Gr-Silver	22	12.5	1.5	52	9	--
	122	116	-0.013	0.024	Med-Pits	Medium	Gr-Silver						
Inconel®-600	122	116	-0.008	-0.015	Medium	Light	Multi	15.5	--	8	76	--	--
	122	116	-0.002	0.004	Medium	Light	Multi						
Haynes®-188	1134	214	+0.059		Light	Very Light	Bl-Black	22	40	<3	10	--	15
	198	214	+0.004			Light	Bl-Black						
Haynes®-25	1134	214	+0.005	0.008	Light	Light	Bl-Black	21	54	<3	10	--	15
	198	214	+0.003	0.008	Light	Light	Bl-Black						
	60	110	+0.001		None	None	Black						
RA®-330	1134	214	-0.025	0.020	Medium	None	Multi	18	--	47	35	--	--
	198	214	-0.036	0.185	Medium	None	Gr Spots						
RA®-446	1134	214	-0.18	0.145	Heavy	None	Multi	25	--	75	--	--	--
	198	214	-0.17	0.472	Heavy	None	Multi						
Titanium	122	116	-0.063	0.210	Heavy	None	Silver-Brn	--	--	--	--	--	--
Tantalum	122	116	-3.3	>3	Disappeared								

* Feed material sintered on coupon surface.

** Bl - Blue
Blk - Black
Brn - Brown
Gr - Green

®Inconel is a registered trademark of Huntington Alloys, Huntington, West Virginia
®Haynes is a registered trademark of the Cabot Corporation, Kokomo, Indiana.
®RA is a registered trademark of Rolled Alloys, Detroit, Michigan.

17th DOE NUCLEAR AIR CLEANING CONFERENCE

melter service. The most promising alloys are those possessing low iron, high nickel or cobalt and a chromium content greater than 20%. Inconel®-625 and the Haynes® alloys were the most corrosive-resistant materials employed during this study.

VII. Conclusions

The off-gas studies discussed in this report have sought to establish the effluent characteristics of liquid-fed joule-heated ceramic melters. The results of these studies have shown particulate emission to be responsible for most melter effluent losses. Moreover, a large fraction of the total particulate mass evolved from an operating melter is conveyed to the off-gas system by submicron aerosols which are almost exclusively responsible for semivolatile transport. Melter operational conditions have had little effect upon these results as long as quasi steady-state conditions are maintained. Even hot melter idling conditions do not significantly affect the overall melter source term.

Melter-generated gases have been found to be potentially flammable as well as corrosive. Hydrogen generation presents the greatest flammability hazard of the combustibles generated by liquid-fed melters. Off-gas dilution was required during a melter test to maintain the H₂ concentration below 70% of its lower flammability limit in the quench melter exhaust. The combustible gas CO has never achieved a quenched off-gas concentration greater than 1/10 of its flammability limit. Auxiliary plenum heating has been found to significantly reduce melter emission rates of both these combustible gases.

Significant concentrations of acidic volatile compounds of sulfur and the halogens exist in unquenched melter off-gas streams independent of melter operational conditions. These gases have been responsible for extensive corrosion observed in melter plenums and in associated off-gas lines and processing equipment. Alloys possessing low iron, high nickel or cobalt and high chromium content have been found to be most suitable for liquid-fed melter service.

VIII. References

- (1) Buelt, J. L. and C. C. Chapman. Liquid-Fed Ceramic Melter, A General Description Report. PNL-2735, Pacific Northwest Laboratory, Richland, Washington (1978).
- (2) Bonner, W. F. The High-Level Waste Immobilization Program: An Overview. PNL-3094, Pacific Northwest Laboratory, Richland, Washington (1979).
- (3) Conroy, A. R., W. H. Manning and W. C. Bauer. "The Role of Sulfate in the Melting and Fining of Glass Batch." Glass Ind. 47(2):pp 84-89, February-March (1966).

IMMOBILIZATION OF KRYPTON-85 IN ZEOLITE 5A*

A. B. Christensen, J. A. Del Debbio, D. A. Knecht,
J. E. Tanner and S. C. Cossel

Exxon Nuclear Idaho Company
P. O. Box 2800
Idaho Falls, ID 83401

Abstract

This paper describes the technical feasibility and presents a summary of a preconceptual design and cost estimate for a process to immobilize krypton-85 by sintering in zeolite 5A at 700°C and 100 MPa (1000 atm) for 2-4 h. Krypton loading of 30-60 m³ at STP per m³ solid can be achieved. The initial water concentration in zeolite 5A has a catalytic effect on the sintering rate and must be kept at approximately 1 wt% by heating prior to the encapsulation run. High initial water loadings and/or encapsulation times longer than 4 h must be avoided because the sintered zeolite 5A recrystallizes to an anorthite-type feldspar and releases the trapped krypton. Data are presented to show how the process conditions affect krypton encapsulation in zeolite 5A and how to assure the quality of the product. Krypton leakage experiments are used to predict leakage rates of less than 0.03% and 0.3% for 10-year storage at 300° and 400°C, respectively. By adding a powdered glass frit to the commercial zeolite 5A 2 mm beads, a solid mass is formed during encapsulation, which can be further compacted using standard hot isotatic pressing techniques at 33 MPa and 600°C to form a fused glassy matrix enclosing the amorphous zeolite.

A process for encapsulating the annual krypton-85 production at a commercial 2000 metric ton of heavy metal (MTHM) spent fuel reprocessing plant is developed. A hot isostatic press (HIP) with an isolated work zone of 8 or 16 L capacity is required to operate for 600 or 300 cycles per year, respectively. Existing HIP technology uses work zones from 1 to 3500 L capacity at similar production rates. A combined encapsulation/compaction cycle is proposed as an option to most effectively immobilize the krypton and the zeolite. A preconceptual design and cost estimate is given for a commercial-scale Kr encapsulation facility. The facility is designed to withstand a worst case rupture of the HIP. The maximum krypton-85 release is estimated to result in an off-site dose well below accident protective action guidance levels. Major licensing concerns appear to be in compliance with applicable codes for HIP fabrication and with developments associated in scaling up demonstration encapsulation plants.

*Work performed under DOE Contract DE-AC07-79ID01675

I. Introduction

U.S. regulation 40 CFR 190 limits krypton-85 releases to 50,000 Ci per gigawatt-year of commercial electric power production for fuel placed into a reactor after January 1, 1983.¹ For light water nuclear reactors, the release limits would correspond to about 15% of the krypton-85 inventory in the spent fuel. If krypton-85 is recovered, storage methods would be required to meet the overall release limits in the regulation.² While storage in pressurized cylinders is technically feasible, there may be large costs associated with long-term storage.³ By trapping krypton in a solid on an atomic or microbubble scale, a less expensive disposal facility, such as shallow dry wells,⁴ could be used, with potentially low release rates. Ion implantation sputtering^{5,6} and zeolite/glass encapsulation⁷⁻¹¹ are two candidate immobilization processes currently under development. Both have krypton storage volumes comparable to that in pressurized cylinders, low krypton release rates at 300 to 400°C, and mechanically strong structures.

The high temperature/high pressure encapsulation process uses existing technology found in the hot isostatic pressing (HIP) industry, where molds containing metal or ceramic powders are compacted and sintered under high pressure of argon to fabricate items such as tungsten carbide bits, superalloy aircraft components, ferrite ceramics for computer memory and turbine components.^{12,13} Typical commercial-scale HIP work-zone volumes range from 1 to 3500 L.

This paper summarizes recent technical and economic developments in the process to encapsulate krypton in zeolite 5A. The technical feasibility for the encapsulation process and of further immobilizing the granular zeolite 5A material in a compacted glass matrix is demonstrated.

The design and cost estimate of a facility to encapsulate the krypton-85 produced at a 2000 metric ton of heavy metal (MTHM) commercial fuel reprocessing plant is presented, including considerations necessary for obtaining a license to operate the facility. The full-scale process design is based on existing commercial hot isostatic pressing technology, using HIP work zone volumes of 8-16 L.

II. Technical Feasibility

Krypton trapping by sintering at 550°C in zeolite 5A was reported by Penzhorn⁷, and the results were confirmed at the INEL at 700°C.^{8,9} Typical gas loading of 46 cc at STP per gram of solid were obtained in zeolite A samples at various pressures, temperatures, and time ranging from 550-700°C, 1000-2000 atm, and 1-6 hours. A schematic for the process to encapsulate krypton by sintering in zeolite 5A is shown in Figure 1.

Figure 2 shows a structural representation¹⁴ of zeolite A and the relative size of a krypton atom. The room temperature gas kinetic diameter of a krypton atom is 0.35 nm; the zeolite A cage opening and internal diameter is 0.5 nm and 1.1 nm, respectively, for calcium-exchanged zeolite A (zeolite 5A).¹⁴

Krypton trapping will occur by sintering in zeolite 5A. The mechanism in zeolite 5A may involve hydrothermal decomposition to form an amorphous structure, which is catalyzed by residual water.^{14,15,16} Recrystallization from the amorphous phase to an anorthite type feldspar occurs at high temperatures. The rate of recrystallization is directly dependent on initial water loadings. Hoss and Roy found that calcium-exchanged zeolite A transforms to a silicate whose X-ray pattern resembled that of anorthite after being exposed to 1000 atm H₂O vapor at 270°C for 10 days.¹⁶

Experimental

Zeolite 5A was obtained from W.R. Grace Co. in 2 mm spheres and is produced by a 67% exchange of calcium for sodium in zeolite 4A. Zeolite 5A spheres are activated for a minimum of 24 hours in the atmosphere at 460°C (1k Pa water vapor pressure) to remove the adsorbed water so that the equilibrium water loading of 0.8 wt% is achieved. Following drying, the sample is quickly transferred into a glovebox with water vapor partial pressure of 10 Pa, where it is weighed, loaded into sample holders, and sealed inside the autoclave.

The experimental system for krypton encapsulation has been described elsewhere¹⁷. The pressure vessel used for encapsulation studies is a 25 mL Leco pressure capsule, surrounded by a cooling jacket and two independently controlled heaters. Heating and cooling times were 2 and 1 hour, respectively. The encapsulation temperatures were calibrated at the sodium iodide melting point of 651°C.¹¹

Experiments were also carried out using a hot isostatic press (HIP) with a 1.0-litre work-zone volume. Argon was used in place of krypton to minimize costs and because Ar behaves similarly to Kr. The system is shown in Figure 3. The cooled pressure bearing walls of the HIP contain a furnace in the high pressure zone and a heat shield to keep wall temperatures below 200°C. Figure 4 shows the furnace, thermocouples, work package, and heat shield. Heating and cooling times were thirty minutes for the HIP.

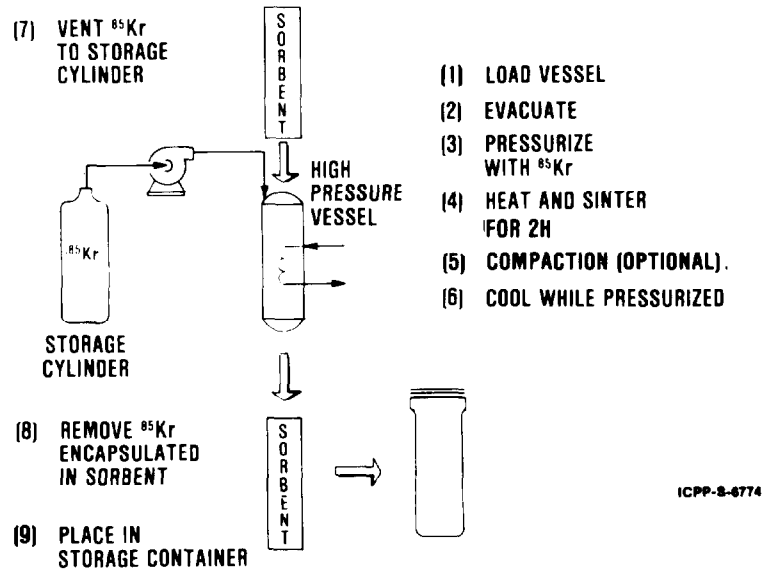


Figure 1. Schematic of the Process Used to Encapsulate Krypton by Sintering in Zeolite 5A.

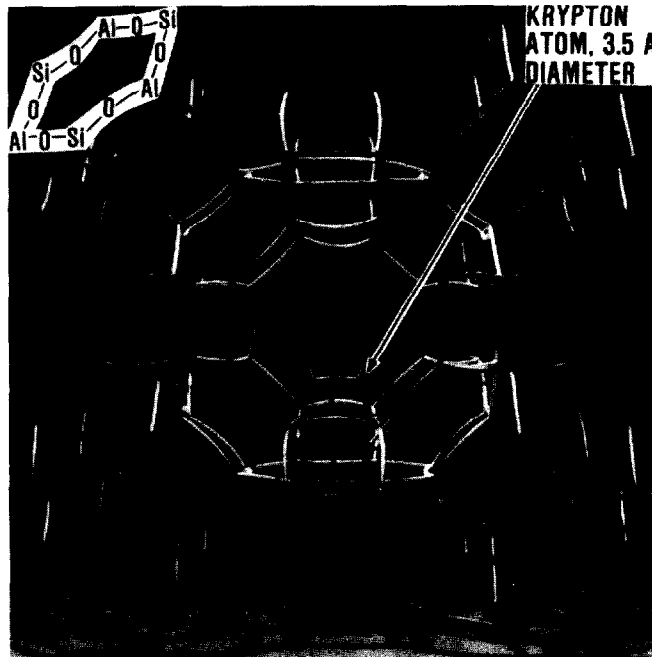
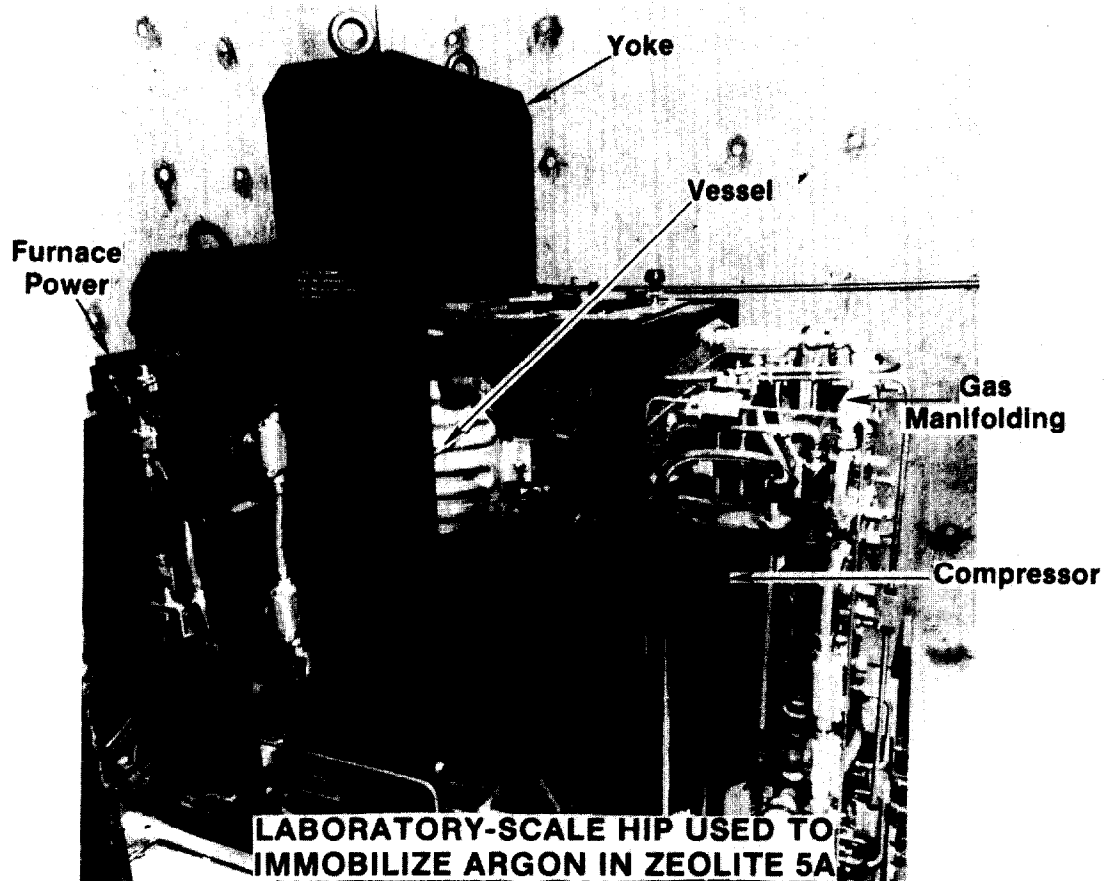


Figure 2. Structural Model of Zeolite 5A Containing a Krypton Atom Encapsulated in the Middle Alpha Cage (0.5 nm Opening).



Routine analysis of sintered zeolite 5A samples after encapsulation use mass spectrometry to determine gas loading, x-ray powder diffraction to determine zeolite 5A structure, and thermogravimetric analysis (TGA) to determine gross gas leakage. Krypton and argon leakage rates were measured by gas chromatography and mass spectrometry at 150 to 800°C.^{11,17}

Results of Encapsulation Tests

Approximately 46 and 70 cm³/g STP of krypton or argon are encapsulated in zeolite 5A at 1000 and 2000 atm, respectively, at the sintering conditions of 650-700°C, 1-6 h, and 0.7 wt% residual water content in zeolite 5A. The effect of initial water loading on product form is shown in Figure 5. Amorphous product containing large amounts of encapsulated krypton was typically formed at 700°C, 102 MPa (1020 atm), and 2-4 h with Grace-Davison zeolite 5A containing 0.8 wt% water in this work, while a similar product was formed by Penzhorn at 520°C 100 MPa, and 2 to 4 h with Bayer zeolite 5A containing 3 wt% water.^{7,11}

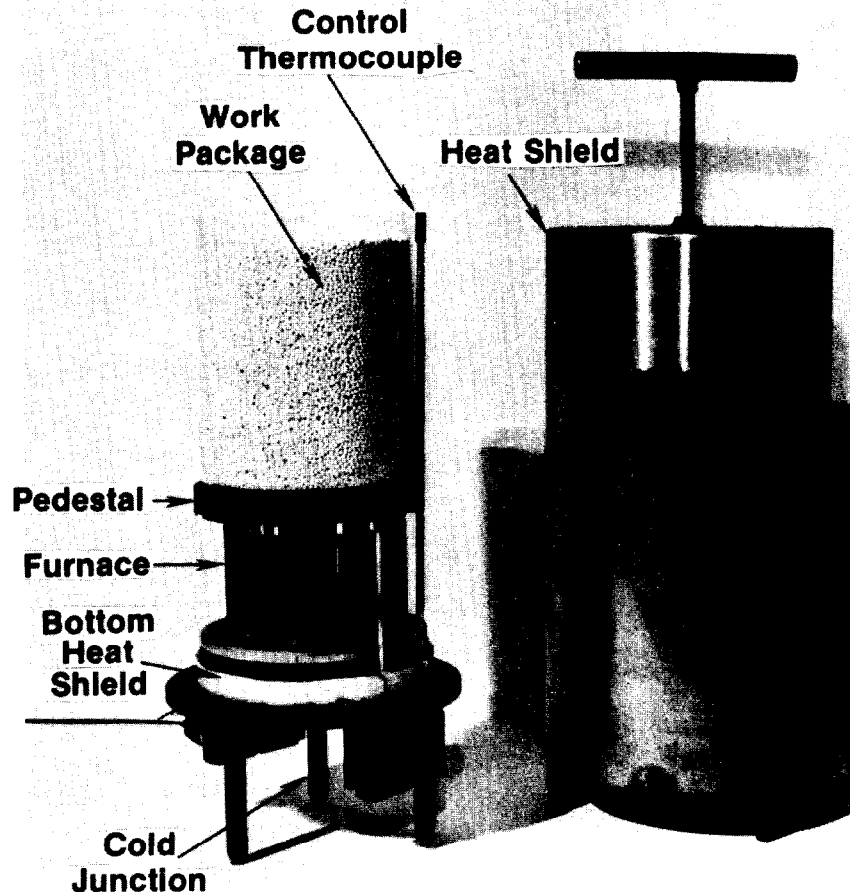


Figure 4. Interior Components of the Laboratory-Scale HIP.

Thermogravimetric analysis (TGA) measures weight changes to within 1% of the total sample weight. Kr loaded in crystalline zeolite 5A quickly leaks out upon heating. As the zeolite becomes amorphous to x-rays, the rate of leakage decreases until no leakage is seen for samples heated to 750°C.

Figure 6 shows x-ray powder diffraction scans for zeolite 5A, amorphous product, recrystallized product, and an anorthite reference material. Based on the encapsulation experiments, the crystalline zeolite 5A appears to pass through the amorphous state, which traps krypton, before it recrystallizes to an anorthite material, which does not trap krypton.

Infrared scans of unsintered and sintered zeolite 5A show a large broadening of the asymmetric stretching and bending vibrations as a result of sintering.¹¹ This broadening and the almost complete loss of the vibrations assigned to double ring structures indicate that the zeolite structure has been eliminated.

Differential thermal analysis (DTA) of untreated zeolite 5A show that the crystalline to amorphous (exothermic) transition occurs at a higher temperature (825°C) than during encapsulation (650-700°C), probably due to lower water concentration in the

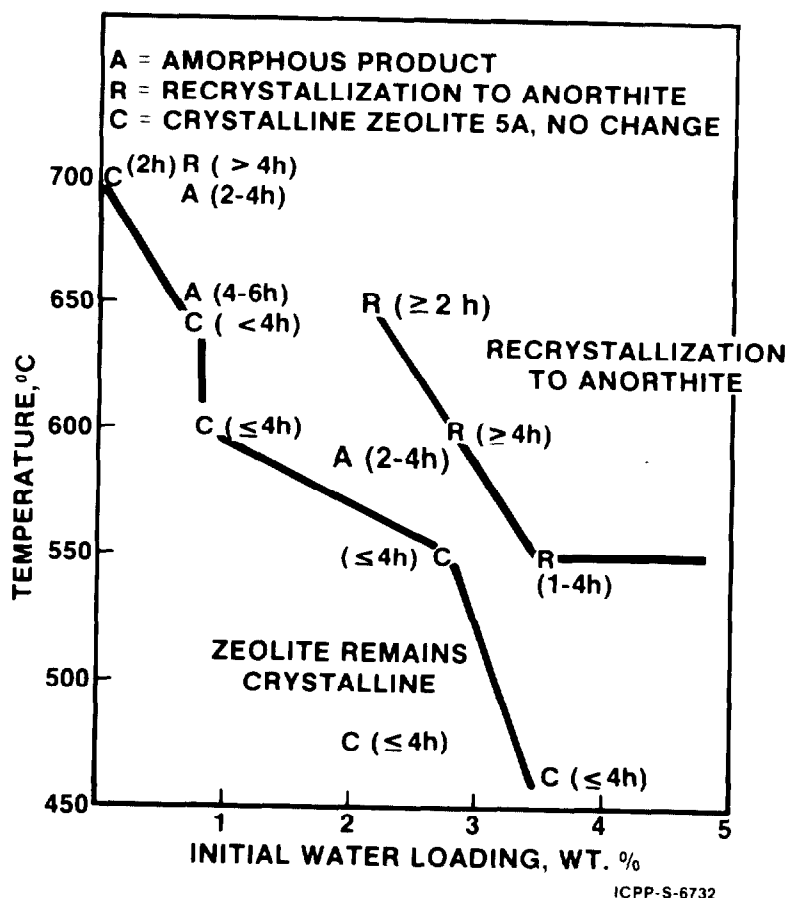


Figure 5. Effect of Encapsulation Temperature, Time, and Initial Water Loading on the Product Formed from Grace-Davison Zeolite 5A.

DTA analysis. The amorphous transition is not observed in sintered zeolite 5A, indicating that the sintered material is already amorphous. A small endotherm is observed due to the krypton release in the sintered sample. Both untreated and sintered zeolites show an exothermic transition due to recrystallization at 800°C for untreated and 1000°C for sintered samples.

Gas pressure does not seem to affect the sintering rate of zeolite 5A; however, it strongly affects gas loading. The Kr loading increases nonlinearly with gas pressure, but almost linearly with gas density, indicating that the sorbed gas is at the same density in the zeolite structure as in the gas surrounding it.

The effect of gas composition on Kr loading in zeolite 5A was studied using gas mixtures composed of N₂, O₂, Ar, Kr, and Xe, with Kr content of 54 or 68%. The encapsulation runs were made using zeolite 5A containing 0.8 wt% H₂O and sintered at 700°C and 100 MPa (1000 atm). Compared to the partial pressures during encapsulation, the component gases are loaded at slightly larger

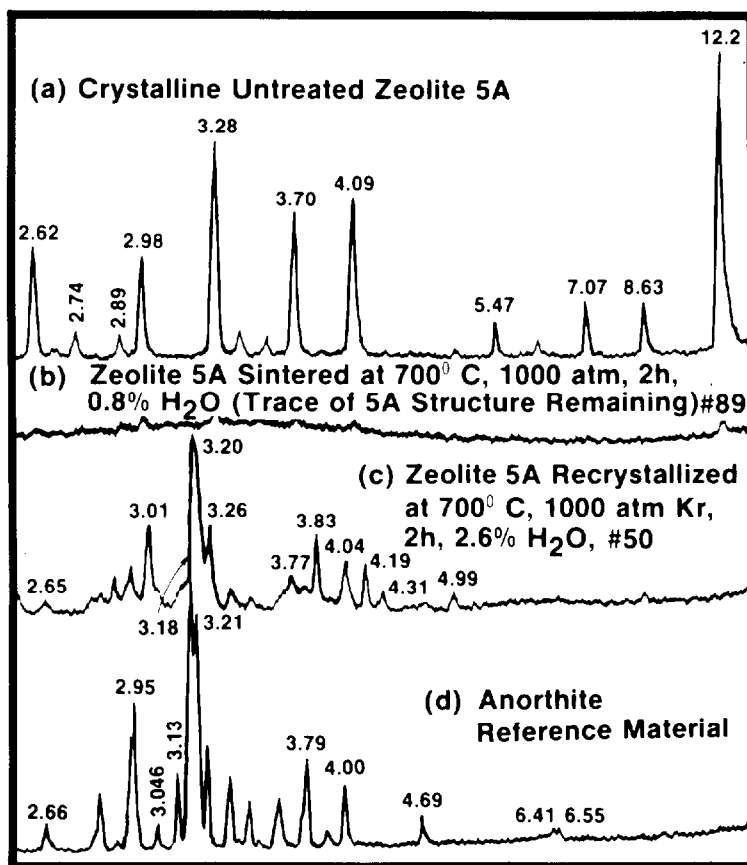


Figure 6. X-Ray Analysis of (a) Crystalline Zeolite 5A, (b) Sintered Product, (c) Recrystallized Product, and (d) an Anorthite Standard.

amounts for larger atoms (Kr and Xe) and at slightly smaller amounts for smaller atoms (Ar, O₂, and N₂). The Kr loading per atmosphere of Kr gas partial pressure (0.05 cm³STP/g/atm) in the gas mixture is the same as for pure Kr gas, and total leakage using TGA analysis is as low as from runs using pure Kr as the encapsulated gas.

The structural transformations occurring in zeolite 5A during the encapsulation process are depicted in the electron micrographs and electron diffraction patterns shown in Figure 7. Based on lower resolution micrographs not shown, atoms are not pulled apart sufficiently during sintering to cause a complete breakdown of the larger structure of the crystal. The high resolution transmission electron microscope (TEM) image shown in Figure 7a is a two-dimensional structural image of zeolite 5A for the (001) orientation which is parallel to the sides of the unit cell. The white dots represent channels 1.1 nm in diameter formed by the alpha cages (see the zeolite 5A model in Figure 2). This picture is similar to one obtained by L. A. Bursill of zeolite 3A.¹⁸ Amorphous areas where the crystal lattice has collapsed due to the energy of the electron beam (200 kV) can be seen as dark patches. Figure 7b and c shows the difference between partial and complete sintering. A sharp interface between the amorphous (glassy) and crystalline areas can be seen in 7b, whereas complete loss of crystallinity is evident

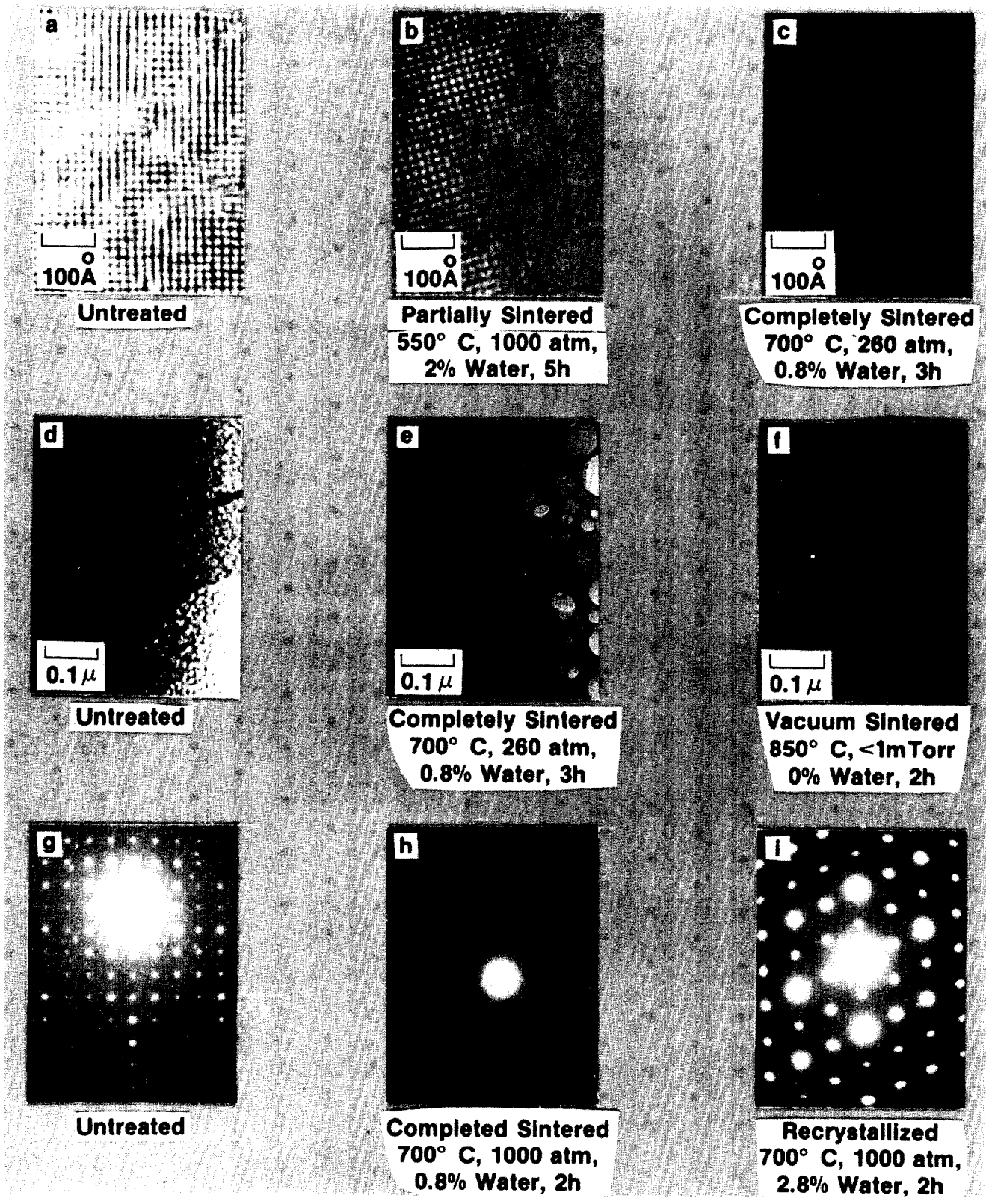


Figure 7. Electron Micrographs and Electron Diffraction Patterns of Zeolite 5A.

in 7c. Krypton leakage on the TGA for the partially sintered zeolite was 21% Kr lost below 825°C, as compared with less than 1% for the completely sintered material. Lower magnification images of untreated and sintered zeolite are shown in Figure 7d through f. Numerous irregularly shaped bright areas can be seen in 7d. These represent amorphous material caused by electron beam damage. The zeolite sintered at 700°C under krypton pressure shown in 7e contains bubbles from 5 to 100 nm in diameter while the vacuum sintered sample (7f) has none. These bubbles probably contain krypton gas under the run pressure of 26 MPa (260 atm). Electron micrographs of zeolite sintered at low pressure (20 atm) and 3.5 wt% water also showed bubbles, indicating that pressure has no effect on the structure of the sintered zeolite.

The appearance of the recrystallization product anorthite type feldspar, which results from too much water (2.8 wt%) being present at 700°C, is seen in other micrographs not shown here.¹¹ The large grains are observed with no bubbles and no uniform contrast, suggesting a sponge-like porous structure, which accounts for krypton leakage. The halo electron diffraction pattern in Figure 7h indicates an amorphous structure, while the pattern in Figure 7g and i indicates crystallinity.

Preliminary compaction tests of zeolite 5A have been carried out, before and after encapsulation with argon or krypton. Figure 8 shows samples of zeolite 5A compacted after encapsulation. In pellets which were formed before encapsulation, the krypton loadings varied, presumably depending on the initial water content; further work is required to determine conditions for obtaining the proper initial water loading. In compaction tests after encapsulation, activated Grace-Davison zeolite 5A beads were mixed with a borosilicate glass frit powder of composition in wt%: SiO₂-57.7, B₂O₃-19.4; Na₂O-16.1; CuO-1.7; Li₂O-5.1 and encapsulated at 700°C and 100 MPa (1000 atm) for 2-4 hours. During the encapsulation the powdered glass frit fused. The mass was further compacted isostatically at 700°C, 1000 atm, and 2 h. Figure 8 shows the reactants before and products after encapsulation and compaction.

Samples of sintered zeolite 5A having krypton loadings of 30-50 STP cm³/g were stored at 460 and 600°C in ovens open to the atmosphere for eight months. X-ray analysis after storage revealed no structural changes. Amorphous samples showed no evidence of recrystallization and samples which initially had traces or significant amounts of anorthite (a recrystallization product) showed no further recrystallization. Apparently the amorphous product recrystallization rate is reduced significantly below 700°C.

Results of Leakage Measurements

Argon and krypton leakage results are reported for zeolite samples which appear by X-ray diffraction to be totally amorphous. Samples which have an amount of crystallinity detectable by X-ray diffraction show much higher initial gas leakage rates during TGA and are not suitable products. Long term immobilization of krypton-85 would require a fully amorphous product.

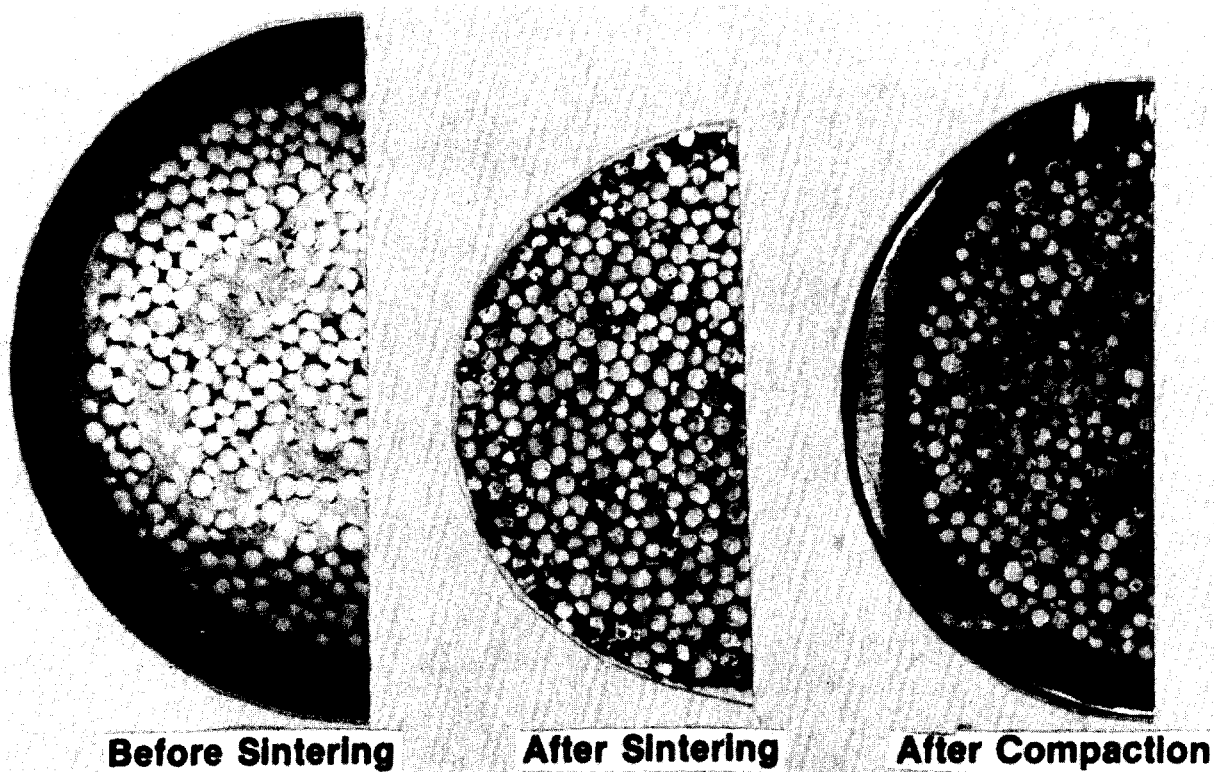


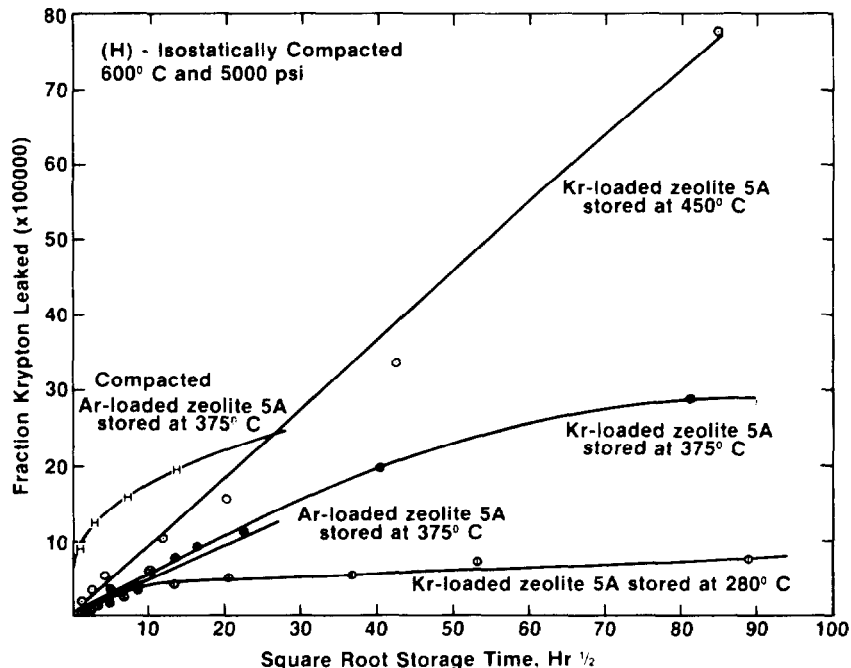
Figure 8. Zeolite 5A Samples Compacted After Encapsulation.

Initial diffusion from a homogeneous body is proportional to the square root of time, according to

$$Q_t/Q_\infty = (\alpha Dt)^{\frac{1}{2}}$$

The fractional leakage of krypton encapsulated in zeolite 5A is shown as a function of the square root of time in Figure 9 at 280, 375, and 450°C for samples which were heated to 600-700°C under vacuum for 1-4 h. The heat treatment apparently removes loosely held krypton from the solid surface, cracks or unsintered portions, resulting in initial constant slopes in Figure 9 when cumulative release is plotted as a function of square root of time. In samples which are not heat treated, the constant slopes are also apparent after a small initially rapid release of krypton. The loosely held krypton does not exceed a few tenths of a percent of the immobilized gas in a sintered sample and can be removed following encapsulation by heating the sample under vacuum for a short time. For samples which are encapsulated at 700°C and then compacted at 600°C and 33 MPa (5000 psi), the leakage rate is the same, after a slightly larger initial release of loosely held gas. The initial leakage data

in Figure 9 can be extrapolated to give leakage rates of less than 0.03% in 10 years' storage at 300°C; based on the observed curvature at later times, these predicted values are clearly overpredictions.



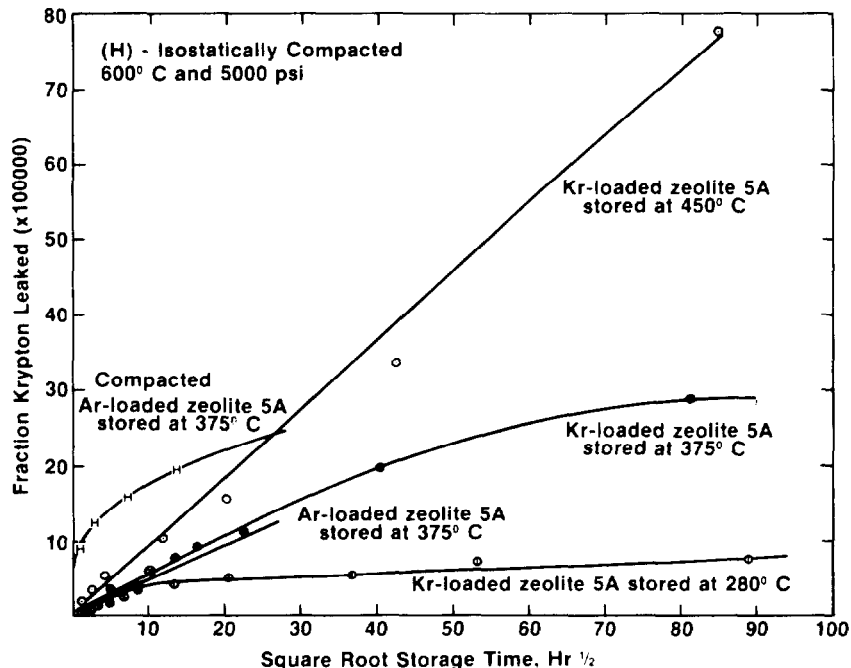
ICPP-S-8859

Figure 9. Fractional Leakage of Tightly Held Krypton from Sintered Zeolite 5A Samples (Heated to 700°C for 2-4 h).

Figure 10 shows the temperature behavior of the diffusivity. The activation energy of 197 kJ/mole was calculated from the leakage rate data, which is similar to a value of 209 kJ/mole obtained by Penzhorn.⁷ Similar results are observed in Figure 10 using sintered porous Vycor containing krypton.

Long-term leakage studies were made using sintered zeolite 5A samples immobilized with Kr, Xe, Ar, N₂ and O₂. Gas loadings were proportional to the partial pressure of the component in the gas phase. The relative leakage rates of these gases from sample stored at 370°C show that, except for an initial release of loosely held gas, the release rate of each component is linear with the square root of the storage time. A similar result was obtained at 700°C. Generally, the gases leak with rates inversely proportional to their smallest molecular dimension. The presence of other gases does not influence the leakage of Kr. The diffusivities calculated for gas mixture components are included in Figure 10.

in Figure 9 can be extrapolated to give leakage rates of less than 0.03% in 10 years' storage at 300°C; based on the observed curvature at later times, these predicted values are clearly overpredictions.

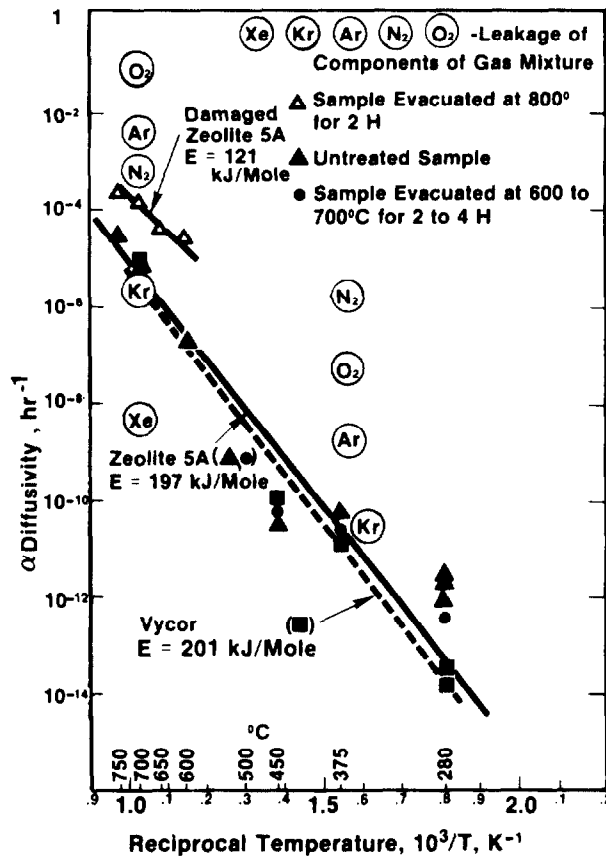


ICPP-S-8859

Figure 9. Fractional Leakage of Tightly Held Krypton from Sintered Zeolite 5A Samples (Heated to 700°C for 2-4 h).

Figure 10 shows the temperature behavior of the diffusivity. The activation energy of 197 kJ/mole was calculated from the leakage rate data, which is similar to a value of 209 kJ/mole obtained by Penzhorn.⁷ Similar results are observed in Figure 10 using sintered porous Vycor containing krypton.

Long-term leakage studies were made using sintered zeolite 5A samples immobilized with Kr, Xe, Ar, N₂ and O₂. Gas loadings were proportional to the partial pressure of the component in the gas phase. The relative leakage rates of these gases from sample stored at 370°C show that, except for an initial release of loosely held gas, the release rate of each component is linear with the square root of the storage time. A similar result was obtained at 700°C. Generally, the gases leak with rates inversely proportional to their smallest molecular dimension. The presence of other gases does not influence the leakage of Kr. The diffusivities calculated for gas mixture components are included in Figure 10.



ICPP-5-6759

Figure 10. Temperature Dependence of Diffusivity of Krypton from Sintered Zeolite 5A.

III. Preconceptual Design And Cost Estimates For A Krypton Encapsulation Facility

A preconceptual design and cost estimate of a facility to encapsulate the krypton-85 produced at a 2000 MTHM per year spent fuel processing plant was prepared under contract by the R. M. Parsons Co. The basis for a commercial-scale encapsulation facility is shown in Table I. The facility is assumed to be located with the reference commercial spent fuel reprocessing plant and noble gas cryogenic separation facility described in the DOE draft environmental impact statement on waste management.³

The flow scheme for ⁸⁵Kr encapsulation is shown in Figure 11. Zeolite is loaded into a capsule, activated and the capsule loaded into the HIP. Krypton is pumped from two storage cylinders into the HIP isolation work-zone, simultaneously with a balancing pressure of He or Ar around the work-zone. After the soak time, Kr and balancing pressure gas are vented to storage. The capsule containing the sintered zeolite is removed and placed into a storage container, which is then welded shut. After inspection the storage container is placed into storage. Transportation casks are used to transport the containers to long-term storage. One year's production is estimated at 5 m³ of sintered zeolite.

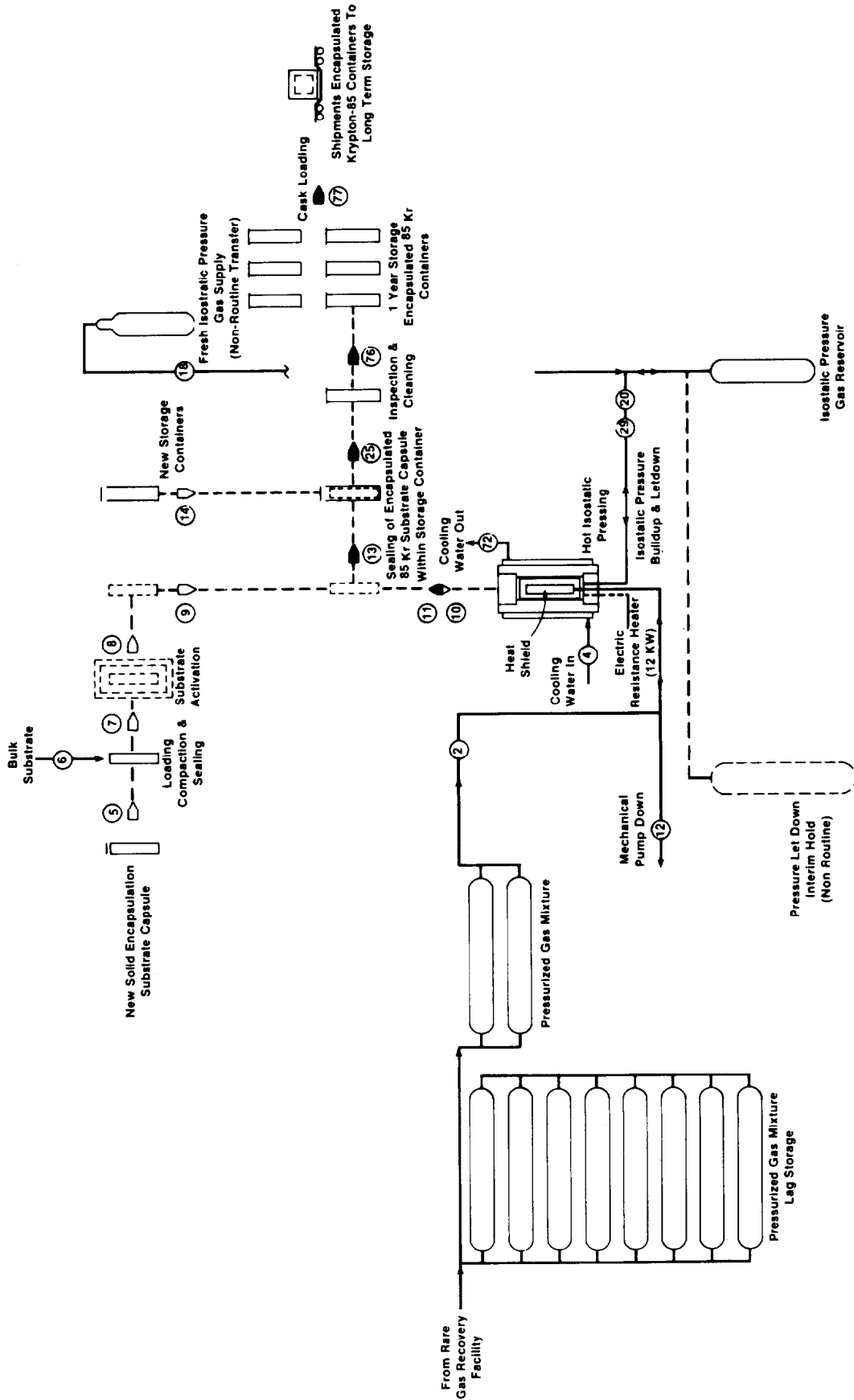


Figure 11. Krypton Encapsulation Process flow Diagram

A HIP containing an isolated work zone, similar to one in operation at General Electric Aerospace Company in Valley Forge, PA, is used to confine krypton-85 and the zeolite 5A. A schematic of an isolation work zone HIP is shown in Figure 12. The isolation work zone contains the work-load of zeolite 5A and krypton-85 gas during encapsulation and is surrounded by a balancing pressure of inert gas, such as helium or argon. As a result the krypton-85 inventory is reduced, and the corrosion of the pressure-bearing vessel walls by the decay product rubidium is eliminated.

The work-load may be preheated before placement to speed the heating time, and the heat-shield, work-load, and furnace may be placed into the HIP in one package, if desired. A crane is normally used to load and unload a HIP. HIPs are placed in concrete pits to facilitate work-package handling and minimize hazards from accidental failure at high pressures.

TABLE I

DESIGN BASIS FOR A COMMERCIAL-SCALE KRYPTON-85
ENCAPSULATION FACILITY

Process Throughput:	110% of 17 MCi/yr of ⁸⁵ Kr, Based on Reprocessing 2000 MTHM/Year of LWR Fuel
Total Volume of Feed Gas: (at 110% Capacity)	230 m ³ at STP
Feed Gas Composition: (by Volume)	2% Xenon 8% Argon 90% Krypton, with ⁸⁵ Kr Making up 6% of the Total Kr
Operation:	Batch Operation Using HIP
Lifetime:	24 Hours/Day, 300 Days/Yr, for 30 Yr
HIP Operating Parameters:	100 MPa and 700°C
Zeolite 5A Material Characteristics:	Bulk Density of 1.0 g/cm ³ Void Fraction of 40%
Gas Lag Storage:	60 Days' Production from Rare Gas Plant or 3.6 MCi
Product Storage:	1 Yr Production or 5 m ³ Sintered Zeolite

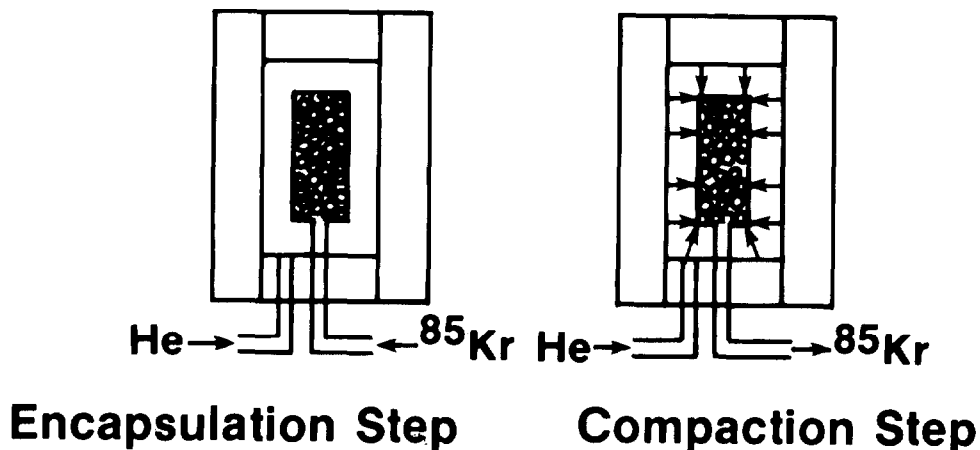


Figure 12. Schematic of ^{85}Kr (A) Encapsulation and (B) Compaction in the Isolation Work Zone of a Hot Isostatic Press. In (A), Pressures Are Balanced; in (B) ^{85}Kr is Withdrawn, Causing Isostatic Compaction of the Work Volume

The laboratory-scale HIP shown in Figures 3 and 4 has recently been modified to accept an isolation work zone for radioactive krypton-85 experiments. A photograph of the modified bottom cover and isolation work zone canister is shown in Figure 13. The two sets of inlets allow simultaneous pressurization of the isolation work zone canister with krypton-85 and of the surrounding volume with helium.

Mock-up vessels which simulate the laboratory-scale HIP vessel, isolation work zone canister, and heat shield were tested for remote operation. An additional alignment fixture, removable bayonet fixture, and manipulator extension fingers (Figure 14) were designed and fabricated. The remote tests demonstrated that the isolation work zone canister containing krypton-85 sintered in zeolite 5A can be remotely loaded and unloaded in the lab-scale, HIP. Radioactive krypton-85 tests are currently under way using this equipment. Modifications for full scale remote operation appears to be feasible, based on the lab scale tests and available HIP technology.

Figure 15, shows the conditions as a function of time during a commercial scale encapsulation process, including temperature, krypton pressure in the isolation work zone, and argon or helium pressure in the volume surrounding the isolated work-zone. The isolation work package is filled with zeolite beads, zeolite bead-glass frit powder mixture or compacted zeolite and heated at conditions necessary to give a residual water loading of approximately 1%. In order to avoid loss of solid material, a porous metal filter is enclosed in the tubing connected to the isolated work package.

Isolation Canister For Krypton Encapsulation System

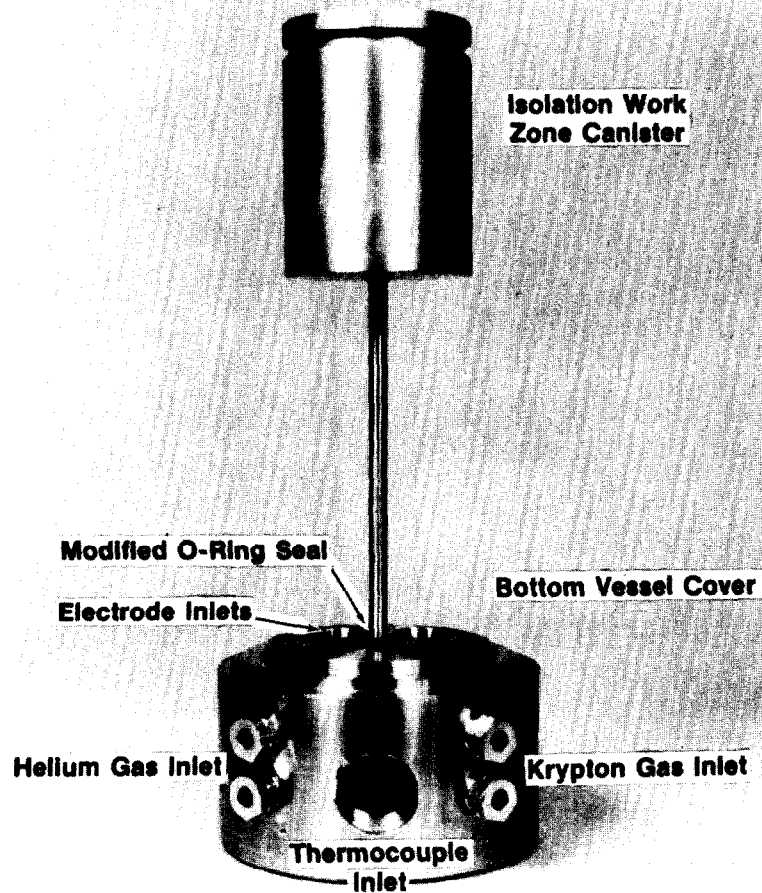


Figure 13. Photograph of Modified Bottom Cover to Lab-Scale HIP with Isolation Work Zone Canister Inserted

During the encapsulation soak time, the krypton pressure inside the work package and the argon or helium pressure outside the work package remain balanced. After the encapsulation soak time, the inner krypton gas can be vented back to storage, resulting in a compaction of the solid in the canister to form a monolithic block. If no compaction is desired, both gases can be vented and the work package cooled. The compaction step is included in the processing conditions shown in Figure 15 and is illustrated schematically in Figure 12. The compacted work package can then be removed remotely and sealed into a second container for long term storage. The total time required for the encapsulation and compaction cycle is about ten hours, including loading and unloading the isolated work package.

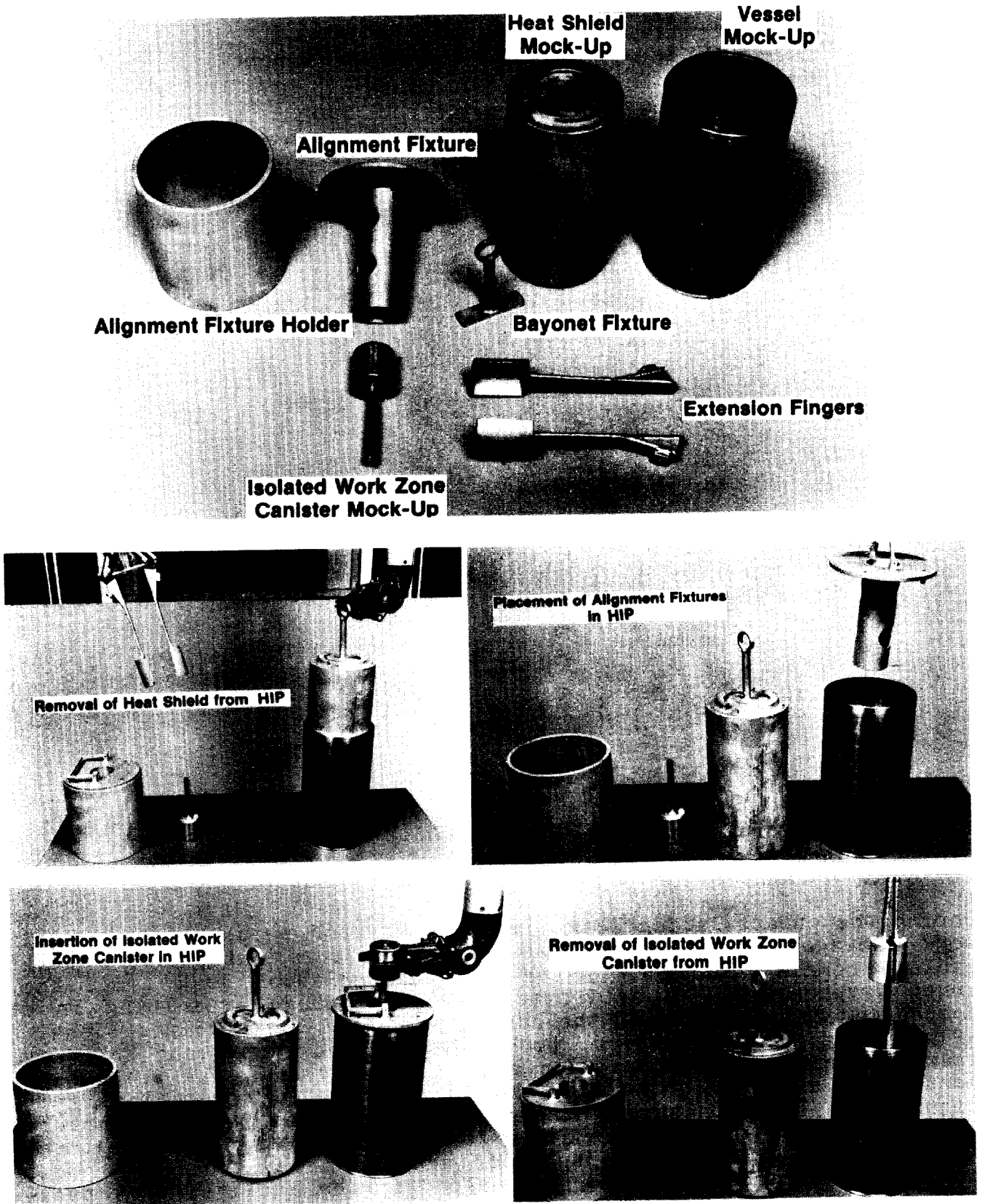
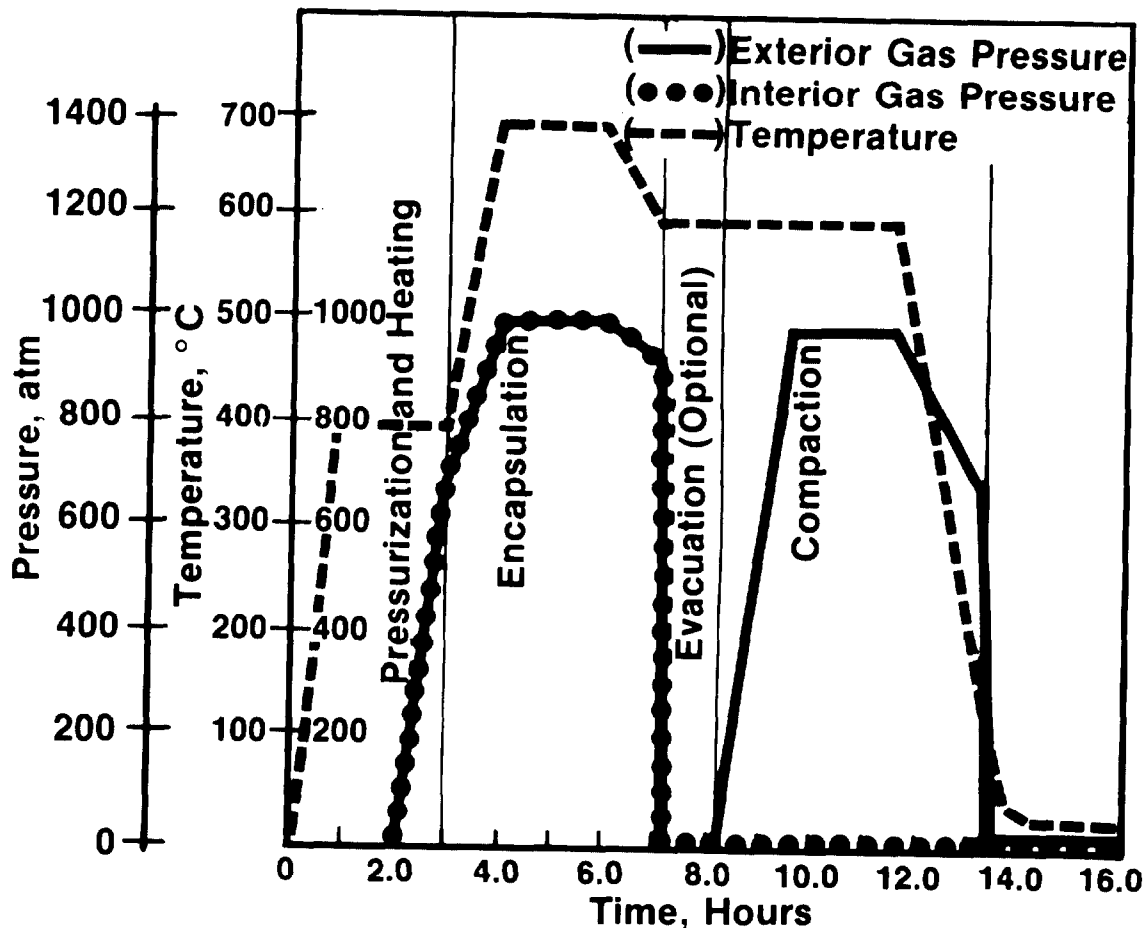


Figure 14. Mock-up of Lab-Scale HIP Components and Tools Required for Remote Operations



ICPP-S-6757

Figure 15. Temperature and Pressure Inside and Outside the Isolated Work Zone as a Function of Time for a Commercial-Scale Krypton-85 Encapsulation Process

The facility floor plan is shown in Figure 16. The facility is rectangular with dimensions 84 feet long by 52 feet wide and a total floor area of 4,368 square feet. All radiation areas are constructed with reinforced concrete. The facility consists of cells to contain the HIP processing, krypton-85 gas storage, immobilized product storage, and other support activities. The structure was designed to withstand and contain the dynamic and static overpressure and fragments resulting from a worst case rupture of the HIP.^{11,20}

A krypton-85 release of $\sim 128,000$ Ci is estimated to result in an off-site dose at 3 km of ~ 17 mrem for an ORNL Hydrofracture facility.²¹ A maximum krypton-85 accidental release from an encapsulation facility is expected to be similar, resulting in a similar off-site dose.¹¹ Thus the maximum emergency off-site dose is well below the emergency protective action guide level of 5 rem thyroid and 1 rem whole body.²²

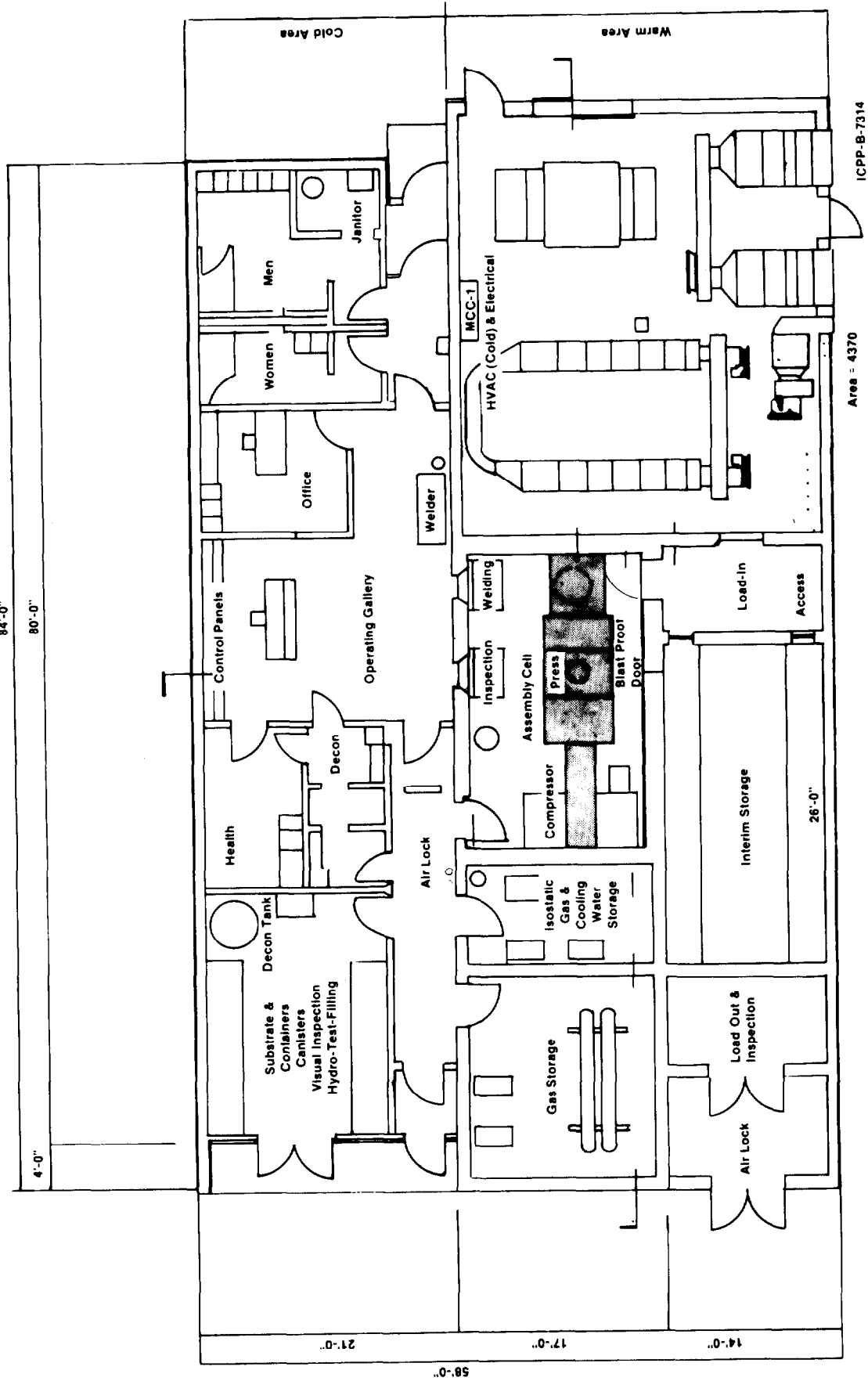


Figure 16. Krypton Encapsulation Facility Floor Plan

17th DOE NUCLEAR AIR CLEANING CONFERENCE

Based on a review of nuclear licensing procedures and requirements, it was concluded that major concerns appear to be in compliance with applicable codes for HIP fabrication and with developments associated in scaling up demonstration plants.¹¹ The licensing of a krypton-85 encapsulation facility should not be excessively expensive or lengthy.¹¹

Total facility and operating costs were evaluated on a life-cycle cost basis, following procedures of the Life-Cycle Manual for the Federal Energy Management Program.²³ The manual specifies that the total present value of the facility is calculated, using a 7 percent per year discount rate for annual costs. The facility was assumed to operate for 30 years, with no salvage value remaining thereafter.

The costs of a Kr encapsulation facility described above are provided in Table II for two sets of design conditions, operating at 300 and 600 cycles per year. Details are provided elsewhere.¹¹

TABLE II
KR ENCAPSULATION PROCESS LIFE-CYCLE COSTS

	<u>300 cycles/yr^a</u>	<u>600 cycles/yr^b</u>
1. Present Value Initial Capital Investments (90% of total)	9.1	9.5
2. Present Value of Life Cycle	0.5	0.6
3. Present Value of Life Manpower	5.1	6.8
4. Present Value of Life Cycle Materials	4.1	4.1
5. Present Value of Life Cycle Replacement/Maintenance	0.9	0.9
6. Present Value of Life Cycle Replacement/Insurance	0.1	0.1
Total Present Value of All Life Cycle Costs	19.8	22.0

^a Calculated using the base case from Parsons¹¹.

^b Base case from Parsons¹¹.

IV. Conclusions

The process to encapsualte krypton-85 in zeolite 5A is technically and economically feasible and can be used to produce a product with a compact solid mass at 700 °C and 100 MPa. A 2000 MTHM per year reprocessing plant would result in up to 5 m³ of zeolite containing krypton-85. At long term storage conditions of 300 or 400°C, less than 0.03% or 0.3% of the krypton inventory, respectively, will leak from sintered zeolite 5A.

The encapsulation process requires a hot isostatic press (HIP) with an 8 or 16 L isolated work zone to operate for 600 or 300 cycles per year, respectively. Since existing HIP technology uses work zones ranging from 1 to 3500 L in capacity at similar production rates, a great deal of flexibility is available, such as operating with a larger volume work zone, fewer cycles per year, or lower encapsulation pressures.

Based on a preconceptual design and cost estimate of a krypton encapsulation facility, the process is economically feasible. No major technology development is required for the process. Maximum krypton-85 release from a worst-case incredible accident would result in maximum doses at the site boundary which are well below the Protective Action Guides for accidental releases. The licensing of a krypton encapsulation facility should not be inordinately lengthy or excessively expensive.

Acknowledgment

The assistance of the following is gratefully acknowledged: H. S. Cole, J. R. Delmastro, E. S. Dickerson, L. L. Dickerson, N. S. Graham, S. H. Hinckley, J. C. Mittl, R. A. Rankin, and E. S. Wade of Exxon Nuclear Idaho Co.; Dr. R. D. Penzhorn of Karlsruhe KfK, Germany; Dr. S. Iijima of Arizona State University; Dr. A. Ruoff of Cornell University; and Dr. G. L. Messing of Pennsylvania State University.

V. References

1. Code of Federal Regulations, 40 CFR 190 (1977).
2. National Council on Radiation Protection and Measurements, Krypton-85 in the Atmosphere. Accumulation, Biological Significance, and Control Technology, NCRP Report No. 44 (July 1, 1975).
3. Management of Commercially Generated Radioactive Waste, Draft Environmental Impact Statement, DOE/EIS-0046-D (April 1979).
4. R. D. Klett, ed., Krypton-85 Disposal Program Conceptual Design Phase: Final Report, SAND-81-1957 (December 1981).

17th DOE NUCLEAR AIR CLEANING CONFERENCE

5. D. S. Whitmell, R. S. Nelson, and M. J. S. Smith, "Containment of krypton in a metallic matrix by combined ion implantation and sputtering," Management of Gaseous Wastes from Nuclear Facilities, IAEA-SM-245/7, 263-278 (December 1980).
6. G. L. Tingey et al., Entrapment of Krypton in Sputter Deposited Metals - A Storage Medium for Radioactive Gases, PNL-2879 (April 1979).
7. R. D. Penzhorn, "Long-term storage of ^{85}Kr in zeolite 5A," Proceedings of the 16th DOE Air-Cleaning Conference, CONF-801038, 2, 1047-1058 (October 1980).
8. A. B. Christensen, J. A. Del Debbio, J. E. Tanner and D. A. Knecht, "Loading and leakage of krypton immobilized in zeolites and glass," Sci. Basis Nucl. Waste Mgmt., 3, 251-8 (1981).
9. A. B. Christensen, J. A. Del Debbio, D. A. Knecht, and J. E. Tanner, "Immobilization and leakage of krypton encapsulated in zeolite or porous glass", ibid, 4 (to be published 1982).
10. G. L. Tingey et al., Solid State Storage of Radioactive Krypton in a Silica Matrix, PNL-3612 (December 1980).
11. A. B. Christensen, J. A. Del Debbio, D. A. Knecht, J. E. Tanner, and S. C. Cossel, The Immobilization of Krypton-85 in Zeolite 5A and Porous Glass, ENICO - 1102 (December 1981).
12. H. D. Hanes et al., "Hot isostatic processing", High-Pressure Science and Technology, 2 (1979).
13. H. T. Larker, "Hot isostatic pressing for the consolidation and containment of radioactive waste", Sci. Basis Nucl. Waste Mgmt., 1, 207-10 (1979).
14. D. W. Breck, Zeolite Molecular Sieves, John Wiley and Sons, New York (1974).
15. G. Denny, J. Wyart, and G. Sabatier, "Structural mechanism of thermal and compositional transformations in silicates", Z. Kristallographie, 112, 161-168 (1959).
16. H. Hoss and R. Roy, "Zeolite studies III: On natural phillipsite gismondite, harmatome, chabazite, and gmelinite", Beitr. Minem U. Petrogr., 7, 389 (1969).
17. R. W. Benedict, A. B. Christensen, J. A. Del Debbio, J. H. Keller, and D. A. Knecht, Technical and Economic Feasibility of Zeolite Encapsulation for Krypton-85 Storage, ENICO-1011 (September 1979).
18. L. A. Bursill, E. A. Lodge, and J. M. Thomas, "Zeolite structures as revealed by high-resolution electron-microscopy", Nature, 286, 111 (July 1980).

17th DOE NUCLEAR AIR CLEANING CONFERENCE

19. J. Crank, The Mathematics of Diffusion, Clarendon Press, Oxford (1956).
20. A. B. Christensen, J. E. Tanner, and D. A. Knecht, Preliminary Safety Evaluation of a Commercial-Scale Krypton-85 Encapsulation Facility, ENICO-1055 (September 1980).
21. F. J. Peretz et al., ^{85}Kr Hydrofracture Engineering Feasibility and Safety Evaluation, ORNL/ENG/TM-22 (July 1981).
22. US Environmental Protection Agency, Manual of Protective Action Guides and Protective Actions for Nuclear Incidents, EPA-520/1-75-001 (June 1980).
23. Life-Cycle Cost Manual for Federal Energy Management Program, NBS Handbook 135.

DISCUSSION

SIEGLER: What is the feed stream and where do you get the concentrated feed streams?

KNECHT: The compositions are given in the paper. We have encapsulated mixtures of N₂, O₂, Ar, Kr, and Xe with a Kr content of 54 or 68%. The Kr loading and leakage were not affected by the added components if based on the partial Kr pressure. There does not seem to be a limitation on the source of a concentrated feed stream. It could come from a Kr recovery facility using cryogenic distillation or fluorocarbon absorption.

MONSON: Why did you choose zeolite 5A over all other materials and what is the krypton loading capacity for zeolite 5A encapsulation?

KNECHT: We initially used sodalite, which trapped krypton physically and did not change its structure. Dr. Penzhorn at KFK discovered that zeolite 5A could be sintered in the presence of krypton, trapping the gas atoms by changing the alumino-silicate structure. We find that the sintered zeolite 5A exhibits much lower leakage rates than sodalite and is available commercially at low cost. The krypton loading capacity is quite high, 30 to 60 m³ of gas at STP per m³ of zeolite solid. This density is equivalent to krypton storage in pressurized cylinders at 1,000 psi.

MOELLER: Would it be practical to use this system for the immobilization of ⁸⁵Kr from commercial nuclear power plants?

KNECHT: Yes. This system is being designed for a 2,000 MTHM per year commercial-scale reprocessing plant which would reprocess the fuel from 67 commercial nuclear power plants.

KABAT: Have you considered that there is any need for krypton-85 removal from the nuclear power plant?

KNECHT: No. The U.S. regulation, which applies to nuclear fuel in the reactor and goes into effect on January 1, 1983, limits the amount of krypton-85 that you can release to 50,000 curies per gigawatt year of electrical generation. About 86% of the krypton that is in the fuel cannot be released. The regulation does not say exactly when the release can take place, so presumably you could recover more of it and then release it later, or use some other arrangement. The regulation is there even though most people recognize that the fuel cladding will retain most of the krypton within the reactor core.

BONKA: I want to comment on the last question. The retention of ⁸⁵Kr at nuclear power plants is not important. The emission rate is only approximately 20 Ci/GW(e). Without ⁸⁵Kr retention, the emission rate at a reprocessing plant with 1,400 T/y is nearly 10⁷ Ci/y

THE LONG-TERM STORAGE OF RADIOACTIVE KRYPTON BY FIXATION
IN ZEOLITE 5A⁺.

R.-D. Penzhorn, H. Leitzig, K. Günther, P. Schuster and H.E. Noppel

Kernforschungszentrum Karlsruhe, IRCh/PWA , 7500
Karlsruhe, Postfach 3640, Federal Republic of Ger-
many.

ABSTRACT

A process developed in Karlsruhe for the long-term storage of radioactive krypton is based on the observation that, in the temperature range 340 - 650 °C and at pressures above 100 bar, krypton can be trapped efficiently in zeolite 5A. The fixation involves a transformation of the original crystal framework into an amorphous state of the solid substrate. After conditioning the gas is neither liberated by elevated temperatures, liq. Rb at 150 °C nor gamma radiation.

In this report data are presented on the presumable temperature profiles in a final storage vessel, expressed as a function of the immobilized Kr-85 inventory. The obtained results correlate well with data estimated from measured thermal conductivities of zeolite 5A.

To verify the process hot experiments were carried out that so far have led to samples with up to 0.03 [Ci/g]. Qualitatively, these samples were shown to be stable. A quantitative evaluation, also with samples having much higher specific activity, is in progress.

A demonstration facility is now under construction. The immobilization of Kr will be carried out at $t < 520$ °C and $p < 300$ bar in a thick-walled one-way autoclave, having a capacity of 5 litres. Gas pressurization will take place by one of two alternatives: a] sorption/desorption of Kr in zeolite 5A at above atmospheric pressure and room temperature or b] sorption/desorption of Kr in zeolite 5A at low temperature and atmospheric pressure. The one-way autoclave concept leads to a very simple process and provides a highly safe second containment during final long-term storage.

+ Supported in part by the Commission of the European Communities under its program on radioactive waste and storage.

INTRODUCTION

Zeolite 5A was recently proposed as a matrix for the long-term storage of ^{85}Kr , after it was discovered that noble gases can be immobilized in this molecular sieve by hydrothermal chemifixation and it was shown that the conditioned gas is very stable towards elevated temperatures, radioactive radiation and certain chemicals [1,2,3]. Work carried out in Idaho has confirmed and extended these first observations [4].

The present paper contains results on the chemifixation of Kr in compacted zeolite 5A. Data are also given on the thermal conductivity of zeolite 5A, the transport of heat in the final storage vessel and the fixation of radioactive krypton in zeolite 5A. In addition, the demonstration facility presently under construction is discussed.

RESULTS AND DISCUSSION

Krypton fixation in compacted zeolite 5A

The bulk density of 2 mm 5A zeolite pellets and the density of activated pellets, measured pycnometrically in toluene, were found to be 0.83 and 1.58 [g/cm^3] respectively. The resulting external void fraction is 0.47. If this void fraction is reduced by compaction a decrease in free ^{85}Kr inventory during chemifixation is achieved. Also, heat transport during final storage is improved and less waste is obtained. Therefore, it appeared interesting to examine compaction techniques like mechanical compression and dessication of a slurry. By mechanical compression of 2 mm zeolite pellets, with pressures up to 178 [kN/cm^2], tablets having diameters between 12 and 50 mm and heights up to 30 mm were prepared. Application of progressively increasing hydraulic pressures yielded tablets showing a regular increase in bulk density [see table 1]. As apparent from the data, the specific BET surface area experiences a significant decrease only, when the employed hydraulic pressure exceeds 100 [kN/cm^2]. In consequence, since the BET determination is carried out at atmospheric pressure, it is anticipated that at several hundred bar pressure,

Table I . Manufacture of tablets from 2 mm 5A zeolite pellets

Hydraulic pressure [kN/cm ²]	Density [g/cm ³]	Specific surface area [m ² /g] ⁺
25	1.31	479.0 ± 10.9
50	1.40	-
75	1.46	458.4 ± 8.4
100	1.52	445.8 ± 12.0
125	1.56	367.1 ± 10.6
175	1.66	-

+ the specific surface area of 2 mm 5A zeolite pellets, determined with N₂ at -196 °C, is 459.9 ± 10.2 [m²/g].

i.e. during chemifixation, compaction will have little influence on the rate of gas diffusion into the zeolite crystals. That this is indeed the case is apparent from the results compiled in table II. They demonstrate that under identical fixation conditions the volu-

Table II . Krypton fixation in various Ca exchanged type 5A zeolites [p = 1000 bar]

Zeolite [MO/Al ₂ O ₃ , M = Ca]	Loading [cm ³ STP Kr/cm ³ zeolite]	
	2 mm pellets	tablets ⁺
0.102	1.4	1.12
0.298	8.4	52.4
0.466	26.6	43.4
0.550	35.7	69.7
0.600	35.7	71.2
0.910	22.4	67.1

+ tablets with $\rho = 1.4$ [g/cm³], prepared with a hydraulic pressure of 50 [kN/cm²]

metric loading of tablets is at least twice as high as that of 2 mm pellets.

In one run Kr was trapped in a desiccated 5A zeolite slurry. Employing a fixation pressure of 1000 bar at a temperature of 520 °C, a loading of 57.3 [cm³ STP Kr/g] was obtained, which is higher by a factor 1.8 than that achieved under identical fixation conditions in 2 mm pellets.

The effect of compaction on the volumetric loading of an autoclave is illustrated in table III.

Table III Degree of filling of an autoclav

Aggregation form of matrix	Density of matrix [kg/l]	Filling [kg/l autoclav]	Loading ⁺ [l STP Kr/l autoclav]
2 mm pellets	1.4	0.7	14
slurry	1.0	1.0	20
tablets ⁺⁺	1.4	1.1	22
tablets + pellets	1.4	1.2	24

+ based on a loading of 20 [cm³ STP Kr/g zeolite]

++ \varnothing tablet/ \varnothing autoclav = 0.33

The highest loading is achieved when the autoclav is filled with a combination of pellets and tablets. Filling can also be improved when pellets of two different diameters are employed [5] .

Thermal conductivity of zeolite 5A

Because most of the β -radiation [average energy = 0.246 MeV] emitted by ⁸⁵Kr is absorbed by the solid matrix a temperature rise in the fixation media is expected. For a reliability assesment, but also to maximize loading without sacrificing safety gained by immobilization, it is necessary to know the temperature profile that developes. The maximum temperature will depend upon the specific ⁸⁵Kr activity, the thermal conductivity of the fluid media surrounding the solid, the void fraction of the solid and the thermal conductivity of the solid. At atmospheric pressure the heat conductivity of most gases is low. Therefore, heat transport will take place essentially near the contact points of the granular material.

To measure the thermal conductivity of zeolites a comparison method was chosen, which involves a measurement of the temperature difference between two points in a material when, under steady state conditions, heat flows linearly from one point in the direction of the other. The temperature difference is related to the heat flow by Fourier's equation. Several types of samples were examined, employing Pyrex 7740 as the reference material: fluid medium/fiber glass, 2 mm 5A pellets in several fluid media and zeolite 5A tablet. No attempt was made to determine accurate thermal conductivity values of the gases. A few measurements with argon, krypton and air were only carried out to calibrate the system. For this purpose, a fiber glass filling material, having a bulk density of $0.1 \text{ [g/cm}^3\text{]}$ and a thermal conductivity about 25 times lower than that of Pyrex 7740, was placed between the reference cylinders.

One aspect that needs to be considered when determining the thermal conductivity of zeolites is the high affinity of these molecular sieves for water. For instance, a activated sample, left under ambient conditions for several hours, will sorb up to 21 weight % of water. It is thus clear that, in a study on the temperature dependence of the thermal conductivity, the initial water content of a non activated zeolite will not remain constant. Since the water content in the crystalline framework has an influence on the thermal conductivity it is difficult to obtain meaningful results. These considerations may explain the observation that, whereas at low temperature, i.e. 300 K, the thermal conductivity of non activated 5 A tablets [$\emptyset = 50 \text{ mm}$, height = 15.8 mm and $\rho = 1.5 \text{ [g/cm}^3\text{]}$] is higher by approx. 0.03 [$\text{w/m} \cdot \text{deg}$] than that of a pretreated tablet [0.19 [$\text{w/m} \cdot \text{deg}$], at temperatures above 550 K both samples have about equal thermal conductivity [at 550 K 0.25 [$\text{w/m} \cdot \text{deg}$].

Zeolite 5A containing trapped gas will no longer sorb water [2]. Its internal void fraction is nearly zero as indicated by the specific surface area, which decreases from an initial 450 [m^2/g] of the pretreated, unloaded 5A zeolite to about 2 - 3 [m^2/g] after noble gas fixation. Thus the thermal conductivity in air of zeolite 5A containing 43 [$\text{cm}^3\text{STP/g}$] noble gas was measured both in form of 2 mm pellets and as a tablet [dimensions as above]. It was found that the thermal conductivity of the pellets increases linearly with temperature from 0.11 up to 0.16 [$\text{w/m} \cdot \text{deg}$] in the range 20 - 280 °C. In the same temperature

range the thermal conductivity of the tablet was about twice as high.

The thermal conductivity of zeolite pellets increases in the order 1 : 1.3 : 1.5 when the measurement is carried out in the presence of Kr, Ar or air. Analogous measurements with a monolithic zeolite block indicate that after compaction the influence of the surrounding fluid medium becomes negligible

A very crude estimation of the absolute thermal conductivity of zeolite type A gives a value of about 1 [W/m · deg] at 300 °C, similar to that glass or quartz

Heat transport measurements

Christensen [6] calculated the heat transport through cylinders containing piled zeolites cooled by natural heat convection. He examined the interaction of cylinder radius, ^{85}Kr loading, and centerline temperature for sodalite pellets. An experimental verification of the calculation was however not carried out.

To simulate a final storage vessel two stainless steel cylinders of equal length [1000 mm] but different diameters, i.e. 89 and 134 mm, were employed. The respective wall thicknesses were 3 and 4.5 mm. Each cylinder was provided with 12 axially and radially distributed Fe/constantan thermocouples as well as four heating coils [see fig. 1 , which shows zeolite pellets in a pyrex glass tube]. All measurements were carried out with activated, unloaded 2 mm 5A zeolite pellets. Cooling occurred by natural convection. Fig. 2 shows a tridimensional plot giving the axial cylinder temperatures vs the radioactive gas loading and the cylinder radius of the larger vessel. Fig. 3 shows similar data together with temperature profiles [dotted lines] estimated with thermal conductivity values obtained in this work. The agreement between the experimental temperature profiles and those calculated employing appropriate heat conduction equations, is satisfactory. It is seen that natural convection will remove the heat generated by radioactive ^{85}Kr decay and will maintain the maximum centerline temperature in a 134 mm \varnothing storage vessel at temperatures below 80 °C, provided the specific loading is lower than 30 [cm³ STP/g]. These temperatures are to be considered upper limits, because activated zeolites conduct heat less

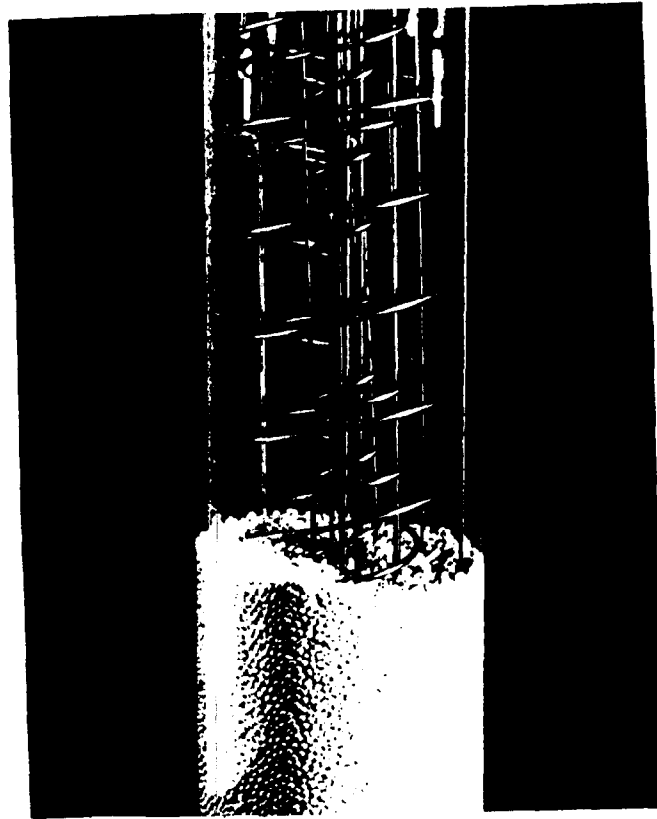


Fig. 1 Experimental set-up showing heating coils, and thermocouples.

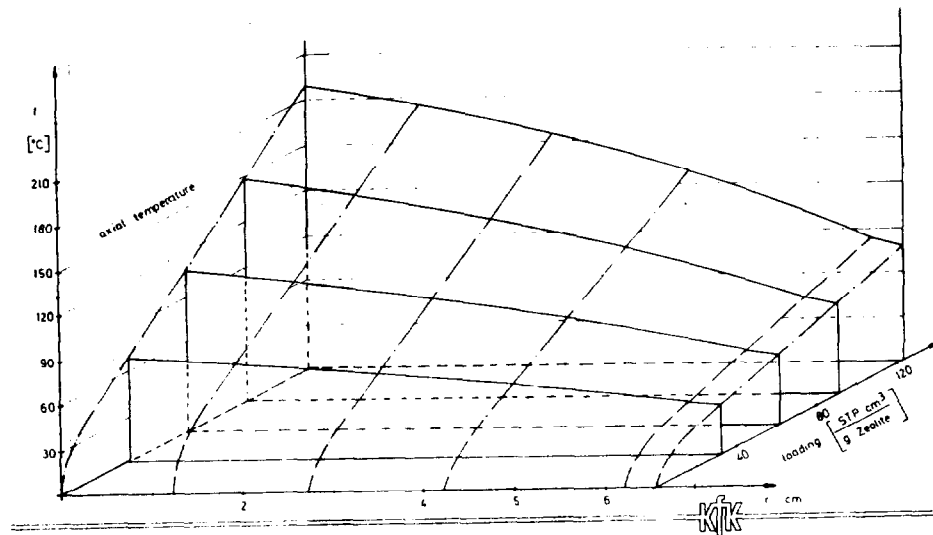


Fig. 2 Tridimensional graph of the axial temperature vs loading and radius of a 134 mm \varnothing vessel containing 2 mm 5A zeolite pellets.

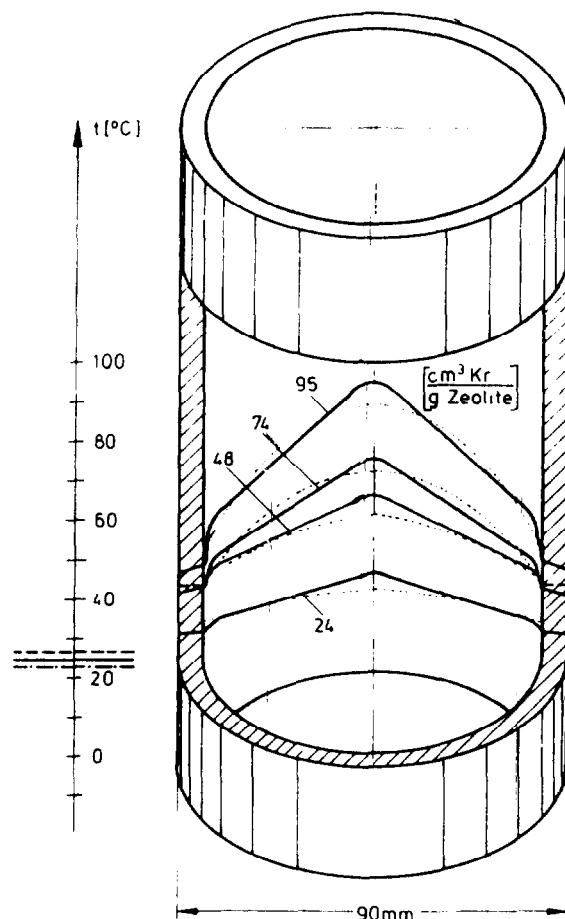


Fig. 3 Temperature profile in a 90 mm \varnothing cylinder as a function of zeolite loading with radioactive krypton. The dotted lines correspond to temperatures calculated with thermal conductivity values obtained in this work.

efficiently than non activated zeolites or zeolites containing trapped noble gas. Furthermore, for commercial krypton disposal, some form of compacted zeolite, having higher thermal conductivity, will probably be employed.

Chemifixation of radioactive krypton

To verify the process and obtain a product for observing the long-term effects of decaying radioactive krypton several hot samples have been prepared. The employed equipment, shown in fig. 4, is very simple. It consists essentially of a one liter storage cylinder, a 4 cm³ pressurization vessel and a 1 cm³ autoclave, containing the zeolite. To carry out a fixation the system is first evacuated. Then the zeolite is activated and radioactive krypton ex-

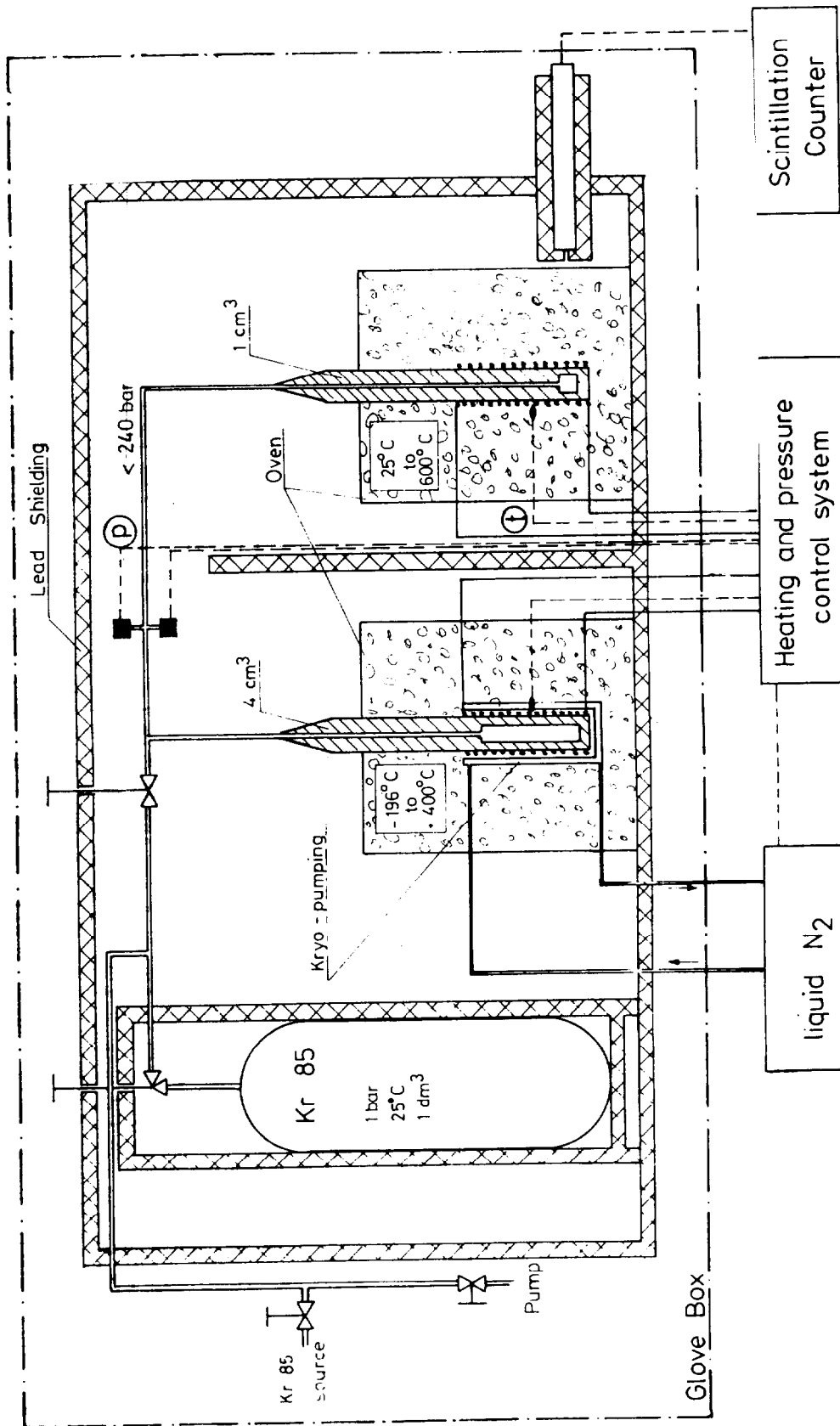


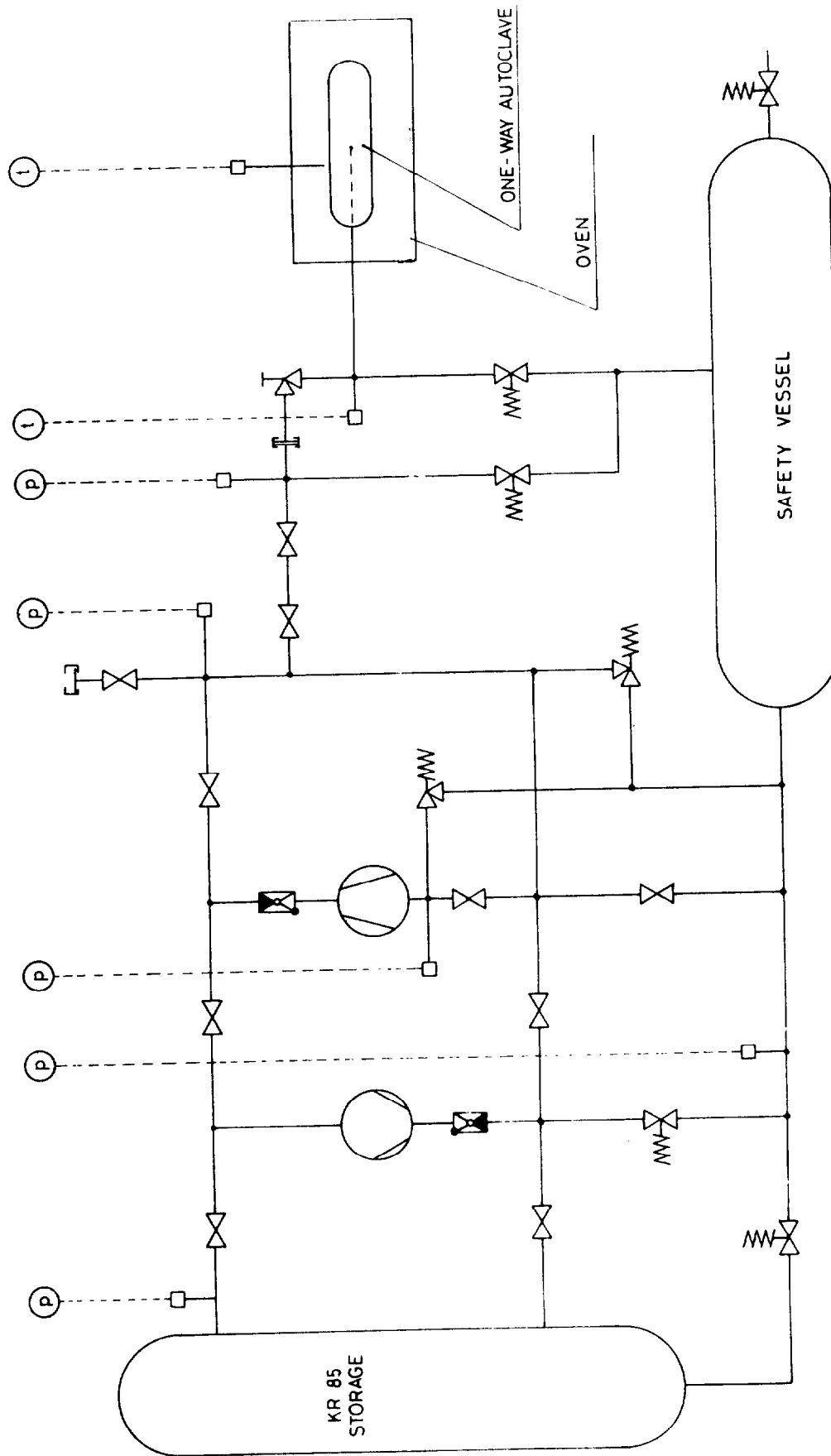
Fig. 4 Fixation of radioactive krypton

panded into the storage cylinder until a pressure of about 1 bar is reached. Next, Kr is frozen out with liq. N_2 in the pressurization vessel and, after closing the appropriate valve, expanded into the pressurization vessel and the autoclave. When the pressurization vessel is heated up to $400^\circ C$ a pressure of approx. 180 bar builds up. At the same time Kr is sorbed by the zeolite [still at room temperature]. Fixation takes place when, finally, the autoclave is heated up to $520^\circ C$. By the above procedure three active samples have been prepared. Their loading and specific activity were 19.6, 20.6 and 19.4 [cm^3 STP $^{85}Kr/g$] and 3.2, 28.3 and 24.3 [mCi/g] respectively. Qualitative inspection of these samples for a period of approx. three month showed them to be stable. A quantitative evaluation, designed to examine leakage [effect of temperature] and chemical stability is in progress.

Within the next few month's additional samples, having a specific activity of the order of 3 - 10 [Ci/g] will be produced. This specific activity is equal or higher than that expected during final storage.

Facility for the immobilization of krypton

A facility, illustrated schematically in fig. 5, is presently under construction. The major equipment includes an thick-walled externally heated one-way autoclave provided with a quick connector, an oven for the pretreatment of the zeolite also to be employed for the hydrothermal krypton fixation, several pumps, a compressor [up to 7 bar], several storage cylinders manifolded together with stainless steel lines, safety devices, temperature and pressure registration, etc. Gas densification will be achieved by sorption/desorption either at 4.5 bar and room temperature or at 1 bar and $-20^\circ C$ [see fig. 6]. Under these conditions enough gas will be sorbed by the zeolite so that, upon raise of temperature up to $520^\circ C$, a pressure of approx. 300 bar will build up in the autoclave due to desorption, and about 22 [cm^3 STP/g] noble gas will be immobilized by chemifixation. By this procedure the process is considerably simplified, because gas pressurization is achieved without a high pressure compressor or a complicated cryopump. The facility will provide information on large scale pretreatment, heat transport, material behaviour, energy consumption, operation time, loading homogeneity, safety devices, etc.



KJK

Fig. 5

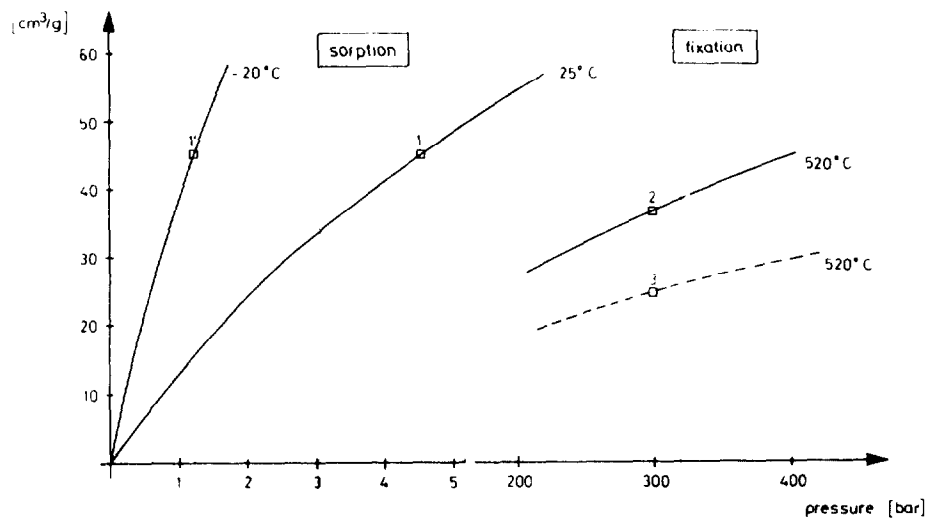


Fig. 6 Sorption and fixation isotherms for krypton in zeolite 5A

The main advantage of the one-way autoclave concept is seen in the simplicity of the process. In addition, the one-way autoclave can be considered a highly safe secondary containment during final disposal because of its inherent resistance towards internal and/or external corrosion, mechanical destruction and temperature excursions.

REFERENCES

- [1] R.-D. Penzhorn, P. Schuster, H.E. Noppel, L.M. Hellwig
Int. Symp. on Management of Gaseous Wastes from Nuclear Facilities, Vienna, Feb. 18-22 [1980]
- [2] R.-D. Penzhorn
16th DOE Nuclear Air Cleaning Conf., San Diego, Calif., Oct. 20-23 [1980]
- [3] R.-D. Penzhorn, P. Schuster, H. Leitzig, H.E. Noppel
to be published in Ber. Bunsen Gesellschaft [1982]
- [4] A.B. Christensen, J.A. DeDebbio, D.A. Knecht, J.E. Tanner, S.C. Cossel
ENICO 1102 [1981]
- [5] A. Kaupa
IMF-Arbeitsbericht Nr 4/65 KFK [1965]
- [6] A.B. Christensen
ICP - 1128 [1977]

DISCUSSION

KNECHT: I would like to comment on the differences in scale of your and our envisioned commercial-scale encapsulation facilities. We are considering a design for a Kr immobilization facility for a 2,000 MTHM per year reprocessing plant while you are considering a design for a 300 MTHM per year reprocessing plant.

PENZHORN: That is correct. We believe that the one-way autoclave concept will be particularly suitable for conditioning the krypton-85 produced in small reprocessing plants (300-350 MTHM per year).

EBY: What do you see as the primary contributing factor for the improvement in loading capacities that you have observed in your recent work as compared to the 1978 studies?

PENZHORN: I like to distinguish between 1) totally reversible sorption, 2) encapsulation, which involves trapping without destruction of the crystal framework and 3) chemifixation, an irreversible process which takes place after the pores to the cavities are closed by a hydrothermal reaction. It was the discovery of the latter form of immobilization that led to improvements of the sorption capacities. By chemifixation, gases can be trapped efficiently in large cavities with large pore openings as opposed to encapsulation where you look for pore openings smaller than the effective kinetic diameter of the gas to be immobilized. Also, in chemifixation, high pressures are no longer required because loading occurs by sorption and not by activated diffusion.

VIKIS: Is the chemical purity of krypton, particularly with respect to the air components, critical to the success of this method?

PENZHORN: No. We think that the composition of the gas to be conditioned is of no consequence to the process. In fact, we have shown that Ne, Ar, Kr and Xe can be trapped in zeolite 5A. Also, 1:1 mixtures of Ar and Xe, as well as Kr and Xe, have been immobilized. In this case, however, we noticed an enrichment of Xe in the zeolite. This is due to the fact that Ar and Kr are sorbed less efficiently by zeolite 5A than Xe.

17th DOE NUCLEAR AIR CLEANING CONFERENCE

VOLATILIZATION AND TRAPPING OF RUTHENIUM IN HIGH TEMPERATURE PROCESSES

M. Klein, C. Weyers, W.R.A. Goossens
SCK/CEN, Nuclear Energy Center
200, Boeretang
B-2400 MOL, Belgium

Work performed within a contract with DWK in Germany in the framework of the HAW technological programme for the vitrification of HLW.

I. Introduction

Solid radioactive aerosols and semi-volatile fission products e.g. Ru, Cs, Sb are generated during high level waste calcination and vitrification processes. The retention of Ruthenium has first been studied because of its strong tendency to form volatile compounds in oxidative media. Since RuO_4 was the suspected form for the high degree of volatilization during high temperature processes, the study has started with testing of capture materials for the trapping of RuO_4 .

II. Materials for the retention of RuO_4

Two types of trapping materials were tested, either adsorbants such as Silica-gel operating above the dew point of the gas, either catalysts such as ferric-oxide/chromium oxide catalyst operating at 300 °C. Detailed results of this laboratory study are reported elsewhere (1) (2).

Three different cases were considered for the carrier gases :

- RuO_4 mixed with dry air ;
- RuO_4 mixed with moist air till a dew point of 85 °C ;
- RuO_4 mixed with NO_x and water vapour produced by high temperature calcination of nitric acid.

For the adsorption on Silica-gel, the bed temperature, which must be higher than the gas dew point, determines the adsorption capacity and the DF. At room temperature, an adsorption capacity of 1 mg/g and a DF of 1000 were obtained for an inlet concentration of 100 mg/m³. At 100 °C, with or without water vapour, the adsorption capacity is lower than 0.2 mg/g and the bed is very rapidly saturated, moreover the presence of high concentrations of water vapour decreases the adsorption capacity of the bed for RuO_4 . For the adsorption of the volatile ruthenium on silica-gel at 100 °C, the presence of NO_x greatly improves the performance of the bed. Indeed, with NO_x , no breakthrough of the bed could be measured and the DF of the bed increased with time (DF from 10 to 100).

In all the cases, the adsorbed species on the bed is slowly reduced into a more stable species, probably ruthenium oxides. Without NO_x , the adsorbed species on the bed can generally be desorbed nearly quantitatively (till 75 %) ; in presence of NO_x , the desorption is limited to 5 % maximum.

For the retention on a ferric oxide/chromium oxide catalyst, in all the cases the capture mechanism is a catalytic decomposition of the volatilized species which is transformed into solid oxides. The deposit of ruthenium oxides enhances the reaction rate so that the DF increases with time. The capacities are higher than 10 mg/g since no bed breakthrough are observed. The initial DF is one order of magnitude lower in presence of NO_x which indicates that the reaction rate is lower. Consequently the RuO_4 very unstable at 300 °C is easily trapped, but in presence of NO_x the species formed is more stable and so has a lower decomposition rate.

A general conclusion of this study is, that in presence of NO_x , the concept of a stable RuO_4 is not any more valid and that the volatile species is probably a nitrosyl ruthenium compound more stable, and more easily adsorbable but more difficulty decomposable than RuO_4 . As a consequence, RuO_4 trapping study was stopped and a study on Ru behaviour during high temperature calcination or vitrification of nitric acid solution of Ru was started.

III. Calcination of nitric acid containing ruthenium

In the CALCILAB laboratory unit described in (2), nitric acid solutions containing $\text{RuNO}(\text{NO}_3)_x(\text{OH})_{3-x}$ complexes are calcined in an inconel calciner with a through-put of about 50 ml/h. The Ru-volatility varies between 50 and 70 % at 600 °C and decreases to 30 % at higher calcination temperatures of 800 to 1000 °C.

The nature of the volatilized species depends also on the calcination temperature ; at 600 °C, the Ru coming out of the calciner is almost completely condensed (DF condensor 360) and only a minute fraction is in aerosol form (0.2 %). If the calcination temperature increases, the % of Ru in aerosol form increases exponentially and reaches respectively 1 and 8 % at 800 °C and 1100 °C. That means that the condensor DF decreases from 80 at 800 °C to 13 at 1100 °C. The condensed form of Ru is soluble in the acidic condensate (pink purple colour) but is slowly reduced to an insoluble oxide. In these conditions, if a specific Ru filter is placed at the exit of the condensor, the efficiency of the bed will be very small since only the aerosol form of Ru is still present in the off-gases.

If the specific Ru filter is placed directly at the exit of the calciner, the volatile species can be trapped. A silica-gel adsorbant bed operating at 100 °C shows an efficiency from 10 to 100 which increases with time. Saturation of this bed is not observed so that the silica-gel capacity is at least higher than 1 mg/g. The adsorption mechanism seems to be similar to the mechanism occurring when RuO_4 and NO_x are mixed together.

A ferric oxide/chromium oxide catalyst can also achieve DF's higher than 10. The mechanism is also similar to these observed when RuO_4 and NO_x were mixed namely :

- increase of the DF with time i.e. with increasing ruthenium oxides deposits ;
- irreversibility of the trapping by catalytic decomposition into stable ruthenium oxides.

IV. Behaviour of Ru in a liquid fed melter

In order to simulate the PAMELA concept for the vitrification of H.L.W., a laboratory unit called VITRILAB with a 2 kg glass capacity and with liquid feed on the molten glass surface has been constructed. The off gas purification line comprises in series a packed bed dust scrubber, a specific Ru filter, an ejector venturi, a condenser and finally a washing bottle and an absolute filter. The liquid feed is a simulated LEWC solution containing traced ruthenium species. The flow sheet of the laboratory VITRILAB unit is given in fig. 1 and the composition of the simulated LEWC solution is given in table I.

Volatilization of Ru from the glass melter

Volatility of Ruthenium with an LEWC liquid feed. The volatility of Ru in a liquid fed melter depends on a number of factors such as liquid flow rate, degree of coverage of the glass pool with a molten salt layer and air sparging flow rate. With a liquid flow rate of 0.14 l/h and an air sparging of 90 l/h, the volatility ranges from 15 to 20 % in the begin of a run but rapidly decreases to values ranging from 10 to 7 % when a molten salt layer covers the glass surface. An increase of the liquid flow rate from 0.14 to 0.17 l/h and a decrease of the sparging air flow from 90 to 60 lN/h result in a decrease of the mean volatility till values of 7 to 3 %.

Table I. Composition of simulated LEWC solution.

NaNO ₃	154	g/l
Fe(NO ₃) ₃ · 9H ₂ O	75	
Al(NO ₃) ₃ · 9H ₂ O	68	
Ni(NO ₃) ₂ · 6H ₂ O	9.5	
Na ₂ MoO ₄ · 2H ₂ O	9	
Ce(NO ₃) ₃ · 6H ₂ O	7.9	
Cr(NO ₃) ₃ · 9H ₂ O	7.4	
Ba(NO ₃) ₂	3.3	
La(NO ₃) ₃	4	
CsNO ₃	3.6	
Y(NO ₃) ₃ · 6H ₂ O	1.9	
Sr(NO ₃) ₂	1.9	
Zn(NO ₃) ₂ · 6H ₂ O	1.2	
RuNO(NO ₃) ₃	6.3	
Specific activity of traced Ru solution		
0.1 to 210 ⁶ Bq/l		

Special care is necessary to avoid blockage of the off gas outlet pipe by ruthenium oxides and dust deposition. In order to prevent the formation of a dust layer in the off gas pipe, a small fraction of the circulating liquid of the dust scrubber is fed countercurrent into the outlet pipe, vaporizes in contact with the outlet tube and so washes out the deposit.

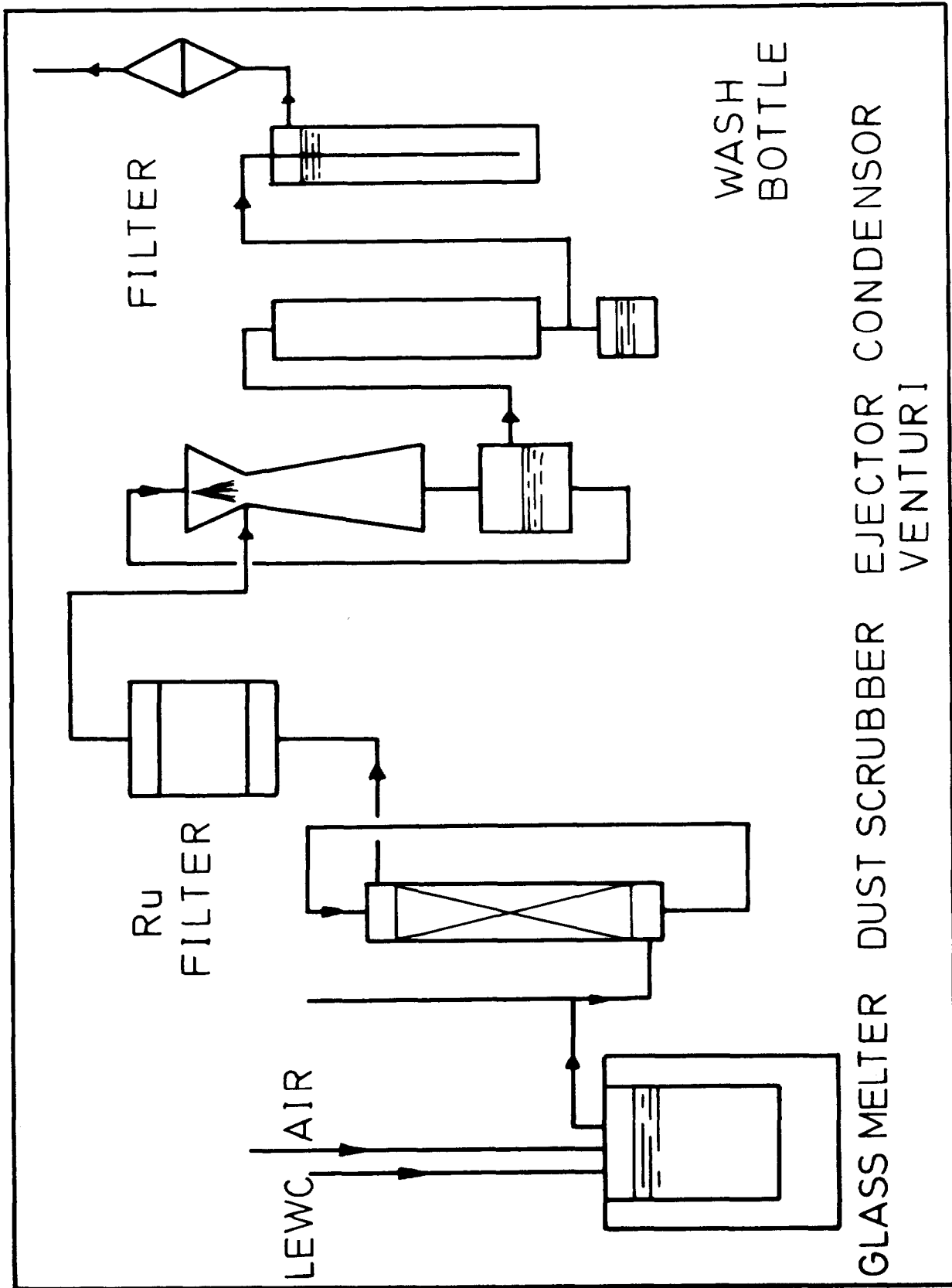


Fig. 1. Flow sheet of VITRILAB laboratory unit

17th DOE NUCLEAR AIR CLEANING CONFERENCE

The distribution of Ru present in the off-gases between the aerosol and the volatile form have been determined by sampling with a cascade impactor followed by a condenser, a wash bottle and a final fiber filter. The flow sheet of the sampling unit is given in Fig.2. Very short sampling times (a few minutes) can only be used with the cascade impactor due to clogging of the jet nozzles of the two last stages (ϕ 1 and 0.6 mm) so that the representativity of the sample is not excellent. Moreover, the impactor must be heated up till 150 °C, in order to prevent water condensation, so that volatile Ru present in the off-gases could be partly decomposed on the walls of the impactor. Nevertheless, it seems that the fraction of Ru still volatile is smaller than 10 % (values down to 0.1 % have been obtained). This fraction, passing through the impactor, is trapped in the condenser and no Ru is found in the wash bottle and in the final filter. The activity mass median aerodynamic diameter of the aerosol at the exit of the oven lies between 1 and 7 μ m and the distribution is quite large (geometric standard deviation $S_g = 3$)

Volatility of different Ru species. Experiments have been performed with the aim of comparing the volatilities of different Ru species fed simultaneously with LEWC on a glass pool.

The different tests were :

- RuNO(NO₃)_x(OH)_{3-x} 2 g/l ruthenium in LEWC at a flow rate of 0.14 l/h corresponding to 280 mg Ru/h ;
- RuO₂ 2 g/l as a suspension in LEWC at the same flow corresponding to 280 mg Ru/h ;
- RuO₄ 280 mg Ru/h sparged with air, fed at the top of the glass oven and mixed with the off-gases coming from the LEWC feed ;
- RuNO(NO₃)_x(OH)_{3-x} 2 g/l in LEWC and with the addition of 100 g/l SUGAR (SACCHAROSE) in the LEWC solution.

Clogging problems at the Ru inlet and at the off-gases outlet' appeared during the RuO₄ tests. High dust concentration during the sugar test lead also to clogging problems at the outlet of the oven. Due to these experimental difficulties, the interpretation of the results is not simple, nevertheless it seems clear that the DF of the oven varies in function of the Ru species fed. With RuNO(NO₃)_x, the mean DF is 13 ; for RuO₂ the DF is much higher and reaches a value of 40 ; for RuO₄, the error on the DF is great but it seems that before clogging, the DF lies between 3 and 8. For RuNO(NO₃)_x + SUGAR, the DF of the glass oven is 1, for the packed bed scrubber 6 and for the venturi ejector 400. The washing solutions contain a very great amount of insolubles. The addition of sugar seem to induce the formation of a great amount of dust which is not trapped in the molten glass layer.

Volatility of Ru from the glass-oxide melt. When the glass oven containing molten glass and waste oxides is sparged with air a reentrainment of Ru occurs. The fraction of Ru present in the sparging air represents a release of 0.1 to 0.01 % pro hour of the Ru activity in the glass. The release increases with the gas flow rate so that the activity released pro hour increases linearly with the square of the gas flow rate. A decrease of the glass temperature from 1100 °C to 800 °C result in a decrease of the Ru entrainment by a factor of 10 to 100.

17th DOE NUCLEAR AIR CLEANING CONFERENCE

Packed bed dust scrubber for the capture of Ru

The characteristics of the glass packed bed dust scrubber, used as first purification device in the off gas line, are given hereafter -

- geometric characteristics : diameter : 5 cm
- height : 25 cm
- packing : Rashig rings
- outside diam. : 0.7 cm
- height : 0.7 cm
- inside diam. : 0.4 cm ;
- liquid flow rate : 100 l/h.

In order to avoid an increase of the volume of the circulating solution, the scrubber operates at a temperature regulated in such a way that the water vapour content of the off gases does not condense out in this scrubber. Therefore, the operating temperature depends on the LEWC liquid feed rate and on the sparging air flow rate. The table II gives the operating temperature for different LEWC and air flow rates.

Table II

LEWC liquid feed l/h	Air gas feed lN/h	Operating temperature °C	Water content % V/V
0.14	90	89	65
0.17	60	93	78

The operation of the dust scrubber is very sensitive to variation in the operating temperature since a 4 degrees variation means an increase of the total gas flow through the scrubber by a factor 1.6. The liquid flow rate is chosen to work below flooding conditions for the highest operating temperature. The representativity of the liquid sampling during a test is doubtful due to the presence of insolubles and to the deposit of ruthenium on the Rashig rings. A mean global DF is determined after each test by measurements of the circulating solution and of two successive rinsing solutions. The distribution between soluble and insoluble fraction is generally 1/1 and the fraction of Ru deposit on the Rashig rings can reach 25 % of the total quantity of Ru trapped in the scrubber. The global DF of the dust scrubber varies between 10 to 50 with a mean value about 20. The activity mass median aerodynamic diameter of the aerosol leaving the dust scrubber lies between 0.3 and 0.6 μm and the distribution is quite narrow ($S_g = 2$).

No significant quantities were found after the cascade impactor which means that the ruthenium at the outlet of the dust scrubber is only in aerosol form.

Specific volatile ruthenium trapping bed

The second barrier for Ru in the off gas line as initially foreseen in the Pamela project, was a silica-gel bed operating at 120 °C in order to avoid condensation problems. Such a filter, which had given favourable results when placed at the exit of a calciner appeared useless in the Vitrilab off gas purification line. The

17th DOE NUCLEAR AIR CLEANING CONFERENCE

ferricoxide-chromiumoxide catalyst gave also very low decontamination factors.

Preheating of the gases between the outlet of the dust scrubber and the inlet of the silica-gel bed resulted in an increase of the DF of the bed with an optimum preheating temperature of 400 - 600 °C. In these conditions, DF higher than 10 could be achieved. In spite of the improvement of the bed efficiency, it has been noted that the activity first decreases with the length of the bed till a minimum and then again increases till the end of the bed. In the last layer, a loose dust deposit containing Ru oxides is accumulated and represents the majority of activity of this layer, whereas in the first layer the Ru is trapped on the silica-gel pellets and reduced to a gray deposit. These observations have led to a modification of the installation in order to determine the distribution of Ru between the aerosol and the volatile form in function of the preheating temperature.

A flow sheet of the modified installation is described in figure 3 and in table III are given for preheating temperatures of 180, 400 and 600 °C :

- the ratio O/I which represents the ratio of the quantity of Ru in the off gases after the preheater to the quantity present at the inlet of the preheater ;
- the distribution of Ru after the preheater between the filter F, the condensor C, the caustic washing bottle B, and the final fiber filter FF.

Table III. Distribution of Ru after the preheater

	Preheating temperature °C		
	180	400	650
O/I	0.8 - 0.9	0.8 - 0.9	0.3 - 0.5
F %	99.7	99.7	93.1
C %	0.2	0.15	6.6
B %	0.1	0.15	0.3
FF	BG*	BG	BG

*BG : measurement not significantly different than the background.

At preheating temperatures from 180 °C to 400 °C, only a small difference was observed between the activity in the off-gases before and after the preheater. But at 650 °C, the activity after the preheater was 30 to 50 % of the activity before ; this means that ruthenium is deposited on the surface of the preheater. Washing of the preheater with water removes only 15 % of the total activity deposited, the rest is only removed from the surface by chemical attack of the stainless steel. At 650 °C the DF of the glass fiber filter is quite lower (15) than for the lower preheating temperatures (DF greater than 300). The ruthenium not trapped by the filter is mainly trapped in the condensor.

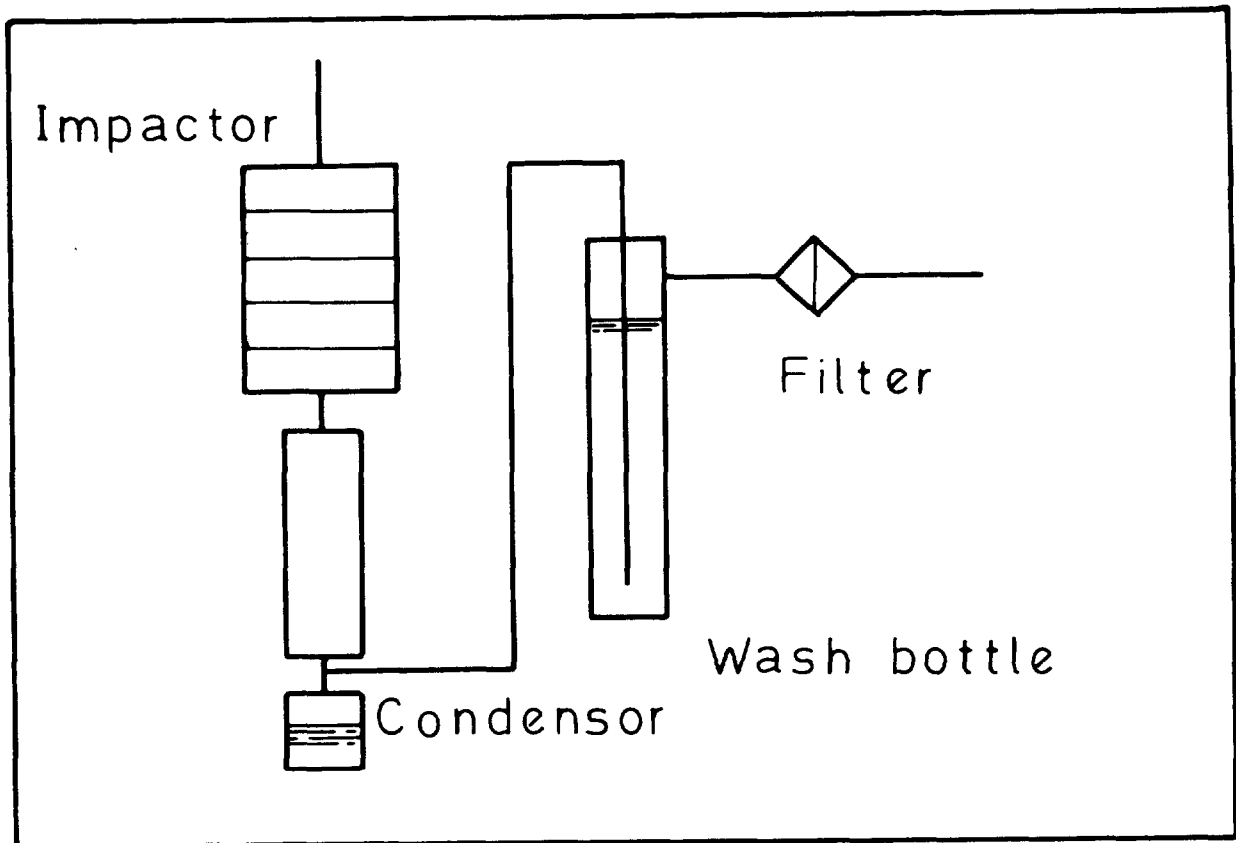


Fig. 2. Flow sheet of the sampling unit

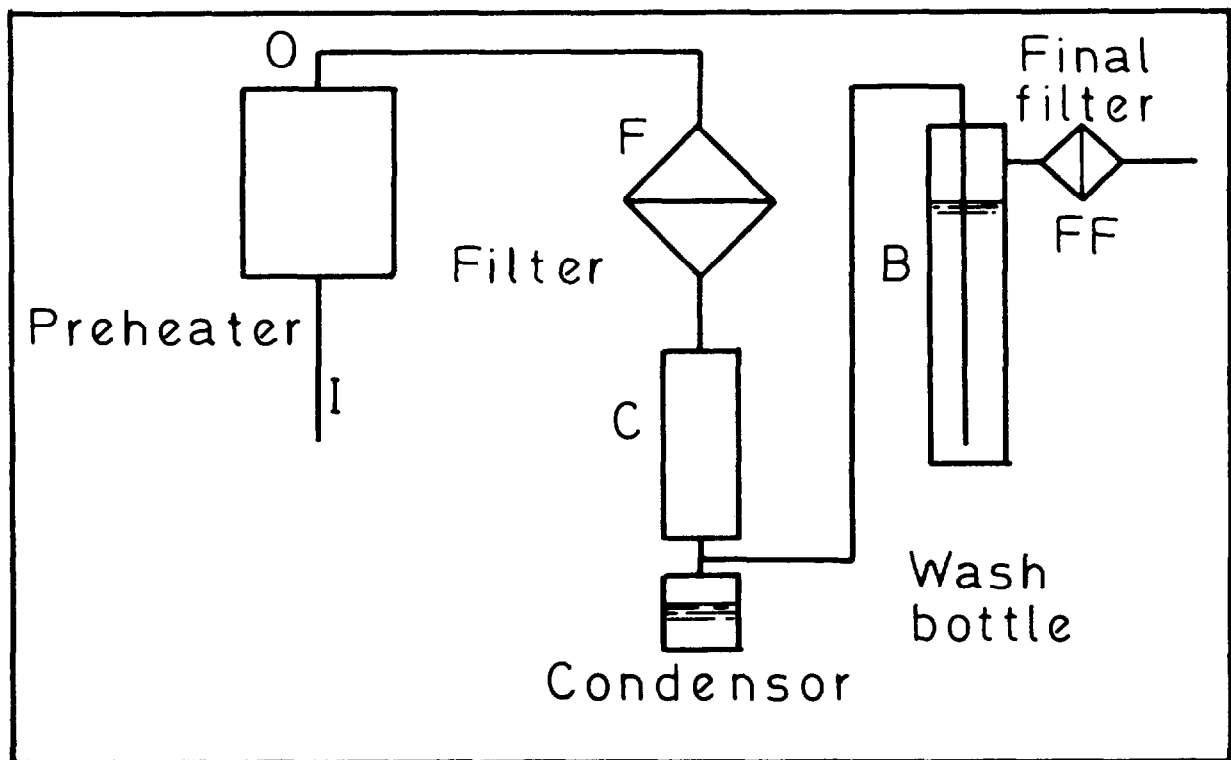


Fig. 3. Modified installation for the study of the influence of the preheating temperature

17th DOE NUCLEAR AIR CLEANING CONFERENCE

Some qualitative observations can be made on the basis of these experimental results :

- at 650 °C, there is a chemical reaction between the Ru and stainless steel (in the literature, the optimum temperature for volatile Ru deposit lies in the range 400-650 °C) ;
- at 650 °C, there could occur a partial volatilization of the aerosols of oxides of ruthenium by the combined action of NO₂ and O₂. This volatile species is not stable at high temperature and reacts with stainless steel, this species at low temperature is condensable and soluble in the acidic condensate.

Ejector venturi

The ejector venturi operates with a nozzle pressure of 3 bars and a liquid flow rate of 300 l/h. The circulating solution is saturated with nitrates to avoid NO degassing problems in the pump. When the ejector venturi is not cooled, the temperature of the circulating solution stabilizes at 84-86 °C so that the volume of the circulating solution is nearly constant. When the circulating solution is cooled, the temperature is stabilized at 50 °C so that the % of water vapour in the off-gases decreases from 55 % to 12 %. The DF of the ejector venturi increases when the DF of the system glass oven-dust scrubber decreases, but decreases in the opposite case so that the over-all DF glass oven-dust scrubber - venturi ejector remains high. During the experimental campaign, over-all DF of $5 \cdot 10^3$ to $2 \cdot 10^4$ were obtained for the three units in series which corresponds to DF's for the ejector ranging from 10 to 50.

V. Conclusion

This experimental study has indicated the importance of moisture and NO_x vapours on the volatility and trapping conditions of ruthenium in high temperature processes. Also the process operating conditions have a great influence on the ruthenium behaviour in the off-gas purification units.

Of particular interests is the observation that the ruthenium release during direct vitrification of simulated high-level liquid waste is a factor of about 5 smaller than the ruthenium release during calcination of this type of waste. Moreover, in the direct vitrification case the ruthenium escapes mostly in the form of an aerosol whereas in the calcination case a volatile ruthenium compound is dominating. Consequently, a specific ruthenium filter is not any more needed in the off-gas line of a direct vitrifier simplifying in this way the number of units in this off-gas line and avoiding the handling and controlling problems of such a ruthenium filter.

In the future, a similar programme will be started on the volatility of cesium and antimony in a liquid fed melter and on the technical reliability of the liquid fed melter and its associated gas purification units on a semi-pilote scale under simulated conditions.

References

- (1) KLEIN, M., "Filtration and capture of semi-volatile nuclides" IAEA-SM-245/51 (1980).
- (2) KLEIN, M., "Volatilization and trapping of ruthenium during calcination of nitric acid solutions". IAEA-SR-72/03 (1982).

DISCUSSION

CHRISTIAN: With regard to the suggested ruthenium nitrosyl vapor species in the presence of NO_x , I obtained spectral evidence for chemical interaction between gaseous ruthenium tetroxide and nitrogen dioxide. When the two gases are placed at measured concentrations in a quartz cell, the uv-visible spectra of both $\text{RuO}_4(\text{g})$ and $\text{NO}_2\text{-N}_2\text{O}_4(\text{g})$ are diminished and a new strong charge transfer band appears. Similarly, the infrared spectrum of the system exhibits no vibrational bands of RuO_4 or nitrogen oxide species and two uncatalogued bands appear. Also, the equilibrium pressure of RuO_4 over RuO_2 in O_2 or NO_2 is insufficient to account for the observed partial pressure of ruthenium in the offgas of a fluidized-bed calciner. This provides additional evidence of the formation of a more volatile, stable species than RuO_4 in the presence of NO_x .

KLEIN: Our observations were quite similar. The following observations, not mentioned in the paper, were made. RuO_4 and NO_x , mixed in the presence of air, react to give a product which deposits in the glass tubing. This deposit is not stable; indeed this deposit is only soluble in nitric acid solution when tube washing is performed immediately. Otherwise, insoluble compounds are formed if the washing is not performed immediately. RuO_4 and NO_x , mixed in the presence of air in a bubbling column containing nitric acid, also react to give various $\text{RuNO}(\text{NO}_3)_x$ compounds soluble in nitric acid.

DEUBER: Did I understand that in your investigations the gaseous Ru specie most difficult to trap was found to be RuO_4 ?

KLEIN: Indeed, the adsorption tendency of RuO_4 on silica-gel is lower than the adsorption tendency of the RuNO complex. However, RuO_4 has a lower stability than the RuNO complex so that, in the case of catalytic beds such as ferric-oxide/chromium oxide catalyst operating at 300°C , RuO_4 is more easily trapped than the RuNO complex.

17th DOE NUCLEAR AIR CLEANING CONFERENCE

PLANT FOR RETENTION OF ^{14}C IN REPROCESSING PLANTS FOR LWR FUEL ELEMENTS

Braun, H.* , Gutowski, H.** , Bonka, H.+ , Gründler, D.**

* Federal Ministry of the Interior, Bonn, F.R.G.

** Linde AG, Höllriegelskreuth, F.R.G.

+ Technical University Aachen, F.R.G.

** Now GRS, Cologne, F.R.G.

ABSTRACT

The ^{14}C produced from nuclear power plants is actually totally emitted from nuclear power plants and reprocessing plants. Using the radiation protection principles proposed in ICRP 26, ^{14}C should be retained at heavy water moderated reactors and reprocessing plants due to a cost-benefit analysis. In the frame of a research work to cost-benefit analysis, which was sponsored by the Federal Minister of the Interior, an industrial plant for ^{14}C retention at reprocessing plants for LWR fuel elements has been planned according to the "double alkali process". The "double alkali process" has been chosen because of the sufficient operation experience in the conventional chemical technique. In order to verify some operational parameters and to gain experiences, a cold test plant was constructed. The experiment results showed that the "double alkali process" is a technically suitable method with high operation security. Solidifying CaCO_3 with cement gives a product fit for final disposal.

I. Introduction

Since about 1972 the radiological significance of ^{14}C emissions from nuclear power plants and reprocessing plants is discussed. It started with the expected emission of reprocessing plants for high temperature nuclear reactor fuel elements /1/. Comparative calculations for other reactors and reprocessing plants showed that their emission rates cannot be neglected while considering radiologically all radioactive emissions /2/.

The retention of ^{14}C has been discussed in Germany in connection with the "Gorleben-Project" /3/, which has been upset in the meantime. At that time a decision was not possible, because no technical solution was available. The Federal Ministry of the Interior in the F.R.G. sponsored within the scope of a cost-benefit analysis, made by the Professorial Chair for Nuclear Reactor Technology of the Technical University Aachen /4/, /5/, the Linde company in Höllriegelskreuth, F.R.G., for designing a plant with data for investment and operation costs. Simultaneously special processing problems should be researched in a nonactive plant /6/.

II. Production and release of ^{14}C from nuclear power plants and reprocessing plants

^{14}C is mainly produced in nuclear power plants due to fission and neutron capture in ^{13}C , ^{14}N and ^{17}O in the fuel elements, in the coolant, in the moderator, and in the air respectively the nitrogen at the outside of the reactor pressure vessel.

This work was sponsored by the Federal Minister of the Interior of the F.R.G. under Contract No. St. Sch. 680a and St. Sch. 680b.

17th DOE NUCLEAR AIR CLEANING CONFERENCE

The ^{14}C production rates and the expected emission rates from the different nuclear power plants have been calculated in various publications, see table I. The total results agree quite well, although greater differences for some reaction rates occur. The calculation results agree extensively with the measured results, see e.g. /27/, /28/, /29/, /30/, /31/, /32/. Table II gives a detailed survey of the production rates according to /16/. The calculations were based on the C-, N- and O-impurities listed in table III.

The expected ^{14}C emission rates from nuclear power plants and reprocessing plants during normal operation are listed in table IV. For water-cooled reactors the ^{14}C that is totally produced in the coolant and moderator is emitted from the nuclear power plant. Measurements showed that in boiling water reactors ^{14}C is emitted to up to more than 95 % /28/, /31/, /32/ as CO_2 and in pressurized water reactors to up to more than 90 % as CH_4 , C_2H_6 and other hydrocarbons /27/, /31/, /32/, due to the hydrogen addition. In reprocessing plants the total ^{14}C in the fuel element is released during the dissolution and emitted to more than 99 % as CO_2 , as measurements at the reprocessing plant Karlsruhe showed /29/, /30/.

III. Radiological significance of the ^{14}C emissions

When regarding the maximum possible individual doses in the vicinity of reprocessing plants, it is obvious, that the radiological impacts of an emission rate of 500 Ci/a via a 200 m stack are small. Fig. 1 shows e.g. the average air concentration at ground level in main wind direction (eastern direction), if 500 Ci/a ^{14}C were emitted via a 100 respectively 200 m stack. The meteorological data of Hannover were used for the calculations. Fig. 2 shows the maximum possible total body annual dose according to the specific activity model /33/ for this case. The natural total body annual dose due to ^{14}C is approx. 1.3 mrem/a for a CO_2 concentration in the atmosphere of 330 vppm. Total body annual doses due to globally distributed ^{14}C in the range of 1 up to 2 mrem/a could be possible in the future, if nuclear energy would be used more intensively /34/, /35/. Fig. 3 shows as an example the change of the total body annual doses due to globally distributed ^{14}C , if the total ^{14}C would be emitted from 1000 nuclear power plants with light water reactors with an electric capacity of 1000 MW each and the corresponding reprocessing plants. The changes due to the combustion of ^{14}C -free fossil fuels and the ^{14}C of the nuclear weapon tests /34/, /35/ has been neglected. 50 % of the annual dose occur due to the emissions of nuclear power plants, see table IV.

A totally different impression occurs, when using the new radiation protection principles in ICRP 26 /36/. According to these principles the aspired retention of radioactive material in nuclear power plants should be determined according to a cost-benefit analysis. On the first path exposure the collective dose due to ^{14}C is 3 man·rem/Ci. The global contribution can be taken from fig. 4; for an integration time of 500 years it is 55 man·rem/Ci. Based on a time of e.g. 500 years, the relation between annual costs, see chapter V, and reduced collective dose (cost effectiveness) results a value of approx. 30 \$/man·rem, taking into account that due to a ^{14}C retention facility in a 1400 t/a reprocessing plant 450 Ci/a are retained and finally disposed. For the retention and the final disposal of ^3H , ^{85}Kr , ^{129}I and the aerosols a cost-effectiveness of approx. 200, 250, 5 respectively 20 \$/man·rem /4/, /37/, /38/ occurs. ^{129}I and the aerosols have to be retained independent from a cost-benefit analysis because of the maximum individual dose. That means, ^{14}C has to be retained before ^3H and ^{85}Kr are retained according to the radiation protection principles in ICRP 26. As a standard value for the costs of detriment it is suitable to base on approx. 100 \$/man·rem according to the costs of fatal road accidents /39/. In the literature values of 10 up to 1000 \$/man·rem are used. Argentine demanded first a ^{14}C -retention facility for a nuclear plant in the heavy water moderated reactor Atucha II /40/.

17th DOE NUCLEAR AIR CLEANING CONFERENCE

TABLE I: Calculated production- and release-rate of ¹⁴C in different nuclear reactor types and reprocessing plants /16/

- a) after measurements at /27/ and /28/
- b) 10 % of production rate at fuel
- c) nitrogen impurity at coolant 5 to 40 ppm
- d) only coolant
- e) with graphite moderator
- f) up to 7 Ci/day calculated, most fixed in structural materials

Reactor-type	Thermal efficiency [%]	Calculated production rate [Ci/(GW(e)·a)]							Calculated release into atmosphere		Reference
		Coolant and fuel of fuel element					Air around pressure vessel	Structural material	Reactor	Reprocessing plant	
		Coolant		Fuel and graphite moderator at HTR		Total					
		Assumed N ₂ [ppm]	Activity [Ci/(GW(e)·a)]	Assumed N ₂ [ppm]	Activity [Ci/(GW(e)·a)]		[Ci/(GW(e)·a)]	[Ci/(GW(e)·a)]	[Ci/(GW(e)·a)]	[Ci/(GW(e)·a)]	
BWR	33	5	11.2	6	18.9	30.1	5·E-4	3	11.2	18.9	/2/, /7/
	33	0	11.5	10	32.7	44.2					/8/, /9/
	33		16 a)	20	13.6	29.7				1.5 b)	/10/
	33	1	9.2	20	22	31.2					/11/
	33	0	10.7	0	9	19.7			10.7		/12/
	34	1	8	1	4.9	12.9		20-30			/13/
	34	1	8	10	12.2	20.2		20-30			/13/
	33		4.7	20	14.8	19.5		43.2			/14/
			8	10	16	24					/15/
	33	5	5.7	10	12.6	18.3	5·E-4	17	6-10 c)	12.6	/16/
PWR	33	5	11.1	6	16.1	27.2	0.005	3.8	11.1	16.1	/2/, /7/
	33	0	3.6	10	12.1	15.7					/8/, /9/
	33		6 a)	20	13.6	19.6				1.5 b)	/10/
	33	6.4	18			18 d)			18		/17/
	34	5	5.2			5.2 d)					/18/
	33	1	3.3	20	22	25.3					/11/
	33		5	20	15.7	20.7		30.4			/14/
	33		5	10	12	17					/15/
	33	5	7	10	12.9	19.9	0.005	20	7	12.9	/16/
HWR	30		410		50	460					/15/
	33		557		20	577					/19/, /20/
	32	5	320	6	23	443					/21/
MAGNOX	30	200	3	50	87	90		213 e)			/10/
	30	200	8.5	50	130	140	5·E-4	325 e)	10		/16/
AGR	40	200	7.5	20	11.7	19.2		255 e)			/10/
	41	200	8.1	50	16.8	24.9	0.001	126 e)			/16/
HTR	41				61	61	0.004				/1/, /2/
				26	160	160					/22/
				10	250	250					/23/
	41			25	54	54					/10/
	41		0.05	5	142	142	0.004		0.1	142	/24/
FBR [U ₂ -fuel]	35	1	0.003	6	2.6	2.6	1	14.5	1	2.6	/2/, /7/
	35			10	2.6	2.6		12.5			/14/
[(U, Pu)N-fuel]	35			25	6.3	6.3		12.5			/14/
	35			75	18.5	18.5		12.5			/14/
	41	1	0.02	20	4.8	4.8				4.8	/25/
	41	1	0.003	10	5.5	5.5	1	8			/16/
	41			(U, Pu)N	1.5E4	1.5E4	1	14.5	1	2.6	
FUSION				(U, Pu)N	1.7E4	1.7E4					/25/
							2 500 f)				/26/

17th DOE NUCLEAR AIR CLEANING CONFERENCE

Table II: Calculated production of ^{14}C in the different reactor types in Ci/(GW_e·a) /16/

Specification		^{14}C -Production in Ci/(GW(e)·a)							
		BWR	PWR	HWR	MAGNOX	AGR	HTR	FBR	
Around pressure vessel	^{14}N	$5 \cdot 10^{-4}$	0.005	0.005	$5 \cdot 10^{-4}$	0.001	0.005	1	
	^{13}C	$7 \cdot 10^{-7}$	$8 \cdot 10^{-7}$	$3 \cdot 10^{-5}$	0.06	0.06	$4 \cdot 10^{-7}$	$5 \cdot 10^{-7}$	
	^{17}O	5.1	6.2	175	1.1	1	$5 \cdot 10^6$	$2 \cdot 10^6$	
Coolant	Fission	0.6	0.6	0.6	0.6	0.5	0.5	0.5	
	^{13}C	$2 \cdot 10^{-4}$	$2 \cdot 10^{-4}$	$7 \cdot 10^{-4}$	$8 \cdot 10^{-4}$	$2 \cdot 10^{-4}$	$9 \cdot 10^{-5}$	$1 \cdot 10^{-5}$	
	^{14}N	7.6	7.8	26	130	13	3.1	2	
	^{17}O	4.4	4.5	13	0.01	3.3	1.6	3	
	^{13}C	$3 \cdot 10^{-4}$	$5 \cdot 10^{-4}$	$7 \cdot 10^{-4}$	$4 \cdot 10^{-4}$	$6 \cdot 10^{-4}$	—	$1 \cdot 10^{-5}$	
	^{14}N	17	20	34	35	32	—	8	
Fuel element	Fuel	^{13}C	2.10 ⁻⁴	2.10 ⁻⁴	7.10 ⁻⁴	8.10 ⁻⁴	2.10 ⁻⁴	9.10 ⁻⁵	1.10 ⁻⁵
		^{14}N	7.6	7.8	26	130	13	3.1	2
		^{17}O	4.4	4.5	13	0.01	3.3	1.6	3
Fuel element	Canning	^{13}C	$3 \cdot 10^{-4}$	$5 \cdot 10^{-4}$	$7 \cdot 10^{-4}$	$4 \cdot 10^{-4}$	$6 \cdot 10^{-4}$	—	$1 \cdot 10^{-5}$
		^{14}N	17	20	34	35	32	—	8
		^{17}O	0.015	0.02	0.03	0.003	0.003	—	$2 \cdot 10^{-4}$
Graphite moderator	^{13}C	—	—	—	110	35	32	—	
	^{14}N	—	—	—	180	59	54	—	
	^{17}O	—	—	—	0.02	$7 \cdot 10^{-4}$	$7 \cdot 10^{-4}$	—	
Total production rate		35	40	27%	500	151	91	15	

Table III: C, N and O impurities used to calculate the rate of ^{14}C production in the different reactor types /16/

Reactor-type	Impurities in ppm or vppm								
	Coolant			Fuel elements					
	C	N	O	C	N	O	C	N	O
BWR	1	5	H ₂ O	50	10	UO ₂	270	80	1500
PWR	1	5	H ₂ O	50	10	UO ₂	270	80	1500
HWR	1	5	D ₂ O	50	10	UO ₂	270	80	1500
MAGNOX	CO ₂	200	CO ₂	50	50	U	100	50	Oxidation 100
AGR	CO ₂	200	CO ₂	50	20	UO ₂	100	50	100
HTR	CO 3 vppm CO ₂ 1 .. CH ₄ 0.1 ..	1 vppm	CO 3 vppm H ₂ O 12 .. CO ₂ 1 ..	50	10	UO ₂	Graphite *	10	3 *
FBR	20	1	1	50	10	UO ₂	1000	100	30

Table IV: Expected ^{14}C emission rate of nuclear power plants at normal operation and of a reprocessing plant without ^{14}C retention

Nuclear facility		Emission rate in Ci/a	
		Atmosphere	Surface water
Reactor (1000 MW _e)	BWR	10	0.01
	PWR	7 *	0.01
	HWR	200 - 400	
	MAGNOX	10	
	AGR	10	
	HTR	1	
	FBR	1	
Reprocessing plant (40000 MW _e) full load	BWR u. PWR	500	
	HTR	3600	
	FBR	220	

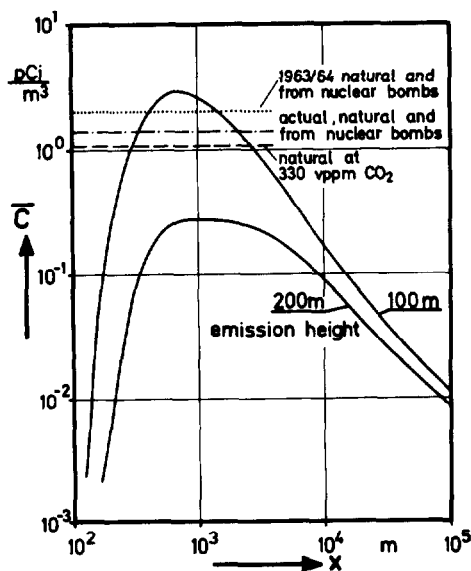


Fig. 1: ^{14}C concentration of the air near ground level in the main wind direction (east), $\dot{E} = 500 \text{ Ci/a}$

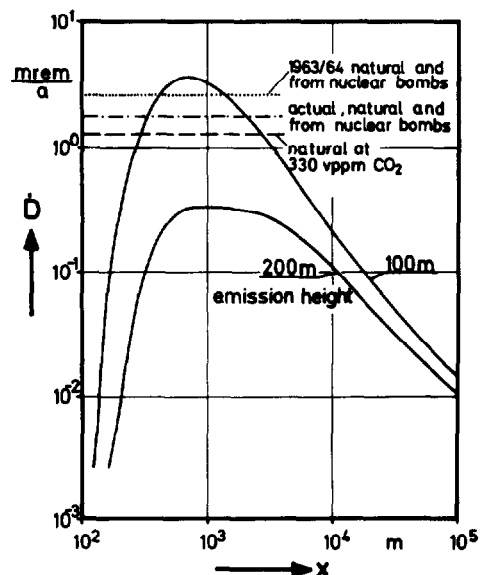


Fig. 2: Maximum radiation exposure due to ^{14}C of an adult in main wind direction (east), $\dot{E} = 500 \text{ Ci/a}$

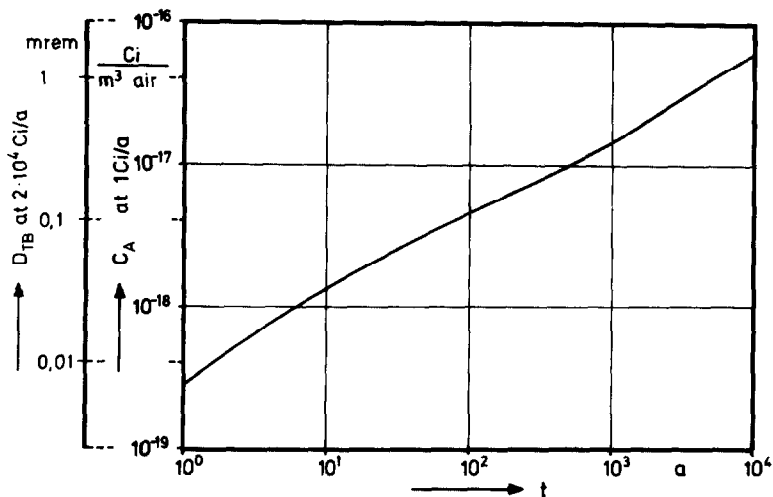


Fig. 3: ¹⁴C activity in the air at ground level after global distribution, if 1 Ci ¹⁴C is emitted per year; total body annual dose for an annual emission of $2 \cdot 10^4$ Ci without ¹⁴C-concentration changes due to nuclear weapon tests; CO₂ concentration in the air 330 vppm = const.

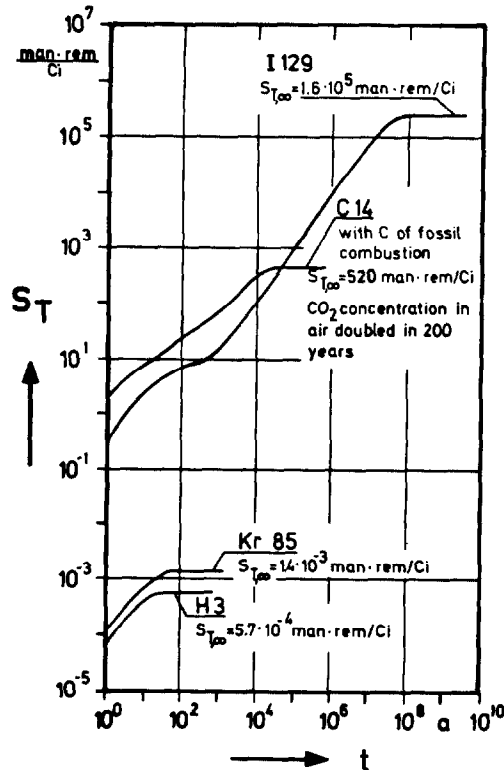


Fig. 4: Total collective effective dose equivalent commitment S_T from globally distributed radionuclides in dependence of integration time (world population $1 \cdot 10^{10}$)

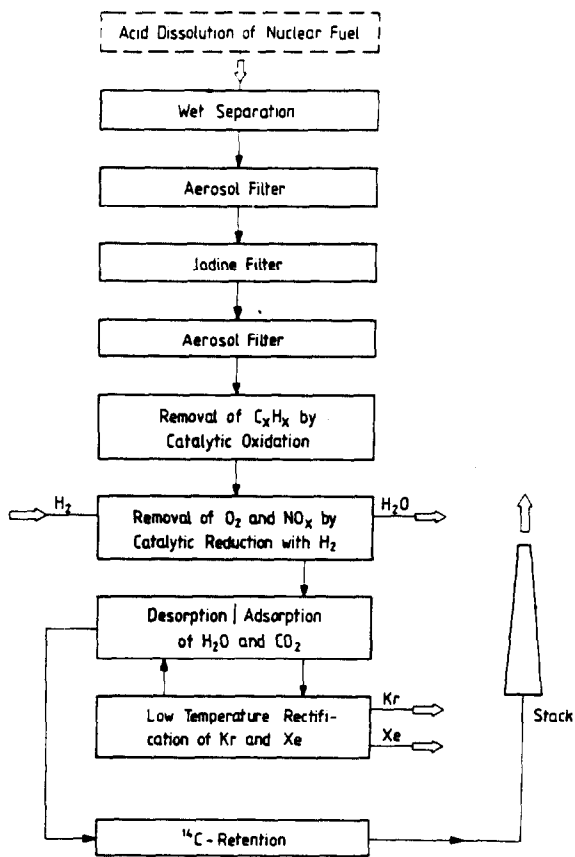
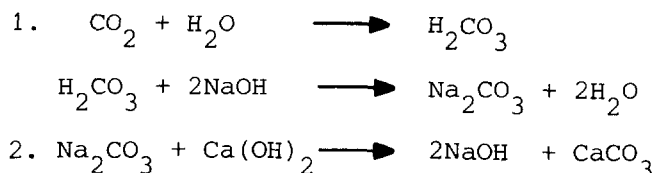


Fig. 5: Scheme for off-gas cleaning for a fuel reprocessing plant for LWR

IV. Methods for ^{14}C separation in reprocessing plants

As carried out in chapter II, in reprocessing plants the ^{14}C is practically released to 100 % as CO_2 into the dissolver-off gas during the dissolution of the fuel. For a reprocessing plant of 1400 t/a the dissolver-off gas amount is approx. 300 m^3/h . CO_2 is adsorbed at the molecular sieve beds installed in front of the low temperature rectification facility for ^{85}Kr separation, if a ^{85}Kr retention is assigned. Fig. 5 shows the conducting of the dissolver-off gas, as it had been designed in the "Entsorgungszentrum" Gorleben /41/. Here, the ^{14}C release occurs with regeneration gas (mainly N_2) of the molecular sieve beds. The CO_2 concentration in the nitrogen varies considerably during the regeneration phase. It mounts up to approx. 3600 vppm at the beginning of the regeneration and then slowly falls down to a few vppm at the end of the regeneration process.

The retention of CO_2 of the regeneration gas can be carried out by absorption in liquids /42/, /43/ or solids /44/, /45/, /46/. Because of the reliability of all operating conditions, the high separation degree, and the high standard of operating experience in the conventional chemical technique, the "double alkali process" has been chosen as reference process, which works according to the following chemical reactions:



The resulting CaCO_3 is chemically stable and after appropriate conditioning it is suitable for final disposal. The use of other alkali or earth alkali metals than Ca, e.g. Ba, is possible. In Argentine Barium is used for the ^{14}C retention of the heavy water moderated reactor Atucha II /40/.

V. Layout for a ^{14}C retention facility for a 1400 t/a reprocessing plant for LWR-fuel elements

The Federal Ministry of the Interior ordered to Linde AG, Werksgruppe TVT, München, a basic engineering of a ^{14}C retention facility according to the "double alkali process" in order to obtain from the industrial point of view technical data and realistic costs. In addition, the results from the Linde-engineering for a ^{85}Kr separation based on the low-temperature rectification /47/ should be taken into consideration and a suitable connection point at the dissolver-off gas system should be determined.

Fig. 5 shows a block diagram with ^{85}Kr separation by low-temperature rectification and ^{14}C retention. After the uranium dissolution the off-gas consists of air as carrier gas, aerosols, iodine, NO_x , Kr, Xe, CO_2 , C_xH_y and H_2O . First, the aerosols and the iodine compounds are separated in the aerosol- and iodine filter train. The hydrocarbons are removed by catalytic oxidation; oxygen and rest parts of NO_x are removed by catalytic reduction. H_2O and CO_2 are retained by the adsorption stretch. The pre-purified off-gas is then fed into the low temperature section which consists of two columns. The Kr-Xe-collecting in the bottom of the first column is separated in the second column, thus removing Kr as the head product from the top. The N_2 that appears at the top of the first column is used to regenerate the H_2O - and CO_2 -loaded adsorbers and is then fed into the ^{14}C retention facility. This connection point was chosen, because the iodine, aerosol as well as Kr-activity has been separated already and carbon 14 appears nearly exclusively as CO_2 . A rest volume of approx. 15 vppm CO results from the catalytic reduction of oxygen and NO_x that is carried out with surplus H_2 . Assuming a reprocessing plant with an annual capacity

17th DOE NUCLEAR AIR CLEANING CONFERENCE

of 1400 t uranium, the gas mixture entering the ^{14}C retention facility has the following compounds (at balance point \diamond of fig. 6):

N_2	0.0937 kg/s
CO_2 max.	(3650 vppm) 0.0006 kg/s
H_2O	$1.4 \cdot 10^{-4}$ kg/s
pressure	1.5 bar
temperature	approx. 573 K up to 283 K

In the heat exchanger, position 1, this gas mixture is cooled down to a temperature of approx. 313 K and is transported to the scrubbing column, position 2, together with the H_2O condensate produced there. In this packed tower the CO_2 is scrubbed with NaOH (6 wt %) up to a residue of approx. 15 vppm (achieved decontamination factor max. 240).

In the head of the column the water is condensed to saturation point at a temperature of approx. 288 K and a pressure of 1.47 bar. The leaving nitrogen is controlled regarding its CO_2 -contents, then heated up in the heat exchanger, position 1, (balance point \diamond), and mixed with other waste air it is emitted via the stack:

N_2	0.0937 kg/s
CO_2 max.	$2.45 \cdot 10^{-6}$ kg/s
H_2O	$0.69 \cdot 10^{-3}$ kg/s
pressure	1.47 bar
temperature	approx. 548 K up to 288 K

The lye circuit is maintained by a caustic solution pump, position 4. $9 \text{ m}^3/\text{h}$ caustic solution with a total volume of 2.25 m^3 are recycled in the washing circuit.

After about 9 days 62 % of the caustic solution is used. Up to this point it is guaranteed that the CO_2 content in the cleaned gas does not exceed 15 vppm.

The composition of the caustic solution which has been used to 62 % is:

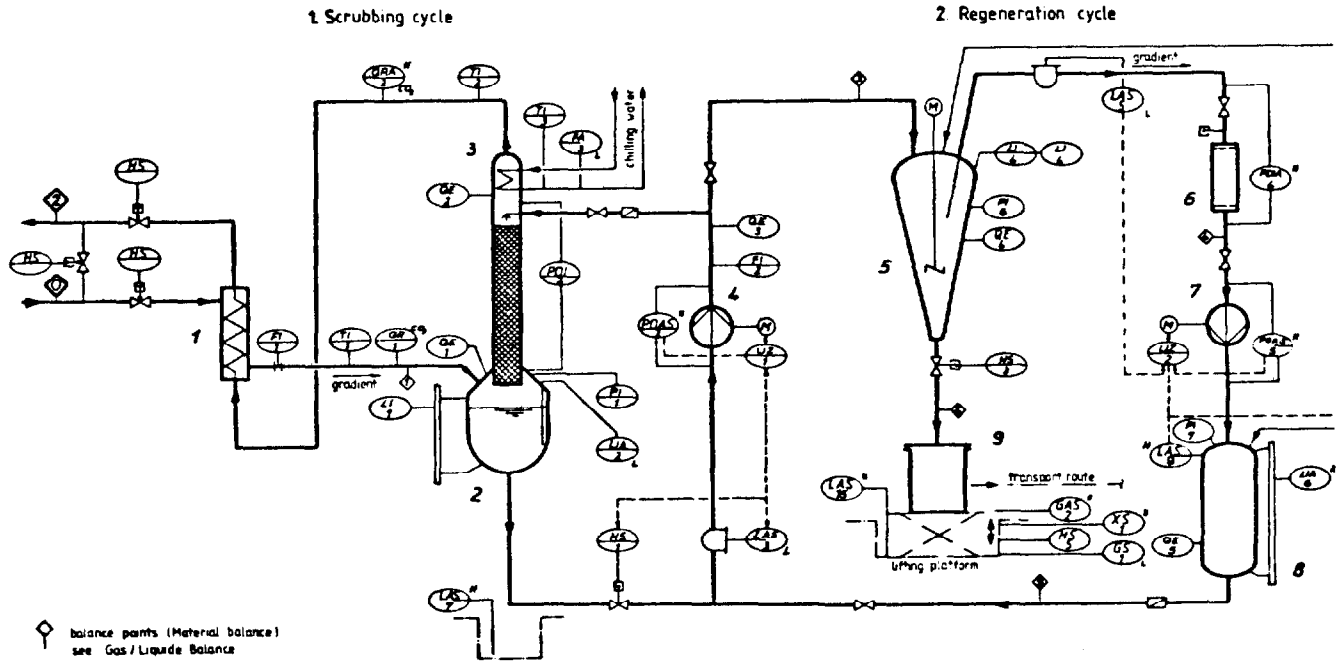
NaOH	54.7 kg
Na_2CO_3	118.4 kg
H_2O	1849.1 kg

This caustic solution is transported into the recovery stirring vessel, position 5, by the caustic solution pump. Then, with the same pump, a second charge of NaOH is drawn from the caustic solution vessel, position 8, in order to substitute the scrubbing solution to be regenerated. The addition of the fresh caustic solution is carried out during CO_2 -free operation. (Only during approx. 3 hours CO_2 is desorbed in an 8-hours cycle).

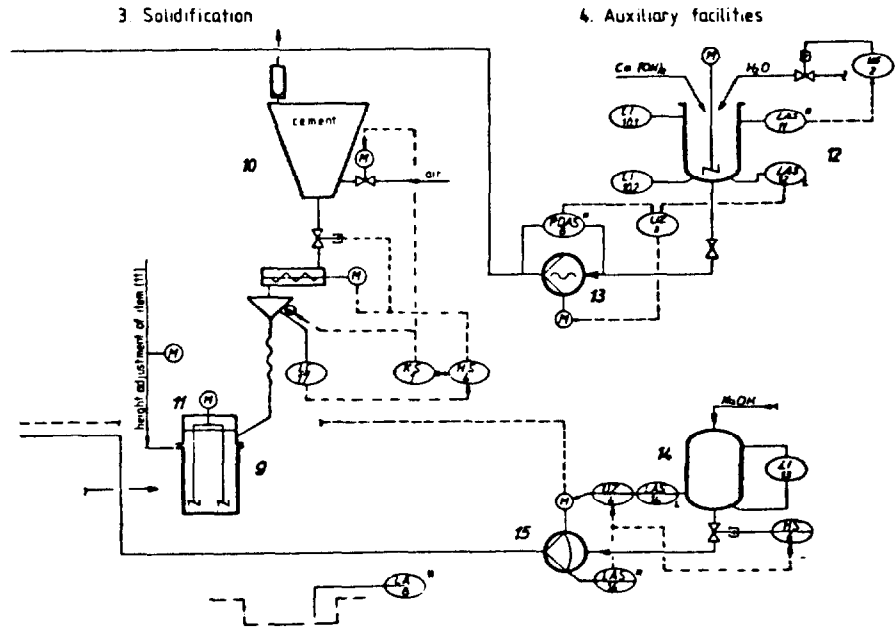
In the suspension stirring vessel, position 12, 74.5 kg of $\text{Ca}(\text{OH})_2$ are suspended in 434 kg H_2O which is then transported into the recovery stirring vessel by a spiral pump, position 13.

To avoid possible clogging of the scrubbing column by non-reacting $\text{Ca}(\text{OH})_2$ that remains in the caustic solution, the addition of $\text{Ca}(\text{OH})_2$ (90 %) is carried out non-stoichiometrically. Accordingly, a residue of Na_2CO_3 can be detected in the regenerated caustic solution.

17th DOE NUCLEAR AIR CLEANING CONFERENCE



1	2	3	4	5	6	7	8
Heat exchanger	Scrubbing column	Condenser	Lye pump	Regenerator	Filter	Lye pump	Lye storage tank



9	10	11	12	13	14	15
waste tank	Cement feed	Stirring apparatus	Suspension tank	Screw pump	Lye storage tank	Diaphragm metering pump

Fig. 6: Processing scheme of the ¹⁴C retention and solidification

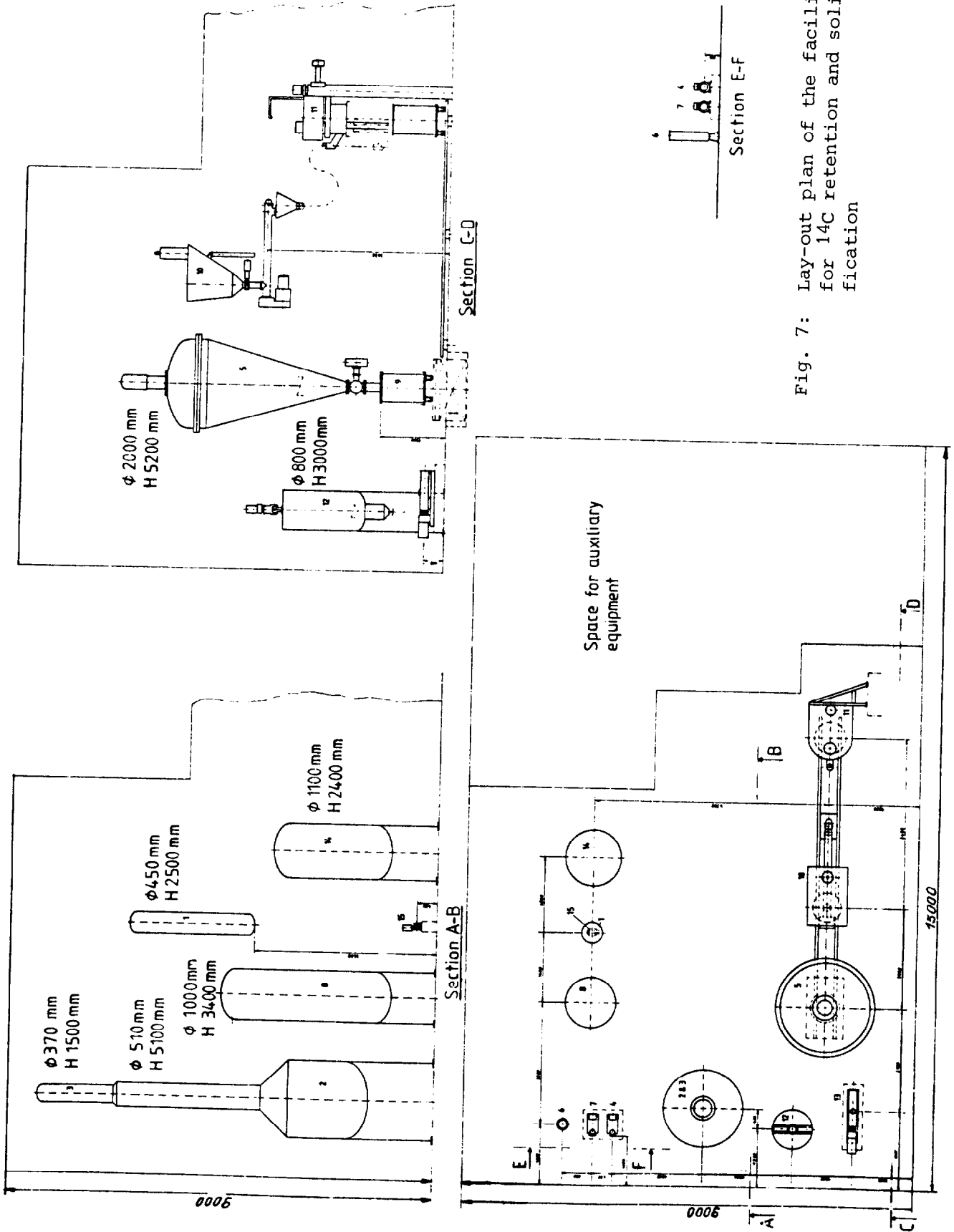


Fig. 7: Lay-out plan of the facility for ¹⁴C retention and solidification

17th DOE NUCLEAR AIR CLEANING CONFERENCE

When the stirring of approx. 1 hour is completed, the crystallized CaCO_3 floating in the caustic solution deposits to the bottom of the recovery stirring vessel. This deposition procedure is completed after approx. 2 hours. The regenerated caustic solution is pumped into the NaOH-vessel via a suction tube by the pump, position 7, except for a residue of approx. 70 kg (rest-moisture and caustic solution column). The retention of non-deposited CaCO_3 -particles within the lye is carried-out in the filter, position 6.

As a substitute of the remainder of the lye in the recovery stirring vessel, approx. 42 litres of soda lye (25 wt %) is pumped from the vessel, position 14, into the caustic solution storage with the aid of a metering pump, position 15. Thus, together with the caustic solution removed from the recovery stirring vessel, a 6 wt % fresh caustic solution is obtained.

After the removal described above, the waste to be solidified remains in the recovery stirring vessel with the following compounds:

NaOH	2.2 kg
Na_2CO_3	0.2 kg
H_2O	37.8 kg
CaCO_3	100.6 kg

Once the waste discharge has been completed, the waste container is transported to the mixing station, position 11, with the aid of a transfer car. There, 50 kg cement is metered off and added to the sludge in the waste container. The mixing of the waste material with the cement is carried-out with counter-current, intermeshing mixing elements, thus reaching all parts of the vessel.

After a mixing time of approx. 15 minutes, the mixing elements are turned aside and the vessel with the solidified waste and an activity of approx. 14 Ci are removed from the mixing station.

After the waste has been hardened, the vessel is closed and can be transported to a deposit.

The dimensions of the most important equipments and the space requirements of the complete facility can be taken from the lay-out plan in fig. 7.

The investment costs for this plant including installation and start-up amounts to approx. DM 6.1 million, taking into account the regulations, standards, and guidelines applicable to the construction and operation of nuclear facilities. The annual operation costs are approx. DM 1.1 million (cost index August 1982).

VI. Cold experiments for the "double alkali process"

In order to gain operating experiences, a testing facility according to the "double alkali process" has been built at the professorial chair for nuclear reactor technology of the technical university Aachen.

Experimental setup

Fig. 8 shows the flow scheme and Fig. 9 a photograph of the facility.

The gas which contains CO_2 (generally air with a CO_2 concentration of 330 vppm) flows - after having passed the pre-pressure regulation (1) - in reverse direction to the caustic solution through the caustic solution scrubber (2). If necessary, the CO_2 concentration can be varied via the feed-in (7). The adjustment of the gas mass flow is carried out via throttle (3) and flow meter (4). A part of the off-gas

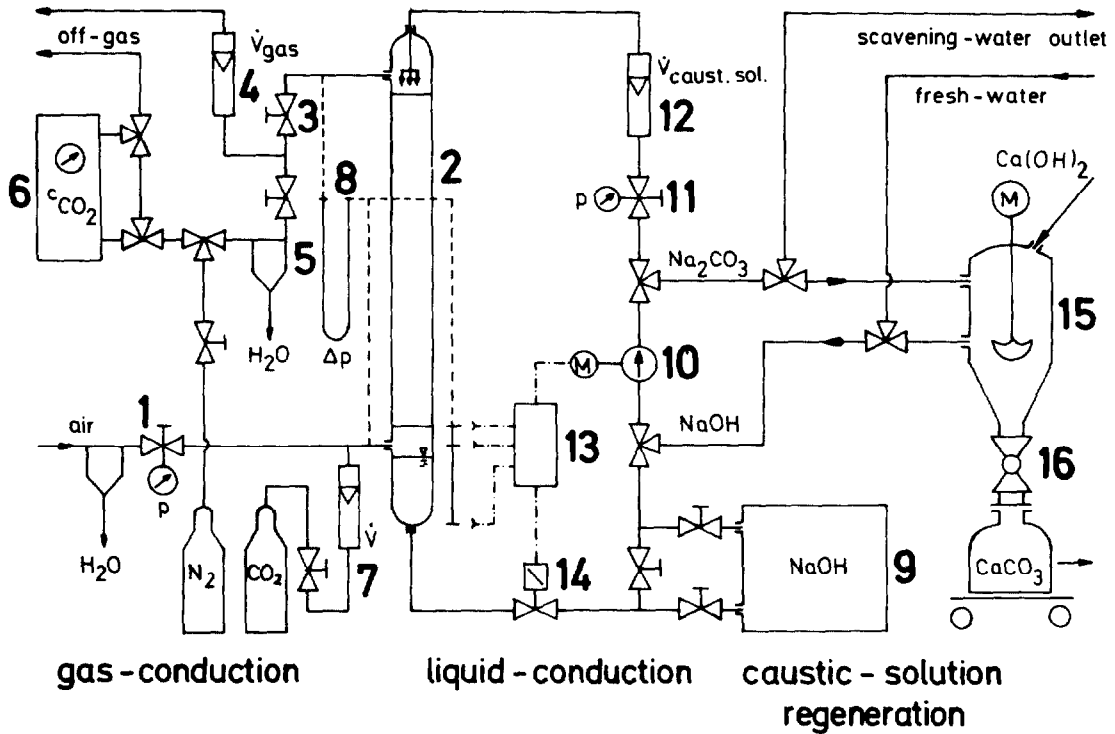
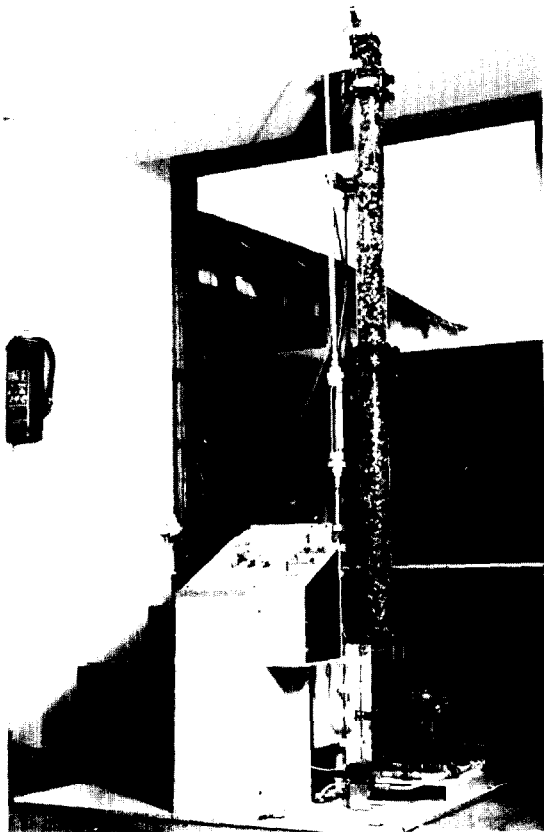


Fig. 8: Flow sheet of the experimental set-up for CO₂-separation



packing volume	: 15,9 l
diameter	: 100 mm
packing height	: 2000 mm
filling bodies	: Pall rings \emptyset 15 mm, stainless steel
caustic solution volume of the facility	: 120 l
caustic solution flow rate	: 0 - 700 l/h
gas flow rate	: 0 - 40 Nm ³ /h at 2.5 bars
CO ₂ -feed	: 0 - 86 Ndm ³ /h at 2.0 bars
design pressure	: 2.5 bars
volume recovery stirring vessel	: 120 l

Fig. 9: Photograph of the test facility with main data

17th DOE NUCLEAR AIR CLEANING CONFERENCE

is analyzed after a water separation (5) with an infrared gas analyzer (6) in order to determine the CO₂-rest concentration. The current resistance at the gas side is determined with the aid of an u-pipe manometer (8).

With the aid of a pump (10) the caustic solution is fed from the storage vessel (9) into the head of the column. The flow rate is regulated with a regulating valve with pressure indication (11) and a flow meter (12). The caustic solution discharge has been adapted to the inlet via an opto-electronical detector (13) and a magnetic valve (14). In danger of flooding, danger-off is initiated by the detector.

The regeneration facility which is made of the settling tank (15) with ball valve (16) for sediment deduction, Ca(OH)₂-feed-in and electric stirrer, is adapted to the caustic solution circuit in that way that a continuous as well as a discontinuous regeneration is possible. The inlet and outlet of further process media - e.g. cleaners - into as well as out of the caustic solution circuit is possible via intersecting points.

Test results

Fig. 10 shows some results for a constant CO₂-inlet concentration of 330 vppm. A better absorption reaction can be stated for higher pressures, higher caustic solution concentration and lower gas flow rate. Fig. 11 shows the mass transfer constant $K_G \cdot a$ of the facility according to the equation /41/:

$$G \cdot dy = K_G \cdot a \cdot p \cdot (y - y_G) \cdot dh \quad (1)$$

- G : gas load (kmol/h m² tower cross section)
K_G : mass transfer value on the gas side (kmol/h m² bar)
a : exchange surface in the scrubbing tower (m²/m³ tower volume)
p : total pressure (bar)
h : height of the exchange layer in the scrubbing tower
y : breaking up of the mole of the gas to be scrubbed out
Y_G : breaking up of the mole of the gas to be absorbed at the phase boundary layer in the gas.

The change of the mass transfer constant in dependence of the CO₂-inlet concentration, of the caustic solution flow rate, and the caustic solution concentration is shown in Fig. 12 for a constant pressure of 2 bars. Only a small decrease of the mass transfer constants can be stated for high CO₂-entering concentrations. If the caustic solution flow rate is increased, the mass transfer constant is improved.

Experiments showed that for an operating pressure of 2 bars and gas flow rates of 20 to 30 kg/h for the test facility used here, the optimum caustic solution concentration lies between 1.5n and 1.7n NaOH.

A further analysis was made in order to determine the flow processes in a packed column which is flown through by gas and trickling liquid in counterflow. The processes can be described very well with the aid of the flow pressure loss in dependence of the gas flow rate and the caustic solution flow rate. The caustic solution flow rate has been increased up to the flood point while keeping the gas flow rate constant. Fig. 13 shows the current density curves for 2 operation pressures with the gas speed as a parameter. Up to line AA no fundamental difference of the facility could be stated. After that the liquid volume mounts in the scrubbing tower. In process engineering line BB is called flood limit respectively highest dead load limit.

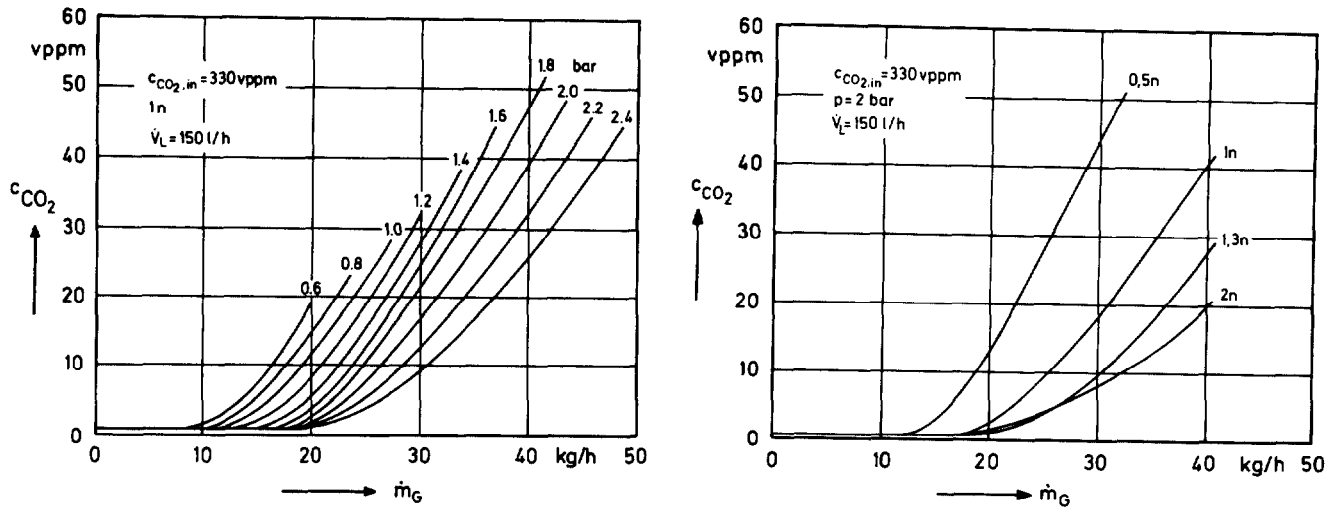


Fig. 10: CO₂ off-gas concentration c_{CO_2} in dependence of the gas flow rate \dot{m}_G , the pressure and the caustic solution concentration at a constant feed concentration of 330 vppm

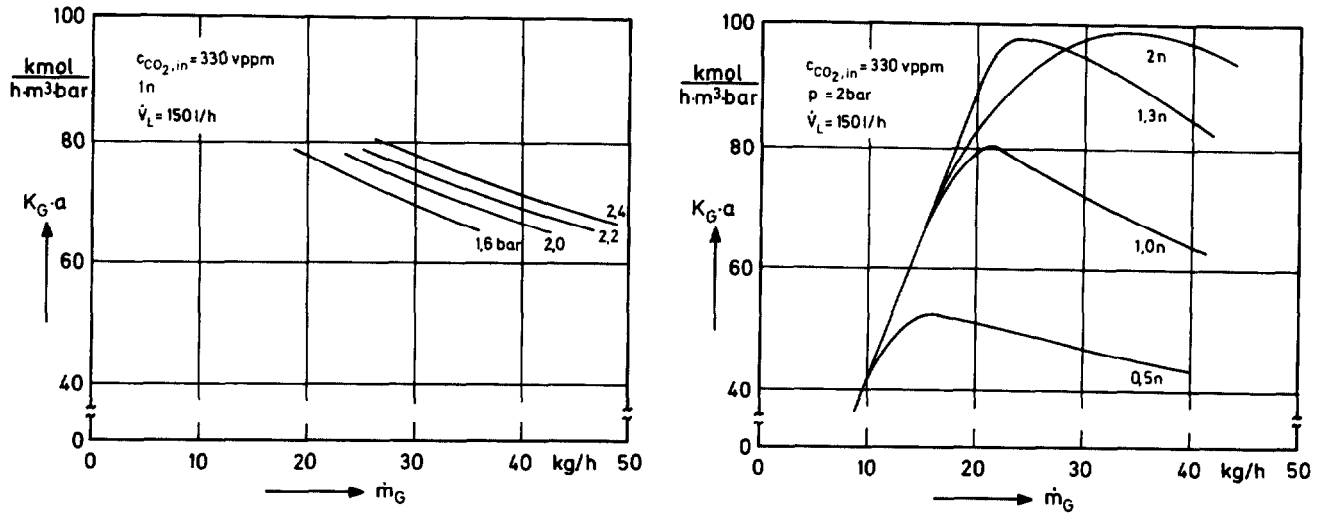


Fig. 11: Mass transfer constant $K_G \cdot a$ in dependence of the gas flow rate \dot{m}_G , the pressure and the caustic solution concentration at a constant feed concentration of 330 vppm

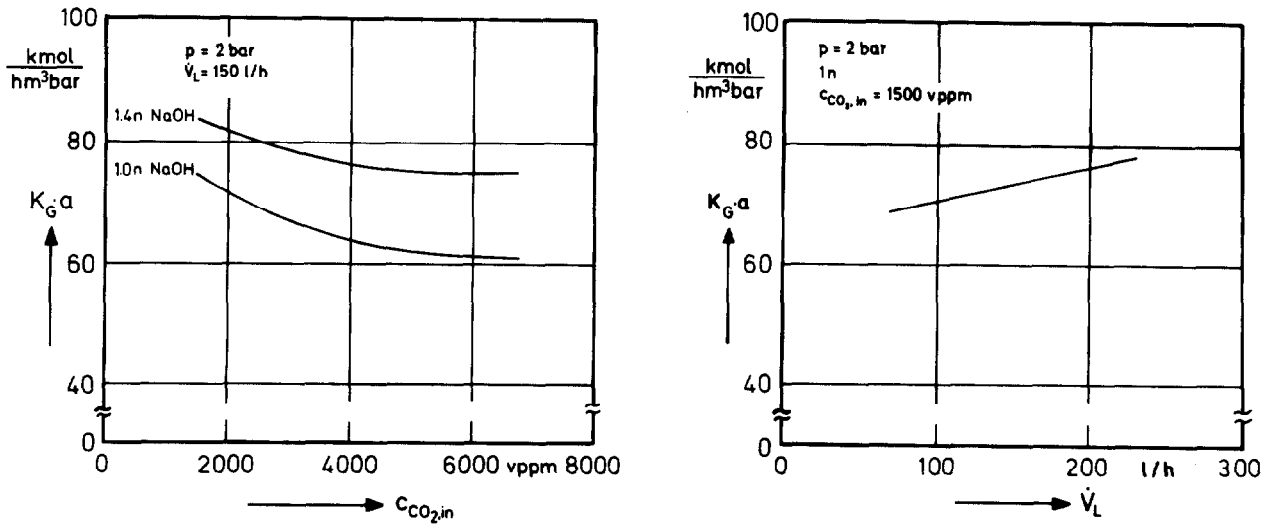


Fig. 12: Mass transfer constant $K_G \cdot a$ in dependence of the feed concentration c_{CO_2} , the caustic solution flow rate \dot{V}_L and the caustic solution concentration

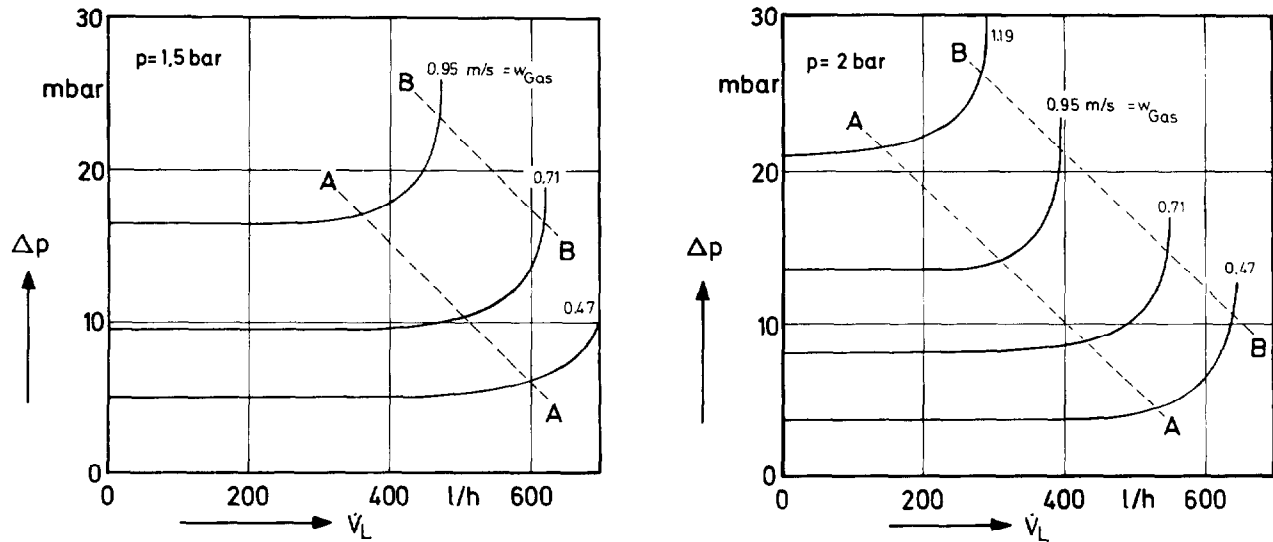


Fig. 13: Pressure drop Δp in dependence of the caustic solution flow rate \dot{V}_L

Operation behaviour

Extensive measurements to test normal behaviour and to determine operation parameters and a stationary long-time test of 200 hours at constant operating conditions (gas flow rate $20 \text{ Nm}^3/\text{h}$, caustic solution flow rate 150 l/h , facility pressure 1.5 bar) were carried out. The test facility is distinguished by the fact that it reacts nearly immediately selfregulating with additional feed, when outer interventions like e.g. change of the gas- and caustic solution flow rate respectively of the CO_2 concentration occur. This flexibility towards given operating conditions allows its use at varying demands. Because of the simple starting and stopping processes, it is also very suitable for discontinual operation. Undesired influences, like variations of pressure, which would have influenced the stationary behaviour, have been compensated with the advanced pressure regulator.

For discontinual operation the regeneration which is necessary in time intervals, allows a regular cleaning of the filling material column. Sedimentations on filling materials and on the bottom of the storage bunker were removed with repeated scrubbing with water. The impurity of the facility, however, remained within certain limits. Even after numerous regeneration periods a CaCO_3 sedimentation could not be noticed. Because of the very good solubility of Na(OH)_2 the danger of obstruction of the filling material column did never occur.

Regeneration of the used caustic solution

In order to determine the optimum process conduction for caustification parameter studies were carried out. The analysis of the sedimentation behaviour of the CaCO_3 were of particular interest. The studies were carried out in a sedimentation vessel - according to Imhoff - with a content of 1000 ml .

After the reaction participants had been mixed with the aid of air stirrers or with electric stirrers, a compression zone was built nearly without transition in about 30 s (no sedimentation zone). The hydrous Na-solution above this zone is clear.

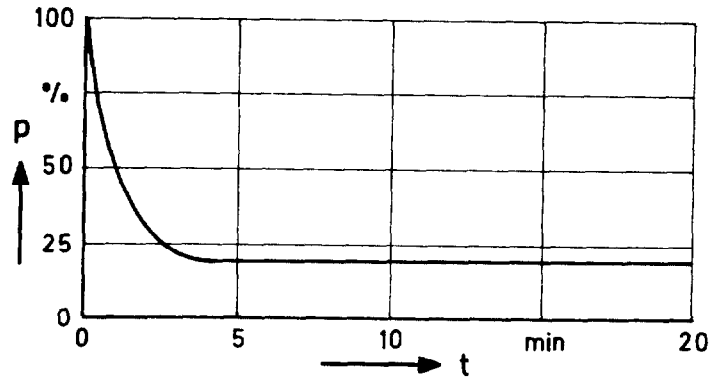


Fig. 14: Conversion in the compression zone, if 1 l poudorous 0.5 mol $\text{Ca}(\text{OH})_2$ is added to 0.5m Na_2OH -solution ans is mixed for 1 minute

Fig. 14 shows e.g. the reaction in the compression zone, if 1 l 0.5m- Na_2CO_3 -solution with 0.5 mol pulverized $\text{Ca}(\text{OH})_2$ is regenerated and mixed for 1 minute with the aid of an air stirrer.

The caustifications carried out in the test time showed that 20 minutes after the stirring period the bottom body is comprised to 80 % of the final density in the liquid. The final density was achieved after approx. 24 hours. The regenerated caustic solution above the bottom body can already be sucked off 20 minutes after the stirring operation is finished and is so clear that it can again be fed into the caustic solution circuit without further filtering. Experiments showed that even after 200 hours CaCO_3 flowed off without problems as viscous mud.

Conditioning for final disposal

It has to be guaranteed by conditioning and final disposal of the precipitated CaCO_3 that ^{14}C is sealed off biosphere for a period of approx. 50.000 years (that is approx. tenfold half life period). The secure sealing off is mainly detracted from two effects: possible solution of CaCO_3 in water which contains CO_2 constituting $\text{Ca}(\text{HCO}_3)_2$; possible exchange of isotopes with C-compounds in other phases, particularly with atmospheric ^{12}C .

Taking these effects into consideration, the above-ground final disposal and the dumping into the deep sea are not suitable for the final disposal of ^{14}C . The best is the final disposal in salt rock. Actually the salt dome in Gorleben is analyzed to determine its suitability for the final disposal of radioactive material in the Federal Republic of Germany.

For final disposal CaCO_3 is homogenized with cement glue and filled into flange top casks, where the mixture can harden. After that the casks are placed into the underground final depot. The conditioning, packing and final disposal is carried out together with the final treatment of the remaining radioactive waste. Approx. 7 m^3/a of waste containing ^{14}C with a specific activity of approx. 65 Ci ^{14}C per m^3 result from ^{14}C retention.

References

- /1/ Bonka, H., Schwarz, G., Wibbe, H.-B.:
Umweltbelastung durch in Hochtemperaturreaktoren entstandenen Kohlenstoff 14;
Kerntechnik 15 No.7 (1973), S. 297-300

17th DOE NUCLEAR AIR CLEANING CONFERENCE

- /2/ Bonka, H., Brüssermann, K., Schwarz, G.:
Umweltbelastung durch Radiokohlenstoff aus kerntechnischen Anlagen;
Reaktortagung, Berlin (1974), S. 454-457
- /3/ RSK und SSK:
Grundsätzliche sicherheitstechnische Realisierbarkeit des Entsorgungszentrums,
Beurteilung und Empfehlung der Reaktor-Sicherheitskommission (RSK) und der
Strahlenschutzkommission (SSK);
Köln, Gesellschaft für Reaktorsicherheit (1977)
- /4/ Horn, H.-G., Gründler, D., Bonka, H.:
Kosten-Nutzen-Analyse zur Rückhaltung radioaktiver Stoffe in Kernkraftwerken
und Wiederaufarbeitungsanlagen;
Bericht zum Forschungsvorhaben St.Sch. 680a, RWTH Aachen (1982) (Bericht in
Vorbereitung)
- /5/ Horn, H.-G., Bonka, H., Gründler, D.:
Will the Cost-Benefit Analysis Give an Additional Decision-Aid to the Reten-
tion of Radioactive Effluents in Nuclear Facilities?
IAEA-SM-258/3 (1981)
- /6/ Gründler, D., Michaelis, W., Hunsänger, K., Bonka, H.:
Versuchsanlage zur Rückhaltung von C 14 bei Wiederaufarbeitungsanlagen für
LWR-Brennelemente nach dem "Doppelten Alkali-Prozeß";
Bericht zum Forschungsvorhaben St.Sch. 680a, RWTH Aachen (1982) (Bericht in
Vorbereitung)
- /7/ Bonka, H., Brüssermann, K., Schwarz, G., Willrodt, U.:
Production and Emission of Carbon-14 from Nuclear Power Stations and Repro-
cessing Plants and its Radioecological Significance;
IV. IRPA Congress, Paris (1977), Vol. 3, S. 945-947
- /8/ Hayes, D.W., Mac Murdo, K.W.:
Carbon 14 Production by the Nuclear Industry;
Savannah River Laboratory, Aiken, South Carolina, DP-MS-74-33 (1975)
- /9/ Hayes, D.W., Mac Murdo, K.W.:
Carbon-14 Production by the Nuclear Industry;
Health Physics 32 (1977), S. 215-219
- /10/ Kelly, G.N., Jones, J.A., Bryant, P.M., Morley, F.:
The Predicted Radiation Exposure of the Population of the European Community
Resulting from Discharges of Krypton-85, Tritium, Carbon-14 and Iodine-129
from the Nuclear Power Industry to the Year 2000;
Commission of the European Communities, Doc.V/2676/75 (1975)
- /11/ Fowler, T.W., Clark, R.L., Gruhlke, J.M., Russel, J.L.:
Public Health Considerations of Carbon-14 Discharges from the Light-Water-
Cooled Nuclear Power Reactor Industry;
USEPA, ORP/TAD-76-3, Washington, D.C. (1976)
- /12/ Skafi, M.:
Bestimmung der C 14-Aktivität in der Abluft von deutschen und ausländischen
Leichtwasserreaktoren (LWR) und die daraus resultierende Strahlenbelastung;
KWU-Bericht R 315-12-1976 (1976)

17th DOE NUCLEAR AIR CLEANING CONFERENCE

- /13/ Olsson, G.:
C 14-Bildning i Kraftreaktorer, Aktiebolaget Atomenergi;
Studsvik, Nyköping, Schweden, S-541 (1976)
- /14/ Davis, W.Jr.:
Carbon-14 Production in Nuclear Reactors;
ORNL/NUREG/TM-12 (1977)
- /15/ UNSCEAR:
Sources and Effects of Ionizing Radiation;
United Nations (1977)
- /16/ Bonka, H.:
Produktion und Freisetzung von H 3 und C 14 durch Kernwaffenversuche und
kerntechnische Anlagen, einschließlich Wiederaufarbeitungsanlagen;
in: Strahlenschutzprobleme im Zusammenhang mit der Verwendung von Tritium
und Kohlenstoff 14 und ihren Verbindungen;
Institut für Strahlenhygiene des Bundesgesundheitsamtes, STH-Bericht 12/1980
(1980) S. 17-26
- /17/ Martin, H.:
Bildung von C 13 und C 14 in wassergekühlten Reaktoren;
KWU-Bericht R 513 - 198/75 (1975)
- /18/ Apelqvist, G.:
Beräkning av ¹⁴C-Bildningen i Lättvattenreaktorer
Vattenfall PM ER-27/75 (1975-09-17)
Vattenfall PM ER-35/75 (1975-11-19)
- /19/ Kabat, M.J.:
Monitoring and Removal of Gaseous Carbon-14 Species;
15th DOE Nuclear Air Cleaning Conference (1978)
- /20/ Kabat, M.J.:
Ontario Hydro, Canada, private Mitteilung (1979)
- /21/ Bonka, H.:
C 14-Produktionsrate in Schwerwasserreaktoren;
(1978), (unveröffentlicht)
- /22/ Brooks, L.H., Heath, C.A., Kistein, B., Roberts, D.G.:
Carbon-14 in the HTGR Fuel Cycle;
GA-A 13174, UC-77 (1974)
- /23/ Magno, P.J., Nelson, C.B., Ellett, W.H.:
A Consideration of the Significance of Carbon-14 Discharges from the Nuclear
Power Industry;
in: Proceedings of the Thirteenth AEC Air Cleaning Conference, San Francisco,
1974, U.S. Atomic Energy Commission report CONF-740807 (1975) S. 1047-1054
- /24/ Schwarzer, K.:
Abschätzung der C 14-Produktion in einem Hochtemperaturreaktor im Hinblick
auf die Wiederaufarbeitung;
Reaktortagung, Düsseldorf 30. März - 2. April (1976) S. 518-521

17th DOE NUCLEAR AIR CLEANING CONFERENCE

- /25/ Till, J.E., Bomar, E.S., Morse, L.E., Tennery, V.J.:
A Radiological Assessment of Reprocessing Advanced Liquid-Metal Fast Breeder Reactor Fuels;
Nuclear Technology, Vol. 37 (1978) S. 328
- /26/ Young, J.R.:
Fusion Reactor Environmental Effects;
in: Pacific Northwest Laboratory Report on Fusion Energy, July 1976 - September 1976, BNWL - 1939-5
- /27/ Kunz, C.O., Mahoney, W.E., Miller, T.W.:
C 14 Gaseous Effluents from Pressurized Water Reactors;
8. Midyear Topical Symposium, Knoxville, CONF-741018 (1974)
- /28/ Kunz, C.O., Mahoney, W.E., Miller, T.W.:
C 14 Gaseous Effluents from Boiling Water Reactors;
ANS Meeting, New Orleans (1975)
- /29/ Schüttelkopf, H.:
Die Emission von $^{14}\text{CO}_2$ mit der Abluft kerntechnischer Anlagen;
KfK 2421 (1977)
- /30/ Schüttelkopf, H., Herrmann, G.:
 $^{14}\text{CO}_2$ - Emissionen aus der Wiederaufarbeitungsanlage;
Seminar on Radioactive Effluents from Nuclear Fuel Reprocessing Plants,
Commission of the European Communities, Karlsruhe (1977) S. 189-201
- /31/ Riedel, H., Gesewsky, P., Schwibach, J.:
Untersuchungen über die Emission von Kohlenstoff-14 mit der Abluft aus Kernkraftwerken;
Institut für Strahlenhygiene des Bundesgesundheitsamtes, STH-Bericht 13/76 (1976)
- /32/ Riedel, H., Gesewsky, P.:
Zweiter Bericht über Messungen zur Emission von Kohlenstoff 14 mit der Abluft aus Kernkraftwerken mit Leichtwasserreaktor in der Bundesrepublik Deutschland;
Institut für Strahlenhygiene des Bundesgesundheitsamtes, STH-Bericht 13/77 (1977)
- /33/ Bonka, H.:
Berechnung der Dosiswerte nach dem spezifischen Aktivitätsmodell für H 3 und C 14;
Symposium "Strahlenschutzprobleme im Zusammenhang mit der Verwendung von H 3 und C 14 und ihren Verbindungen" (1979), Institut für Strahlenhygiene des Bundesgesundheitsamtes, SHT-Bericht 12/1980 (1980), S. 129-136
- /34/ Bonka, H., Gründler, D., Hesel, D., Münster, M., Schmidlein, P., Sünder, B.:
Radiologische Auswirkungen der Emissionen aus Wiederaufarbeitungsanlagen im bestimmungsgemäßen Betrieb;
Seminar on Radioactive Effluents from Nuclear Fuel Reprocessing Plants,
Commission of the European Communities, Karlsruhe (1977) S. 219-246
- /35/ Bonka, H.:
Strahlenexposition durch radioaktive Emissionen aus kerntechnischen Anlagen im Normalbetrieb;
Verlag TÜV Rheinland (1982)

17th DOE NUCLEAR AIR CLEANING CONFERENCE

- /36/ ICRP:
Recommendations of the International Commission on Radiological Protection;
ICRP Publication 26, Pergamon Press, Oxford (1977)
- /37/ Gründler, D.:
Kosten-Nutzen-Analysen zur Rückhaltung von Tritium, C 14 und Krypton 85 aus
Wiederaufarbeitungsanlagen für LWR-Brennelemente;
Dissertation RWTH Aachen (1981)
- /38/ Horn, H.-G.:
Einfluß verschiedener Dosisbegrenzungskonzepte auf die Rückhaltung von Aero-
solen und Jod bei Wiederaufarbeitungsanlagen;
Dissertation RWTH Aachen (in Vorbereitung)
- /39/ Bonka, H., Gründler, D., Horn, H.-G.:
Use of Optimization Methods in the Field of Radiation Protection for Nuclear
Facilities; Radiation Protection Optimization - Present Experience and Methods;
Proceedings of the European Scientific Seminar held in Luxembourg, Pergamon
Press (1979), S. 112-152
- /40/ Beninson, D.J., González, A.J.:
Application of the Dose Limitation System to the Control of Releases of Car-
bon-14 from Heavy Water Moderated Reactors;
IAEA-SM-258/53 (1981)
- /41/ DWK:
Bericht über das in der Bundesrepublik Deutschland geplante Entsorgungszentrum
für ausgediente Brennelemente aus Kernkraftwerken;
Deutsche Gesellschaft für Wiederaufarbeitung von Kernbrennstoffen mbH,
Hannover (1977)
- /42/ Ullmanns:
Encyklopädie der technischen Chemie - Verfahrenstechnik I;
Verlag Chemie, Weinheim (1977), S. 575-585
- /43/ Schmidt, P.C.:
Alternativen zur Verminderung der C 14-Emissionen bei der Wiederaufarbeitung
von HTR-Brennelementen;
JÜL-1567 (1979)
- /44/ Von der Decken, C.B., Engel, R., Lange, G., Rausch, W.:
Untersuchungen zur Gasreinigung des THTR-Reaktors;
EURATOM 10.5, 1327 (1966)
- /45/ Haag, G.L.:
Carbon-14 Immobilization via the $\text{CO}_2\text{-Ba(OH)}_2$ Hydrate Gas-Solid Reaction;
16th DOE Nuclear Air Cleaning Conference (1981)
- /46/ Cheh, C.H., Glass, R.W., Chew, V.S.:
Removal of Carbon-14 from Gaseous Streams;
IAEA-SM-72/O7 (1982)
- /47/ Gutowski, H., Schröder, E.:
Angewandte Tieftemperatur-Technik zur Kryptonabscheidung in Wiederaufarbei-
tungsanlagen unter kerntechnischen Bedingungen;
Atomenergie, Kerntechnik Bd. 33 (1979), S. 277-280
- /48/ Croff, A.G.:
An Evaluation of Options Relative to the Fixation and Disposal of ^{14}C -Con-
taminated CO_2 as CaCO_3 ;
ORNL/TM-5171 (1976)

MECHANISM OF THE $\text{CO}_2\text{-Ca(OH)}_2$ REACTION

V.S. Chew, C.H. Cheh and R.W. Glass
 Ontario Hydro Research Division
 800 Kipling Avenue
 Toronto, Ontario, Canada M8Z 5S4

Abstract

Recent studies clearly showed the importance of moisture in achieving high Ca(OH)_2 absorbent utilization for removing CO_2 from gas streams at ambient temperatures. However, the role of moisture and the mechanism of the reaction was not well understood. This paper summarizes the results of a study of the mechanism of the $\text{CO}_2\text{-Ca(OH)}_2$ reaction with emphasis on the role of moisture. The reaction between Ca(OH)_2 and CO_2 in moist N_2 was found to be first order with respect to the reactants with a rate constant of about 100 min^{-1} . At high humidities, the rate of reaction was chemically controlled, but at low humidities, the reaction rate was limited by the diffusion through the carbonate layer formed by the reaction. Calculations showed that capillary condensation could have occurred only in about 2% of the pore volume and was unlikely to have affected the reaction rate significantly by allowing the reaction to occur in the liquid phase. It was, therefore, concluded that the main role of moisture was to improve the Ca(OH)_2 utilization by lowering the resistance to diffusion through the carbonate layer.

Nomenclature

C_A	= concentration of gas phase reactant A
k	= rate constant
k_g, k_d, k_s	= rate constants
R	= particle radius
t	= reaction time
T_5	= time at 5% breakthrough
X	= fraction of gas at bed outlet
X_B	= fraction conversion of B
ρ_B	= molar density of B in the solid
τ	= time/(time at $X = 0.5$)
\emptyset	= bed volume/volumetric gas flow

I. Introduction

Recently we presented performance data on an ambient temperature, fixed bed, $\text{Ca}(\text{OH})_2$ absorber developed to remove $^{14}\text{CO}_2$ from the moderator cover gas system of CANDU nuclear reactors.⁽¹⁾ During the development of this process the importance of moisture in achieving high absorbent utilization and, to some extent, removal efficiency, was clear; however the role of moisture in the reaction was not. The present work was conducted to study the mechanism of the reaction, with particular emphasis on the role of moisture.

II. Previous Studies

The reaction of CO_2 with a suspension of $\text{Ca}(\text{OH})_2$ in water has been well studied since early this century⁽²⁾. The absorption of CO_2 by dry sorbents, in particular soda lime, has been known for many years and this material is widely used today in medical anaesthetic applications and has been extensively studied in divers' re-breather apparatus⁽³⁾. Nevertheless, the mechanism of the reaction between CO_2 and soda-lime is not well understood. $\text{Ca}(\text{OH})_2$ has been used at elevated temperatures to absorb CO_2 ⁽⁴⁾⁽⁵⁾ but the mechanism was not well understood. $\text{Ba}(\text{OH})_2$ has been studied by Haag et al⁽⁶⁾ where again moisture appears to play an important role in the mechanism of the reaction.

Theory

For the reaction:



a first order reaction in a fixed bed reactor is given by⁽⁷⁾:

$$\ln \frac{X}{1-X} = k\theta(\tau - 1) \quad (2)$$

Thus a plot of $\ln(X/(1-X))$ versus $(\tau - 1)$ will give a straight line of slope k , the rate constant.

To identify the rate controlling step in the reaction, the "shrinking unreacted core" model appears to be appropriate⁽⁸⁾. In this model, the major controlling resistances are, gas film diffusion, diffusion through product layer and chemical reaction.

Gas film diffusion is given by:

$$t = \frac{\rho_B R}{3b k_g C_A} \cdot X_B \quad (3)$$

Diffusion through product:

$$t = \left(\frac{1}{2} - \frac{1}{3}X_B - \frac{1}{2}(1 - X_B)^{2/3} \right) \frac{\rho_B R}{b k_d C_A} \quad (4)$$

Chemical reaction:

$$t = (1 - (1 - X_B)^{1/3}) \frac{\rho_B R}{b k_s C_A} \quad (5)$$

Although the gas film resistance remains unchanged throughout the reaction, the resistance to chemical reaction increases as the surface of the unreacted core decreases and the resistance to diffusion through the product layer increases as the product layer builds up. The mean rate constant, \bar{k} , defined as the average over the time necessary for the reaction to go to completion, is given by (8)

$$\bar{k} = \frac{1}{1/k_g + 1/k_d + 3/k_s} \quad (6)$$

\bar{k} can be calculated if k_g , k_d and k_s are known. k_g , k_d and k_s can be calculated from Equations (3), (4) and (5). It should be noted that the mean rate constant, \bar{k} , and the rate constant, k , from Equation (2) are related to each other by the total surface area in a unit volume of packed bed⁽⁹⁾.

III. Experimental Studies

The Ca(OH)_2 was prepared using a technique described earlier⁽¹⁾. The physical characteristics of the Ca(OH)_2 are listed in Table I and a typical chemical composition, determined by a thermal gravimetric analyzer (TGA), is shown in Table II. The pore size distribution of the absorbent by volume and by area is plotted in Figures 1 and 2, respectively.

Table I Calcium hydroxide characteristics.

Bulk density	0.56 kg/L
Particle size	-2.38 + 0.50 mm
Apparent (skeletal) density	197 kg/L
BET surface area	28.5 m ² /g
Total intrusion volume	1.29 mL/g
Total pore area	36.1 m ² /g
Median pore diameter (volume)	2.46 μm
Median pore diameter (area)	11.1 nm
Porosity	0.718

17th DOE NUCLEAR AIR CLEANING CONFERENCE

Table II Thermal gravimetric analysis of $\text{Ca}(\text{OH})_2$ samples(1).

	Moisture (g/kg)	$\text{Ca}(\text{OH})_2$ (g/kg)	CaCO_3 (g/kg)	CaO (g/kg)
February, 1981	13	906	57	24
	13	877	86	33
March, 1981	13	898	57	33
July, 1981	21	923	18	38
	16	898	45	50
	13	894	50	43
	12	906	52	30
March, 1982	16	896	51	37

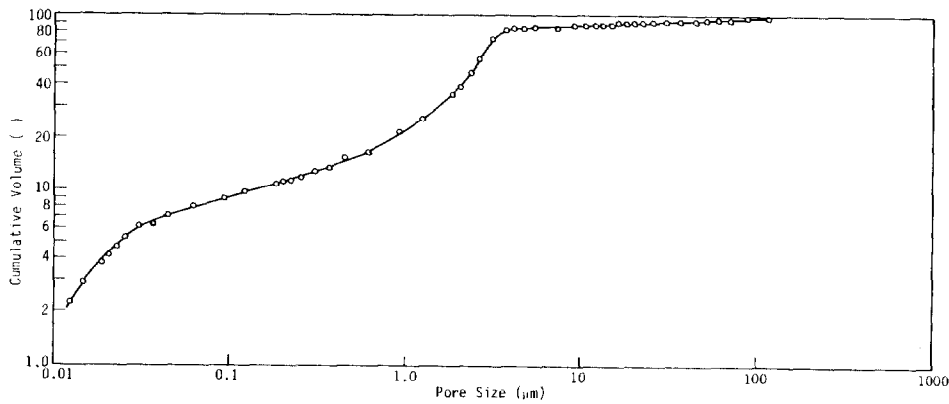


FIGURE 1
PORE SIZE DISTRIBUTION (BY VOLUME) OF $\text{Ca}(\text{OH})_2$ ABSORBENT

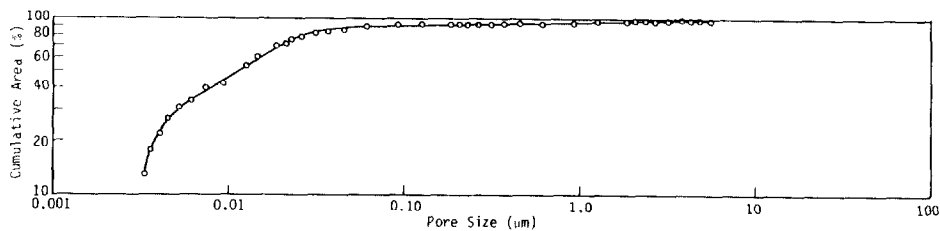


FIGURE 2
PORE SIZE DISTRIBUTION (BY AREA) OF $\text{Ca}(\text{OH})_2$ ABSORBENT

Procedure

A bench scale flow reactor described earlier⁽¹⁾ was used to determine the breakthrough characteristics of the $\text{Ca}(\text{OH})_2$ bed to test the assumption of a first order reaction between CO_2 and the number of moles of $\text{Ca}(\text{OH})_2$ available for reaction per unit bed volume (Equation 2).

The rate constants k_g , k_d and k_s were determined using thermal gravimetric analysis. For these experiments, about 50 mg of $\text{Ca}(\text{OH})_2$ particles (-2.38 + 2.00 mm) were supported on glass wool on the microbalance pan. Moist nitrogen gas was then passed through the system for about one hour to hydrate any remaining CaO present in the $\text{Ca}(\text{OH})_2$ sample and to condition the sample. A N_2/CO_2 mixture was then passed through a water bath and the humidity of the gas stream measured using a dewpoint hygrometer (General Eastern; model 1100AP). This humidified stream entered the microbalance system and the weight change of the $\text{Ca}(\text{OH})_2$ sample was recorded continuously at constant temperature until no further change in weight was observed. The used sample was then transferred to a platinum pan and analyzed for its chemical composition using the TGA.

IV. ResultsOrder of Reaction

The data from bench scale experiment No L-32 (see Table III) were used to construct a plot of $\ln(X/X-1)$ versus $(\tau-1)$ to test the validity of Equation 2 for the reaction. Figure 3 shows that the experimental data fit Equation 2, hence the reaction is first order with respect to the two reactants and the rate constant, k , is 100 min^{-1} .

Table III Summary of bench scale experimental conditions and results.

Experiment No	Gas Flow Rate (ℓ/min)	CO_2 Concentration ($\mu\ell/\ell$)	Bed Height (cm)	Utilization at T_5 (g/kg)	Length of Unused Bed, (LUB) (cm)	Bed Height / LUB
L-13	2.0	330	4.5	495	2.0	2.25
L-20	1.6	308	4.0	538	1.6	2.5
L-21	4.0	300	3.8	101	3.4	1.1
L-22	1.0	300	1.9	514	0.81	2.3
L-23	4.0	305	7.6	550	3.0	2.5
L-32	2.0	415	8.0	660	2.0	4.0

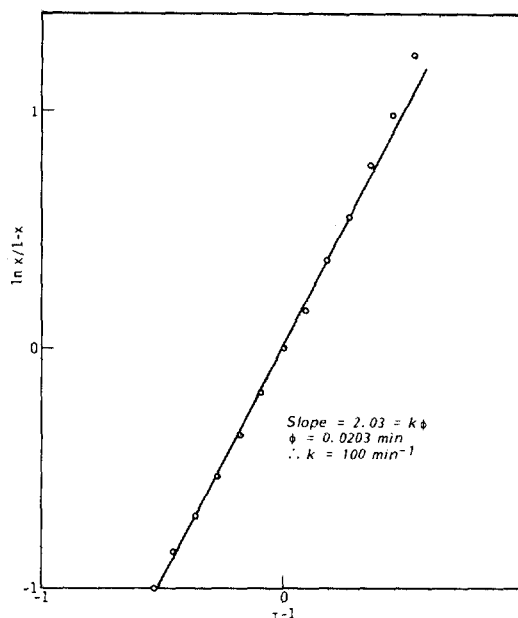


FIGURE 3

DETERMINATION OF REACTION ORDER AND RATE CONSTANT

Rate Controlling Step

Bench scale experiments (Nos L-13, L-22 and L-23) were conducted at a constant gas residence time (0.6 s) but different flow rates (1 to 4 l/min). The results summarized in Table III show that the $\text{Ca}(\text{OH})_2$ utilization remained the same for the gas flow rates studied indicating that gas film resistance does not influence the rate of the reaction.

Typical data obtained from TGA experiments at high humidities and CO_2 concentrations of $400 \mu\text{l/l}$ are shown in Figures 4 to 6. The results show that there is a linear relationship between $1 - (1 - X_B)^{1/3}$ and time; ie, the reaction rate is chemically controlled (Equation 5) depending mainly on the surface area of the unreacted $\text{Ca}(\text{OH})_2$. It is only in the latter stages of the reaction that the $(1/2 - 1/3 X_B - 1/2 (1 - X_B)^{2/3})$ versus t plot becomes linear; ie, the resistance caused by diffusion through the carbonate layer becomes significant. It is primarily because of this resistance that only $\sim 850 \text{ g/kg}$ of $\text{Ca}(\text{OH})_2$ is reacted at the end of typical TGA experiments.

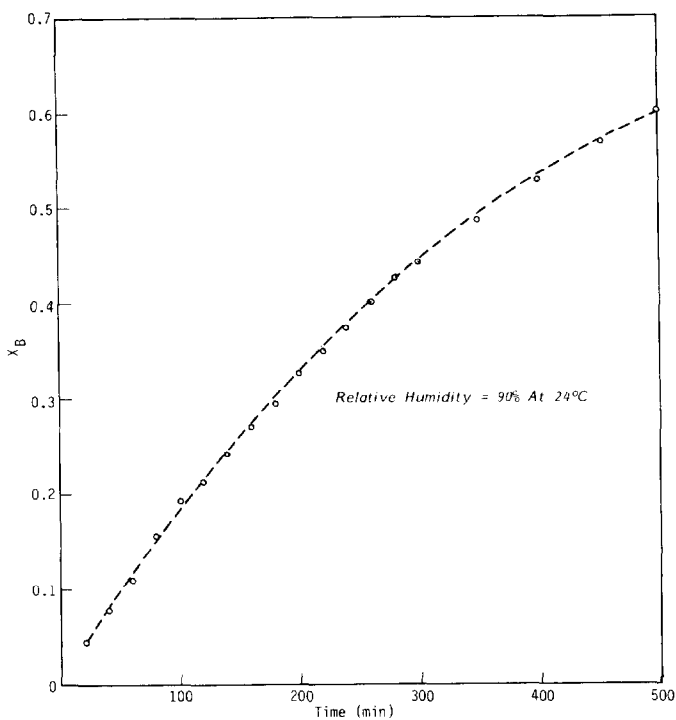


FIGURE 4

DETERMINATION OF RATE CONTROLLING STEP FOR HIGH HUMIDITY EXPERIMENT (G642) (ASSUMING GAS DIFFUSION CONTROLLED)

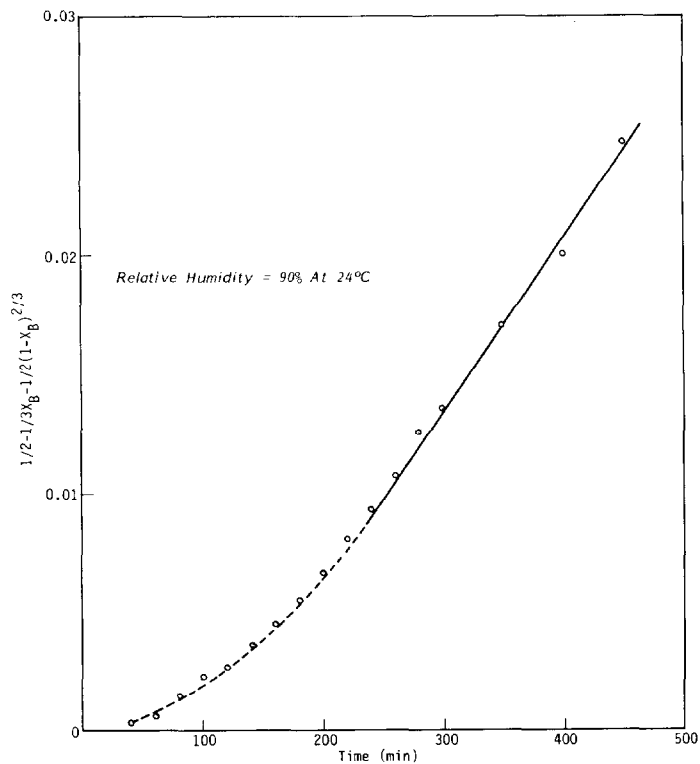


FIGURE 5

DETERMINATION OF RATE CONTROLLING STEP FOR HIGH HUMIDITY EXPERIMENT (G642) (ASSUMING DIFFUSION THROUGH PRODUCT LAYER CONTROLLED)

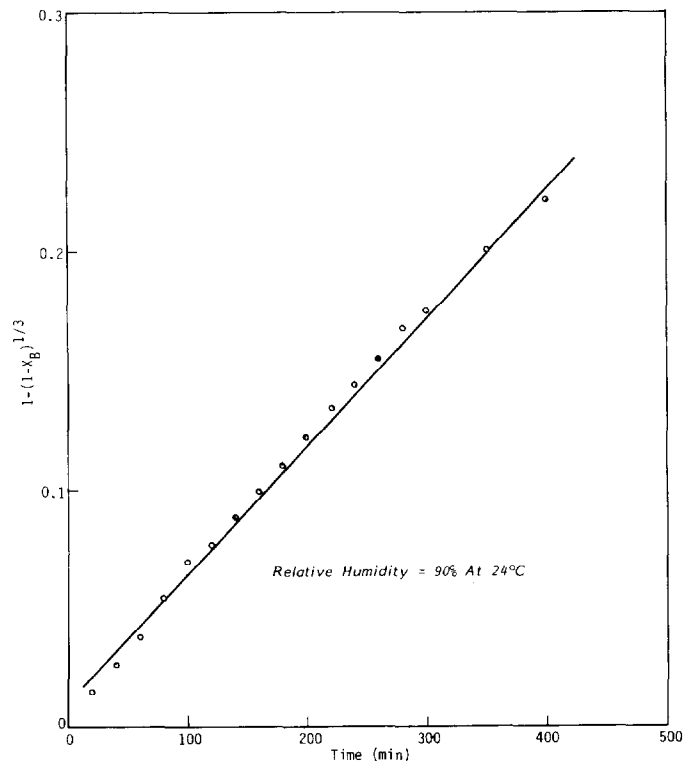


FIGURE 6

DETERMINATION OF RATE CONTROLLING STEP FOR HIGH HUMIDITY EXPERIMENT (G642) (ASSUMING CHEMICAL REACTION CONTROLLED)

17th DOE NUCLEAR AIR CLEANING CONFERENCE

Table IV lists the values obtained for k_s , k_d and k_g under different experimental conditions. These data suggest that k_g is relatively constant in the gas velocity range of 0.8 to 3.3 cm/s and was estimated to be about 28.8 cm/min. It should be noted that the maximum gas velocity that could be used in the TGA system was 3.3 cm/s which is only half of the superficial gas velocity used in the fixed bed bench scale experiments and the actual velocity across the particles in the bed could be much higher. k_d has an average value of 6.24 cm/min for the high relative humidity condition (90% at 24°C). k_s is relatively independent of CO_2 concentrations in the range 400 to 1000 $\mu\text{l}/\text{l}$ and has an average value of 23.1 cm/min.

These TGA results indicate that the mean rate constant is 3.0 cm/min (or 77 min^{-1}) for the -2.4 and 2.0 mm $\text{Ca}(\text{OH})_2$ particles at 24°C. This is somewhat lower than the mean rate constant obtained from the fixed bed bench scale system (100 min^{-1}) probably due to the lower gas velocity in the TGA apparatus.

Table IV Summary of TGA experimental conditions and results.

Experiment No	G635	G636	G639	G647	G642	G643	G644	G640	G657	G658
$\text{Ca}(\text{OH})_2$ Size (mm)	2.38+2.00	2.38+2.00	2.38+2.00	2.38+2.00	2.38+2.00	2.38+2.00	2.38+2.00	2.38+2.00	2.38+2.00	2.38+2.00
Temp (°C)	24	24	24	24	24	24	24	24	51	55
RH (%)	90	90	90	90	90	90	90	50	60	24
CO_2 conc ($\mu\text{L}/\text{L}$)	1000	1000	1000	1000	400	400	400	400	400	400
Flowrate (L/min)	1.0	0.6	0.4	0.25	1.0	0.6	0.25	1.0	1.0	1.0
Slope g^* (min^{-1})	4.5×10^{-3}	3.3×10^{-3}	3.4×10^{-3}	3.3×10^{-3}	1.7×10^{-3}	1.7×10^{-3}	1.8×10^{-3}	-	2.1×10^{-3}	-
Slope d^{**} (min^{-1})	1.25×10^{-4}	1.32×10^{-4}	1.59×10^{-4}	1.99×10^{-4}	7.2×10^{-5}	8.0×10^{-5}	8.3×10^{-5}	2.7×10^{-6}	2.1×10^{-4}	3.2×10^{-5}
Slope c^{***} (min^{-1})	1.3×10^{-3}	1.4×10^{-3}	1.6×10^{-3}	1.3×10^{-3}	68×10^{-3}	6.1×10^{-4}	6.1×10^{-4}	-	31.3	-
k_g (cm/min)	27.3	20.0	20.6	20.0	25.8	25.8	27.3	-	18.9	-
k_d (cm/min)	4.55	4.80	5.79	7.24	6.55	7.24	7.50	0.244	43.5	0.288
k_s (cm/min)	24.2	20.7	20.9	21.3	34.4	25.2	24.9	-	-	-

- * Slope g = initial slope of X versus time
 ** Slope d = slope of $1/2 - 1/3 X^{-1/2}(1-X)^{1/3}$ versus time
 *** Slope c = slope of $1-(1-X)^{1/3}$ versus time

Role of Moisture

The $\text{Ca}(\text{OH})_2$ samples (with an initial moisture content of -14 g/kg) were exposed to CO_2 -free nitrogen of different humidities and the moisture absorbed by or desorbed was determined by TGA (see Figure 7). The weight gain of the sample increased sharply as the relative humidity of the gas stream increased beyond 80% at 25°C.

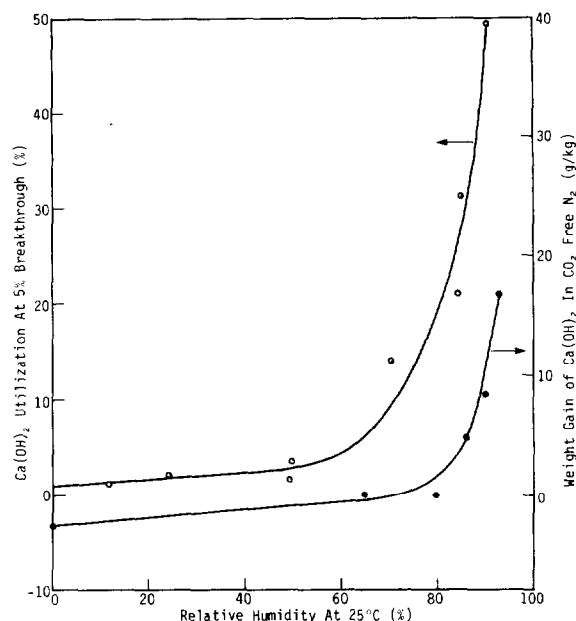


FIGURE 7
THE EFFECT OF HUMIDITY ON THE WEIGHT GAIN
AND UTILIZATION OF $\text{Ca}(\text{OH})_2$

Previous bench scale experiments showed that the $\text{Ca}(\text{OH})_2$ utilization (at 5% breakthrough) also increased sharply as the relative humidity increased beyond 80%⁽¹⁾. This seems to indicate that the increase of utilization is directly related to the increase of moisture content at high relative humidities.

Since the $\text{Ca}(\text{OH})_2$ absorbent used was very porous (porosity ≈ 0.72), it is possible that capillary condensation could have occurred in the small pores and the reaction between CO_2 and $\text{Ca}(\text{OH})_2$ could have proceeded in the liquid phase. However, calculations using a simplified Kelvin equation⁽¹⁰⁾ show that at a relative humidity of 85% at 25°C, capillary condensation can only occur in pores with diameters less than 13 nm, but only 2.5% of the total pore volume of the $\text{Ca}(\text{OH})_2$ samples was found to be less than 13 nm (see Figure 1) as determined by mercury porosimetry. Furthermore, according to the Kelvin equation, the extent of capillary condensation occurring at 45 and 25°C (identical relative humidities) would be approximately the same, but the bench scale experiments showed that the utilization of the $\text{Ca}(\text{OH})_2$ bed was considerably better at 45°C and 65% relative humidity than that at 25°C and at the same relative humidity⁽¹⁾. Again, this suggests that capillary condensation does not play an important role in the present reaction.

It has been suggested that water vapour can increase the porosity of the carbonate layer by modifying its microstructure⁽⁵⁾, thus permitting CO_2 gas to penetrate the carbonate layer. As discussed earlier, the reaction rate for high relative humidity (90%) experiments is chemically controlled. When the relative humidity is lowered from 90% to 50% at 25°C, the reaction is no longer chemically controlled. Instead, the reaction is controlled by diffusion through the product layer (see Figures 8 and 9) and the reaction rate is much

lower. Therefore, the main role of moisture in the reaction is to increase the reaction rate and improve the $\text{Ca}(\text{OH})_2$ utilization by decreasing the resistance to diffusion through the carbonate layer.

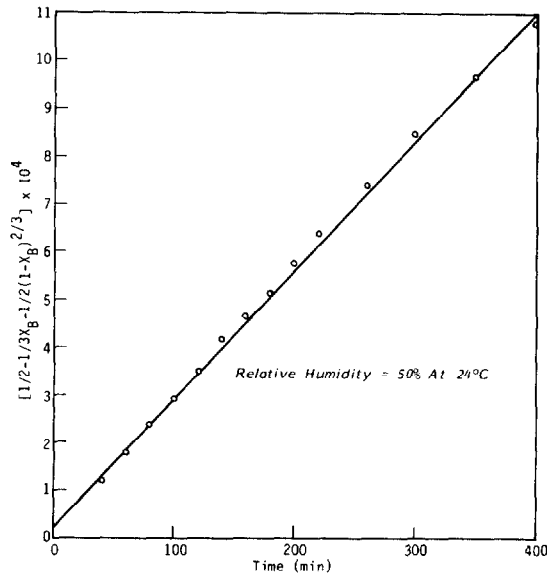


FIGURE 8
 DETERMINATION OF RATE CONTROLLING STEP
 FOR LOW HUMIDITY EXPERIMENT (G640)
 (ASSUMING DIFFUSION THROUGH PRODUCT LAYER CONTROLLED)

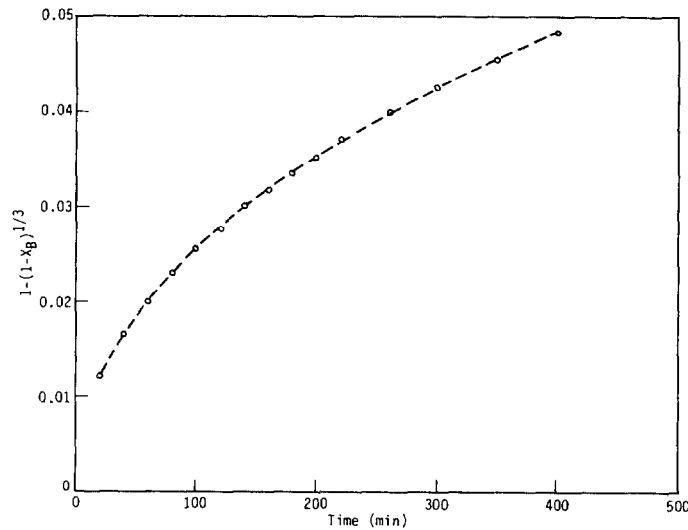


FIGURE 9
 DETERMINATION OF RATE CONTROLLING STEP
 FOR LOW HUMIDITY EXPERIMENT (G640)
 (ASSUMING CHEMICAL REACTION CONTROLLED)

At 50°C, TGA experiments (see Table IV experiment No G658 and G657) show that increasing the relative humidity from 24% to 60% is sufficient to change the reaction rate diffusion control through the product layer to chemical control. This is probably because the vapour pressure of water at a relative humidity of 60% at 50°C is sufficiently high to modify the microstructure of the carbonate layer and improve diffusion through the layer.

Reactor Design Considerations

Results of the bench scale experiments showed that the Length of Unused Bed (LUB) was independent of the bed height and was only a function of the gas velocity - the higher the gas velocity, the longer the LUB⁽¹⁾. As the gas velocity was increased from 3.3 to 13.3 cm/s, the LUB increased from 0.8 to over 3 cm (see Table IV). furthermore, the utilization of the Ca(OH)₂ at 5% breakthrough increased from 100 g/kg to 660 g/kg as the bed height-to-LUB ratio increased from 1 to 4 (see Figure 10). Hence, in order to achieve good utilization (eg, utilization of over 600 g/kg), the bed height-to-LUB ratio should be maintained at above 4 by either increasing the bed height or reducing the gas velocity (to reduce the LUB).

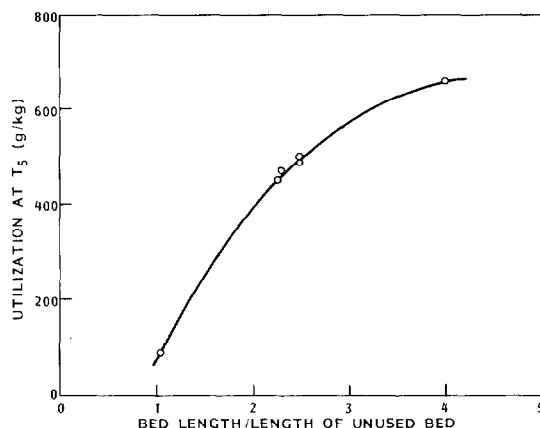


FIGURE 10

THE EFFECT OF (BED HEIGHT/LUB) RATIO ON Ca(OH)₂ UTILIZATION

V. Conclusions

1. The reaction between Ca(OH)₂ and CO₂ in moist N₂ is first order with respect to the two reactants with a rate constant of 100 min⁻¹.
2. The main role of moisture in the reaction is to improve the Ca(OH)₂ utilization by lowering the resistance to diffusion through the carbonate layer formed by the reaction.
3. The Ca(OH)₂ absorbent used was very porous with a porosity of 0.72 and a surface area of 36.1 m²/g.

17th DOE NUCLEAR AIR CLEANING CONFERENCE

4. Capillary condensation could have occurred only in about 2% of the pore volume and was unlikely to affect the reaction rate significantly by allowing the reaction to occur in the liquid phase.
5. At high humidities, the rate of reaction is chemically controlled but at low humidities, the reaction rate is limited by the diffusion through the carbonate layer.
6. The bed height-to-LUB ratio should be kept above 4 in order to achieve good utilization of Ca(OH)_2 .

References

1. Cheh, C.H., Glass, R.W. and Chew, V.S. "Removal of Carbon-14 from Gaseous Streams." Paper presented at the IAEA Seminar on the Testing and operation of Off-Gas Cleaning Systems at Nuclear Facilities, Karlsruhe; FRG. May 3-7, 1982.
2. Statham, N. US Patent 1,178,962. 1916.
3. Veinot, D.E. Defence Research Establishment Atlantic, Canada. Private Communication.
4. Engel, R. and Decken, C.B. "Removing Carbon Dioxide and Water from a Gas Stream." US Patent 3,519,384.
5. Mozes, M.S. Ontario Hydro Research Division Report 80-509-K. 1980.
6. Haag, G.L. "Carbon-14 Immobilization Via the CO_2 - Ba(OH)_2 Hydrate Gas-Solid Reaction." Proc 16th DOE Nuclear Air Cleaning Conference, San Diego, California. October 20-23, 1980.
7. Karlsson, H.T., Klingspor, J. and Bjerle, I. "Adsorption of Hydrochloric Acid on Solid State Lime for Flue Gas Clean Up." J. Air Pollution Control Association 31. pp 1177-1180. 1981.
8. Levenspiel, O. "Chemical Reaction Engineering." p 341. John Wiley and Sons Inc. 1962.
9. Sherwood, T.K. Pigford, R.L. and Wilke, C.R. "Mass Transfer." p 555. McGraw Hill.
10. Gregg, S.J. "The Surface Chemistry of Solids." Chapman & Hall Ltd. 1951.

DISCUSSION

RINGEL: In the process, water is needed for high utilization and reaction. What would it mean if you used $\text{Ca}(\text{OH})_2$ slurry instead of $\text{Ca}(\text{OH})_2$ particles?

CHEH: The dry $\text{Ca}(\text{OH})_2$ process developed by Ontario Hydro has the advantages of a $\text{Ca}(\text{OH})_2$ slurry process, such as high absorbent utilization and high DFs, but avoids the many disadvantages of a wet process which involves more complicated operations such as filtration and handling of contaminated liquid and slurry streams.

HAAG: What is the assumed particle geometry in your studies? What is the maximum reactant utilization and required relative humidity? Is caking a problem at 100% relative humidity?

CHEH: The particles are assumed to be spherical in this study. Utilization of the $\text{Ca}(\text{OH})_2$ absorbent can be as high as 85% and the relative humidity should be in the range of 85-100% at 25°C for the same bed temperature. Our pilot plant results showed that caking is not a problem at 100% relative humidity if the bed temperature is 20-25°C. This result is reported in another paper presented at the IAEA Seminar on the Testing and Operation of Off-gas Cleaning Systems at Nuclear Facilities, 3-7 May, 1982.

HAAG: Just a point of observation. In our studies on the barium hydroxide system, we noticed that our surface area is a definite function of relative humidity. Dr. Paul Edment of Oregon State University has observed in his systems that when he obtained two or three monolayers of water on the surface, it acted as if it were a liquid solution with respect to transport properties. In our own studies, what we feel to be happening is that solution is resulting in transport of the barium ions and hydroxide ions, and our surface does decrease as our humidity increases. So, it is almost as if there is a liquid solution sitting there on the surface. Also, we have noticed that our surface area tends to decrease as the rate of reaction decreases. It appears that the slower the rate of reaction the more defined the crystal structure is within the material. In essence, if the reaction takes place in a more orderly environment, our crystalites are much bigger. I think what you are seeing, and what we are seeing, are very closely parallel.

CHEH: It makes sense that the CO_2 and the calcium hydroxide react in the liquid phase, but we don't seem to get evidence of it in our studies. Perhaps a study similar to yours could tell us a bit more on this point.

BONKA: The highest ^{14}C emission rates from nuclear power plants are from heavy water reactors. Argentina decided after a cost-benefit analysis to retain ^{14}C at the reactor Atuche II. Has there been a similar decision or discussion in Canada?

CHEH: Although the ^{14}C emissions from Ontario Hydro's nuclear generating stations are below 1% derived emission limit, an

17th DOE NUCLEAR AIR CLEANING CONFERENCE

effort has been devoted by Ontario Hydro to further reduce ^{14}C emissions. The development of the dry air ambient temperature $\text{Ca}(\text{OH})_2$ system for the moderator cover-gas and nitrogen annulus gas of the Candu reactor is part of this effort. An engineering design of this procedure is being prepared and testing of this system in our nuclear stations is under consideration.

KABAT: I have a comment to this point, too. Carbon-14 removal in Canada is not officially required by regulation. It is a voluntary action of Ontario Hydro to reduce the carbon-14 stack emissions in order to remove ^{14}C from the systems. The moderator system is the major contribution to the stack. In Pickering, where we have a nitrogen annulus gas in two units, a carbon-14 recovery system will be installed on the annulus gas systems, eventually. The point is that, since the process we developed is so simple and reliable (we tested it for a long period of time) with very little maintenance required, if we put it in the moderator cover gas system it would probably last well over two years before it will need to be changed. This is one of the main reasons we are thinking that perhaps we should put it in anyway.

17th DOE NUCLEAR AIR CLEANING CONFERENCE

^{14}C RELEASE AT LIGHT WATER REACTORS

C. Kunz
Center for Laboratories and Research
New York State Department of Health
Albany, New York 12201

Abstract

The quantity, discharge pathway, and chemical form were determined for the ^{14}C released from two pressurized water reactors (PWR) and one boiling water reactor (BWR) in northeastern U.S. Continuous stack samplers were used to measure either total ^{14}C or $^{14}\text{CO}_2$ in the gaseous effluent. In addition, grab samples were taken of stack gas, containment air, and gas in decay tanks and analyzed for ^{14}C in specific chemical species such as CO_2 , CH_4 , C_2H_6 , C_3H_8 , and C_4H_{10} . Samples of primary coolant taken before and after passage through the clean-up demineralizers were also analyzed to determine the ^{14}C in the coolant and the decontamination factors for the demineralizers.

The ^{14}C gaseous discharge rate for a 490 MW(e) PWR was 11.6 Ci/GW(e)-yr. Venting of gas decay tanks accounted for 42% of the total ^{14}C released; 35% was discharged through auxiliary building ventilation and 23% through containment venting. The average chemical composition was 69% as $^{14}\text{CH}_4$, 16% as $^{14}\text{C}_2\text{H}_6$, 5% as $^{14}\text{C}_3\text{H}_8$ and $^{14}\text{C}_4\text{H}_{10}$, and 10% as $^{14}\text{CO}_2$.

The ^{14}C gaseous discharge rate for a 1000 MW(e) PWR was 8.0 Ci/GW(e)-yr. Venting of gas decay tanks accounted for about 7% of the total ^{14}C released. The predominant pathway for ^{14}C gaseous discharge at this PWR was pressure relief venting and purging of the containment air. $^{14}\text{CO}_2$ made up 19% of the total ^{14}C , with the balance as $^{14}\text{CH}_4$ and other hydrocarbon gases.

The ^{14}C gaseous discharge rate for an 850 MW(e) BWR was 12.3 Ci/GW(e)-yr. Approximately 97% of the gaseous ^{14}C release was as off-gas discharge, and the chemical composition of the discharge was about 98% $^{14}\text{CO}_2$.

There was no measurable removal of ^{14}C by the coolant demineralizers for the PWRs. A decontamination factor of 7 was observed for the clean-up demineralizer at the BWR, resulting in a ^{14}C removal rate of approximately 0.5 Ci/GW(e)-yr.

Introduction

In light water reactors ^{14}C is produced as an activation product in the coolant, fuel, and structural material. The most important production reactions and their thermal neutron cross-sections for ^{14}C formation in light water reactors are:



The isotopic abundance of ^{17}O is 0.04% of oxygen, which is a major constituent of the coolant water and oxide fuel. Production of ^{14}C from ^{17}O is therefore unavoidable. The isotopic abundance of ^{14}N is 99.62% of the nitrogen, which is present as an impurity in both the coolant and fuel. Production of ^{14}C through the activation of ^{14}N is difficult to estimate, since the nitrogen concentrations in the coolant water and the fuel are not well known. If approximately 50 ppm of atomic nitrogen is present in the coolant, the amount of ^{14}C produced from

17th DOE NUCLEAR AIR CLEANING CONFERENCE

dissolved ^{14}N is about equal to that from the activation of the ^{17}O in the H_2O .

In 1974 Bonka et al.⁽¹⁾ estimated the rate of formation of ^{14}C in nuclear reactors; Magno et al.⁽²⁾ discussed the radiological significance of ^{14}C discharges; and Kunz et al.⁽³⁾ reported on measurements of ^{14}C at pressurized water reactors (PWRs). Since 1974 there have been a number of publications on the calculated and measured production and discharge of ^{14}C at light water reactors. The most extensive measurements have been made in the Federal Republic of Germany.⁽⁴⁾

Bonka⁽⁵⁾ has summarized eight studies, including his own work, to calculate estimates of the production of ^{14}C in light water reactors. The average calculated production rates in the primary coolant were 6.7 and 8.2 Ci/GW(e)-yr for PWRs and boiling water reactors (BWRs) respectively. Although ^{14}C is also formed in the fuel and the structural material of the core, only the ^{14}C formed in the coolant is subject to release during normal plant operation.

Two-year studies of the ^{14}C discharge have been conducted at each of three light water reactors; a 490 MW(e) PWR, a 1000 MW(e) PWR, and an 850 MW(e) BWR. The studies at the 490 MW(e) PWR have been completed, and the results are discussed here in detail. Samples and data are still being analyzed for the 1000 MW(e) PWR and the 850 MW(e) BWR, so only the results obtained as of this writing will be summarized here.

Experimental

Stack samplers were operated continuously to obtain integrated samples for measurement of total ^{14}C or $^{14}\text{CO}_2$ in the gaseous effluent. In addition, grab samples of stack gas, containment air, off-gas, and gas in decay tanks were analyzed for ^{14}C content as specific chemical species: CO_2 , CH_4 , C_2H_6 , C_3H_8 , and C_4H_{10} . The several chemical species were separated by gas chromatography,⁽⁶⁾ and the ^{14}C was measured by internal gas proportional counting.⁽⁷⁾

A schematic of the continuous sampler is shown in Fig. 1. A sample flow of 100 cc/min is maintained in the sampler by using a diaphragm pump. The sampled gas is drawn through a tube furnace at 600°C containing palladium-on-alumina and platinum-on-alumina pellets. All carbon species, such as CH_4 , C_2H_6 , and CO , are oxidized to CO_2 . From the furnace the gas flows through a solid absorbent, such as Drierite, to remove the water vapor and then through a cartridge containing a solid absorbent of 8- to 20-mesh Ascarite, which contains NaOH on a solid support material to trap CO_2 . Water vapor must be removed, prior to the Ascarite step, in order to avoid dissolving the NaOH and clogging the tube. The CO_2 absorbent cartridges contain 25 g of Ascarite and are changed at biweekly intervals.

To prepare the sample for measurement of ^{14}C content, CO_2 must first be evolved by acidifying the Ascarite. The 25 g of Ascarite are added to 50 ml of water in a flask attached to the gas flow apparatus, and helium is bubbled through the mixture. Approximately 50 ml of concentrated HCl is added to the Ascarite-water mixture, and the helium flow is maintained for 30 min. The helium containing the evolved CO_2 is passed through a cold water condenser and a cold trap at approximately -60°C to remove water vapor and finally through a liquid nitrogen cold trap to collect the CO_2 . The volume of collected CO_2 is measured (~ 650 cc for a 2-week sampling period), and about 50 cc is chromatographically purified and loaded into an internal gas proportional tube for counting.

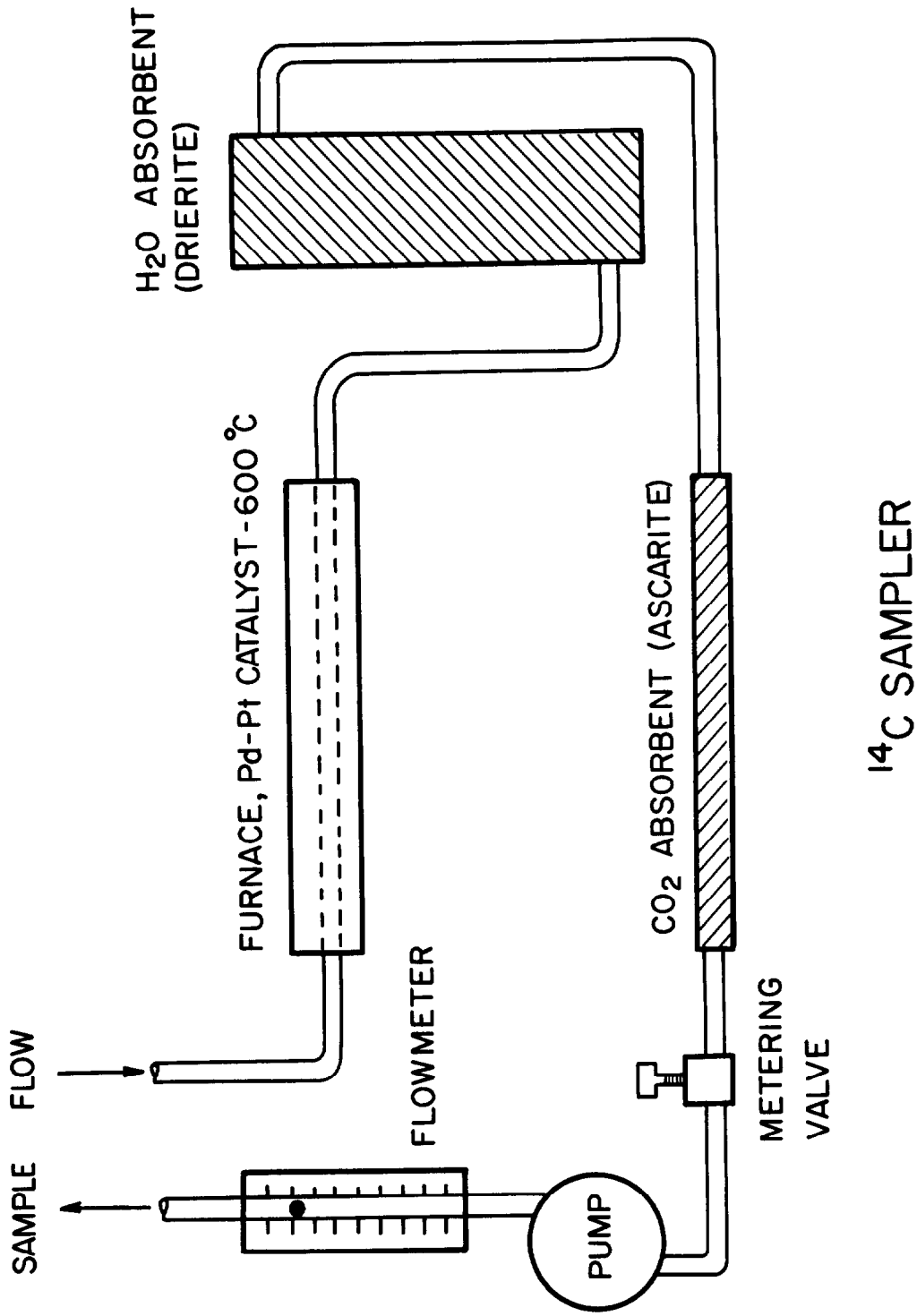


Figure 1 ^{14}C sampler used to continuously sample vented gases. All carbon species are oxidized to CO_2 and trapped on a solid absorbent.

17th DOE NUCLEAR AIR CLEANING CONFERENCE

The specific activity ($^{14}\text{C}/\text{cc}$ of CO_2) is measured, and the ^{14}C concentration per cubic centimeter of vent gas is calculated. The volume of air sampled is determined from the sampler flow rate and also from the total amount of CO_2 trapped, assuming that the sampled gas contains the ambient concentration of CO_2 in air (325 ppm).

The analytical uncertainty associated with the measurement of the concentration of ^{14}C in each 2-week sample is less than $\pm 10\%$. In determining the quantity of ^{14}C discharged, additional uncertainties are associated with determining the volume of gas sampled and the flow rate of the plant vent. Considering these three factors, the uncertainty in determining the quantity of ^{14}C released is estimated at $\pm 25\%$.

Results and Discussion

490 MW(e) PWR

Plant Ventilating System. The two main vents at this plant - the plant vent and the containment vent - are both rooftop vents discharging gas at a height of about 45 m. Four gas decay tanks are used to hold cover gas from the primary system to allow time for short-lived gaseous radionuclides to decay prior to discharge. The gas decay tanks and all building ventilation air except for containment are exhausted through the plant vent at a flow rate of 2.97×10^7 cc/s. The building air is exhausted continuously. The gas decay tanks are vented approximately 20 times each year, and about 10 h are required to vent each tank. The containment building is vented at 1.18×10^7 cc/s during refueling outages and some repair outages. When the plant is operating, containment is not vented. All releases through the plant vent and containment vent pass through charcoal and HEPA filters to remove radioactive iodine and particulates.

Gaseous Grab Samples. Grab samples of decay tank gas, containment air, and stack gas have been collected at various times since 1973 and analyzed for the concentration of ^{14}C as CH_4 , C_2H_6 , C_3H_8 , C_4H_{10} , and CO_2 . For some of the samples aliquots were passed through a combustion furnace to oxidize all carbon compounds to CO_2 which was measured for ^{14}C . These results were compared to the total ^{14}C obtained by summing the specific chemical species measured separately. The results agreed within 10%, indicating that all major species of ^{14}C were accounted for.

The average chemical composition of the ^{14}C in the gas decay tanks was 74% as $^{14}\text{CH}_4$, 16% as $^{14}\text{C}_2\text{H}_6$, 6% as $^{14}\text{C}_3\text{H}_8$ and $^{14}\text{C}_4\text{H}_{10}$, and 4% as $^{14}\text{CO}_2$.

The cover gas for the primary coolant was predominantly hydrogen. In this hydrogen atmosphere and under the intense radiation of the reactor core any carbon present tends to be reduced to form hydrocarbons. Our results indicate that the more hydrogen-saturated volatile species, CH_4 and C_2H_6 , were preferentially formed.

The average concentration of total ^{14}C in the gas decay tanks was 1×10^{-3} $\mu\text{Ci}/\text{cc}$. During an 88-week period when the discharge of ^{14}C was measured with continuous stack samplers, gas decay tanks were vented 31 times. The volume of each tank is 13.3m^3 and they are normally filled to a pressure of 6.3×10^5 Pa (92 psi). The average concentration of ^{14}C and the total volume of gas released corresponds to a release rate of 1.5 Ci/yr from the gas decay tanks.

In the containment air the total ^{14}C concentration ranged from 8×10^{-7} to 6×10^{-6} $\mu\text{Ci}/\text{cc}$. The chemical composition of the ^{14}C in containment averaged

17th DOE NUCLEAR AIR CLEANING CONFERENCE

74% as $^{14}\text{CH}_4$, 21% as $^{14}\text{C}_2\text{H}_6$, 3% as $^{14}\text{C}_3\text{H}_8$ and $^{14}\text{C}_4\text{H}_{10}$, and 2% as $^{14}\text{CO}_2$. This is similar to the chemical composition of the ^{14}C in the gas decay tanks, with only a small percentage as $^{14}\text{CO}_2$. Apparently the ^{14}C found in the containment air is formed in the reactor vessel and leaks into the containment building. If the ^{14}C were formed in containment by interaction of neutrons with containment air, the predominant gaseous chemical species should be $^{14}\text{CO}_2$ and ^{14}CO , due to the oxidizing conditions of the containment air.

Containment is purged during shutdowns and isolated when the reactor is operating. The rate of accumulation of ^{14}C in containment can be estimated from the length of time containment is isolated before grab samples are taken, assuming that containment was well purged of radioactive gas during venting. The average rate of accumulation determined from three containment samples was 0.4 Ci/yr. This corresponds to the amount of ^{14}C leaking into the containment building when the reactor is operating. It does not include ^{14}C leaking into containment during an outage.

Two samples of building ventilation air from the main plant vent were taken when the gas decay tanks were not being vented. The chemical composition of the ^{14}C in one sample was similar to that found in the decay tank and containment samples. However, in the other sample the $^{14}\text{CO}_2$ comprised 49% of the total ^{14}C . The origin of the higher fraction of $^{14}\text{CO}_2$ in the main plant vent is not known.

Continuous Gas Sampling. To more accurately measure the rate of discharge of gaseous ^{14}C , samplers were used to draw off continuously a small flow of gas from the main plant vent and the containment vent. The main plant vent is the discharge point for the gas decay tanks and for all building ventilation except in the containment building, which is vented through the containment vent. The containment vent is normally operated only during refueling operations and other outages. At such times containment is continuously vented; it is then isolated when the reactor is started up.

When containment was not being vented, the containment sampler was used to sample the main plant vent for $^{14}\text{CO}_2$ only. This was accomplished by not using the oxidizing furnace. In those periods the main plant vent was thus sampled simultaneously for total ^{14}C and for $^{14}\text{CO}_2$.

The continuous ^{14}C samplers were placed on the vents on 14 March 1980. The results for the next 88 weeks of continuous sampling of the main plant vent are shown in Fig. 2.

During and just before outages the ^{14}C releases were the greatest, most probably for the following reasons: During outages the gases covering and dissolved in the primary coolant system are purged into the gas decay tanks. The tanks are vented to make room for the cover gas, and after a hold-up period the cover is discharged. During an outage, therefore, when radioactive gases that have accumulated in the primary coolant are removed and released from the gas decay tanks, the discharge of ^{14}C is the greatest. After an outage the concentration of radioactive gases in the primary system is reduced, and less ^{14}C is discharged.

The release of ^{14}C is greater during periods when gas decay tanks are vented. However, even when decay tanks are not being vented, a substantial quantity of ^{14}C is discharged. The release of ^{14}C during such periods indicates that ^{14}C is leaking from various reactor components in auxiliary buildings outside the containment building. For example, there may be some leakage of radioactive gases from

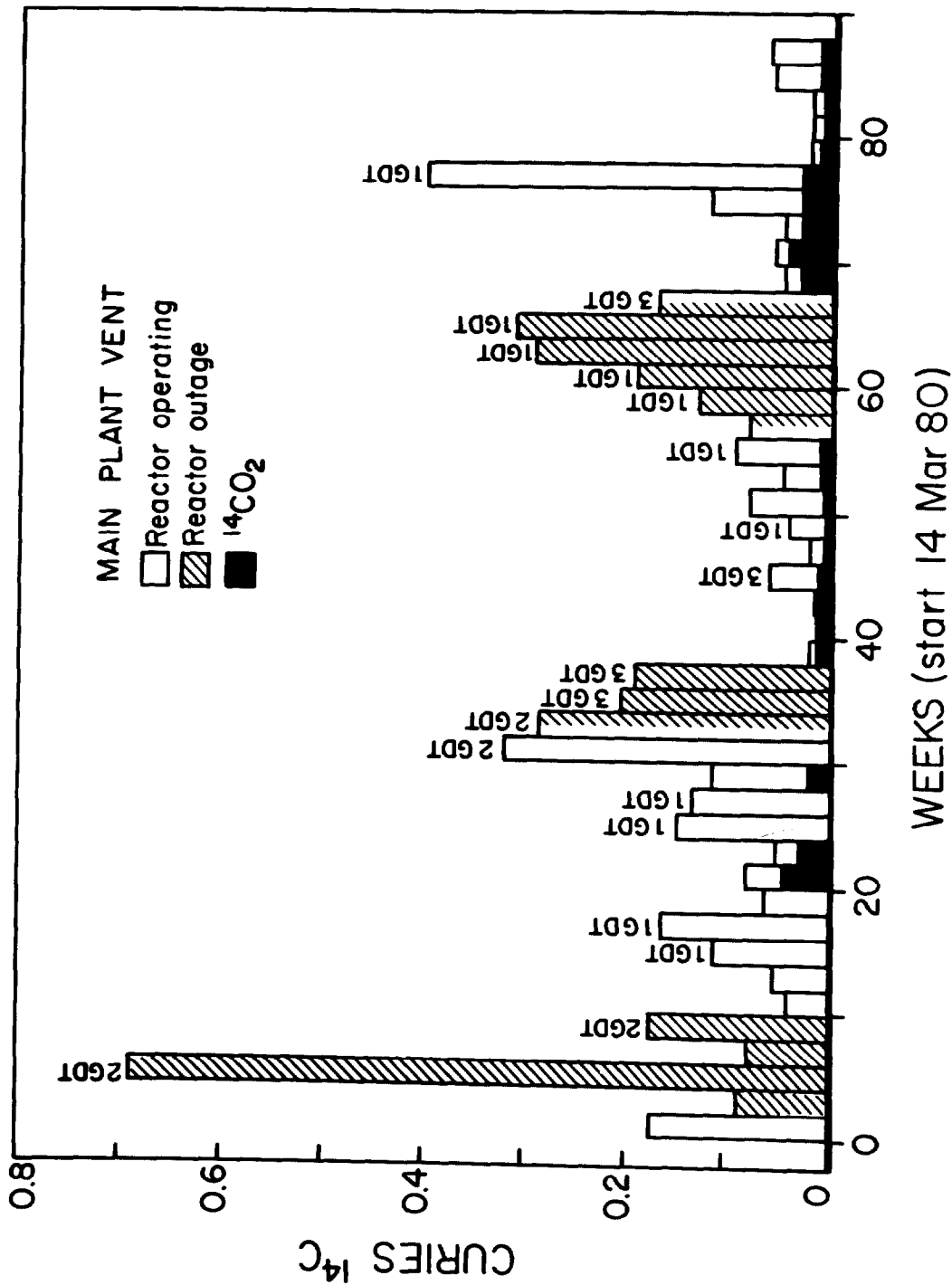


Figure 2 Biweekly measurements of ^{14}C discharge from main plant vent of a 490 MW(e) PWR. Gas decay tank (GDT) releases are indicated for each 2-week period.

17th DOE NUCLEAR AIR CLEANING CONFERENCE

the primary to the secondary coolant, and these gases could be released in buildings outside the containment building. Gases released in auxiliary buildings are discharged through the main plant vent.

During 50 weeks of the 88-week test period there were no releases from the gas decay tanks through the main plant vent. During these 50 weeks a total of 1.48 Ci of ^{14}C were discharged from the main plant vent, for a discharge rate of 1.5 Ci of $^{14}\text{C}/\text{yr}$ from auxiliary building ventilation.

The $^{14}\text{CO}_2$ fraction of the total ^{14}C in the main plant vent was measured during 44 weeks of the test period. A total of 0.37 Ci of $^{14}\text{CO}_2$ was released, which corresponds to a discharge rate of 0.4 Ci of $^{14}\text{CO}_2/\text{yr}$. The concentration of $^{14}\text{CO}_2$ in the main plant vent does not appear to be affected by the release of gas from the decay tanks. This is not surprising in view of the very low concentration of $^{14}\text{CO}_2$ in the grab samples from gas decay tanks. The $^{14}\text{CO}_2$ appears to be associated primarily with the continuous auxiliary building discharge from the main plant vent. The source of the $^{14}\text{CO}_2$ is not known. Analyses of grab samples from gas decay tanks and of containment air indicate that very little $^{14}\text{CO}_2$ is formed in the pressure vessel, decay tanks, or containment building.

The results for continuous sampling of the containment vent are shown in Fig. 3. During the first outage a total of 0.91 Ci was released from this vent. During the second and third outages 0.31 and 0.43 respectively were released. The total amount of ^{14}C released from the containment vent during the 88-week test period was 1.65 Ci, for a rate of 1.0 Ci/yr.

The grab samples indicated that ^{14}C was accumulating in the containment building at a rate of 0.4 Ci/yr during periods when the plant was operating. It appears that over half of the ^{14}C discharged from containment was released from reactor components during the outages. Apparently ^{14}C in the pressure vessel, steam generators, and other reactor components is released during refueling and repairs and is discharged with the containment venting.

Considering the discharge from both the main plant vent and the containment vent (Fig. 4), the total amount of ^{14}C discharged during the 88-week test period was 7.2 Ci. This corresponds to a discharge rate of 4.3 Ci/yr.

The sources or location of the ^{14}C discharges can be roughly apportioned. The ^{14}C release rate from the containment vent was 1.0 Ci/yr. The ^{14}C discharged continuously through the main plant vent from the venting of auxiliary building air was estimated at 1.5 Ci/yr. This leaves a balance of 1.8 Ci/yr for the ^{14}C discharged from the gas decay tanks, a value which agrees within analytical error with the rate of 1.5 Ci/yr estimated from the grab sample data.

Therefore about 58% of the total ^{14}C is discharged by ventilating the containment and auxiliary buildings and about 42% in the gas decay tank releases. The stack flow rates for the containment and auxiliary building vents are 1.18×10^7 and 2.97×10^7 cc/s respectively. These flow rates seem too great to make practical any processing of the gas for ^{14}C removal. However, the discharge from the gas decay tanks could be processed to remove ^{14}C .

The release rate for total ^{14}C , determined by continuous sampling for 88 weeks, was 4.3 Ci/yr. During this test period the reactor operated for about 75% of the time at close to its design power level of 490 MW(e) gross. Therefore the ^{14}C release rate of 4.3 Ci/yr corresponds to a release rate of 11.6

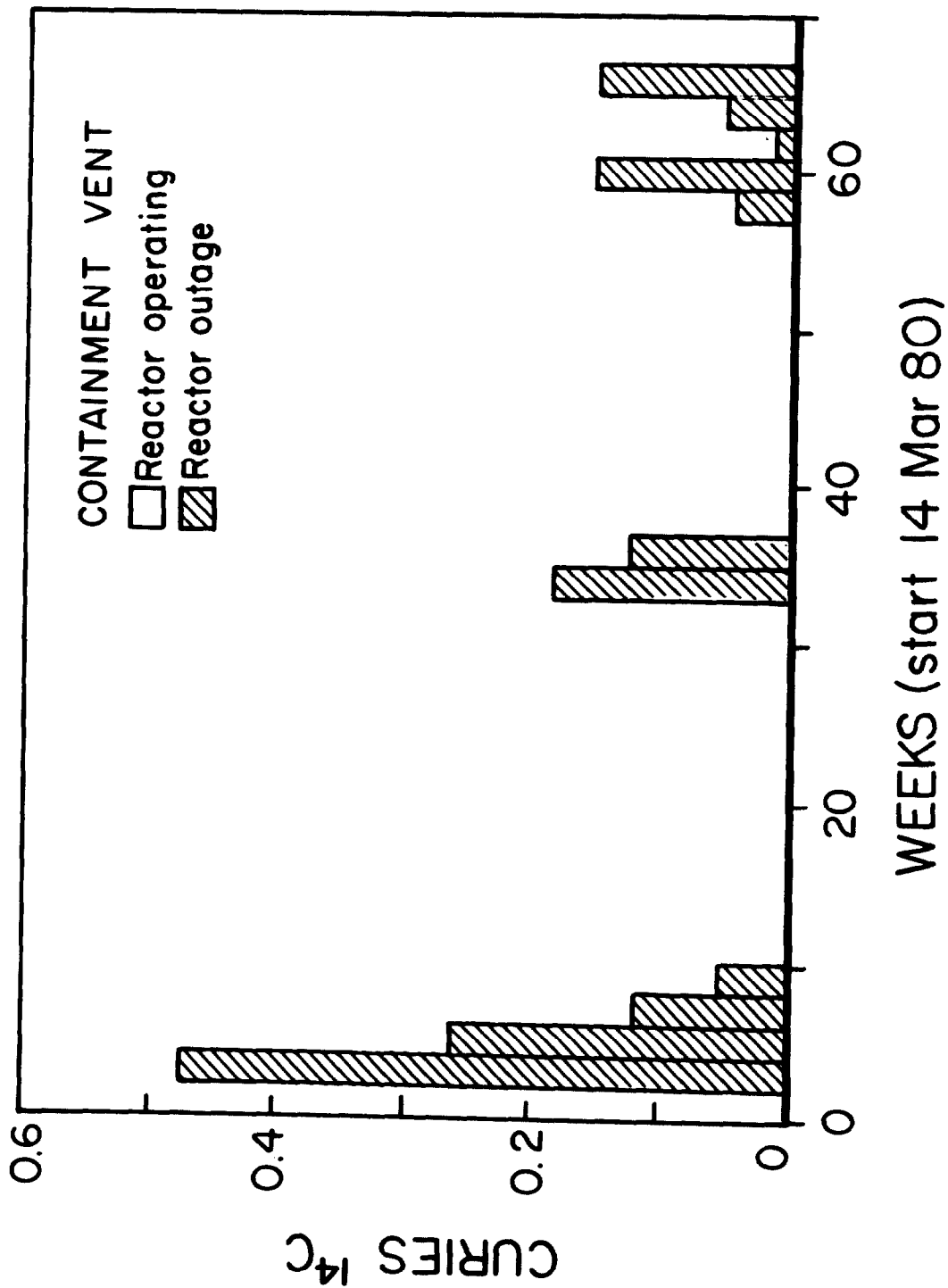


Figure 3 Biweekly measurements of ¹⁴C discharge from containment vent of a 490 MW(e) PWR.

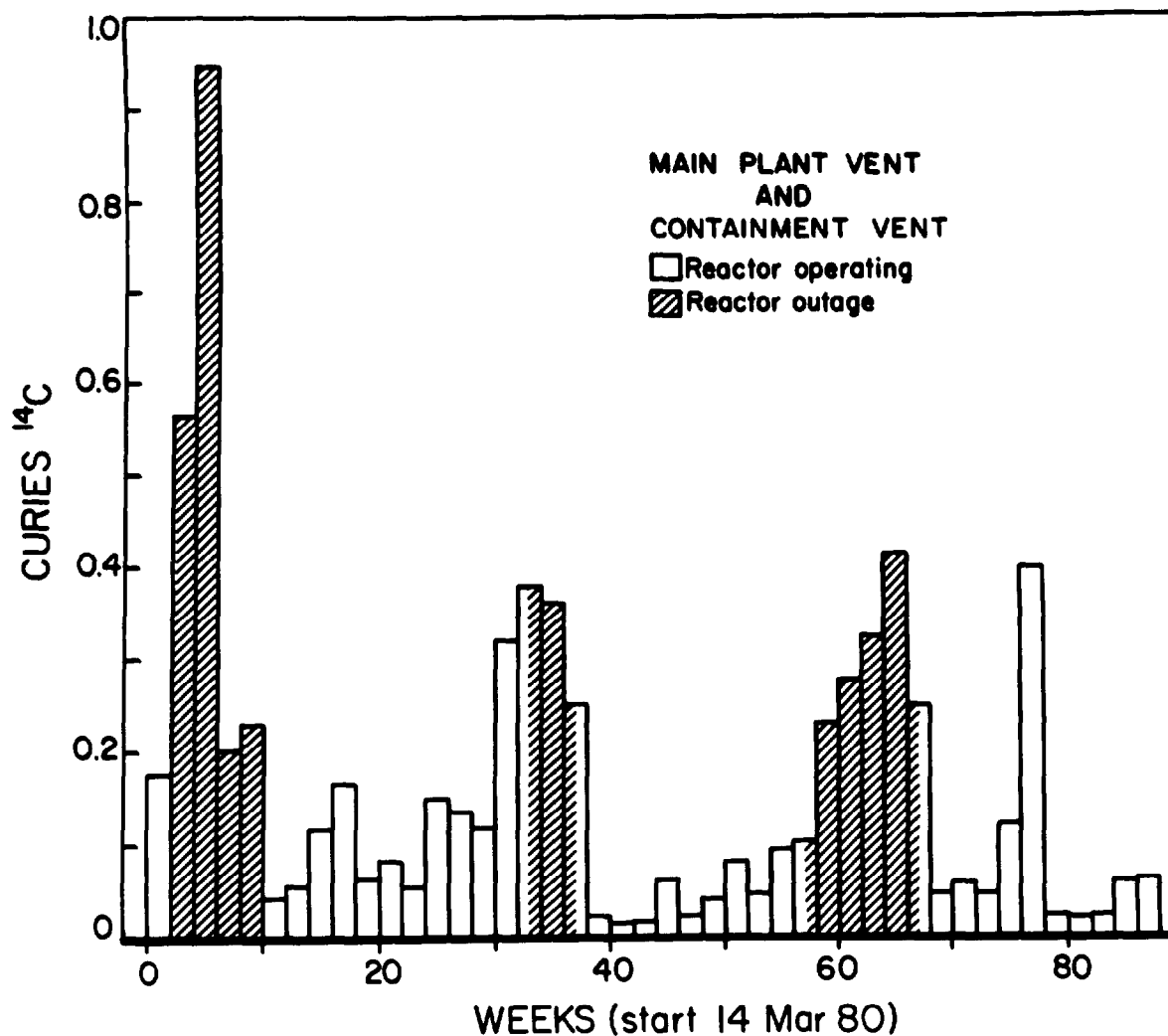


Figure 4 Combined ^{14}C discharge from main plant vent and containment vent of a 490 MW(e) PWR.

Ci/GW(e)-yr.

The average value calculated for production of ^{14}C in the coolant of generic PWRs is 6.7 Ci/GW(e)-yr.⁽⁵⁾ The 490 MW(e) reactor is one of the older reactors and has about one-half the generating capacity of newer PWRs. The unique design of this reactor may result in higher production rates of ^{14}C in the coolant than has been calculated for generic designs.

Liquid Grab Samples. Primary coolant samples were analyzed for inorganic and organic ^{14}C . Samples were taken before and after passage through the primary coolant clean-up demineralizers to determine the decontamination factor for ^{14}C . The total ^{14}C concentration, obtained by adding the inorganic and organic concentrations, indicates that there is no measurable removal of ^{14}C by the ion-exchange resins.

If, however, only 10% of the ^{14}C in the primary coolant were removed in

17th DOE NUCLEAR AIR CLEANING CONFERENCE

passing through the clean-up demineralizers, a quantity not recognizable by differential analysis of the primary coolant, the removal rate would be 1.7 Ci/GW(e)-yr, or about 15% of the gaseous discharge rate. Measurements of the ^{14}C concentrations in the demineralizer resins and filter sludge should be made in addition to the coolant measurements to determine the amount of ^{14}C discharged as low-level solid wastes.

The average concentration of total ^{14}C in the primary coolant was 1.1×10^{-4} $\mu\text{Ci/ml}$ and varied by less than a factor of 2 from sample to sample. By measuring the leak rate of primary coolant, the discharge of ^{14}C via this pathway could be estimated. Assuming a primary coolant leak rate of 130 cc/min and an average concentration for total ^{14}C of 1×10^{-4} $\mu\text{Ci/ml}$, the liquid discharge rate was 0.007 Ci/yr.

A wastewater composite sample was also analyzed for inorganic and organic ^{14}C . The composite included contaminated water from sources such as controlled area equipment and floor drains, radiochemistry laboratory drains, and laundry and shower drains, which is collected in a wastewater hold-up tank. Evaporators are used to concentrate the radioactive material as evaporator bottoms or sludge and to recover the distilled water. The evaporator sludge is packaged in drums for disposal in low-level burial sites. Based on the measured ^{14}C concentration of 5.1×10^{-7} $\mu\text{Ci/ml}$ in the wastewater and assuming that a maximum of 8000 cc of wastewater/min is processed and that all the ^{14}C is collected in the evaporator bottoms, a total of 0.002 Ci/yr would be shipped to burial.

1000 MW(e) PWR

Plant Ventilating System. All building air, containment air, and gas decay tanks at this reactor are vented through the main plant vent at a flow rate of $2-4 \times 10^7$ cc/s. Building air is continuously vented; containment air and gas in decay tanks are released periodically.

Gaseous Grab Samples. Samples of decay tank gas collected in 1976 and 1978 contained 3% to 4% of the total ^{14}C as $^{14}\text{CO}_2$, whereas a sample taken in 1981 contained 25% of the total ^{14}C as $^{14}\text{CO}_2$. The balance of the ^{14}C was in the form of $^{14}\text{CH}_4$ and other hydrocarbon gases. During the recent test period (August 1980-April 1982), gas decay tanks were vented at a rate of 48 tanks/yr. The volume of each tank is 14.9m^3 , and they are normally filled to a pressure of 6.9×10^5 Pa (100 psi). The average concentration of total ^{14}C in the gas decay tanks was 5.3×10^{-5} $\mu\text{Ci/cc}$, which results in a release rate of 0.26 Ci/yr.

The $^{14}\text{CO}_2$ concentration in a sample of containment air collected in 1978 was 7% of the total ^{14}C concentration. In a 1981 sample $^{14}\text{CO}_2$ was 15% of the total, with the balance as $^{14}\text{CH}_4$ and other hydrocarbon gases. The containment air is vented at a rate of 7.1×10^5 cc/s for about 3 h every 3 days to relieve excess pressure. This corresponds to exchanging the containment air every 23 days, or about 16 times each year. In addition the containment is purged two or three times each year. The average concentration of ^{14}C in the containment air was 3.4×10^{-6} $\mu\text{Ci/cc}$, which indicates a ^{14}C discharge rate of 3.5 Ci/yr through pressure relief and purging of containment air.

Continuous Gas Sampling. Continuous samplers were used to measure both total ^{14}C and $^{14}\text{CO}_2$ releases from the main plant during an 84-week period beginning in August 1980. Measurements of total ^{14}C (Fig. 5) show that the rate of discharge of ^{14}C tended to increase with time after an outage. The amount

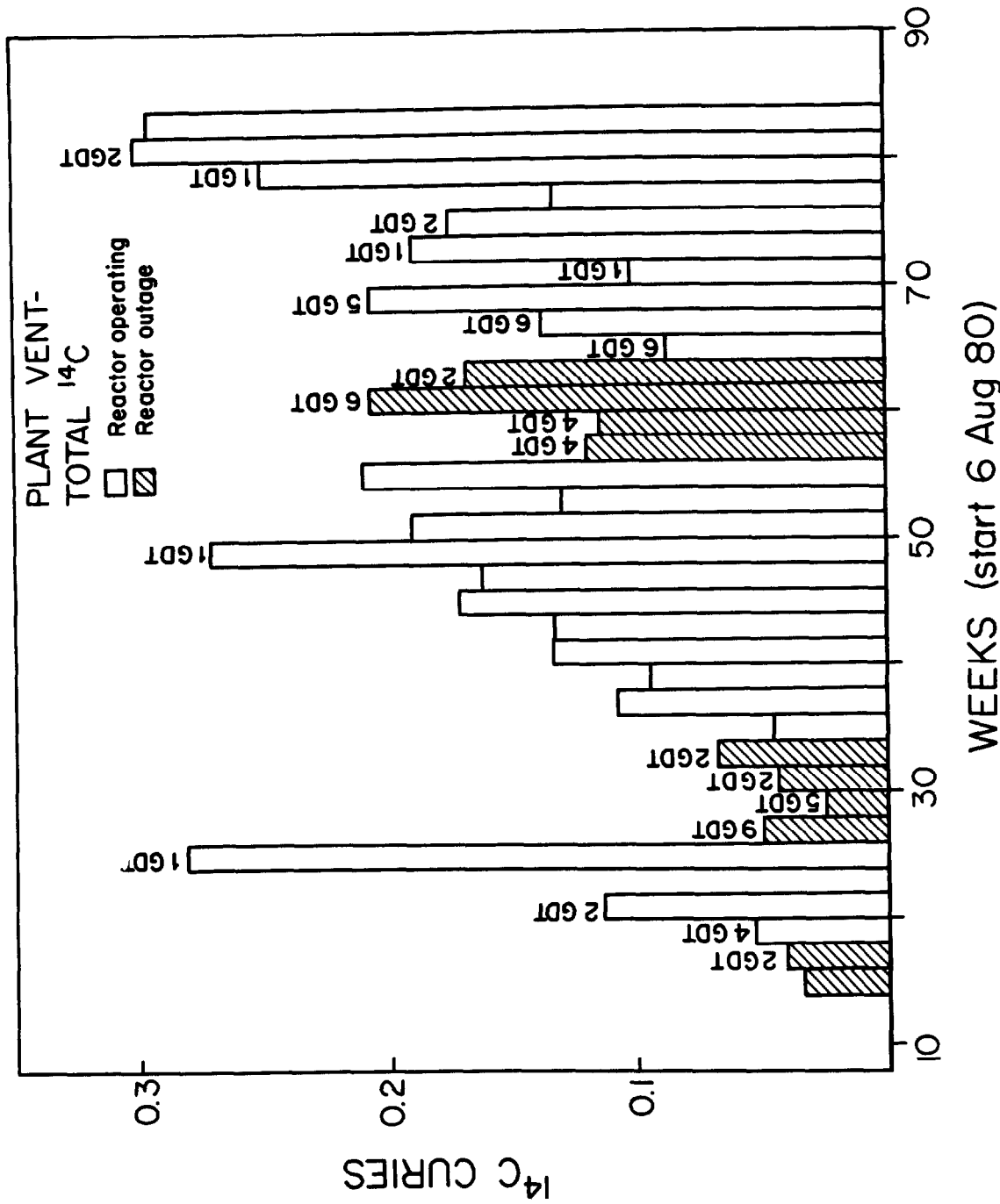


Figure 5 Biweekly measurements of total ¹⁴C discharge from plant vent of a 1000 MW(e) PWR. Gas decay tank (GDT) releases are indicated for each 2-week period.

17th DOE NUCLEAR AIR CLEANING CONFERENCE

of ^{14}C released varied considerably from week to week, with no apparent correlation between the quantity discharged and the gas decay tank releases.

During the 68-week period when total ^{14}C was measured, 4.9 Ci was discharged, a rate of 3.7 Ci/yr. Since the reactor was operating at 48% of full power, this rate corresponds to 8.0 Ci/GW(e)-yr.

During 26 weeks when no gas decay tanks were vented, a total of 1.8 Ci of ^{14}C was released, - a rate of 3.7 Ci/yr - the same rate as for the entire 68-week sampling period. Thus indicating that the amount of ^{14}C discharged via gas decay tank releases was only a small fraction of the total. The grab sample data further indicated that 0.26 Ci/yr, or about 7% of the total ^{14}C , was discharged through gas decay tank releases. The grab sample estimates of ^{14}C released through pressure relief venting and purging of containment indicate that containment releases were the major pathway for ^{14}C discharge.

The amount of ^{14}C discharged as $^{14}\text{CO}_2$ is shown in Fig. 6. The $^{14}\text{CO}_2$ discharge was greatest during outages. For the last 54 weeks of the test period both total ^{14}C and $^{14}\text{CO}_2$ were measured. During this period 0.81 Ci of $^{14}\text{CO}_2$ was discharged, and the total ^{14}C discharged was 4.25 Ci. Therefore $^{14}\text{CO}_2$ represented 19% of the total ^{14}C released.

Liquid Grab Samples. Samples of primary coolant were taken before and after passage through the clean-up demineralizers and were analyzed for inorganic and organic ^{14}C . There was essentially no change in ^{14}C concentration, indicating that the decontamination factor for ^{14}C is small. A decontamination factor of only 10% would be unmeasurable by this method but would result in about 1 Ci of ^{14}C /yr being removed by the clean-up demineralizers. The average concentration of ^{14}C in the primary coolant was 7×10^{-5} $\mu\text{Ci/ml}$, about half organic and half inorganic carbon. Assuming a primary coolant leak rate of 2000 cc/min, a liquid discharge rate of 0.07 Ci/yr is estimated for this possible pathway.

850 MW(e) BWR

Plant Ventilating System. The off-gas stripped from the primary steam at the BWR is released through a 117-m stack. The unprocessed off-gas has a flow rate of about 7×10^4 cc/s, which is reduced to about 2×10^4 cc/s when the advanced off-gas system is used. The off-gas is diluted with outside air, resulting in a stack flow rate of 3×10^6 cc/s. The reactor building, turbine building, refuel floor, and radwaste building each have a separate building vent.

Gaseous Grab Samples. Three samples from the off-gas stack were analyzed for ^{14}C . $^{14}\text{CO}_2$ comprised between 97% and 99% of the total ^{14}C , with the balance as $^{14}\text{CH}_4$ and other hydrocarbon gases. Under the oxidizing conditions in the coolant of a BWR, carbon appears to be predominantly oxidized to CO_2 . The average concentration of total ^{14}C in the off-gas stack was 9×10^{-8} $\mu\text{Ci/cc}$. Since the stack flow rate was 3×10^6 cc/s, the estimated ^{14}C discharge rate was 9 Ci/yr based on grab sample measurements.

Continuous Gas Sampling. The stack gas was sampled for total ^{14}C for 98 consecutive weeks, beginning in July 1980 (Fig. 7). During outages the ^{14}C release dropped rapidly to essentially zero. When the plant was operating, the quantity of ^{14}C released tended to be directly related to the reactor power level. During the 98-week test period a total of 11.9 Ci of ^{14}C was discharged from the off-gas stack, a discharge rate of 6.3 Ci/yr. Since the reactor operated at 61% of full

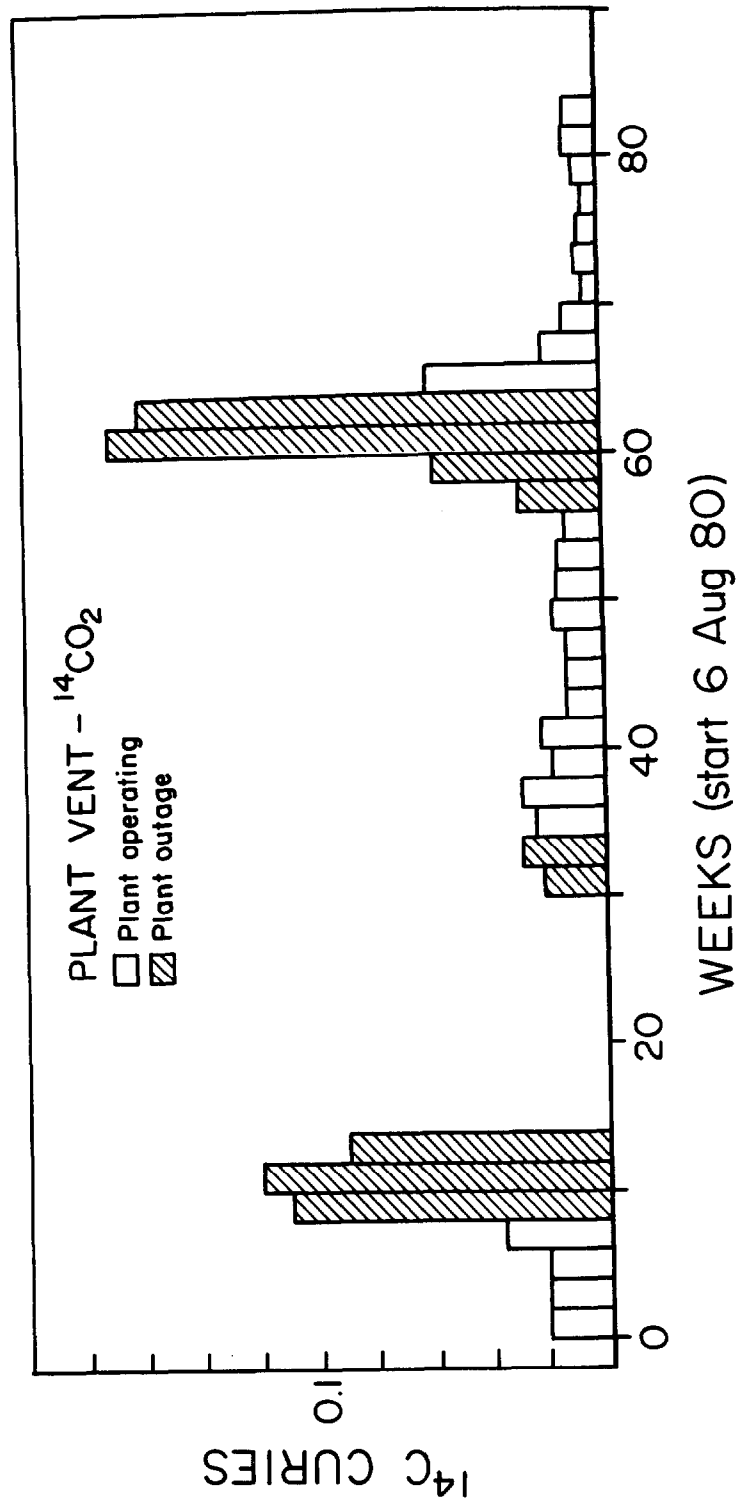


Figure 6 Biweekly measurements of $^{14}\text{C}\text{O}_2$ discharge from plant vent of a 1000 MW(e) PWR.

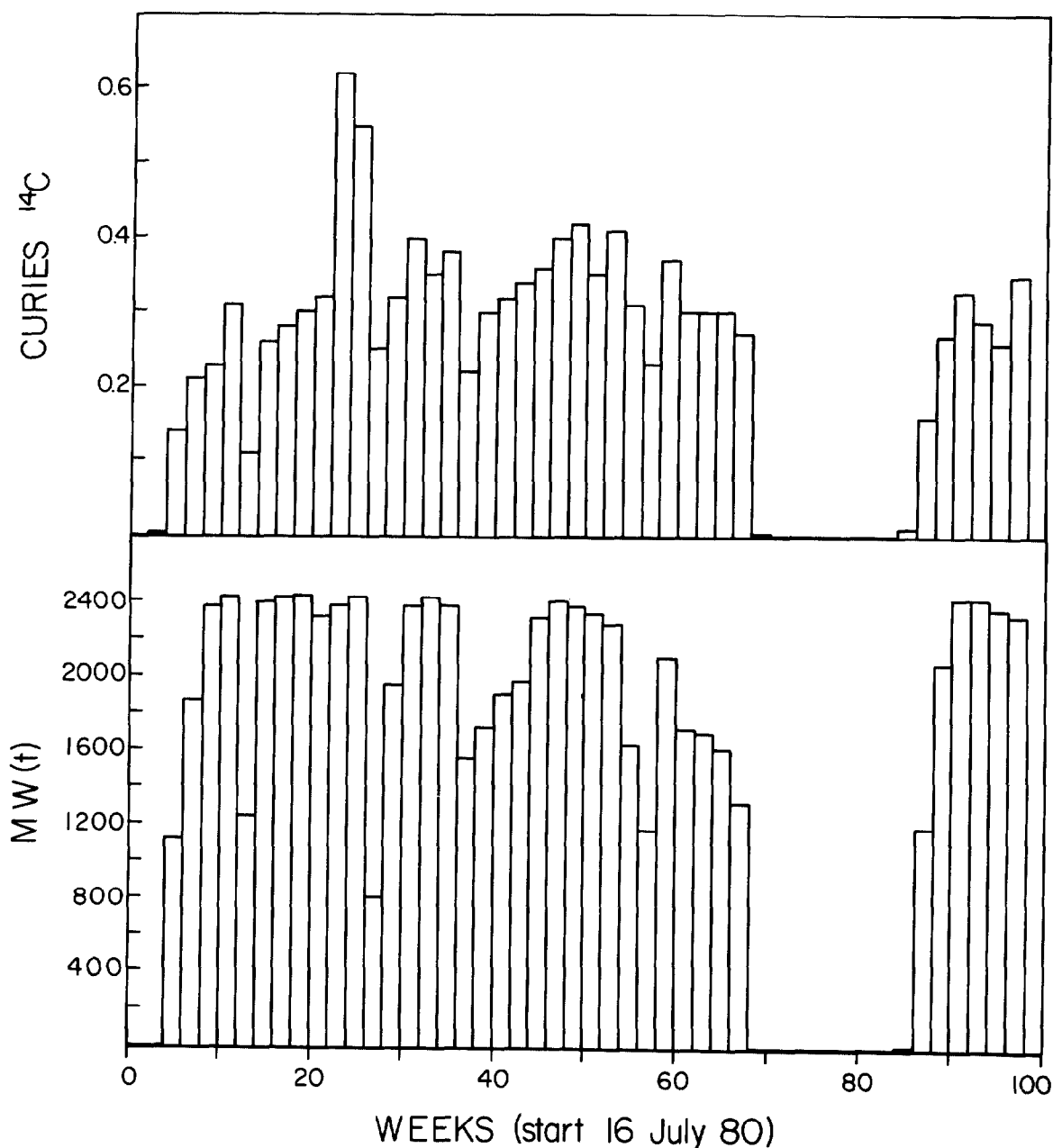


Figure 7 Biweekly measurements of ^{14}C discharge from off-gas stack and average power levels of an 850 MW(e) BWR.

power, the discharge rate is equivalent to 12.3 Ci/GW(e)-yr.

A continuous sampler was used to sample the total ^{14}C discharge from each of the building vents for a period of about 3 months on each vent. The reactor building, turbine building, and radwaste building vents were sampled when the reactor was operating; the refuel floor vent was sampled during an outage. The rates of ^{14}C discharge were 0.018 Ci/yr for the reactor building, 0.035 Ci/yr for the turbine building, 0.048 Ci/yr for the radwaste building, and 0.12 Ci/yr for

17th DOE NUCLEAR AIR CLEANING CONFERENCE

the refuel floor. Thus gaseous ^{14}C appears to be discharged almost entirely via the off-gas stack.

Liquid Grab Samples. One set of coolant samples taken before and after passage through both the clean-up and condensate demineralizers was analyzed for inorganic and organic ^{14}C . A decontamination factor of 7 was found for the clean-up demineralizer, whereas the condensate demineralizer showed no removal of ^{14}C . The concentration of ^{14}C in the coolant before the clean-up demineralizer was 2×10^{-6} $\mu\text{Ci/ml}$, which, when combined with a decontamination factor of 7, results in a ^{14}C removal rate of 0.5 Ci/yr. Additional coolant samples, as well as resins and filter sludge, could be analyzed for ^{14}C to determine more accurately the amount of ^{14}C removed by the demineralizers.

The primary coolant leak rate was about 3×10^4 cc/min. This water is recycled after demineralizer cleanup. Assuming that all the ^{14}C is removed during cleanup, 0.03 Ci/yr would be retained in the recycled water cleanup systems.

Conclusions

Continuous stack samplers with a solid absorbent to trap CO_2 were used to monitor the gaseous ^{14}C released from two PWRs and one BWR. The samplers were run continuously for 84 to 98 weeks at each reactor; sample cartridges were exchanged biweekly.

The ^{14}C discharge rates measured for a 490 MW(e) PWR and a 1000 MW(e) PWR were 11.6 and 8.0 Ci/GW(e)-yr respectively. In other studies the average calculated estimate for the production of ^{14}C in the coolant of a PWR was 6.7 Ci/GW(e)-yr,⁽⁵⁾ and the average measured value for five PWRs in the Federal Republic of Germany was 6 Ci/GW(e)-yr.⁽⁴⁾ The somewhat higher rate of 11.6 Ci/GW(e)-yr determined for the 490 MW(e) PWR may be due to the unique design of this older reactor. Otherwise there is fairly good agreement between the calculated and measured values for PWRs.

The chemical form of the ^{14}C gaseous discharge at the PWRs was over 80% as $^{14}\text{CH}_4$ and other hydrocarbon gases, with the balance as $^{14}\text{CO}_2$. The ^{14}C release was quite variable from week to week, with substantial quantities released during outages. Most of the ^{14}C was released through containment and auxiliary building ventilation, where the large volume flow rates would appear to make ^{14}C removal impractical.

The ^{14}C discharge rate measured for an 850 MW(e) BWR was 12.3 Ci/GW(e)-yr. The average calculated estimate for production of ^{14}C in the coolant of a BWR was 8.2 Ci/GW(e)-yr,⁽⁵⁾ and the average measured value at four BWRs in the Federal Republic of Germany was 14 Ci/GW(e)-yr.⁽⁴⁾ These initial results indicate that the actual production rate for a BWR is over 50% higher than the average calculated estimate. The chemical form was almost entirely $^{14}\text{CO}_2$, and the discharge pathway was almost entirely via the off-gas stack. The off-gas flow rate of $2-7 \times 10^4$ cc/s would appear to be amenable to ^{14}C removal. The release of ^{14}C showed a correlation to reactor power, dropping to essentially zero during outages.

From initial measurements of the ^{14}C decontamination factors for the primary coolant clean-up systems it appears that the discharge of ^{14}C in solid wastes is small compared to the gaseous discharge.

17th DOE NUCLEAR AIR CLEANING CONFERENCE

Acknowledgment

Partial funding of this study was provided by the Rochester Gas and Electric Company and the Power Authority of the State of New York. Staff members at the three nuclear plants were extremely helpful in providing guidance and assistance throughout this study.

References

1. Bonka, H., Brussermann, K., Schwarz, G., "Umweltbelastung durch Radiokohlenstoff aus kerntechnischen Anlagen", Reaktortagung, Berlin (April 1974).
2. Magno, P. J., Nelson, O. B., Ellett, N. H., "A consideration of the Significance of carbon-14 discharges from the nuclear power industry", 13th AEC Air Cleaning Conf., San Francisco (1974).
3. Kunz, C., Mahoney, W. E., and Miller, T. W., "C-14 gaseous effluent from pressurized water reactors", Health Physics Soc. Symposium on Population Exposures, Knoxville, TN, 21-24 October 1974.
4. Schwibach, J., Riedel, H., and Bretschneider, J., "Investigations into the emission of carbon-14 compounds from nuclear facilities", Report No. V-3062/78-EN, Commission of the European Communities, Luxembourg, November 1978.
5. Bonka, H., "Produktion und freisetzung von ^3H and ^{14}C durch kernwaffenversuche, testexplosionen und kerntechnische anlagen", Einschliesslich Wiederaufarbeitungsanlagen, Wissenschaftliches Symposium des Instituts für Strahlenhygiene, Berlin, 14-16 November 1979.
6. Kunz, C., "Separation techniques for reactor-produced noble gases", Proc. Noble Gases Symposium, Las Vegas, NV, pp. 209-217 (1973).
7. Paperiello, C. J., "Internal gas-proportional beta-spectrometry for measurement of radioactive noble gases in reactor effluents", Proc. Noble Gases Symposium, Las Vegas, NV, pp. 239-248 (1973).

DISCUSSION

BONKA: You mentioned that the measured ^{14}C emission rate of boiling water reactors is nearly 50% higher than the calculated rate. The reason should be a higher nitrogen impurity in the water of the primary circuit. In the literature I found one value for the nitrogen impurity in the water. That is a nitrogen measurement in a water sample of the boiling water reactor Muhlegerg/Swiss at a laboratory in New York. The nitrogen impurity was nearly 50ppm.

KUNZ: I am not aware of the Swiss measurement or any other measurement of the nitrogen impurity in the coolant of boiling water reactors. It may be possible to estimate the nitrogen in the coolant from the nitrogen content of the off-gas. Assuming that the source of the nitrogen in the off-gas is the coolant and is not due to air in-leakage to the off-gas stream, I believe the coolant concentration could be as high as 20ppm atomic nitrogen.

17th DOE NUCLEAR AIR CLEANING CONFERENCE

SIEGLER: Commenting on the last question, I believe that the speaker's estimate of 20 ppm N_2 in BWR reactor water is high by a factor of 50 to 100 based on measurements made at operating BWRs. Also, N_2 in off-gas is due to air in-leakage.

HAYES: Can you explain the reason why the 490 MW(e) PWR shows 45% (about 5 Ci/GW(e)-yr) of $C-14$ released from the waste gas decay tanks while the larger (1,000 MW(e)) PWR shows only 7% or 0.56 Ci/GW(e)-yr released from the waste gas decay tanks?

KUNZ: Our results indicate that at the 1,000 MW(e) PWR most of the $C-14$ is leaking from reactor components into the containment air during plant operation. At the 490 ME(e) PWR the radioactive gases are better contained in the primary system during plant operation and a higher fraction of the total $14C$ is transferred to the GDTs.

BANGART: As a further comment on the last question, I would like to add that the amount of $C-14$ released from WG-DT will be dependent upon the type of gas stripping of the let-down flow, i.e., full or partial stripping. Similarly, $C-14$ releases to building ventilation may depend upon the amounts of mainenance being conducted.

CARBON-14 IMMOBILIZATION VIA THE $\text{Ba}(\text{OH})_2 \cdot 8\text{H}_2\text{O}$ PROCESS*

G. L. Haag, J. W. Nehls, Jr., and G. C. Young
Chemical Technology Division
Oak Ridge National Laboratory
Oak Ridge, Tennessee

Abstract

The airborne release of ^{14}C from various nuclear facilities has been identified as a potential biohazard due to the long half-life of ^{14}C (5730 years) and the ease with which it may be assimilated into the biosphere. At Oak Ridge National Laboratory (ORNL), technology is under development, as part of the Airborne Waste Management Program, for the removal and immobilization of this radionuclide. Prior studies have indicated that ^{14}C will likely exist in the oxidized form as CO_2 and will contribute slightly to the bulk CO_2 concentration of the gas stream, which is airlike in nature (~330 ppmv CO_2). The technology under development utilizes the CO_2 - $\text{Ba}(\text{OH})_2 \cdot 8\text{H}_2\text{O}$ gas-solid reaction with the mode of gas-solid contacting being a fixed bed. The product, BaCO_3 , possesses excellent thermal and chemical stability, prerequisites for the long-term disposal of nuclear wastes. For optimal process operation, studies have indicated that an operating window of adequate size does exist. When operating within the window, high CO_2 removal efficiency (effluent concentrations <100 ppbv), high reactant utilization (>99%), and an acceptable pressure drop across the bed (3 kPa/m at a superficial velocity of 13 cm/s) are possible. This paper will address three areas of experimental investigation: (1) microscale studies on 150-mg samples to provide information concerning surface properties, kinetics, and equilibrium vapor pressures; (2) macroscale studies on large fixed beds (4.2 kg of reactant) to determine the effects of humidity, temperature, and gas flow rate upon bed pressure drop and CO_2 breakthrough; and (3) design, construction, and initial operation of a pilot unit capable of continuously processing a $34\text{-m}^3/\text{h}$ ($20\text{-ft}^3/\text{min}$) air-based gas stream.

I. Introduction

The release of ^{14}C from the nuclear fuel cycle has been identified as a potential biohazard because of its long half-life (5730 years) and the ease with which it may be assimilated into the biosphere.¹⁻²⁰ In nuclear reactors, ^{14}C is produced primarily by neutron interactions with ^{13}C , ^{14}N , and ^{17}O , which are present in the fuel, the cladding, and the coolant. The bulk of the ^{14}C is released in gaseous form either at the reactor or when the spent fuel is reprocessed. Presented in Table I are representative release rates at various nuclear facilities.

*Research sponsored by the Division of Waste Products, Office of Nuclear Waste Management, U.S. Department of Energy under contract W-7405-eng-26 with the Union Carbide Corporation.

17th DOE NUCLEAR AIR CLEANING CONFERENCE

Table I. Approximate production and release rates of several types of facilities

Facility	Rate [Ci/Gw(e)yr]
Nuclear reactors	
LWR	8-10
CANDU	500
Reprocessing plants	
LMFBR	6
LWR	18
HTGR	200

Source: ref. 2.

Carbon-14, like ^3H , ^{85}Kr , and ^{129}I , is a global radionuclide. That is, upon release to the environment, its dosage impact is not limited to the region of release, a release which may be legislated by local government, but rather the net dosage is distributed globally in a nearly uniform manner. Furthermore, because of its long half-life, ^{14}C release poses a health hazard to both present and future generations. Modeling studies have been conducted for predicting the dosage effects from ^{14}C release. However, these studies require major assumptions concerning the effects of low-level radiation, future population growth, and time span of dosage integration. Depending upon the assumptions, total dosage estimates typically vary from 400 to 590 man-rem/Ci. In a modeling study by Killough and Rohwer at ORNL, a total dosage estimate of 540 man-rem/Ci was obtained. This study also predicted dosage estimates for time periods of 30 and 100 years of 18 and 23 man-rem/Ci, respectively.¹⁷ More recent modeling studies by Killough et al. have indicated that for ^{14}C release from a 30.5-m (100-ft) stack at the Morris, Illinois, or Barnwell, South Carolina, reprocessing plants, 0.02 and 0.002% of the total dosage would occur within 100 km of the respective points of release.¹⁸ A study by the Nuclear Energy Agency (NEA) on the release of global radionuclides ^3H , ^{14}C , ^{85}Kr , and ^{129}I restricted the time period of interest to 10,000 years. Hence a partial dosage for ^{14}C of 290 man-rem/Ci was used.¹⁶ With knowledge of the worldwide release of ^{14}C , the resulting dosage per curie released, and assuming 146 fatal effects, 105 nonfatal cancers, and 76 serious genetic effects per million man-rem of dosage as estimated by Fowler and Nelson,²⁰ an estimate of the health effects resulting from ^{14}C release may be made. However, these health effects must be placed in proper perspective; that is, they may occur any place and any time within the time limits of dosage integration. For global radionuclides with long half-lives, the often cited cost-effective values for controlling radionuclide release, \$100 to \$1000 per man-rem, may not be justified, as certain questions of a philosophical and technical nature must first be answered. However, if a technology with suitable cost-effectiveness is shown to exist, the control of ^{14}C

release will then be warranted. Therefore, the primary goal of this research effort is to develop such a cost-effective technology.

II. Technology Development

In the development of technology for controlling the release of ^{14}C from the nuclear fuel cycle, we have established the following criteria for candidate processes:

1. acceptable process efficiency, with a nominal decontamination factor of 10;
2. acceptable final product form for long-term waste disposal;
3. excellent on-line process characteristics;
4. process operation at near-ambient conditions; and
5. acceptable process costs (<\$10/man-rem).

Based upon these criteria, an operationally simple process that utilizes fixed-bed canisters of $\text{Ba}(\text{OH})_2 \cdot 8\text{H}_2\text{O}$ has been developed at ORNL. At ambient temperatures and pressures, this process is capable of removing CO_2 (330 ppmv) in air to concentrations <100 ppbv. Thermodynamic calculations indicate equilibrium concentrations to be at the part-per-trillion level.²¹ The product, BaCO_3 , possesses excellent thermal and chemical stability as it decomposes at 1450°C and is sparingly soluble in water, 0.124 mg-mol/L at 25°C .^{22,23} Furthermore, the soluble reactant undergoes 100% conversion, thus ensuring an extremely stable material for final disposal. Gas throughputs are such that reactor size remains practical for the treatment of anticipated process streams. For a design superficial velocity of 13 cm/s, a reactor with a diameter of 0.70 m (27 in.) would be required for the treatment of a $170\text{-m}^3/\text{h}$ ($100\text{-ft}^3/\text{min}$) off-gas stream. Although extensive cost studies have not been completed, initial comparative studies with alternative technologies have indicated the process to be extremely cost competitive.^{16,20,24-31} The estimated process cost is <\$10/man-rem.

This paper highlights the contents of two major technical reports that are in preparation.^{32,33} For additional information, these reports should be consulted. Studies concerning the development of the $\text{Ba}(\text{OH})_2 \cdot 8\text{H}_2\text{O}$ process for $^{14}\text{CO}_2$ removal will be broken into three areas: (1) microscale studies, (2) fixed-bed macroscale studies, and (3) design and operation of a pilot plant.

Experimental studies have concentrated upon the use of flakes of $\text{Ba}(\text{OH})_2 \cdot 8\text{H}_2\text{O}$. As shown in Fig. 1, the material is a free-flowing solid and when reacted with CO_2 under proper conditions, the flake form remains intact upon conversion to BaCO_3 . Vendor specifications indicate that the material is substoichiometric in water and possesses an overall hydration of 7.0 to 7.9 H_2O . Discussions with the vendor indicated that the water deficiency is intentional so as to ensure a free-flowing, nonsticking product.

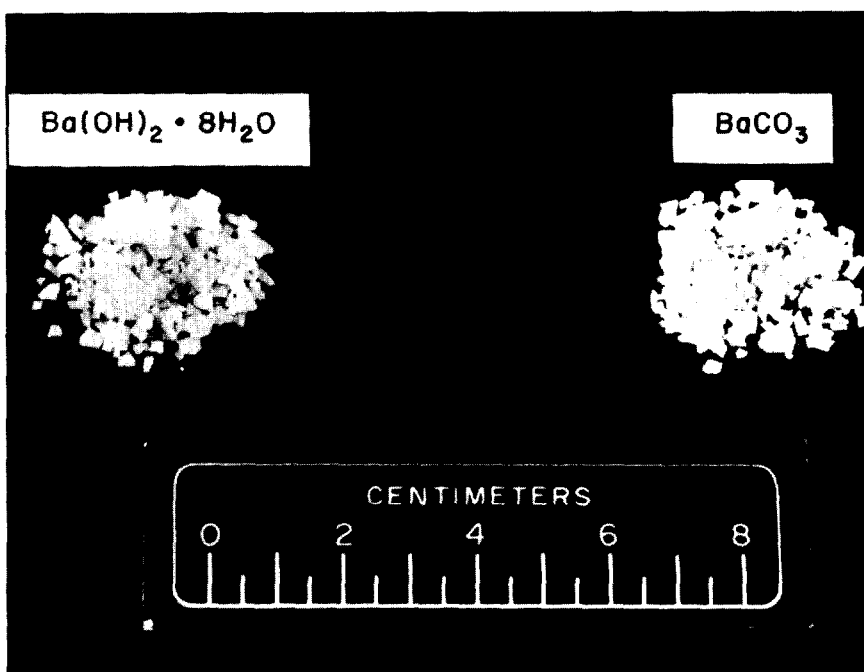


Fig. 1. Commercial $\text{Ba(OH)}_2 \cdot 8\text{H}_2\text{O}$ flaked reactant and BaCO_3 flaked product. The product was obtained at a process relative humidity <60%.

The flakes are prepared by distributing a Ba(OH)_2 hydrate magma ($\sim 78^\circ\text{C}$) on a stainless steel conveyor belt, which is cooled on the underside with cooling water.³⁴ The resulting flakes have variable thicknesses [an average thickness 0.10 cm (1/16 in.)]. The results of a particle-size analysis on material originating from two batches are presented in Table II. Analysis of samples obtained from these batches indicated stoichiometries of approximately 7.5 and 7.0 H_2O

Table II. Particle-size analysis of commercial $\text{Ba(OH)}_2 \cdot 8\text{H}_2\text{O}$ flakes obtained from two different batches

Particle size		Weight percent	
Mesh	mm	Batch 1	Batch 2
4 +	4.75	18.5	5.8
8 + 4	2.36 + 4.75	46.9	33.0
20 + 8	0.850 + 236	31.6	54.5
50 + 20	0.300 + 0.850	2.0	4.9
120 +	0.125 + 0.300	0.4	1.2
+ 120	+ 0.125	0.6	0.6

respectively. For a given batch, little variation was observed in the extent of hydration. X-ray analysis of the two samples failed to confirm the presence of $\text{Ba}(\text{OH})_2 \cdot 3\text{H}_2\text{O}$, the next stable hydrate of lower stoichiometry. However, the existence of a $\text{Ba}(\text{OH})_2 \cdot 3\text{H}_2\text{O}$ - $\text{Ba}(\text{OH})_2 \cdot 8\text{H}_2\text{O}$ eutectic with an overall water stoichiometry of 7.19 has been reported.^{35,36} We speculated that the trihydrate species was not detected because of its extremely small crystallite size. Sorption isotherm studies indicated that the reactant displayed negligible micro-porosity ($d < 2$ nm) or restrictive mesoporosity (2 nm $< d < 150$ nm). Mercury porosimetry studies indicated that the pore size distribution was bimodal with maximas of 0.17 and 1.0 μm and that the flake porosity was 12%. When a flake was exposed to a water vapor pressure less than or greater than the vapor pressure of $\text{Ba}(\text{OH})_2 \cdot 8\text{H}_2\text{O}$, the material either dehydrated to the trihydrate or hydrated to the octahydrate. Rehydration was observed to proceed in one of two regimes and was dependent upon the relative humidity. This factor will be addressed in subsequent sections. The best correlation for predicting the vapor pressure of $\text{Ba}(\text{OH})_2 \cdot 8\text{H}_2\text{O}$ appears to be that presented by Kondakov et al.:³⁷

$$\log P = - \frac{58230}{19.155T} + 13.238 ,$$

where

P = pressure, Pa or nt/m²,

T = temperature, K.

With respect to published vapor pressure data on $\text{Ba}(\text{OH})_2 \cdot 8\text{H}_2\text{O}$, a comprehensive, chronological review of the published vapor pressures is presented in ref. 32.

As shown in Fig. 1, operating conditions exist for which the integrity of the flake form is retained upon conversion to BaCO_3 . Because of the low molar volume of the product as compared to that of the reactant, a ratio of 0.31, and an initial particle voidage of 12%, one would predict a final product porosity of 73%. Mercury porosimetry studies have indicated product porosities of 66 to 72%.^{21,32} Visual evidence of this porosity may be observed by comparing scanning electron micrographs of the reactant and product (Fig. 2).

The following $\text{Ba}(\text{OH})_2$ hydrate nomenclature, will be used in the remainder of this paper: The substoichiometric flakes will be referred to as commercial $\text{Ba}(\text{OH})_2 \cdot 8\text{H}_2\text{O}$ (7.5). Where it is of significance, the term in parenthesis will refer to the initial hydration stoichiometry. The term $\text{Ba}(\text{OH})_2 \cdot 8\text{H}_2\text{O}$ will refer to the stable crystalline species with 8 waters of hydration.

III. Microscale Studies

Realizing that an understanding or at least an awareness of phenomena which occur on the microscale is often required to develop an understanding of macroscale phenomena, basic studies were conducted



Fig. 2. Scanning electron micrographs of a flake of commercial $\text{Ba}(\text{OH})_2 \cdot 8\text{H}_2\text{O}$ (top) and the BaCO_3 product. The product was obtained at a process humidity $<60\%$ (original photo, 8.9 x 11.4 cm; magnification, 5000x).

on the hydrates of Ba(OH)_2 and the BaCO_3 product. Analytical techniques consisted of scanning electron microscopy; mercury intrusion for porosimetry determination; acid-base titrations and overall mass balances to determine the extent of conversion and hydration; x-ray diffraction analysis; single-point BET analysis; and operation of a microbalance system whereby studies of a kinetic, thermodynamic, and surface morphological nature could be performed on 150-mg samples (Fig. 3). Results from these studies were useful in the characterizing the $\text{Ba(OH)}_2 \cdot 8\text{H}_2\text{O}$ reactant, which was reported in the preceding section. The intent of this section is to highlight experimental results from the microscale studies, which are as follows.

1. Methods to prepare $\text{Ba(OH)}_2 \cdot \text{H}_2\text{O}$, $\text{Ba(OH)}_2 \cdot 3\text{H}_2\text{O}$ and $\text{Ba(OH)}_2 \cdot 8\text{H}_2\text{O}$ were developed, and the presence of these species was confirmed.

2. Commercial $\text{Ba(OH)}_2 \cdot 8\text{H}_2\text{O}$ flakes were found to display negligible surface area. Hydration to $\text{Ba(OH)}_2 \cdot 8\text{H}_2\text{O}$ was observed to proceed in one of two regimes. For relative humidities $<60\%$, the increase in surface area was small and the flake form remained intact. For relative humidities $>60\%$, the flake recrystallized in a manner which resulted in greater surface area, but the increase in activity also resulted in a more fragile product.

3. Dehydration of commercial $\text{Ba(OH)}_2 \cdot 8\text{H}_2\text{O}$ to $\text{Ba(OH)}_2 \cdot 3\text{H}_2\text{O}$ and subsequent rehydration to $\text{Ba(OH)}_2 \cdot 8\text{H}_2\text{O}$ at relative humidities $<60\%$ was modeled by a shrinking core model. The relative rate was found to be dependent upon the difference between the water sorbed on the surface for a given P/P_0 value (i.e., relative humidity) and that required on the surface for $\text{Ba(OH)}_2 \cdot 8\text{H}_2\text{O}$ to exist in a stable form.

4. There was evidence of considerable hydrogen bonding within the $\text{Ba(OH)}_2 \cdot 8\text{H}_2\text{O}$ crystal. These results paralleled the crystallography studies of Monohar and Ramaseshan in which they cited difficulty in differentiating the location of the hydroxyl ions from the waters of hydration.³⁸

5. The vapor pressure correlation for $\text{Ba(OH)}_2 \cdot 8\text{H}_2\text{O}$ cited in the previous section was indirectly verified at two temperatures.

6. At low CO_2 vapor pressures, $\text{Ba(OH)}_2 \cdot 8\text{H}_2\text{O}$ was observed to be 3 orders of magnitude more reactive toward CO_2 than either $\text{Ba(OH)}_2 \cdot 3\text{H}_2\text{O}$ or $\text{Ba(OH)}_2 \cdot \text{H}_2\text{O}$.

7. For relative humidities $<60\%$, the increase in surface area with product conversion was found to be a very strong function of the specific rate of reaction and was not a linear function of conversion.

8. The surface area of BaCO_3 product was determined to be a function of relative humidity. In a manner analogous to the dehydration of commercial $\text{Ba(OH)}_2 \cdot 8\text{H}_2\text{O}$ and the rehydration of $\text{Ba(OH)}_2 \cdot 3\text{H}_2\text{O}$, surface water appeared to aid in the transport of the reactant and product species, thus resulting in lower surface areas at higher values of P/P_0 . However, the authors feel that the increase in



Fig. 3. The microbalance system.

surface water could not account for the drastic difference in CO_2 reactivity observed for the various hydrate species. The difference in reactivity appears to result from the additional water in the crystal structure and the greater mobility of the hydroxyl ions.

9. Based upon the analysis of nitrogen sorption isotherm data, there were no indications of hysteresis. Therefore if capillary condensation should occur, one would speculate it to result from the wall effects of noncircular pores (e.g., V-shaped points of intersurface contact).

Detailed information appears in ref. 32, which is as yet unpublished.

IV. Fixed-bed macroscale studies

Over 18,000 hours of experimental operating time have been completed on fixed beds of $\text{Ba}(\text{OH})_2 \cdot 8\text{H}_2\text{O}$. These beds typically contained from 2.9 to 4.3 kg of reactant. A schematic of the experimental system, which has been described in detail in a previous paper,²¹ is presented in Fig. 4. The intent of this aspect of the study was to determine the effects of air flow rate (superficial gas velocities of 7-21 cm/s), operating temperature (22-42°C), and water vapor pressure or relative humidity (0-80%) on the operational characteristics of the fixed bed, most notably the shape of the breakthrough curve and the pressure drop across the fixed bed. Since the reaction is endothermic, the reactor was jacketed and the temperatures of the influent and effluent streams were held constant. Presented in Fig. 5 is a typical breakthrough curve and pressure drop plot. For this particular run, the pressure drop increase was noticeable and was not solely a function of bed conversion.

In the course of these fixed-bed studies, it was observed that for a given mass throughput, certain process conditions resulted in a greater pressure drop than others. In several instances, the increase in pressure drop during a run behaved in an autocatalytic manner and necessitated discontinuation of the run. The increase in pressure drop appeared to result from two phenomena: a slow gradual increase that was a function of bed conversion and a rapid increase that was a function of relative humidity. The magnitude of the latter often overshadowed the former. The observed pressure drop, plotted as a function of relative humidity at two temperatures (295 and 305 K) and a superficial velocity of ~13 cm/s, is presented in Fig. 6. It is significant that the data are consistent at the two temperatures as the saturation vapor pressures differed by a factor of 1.8. Furthermore, the dependency upon relative humidity indicates the presence of a surface adsorption phenomenon. For physical adsorption on surfaces, the extent of adsorption is dependent upon the extent of saturation, P/P_0 , or in the case of water, the relative humidity. The fact that the pressure drop became more severe at ~60% relative humidity indicates that capillary condensation is likely present. Since no hysteresis was observed during nitrogen adsorption studies, we speculate that the condensation occurs at V-shaped contact points or pores. The presence of the condensed water then provides sites of rapid recrystallization. Because the flaked reactant

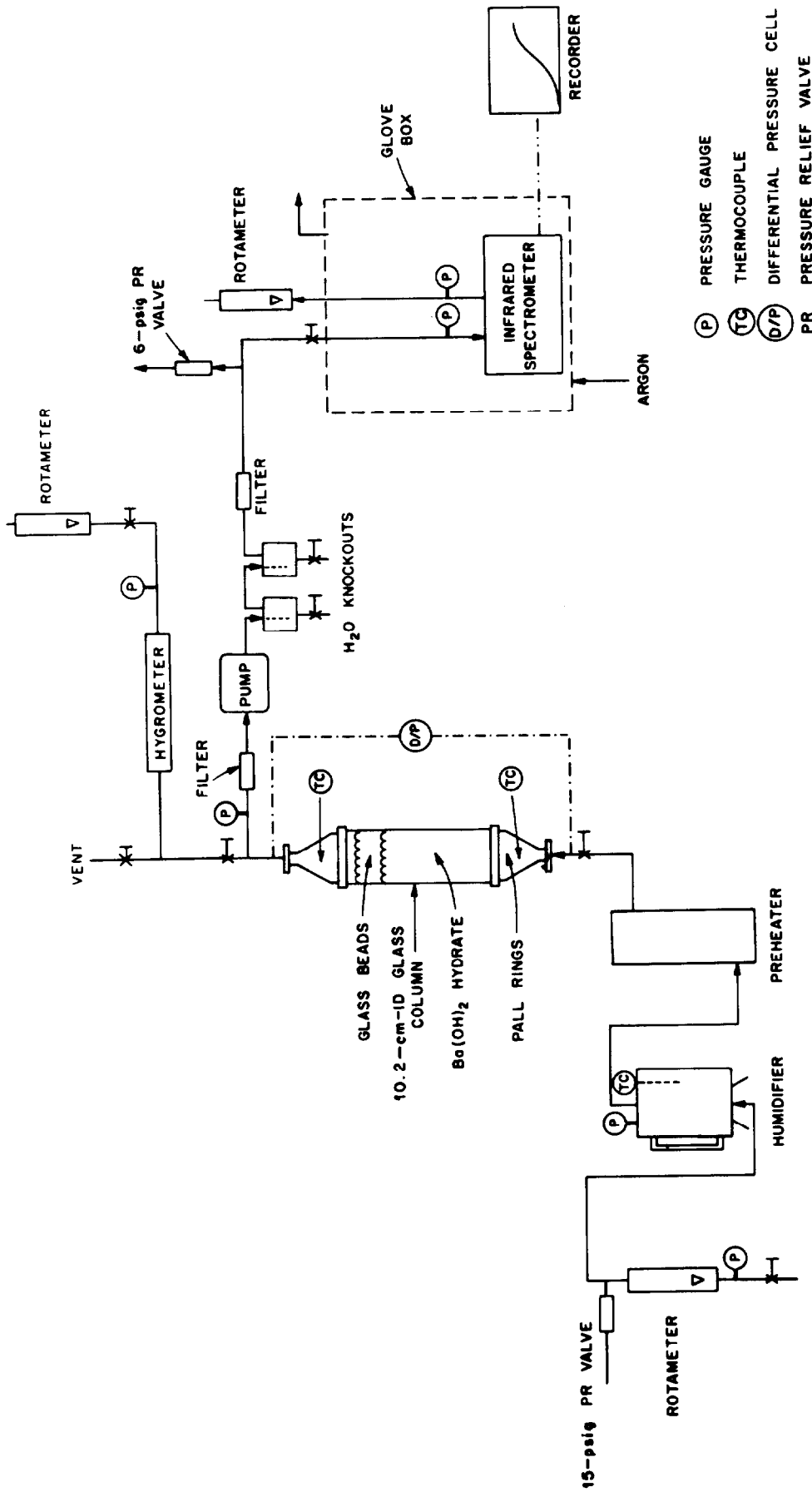


Fig. 4. The fixed-bed experimental equipment.

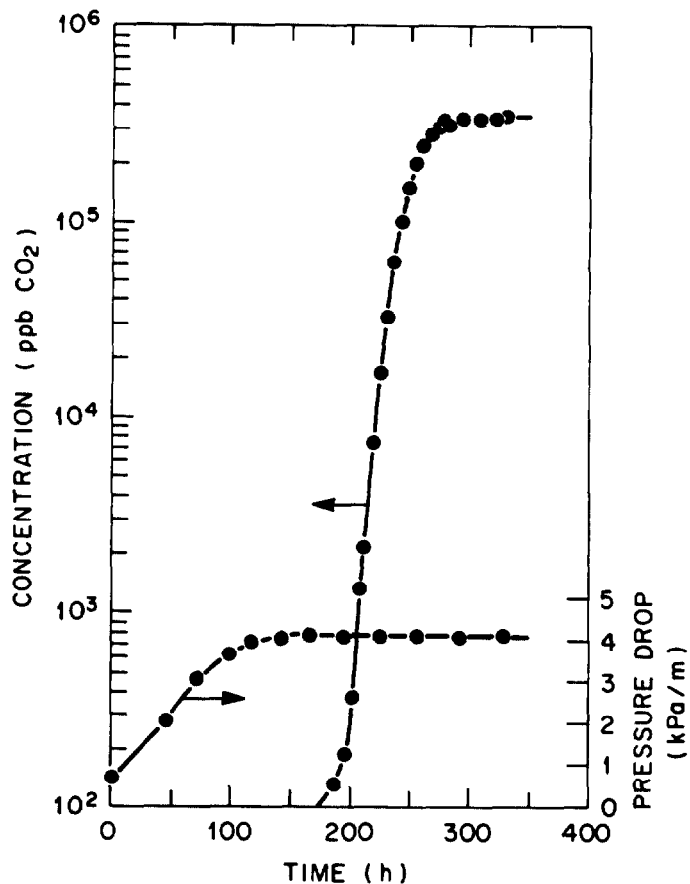


Fig. 5. Logarithm of the experimental breakthrough profile and the change in pressure drop across the bed presented as function of time (superficial gas velocity, ~ 13 cm/s).

was prepared by the rapid cooling of a magma that was substoichiometric in octahydrate (7.0 to 7.9 waters of hydration), the rate of recrystallization is likely enhanced by a need to reduce internal energy locked within the flake. This energy may be present as defects within the crystallites or surface energy resulting from the small size of the crystallites and the presence of the $\text{Ba}(\text{OH})_2 \cdot 3\text{H}_2\text{O}$ – $\text{Ba}(\text{OH})_2 \cdot 8\text{H}_2\text{O}$ eutectic. Photographs of commercial $\text{Ba}(\text{OH})_2 \cdot 8\text{H}_2\text{O}$ flakes after recrystallization at a relative humidity $>60\%$ are presented in Fig. 7. For rehydration at lower humidities, external changes of the flake were small.

The functional dependency of pressure drop upon relative humidity is helpful in understanding the autocatalytic pressure drop behavior observed at high relative humidities. For a fixed influent water vapor concentration, any increase in system pressure at constant temperature will result in an increase in the water vapor pressure and likewise the relative humidity, P/P_0 . Therefore as the pressure drop across the bed increases, so does the relative humidity within the bed and each continues to increase until the run must be terminated. At lower relative humidities, the rate of increase in pressure drop as a function of relative humidity is not sufficient to autocatalyze the process.

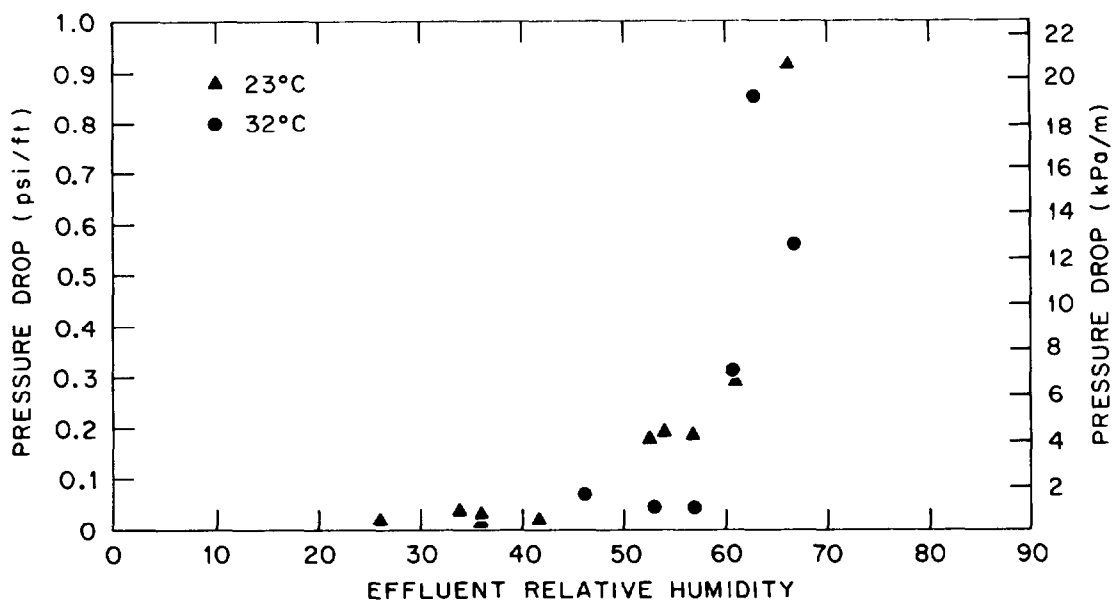


Fig. 6. Pressure drop as a function of relative humidity during fixed-bed studies on commercial $\text{Ba}(\text{OH})_2 \cdot 8\text{H}_2\text{O}$ flakes (superficial gas velocity, ~ 13 cm/s).

The pressure drop dependency upon relative humidity also restricts the upper flow rate that the process may treat. Increased gas flows result in greater pressure drops across the bed (i.e., a greater pressure at the entrance to the bed). Therefore, the relative humidity at the entrance of the bed must be $< 60\%$, but the influent water vapor pressure must be greater than the dissociation vapor pressure of $\text{Ba}(\text{OH})_2 \cdot 8\text{H}_2\text{O}$.

Extensive modeling studies were performed on the breakthrough curves from the fixed-bed studies. Because of the nature of the governing partial differential equations and their respective boundary conditions, solutions were of a numerical nature. An in-depth review of the method of analysis and of the associated assumptions is presented elsewhere.³² The analysis indicated that the rate expression could be modeled by an equation of the form:

$$R = K_F A_0 (1 - X) C ,$$

where

K_F = gas film mass transfer coefficient,

A_0 = initial surface area available for mass transfer,

X = fractional conversion of reactant,

C = bulk CO_2 concentration.

Data analysis indicated $K_F A_0$ to be a weak function of temperature and a strong function of velocity, indicative of gas-film

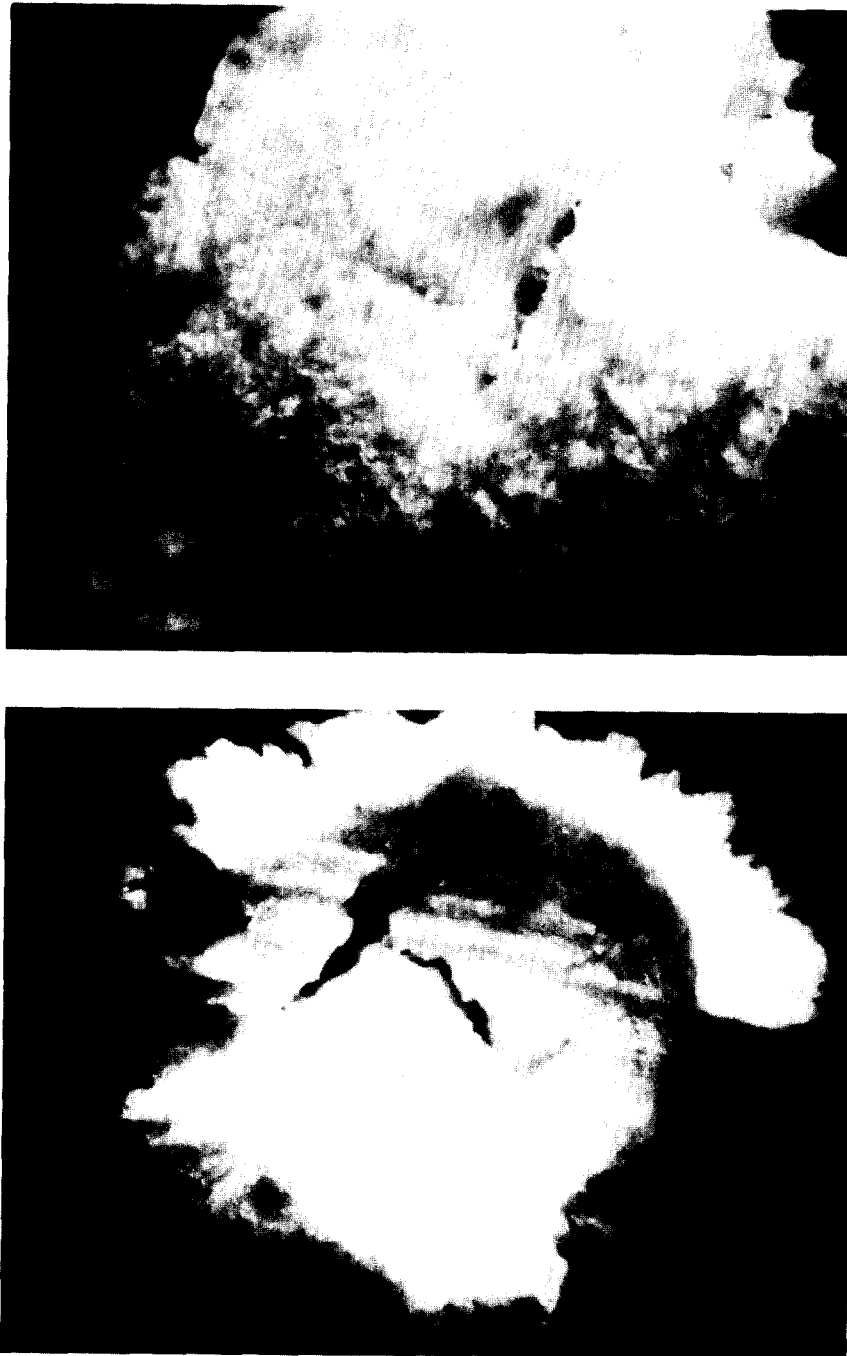


Fig. 7. Top and bottom views of a commercial $\text{Ba}(\text{OH})_2 \cdot 8\text{H}_2\text{O}$ flake subjected to relative humidity $>60\%$.

control. Considerable dispersion in the value of the K_{FA_0} coefficients was observed for a given mass throughput. There were indications that the dispersion resulted from differences in the actual area available for mass transfer and the possible presence of localized channeling. Based upon published correlations for the K_F coefficient, the correlation for the K_{FA_0} coefficient possessed a greater functional dependency upon velocity than expected. Because the studies were conducted on flaked material with considerable interparticle contact, we speculate that the amount of surface area available for mass transfer increased as a function of gas velocity, thus resulting in the greater than anticipated functional dependency of K_{FA_0} upon velocity. This factor may also account for the greater than anticipated dispersion in K_{FA_0} as some localized packing arrangements would be more conducive to restructuring. Representative breakthrough curves and the model-predicted curves are presented in Fig. 8.

V. Pilot Unit Development

In the development of this fixed-bed technology, a pilot unit capable of processing $34 \text{ m}^3/\text{h}$ ($20 \text{ ft}^3/\text{min}$) was designed, constructed, and is currently in operation. Specific goals of this aspect of process development are to provide

1. the basis for the design of a ^{14}C immobilization module for future testing under hot conditions;
2. data at operating conditions not achievable with present bench-scale equipment, in particular operation at near-adiabatic conditions;
3. necessary scale-up data; and
4. operating data on key hardware items and instrumentation.

Presented in Fig. 9 is a flow schematic of the ^{14}C immobilization pilot unit; a photograph of the system is presented in Fig. 10. The designed gas throughput at a superficial velocity of 13 cm/s in the reactor is $34 \text{ m}^3/\text{h}$ ($20 \text{ ft}^3/\text{min}$). The system consists of two reactors which contain canisters loaded with 32 kg (70 lb) of commercial $\text{Ba}(\text{OH})_2 \cdot 8\text{H}_2\text{O}$ reactant. Due to the size of the canisters and the relatively long loading times prior to breakthrough, continuous operation with only two reactors is possible. The steam, air, and CO_2 flow stations are unique to our pilot unit and will not be discussed in detail.

The overall pilot unit is controlled by a 5TI logic controller manufactured by Texas Instruments. The unit is currently capable of monitoring 8 DC and 16 AC input signals and providing 24 DC and 16 AC output signals. The logic controller monitors alarm signals from the CO_2 analyzer, hygrometer, flowmeters, timers, and pressure and temperature sensors. Upon sensing an alarm condition such as a CO_2 concentration of 1 ppmv in the effluent gas stream, valves are actuated

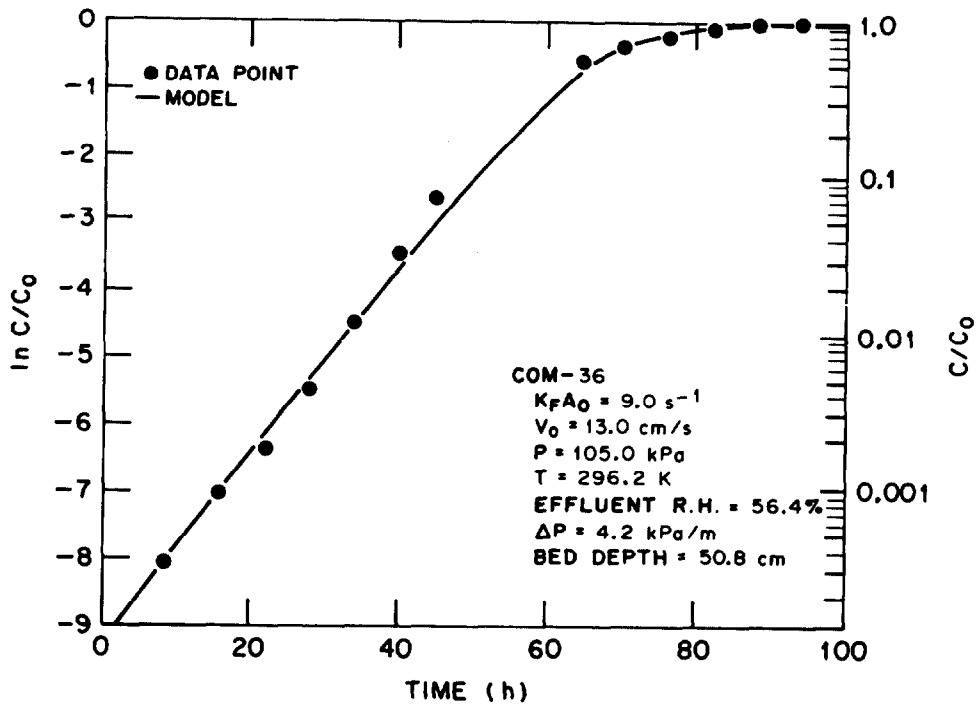
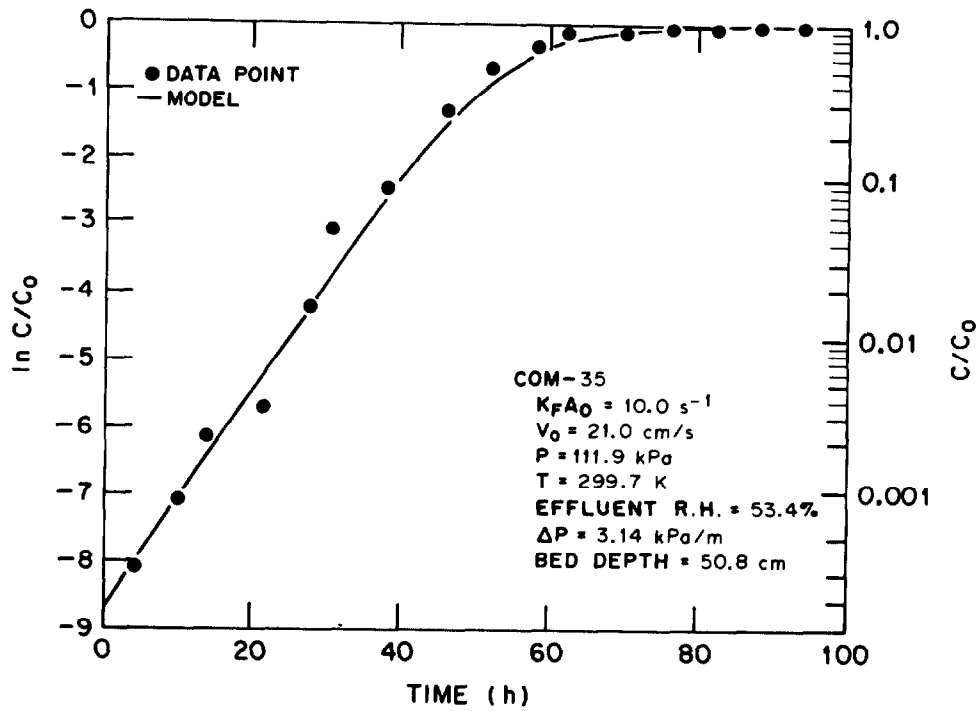


Fig. 8. Breakthrough curves and model-predicted breakthrough curves for typical fixed-bed runs.

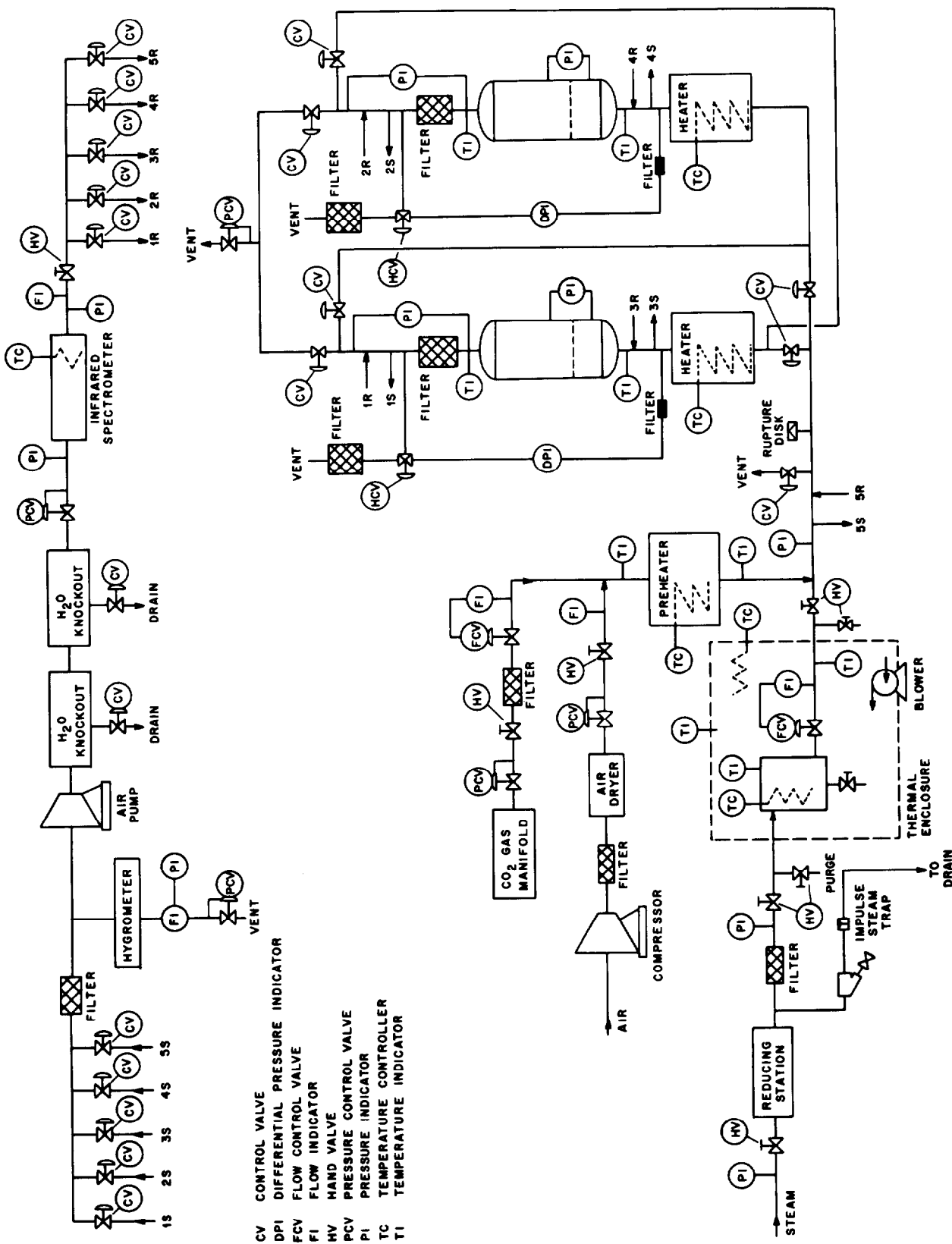


Fig. 9. The ¹⁴C immobilization pilot unit.

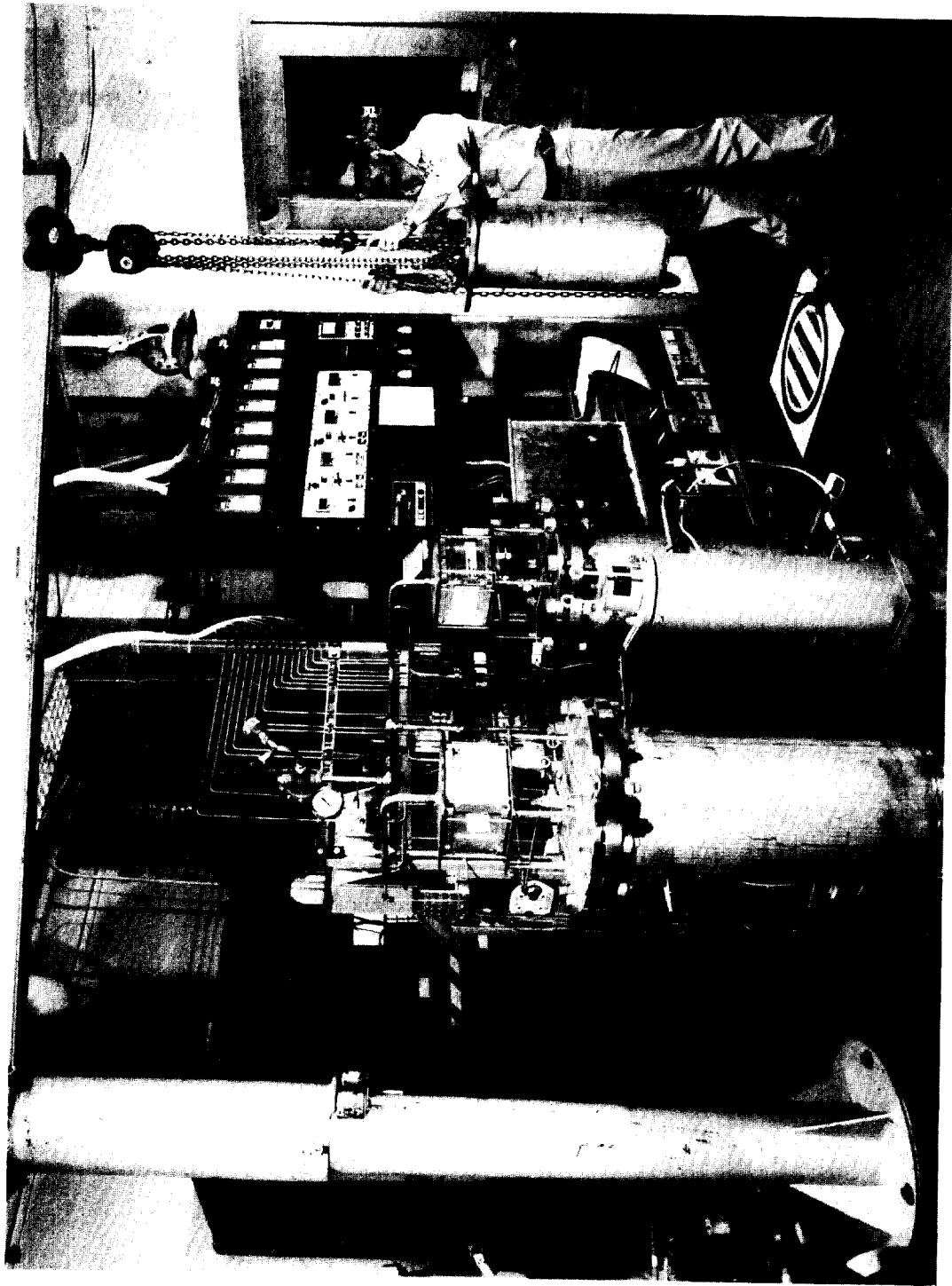


Fig. 10. The ^{14}C immobilization pilot unit.

in the proper sequence at prescribed time intervals thus diverting flow to the second column. Numerous 3/4- and 1/4-in. Whitey ball valves are located within the system for bulk flow control and for gas sampling. For valve actuation, electronic DC signals from the logic controller are converted to pneumatic signals using modular Humphrey TAC³ electric air valves. The Whitey ball valves are then actuated pneumatically via Whitey actuators. Gas samples may be routinely taken and returned from any one of five points within the system. Sampling from these locations may be controlled by the logic controller. The sample gas is filtered and a portion of it fed to a General Eastern model 1200 APS hygrometer sensor. The unit utilizes the "vapor condensation on a mirror" principle, thus providing a true dewpoint determination. Because of the small sensor volume and the resulting small gas throughput (0.5 L/min), this portion of the gas sample is vented to the atmosphere. The remainder of the sample gas is pressurized via a metal bellows pump, fed to two knockout vessels for H₂O removal, and then moves to a Wilks-Foxboro Miran 1A infrared spectrometer. This unit, described elsewhere,^{21,32} is capable of analyzing CO₂ over the continuous 100 ppbv to 330 ppmv CO₂ range. Because of the 5.6-L sensor volume and to ensure an adequate instrument response time, the gas throughput is appreciable and the sample stream is recycled to the pilot unit.

Gas preheaters connected to Barber-Coleman series 520 temperature controllers are located before each reactor to provide the desired influent temperature. The pressure drop across each column and the gauge pressure at the base of the column are monitored via Foxboro model E13DH differential pressure cells. Dwyer Photohelix pressure gauges/switches monitor the pressure drop across the gas distributors and HEPA filters. Thermocouples are located throughout the system for temperature control and sensing. Original plans were to enclose the pilot unit in a thermal-regulated structure so that studies could be conducted at 30 and 40°C under highly controlled conditions. These studies are currently in jeopardy because of funding uncertainties.

Whereas prior studies on the 10.2-cm-I.D. fixed beds were conducted at near-isothermal conditions, the pilot unit studies are being done under near-adiabatic conditions. For the treatment of an air-based (330-ppmv-CO₂) gas stream, one would predict a temperature drop of ~4°C in the gas stream due to the endothermic nature of the reaction (364 kJ/mol). Such a temperature drop has been verified experimentally. Because of the sensitivity of the operational characteristics of the bed (i.e. pressure drop) upon relative humidity and the dependency of relative humidity upon system temperature, the results from these studies are extremely valuable in determining conditions for optimal process operation. Experiments will also be conducted to determine if preconditioning the bed prior to contact with CO₂ is beneficial in reducing pressure drop problems. During the preconditioning step, the substoichiometric commercial Ba(OH)₂·8H₂O will be hydrated to Ba(OH)₂·8H₂O at conditions which ensure the retention of flake integrity (relative humidity <60%). We speculate that pressure drop problems during subsequent CO₂ removal at relative humidities >60% will be reduced.

VI. Conclusions

Extensive studies have been conducted on $\text{Ba}(\text{OH})_2$ hydrates, their reaction with CO_2 , and the operation of a fixed-bed process for CO_2 removal. Microscale studies indicated that (1) the published vapor pressure data for $\text{Ba}(\text{OH})_2 \cdot 8\text{H}_2\text{O}$ is valid, (2) the rate of dehydration or rehydration is proportional to the amount of free water on the surface (i.e. a function of relative humidity), and (3) the reactivity of $\text{Ba}(\text{OH})_2 \cdot 8\text{H}_2\text{O}$ for CO_2 is 3 orders of magnitude greater than that of either $\text{Ba}(\text{OH})_2 \cdot 3\text{H}_2\text{O}$ or $\text{Ba}(\text{OH})_2 \cdot \text{H}_2\text{O}$. Macroscale studies under near-isothermal conditions on 10.2-cm-ID fixed beds of commercial $\text{Ba}(\text{OH})_2 \cdot 8\text{H}_2\text{O}$ flakes indicated that the pressure drop across the bed increased dramatically as 60% relative humidity in the effluent gas was approached. It is speculated that this phenomenon results from the capillary condensation of water at V-shaped contact points or pores and that this facilitates the subsequent rehydration and recrystallization of the flake. Although the resulting flakes have greater external surface area, they are more fragile and degrade more readily upon conversion to BaCO_3 , thus resulting in increased pressure drop across the fixed beds.

Experimental studies indicated that the transfer of the reactant gas through the gas film is the major resistance to mass transfer. A model, assuming gas film control, was developed, and exact numerical solutions were obtained. An excellent correlation between the model-predicted breakthrough curves and the experimental breakthrough curve was obtained when the area available for mass transfer was modeled as a linear function of conversion [i.e. $A = A_0(1 - X)$]. The magnitude of the mass transfer coefficient was characteristic of literature values. There were indications that the magnitude of the initial surface area available for reaction, A_0 , may be a weak function of velocity due to a realignment of the flakes. This realignment results from fluid shear forces and an accompanying reduction in the number of planar contact points between neighboring flakes, thus increasing the area available for mass transfer.

Based upon the experimental data obtained during this study and its subsequent analyses, a window or regime of optimal process operation under near-isothermal conditions was determined to exist for the fixed-bed process. The window is bounded on the lower side by the dissociation vapor pressure of $\text{Ba}(\text{OH})_2 \cdot 8\text{H}_2\text{O}$ and on the upper side by the onset of appreciable capillary condensation and subsequent pressure drop problems (~60% relative humidity). An operating envelope is presented in Fig. 11 for the treatment of a 330-ppmv- CO_2 gas stream at a system pressure of 104.8 kPa (0.5 psig). The relative humidity of the influent gas must fall within the envelope for optimal gas throughput. If changes are made either in the CO_2 concentration, thus affecting the amount of water vapor produced, or in the system pressure, which will affect the partial pressure of the water vapor and subsequently the relative humidity (P/P_0), the operating envelope will change. The operating envelope also demonstrates why operational problems at 22 and 32°C were not severe and why considerable difficulty was encountered when trying to operate the process at 42°C.

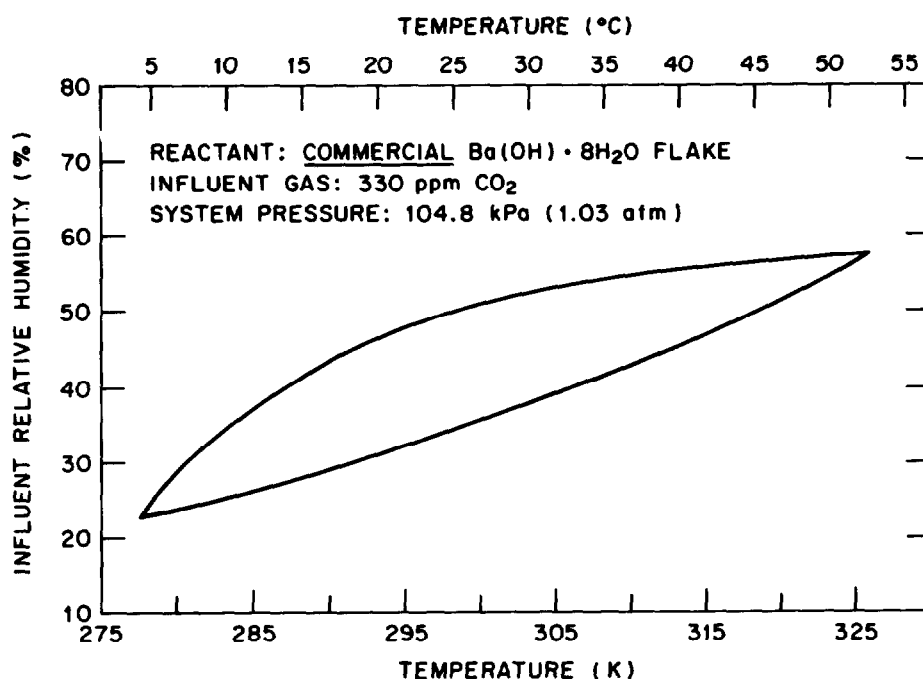


Fig. 11. Operating window for contacting a 330-ppmv CO₂ gas stream with fixed beds of commercial Ba(OH)₂·8H₂O flakes under isothermal conditions.

Successful isothermal operation of the process at higher effluent relative humidities (>60%) is possible by significantly reducing the gas throughput. The effect of operating the bed at conditions of water vapor saturation, whereby the water product would remain in the bed and the reaction would become exothermic, was not examined in detail. However, the reaction does proceed readily at these conditions and the BaCO₃ product is extremely insoluble.

Studies are under way on a pilot unit to determine the effects of operation at near-adiabatic conditions, whereupon the endothermic reaction results in a 4°C drop in the gas temperature upon passing through the bed. We speculate that complete reactant utilization and an acceptable pressure is possible when the relative humidity, based upon the effluent water vapor pressure and the effluent saturation vapor pressure, falls within the operating window. This speculation is based upon a relative comparison of the rate of axial movement of the reaction zone through the bed and the rate of dehydration and accompanying deactivation of commercial Ba(OH)₂·8H₂O flakes. Furthermore, studies are under way to determine if prior hydration of the water-deficient commercial Ba(OH)₂·8H₂O to Ba(OH)₂·8H₂O at conditions which retain the integrity of the flake (a relative humidity <60% and a water vapor pressure greater than the dissociation vapor pressure of Ba(OH)₂·8H₂O), will enable subsequent CO₂ removal at much higher relative humidities in the absence of significant pressure drop problems.

17th DOE NUCLEAR AIR CLEANING CONFERENCE

References

1. H. Bonka et al., "Contamination of the environment by carbon-14 produced in high-temperature reactors," *Kernetechnik* 15(7), 297 (1973).
2. W. Davis, Jr., *Carbon-14 production in nuclear reactors*, ORNL/NUREG/TM-12 (February 1977).
3. C. D. Kunz, "Continuous stack sampling for ^{14}C at the R. E. Ginna pressurized water reactor," *Trans. Am. Nucl. Soc.* 38, 100 (1981).
4. C. O. Kunz, W. E. Mahoney, and T. W. Miller, "Carbon-14 gaseous effluents from boiling water reactors," *Trans. Am. Nucl. Soc.* 21, 91 (1975).
5. C. O. Kunz, W. E. Mahoney, and T. W. Miller, "C-14 gaseous effluent from pressurized water reactors," pp. 229-34 in *Proceedings of the health physics society 8th midyear symposium*, CONF 741018 (1974).
6. M. J. Kabat, "Monitoring and removal of gaseous carbon-14 species," *Proceedings of the 15th DOE nuclear air cleaning conference*, CONF 780819 (1979).
7. H. Schuttelkopf, *Releases of $^{14}\text{CO}_2$ from nuclear facilities with gaseous effluents*, Kernforschungszentrum Karlsruhe KFK 2421, June 1977 (translated from German) ORNL-tr-4527 (1978).
8. *Program strategy document for the management of radioactive airborne wastes - draft*, Exxon Nuclear Idaho Company, Inc., prepared for Department of Energy, Idaho Operations Office (1981).
9. P. J. Magno, C. B. Nelson, and W. H. Ellett, "A consideration of the significance of carbon-14 discharges from the nuclear power industry," p. 1047 in *Proceedings of the thirteenth AEC air cleaning conference*, CONF-740807 (1975).
10. G. G. Killough, *A diffusion-type model of the global carbon cycle for the estimation of dose to the world population from releases of carbon-14 to the atmosphere*, ORNL/TM-5269 (1977).
11. G. G. Killough et al., *Progress report on evaluation of potential impact of ^{14}C releases from an HTGR reprocessing facility*, ORNL/TM-5284 (July 1976).
12. L. Machta, "Prediction of CO_2 in the atmosphere," *Carbon and the biosphere*, G. M. Woodwell and E. V. Pecan, eds., Technical Information Center, Office of Information Services, U.S. Atomic Energy Commission (August 1973).
13. J. W. Snider and S. V. Kaye, "Process behavior and environmental assessment of ^{14}C releases from an HTGR fuel reprocessing facility." Paper presented at and published in the proceedings of the ANS-AIChE topical meeting, Sun Valley, Idaho, Aug. 5-6, 1976.

17th DOE NUCLEAR AIR CLEANING CONFERENCE

14. L. Pauling, "Genetic and somatic effects of carbon-14," *Science* 128, 1183 (1958).
15. J. Schwibach, H. Riedel, and J. Bretschneider, *Studies on the emission of carbon-14 from nuclear facilities (nuclear power plants and reprocessing plants): Its measurement and the radiation exposure resulting from emissions*, Series of the Institute for Radiation Hygiene of the Federal Health Office, No. 20 (translated from German), OLS-80-233 (1979).
16. *Radiological significance and management of tritium, carbon-14, krypton-85, iodine-129 arising from the nuclear fuel cycle*, Nuclear Energy Agency, Organization for Economic Cooperation and Development, Paris, France (1980).
17. G. C. Killough and P. S. Rohwer, "A new look at the dosimetry of ^{14}C released to the atmosphere as carbon dioxide," *Health Phys.* 4, 141 (1978).
18. G. C. Killough, J. E. Till, E. L. Etnier, B. D. Murphy, and R. J. Roridon, "Chapter 11, dose equivalent due to atmospheric releases of carbon," taken from *Models and parameters for environmental radiological assessment*, C. W. Miller, ed., DOE/TIC-11368 (in press).
19. G. C. Killough and J. E. Till, "Scenarios of ^{14}C releases from the world nuclear industry from 1975 to 2020 and the estimated radiological impact," *Nucl. Saf.* 19(5), 602 (1978).
20. T. W. Fowler and C. B. Nelson, *Health impact assessment of Carbon-14 emissions from normal operations of uranium fuel cycle facilities*, EPA 520/5-80-004 (1981).
21. G. L. Haag, "Carbon-14 immobilization via the $\text{CO}_2\text{-Ba(OH)}_2$ hydrate gas-solid reaction," *Proceedings of the 16th DOE nuclear air cleaning conference*, CONF 801038 (1981).
22. *Handbook of chemistry and physics*, 52nd ed., The Chemical Rubber Co., Cleveland, Ohio (1972) pp. 13-70.
23. W. F. Linke and A. Seidell, *Solubilities of inorganic and metal organic compounds*, 4th ed., American Chemical Society, Washington, D.C. (1958).
24. A. G. Croff, *An evaluation of options relative to the fixation and disposal of ^{14}C -contaminated CO_2 as CaCO_3* , ORNL/TM-5171 (April 1976).
25. A. G. Evans, W. E. Prout, J. T. Buckner, and M. R. Buchner, *Management of radioactive waste gases from the nuclear fuel cycle - Volume 1, Comparison of alternatives*, NUREG/CR-1546, DPST-NUREG-80-5, vol. 1 (1980).
26. D. W. Holladay, *Experiments with a lime slurry in a stirred tank for the fixation of carbon-14 contaminated CO_2 from simulated HTGR fuel reprocessing off-gas*, ORNL/TM-5757 (1978).

17th DOE NUCLEAR AIR CLEANING CONFERENCE

27. D. W. Holladay, *An experimental investigation of the distribution of krypton from simulated HTGR fuel reprocessing off-gas during the removal and fixation of CO₂ by the CO₂-Ca(OH)₂ slurry reaction*, ORNL/TM-6539 (in preparation).
28. D. W. Holladay and G. L. Haag, "Removal of ¹⁴C-contaminated CO₂ from simulated LWR fuel reprocessing off-gas by utilizing the reaction between CO₂ and alkaline hydroxides in either slurry or solid form," pp. 548-69 in *Proceedings of the 15th DOE nuclear air cleaning conference*, CONF 780819 (1979).
29. K. J. Notz, D. W. Holladay, C. W. Forsberg, and G. L. Haag, "Processes for the control of ¹⁴CO₂ during reprocessing," paper presented at the International Symposium on Management of Gaseous Wastes from Nuclear Facilities, Vienna, Austria, Feb. 18-22, 1980.
30. G. R. Bray, C. L. Miller, T. D. Nguyen, and J. W. Rieke, *Assessment of carbon-14 control technology and costs for the LWR fuel cycle*, EPA 520/4-77-013 (1977).
31. J. L. Kovach, *Review of carbon-14 control technology and cost*, NUCON 8EP555/01 (1979).
32. G. L. Haag, *Application of the CO₂-Ba(OH)₂·8H₂O gas-solid reaction for the treatment of dilute CO₂-bearing gas streams*, Ph.D. Dissertation, University of Tennessee, Knoxville; and ORNL-5887 (both in preparation).
33. G. L. Haag, G. C. Young, J. W. Nehls, Jr., *Pilot unit development of the Ba(OH)₂·8H₂O-CO₂ gas-solid reaction for ¹⁴C immobilization*, (to be published as ORNL/TM-8433).
34. Jim Nillis, Sherwin Williams Company, Coffeerville, Kansas, personal communication, 1981.
35. M. Michaud, "Contribution to the study of the hydroxides of potassium and barium," *Revue de Chimie Minerale*, t.5, 89 (1968).
36. M. Michaud, "Inorganic Chemistry - Study of the binary water-barium hydroxide system," *C. R. Acad. Sci. Paris* 262.CV, 1143 (1966).
37. B. A. Kondakov, P. V. Kovtunencko, and A. A. Bundel, "Equilibria between gaseous and condensed phases in the barium oxide-water system," *Russ. J. Phys. Chem.* 38(1), 99-102 (1964).

DISCUSSION

CHRISTIAN: With the present concept, most of your water product will result from inactive atmospheric CO₂. Since you obtain less than 100 ppb CO₂ in the exit gas from the Ba(OH)₂·8H₂O bed, the goal DF of 100 could still be obtained if the inlet purge air to a dissolver were treated with molecular sieves to remove atmospheric CO₂ to about 10 ppm and the waste volume might be reduced by a factor of 30. Have you tested the bed at reduced inlet concentrations to verify that this would, indeed, work?

HAAG: This is an excellent point. With present analytical techniques, we are capable of analyzing CO₂ to a lower concentration limit of 100 ppb. Thermodynamic calculations indicate an equilibrium concentration of the order of parts per trillion. Therefore, I see no difficulty in obtaining a DF of 100 or a 1,000 for the treatment of a 10 ppm CO₂ gas stream. Our process model has indicated the rate-controlling steps to be mass transfer across the gas film. Therefore, the major effect may be a slight increase in the length of the mass transfer zone. However, the pretreatment of the dissolver off-gas for a 100 ft³/min off-gas stream would decrease the waste volume from .7 ft³/d to .02 ft³/d, the mass of waste from 26 lb/d to .81 lb/d, and the reactant cost from \$15/d to \$0.45/d.

EBY: As I understand it, your tests were evaluated at 330 ppm. Could you speculate what effects you might expect as far as loading and breakthrough for CO₂ concentrations in the neighborhood of 50%. For instance, if we were to remove CO₂ in a fluorocarbon process and concentrate it prior to final fixation?

HAAG: The bulk of our studies have been conducted with 330 ppm CO₂. However, during initial studies, concentrations as great as 88% were used with excellent removal efficiencies. The difficulty that arises under such conditions results from the fact that 9 molecules of water are released per molecule of CO₂ reacted thus causing water condensation within the bed for higher CO₂ concentrations. The condensation of water causes the reaction to become slightly exothermic rather than endothermic. Because of the low solubilities of Ba(OH)₂ and BaCO₃ in water, and the low gas flow rates required of the system, water condensation was not extremely detrimental to bed operation. However, column cooling capabilities would be required for a 50% CO₂ gas stream. Additional studies are required using a 50% CO₂ gas stream as a reference point. Such a system would be required to handle only 0.03 to 0.33 ft³/min for a typical 1,500 MTHM/y reprocessing plant with a 100-500 ft³/min, 330 ppm CO₂ off-gas stream being fed to the fluorocarbon process.

CLOSING REMARKS OF SESSION CHAIRMAN:

In this session, results were presented from an off-gas study of liquid-fed joule-heated ceramic melters, which established the off-gas and effluent characteristics from which optimal effluent control systems can be designed. The experimental study on the volatilization and trapping of ruthenium resulted in the optimization of airborne ruthenium species removal from high temperature processes.

The major part of this session was related to carbon-14 removal. We were told about three removal systems presently being developed in USA, Germany, and Canada: the double alkali process, which was tested and previously applied on a relatively large scale, and two dry systems, which apparently have very good potential for this application. These dry systems are: the barium hydroxide system which is in the stage of pilot testing at ORNL, and the calcium hydroxide system, which was developed in Canada, initially for the selective sampling of ^{14}C airborne species. This sampler, which requires elevated temperature for the catalytic conversion of hydrocarbons to CO_2 , was developed in 1978 and was described at the 15th Air Cleaning Conference. It was used in 1979-1981 in Candu nuclear power stations for the analysis of ^{14}C species in gaseous effluents. An alternative application is being developed for the removal of $^{14}\text{CO}_2$ from Candu systems at ambient temperature. The results, presented at this session, are also promising for this purpose.

It is apparent from the presentations that all three systems are cost effective, can efficiently remove CO_2 from large streams, and transfer it to solid, insoluble forms which are suitable for long term disposal.

The analysis of ^{14}C sources, its chemical forms and releases from light water reactors, provides data for the evaluation of environmental hazards from ^{14}C and the need for its removal from light water reactor systems.

From two papers, presented at this session, it is also apparent that ^{85}Kr solidification and its long term disposal will be feasible at a reasonable cost in the near future.

Session 5

FILTRATION AND FILTER TESTING I

TUESDAY: August 3, 1982

Co-CHAIRMEN: H.T. Ettinger, Los Alamos
National Laboratory

B.V. Gerber, US Army ARRADCOM
Chemical Systems Lab.

VERTICAL REMOVABLE FILTERS IN SHIELDED CASING FOR RADIOACTIVE
CELLS AND PROCESS GASEOUS WASTES
M. Prinz

DEVELOPMENT OF FILTERS AND HOUSINGS FOR USE ON ACTIVE PLANT
S. Hackney, R.P. Pratt

AEROSOL FILTRATION WITH METALLIC FIBROUS FILTERS
M. Klein, W.R.A. Goossens

EVALUATION OF PERMANENTLY CHARGED ELECTROFIBROUS FILTERS
A.H. Biermann, B.Y. Lum, W. Bergman

EVALUATION OF PROTOTYPE ELECTROFIBROUS FILTERS FOR NUCLEAR
VENTILATION DUCTS
W. Bergman, W.D. Kuhl, A.H. Biermann, J.S. Johnson, B.Y. Lum

A NEW METHOD OF DETERMINING THE OVERALL PARTICLE DECONTAMINATION
FACTOR FOR MULTIPLE OFF-GAS CLEANING COMPONENTS IN REPROCESSING
PLANTS
J. Furrer, A. Linek

IN-SITU CONTROL OF FILTRATION SYSTEMS IN FRANCE: 5 YEARS
EXPERIENCE
J. DuPoux

CONTAMINATION CONTROL AND PERSONNEL PROTECTION

AIR CLEANING PHILOSOPHY IN A NUCLEAR MATERIALS FABRICATION
PLANT
F.Y. Ward, R.E. Yoder

SYSTEM OPERATIONAL TESTING OF MAJOR VENTILATION SYSTEMS FOR
A PLUTONIUM RECOVERY FACILITY
F.J. Linck, Jr.

17th DOE NUCLEAR AIR CLEANING CONFERENCE

VERTICAL REMOVABLE FILTERS IN SHIELDED CASING FOR RADIOACTIVE CELLS AND PROCESS GASEOUS WASTES

M. Prinz
Ventilation Department
S.G.N.
(Société Générale pour les Techniques Nouvelles)
Saint Quentin en Yvelines - France

Abstract

The installation of shielded filtration casing is necessary for highly contaminated active cells (for example, fuel bundle shearing cells of reprocessing plants) and process gaseous wastes containing active aerosols.

SGN and COGEMA have developed a filtration casing equipped with a vertically removable filter element.

Two types of casing have been developed :

- one for a flow rate of 500 m³/hr,
- one for a flow rate of 3000 m³/hr.

The filter elements are fitted with high efficiency glass fibre media. They are cylindrical in shape. The top flange of the filter is equipped with a gasket to ensure sealing between the filter element and its casing.

The filter element is blindly installed and removed and its orientation, inside the casing, is immaterial.

The shielding casing is made of a cast iron, or steel, shielding slab under which is secured the filtration casing itself. This shielding slab is settled on side shielding walls made of concrete or cast iron.

The filter element, integral with a plug, is placed in the horizontal slab.

The attachment of the filter element under the plug is made necessary for the following two reasons :

- a) so that the plug and filter may be removed as one unit,
- b) to keep the filter on its sealing surfaces, according to sealing and seismic resistance requirements.

Filter removal is performed with the help of an intervention cask, centered over a removable trap door provided on the shielding slab of the casing.

First, the plug and filter element assembly is raised into the cask.

Then, the filtering element may be separated from the plug which is decontaminated and salvaged. The whole plug and filter assembly may also be sent to the conditioning waste storage.

The installation of a clean filter element in the casing, is also performed

17th DOE NUCLEAR AIR CLEANING CONFERENCE

with the help of the intervention cask, proceeding as above, but in reverse order.

The same intervention cask may also be used to remove the upstream and downstream dampers from the top of the casing.

The casings are provided with pressure pick-up points enabling pressure measurement on site, in accordance with usual regulations.

I - Introduction

In some cases, the ventilation of active cells and gaseous wastes necessitates the installation of shielded casings.

There exist some shielded casings suitable for 1250 m³/hr output filters, from which the filter element can be removed horizontally.

The intervention cask accommodating the filter is placed against the front face of the casing and enables withdrawal under $\alpha . \gamma$ protection.

The protective doors open vertically or horizontally and the filter element is pulled inside the intervention cask with the help of a rod.

The doors are then shut, awaiting the introduction of a new filter element.

This system is at present in use in French reprocessing plants but its main drawback is the difficult handling of the casing protection door latches and the horizontal withdrawal of the horizontal filter element inside the intervention cask.

A new type of shielded casing has been developed for use in projected new reprocessing plants. This new type of casing enables withdrawal under $\alpha . \gamma$ protection and differs from existing casings in that the filter element can be installed or withdrawn vertically.

II - Why vertical handling ?

Filter element installation or withdrawal operations form part of the installation maintenance program.

Maintenance

This covers all the operations normally carried out to keep the installation in a state of permanent working condition and safety while the plants are in production.

These operations are the object of procedures laid down during plant design and testing.

Personnel protection

Maintenance operations must be carried out in normal working conditions, while observing the following criteria :

- sustained containment,

17th DOE NUCLEAR AIR CLEANING CONFERENCE

- limitation of equivalent activity level sustained by the operator,
- working position and protective clothing as little constraining as possible,
- limitation of risks for the operators, even of non-nuclear nature.

The maintenance operations may be carried out in accordance with established criteria, taking into account the activities and the qualification of anti-radiation equipment.

Risk of external exposure

To remain within the exposure limit of 0.5 Rem/year, the level equivalent per operator is limited, during maintenance operations, to :

- 2.5 mRem/working hour, for the whole body,
- 30 mRem/working hour, for the hands.

Since the collective level is to be kept down to the minimum, the maintenance operations are so designed that the number of operators required is as small as possible.

III - Equipment design for modular exchange

The filtering equipment comes within that group of equipment which can be maintained through an exchange of module.

There are some standardized modular units common to several workshops and to several items of equipment :

- for standardization purposes, a series of devices is designed to enable modular exchange in a remote maintenance cask.

These standardized modular devices are designed in such a way that :

- their role of containment barrier is fulfilled during normal operation,
- their connection with the remote maintenance cask is ensured without containment failure during the maintenance operation,
- the amount of radioactive material they retain is kept down to the minimum,
- they may be rinsed and cleaned, provided that these operations are compatible with the process and with safety.

IV - Application to filtration casing

The filtration casings used on contaminated cells and on gaseous waste systems must be shielded.

Indeed, such filters can trap a high level of activity and the dust retained can be a transmitting source of α . γ radiation.

The installation and the removal of filter elements located inside shielding casings must comply with plant maintenance operation and modular exchange concept criteria.

17th DOE NUCLEAR AIR CLEANING CONFERENCE

In order to use the remote maintenance cask employed for all other modular assemblies, it has been necessary to completely redesign the filtration casings used on the installations.

Since the modular assemblies are evacuated vertically, and blindly, the casing and the filter have been designed accordingly.

The first step was to design a filter element capable of meeting the above requirements.

Determination of filter element output

In the reprocessing plants, the two systems likely to necessitate the presence of shielded filtration casings are those used for processing and gaseous wastes and those used for exhausting areas with a high contamination risk.

In most cases, the gaseous waste systems have a low ventilation flow rate. Following a study of existing plants and another study concerning future plants, it appears that a gaseous waste exhaust flow rate of 500 m³/hr is often used.

The process gaseous waste filter therefore has an output of 500 m³/hr.

The exhaust of cells with a high risk of contamination necessitates a much larger flow rate.

The 610 x 610 x 292 mm HEPA (THE) small pleats filters provide a maximum output of 3000 m³/hr, with a pressure drop of 25 mmCE.

In order to enable the standardization of the installations and for dimensional reasons, a 3000 m³/hr output exhaust filter element has been selected for the ventilation system of cells presenting a high risk of contamination.

V - Why was a cylindrical filter element selected ?

The filter element installation and removal operations are carried out blindly. It is therefore impossible to accurately locate a filter on its sealing surface.

This is the reason why filter elements of cylindrical design have been selected.

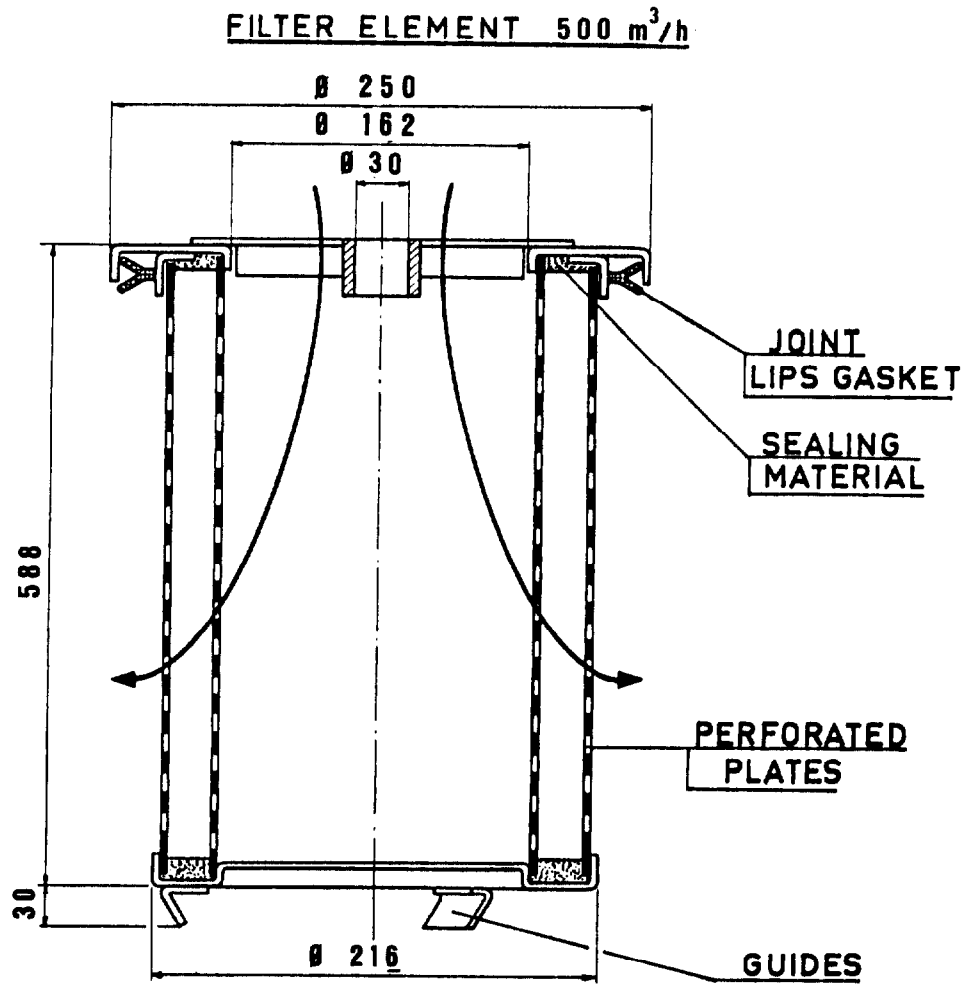
VI - Description of filter elements

500 m³/hr output filter element (see fig. 1)

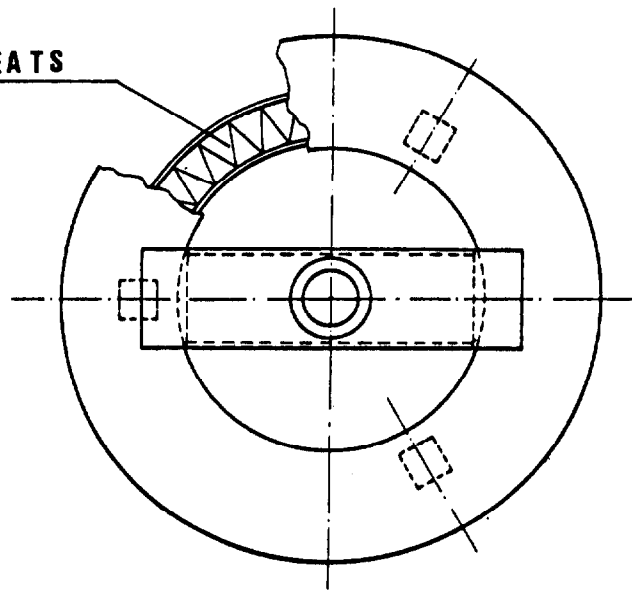
Filtered air characteristics

- | | |
|---------------------------|-------------------------|
| - steady flow temperature | : 50°C |
| - max. temperature | : 120°C |
| - corrosion | : high risk |
| - activity | : greater than 1000 MPC |

— FIGURE.1 —



FILTER IN LITTLE PLEATS



17th DOE NUCLEAR AIR CLEANING CONFERENCE

Dimensions of filter element

- outside diameter	: 250 mm
- height	: 618 mm
- effective area	: 5 m ²
- diff. pressure at nominal flow rate	: 26 mmCE
- velocity over paper	: 2.7 cm/s
- filtering coefficient (average uranine granulometry = 0.15 micron)	: greater than 5000
- decontamination factor	: 99.98% efficiency
- DOP - NaCl. efficiency	: 99.99%
- disposal in a 200 litre capacity drum	: 500 mm dia. x 790 mm high
- weight of filter element	: 5 kg

Description of filter element

The filter element designed and produced by SOFILTRA POELMAN is composed of a layer of glass fibre paper complying with standard MIL F 51079 B, with 20 mm pleats, reinforced with glass thread.

This layer is sandwiched between two perforated stainless steel sheets providing the necessary mechanical strength and protection of the filter paper.

The filter element is fitted with a dished bottom flange and an annular top flange accommodating the sealing gasket.

Sealing, between the filter paper and these stainless steel end fittings is provided by means of a PVC compound with the following characteristics :

- good resistance to acids,
- good resistance to heat (1 hour at 200°C),
- fire-proof.

Sealing between the filter element and its support is by means of a double-lip seal in contact, on the one hand, with the machined face of the casing and, on the other hand, with the top flange of the filter element. Sealing is ensured by the mere weight of the filter element (5 kg).

The grabbing device is welded to the top flange of the filter element.

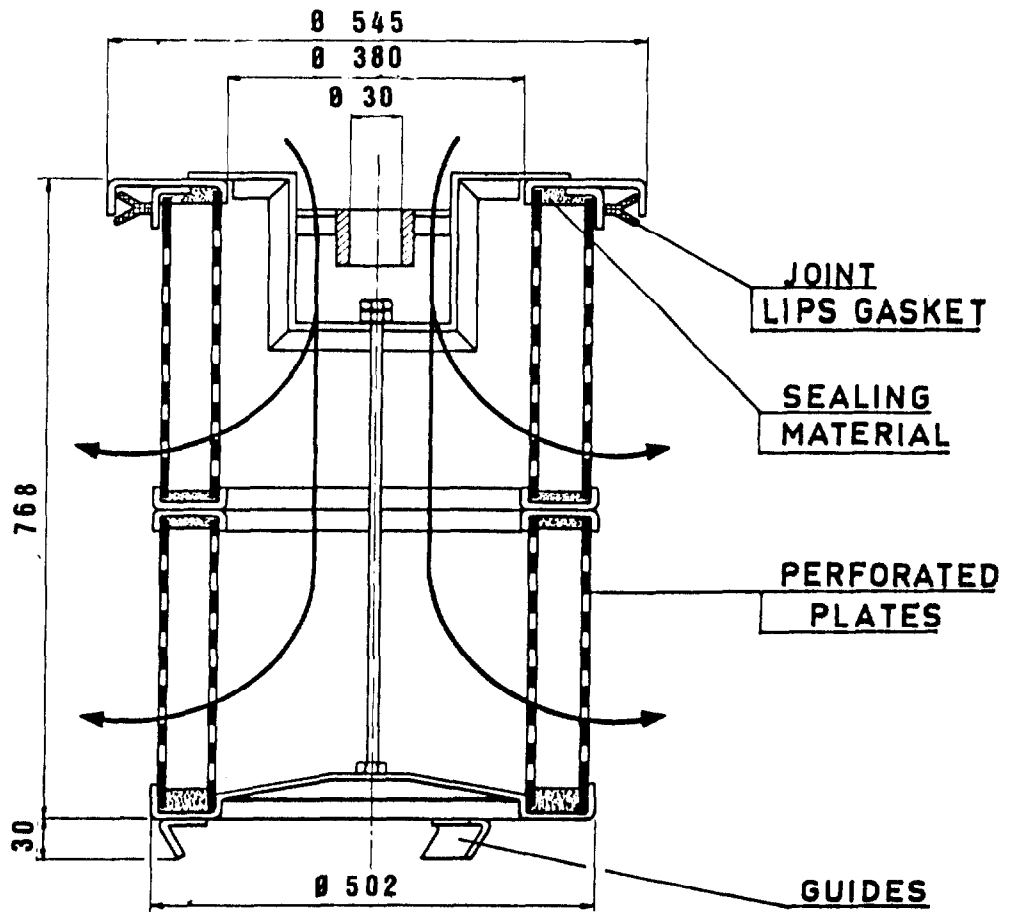
3000 m³/hr output filter element (see fig. 2)

Filtered air characteristics

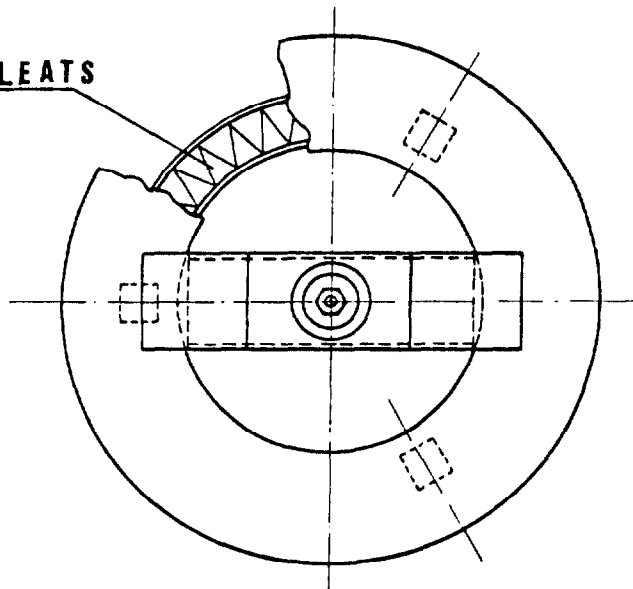
- steady flow temperature	: 12 to 50°C
- max. temperature	: 120°C

— FIGURE.2 —

FILTER ELEMENT 3000 m³/h



FILTER IN LITTLE PLEATS



17th DOE NUCLEAR AIR CLEANING CONFERENCE

- corrosion : high risk
- activity : greater than 1000 MPC

Dimensions of filter element

- outside diameter : 545 mm
- height : 798 mm
- effective area : 33 m²
- diff. pressure at nominal flow rate : 23 mmCE
- velocity over paper : 2.5 cm/s
- filtering coefficient (uranine) : greater than 5000
- decontamination factor : 99.98% efficiency
- DOP - NaCl. efficiency : 99.99%
- disposal in a 400 litre capacity drum : 710 mm dia. x 1100 mm high
- weight of filter element : 20 kg

Description of filter element

The filter element is composed of a layer of glass fibre paper complying with standard MIL F 51079 B, with 50 mm pleats, reinforced with glass thread.

The layers are sandwiched between two perforated stainless steel sheets.

For production reasons, the filter element is made up of two superposed cylindrical sections and an intermediate seal.

A central safety draw-bolt provides the mechanical link between the bottom end of the filter and the grabbing device.

VII - Casing design criteria

Two filtration casings were designed : one accommodating a 500 m³/hr output filter element and the other a 3000 m³/hr output filter element.

Common design for both filtration casings

Design : These casings are designed so as to enable filter element isolation and removal under a remote maintenance cask while keeping contamination containment and protection within regulation limits.

Functional requirements : The air enters at the top of the filter so that the dust remains at the bottom of the filter element.

Seism : In case of seism, the filter elements must remain in their normal working position.

17th DOE NUCLEAR AIR CLEANING CONFERENCE

Weight and size : The size of the filter elements is dictated by the dimensions of the corresponding storage drums which are :

- capacity drum : 200 litre or 400 litre

Operational requirements : Removal of filter element through the top of the casing, under $\alpha . \gamma$ protection.

Availability - Reliability : These filtration casings are used permanently. The continuity of the filtration must be ensured during maintenance and while the filter elements are being changed.

The average service life of the filter elements depends upon :

- clogging, which itself depends on the amount of dust contained in the air to be filtered and on the maximum design pressure differential.
- the rate of irradiation (radioprotection check).

Maintenance : Casing maintenance ensures the highest possible level of availability, consequently :

- the casing is designed so that, in case of breakdown, repair is carried out as quickly as possible,
- the most sensitive elements, such as the isolation dampers, are designed so as to allow easy disassembly in the remote maintenance cask.

Safety - Equipment inherent safety system : The casings are provided with a biological shield, to protect the operators.

Specific precautionary measures : To prevent corrosion, metallic parts will be made of stainless steel.

Behaviour requirements : It must be possible to replace a defective damper. If the filter element is incorrectly installed, the installation operation must be repeated.

VIII - Description of casing (see fig. 3)

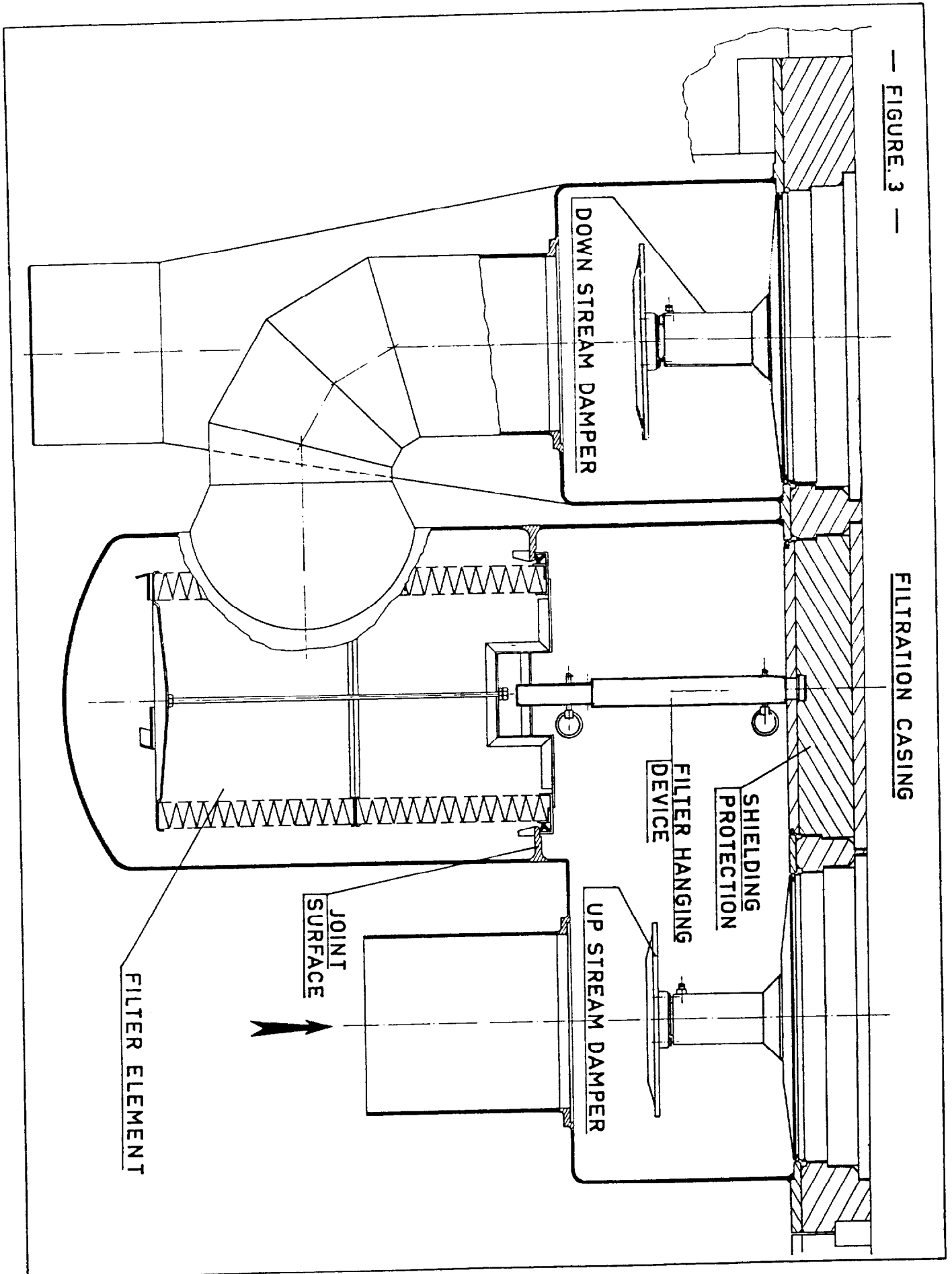
The filtration casing accommodates the filter element and is equipped with isolation valves.

- the 500 m³/hr output casing weighs 500 kg
- the 3000 m³/hr output casing weighs 2000 kg.

The filtration casing is composed of :

- an horizontal, protective cast iron slab.

The casing and its two upstream and downstream dampers are fixed to the protective slab.



— FIGURE 3 —

FILTRATION CASING

DOWN STREAM DAMPER

SHIELDING PROTECTION

FILTER HANGING DEVICE

UP STREAM DAMPER

JOINT SURFACE

FILTER ELEMENT

17th DOE NUCLEAR AIR CLEANING CONFERENCE

The filter element can be secured under a plug located inside the protective slab.

The dampers are secured under the plugs provided in the protective slab.

Attachment of filter element

The filter element is hooked under the plug with the help of an element comprising :

- 1) a link pin, securing the filter element supporting rod to the plug,
- 2) a spring mechanism, pressing the filter element against its sealing surface.
- 3) a link pin, securing the filter element to its supporting rod.

Attachment of dampers :

The dampers are secured under plugs by means of supporting rods allowing them to move vertically in both directions.

The plugs supporting the dampers and the filter element of a 500 m³/hr output casing, are of identical diameter : 300 mm.

Similarly, the plugs supporting the dampers and the filter element of a 3000 m³/hr output filtration casing, are of identical diameter : 580 mm.

- these plugs are fitted in the protective slab where they are adequately secured.
- sealing is obtained by means of a gasket housed in a groove under the plug.
- the damper position is indicated by an index flush with the protective surface when the damper is open.

It is thus possible to know whether the damper is open or shut.

The protective slab, casing and damper assembly may be rested upon lateral steel shields or upon concrete shields, depending upon the amount of space which may be used.

IX - Filter element removal/installation

(see fig.4)

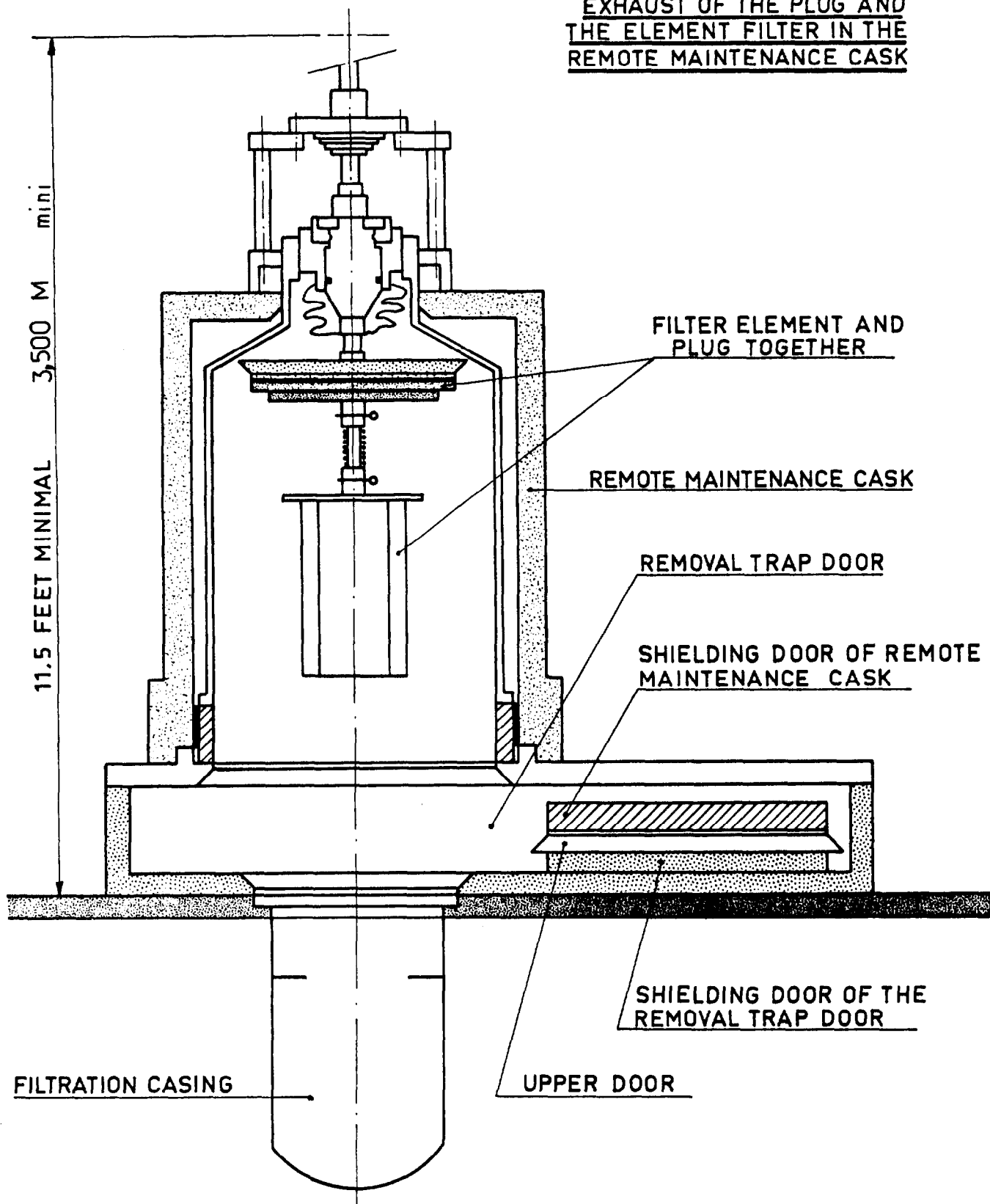
The filter element is removed and installed from the top end of the filtration casing.

The casing isolation dampers are shut and a cover is placed upon the casing to protect the environment.

A remote maintenance cask is then placed over the cover and the trap doors provided on the remote maintenance cask and on the cover are open, to enable the withdrawal of the plug and filter element assembly from the filtration casing, into the maintenance cask.

— FIGURE 4 —

EXHAUST OF THE PLUG AND THE ELEMENT FILTER IN THE REMOTE MAINTENANCE CASK



17th DOE NUCLEAR AIR CLEANING CONFERENCE

The protective trap doors are shut and the remote maintenance cask containing the active filter can be evacuated.

Another remote maintenance cask containing a clean filter and plug assembly is then placed over the cover.

The trap doors of the cover and maintenance cask are opened and the filter element is lowered into the filtration casing, regardless of its orientation, since both the filter element and its plug are cylindrical.

The spring located in the supporting rod presses the filter element against its seat, under the load applied by the plug.

The remote maintenance cask and cover are taken away.

It is then possible to open the filtration casing isolation dampers and carry out the tests which will show whether or not the filter element is correctly seated on its support.

Variant (see figs. 5 and 6)

The plugs may be designed for immediate re-use. In such a case, the filter element is not attached to the plug located in the protective slab. The plug is equipped with a spring rod which presses the filter element against its seat but when the plug is raised by means of a remote maintenance cask, the filter element remains in position. A second remote maintenance cask can then be used to withdraw the filter element provided with a grabbing device.

A new filter element, located in a third remote maintenance cask, is then lowered in position in the filtration casing and the plug lowered on top of it.

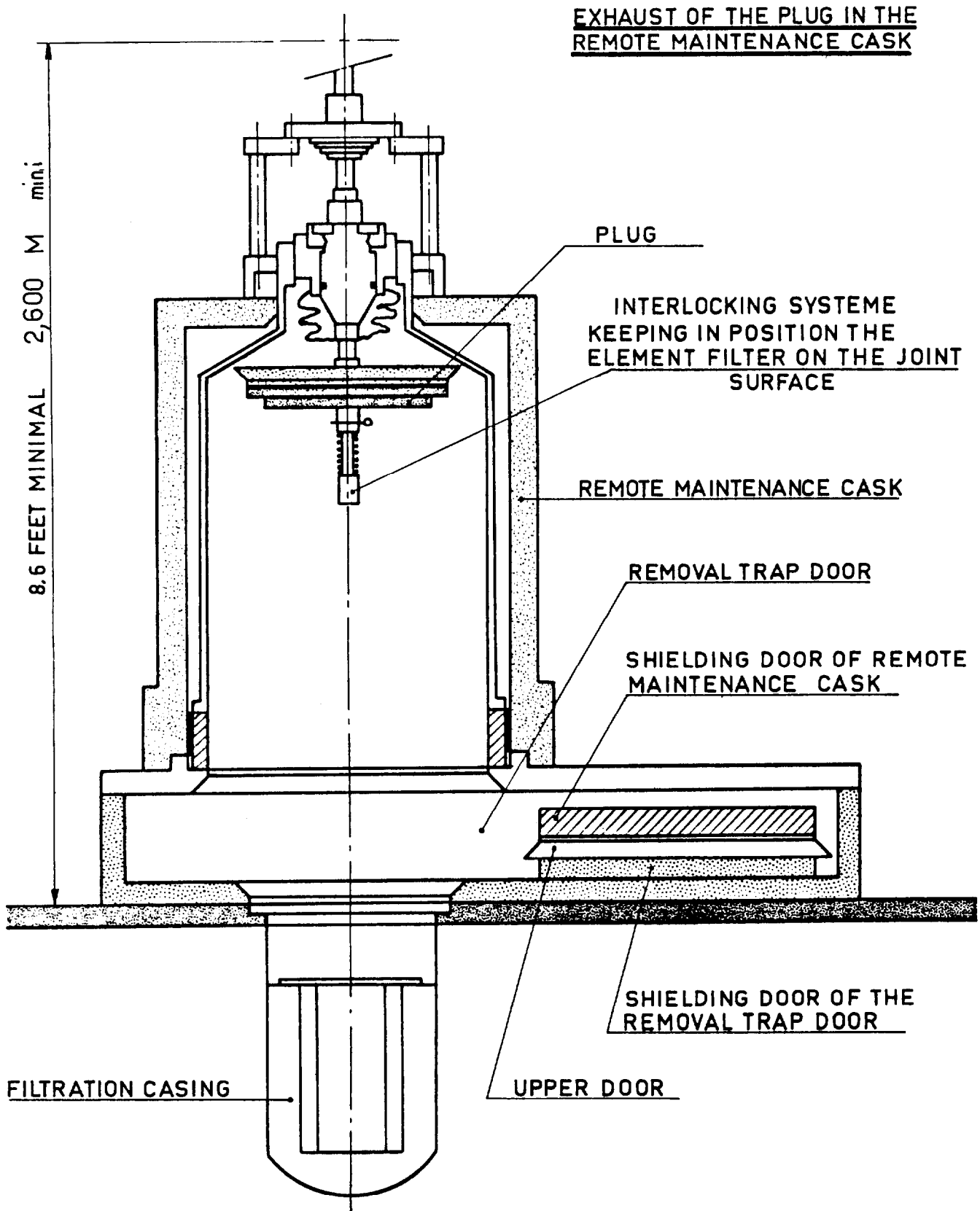
This solution presents the advantage of using lower remote maintenance casks since the absence of the plug enables the vertical stroke of the maintenance cask mechanism to be reduced to the height of the filter element, i.e. 780 mm, plus the height of the grabbing system.

Another advantage of this solution resides in the fact that the plug can be re-used immediately, thus limiting the number of technological wastes.

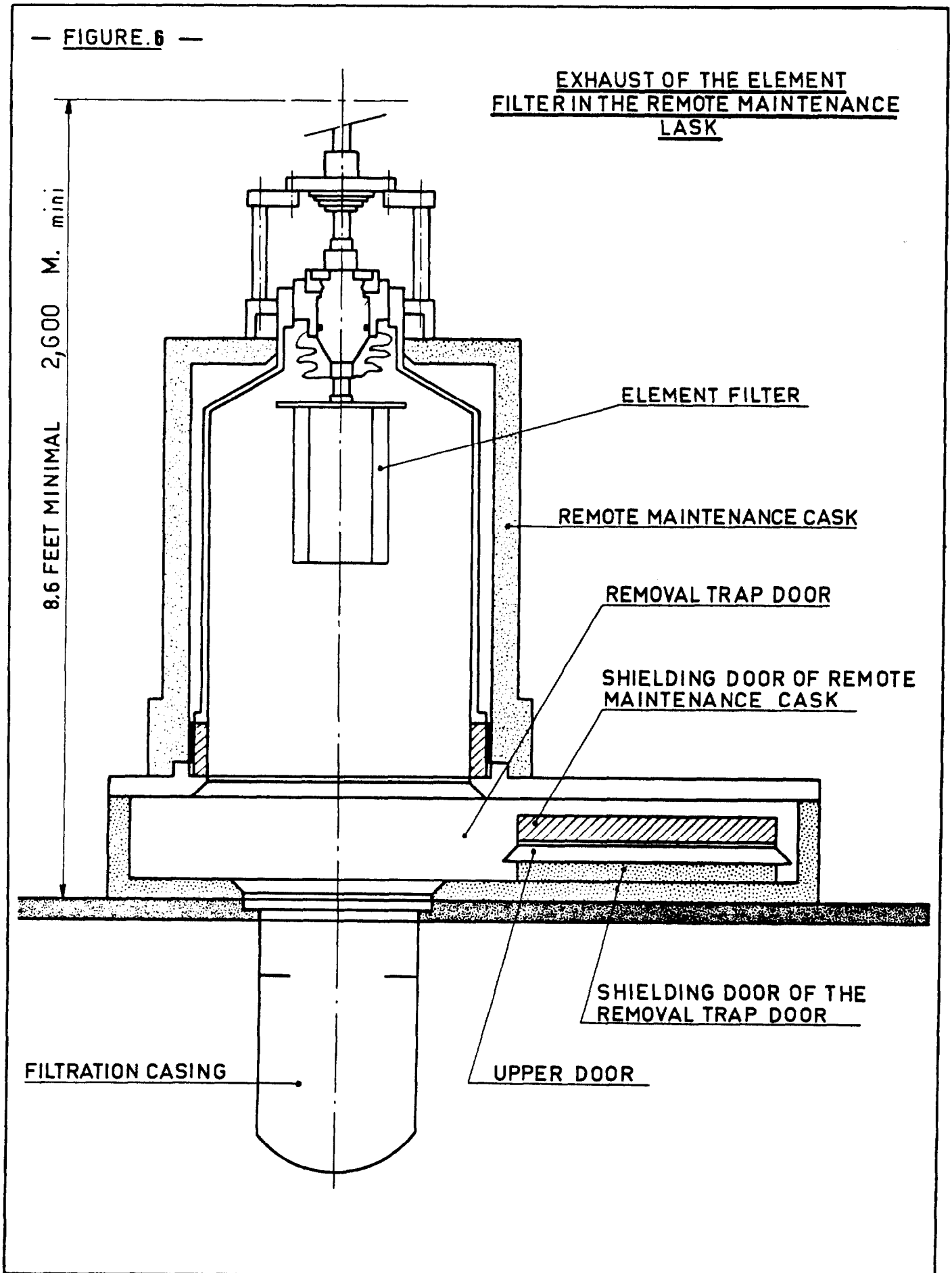
The only drawback of this solution is the increased amount of handling, during filter element removal and installation operations.

Both these solutions may be used with the type of filtration casing described herein.

— FIGURE.5 —



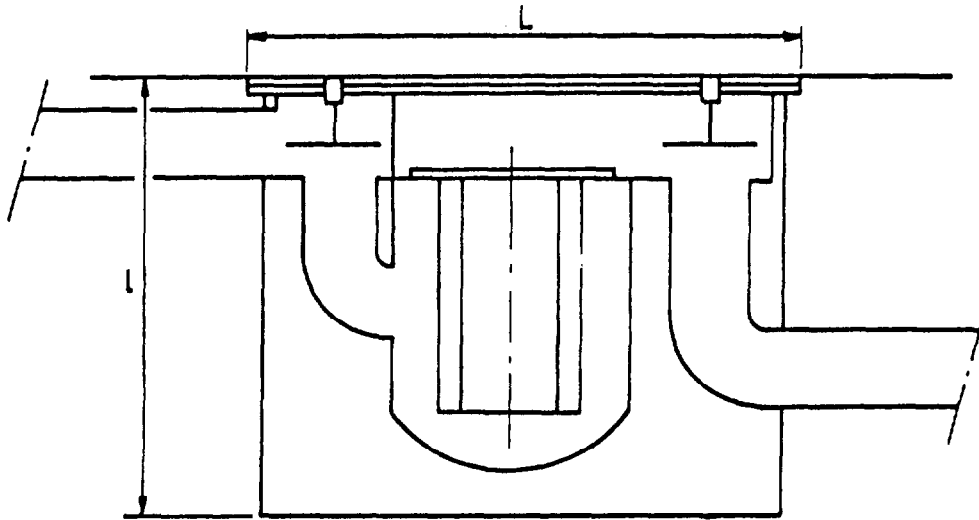
— FIGURE. 6 —



X - DIFFERENT KIND OF USED OF FILTRATION CASING

- ONE STAGE CASING WITH TWO SHIELDED DAMPERS

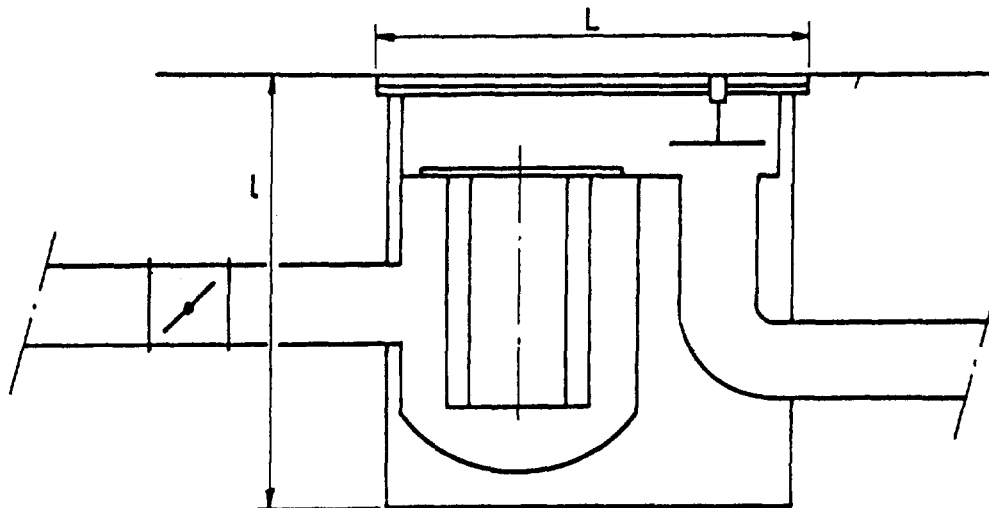
	L	l	D
500 m ³ /h	1400	1030	960
3000 m ³ /h	2450	1520	1560



- ONE STAGE CASING WITH ONE UPSTREAM SHIELDED DAMPER

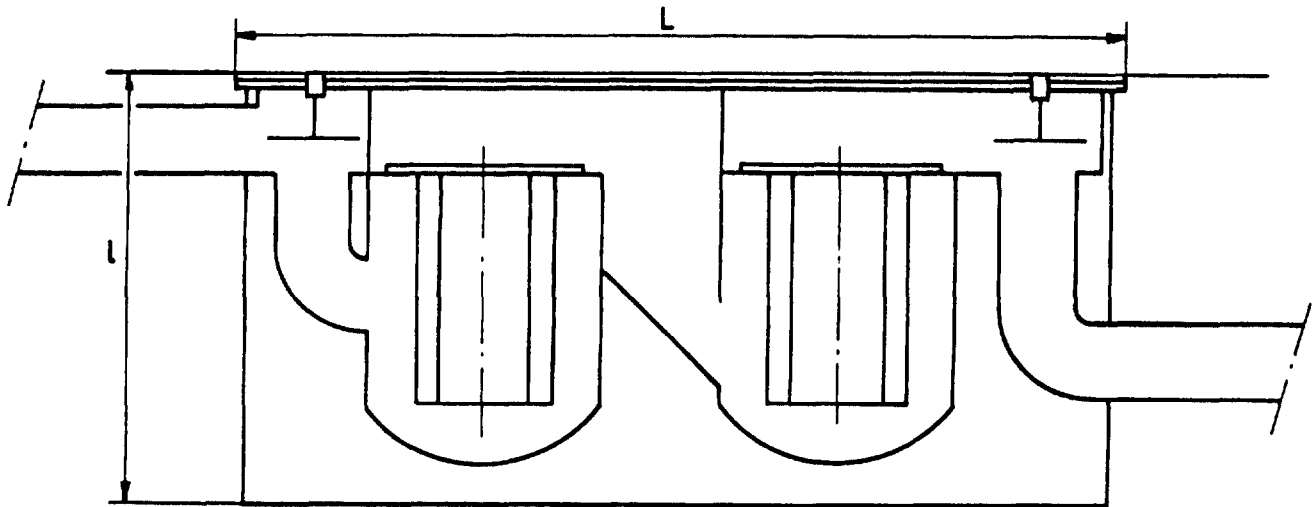
THE DOWN STREAM DAMPER IS CONSTITUTED WITH A NO SHIELDED REMOVAL DAMPER

	L	l	D
500 m ³ /h	1200	1030	900
3000 m ³ /h	2100	1520	1160



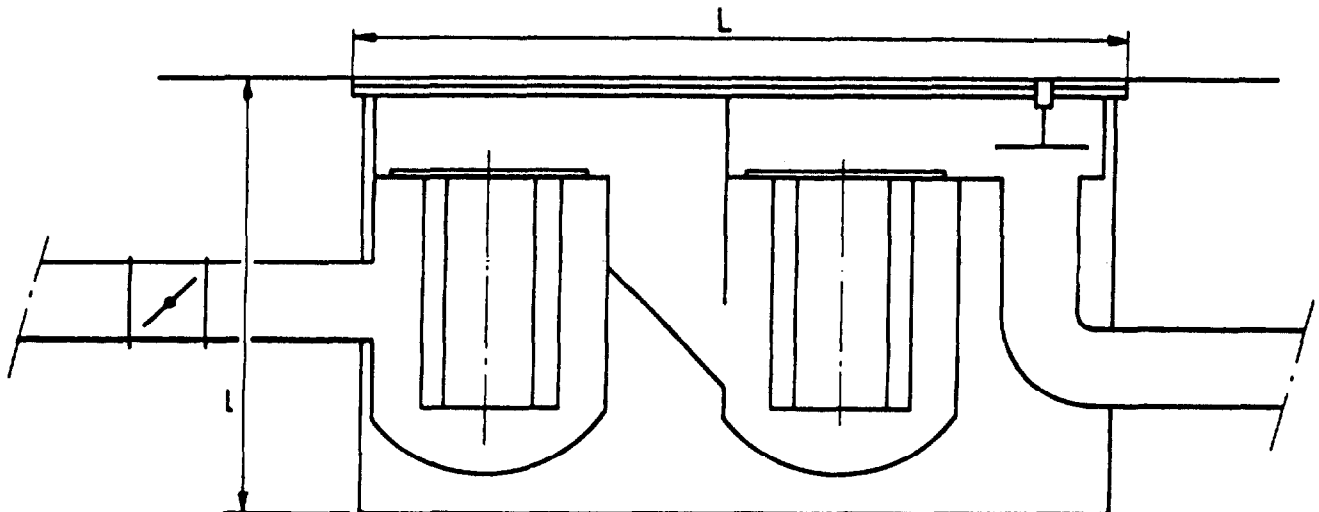
TWO STAGES CASINGS WITH TWO SHIELDED DAMPERS
 IT IS NOT NECESSARY TO PUT THE DAMPERS BETWEEN THE
 TWO STAGES

	L	l	D
500 m ³ /h	1 8 0 0	1 0 3 0	9 0 0
3 0 0 0 m ³ /h	3 2 5 0	1 5 2 0	1 3 7 0



TWO STAGES CASINGS WITH ONE UPSTREAM SHIELDED DAMPER
 THE DOWN STREAM DAMPER IS CONSTITUED WITH A NO
 SHIELDED DAMPER

	L	l	D
500 m ³ /h	1 7 6 0	1 0 3 0	9 0 0
3 0 0 0 m ³ /h	2 7 3 0	1 5 2 0	1 1 6 0



17th DOE NUCLEAR AIR CLEANING CONFERENCE

XI - Filtration casing tests

The 500 m³/hr and 3000 m³/hr filtration casings and their installations are designed to enable testing in situ.

In order to take measurements by the normally used methods, some pressure inlet and outlet points are provided.

Two-stage filtration casing

To enable the testing of the 2nd stage, and improve the homogeneity of the aerosol/air mixture, a metal plate is fitted between the 2 stages in order to set up a turbulence at the outlet of the 1st stage of filtration.

Pressure drop measurements

3000 m³/hr output casing, with clean filter and 2 shielded dampers :

<u>Flow rate</u>	<u>Casing</u>	<u>Filter</u>	<u>TOTAL</u>
2000 m ³ /hr	17.0 mmCE	14.0 mmCE	31.0 mmCE
3000 m ³ /hr	40.0 mmCE	23.0 mmCE	63.0 mmCE
4000 m ³ /hr	70.0 mmCE	31.5 mmCE	101.5 mmCE

500 m³/hr output casing, with clean filter and 2 shielded dampers :

<u>Flow rate</u>	<u>Casing</u>	<u>Filter</u>	<u>TOTAL</u>
400 m ³ /hr	19 mmCE	20 mmCE	39 mmCE
500 m ³ /hr	31 mmCE	26 mmCE	57 mmCE
600 m ³ /hr	45 mmCE	33 mmCE	78 mmCE

3000 m³/hr output two-stage casing, with clean filters and 2 shielded dampers :

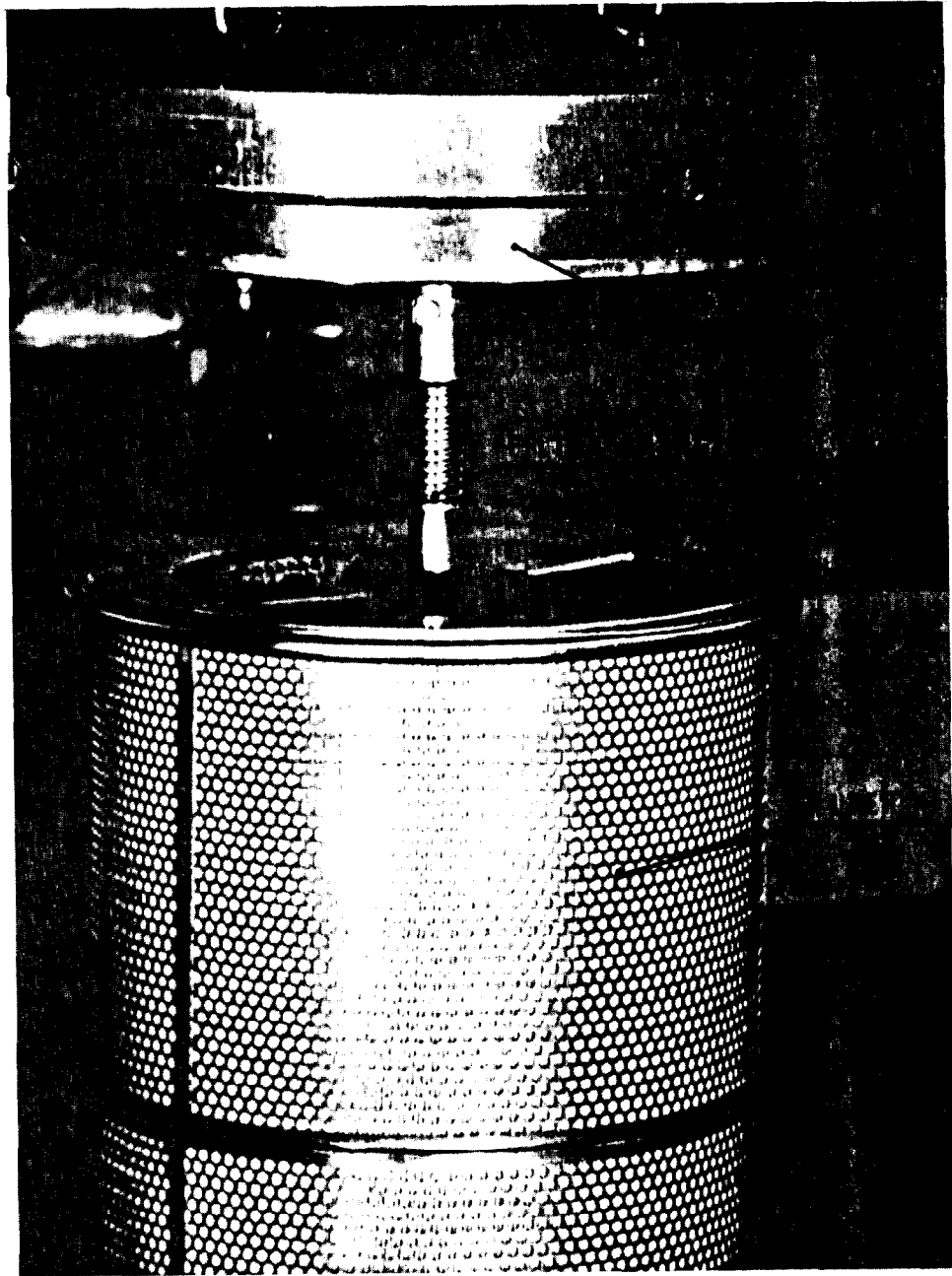
<u>Flow rate</u>	<u>Casing</u>	<u>Filter</u>	<u>TOTAL</u>
2000 m ³ /hr	34 mmCE	28 mmCE	62 mmCE
3000 m ³ /hr	69 mmCE	46 mmCE	115 mmCE
4000 m ³ /hr	117 mmCE	63 mmCE	180 mmCE

XII - French reprocessing plant applications

These filtration casings will be used in the ventilation installations of reprocessing plants, in France.

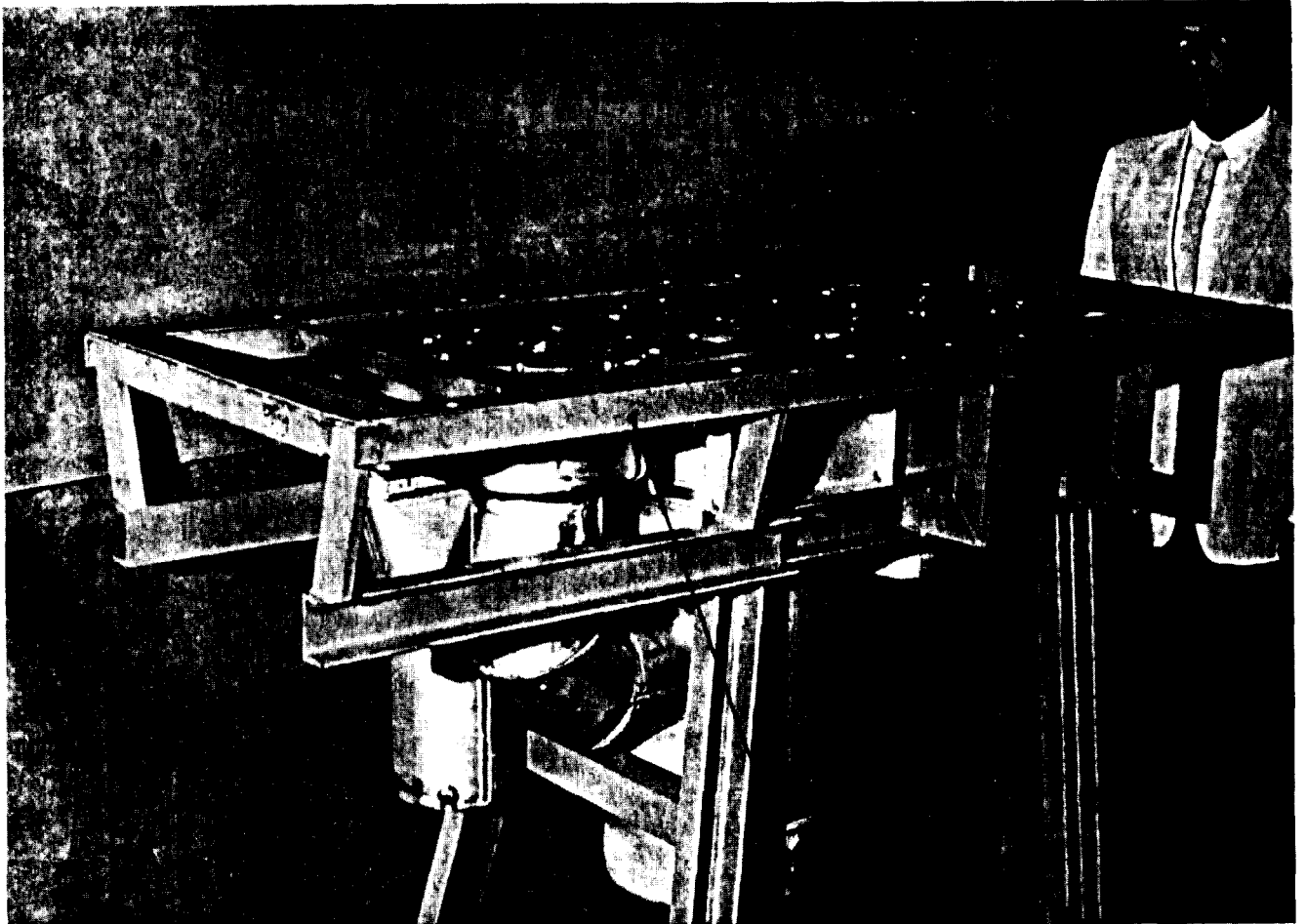
They will be installed in the process wastes ventilation and high-level contamination cell exhaust systems.



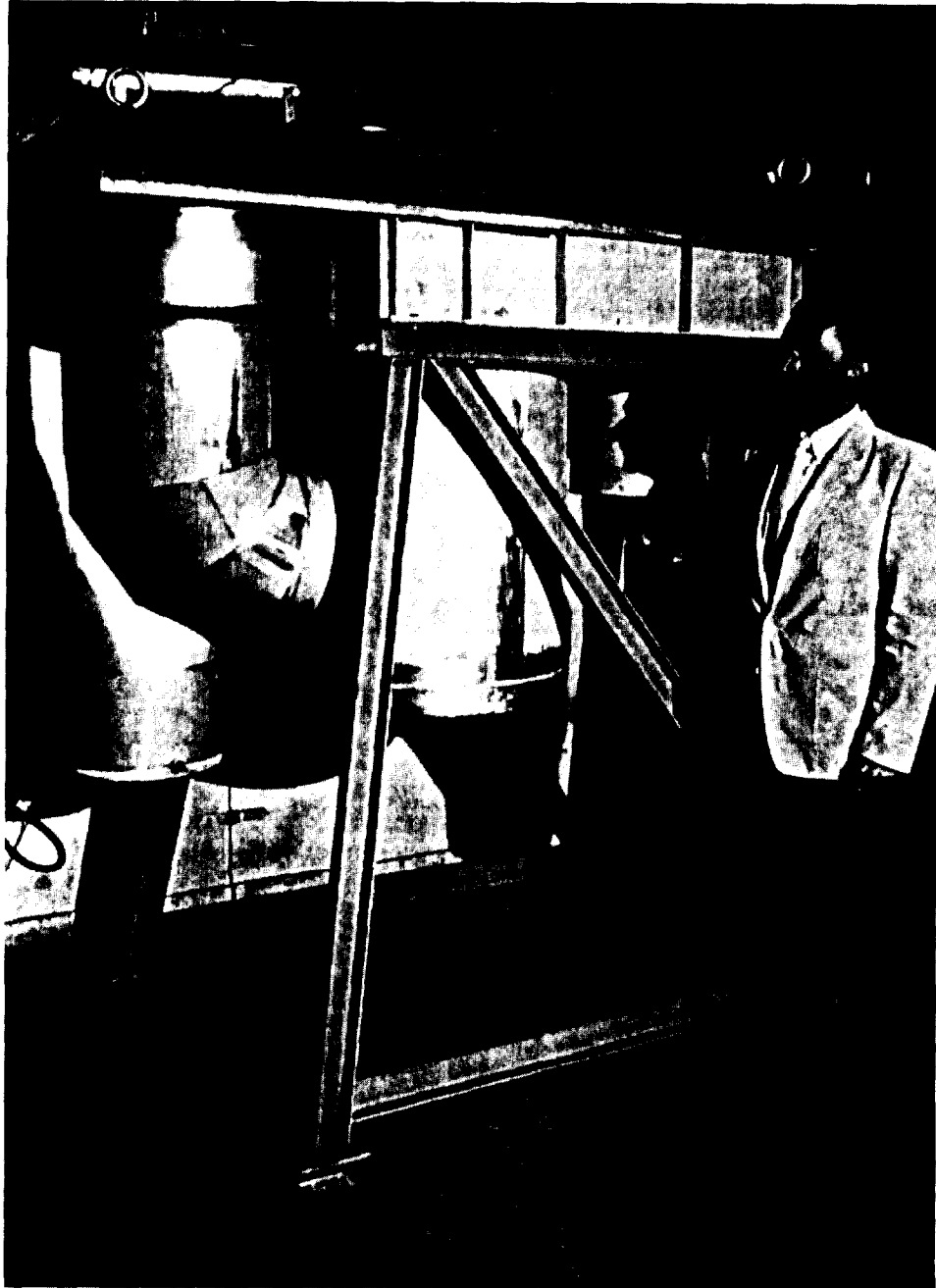




filtration casing 3000 m³/h



filtration casing 500 m³/h



DISCUSSION

GERBER: How has the integrity of the installed filters been measured?

PRINZ: The casing is equipped with inlet and outlet points to verify the integrity of the filtration. The measurement is made by normally used methods with uranium aerosol according to French Standard AFNOR X99011.

BERGMAN: Does the air enter the cylindrical filter from the inside or outside of the cylindrical filter element? The reason I ask is because of the metallic screen on the outside. We have found that if a metallic screen with small openings is on the upstream side of the filter it acts as a template to effectively eliminate large portions of the effective filtering element.

PRINZ: Surely the stainless steel perforated plate acts as a template before the filtering element. Nevertheless, the open section is about 70% of the face area. These plates ensure protection of the filter paper and the rigidity of the filter element. We have decided to direct the flow from the inside to the outside, thereby losing a part of the filtration surface because the dust will then be retained in a sort of pocket and can be better confined, particularly when we move the filter element into the remote maintenance cask, and during the cask travel.

WATSON: How do you dispose of the filters? Can they be compressed?

PRINZ: The 500 m³/h filter element can be disposed of in a 200 liter capacity drum and the 3,000 m³/h filter element can be disposed of in a 400 l capacity drum. These two drums, situated in the decontamination facility, can be compressed. When the remote maintenance cask brings the plug plus the filter element 14 into the decontamination cell, the filter element and its plug are separated by withdrawing the link pin securing the filter element to its supporting rod. The perforated stainless steel plate is not very resistant and we can crush the filter element. It is for this reason that for the 3,000 m³/h element, the safety draw bolt which provides the mechanical link between the bottom end of the filter and the grabbing device is thin.

DYMENT: At its rated flowrate, the resistance of the filter casing is greater than that of the filter element. What is the reason for designing the housing to have such a high resistance?

PRINZ: The filter element has a pressure drop (for normal conditions) of 24 mm WG. The casing has a pressure drop of 40 mm WG. This pressure drop is due to the several changes in the direction of our flow in the casing, especially the last curve after the downstream damper. But if we look at the pressure drop: 40 mm WG for casing + 24 mm WG for filter + 80 or 100 mm WG for reserve logging, we think that it is not necessary to try to reduce the pressure drop of the casing by an increase in the section. More especially, as this type of filter is used for process gaseous wastes which do not have

17th DOE NUCLEAR AIR CLEANING CONFERENCE

very large flow rates. Further, our active cells represent only small part of the ventilation volume of a complete system.

DEVELOPMENT OF FILTERS AND HOUSINGS FOR USE ON ACTIVE PLANT

S. Hackney and R. P. Pratt
United Kingdom Atomic Energy Authority

Abstract

New designs of housings for conventional HEPA filters have been developed and are now in use. A further design is planned for future use. The main features to be developed are the engineering of double door systems to replace bag posting and other methods of filter changing which expose personnel to hazardous environments and the addition of a secondary containment to reduce the role of the gasket seal in the filtration efficiency.

Also under development are circular geometry filters of HEPA standard which offer significant advantages over rectangular filters for applications requiring remote shielded change facilities. Two types of filter construction are being evaluated, conventional radial flow cartridge filters and spiral-wound, axial-flow filters.

The application of circular filters for primary filter systems on active plant is in hand. A push-through change system has been developed for a new cell facility under construction at Harwell. Existing rectangular filters on a high activity cell are being replaced with clusters of small cartridge filters to overcome changing and disposal problems. A similar system but using 1700m³/h filters for large volume off-gas treatment is also being studied.

A remote change shielded filter installation is being developed for use in high alpha, beta, gamma extract systems. The design incorporates large cartridge filters in sealed drums with remote transfer and connection to duct work in the facility. A novel application of the use of double-lid technology removes the need for separate shut off dampers and enables the drums to be sealed for all transfer operations.

I. Square Section Geometry Filter Packs

1.1 Introduction

The particular new designs of filter housings described in this paper came into being from a requirement to eliminate bag-posting of filters in the UK Fast Breeder Reactor Reprocessing and associated facilities programme.

A design was evolved adopting the double door concept of posting which had been in use for some time for the posting of small packages of active materials and waste. A valuable spin-off from this design work, was the introduction of a secondary containment around the filter unit which eliminated the problems associated with the effects of the gasket seal on the filtration efficiency.

The introduction of the secondary containment has lead to design proposals in which filters can be changed without isolating the plant and with no loss of filtration efficiency during the process.

1.2 Design Description

Figure 1 shows the principle of the secondary containment and the double door isolation in schematic form. The filter is housed in a removable box with a gasket seal on both edges of the casing isolating the primary from the secondary containment. Housed in recesses in the ducts are the plugs which are used to isolate the ducts and the filter box such that the box can be removed and transferred to a facility where the used filter is replaced.

In the operating mode the air is drawn through the filter by the extract fans ensuring that both the entry and exits are below atmospheric pressure. Any leakage via the gasket seals will flow from the secondary containment into the primary. Leakage on the active side will pass through the filter whilst leakage on the filtered side is clean air and therefore of no consequence.

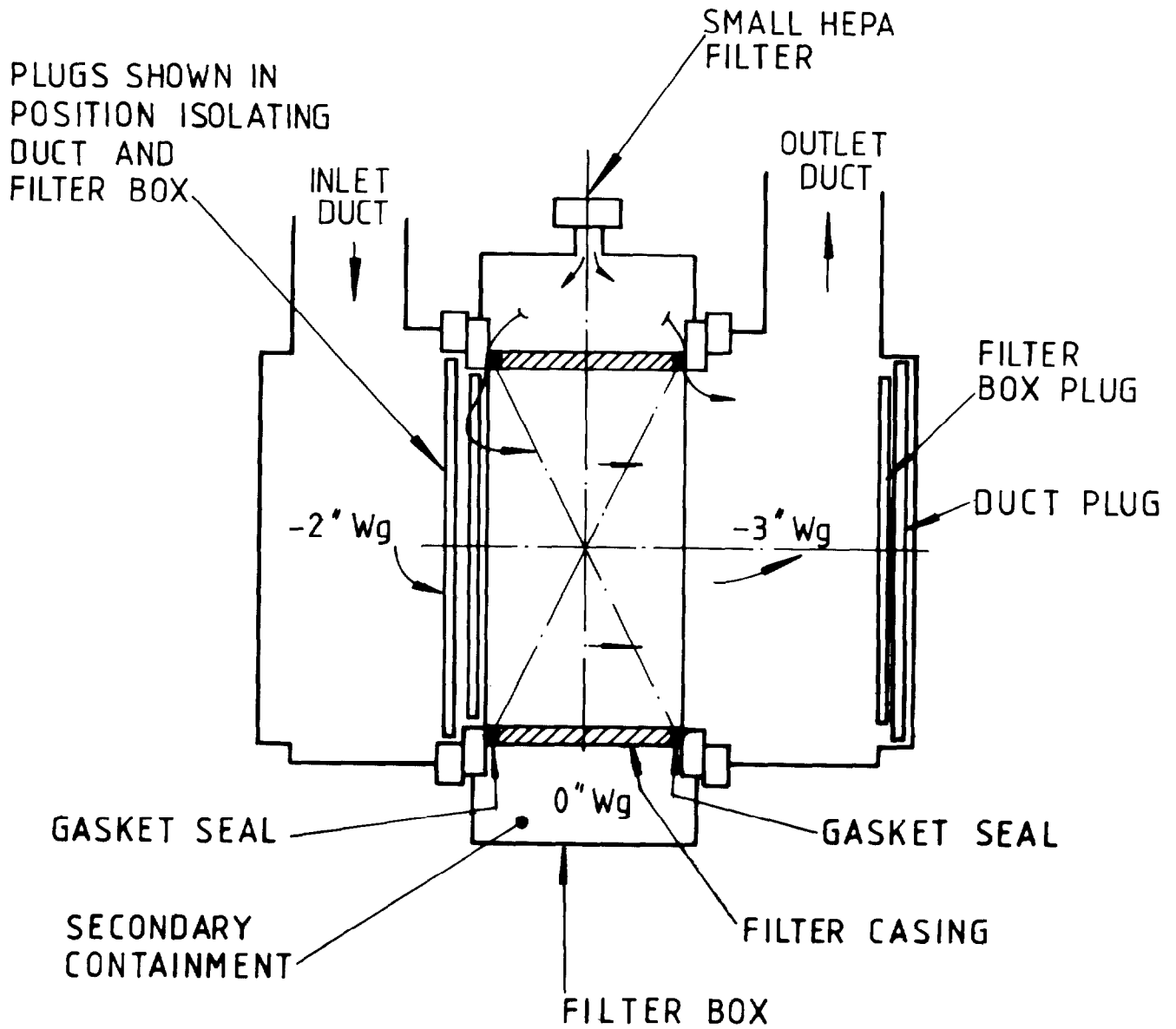


FIGURE 1
HEPA FILTER HOUSING SCHEMATIC

17th DOE NUCLEAR AIR CLEANING CONFERENCE

By-pass of the active air will only occur if the active gasket is leaking and the volume of flow by-passing the gasket on the filtered side is of such a magnitude as to draw down the secondary containment pressure to below the pressure at the filter inlet on the active side. Nominal pressures for each of the air spaces is shown in figure 1 to illustrate the point. The circuit resistance to flow on the secondary containment side is the small filter which is there should a blow-back incident occur. This could be replaced with a flap valve in most cases should it be necessary to increase the by-pass flow capacity.

An alarm can be fitted to the secondary containment, or a monitoring point to detect any pressure difference between that and the atmosphere. This ensures that any gasket deterioration can be detected.

1.3 3×200 cfm Shielded Housing

This unit as shown in figure 2 consists of a leak-tight box with an air inlet and outlet duct running down each side. These ducts can be isolated by moveable plugs to facilitate filter changing. The filter assembly has a similar plug which is attached to the duct plug and withdrawn to the back of the duct to allow air to pass through the filter. With the filter in the operating position any leakage across the filter gaskets is inwards from the secondary containment surrounding the filter. Flow into the secondary containment is filtered and monitored to detect in-leakage into the primary circuit. The filtration efficiency and plugging of the filters can be checked by isolating each filter in turn.

The filter units complete with end plugs are flaked in and out of the housing with no other form of encapsulation being necessary. There are two plants in operation using this type of primary filtration unit.

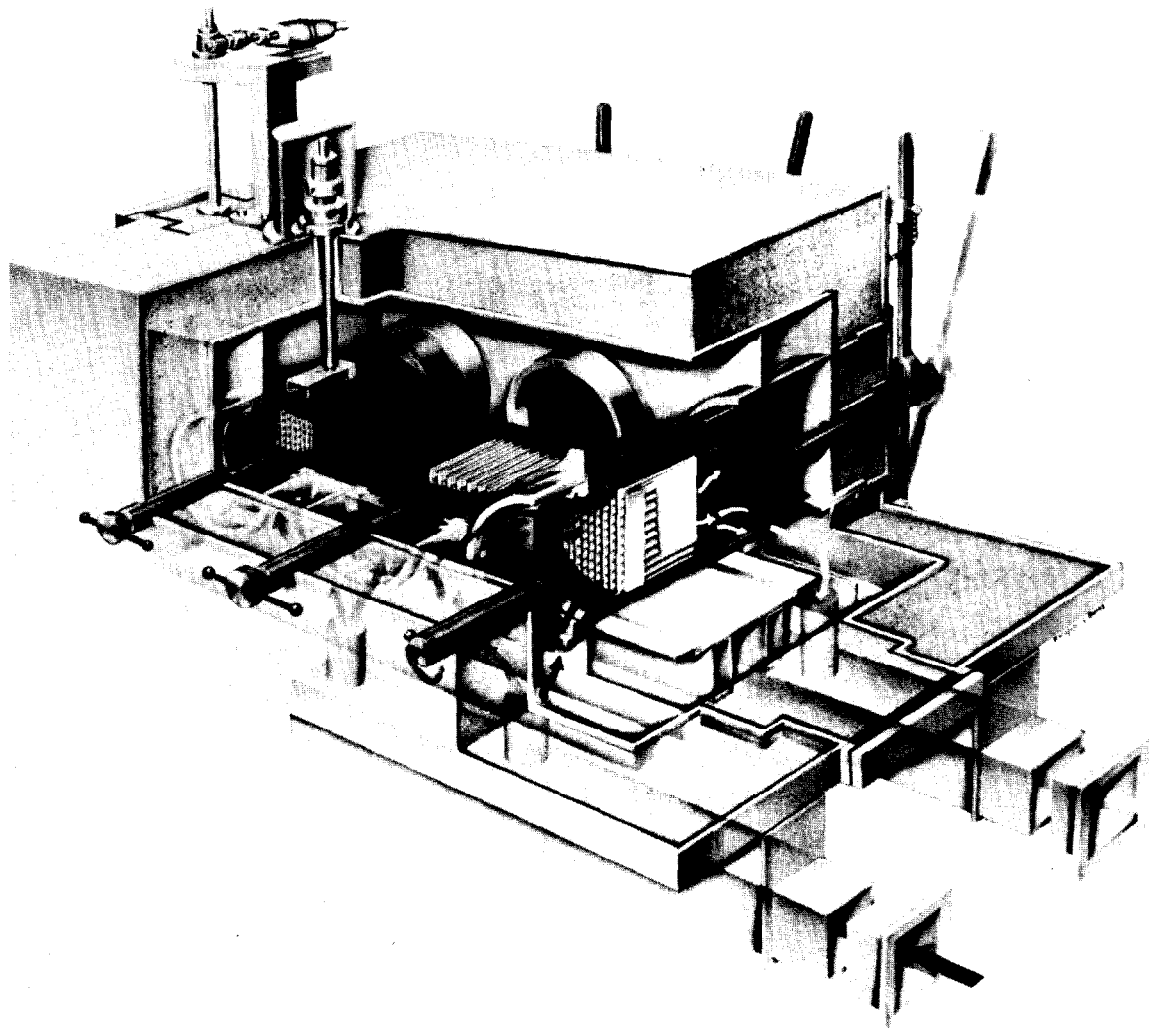


FIGURE 2
FILTER HOUSING

1.4 Unshielded 1000 cfm Filter Housing

The same principles are applied to the 1000 cfm filter units used in non-shielded applications as illustrated in figure 3. The three main components making up one unit are made of cast aluminium. The box containing the filter is inserted between two housings by swinging the filtered side housing on a sponge rubber hinge. The whole assembly is clamped together using four bolts. The isolating plugs are screwed together and removed to the back of the housings during operations.

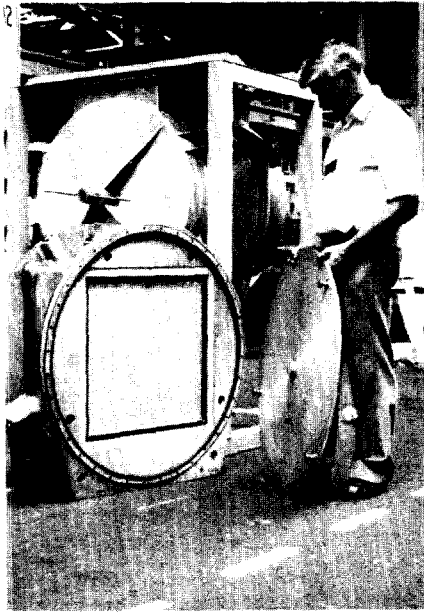


FIGURE 3
1000 cfm UNSHIELDED FILTER HOUSING

1.5 Filter Posting and Breakdown Facility

The filter box containing the filter is removed to a glove box filter break down facility (see figure 4) where the used filter is replaced with a new one and then the used one is broken down to reduce the waste volume. The filter in its box is inserted between the two glove boxes. Using the gloves the blanking plugs are removed from the glove box and the filter box to gain access to the filter. The filter is removed by inserting the clean filter via the new filter glove box and pushing the spent filter into the breakdown box. The gaskets and blanking plugs are replaced and the filter box is returned with the new filter installed back to the filtration plant.

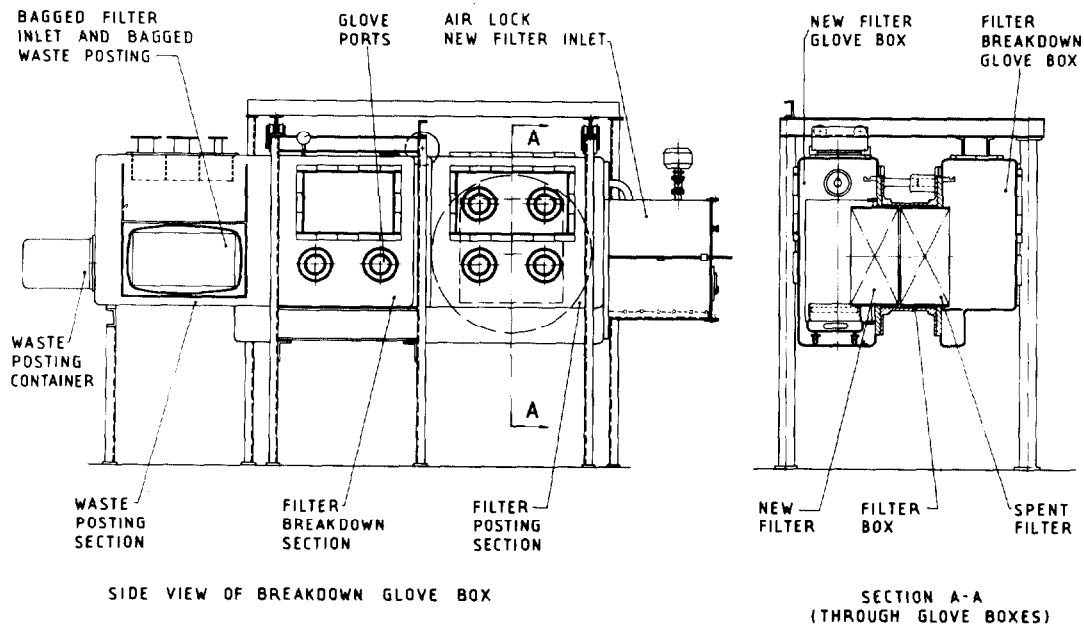


FIGURE 4
FILTER POSTING AND BREAKDOWN FACILITY

There is something like a total of 24,000 cfm installed capacity in operation at the present time. Figure 5 shows a large proportion of this installed capacity at Dounreay, UK. Consideration is being given to using the high flow filter packs to increase the capacity of the existing plants.

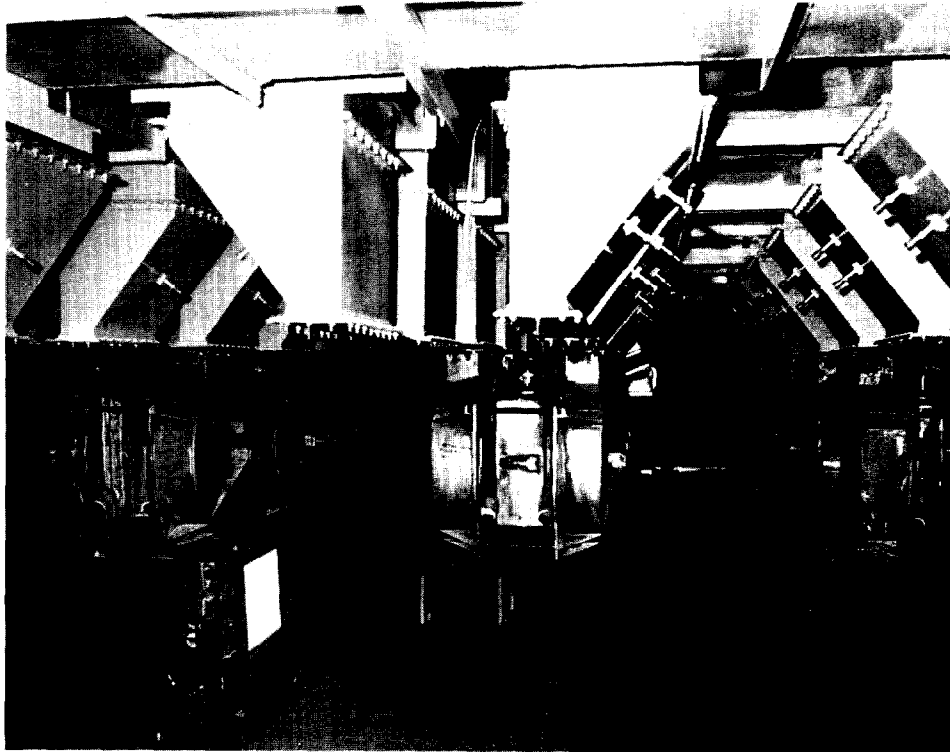


FIGURE 5

1.6 Application of the Air Purge to Multi-Unit Plants

The principle of reducing the gasket seal on the filter pack to an order of secondary importance removes some design limitations and results in a much simpler design which is essential for shielded applications.

The improvements are related to the method of mounting and the replacement of the filter pack.

The assembly as illustrated in figure 6 consists of 2 rectangular steel boxes which extend through the shielding and terminate in flanges against which shield doors at either end are sealed. The box is made to contain the filter packs with the gap between the plates maintained to such tolerances as to ensure the gasket seal is compressed enough to maintain a measure of sealing to isolate the primary from the secondary circuits. Flow apertures are cut in the plates in the form of narrow slots to allow the air to flow through the filters. The unit illustrated has an installed capacity of 10×1000 cfm filter packs. The filter units are surrounded by a secondary containment in the form of a shield wall which is held at atmospheric pressure, with a filtered air inlet.

The filter packs are replaced by inserting a new filter at one end and discharging a used one into the transport flask at the other. This procedure is repeated five times to replace one bank. When the filter packs are traversing the inlet and outlet apertures the gap between the units is prevented from allowing active air to by-pass the filter by the differential pressure sucking clean air from the secondary containment both into the active and non-active sides of the filtration system.

The spent filter is discharged into a box of similar dimensions to the filter housing. This ensures that when the filter is in the box the gaskets are again isolating the active side of the filter paper. During the transition from the housing to the box an air purge is introduced at the joint between the housing and box flange to ensure the sealing faces external to the containment are not contaminated. When the filter has been pushed

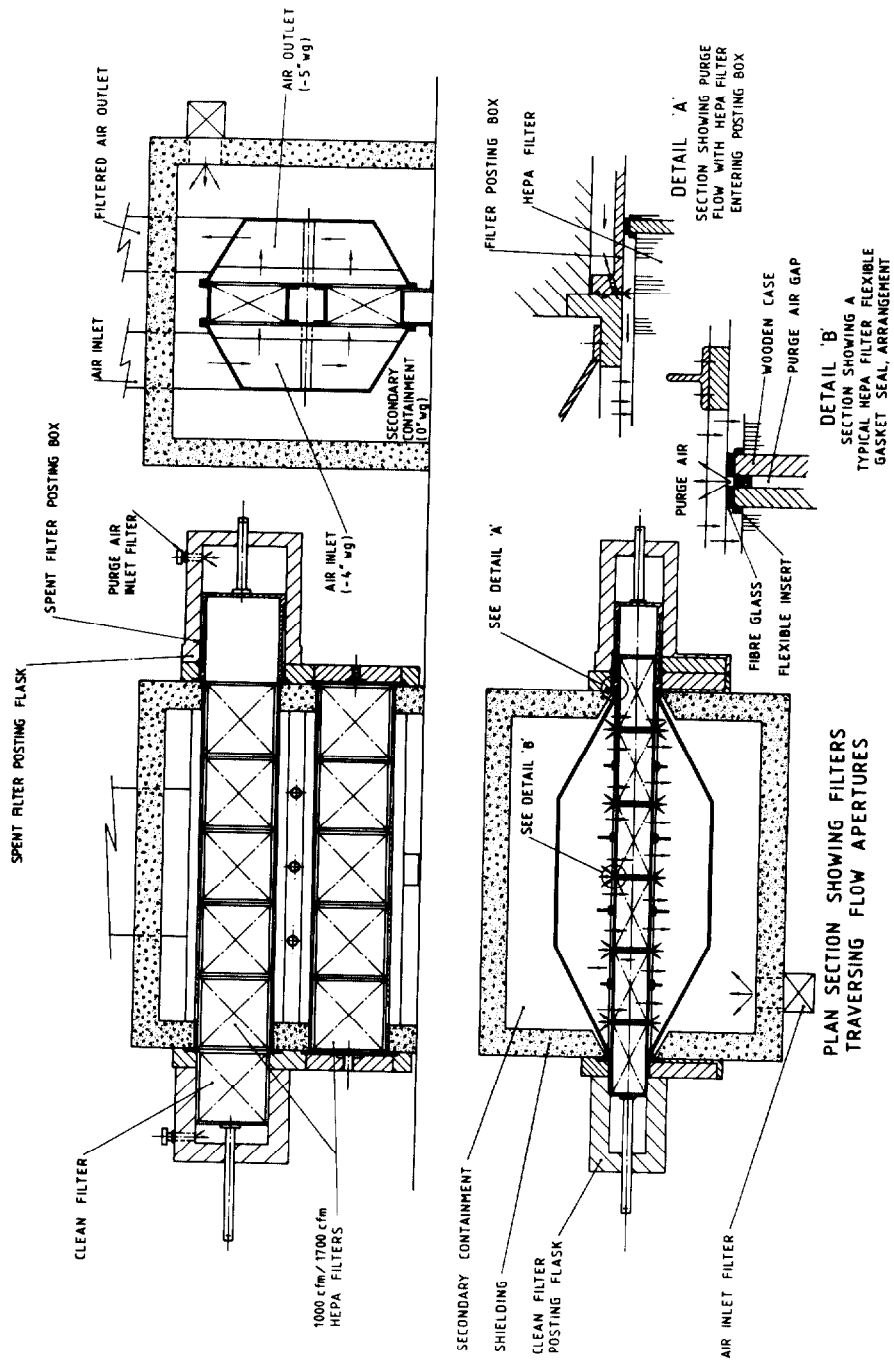


FIGURE 6
MULTI-HEPA FILTER ARRANGEMENT WITH BAG-LESS TRANSFER

17th DOE NUCLEAR AIR CLEANING CONFERENCE

into the filter box the latter is withdrawn into the flask and both shield doors are closed and sealed to maintain containment. The used filter is discharged from the flask at some central waste treatment facility.

Further development is necessary on the flexible gasket seal to ensure flexibility to maintain an acceptable seal and at the same time have a frictional resistance to movement that will allow the filter packs to be moved along during replacement. The design illustrated in figure 5 shows a wooden case filter with a glass fibre cloth outer skin to the gasket seal similar to the existing high temperature seals, the cloth edges being retained by a wooden beading to form a firm fixing. If a more flexible filler than the glass-wool used at present is required possibly sponge rubber could be substituted.

II. Circular Filter Development

2.1 Introduction

An assessment of the problems associated with the installation, removal and ultimate disposal of standard deep-pleat rectangular filters has highlighted the need for alternative designs of filter inserts for remote change filter systems where high levels of alpha, beta, gamma activity can be expected. The main disadvantages of the standard filter insert result from its physical shape.

The rectangular filter is difficult to handle and position remotely, requires a high degree of flatness for the sealing face of the housing, is difficult to post into and out of a containment and produces severe problems in terms of its ultimate disposal into the standard 200 litre drum used by the UK nuclear industry.

An examination of alternative filter geometries highlighted several advantages for filters of circular geometry. These were:-

1. Circular filters would be compatible with developed double-lid posting and containment systems.
2. Circular filters would be compatible with existing waste treatment facilities and disposal routes based on 200 litre drums without breakdown or physical manipulation.
3. Circular filters could be sealed into the housings with circular pistons seal rings onto cylindrical sealing surfaces which would be easy to generate to the required tolerances and surface finishes. They could be designed such as to require no sophisticated clamping systems to effect a seal between filter and housing.
4. Circular filters would be easier to handle and move remotely.
5. Appropriate design considerations would lead to cylindrical filters significantly weaker in strength than conventional rectangular filters with subsequent ease of volume reduction by crushing prior to ultimate disposal should this be required.

Examination of current filter manufacturing technology and expertise suggested that production of radial flow cartridge filters of HEPA standard was entirely feasible at the required ratings up to $1700\text{m}^3/\text{h}$. Some companies had been producing high integrity filters of this type with ratings up to $200\text{m}^3/\text{h}$ for some time, and with the introduction of manufacturing capability for pleated panels as used in high-capacity filters no difficulties were anticipated in scaling up to $1700\text{m}^3/\text{h}$.

One possible disadvantage of the radial flow filter for some applications is that an air plenum is required within the housing to collect the flow after its passage through the filter prior to ducting away to extract. A much simpler, smaller and therefore cheaper housing could be envisaged if a cylindrical filter with axial flow characteristic were developed. Designs available were found to be limited to a small respirator filter approximately 100 mm diameter by 25 mm deep produced by spiral winding techniques, or to the use of a rectangular deep pleat element set into a cylindrical case.

It was therefore decided that two parallel lines of development would be followed to produce circular filters. Firstly in conjunction with the industry existing technology would be used to develop $1700\text{m}^3/\text{h}$ radial flow cartridge filters. Secondly the spiral winding technique would be developed to produce axial flow circular

filters in a range of sizes from 200 mm ϕ to 500 mm ϕ , with target rated air flows of 200 to 2000 m³/h respectively.

2.2 Progress to Date

2.2.1 Radial flow cartridge filters. This filter design has been developed in collaboration with two British manufacturers, Temperate Filtration Ltd and Machine Control Ltd. The target size for a rated flow of 1700 m³/h was 500 mm ϕ by 620 mm long, compatible with the 200 litre waste drum for ease of disposal. This target has been achieved by both companies, and a prototype filter is shown in figure 7. The filters consist simply of an annulus of pleated paper supported within a perforated metal tube and sealed top and bottom, the lower end being solid. Both companies are able to produce filters with conventional metal trays and sealed with adhesives or with stiff polyurethane mouldings. In addition to the simple single annulus design Machine Control has developed an extended life version⁽¹⁾ incorporating a second annulus of pleated paper inside the main annulus, figure 8. Flow distribution for this filter is shown in figure 9. Performance testing of the filters has demonstrated that the life of the extended-life design, in terms of dust loading versus pressure drop, is increased significantly for both sub-micron carbon black and for BS No. 2 test dust (5 μ mean size). Results of the test programme are given in Table I.

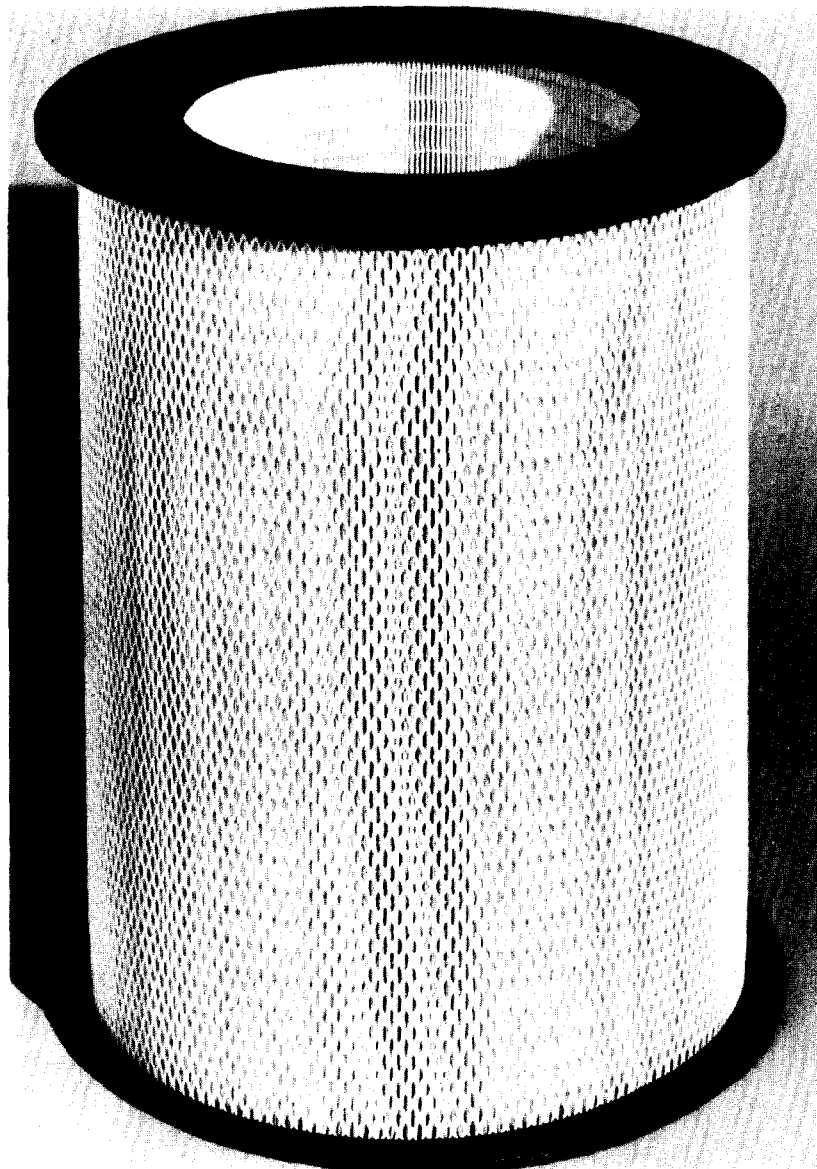


FIGURE 7
RADIAL-FLOW CIRCULAR FILTER RATED AT 1700 m³/h

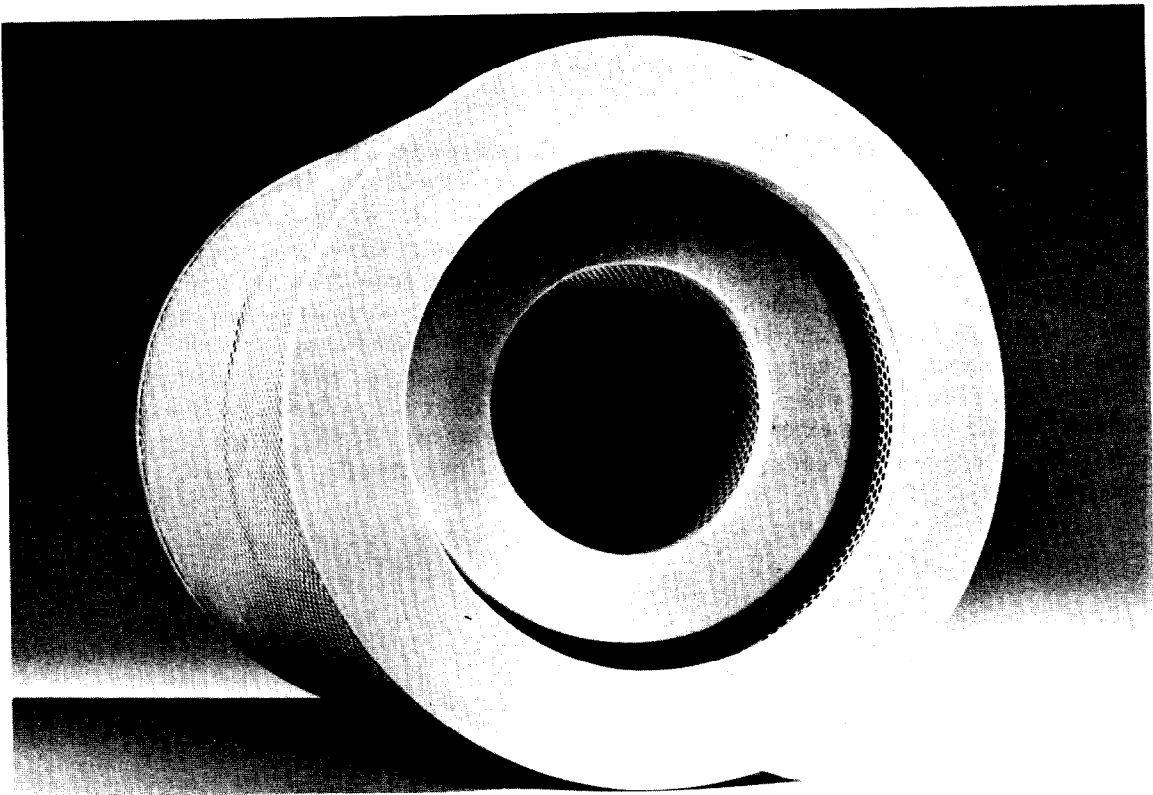


FIGURE 8
EXTENDED LIFE RADIAL FLOW CIRCULAR FILTER RATED AT $1700\text{m}^3/\text{h}$

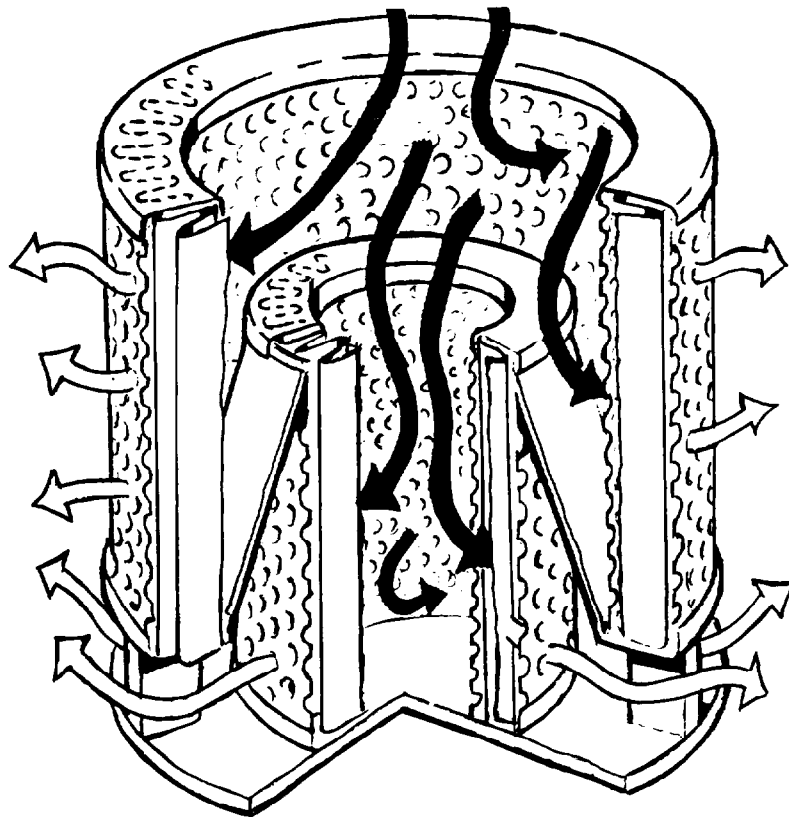


FIGURE 9
AIR-FLOW DISTRIBUTION WITHIN AN EXTENDED-LIFE RADIAL-FLOW
CIRCULAR FILTER

Table I. Performance of Circular Filters

<u>Parameter</u>	<u>Radial Flow Cartridge Type</u>		<u>Axial Flow Type</u>
	<u>Standard</u>	<u>Extended Life</u>	
Physical size mm	430 ϕ \times 610	480 ϕ \times 610	450 ϕ \times 300
Rated Flow (m ³ /h)	1700	1700	800
Pressure Drop at Rated Flow (mm water gauge)	25	25	25
Efficiency (BS Sodium Flame)%	99.95	99.95	99.95
Burst Strength (mm water gauge)	300	300	300
Dust loading to 150 mm water gauge BS Nos 2 (Kg)	13	18	
Dust loading to 150 mm water gauge (Carbon block) (Kg)	0.4	0.65	0.36

Preliminary work has been carried out to assess the potential of volume reduction of the filter prior to drum disposal. It has been shown that the filter can be reduced to one quarter of its initial volume by simple compaction by a hydraulic ram within the 200 litre drum (figure 10).

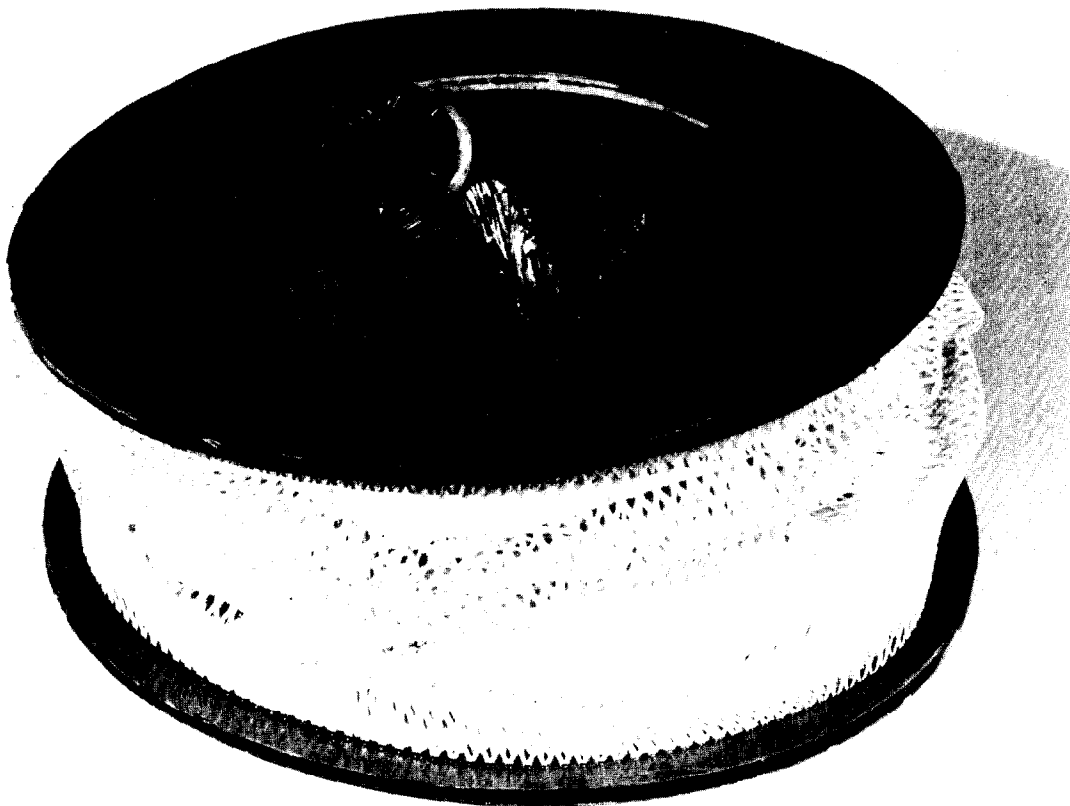


FIGURE 10 CIRCULAR FILTER CRUSHED TO 25% OF ORIGINAL VOLUME

Work is still progressing on the optimum design of gasket for this design of filter. Whilst the gasket design has to be complementary to the housing design, it is anticipated that the best solution will be the use of a "C" section ring in the inlet throat of the filter, (figure 11) enabling the filter to be sealed purely through the location of the insert in the housing, and requiring minimum dimensional tolerancing of the insert except for the inlet throat itself. No clamping would be necessary to effect a seal and the use of generous tapers on the seal spigot of the housing would simplify remote positioning.

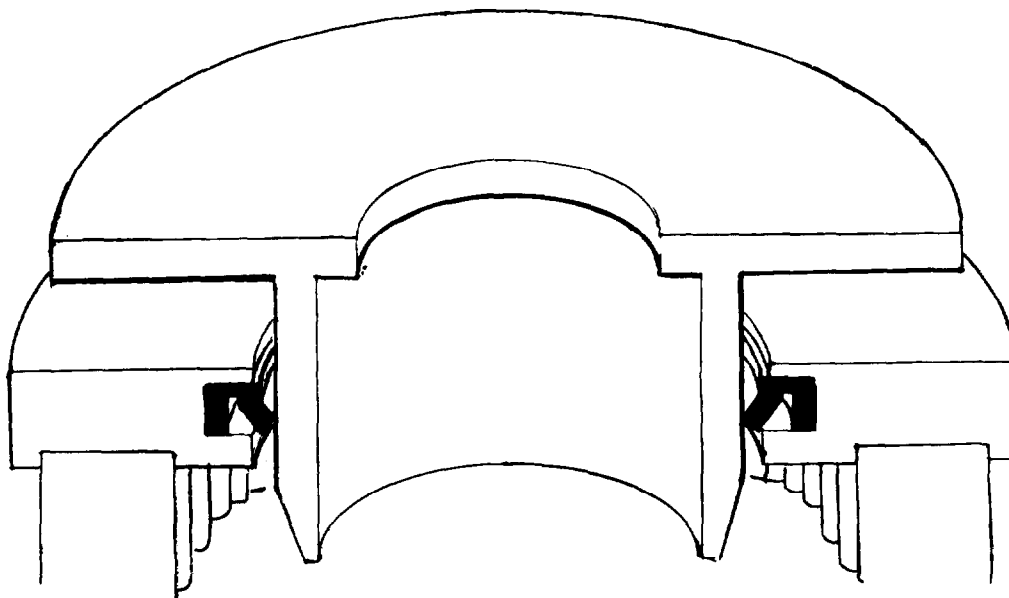


FIGURE 11
RADIAL FLOW FILTER SEAL CONFIGURATION

2.2.2 Axial Flow Filters. The flow distribution and construction of the spiral wound filter is shown in figure 12. Preliminary work was aimed at scaling up the existing respirator filter to provide a 200 mm ϕ \times 300 long filter with a target rating of 200 m³/h.

However, although from a production point of view there were few problems in producing larger prototype filters, flow tests verified the need to provide spaced flow channels in filters longer than 50 mm to reduce the pressure drop through the filter.

Filters have been produced in limited numbers for evaluation in two sizes, 200 mm ϕ and 500 mm ϕ , both 300 mm long (figure 13). The volumetric flow rate for a differential pressure of 25 mm water gauge is 300 m³/h and 800 m³/h for the 200 mm diameter and 500 mm diameter filters respectively. Performance data for the 500 mm diameter filter is given in Table 1.

It is anticipated that these filters when fully developed will be fitted into open ended ducts with simple 'C' section piston seals (figure 12). The installation will therefore be extremely simple and no clamping will be required to effect a seal. The strength of the filter case need be sufficient only to overcome the friction of the seals in the housing, allowing a low strength filter to be produced which would be correspondingly easy to volume-reduce by crushing prior to disposal if required.

III. Application of Circular Filters

3.1 Glove Box Filters

The first circular-bodied filters used in the UK nuclear industry were small 5 m³/h glove box filters, introduced in the mid sixties. The filter element was a hand-folded radial-pleated glass fibre paper element

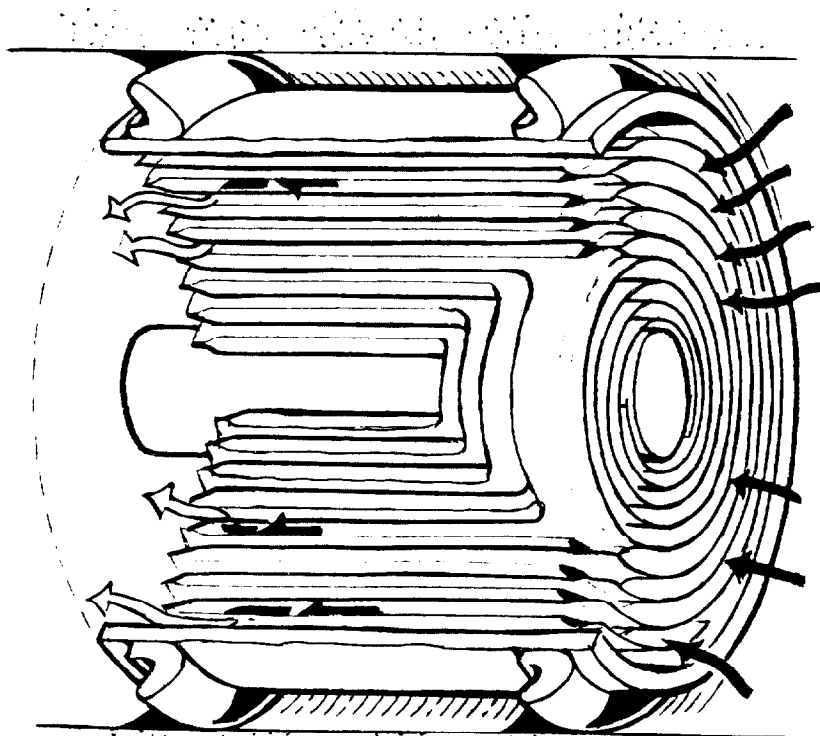


FIGURE 12
AIR-FLOW DISTRIBUTION WITHIN AN AXIAL-FLOW CIRCULAR

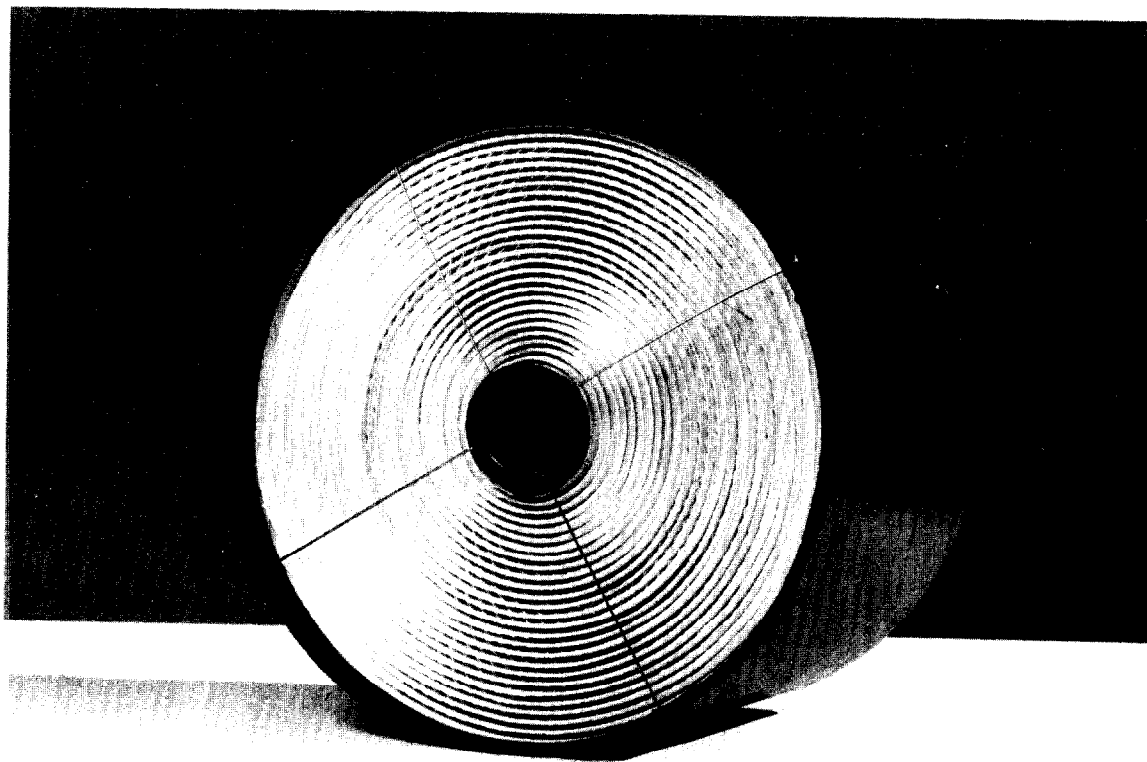


FIGURE 13
PROTOTYPE AXIAL-FLOW CIRCULAR FILTER

sealed into moulded housings to provide an axial flow through the unit. Recently the filter element has been redesigned and is now constructed from an annulus of machine pleated glass-fibre paper sealed into the same mouldings. The use of machine pleated paper has enabled a greater area of paper to be used with the result that the filter is uprated to $20 \text{ m}^3/\text{h}$. The efficiency and pressure drop at rated flow is unchanged at 99.998% and 10 mm water gauge respectively.

3.2 High-level Active Cell Primary Filters

The primary extract filters for a suite of high activity cells were designed to fit in a well under the cell floor.

The filters specified are 2 standard deep-pleat filters measuring $380 \times 380 \text{ mm} \times 220 \text{ mm}$ rated at $400 \text{ m}^3/\text{h}$ and rely on their weight and generated pressure drop to effect a seal onto a feature in the well by conventional gaskets. Operating experience has revealed that on two cells of the suite activity levels on the primary filters were such that posting and transfer for ultimate disposal was restricted to the use of standard $7'' \phi$ containers within a shielded flask. Thus it has been necessary to dismantle the filters remotely within the cell after a filter change into pieces small enough to be accommodated within the $7'' \phi$ containers.

The primary filters are now being replaced with a cluster of 10 radial flow cartridge filters, (figure 14) measuring $165 \text{ mm } \phi \times 200 \text{ mm}$ long rated at $85 \text{ m}^3/\text{h}$ each. The filters are sealed into a plate sealed into holes in a metal plate by piston 'O' ring seals fitted in the top flange of each filter. The plate is sealed onto a feature of the well using conventional gaskets which provides a lower plenum for the filtered air and space for the filter bodies. Thus a seal is effected which requires no clamping, and which enables the filter to be changed easily using cell master-slave manipulators. Disposal is directly into the container with no dismantling being necessary.

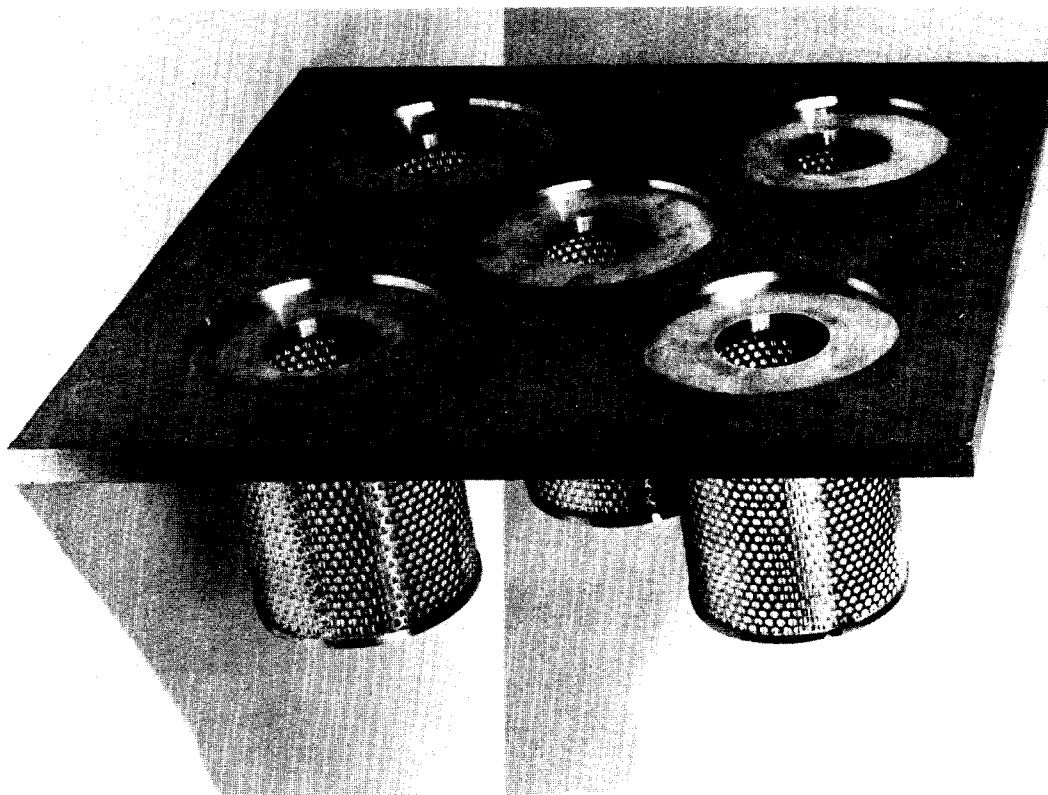


FIGURE 14
CLUSTER OF RADIAL-FLOW FILTERS FOR ACTIVE CELL PRIMARY FILTER INSTALLATION